Evaluation of two novel perimetric techniques for the detection of open angle glaucoma – an in-depth analysis

Christoph Andrea Castelberg
Doctor of Philosophy

Cardiff University 2010

ProQuest LLC
789 East Eisenhower Parkway
P.O. Box 1346
Ann Arbor, MI 48106-1346

Christoph Andrea Castelberg
Doctor of Philosophy
Cardiff University 2010

Evaluation of two novel perimetric techniques for the detection of open angle glaucoma – an in-depth analysis

The aim of this thesis was to evaluate two novel forms of perimetry for the detection of open angle glaucoma; namely Short-wavelength Automated Perimetry (SWAP) using the Swedish Interactive Threshold Algorithm (SITA) and Pulsar perimetry using Tendency Oriented Perimetry (TOP).

The evaluation of SITA SWAP was undertaken on 29 normal individuals naïve to perimetry; 25 individuals with ocular hypertension (OHT), and 25 with open angle glaucoma (OAG) all of whom were experienced in Standard automated perimetry (SAP). All individuals underwent SITA SWAP, SITA Standard and SITA Fast perimetry in each eye at each of five weekly visits. The results of the investigations revealed a greater learning effect, a greater between-examination variability and a greater between-individual within-visit between-algorithm variability and no indication of a better structure function relationship (as assessed by the Heidelberg Retina Tomograph II) with SITA SWAP compared to either SAP algorithm.

The evaluation of Pulsar perimetry was undertaken on 25 normal individuals naïve to perimetry, 26 individuals with OHT and 27 individuals with OAG. All individuals underwent SITA Standard and Pulsar perimetry in each eye at each of five weekly visits. The apparent heterogeneity in any learning effect (overall demonstrated by the Bland and Altman plots) limits the utility of Pulsar perimetry for follow-up examinations.

The influence of defocus on Pulsar perimetry was evaluated on 17 normal individuals naïve to perimetry and 14 individuals with OAG. All individuals underwent SITA Standard and Pulsar perimetry in one designated eye at each of five weekly visits using 4 different defocus levels for Pulsar perimetry. The slopes of degradation in the group mean MS and mean MD revealed that an appropriate correction for viewing distance is mandatory with Pulsar perimetry.

SAP, SITA, SWAP, Pulsar perimetry, TOP, HRT, learning effect, defocus

To Ursula

ACKNOWLEDGEMENTS

I would like to thank the following persons without whose help and input this thesis would not have been completed.

Firstly, I would like to extend my very special thanks to my supervisor, Prof. John M. Wild, for his endless patience; his guidance; and his scientific, as well as his personal, support.

Secondly, I am very grateful to PD Dr. med. Mario Zulauf for his intellectual contribution, his vast expertise in ophthalmology and his help in recruiting patients with ocular hypertension and with glaucoma.

I also wish to thank Ms Bea Thöny, the nurse who organised appointments for the patients and who carried out some of the perimetry; Peter and Ivan Grischott for their computer assistance; Mr. David Shaw, Senior Medical Statistician, for the Analyses of Variance; to the two mathematics experts, Dr. Martin Kern and Dr. Frank Rakebrandt who provided a mathematical basis for the Learner's Index; and to Hector Alvarez, my English teacher, for his coaching of English, a foreign language to me.

I would also like to thank the staff of my practice who covered for me during my commitment to this thesis.

Finally, I would especially like to thank my wife, Ursula, and also Carlo and Sidonia, my children, for all their personal support and encouragement during this demanding period.

Declaration

This thesis has not been previously presented with the expectation of receiving any degree elsewhere and is not being submitted now in order to receive any degree from any institution other than from Cardiff University.

Signed.....Ov. Callberg..... **(candidate)**
Date.....Landgraaf, 14 th February 2010

Statement 1

This thesis is based on my own studies and research, except where I state the source with the clearly corresponding references. A full list of references is found as an appendix.

Signed.....Ov. Callberg..... **(candidate)**
Date.....Landgraaf, 14 th February 2010

Statement 2

If my thesis is accepted, I give permission for it to be available for photocopying, for inter-library loan and for the title and the abstract to be made accessible to outside institutions.

Signed.....Ov. Callberg..... **(candidate)**
Date.....Landgraaf, 14 th February 2010

Statement 3

If my thesis is accepted, I agree to make the entirety of the data collection derived from my own investigations available to any who might use it for further exploration.

Signed.....Ov. Callberg..... **(candidate)**
Date.....Landgraaf, 14 th February 2010

LIST OF CONTENTS

LIST OF TABLES

LISTE OF FIGURES

KEY TO THE ABBREVIATIONS USED IN THE TEXT

ACAT	**Age-corrected average threshold**
AGIS	**Advanced Glaucoma Intervention Study**
ANCOVA	**Analysis of Co-Variance**
ANOVA	**Analysis of Variance**
ARA	**Abnormal response area**
CDAR	**Cup-disc Area Ratio**
CFF	**Critical flicker fusion**
CFFT	**Critical flicker fusion thresholds**
CI	**Confidence interval**
CIGTS	**Collaborative Initial Glaucoma Treatment Study**
CLM	**Contour Line Mean Height**
CLV	**Corrected Loss Variance**
CMS	**Central mean sensitivity**
CoV	**Coefficient of Variation**
CPSD	**Corrected Pattern Standard Deviation**
CSF	**Contrast sensitivity function**
CSM	**Cup Shape Measure**
CV	**Cup Volume**
DA	**Disc Area**
dB	**Decibels**
DDc	**Diffuse Defect Index**
DS	**Dioptres**
EMGT	**Early Manifest Glaucoma Trial**
ERF	**Error Related Factor**
FDT	**Frequency-Doubling Technology**
FOS	**Frequency of seeing curve**
FSM	**Mikelberg Discriminate function**
GCP	**Glaucoma Change Probability analysis**
GH	**General Height Index**
GHT	**Glaucoma Hemifield Test**
GPA	**Glaucoma Progression Analysis**
GPI	**Glaucoma Progression Index**
GPS	**Glaucoma Probability Score**
HFA	**Humphrey Field Analyzer**
HRP	**High-pass Resolution Perimetry**
HRT	**Heidelberg Retina Tomograph**
HVC	**Height Variation Contour**
IOP	**Intra ocular pressure**
K-cell	**Small bistratified cells (koniocellular pathway)**
LD	**Localised Defect Index**
LF	**Long-term fluctuation**
LE	**Left eye**
LI	**Learner's Index**
LOCS	**Lens Opacities Classification System**
LV	**Loss Variance**
M-cell	**Parasol cells (magnocellular pathway)**
MD	**Mean Defect/ Mean Deviation**
MRA	**Moorfields Regression Analysis**

MRH	**Mean Retinal Height**
MS	**Mean Sensitivity**
OCT	**Optic coherence tomography**
OAG	**Open angle glaucoma**
OHT	**Ocular hypertension**
OHTS	**Ocular Hypertension Treatment Study**
OMA	**Ocular media absorption**
ONH	**Optic nerve head**
PD	**Pattern Deviation**
PMS	**Peripheral mean sensitivity**
P-cell	**Midget cells (parvocellular pathway)**
PSD	**Pattern Standard Deviation**
RA	**Rim Area**
RB	**Burk Discriminate function**
RE	**Right eye**
RF	**Reliability factors**
RNFL	**Retinal nerve fiber layer**
ROC	**Receiver operating characteristic**
RP	**Reference Plane**
RV	**Rim Volume**
src	**Spatial resolution and contrast units**
SAP	**Standard automated perimetry**
SASP	**Semi-automated static perimetry**
SF	**Short-term fluctuation**
SR	**Spatial resolution**
SITA	**Swedish Interactive Threshold Algorithm**
SKD	**Stato-kinetic dissociation**
SKP	**Semi-automated kinetic perimetry**
SLP	**Scanning laser polarimetry**
SLT	**Scanning laser tomography**
SRP	**Standard Reference Plane**
sLV	**Square root of the Loss Variance**
SWAP	**Short-wavelength Automated Perimetry**
SWS	**Short-wavelength sensitive**
TCA	**Topographic Change Analysis**
TD	**Total Deviation**
TMP	**Temporal Modulation Perimetry**
TOP	**Tendency Oriented Perimetry**
TSF	**Temporal sensitivity function**
v	**versus**
VA	**Visual acuity**

CHAPTER 1

FUNDAMENTALS OF PERIMETRY

1.1 Introduction

1.1.1 The visual field

The visual field is that part of the environment which is visible to the steadily fixating eye. The maximum extent of the monocular visual field is 60° superiorly, 60° nasally, 70° inferiorly and 90° temporally. The field within 30° eccentricity from fixation is termed the central field and that beyond 30° eccentricity is termed the peripheral field (Anderson and Patella 1999).

Every point in the retina corresponds to a defined location in the visual field. Objects seen in the superior visual field are imaged on the inferior retina and vice versa. Objects seen in the temporal visual field are imaged on the nasal retina and vice versa.

1.1.2 The differential light threshold

The visual field is assessed by measuring the differential light threshold at different locations within the field. The differential light threshold is the minimum stimulus luminance (ΔL), against a constant background luminance (L), necessary to elicit a visual response and is expressed as ($L/\Delta L$) (Anderson and Patella 1999). The differential light sensitivity is the reciprocal of the differential light threshold and is expressed as ($\Delta L/L$).

1.1.3 The island of vision

The 'island of vision surrounded by a sea of blindness' (Traquair 1927) is a three-dimensional schematic analogy of the visual field, whereby increasing differential light sensitivity to the stimulus is represented along the z-axis and the stimulus location is represented along the x and y axes, respectively. Under photopic conditions, the island of vision exhibits a peak of sensitivity, which corresponds to the fovea, and progressively reduces in height towards the shoreline of the sea of blindness. The slope of the island of vision is steepest nasally and flattest temporally. Within the island of vision at approximately 15° temporally, and 1.5° inferiorly, to fixation lies the physiological blind spot. This represents the projection, through the optics of the eye, of the optic nerve head. The blind spot extends 5.5° degrees horizontally and 7.5° vertically.

The analogy of the island of vision surrounded by a sea of blindness is a useful and easily-understood way to describe visual field loss to a patient; however, the concept is of little clinical use for the detection and follow-up of visual field loss.

The aim of perimetry is to assess the dimensions of the hill of vision and, hence, the integrity of the visual system as a whole; the latter involves pre-retinal factors, the retina, the optic nerve and the pathways to the visual cortex.

A localised, or focal, area of reduced sensitivity is termed a relative scotoma, or relative defect, and is analogous to a valley or crater, of variable depth, within the island of vision. An absolute defect exhibits no perception to the maximum stimulus luminance of the given perimeter. A general reduction in sensitivity across the visual

field is termed a generalised, or diffuse, loss and is analogous to an overall reduction in the height of the island of vision. The loss of the peripheral field in the presence of a normal central field of varying extent is termed a constriction and is analogous to an erosion of the shore line of the island of vision. The constriction may be localised to a specific region or may be generalised affecting the whole field, as in a concentric constriction. The type of visual field abnormality is determined by the location of the lesion and is governed by the underlying anatomy of the visual pathway. All visual field defects can be categorised as either pre-chiasmal, chiasmal or post chiasmal. A pre-chiasmal defect includes those arising from pre-retinal abnormally, such as a media opacity; a retinal nerve fibre layer abnormality; an outer retina abnormality involving the receptors; or an optic nerve abnormality. An arcuate defect, for example, which respects the horizontal midline, can arise from glaucomatous damage to the retinal nerve fibre layer; a bilateral quadrantanopia (which respects the vertical midline and affects one quadrant of the visual field) and which is homonymous (i.e. affects the same side of the field in both eyes) and congruous (i.e. is symmetric between the two eyes) and is present superiorly arises from a post chiasmal abnormality in the temporal lobe of the cortex.

1.1.4 Kinetic and static perimetry

There are two types of perimetry, kinetic and static perimetry. Kinetic perimetry describes the presentation, and movement, of a stimulus usually from the non-seeing to the seeing region of the visual field. The eccentricity at which the stimulus is first detected is designated as the differential light threshold. A line joining locations of equal sensitivity is termed an isopter and is analogous to the contour line on a map. As the stimulus is moved in a centripetal manner from the threshold location

towards fixation the stimulus becomes increasingly visible. By varying the size and luminance of the stimulus, the topography of the island of vision can be determined.

Static perimetry utilises a stationary stimulus within the normal extent of the visual field and the stimulus luminance is either increased until a 'seen' response is obtained or decreased until a 'not seen' response is obtained, i.e. the threshold is 'crossed'. There are two types of static perimetry: threshold perimetry and suprathreshold perimetry. Threshold perimetry estimates the differential light threshold (i.e. the topography) at each stimulus location. Suprathreshold perimetry utilizes a stimulus at one or more known levels of measurement brighter than the expected normal threshold. Usually, the initial luminance is between 5dB and 6dB brighter than threshold, depending upon the type of instrument, and the second luminance level is at the maximum for the instrument. Thus, any potential field loss can be graded as normal (i.e. seen at the initial luminance setting), relative (i.e. not seen at the initial luminance setting but seen at the maximum setting) or absolute (i.e. not seen at the maximum setting). The advantage of a suprathreshold strategy is that the examination duration for the normal eye can be shorter than that for the corresponding threshold strategy. However, the reduction in examination duration is at the expense of the ability of the technique to identify shallow/ early abnormality.

Shallow and/ or small areal extents of visual field loss can be easily overlooked with kinetic perimetry due to the movement of the stimulus and the resulting successive lateral summation and, therefore, the technique is not as sensitive as threshold static perimetry (Heijl 1976; Bynke and Heijl 1978; Katz et al 1995a). However, kinetic perimetry is more useful than static perimetry for the examination of steeply

bordered advanced loss (Vonthein et al 2007) and is currently more useful for examination of the peripheral field (Choplin and Edwards 1999) However, the recent development of the GATE (German Adaptive Thresholding Estimation) strategy may enable threshold perimetry to be a viable technique for examination of the peripheral field (Schiefer 2009).

Compared to manual kinetic perimetry, static perimetry is independent both of the patient's and the perimetrist's reaction time and, of course, of the stimulus velocity (Greve 1975; Trope and Britton 1987). By variously reversing the direction of presentation, the threshold can be crossed several times. Normally, static perimetry is more sensitive and precise than kinetic perimetry and therefore can detect early/ shallow visual defects much more readily.

The 'gold standard' instrument for kinetic perimetry is the Goldmann perimeter (Goldmann 1945; 1946). The perimeter utilises one of six stimulus sizes which are described in terms of Roman numerals. Each successively larger stimulus subtends a visual angle twice, and an area four times, larger than that of the immediately smaller stimulus. The angle subtended by the smallest stimulus, Size 0, is 0.054° and by the largest, Size V, is 1.732°. The stimulus luminance is described in terms of Arabic numerals, 1 to 4, and in terms of letters, a to e. The maximum luminance (1000asb) is represented by 4e. A reduction of one number represents a 0.5 log unit reduction in luminance and a reduction of one letter (e.g. e to d) represents a reduction of 0.1 log units. The dynamic range of the Goldmann perimeter, from the smallest and dimmest stimulus (01a) to the largest and brightest (V4e), is greater than 4 log units. The outcome with the Goldmann perimeter is highly dependent

upon the influence of the perimetrist. As a consequence, a number of attempts have been made to automate kinetic perimetry. The first attempts at automation included the Perimetron (Portney and Krohn 1978), the Squid (Lewis et al 1986) and the Perikon (Marraffa et al 1989) perimeters. The current approach to the automation of kinetic perimetry is that of semi-automated kinetic perimetry (SKP) with the Octopus 101 and 900 perimeters (Schiefer et al 2001; 2004; 2006; Nowomiejska et al 2003, 2004a,b,c; 2005; Hashimoto et al 2003; Dolderer et al 2007; Vonthein et al 2007).

Static threshold perimetry was not clinically viable before the advent of automated perimetry. The principles and concepts of automated perimetry were first described in 1972 (Fankhauser et al 1972). The first commercially available automated perimeter, the Octopus 201 automated perimeter, became available in 1974 (Spahr and Fankhauser 1974a,b). The introduction of the Octopus perimeter was closely followed by that of the Competer (Heijl and Krakau 1975a; 1975b), and subsequently the Fieldmaster (Keltner et al 1979), the Peritest (Greve 1980), the Dicon (Hart and Gordon 1983; Mills 1984) and the Humphrey Field Analyzer (HFA) (Heijl 1985).

1.2 Principals of perimetry

1.2.1 Perimetric units of measurement

The properties of the differential light threshold were first described towards the end of the nineteenth century by Ernst Weber and by Gustav Fechner and can be summarised in terms of the Weber-Fechner Law namely:

$$\Delta L/L=K$$

where ΔL and L are as described previously and K is a constant.

For a logarithmic scale:

$$\text{Sensitivity (dB)} = k + 10 \log (\Delta L/L)$$

Normally, the conventional units of luminance in perimetry are the candela per square meter (cdm^{-2}) or the apostilb (asb). The apostilb corresponds to 1 lumen of total emittance per square metre of an illuminated surface, or $1/\pi$ lumens per steradian per square meter of a perfect Lambertian surface. To convert asb into cdm^{-2}, it is necessary to divide by π. Thus, a 10,000asb luminance corresponds to $3183cdm^{-2}$.

The Weber-Fechner Law is valid at background luminances of $10cdm^{-2}$ and greater (Aulhorn and Harms 1972; Greve 1973). In the mesopic range of luminances, the response can be adequately described by the Rose – de Vries Law where:

$$\Delta L/L^{0.5} = K$$

At scotopic levels of luminance, i.e. below $0.3cdm^{-2}$, the response is linear and $\Delta L = K$.

The decibel (dB) is a relative measurement and is used in perimetry to describe the differential light sensitivity. The dB scale is a logarithmic scale whereby 1.0dB represents 0.1 log unit and 10dB represents 1.0 log unit. A 1.0 log unit neutral density filter therefore attenuates the stimulus luminance to one tenth of its original value and a 2.0 log unit filter to one hundredth of its original value. Sensitivity in dB is referenced to the maximum luminance of the perimeter which is represented as 0dB. Consequently, an increase in the dB scale corresponds to an increase in the differential light sensitivity.

In the former, and in the current, versions of the Humphrey Field Analyzer (HFA), the maximum luminance of the white stimulus is 10,000asb whereas for the Goldmann perimeter and for the Octopus 201 and 101 perimeters, the maximum stimulus luminance corresponds to 1000asb. Clearly, a particular dB value in one type of perimeter may not correspond (in terms of the absolute measure of luminance) with the same dB value in another type of perimeter. The background luminance (L) is $10cdm^{-2}$ (31.5asb) for the HFA and for the Octopus 900 perimeter and therefore the constant (k) corresponds to 5.

With the HFA, one asb is equivalent to a 40dB stimulus and is therefore 1/10,000 less intense than the maximum luminance. The default stimulus size is Goldmann size III for both the HFA and Octopus perimeters. With the HFA and stimulus size III, a sensitivity of 40dB can be achieved at the fovea in young normal observers who are experienced in perimetry.

1.2.2 Definition of the threshold

For static perimetry, threshold is usually defined as the stimulus luminance which has a 50% probability of detection. The probability of detection is determined by the Frequency of Seeing (FOS) curve where the percentage of seen responses is plotted against the log of the stimulus luminance. The FOS is typically S-shaped (sigmoidal) in appearance (Weber and Rau 1992). The slope of the curve is an indication of the variability associated with the estimation of threshold. An increasingly flatter slope indicates increasing variability of the threshold estimate whereas an increasingly steeper slope indicates increasingly less variability. The magnitude of the slope is often also described in terms of the inter-quartile range i.e. the difference between the sensitivity values corresponding to the 25% and 75% seen responses. The magnitude of the variability is dependent upon a number of factors (Section 1.2.3); it varies between individuals of the same age, increases with age, and increases with increase in eccentricity of the stimulus location (Weber and Rau 1992; Olsson et al 1993; Chauhan et al 1993b).

1.2.3 Factors influencing stimulus visibility

1.2.3.1 Stimulus size

The apparent size of the stimulus depends upon its areal size and upon the viewing distance of the perimeter. The latter is constant for any one type of automated perimeter (i.e. 30cm in the case of the HFA 700 series). However, the relative visibility of the stimulus is also affected by the reduction in the effective retinal illumination which arises from the reduction in the apparent pupillary area with increasing peripheral angle of the stimulus presentation (Wild et al 1987). However, the reduced retinal image projection (Drasdo and Fowler 1974) compensates for this latter effect such that the retinal illumination is approximately constant out to an eccentricity of 80° (Bedell and Katz 1982; Koojiman 1983).

A well defined relationship exists between stimulus size and stimulus intensity. Due to the convergent nature of the neural processing within the retina, a ganglion cell is able to respond equally to a small bright stimulus and to a larger dimmer stimulus. This phenomenon is known as spatial summation (Flanagan et 1988; Latham et al 1993). The magnitude of the differential light sensitivity as a function of stimulus area is defined in the normal eye by:

$$\Delta L \times A^k = \text{Constant}$$

Where A is the area of the stimulus, ΔL is the stimulus luminance and k is the summation coefficient. When k=1, complete spatial summation is present and Ricco's Law applies. Partial summation occurs when the stimulus area exceeds a critical area known as Rocco's area. In such cases, k is less than unity and the relationship is no longer a reciprocal function. Partial summation has been described variously by Pieron's Law (k=0.3), by Piper's Law (k=0.5) and by Goldmann who used a value of k=0.8. When k=0, the Weber-Fechner Law applies. The suitability of Goldmann's approximation has been confirmed independently (Choplin et al 1990). The coefficient, k, varies physiologically between normal individuals and in ocular disease (Garway-Heath et al 2000).

As mentioned previously, the default stimulus size for automated static perimetry is Goldmann size III. However, for patients with end-stage glaucoma and with apparent absolute defects using stimulus size III, threshold perimetry can usefully be undertaken with either stimulus size IV or V in order to increase the dynamic range and therefore probe the depth of the defect(s). The within-examination variability of

the threshold estimate is also reduced with size V compared to size III in patients with OAG at stimulus locations exhibiting normal sensitivity and at locations exhibiting moderate damage (Wall et al 1997b). However, the use of large stimuli may fail to detect small focal defects discernable with smaller stimuli (Gramer et al 1981).

The differential light sensitivity derived with small stimuli is more affected, compared to large stimuli, by optical defocus and by refractive error (Ogle 1960; 1961a,b) and by media opacity (Wood et al 1987a).

1.2.3.2 Background luminance

The level of background luminance determines the degree of light or dark adaptation of the retina. The height and extent of the island of vision successively increases with decrease in the background luminance from photopic through mesopic to scotopic levels. However, the increase in sensitivity is not uniform across the field. The foveal peak disappears due to the absence of rods and the more peripheral field exhibits a greater increase than the more central field, with reduction in luminance, due to the greater prevalence of the rods in the peripheral retina.

As was mentioned previously, the default background luminance of the Goldmann perimeter, of the HFA and of the Octopus 900 series perimeter is 31.5asb ($10cdm^{-2}$). This value ensures the maximum dynamic range of the stimulus, in terms of the contribution of the background luminance, whilst remaining within range over which the Weber-Fechner Law is operative.

1.2.3.3 Stimulus luminance

As was also mentioned previously, the HFA and the Octopus 900 utilize a maximum luminance of 10,000 apostilbs (asb); thus 0dB represents 10,000asb. Zero dB for the Octopus 101 corresponds to 1,000 asb, whereas 0dB corresponds to 4,800 asb for the Octopus 300.

The maximum stimulus luminance should not be sufficiently high as to induce stray light effects whereby the light from a stimulus presented at a location exhibiting deep loss is scattered to adjacent locations exhibiting higher sensitivity and thus elicits a 'seen response' (Fankhauser 1979).

1.2.3.4 Stimulus duration

With increase in stimulus duration, the stimulus appears to become increasingly brighter and can therefore be seen more easily. However, when the duration exceeds a critical value, the perceived luminance becomes independent of the duration. The relationship between duration (T) and the differential light threshold (ΔL) can be described by Bloch's Law (Bloch 1885):

$$\Delta L \times T^k = C$$

where k is the temporal summation coefficient and C is a constant. If the stimulus duration is less than the critical duration, complete temporal summation occurs. If the stimulus presentation exceeds the critical time, partial temporal summation occurs and k tends toward zero. In the case where $k = 0$, and all other stimulus parameters remain constant, an increase in stimulus duration has no further effect on the differential light sensitivity.

1.2.3.5 Stimulus colour

The visibility of the stimulus is affected by the colour of the stimulus and by the reduced luminance associated with the given colour. A red stimulus on a white background has been advocated for assessing the field of those exposed to chloroquine (Easterbrook and Trope 1989) or to phenothiazines (Boet 1970). However, for the assessment of a given colour pathway it is necessary to saturate the opponent pathway by an appropriate choice of stimulus and background wavelengths. However, some degree of long-wavelength sensitive (LWS) pathway isolation can be achieved with an achromatic background (Harwerth et al 1999).

Threshold perimetry of the short-wavelength sensitive (SWS) pathway can be undertaken using a blue stimulus presented against a high luminance yellow background. The blue stimulus examines the SWS pathway, the high luminance saturates the rod pathway and the yellow background saturates the medium-wavelength sensitive (MWS) and the LWS pathways. The technique, known as Short-wavelength Automated Perimetry (SWAP) will be discussed in detail in Chapter 3. It has been used for the investigation of OAG on the basis either that the axons of the ganglion cells responsible for processing blue stimuli, the koniocellular ganglion cells, are preferentially damaged (Quigley et al 1987; 1988; Glovinsky et al 1991; 1993; Kerrigan-Baumrind et al 2000) compared to the other ganglion cell types or that the reduced redundancy of the sparse koniocellular ganglion cells enables the visual dysfunction to be detected earlier than that of SAP which is largely mediated by the numerous parvocellular ganglion cells (Ansari et al 2002; Spry et al 2005a).

1.2.3.6 Other factors

The Perimetric Learning effect

A learning effect is present in perimetry whereby the differential light sensitivity can improve during the examination of the first eye at the first visit for perimetry. The effect can be transferred between eyes at the first visit and between visits for each eye upto the third or fourth visit (Searle et al 1991). In general, an improvement of about 1 to 2dB in the MS and in the MD for SAP occurs between the first and the second visit (Werner et al 1988; 1990). The improvement in sensitivity increases with increase in eccentricity and is more pronounced in the superior field compared to the inferior field (Wood et al 1987b; Wild et al 1989; Heijl et al 1989b; Werner et al 1990; Searle et al 1991). It is greatest in areas of relative loss i.e. intermediate levels of defect depth (Wild et al 1989; Heijl et al 1989b; Heijl and Bengtsson 1996) and is independent of age (Heijl et al 1989b; Kulze et al 1990). The learning effect occurs in normal individuals (Wood et al 1987b; Heijl et al 1989c, Searle et al 1991), in patients with ocular hypertension (Werner et al 1990; Searle et al 1991; Wild et al 1991) in patients with glaucoma (Werner et al 1988; Kulze et al 1990; Wild et al 1991; Heijl and Bengtsson 1996).

The Learner's Index (LI)

A Learner's Index (LI) has been proposed to quantify the extent of the learning effect for SAP (Olsson et al 1997b) whereby a value tending to zero corresponds to a normal visual field and a value tending to 1.0, in an otherwise normal individual, suggests that the visual field is likely to be normal but exhibits an 'average' amount of 'learning'. It is important to distinguish the learning effect from the LF, which represents the variability of the threshold measurement among several tests.

A learning effect is also present for SWAP in normal individuals and in individuals with OHT or with OAG over short-term follow-ups ranging from between one and three weeks (Zhong et al 2008) and weekly over five weeks (Wild et al 2006) both in those experienced in SAP and also in those without previous experience of any type of perimetry. The effect is also present over the long term, improving at each yearly visit over a period of six years (Gardiner et al 2008).

The learning effect for both SAP and SWAP is discussed in more detail in Chapter 3 and the LI in Appendix B1.

The Fatigue Effect

A fatigue effect is also present in perimetry whereby the differential light sensitivity deteriorates during the examination (Heijl 1977a; Heijl and Drance 1983; Hudson et al 1994). It is present in normal individuals (Heijl 1977a,b; Suzumura 1988; Johnson et al 1988a, Searle et al 1991), in individuals with OHT (Langerhorst et al 1987; Suzumura 1988), with OAG (Heijl 1977a,b; Suzumura 1988; Johnson et al 1988a) and with optic neuropathy (Wildberger and Robert 1988; Keltner and Johnson 1995). It exacerbates the apparent depth of existing loss. The fatigue effect increases with increase in the duration of the examination and is often greater for the second eye examined. It is more pronounced with examination durations greater than 5 minutes. The overall magnitude, on average, ranges between 1.0 and 2.5dB in normal individuals (Johnson 1988a; Hudson et al 1994) and is similar in magnitude, on average, for individuals with OHT and possibly slightly greater for individuals with OAG. The fatigue effect is more pronounced in abnormal regions of the visual field (Heijl 1977a,b; Holmin and Krakau 1979; Heijl and Drance 1983; Suzumura

1988). It can be reduced by the introduction of rest periods during the examination and/ or by the use of shorter examination durations. In the former case, care should be taken to ensure that retinal adaptation is maintained. In the latter case, the reduction in examination duration by the use of an alternative algorithm may be at the expense of a loss of accuracy in the threshold estimate. The various types of algorithm for determining the threshold estimate are discussed in Section 1.2.5. The fatigue effect is associated with a higher SF and an increased number of incorrect responses to the false-negative catch trials and is more pronounced with increase in age (Langerhorst et al 1987; Gonzalez de la Rosa and Pareja 1997). The fatigue effect is apparently counteracted by the opposing vector of the learning effect (Hudson et al 1994).

Defocus

The magnitude of the differential light sensitivity reduces with increase in defocus (Weinreb and Perlman 1986; Goldstick and Weinreb 1987; Heuer et al 1987; Herse 1992; Gaffney 1993; Wang et al 1997). The smaller Goldmann stimuli are more prone to the effects of defocus than are the larger stimuli (Ogle 1960; 1961a,b). The influence of defocus on the visual field is discussed in detail in Chapter 5.

1.2.4 Suprathreshold and threshold perimetry

Suprathreshold perimetry utilises a stimulus which is presented at a given suprathreshold level (i.e. at a higher luminance than the threshold) and therefore should be readily visible to the observer. Such an approach is frequently adopted for the examination of the visual field of those who exhibit a high index of suspicion of normality. A variety of approaches have been adopted for the setting, and the magnitude, of the threshold increment. The suprathreshold value is usually

referenced to the age-corrected normal value at each location across the field (Siatkowski et al 1996) but can also be referenced to the threshold of the individual (Henson and Artes 2002). The latter can be estimated by a variety of means and is usually determined for a number of locations within the paracentral region. These values are the used to derive the subsequent values across the field. The magnitude of the suprathreshold setting varies within- and between-types of perimetry. For example, the suprathreshold increment for the Humphrey Field Analyzer is 6dB relative to the estimated individual threshold or 8dB relative to the age-corrected normal threshold whilst that for the Henson perimeters is 5dB relative to the estimated individual threshold. The response from the patient can be graded in a number of ways. The simplest approach is to adopt a 'one level' strategy whereby the outcome is graded as either 'seen' or 'not seen' at the initial threshold increment. With such a procedure, the magnitude of sensitivity at the location exhibiting a 'not seen' response is unknown. An alternative approach is to adopt a 'two level' strategy whereby those locations at which the initial suprathreshold luminance was 'not seen' are re-examined using the maximum stimulus luminance of the perimeter. The outcome at any given location can thus be graded as 'seen' at the initial suprathreshold increment or as 'not seen' at the initial suprathreshold increment but 'seen' at the maximum stimulus luminance (i.e. the defect is relative) or as 'not seen' at both the initial suprathreshold increment and the maximum stimulus (i.e. the defect is relative). The Henson perimeters, for example, in addition to the suprathreshold increment of 5dB use further increments of 8dB and 12dB. These suprathreshold strategies were faster than the first generation of threshold algorithms but exhibited poorer sensitivity for the detection of OAG (Mills et al 1984) and in neuro-ophthalmological disease (Siatkowski et al 1996).

1.2.5 Conventional methods (algorithms) for estimating threshold

It is not practical in clinical perimetry to determine the threshold by the use of the FOS curve due to the length of time necessary to obtain the outcome. As a consequence, the threshold is estimated using a bracketing, or staircase, technique whereby the threshold is approached in intervals, or steps, of equal luminance from either the 'seeing' to 'non-seeing' direction or from the 'non-seeing to seeing' direction. Once a change in response has been obtained from the observer, i.e. the threshold has been 'crossed', the magnitude of the stimulus luminance is usually halved and the direction of approach towards the threshold is reversed until the threshold is crossed once again. The accuracy of the threshold estimate increases with the number of crossings of threshold, with a reduction in the step size and with the number of estimates of threshold. However, such an increase in accuracy is at the expense of an increase in examination duration (Bebié et al 1976a).

1.2.5.1 Normal Threshold algorithm

The original threshold algorithm of the Octopus perimeter, Normal strategy, utilized steps of 4dB, 2dB and 1dB. Although this approach remains unchanged, the subtleties of the algorithm have been modified over the years. The algorithm currently begins at the age-corrected normal value, less 4dB, at each of four primary points (anchor points) located at 9°, 9° eccentricity in each quadrant for Program 32 and at 8°, 8° for Programs G1 and G2, respectively. If the patient does not respond to this initial stimulus luminance at any of the four anchor points, the subsequent stimulus luminance is increased by 6dB. Thereafter, if the patient continues to fail to respond, the steps are successively increased by 8dB until a response is obtained. The luminance is then decreased in steps of 4dB until a 'non-seen' response is obtained. The stimulus luminance is then increased in 2dB steps until a 'seen' response is obtained and this is followed by a 1dB adjustment in the opposite

direction. The outcome at the anchor points determines the start level at each of the surrounding locations and the outcomes at each of these surrounding locations determine the start level at each of the immediate neighbouring locations and so on. If the patient responds to the initial stimulus luminance, the luminance is reduced by 4dB until the threshold is crossed and the subsequent reversals are in 2dB and 1dB steps. The algorithm can also be used with a 4-2-2dB double crossing of threshold (Hermann et al 2008).

Full Threshold algorithm

The initial algorithm for the HFA, Full Threshold, utilizes a double crossing of threshold with steps of 4dB and 2dB. The start luminance at each of four seed points situated at 9°, 9° eccentricity in each quadrant is 25dB, irrespective of the age of the patient, and the threshold is estimated twice at each of these four locations. The start level at each of the immediate surrounding locations is determined by extrapolation from the outcome at the corresponding seed location (Fingert and Lewis 2001). The threshold is designated as the last 'seen' stimulus luminance (Wild et al 1999a,b). The Short-term fluctuation (SF) (see Section 1.3.6.3) is calculated from the threshold estimate obtained twice at each of ten pre-defined stimulus locations.

1.2.5.2 FASTPAC

The FASTPAC algorithm for the HFA, introduced in 1991, utilizes a 3dB step in either an ascending or a descending direction, respectively, and threshold is crossed once (Flanagan et al 1993b). Like the Full Threshold algorithm, FASTPAC also uses the four primary seed points to determine the initial stimulus luminance for the neighbouring stimulus locations. The luminance presented at the neighbouring points is 1dB brighter when the expected threshold is an even number and 2dB

dimmer when the expected threshold is an odd number (Flanagan et al 1993b). The threshold is also designated as the 'last seen' stimulus luminance (Wild et al 1999a,b).

The examination duration of the FASTPAC algorithm is approximately 35% shorter than that of the Full Threshold algorithm but is at the cost of an approximate 25% increase in the SF (i.e. the within-test variability) and an apparent underestimation of focal loss in glaucoma (Flanagan et al 1993b; O'Brien et al 1994; Glass et al 1995). The underestimation of focal loss, combined with the larger SF is influenced by the magnitude of the difference between the starting value and the estimated/ measured threshold. A negative difference leads to an underestimation of the threshold whilst a positive difference leads to an overestimation of threshold (Glass et al 1995).This effect is more pronounced for the FASTPAC algorithm than for the Full Threshold algorithm.

For the Full Threshold and the FASTPAC algorithms, the average response time to the first 10 stimulus presentations is calculated. A value of 0.85sec is added to the average response time and the resultant is then used as the between-stimulus interval.

The Full Threshold and FASTPAC algorithms have also been applied to SWAP with the HFA and this is discussed in Chapter 3.

1.2.5.3 SITA (Swedish Interactive Threshold Algorithm)

Two Swedish Interactive Threshold Algorithms (SITA), SITA Standard and SITA Fast, were introduced in 1997 for SAP with the HFA (Bengtsson et al 1997b). The object of each of the two SITA algorithms was to shorten the examination duration without a loss in accuracy of the threshold estimate. The SITA Standard algorithm uses 4dB and 2dB steps, and is analogous to the Full Threshold algorithm, whilst SITA Fast uses a 4dB step, only, and is analogous to the FASTPAC algorithm (Bengtsson et al 1997b; Bengtsson and Heijl 1998b). The SITA SWAP algorithm (Bengtsson 2003), which became commercially available in 2006, and which will be discussed later in Chapter 3 was a replacement for the Full Threshold and FASTPAC algorithms previously used for SWAP.

The SITA algorithms each utilize two Bayesian posterior probability, or likelihood, functions (models) at each stimulus location. One function is a distribution of the probability of the likelihood of a seen response at any given value of sensitivity in the normal eye and the other function is an equivalent distribution in the glaucomatous eye (Olsson and Rootzen 1994). The two probability models are based upon knowledge of the age-corrected threshold value, the between-individual variability in the estimation of threshold, the variation in the shape of the FOS curve between stimulus locations and the correlation of sensitivity between neighbouring stimulus locations. Each function is adjusted continuously as the examination proceeds, i.e. following the positive or negative response to each individual stimulus presentation, and the shape of each function continually changes as the examination progresses. At any given moment in the examination, the height of the function describes the most likely threshold at the given location and the width describes the accuracy of the threshold estimate.

The thresholding procedure at any given location is terminated when a predetermined level of accuracy, as predefined by the Error Related Factor (ERF), is obtained (Bengtsson et al 1997b). The magnitude of the ERF at each stimulus location represents a balance between accuracy and test time. Threshold estimation with the SITA Standard algorithm cannot be terminated unless there has been at least one crossing of the threshold (Bengtsson et al 1997b). However, the threshold estimation with the SITA Fast algorithm can be terminated at any given location without a crossing of threshold (Bengtsson et al 1997b; Bengtsson and Heijl 1998b).

The SITA algorithms determine the response time to each stimulus presentation (Bengtsson et al 1997b) and the subsequent inter-stimulus interval is based upon this individual response time window. Responses which occur within a 'listen time' window of 180msec, which immediately follows the onset of the stimulus presentation, and also those which occur within a further 'listen time' window (which commences at a fixed time after the response window and which runs into the 'listen window' associated with subsequent stimulus) are designated as false-positive responses (Olsson et al 1997a).

At the end of the examination, the estimate of sensitivity at each stimulus location is recalculated utilizing all the response information obtained during the examination (Bengtsson et al 1997b; McKendrick 2005). This process enables, in particular, the thresholds estimated at the beginning of the examination to be recalculated from all available response information.

The post-processing procedure also identifies and excludes those responses which occur within the 'listen time' window, i.e. the false-positive responses (Olsson et al 1997a), thereby providing a better estimate of threshold. The use of this approach also obviates the necessity for the traditional false-positive catch trials (Section 1.3.9.2) and therefore permits a slight reduction in the examination duration. The rate of the false-positive responses appears on the print-out. The response time of the patient can be affected by the magnitude of the stimulus luminance and the stimulus location and may alter during the examination (Wall et al 1996).

The resultant threshold estimate derived by either SITA algorithm is assumed to represent the stimulus luminance corresponding to a 50% probability on the FOS curve (Bengtsson and Heijl 1998a, Bengtsson et al 1998c).

Overall, the SITA Standard and SITA Fast algorithms exhibit good sensitivity and specificity for the detection of glaucomatous visual field loss, and a considerable reduction in the examination duration, relative to the older algorithms (Bengtsson and Heijl 1999a; Wild et al 1999b; Sharma et al 2000; Budenz et al 2002; Schimiti et al 2006). The confidence limits for normality are greater for the SITA Fast algorithm than for the SITA Standard algorithm. The between-examination variability of the SITA Fast algorithm is also greater than that of the SITA Standard algorithm (Nordmann et al 1998; Sekhar et al 2000; Artes et al 2002).

The SITA algorithms cannot be used with the HFA 600 series due to the limited speed of the older processors and are only available for the HFA 700 series (Johnson et al 1997).

1.2.5.4 Dynamic strategy

Weber (1990) suggested that the step size should be varied according to stimulus eccentricity, i.e. the steps should increase with decline in the differential light sensitivity.

The Dynamic strategy, which is available in the Octopus perimeters, adjusts the step size according to the slope of the FOS curve at the given location (Weber and Klimaschka 1995; Madea et al 2000). The step size increases from 2dB to 10dB with increase in defect depth. The threshold is crossed only once and is designated as the average luminance of the last two stimuli following a change in response (Klimaschka and Weber 1994; Weber and Klimaschka 1995).

The benefit of the Dynamic strategy compared to the Threshold algorithm of the Octopus is a reduction of approximately 30-40% in the examination duration for the normal field (Zulauf et al 1994; Weber and Klimaschka 1995) and 40-50% in advanced loss. The variability with the Dynamic strategy is markedly lower over the range of normal sensitivity (by approximately 60%) compared to that for the Octopus Normal Threshold algorithm, but is, unfortunately, greater (by approximately 150%) at locations exhibiting relative loss. The SF and the LF of the Dynamic strategy are also greater than those of the Normal Threshold algorithm by 15% and 21%, respectively (Zulauf et al 1994; 1996a).

1.2.5.5 TOP (Tendency Oriented Perimetry)

Tendency Oriented Perimetry (TOP) was introduced in 1996 (Gonzalez et al 1996; Martinez et al 1996) for the Octopus perimeters and is based upon the correlation of sensitivity between neighbouring stimulus locations.

The TOP strategy subdivides the various stimulus locations within the given stimulus program into four overlapping sub-matrices such that the between-stimulus separation is 12° (Anderson 2003). For example, in the case of Program 32, each grid comprises 19 stimulus locations. Each matrix is examined sequential order. The stimulus luminance at each of the locations in the first sub-matrix is presented at half (8/16) that of the age-corrected value of normal sensitivity at the given location.

A 'seen' response is then recorded as +4/16 of the age-corrected value of normal sensitivity at the given location. A 'not seen' response is recorded as -4/16 of the age-corrected value of normal sensitivity at the given location. Each location in the first sub-matrix is examined once. As a consequence of the responses derived for the locations in the first sub-matrix, the expected value of sensitivity at any given location in the second sub-matrix is modified by the average of the response derived by the first sub-matrix at any locations situated within 3° vertically and 3° horizontally of the given location in the second sub-matrix. The stimulus luminance at each of the locations in the second sub-matrix is presented at 3/16 that of the expected value of normal sensitivity at the given location. A 'seen' response is then recorded as +3/16 of the expected value of normal sensitivity at the given location and a 'not seen' response as -4/16 of the expected value of normal sensitivity at the given location. The locations in the third sub-matrix are adjusted by the average of the response derived by the second sub-matrix at any locations situated within 3° vertically and 3° horizontally of the given location and the threshold estimate for all the locations within the third sub-matrix is recorded as +/- 2/16 of the expected value of normal sensitivity at the given location. The cycle is repeated for those locations in the fourth sub-matrix and sensitivity is recorded as +/- 1/16 of the expected value of normal sensitivity at the given location.

The TOP strategy is appropriate for patients in whom time-consuming perimetry is not possible or who exhibit advanced loss (Maeda et al 2000). The algorithm can be easily applied to other perimetric methods such as Flicker perimetry, SWAP and Pulsar perimetry (Chapter 4 and 5). The TOP algorithm yields shallower defects compared to the Threshold algorithm (Lachkar et al 1998; Maeda et al 2000) and the SITA Fast algorithm of the HFA (King et al 2002). The examination duration is between 75% and 80% less compared to the Threshold strategy both in normal individuals and in individuals with OAG (Morales et al 2000; Kratochvilova 2002; Gonzalez de la Rosa et al 2003a).

1.2.5.6 GATE/ GATE-i (German Adaptive Thresholding Estimation)

The GATE-i algorithm (Schiefer et al 2009) starts by determining the sensitivity at each of five predefined seed locations. The measured sensitivity at each seed location is compared to the corresponding age-corrected normal value. The smallest deviation between the measured and age-corrected values of sensitivity is then used to adjust the overall height of the expected visual field. The initial stimulus luminance at each subsequent stimulus locations is slightly infraliminal to the expected value. If the stimulus is 'seen', the luminance is reduced in 4dB steps until a 'non-seen' response is obtained after which the luminance is increased until a 'seen' response is obtained. If the initial luminance is 'not seen', the subsequent stimulus is presented at the maximum luminance. If the latter is 'not seen', the thresholding process is terminated at the given location. If the maximum luminance is 'seen', the subsequent stimulus is presented at 4dB brighter than the initial presentation and the luminance is increased in 4dB steps until a 'seen' response occurs. The stimulus is then presented 2dB dimmer than the level at which the

'seen' response occurred. The threshold is defined as the mean of the dimmest 'seen' stimulus and the brightest 'not seen' stimulus.

The GATE algorithm is similar to the GATE-i algorithm but differs only in that the reference field is based upon the previously determined thresholds for the given individual rather than upon the age-corrected normal values.

The characteristics of the threshold recorded with the GATE-i and GATE algorithms compare favourably with that obtained with the Full Threshold algorithm despite the approximate halving of the examination duration. The mean sensitivities of 60 individuals (40 with OAG, 10 with suspected OAG and 10 with OHT) derived with Program 24-2 and with the SITA Standard, GATE-i and GATE algorithms were 1.2dB, 0.6dB and 0.0dB higher, respectively, than with the Full Threshold algorithm. The standard deviation of the difference in the mean sensitivity obtained at two examinations within a period of 14 days was 3.9dB for the Full Threshold algorithm, 4.5dB for GATE-i, 4.2dB for GATE and 3.1dB for the SITA Standard algorithm. Test-retest agreement, as measured by the 95% reference interval of the differences, were -7.69dB to 7.69dB, -9.76dB to 9.0dB, -8.40dB to 8.56dB and -7.01dB to 7.44dB, respectively. The examination durations were 9.0, 5.7, 4.7 and 5.6 minutes, respectively.

1.2.6 Stimulus grid

The stimulus configuration used for perimetry is generally based upon a square grid with an inter-stimulus separation of 6°. The separation is based upon a 95% probability of detection of a focal defect which is as large as the blind spot

(Fankhauser and Bebié 1979) and 100% probability (certainty) of detecting a focal defect of 8.4° or more in diameter scotoma. For the HFA, four grids are based upon a separation of 6°, namely Programs 30-1, 30-2, 24-1 and 24-2. The '1'designation signifies that the locations are referenced (or centred) upon the horizontal and vertical midlines, respectively, whilst the '2' designation signifies that the locations are referenced (or centred) upon a 3° offset on either side of the horizontal and vertical midlines, respectively. Program 30-2 comprises 76 stimulus locations out to a maximum eccentricity of 27°, whilst Program 24-2 comprises 54 stimulus locations out to a maximum eccentricity of 27° on either side of the midline along the nasal meridian and elsewhere out to a maximum eccentricity of 21°. Program 32 of the Octopus perimeter is analogous to Program 30-2 of the HFA in terms of the stimulus locations. The stimulus locations of Program G1 of the Octopus perimeters are not based upon a formal geometric arrangement but are based upon the anatomical distribution of the retinal nerve fibre layer.

Program 10-2 of the HFA comprises 68 stimulus locations out to a maximum eccentricity of 9°. The inter-stimulus separation is 2° and the stimuli are offset by 1° on either side of the horizontal and vertical midlines.

The selection of the appropriate stimulus program for individuals with OAG is dependent upon the stage of the disease. In the early stages of OAG when field loss is either absent or minimal, Programs 30-2 or 24-2, the case of the HFA, are utilized. Program 24-2 should be used when the field loss becomes more advanced and Program 10-2 should be utilized in end-stage OAG.

1.3 Representation of the estimated differential light sensitivity – the single field print out

1.3.1 Raw data and grey scales

The fundamental representation of the visual field recorded by threshold perimetry is the absolute value of sensitivity displayed as a function of stimulus location. Such a display of the numerical values can be difficult to interpret and the values, themselves, are not subjected to statistical analysis.

The gray scale, whereby the various magnitudes of sensitivity are represented in terms of various levels of gray, was originally designed to be analogous to the isopter plots of kinetic perimetry. By convention, light shading represents high values of sensitivity and dark shading low values. The gray scale provides an overall impression of the vision field. However, caution needs to be exercised when interpreting the visual field by means of the gray scale, alone, as the range of sensitivity within each level of gray covers 5dB. The difference between two successive shades of gray can therefore range from 1 to 9dB. The gray scale merely represents the absolute values of sensitivity and the scale is neither age nor eccentricity corrected. Thus, the gray scale is darker for the elderly normal individual than for the young normal individual. The scale appears darker at the edges of the central field than in the centre with increase in age due to the normal age-related steepening of the island of vision. The absolute values of sensitivity, and the associated gray scale representation, cannot separate the attenuation in sensitivity arising from pre-retinal factors from that arising due to neural damage.

1.3.2 Total Deviation-values/ Comparison tables and Total Deviation probability map/ Comparison probability plot

A more useful representation of sensitivity, compared to that of the gray scale, is in terms of the difference between the measured sensitivity at the given stimulus

location and the corresponding age-corrected normal value. With the HFA, a negative value indicates a reduction in the measured sensitivity compared to the age-corrected normal value and a positive value an enhanced sensitivity. The representation at each stimulus location is displayed as the Total Deviation probability map. The equivalent representation for the Octopus perimeters is the Comparison table. Measured values within +/-4dB of the age-corrected normal value are considered to lie within normal limits and are designated with a plus sign (+). An integer at any given location represents a reduction in sensitivity from the age-corrected normal value. The use of the plus sign is to avoid an 'overloading' of the representation.

The probability that the deviation at each location lies within the normal range of deviations is displayed in the Total Deviation probability map of the HFA (Heijl et al 1987b) and in the Comparison probability plot of the Octopus (Weijland et al 2004). A statistically significant deviation at the given location (i.e. $p<5\%$, $p<2\%$, $p<1\%$ or $p<0.5\%$) is indicated in terms of a symbol which increase in the level of grey as the magnitude of the probability level becomes increasingly smaller.

1.3.3 General Height Index

The absolute value of sensitivity and the deviation of the given value from the age-corrected normal value, either in absolute terms or as a probability level, do not separate the generalised component of field loss (i.e. generalised/ diffuse loss occurring throughout the field) from localised loss (i.e. focal loss). Such an approach can be achieved by the use of a normalising process whereby the generalised component of loss is estimated and then removed from the measured sensitivity at each location. The resultant magnitude of sensitivity at each location is then

considered in terms of the deviation from the age-corrected normal value and in terms of the statistical probability accompanying the deviation. A similar approach is applied to those clinically less common cases where the overall visual field exhibits a higher sensitivity than the age-corrected normal field. The GH index is the technique used to estimate the magnitude of the generalised component with the HFA. It is defined as the seventh most positive/ least negative measured value of sensitivity derived from the stimulus locations representing the Program 24-2 grid. The seventh highest deviation represents the 85th percentile of the 56 locations of the Program 24-2 grid (the location above the blind spot at x=15° and y=3°) and the two location below the blind spot at x=15° and y=-3° and x=15° and y=-9° are not considered in the calculation.

1.3.4 Pattern Deviation-values/ Corrected Comparison tables and Pattern Deviation probability map/ Corrected Comparison probability plot

The measured sensitivity, adjusted by the value of the 85th percentile, at each stimulus location is displayed in terms of the Pattern Deviation-values. The accompanying probability analysis is displayed as the Pattern Deviation probability map.

The corresponding approach for the Octopus perimeters utilises the difference between the 10th and 95th percentiles of the distribution of the deviations from the age-corrected normal value at the location which exhibits the 6th least positive (best) deviation (having excluded negative values) for Program G1 and the 8th ranked location for Program 32. The adjusted values of the measured sensitivity are displayed in terms of the Corrected Comparison table and the Corrected Comparison probability plot.

1.3.5 Cumulative defect (Bebié) curve

The Cumulative defect curve, also called the Bebié curve (Bebié et al 1989) is a graphical representation of the measured sensitivity at each location which is available with the Octopus perimeters. The measured sensitivity is ranked from the most sensitive (upper left) to the least sensitive (lower right). The normal range of sensitivity at any given value of sensitivity is defined by the respective 5^{th} and the 95^{th} percentiles. The shape and the vertical position of the defect curve provide an overview of focal and generalized loss, respectively. A focal defect is indicated with a sharp fall of the defect curve towards the right side of the graph, whilst, in the case of diffuse field loss, the defect curve runs below but parallel to the normal curve. Unfortunately, the defect curve does enable a representation of the spatial characteristic of the field loss. It can also be difficult to identify the difference between focal and a diffuse loss (Funkhouser 1991; Funkhouser et al 1992a,b).

1.3.6 Global indices

The value of sensitivity across the field can be described by various summary statistics.

1.3.6.1 Mean Deviation and Mean Defect indices

The Mean Deviation (MD) is an index used with the HFA. It is the weighted mean of the deviations of the measured value of sensitivity from the corresponding age-corrected normal value of sensitivity across all the stimulus locations (Heijl et al 1987b). The weighting function emphasizes the contribution of the more centrally situated locations. An increasingly negative value indicates increasing severity of field loss. The corresponding index for the Octopus perimeters is the Mean Defect (MD) (Weijland et al 2004). It is the unweighted mean of the deviation of the age-corrected normal sensitivity from the measured value of sensitivity across all

locations. An increasingly positive value indicates increasing severity of field loss. The MD indices are sensitive to generalized loss.

The Mean Deviation is expressed as:

$$MD = \left\{ \frac{1}{n} \sum_{i=1}^{n} \frac{(x_i - z_i)}{s_{1i}^{\ 2}} \right\} / \left\{ \frac{1}{n} \sum_{i=1}^{n} \frac{1}{s_{1i}^{\ 2}} \right\}$$

Where n is the number of stimulus locations excluding those corresponding to the blind spot; x_i is the measured value of sensitivity at stimulus location i; z_i is the age-corrected normal value of sensitivity at stimulus location i; and s_{li}^2 is the variance of normal sensitivity at location i; The MD is weighted at each stimulus location, i, for the variation of the threshold which increases with increase in eccentricity.

The Mean Defect is expressed as:

$$MD = \frac{1}{n} . \sum_{i=1}^{n} (z_i - x_i)$$

Where n is the number of stimulus locations excluding those corresponding to the blind spot; z_i is the age-corrected normal value of sensitivity at stimulus location i and x_i is the measured value of sensitivity at stimulus location i.

1.3.6.2 Pattern Standard Deviation and Loss Variance

The Pattern Standard Deviation (PSD) index represents the weighted standard deviation of the deviation values between the measured sensitivity and the corresponding age-corrected normal sensitivity across all locations (Heijl et al 1987b). It is an indicator of the non-uniformity of the measured sensitivity across the visual field. An increasingly positive value indicates an increasing non-uniformity of the field. The corresponding index for the Octopus perimeters is the Loss Variance (LV) (Weijland et al 2004). The LV represents the variance of the deviation between the age-corrected normal sensitivity and the measured value of sensitivity across all locations. It should be noted that the PSD is a standard deviation whilst the LV is a variance and, therefore, neither index can have a negative value. An increasingly positive value for either index indicates an increasing non-uniformity of the field. The PSD and LV are therefore sensitive to localized loss. The PSD is expressed as:

$$PSD = \sqrt{\left\{\frac{1}{n}\sum_{i=1}^{n} {s_{1i}}^2\right\}\left\{\frac{1}{n-1}\sum_{i=1}^{n}\frac{(x_i - z_i - MD)^2}{{s_{1i}}^2}\right\}}$$

Where n is the number of stimulus locations excluding the blind spot; x_i is the measured value of sensitivity at stimulus location i; z_i is the age-corrected normal value of sensitivity at stimulus location i; $s_{li}^2$is the variance of the normal sensitivity at location i; and MD is the Mean Deviation.

LV is expressed as:

$$LV = \frac{1}{(n-1)} \sum_{i-1}^{n} (x_i - MD - z_i)^2$$

Where n is the number of stimulus locations excluding the blind spot; x_i is the measured value of sensitivity at stimulus location I; MD is the Mean Defect; and z_i is the age-corrected normal value of sensitivity at stimulus location i.

1.3.6.3 Short-term fluctuation

The Short-term fluctuation (SF) is a measure of the within-examination variability of the threshold estimate (Bebié et al 1976b; Flammer et al 1984b). The SF is expressed as the standard deviation of the estimates of threshold at a given number of stimulus locations within the visual field. The Short-term fluctuation increases with increase in eccentricity and with increase in relative loss (Brenton and Phelps 1986; Heijl et al 1987b). The SF for the HFA is calculated from double determinations of threshold at each of 10 designated stimulus locations and differs from the Octopus calculation in that the SF is weighted by the within-examination normal variance at each given specific location. It is expressed as:

$$SF = \left[\left[\frac{1}{10} \sum_{i=1}^{10} s_{2i}^2 \right] \cdot \left[\frac{1}{n} \sum_{i=1}^{n} \frac{\sum (x_{i1} - x_{i2})^2}{2.s_{2i}^2} \right] \right]^{\frac{1}{2}}$$

Where s^2_{2i} is the normal within-examination variance at location i; and x_{i1} and x_{i2} are the first and second threshold estimates, respectively, at location i.

The SF for the Octopus perimeter is defined by the equation:

$$SF = \left[\frac{1}{m} \sum_{i=1}^{m} \frac{\sum_{k=1}^{R} (x_{ik} - \bar{x}_i)^2}{R-1} \right]^{\frac{1}{2}}$$

Where m is the number of locations with repeated measurements, x_{ik} represents the sensitivity at location i with repeated measurement k; $\bar{x}_i$ is the MS at location i, and R is the number of repeated measurements.

The magnitude of the SF in normal individuals experience in perimetry is approximately 1.0dB and does not approach zero due to the normal physiological variability associated with the estimate of threshold which increases within increase in eccentricity. The weighting function present in the formula for the SF used by the HFA minimizes the influence of the regional differences in the physiological variability associated with the threshold estimate. The magnitude of the SF is increased in areas of relative loss (i.e. as sensitivity declines) and also at the border of a defect due to the influence of fixation instability. The magnitude of the SF which, in essence, is an indication of the measurement error associated with the threshold estimate, is highly influenced by the patient's understanding of, and attentiveness during, the examination (Heijl and Drance 1983). An elevated SF accompanied by an excessive number of incorrect responses to the false-positive catch trials (see Section 1.3.9.2) is indicative of poor cooperation by the patient. Alternatively, an elevated SF accompanied by an excessive number of incorrect responses to the false-negative catch trials can be due to the fatigue effect but can

also be associated with substantial field loss in co-operative individuals (Flammer et al 1984b). The SF is not calculated with the SITA strategies or with the TOP strategy.

1.3.6.4 Corrected Pattern Standard Deviation and Corrected Loss Variance

The Corrected Pattern Standard Deviation (CPSD) removes the effect of the SF. The CPSD is defined as:

$$CPSD^2 = PSD^2 - k(SF)^2$$

where PSD is the Pattern Standard Deviation, k is a correction factor and SF is the Short-term fluctuation.

The correction factor is 1.28 for Program 30-2 and 1.14 for Program 24-2. The difference between the two values merely reflects the difference in the proportionate spatial contribution of the SF to each Program.

The Corrected Loss Variance (CLV), used by the Octopus perimeters, is equivalent to the CPSD used by the HFA SF. CLV is defined as:

$$CLV=LV-(SF)^2$$

Where LV is the Loss Variance.

1.3.7 The Glaucoma Hemifield Test

The concept of the Glaucoma Hemifield Test (GHT) used for the HFA is based upon the assumption that glaucomatous field loss is asymmetric between the superior and inferior hemi-fields (Hart and Becker 1982; Mikelberg and Drance 1984; Duggan et al 1985; Chen 1992; Åsman and Heijl 1992a; Åsman and Heijl 1992b).

The difference between the superior and inferior hemifield is evaluated by comparing the differences in the magnitude of the Pattern Deviation probability level at mirror-image locations in each of five zones on either side of the midline (Åsman and Heijl 1992b). Each zone contains between 3 and 6 stimulus locations. A probability score, the sum of the reciprocal of each of the given Pattern Deviation probability levels, is calculated for each zone and then compared to the mirror image probability score (Åsman and Heijl 1992a; 1992b). The outcome of the comparison of the difference between the two hemifields is described in qualitative terms on the print-out. 'Outside Normal Limits' indicates an overall asymmetry which is statistically significant at $p<0.01$ or an asymmetry in one zone which is statistically significant at $p<0.005$. 'Borderline' indicates that the asymmetry occurs with a probability level of $p<0.03$. 'General Reduction of Sensitivity' indicates, as the name suggests, an overall reduction in sensitivity across the field which occurs when the GH index is positive and exhibits a probability level of $p<0.005$. 'Abnormally High Sensitivity' occurs with a negative GH index at a probability level of $p<0.005$. 'Within Normal Limits' occurs when none of the criteria reach statistical significance.

The 'Outside Normal Limits' criterion of the GHT exhibits a sensitivity of 92% and a specificity of 87% for OAG in individuals naïve to automated perimetry but with

experience of manual perimetry. The inclusion of 'Borderline' outcomes marginally improved the sensitivity (94%) but reduced the specificity (81%) (Katz et al 1991b).

The repeatability of the GHT over two visual field examinations separated by one year was investigated by Katz et al (1995b). Their cohort comprised 41 normal individuals 407 individuals with OHT and 95 individuals with OAG. The proportion of the 41 normal individuals who exhibited abnormality by the GHT on two consecutive tests was 2.4%. Of the 95 individuals with OAG, 10.5% exhibited a normal visual field. The specificity at the second visit increased from 80.8% to 89.9%, with a modest loss of sensitivity, namely from 84.2% to 80.0%. The percentage agreements between the outcome of the GHT over the two visits was 83% for normal individuals, 80% for individuals with OHT and 91% for individuals with OAG, respectively.

The mirror hemifield comparison of nerve fiber zones, as made with the GHT, would seem to be a useful method for determining the presence of glaucomatous visual field loss.

1.3.8 Diffuse Defect Index

The Diffuse Defect Index (DDc) is available for the Octopus 300 and 900 perimeters (Monhart et al 2006). It compares the magnitude of the 50% percentile of the distribution of the average normal age-corrected sensitivity, associated with the 12^{th} to the 16^{th} ranked deviations in the Bebié curve for Program G1, with the mean of the measured sensitivity at the corresponding ranks. The DDc Index can be either positive or negative. The 20^{th} to 27^{th} is used for all remaining programs.

1.3.9 Localised Defect Index

The Localised Defect Index (LD) is also available for the Octopus 300 and 900 perimeters (Monhart et al 2006). It represents the area under the Bebié curve, having corrected for the magnitude of the DDc, between the 50^{th} percentile of the age-corrected normal sensitivity and the measured sensitivity at each stimulus locations and the measured sensitivity. The LD Index is also known as the abnormal response area (ARA). The LD Index is similar to the sLV (PSD) but the influence of false-positive responses is minimised due to the exclusion of the first 20% of the ranks in the calculation of the DDc (Buerki and Monhart 2007).

1.3.10 The Cluster Graph

The Cluster Graph analysis is available for the Octopus 300 and 900 series perimeters. It displays the LD of each of 10 regions designated on the basis of the distribution of the retinal nerve fibre layer (Buerki 2006).

1.3.11 Reliability parameters

A number of methods have been developed for estimating the reliability of the response from the patient during the visual field examination.

1.3.11.1Fixation stability

The Heijl-Krakau technique for estimating fixation stability (Heijl and Krakau 1975b; 1977) positions a stimulus of maximum luminance at the centre of the blind spot at pseudo-random time points during the examination. If the patient detects the stimulus, a fixation loss is recorded. If the number of fixation losses by the Heijl-Krakau technique exceeds more than 20%, the examination is normally be classed as unreliable. However, increasing the criteria to 33% has minimal effect on the sensitivity and specificity for the detection of field loss in individuals with OHT

(Bickler-Bluth et al 1989) and individuals with glaucomatous field loss (Bickler-Bluth et al 1989; Birt et al 1997) despite the fact that the number of incorrect responses to the fixation loss catch trials is considered to be greater in patients with OHT and in patients with OAG (Katz et al 1991a).

The outcome of the Heijl-Krakau technique is dependent upon the stimulus size (Fankhauser and Haeberlin 1980; Bengtsson and Heijl 2006), the size of the blind spot (Fankhauser 1993), the maximum luminance of the stimulus (Moss et al 1995; Wild et al 1995) and the correct initial location of the blind spot (Sanabria et al 1991). Stray light originating from the ocular media (Fankhauser and Haeberlin 1980) or reflected from the blind spot, itself, can also affect the outcome of the Heijl-Krakau technique. Approximately 10% of the total number of stimuli are presented at the blind spot location during examination with Program 30-2 of the HFA (Katz and Sommer 1988). Thus, only 90% of the examination duration is concerned with measurement of the differential light sensitivity.

The 'gaze tracker' system used with the HFA 700 Series measures the distance between the centre of the pupil and the first corneal reflex (Purkinje image) during steady gaze of the fixation target. The corneal reflex is produced by an infrared source in the perimeter bowl. The deviation from the base line, i.e. an increase in the distance between the pupil centre and the corneal reflex which occurs during an eye movement, is represented graphically as an upward deflection which is truncated at an amplitude of 10°. Deviations produced by head movements of less than 1° are not recorded. Eyelid closure or tear film rupture is represented by a downward deflection. The advantage of the gaze tracker over the Heijl-Krakau blind spot

method is that fixation quality is determined over the entire examination and the technique is less time consuming since it does not involve the use of additional stimuli.

The Octopus perimeters continuously monitor the position of the pupil with an infrared system. The stimulus is not presented during a loss of fixation or during eyelid closure (Fingert and Lewis 2001; Weijland et al 2004).

The use of a moving fixation target between stimulus presentations has been advocated (Reitner et al 1996). Such a strategy has been used in patients with neuro-ophthalmic disorders where the average examination duration of 14.9 minutes was reduced by 3.9 minutes (Reitner et al 1996). The acceptance of perimetry by these latter patients was greater with the moving fixation target due to less fatigue and a more interesting task. However, relative to static fixation, kinetic fixation is associated with fixation inaccuracy and an underestimation of the absolute scotoma at the physiologic blind spot (Åsman et al 1999).

1.3.11.2 False-positive catch trials

A false-positive response is defined as the designation of a 'seen' response despite the non-presentation of the stimulus. The original criterion for an unreliable outcome to the visual field examination was 33%, or more, incorrect responses to the false-positive catch trials. However, with the advent of the SITA algorithms and the associated change in the method of assessment of false-positive responses (Section 1.2.5.3), the criterion has been reduced to greater than, or equal to, 20%. False-positive responses are associated with an artificially elevated sensitivity and therefore yield a more positive Mean Deviation with the HFA and a more negative Mean Defect with the Octopus perimeter both in normal individuals and in

those with OAG (Katz and Sommer 1990; Cascairo et al 1991; Olsson et al 1997a; Newkirk et al 2006). High values of sensitivity occurring beyond the normal range can be immediately identified by the 'white' designation on the grey scale. The 'listen time' assessment of false positive responses used by the SITA algorithms tends to underestimate false-positive errors, particularly in normal individuals compared to individuals with OAG (Newkirk et al 2006).

A high number of incorrect response to the false-positive catch trials can be present in patients who are anxious or who tend to be 'trigger happy' because they are under the impression that they must act with haste. In such cases, it is important to reinstruct the individual to be slower and to be more deliberate in their response. The influence of moderate alcohol ingestion, which leads to 10% increase in the number of incorrect responses to the false-positive catch trials (Zulauf et al 1986), results in an improvement in sensitivity of 1dB. It seems that the negative influence of alcohol, i.e. the diminution of attentiveness, is apparently compensated by the increase in sensitivity associated with the increase in the number of false-positive responses.

1.3.11.3 False-negative catch trials

A false-negative response occurs when the patient fails to respond to a stimulus which was previously seen when presented at a lower luminance earlier in the examination. A false-negative response can be indicative of inattention. The stimulus luminance used for the false-negative catch trials, at any given stimulus location, with the Full Threshold and FASTPAC algorithms of the HFA is 9dB brighter than the initial value of sensitivity measured at an earlier stage in the

examination. The corresponding approach for the Octopus perimeters utilizes the maximum stimulus luminance.

The SITA algorithms of the HFA utilize a modified approach for the assessment of the false-negative response based upon the likelihood functions (Section 1.2.5.3) and upon a small number of specific false-negative catch trials based around a knowledge of the shape of the FOS curve at the given location which, itself, is determined by assumption from the current threshold estimate at the location (Olsson et al 1988; 1994).

Unreliable and/ or tired patients with visual field loss frequently exhibit a high number of incorrect responses to the false-negative catch trials (Katz and Sommer 1988; 1990; Katz et al 1991a; McMillan et al 1992; Bengtsson and Heijl 2000). An extreme manifestation of such an outcome in the normal eye is associated with a 'clover leaf' field. However, the number of incorrect responses to the false-negative catch trials is moderately correlated with increasing severity of the field loss, itself, which co-varies with an increase in the within-examination variability such that at some locations the latter can be larger than the 9dB increment. For the same reason, a high number of incorrect responses to the false-negative catch trials are often associated with an elevated SF.

1.3.11.4 Reliability factor

The Reliability factor (RF), which is used with the Octopus perimeters, is an overall indication of the patient's cooperation and is expressed as the total number of

incorrect responses to the false-positive and to the false-negative catch trials divided by the total number of trials. Normally, the RF should not exceed 15%.

1.3.11.5 Long-term fluctuation

The Long-term fluctuation (LF) is the variability in the threshold estimate additional to that of the SF and occurs between examinations (Bebié et al 1976a; Flammer et al 1984a) The LF comprises two components, the Homogeneous (Ho) and the Heterogeneous (He) LF (Bebié et al 1976b; Hutchins et al 2001). The LF (Ho) affects all locations, equally, whereas the LF (He) varies between different locations (Hutchings et al 2000). The two components are summary measures of the variance across all the specified locations. Several alternative measures of the between-examination variability, as a single entity, have been described (Katz and Sommer 1987; Young et al 1990) or for a single stimulus location (Katz and Sommer 1987; Werner et al 1989; Rutishauser et al 1989; Heijl et al 1987a; Zulauf et al 1990; Boeglin et al 1992; Blumenthal et al 2000). These measures describe the total between-examination variability and do not differentiate between the overall variance (i.e. the LF [Ho]) and the localised variance (i.e. the LF [He]).

The calculation of the LF (Ho) and the LF (He) require two or more estimates of threshold at the given locations between each of the two or more examinations. With either the Full Threshold or the FASTPAC strategies and either Program 30-2 and 24-2, the calculation of the SF and the LF is limited to the 10 double determinations of threshold at the standard locations. The SITA algorithms do not provide a second estimate of threshold at any given location and neither the SF nor either component of the LF can be calculated.

The 90% confidence limits for the LF (Ho) and LF (He) in individuals with stable OAG are 3.3dB and 3.6dB, respectively (Hutchings et al 2000). Individuals with OHT exhibit a statistically significantly higher LF (Ho) than normal individuals. The magnitudes of both components for those with OAG is statistically significantly higher than for those of normal individuals (Flammer et al 1985). Furthermore, little correlation is present between the magnitude of the LF and the magnitude of the SF or the severity of the field loss (Hutchings et al 1993).

The between-examination variability increases with increase in age (Heijl et al 1987a; Katz and Sommer 1987) and with increase in eccentricity for normal individuals (Heijl et al 1987a) and for patients with OAG (Boeglin et al 1992). The magnitude of the between-examination variability is influenced by the length of the interval between the examinations. It is lower in magnitude over short intervals than for longer intervals (Katz and Sommer 1987; Boeglin et al 1992).

The SF and the LF reflect the physiological variation in the threshold estimate. Certain factors, e.g. exercise (Koskela et al 1990), the menstrual cycle (Akar et al 2005) and certain drugs can all affect the magnitude of the threshold estimate (Flammer and Drance 1983a,b; Flammer et al 1986; Caprioli and Miller 1988; Wild et al 1988; Fogagnolo et al 2007).

1.4 Determination of progressive visual field loss

The earliest detection of deterioration in the visual field over time is a difficult task in that the change in the visual field has to be separated from the within- and between-variability associated with the threshold response. In addition,

physiological factors associated with aging, particularly that of cataract or increasing cataract (Greve 1979; Guthauser et al 1987; Heuer et al 1988; Wood et al 1989; Dengler-Harles et al 1990; Bengtsson et al 1997a), and reduction in pupil size (Mikelberg et al 1987; Lindenmuth et al 1989; Lindenmuth et al 1990; Edgar et al 1999) influence the magnitude of threshold and can mimic or mask 'true' change. Other factors, such as reduced vigilance (Langerhorst et al 1987; Johnson et al 1988a; Suzumura 1988), and reduced manual dexterity e. g. due to arthritis (Tremblay et al 2002; Durez et al 2006) and stroke (Nowak et al 2007; 2008) influence the measurement of threshold and can also mimic or mask 'true' change. In addition, the variability of the threshold estimate increases with increase in defect depth both within- (Werner et al 1989; Heijl et al 1989b) and between-examinations (Gloor and Vokt 1985).

The initial visual field examination, frequently carried out at the time of diagnosis, is not, for a number of reasons, the ideal baseline for which to compare subsequent follow-up examinations. The perimetric learning effect (see Section 1.2.3.6) generally renders the first, or even the first two, examinations obsolete. In addition, neurophysiologic and/ or psychophysical changes due to the medical lowering of IOP can markedly alter the initial visual field (Flammer and Drance 1983a,b; Spaeth 1985; Flammer et al 1986; Caprioli and Miller 1988; Fogagnolo et al 2007). IOP lowering agents can also have an influence on vascular physiology (Martin and Rabineau 1989; Evans et al 1999; Gherezghiher et al 2009), serum electrolytes (Spaeth 1967; Cowan et al 1984; Chapron et al 2004) and pupil size (Mikelberg et al 1987; Lindenmuth et al 1989; Lindenmuth et al 1990, Edgar et al 1999). As a consequence, it is generally clinically necessary to administer at least a second and possibly also a third visual field examination (the latter to confirm the results of the

second examination) which then serve as the baseline. Any change in the field at a follow-up examination should be confirmed by a repeat examination. The baseline to which the subsequent fields are referenced can be reset as appropriate.

1.4.1 Overview and Series displays

The Overview print-out of the HFA describes the salient features of each of a series of visual fields including the gray scale, the threshold values and the Total and Pattern Deviation probability maps. Additional information, such as pupil size, VA, the proportion of incorrect responses to the fixation loss, false-negative and false-positive catch trials, the global indices and the GHT messages are also displayed. The equivalent print-out of the Octopus perimeters, the Series display, also contains the Cumulative defect curve (Bebié curve).

1.4.2 Change Analysis and Trend displays

The Change Analysis print-out of the HFA graphically illustrates each of the global indices as a function of the time at which the visual field examination was undertaken. The linear regression characteristics, including the statistical significance of the slope, of the MD index against the times to the follow-up examinations are displayed for five or more visual field examinations. A box plot of the threshold values is also included in the Change Analysis print-out. The upper and lower limits and the middle of the box represent the eighty-fifth, fifteenth and fiftieth percentiles, respectively, of the distribution of the threshold estimates across the field. The top and bottom of the whiskers represent the highest and lowest values of sensitivity, respectively. An identical shaped box plot but with a lower sensitivity indicates a general depression such as that resulting from a cataract. A downward more extended lower tail to the box represents a focal defect. Visual field

progression can be identified by the change in the appearance of the box plot between follow-up examinations. However, the resolution of this technique for the identification of early/ small loss is poor.

The Bebié curve for the Octopus perimeters (Bebié et al 1989; Bebié 1990), described earlier (Section 1.3.3), is analogous to the box plot. A downward displacement of the Bebié curve, without a change in shape, indicates a general reduction in sensitivity. A dip commencing anywhere along the curve indicates focal loss and corresponds to a lengthening of the lower tail of the box plot.

The Trend display for the Octopus perimeters is the equivalent of the Change analysis for the HFA. The regression lines of the MD and of the sLV against time to follow-up are colour coded. Green represents a statistically significant negative (improving in the case of the MD) slope, red represents a statistically significant positive (deteriorating in the case of the MD) slope and blue, a slope which does not reach statistical significance, i.e. is clinically stable. It should be noted that a positive MD with the Octopus perimeters represents abnormality.

The MD indices are referenced to the age-matched normal values of sensitivity and, as such, the slope of the regression line should be independent of the effects of aging. The MD indices quantify the overall visual field loss and subtle localized glaucomatous progression may be masked by the insensitivity of the use of the MD index, itself, or by extraneous factors e.g. by cataract or by senile miosis (Spry and Johnson 2002). In addition, a minimum of five examinations are necessary to derive a statistically robust slope of the regression line.

1.4.3 Pointwise linear regression

Linear regression of the outcomes of the given visual field examinations against the times to follow-up have been undertaken for the various global indices (Chauhan et al 1990; Heijl et al 2009), for the mean or overall sensitivity of various sectors of the visual field (Wu et al 1987; Katz et al 1997; Nouri-Mahdavi et al 1997) and for each individual stimulus location–pointwise linear regression analysis (Wu et al 1987; O'Brien and Schwartz 1992; McNaught et al 1995; Fitzke et al 1996; Wild et al 1997; Gardiner and Crabb 2002a,b; Spry et al 2002; Strouthidis et al 2007). Generally, a deterioration of 1dB per year (McNaught et al 1995; Wild et al 1997) or 2dB per year (Gardiner and Crabb 2002a) is considered to represent clinically significant visual field progression.

The advantage of pointwise linear regression analysis lies in the capability of the technique to evaluate potential progression of the visual field in terms of the individual him/ herself rather than referenced to some population-derived characteristic. Such an approach can be very useful in those individuals who exhibit good within- and between-examination variability in response. Conversely, the utility of the technique is impaired in those who exhibit excessive variability. As a consequence, various forms of spatial and/ or temporal filtering of the measured response have been proposed with varying degrees of success (Gardiner and Crabb 2002b; Spry et al 2002; Strouthidis et al 2007).

The sensitivity of pointwise univariate regression analysis for identifying progressive loss increases with the frequency of the examinations but at a cost of a reduction in specificity. At a rate of 2dB per year, three examinations per year

represent a compromise for the optimum sensitivity and specificity (Gardiner and Crabb 2002a).

1.4.4 Glaucoma Change Probability analysis

The GCP analysis of the HFA compares the difference between the sensitivity at a given stimulus location at a given examination and the mean sensitivity at the same location obtained at two baseline examinations. A location which exhibits a negative difference in sensitivity from baseline which lies outside the 95% confidence interval of the test-retest variability for individuals with stable OAG is designated as such with a black triangle. An open triangle is used to designate a location which exhibits a positive difference in sensitivity from baseline which lies outside the corresponding 5% confidence interval. The GCP print-out also contains the gray scale representation of the sensitivity at the given examination and the corresponding Total Deviation probability map (Morgan et al 1991; Heijl et al 1990a; 1990b). Unfortunately, such an approach does not differentiate a deterioration in sensitivity due to a (progressing) cataract from that due to the glaucomatous process (Bengtsson et al 1997a; Bengtsson and Heijl 2008).

1.4.5 Glaucoma Progression Analysis

The Glaucoma Progression Analysis (GPA) compares the difference between the Pattern Deviation values at a given stimulus location at a given examination and the mean of the Pattern Deviation values at the same location obtained at two baseline examinations. At any given examination, a location which exhibits a negative difference in sensitivity from baseline which lies outside the 95% confidence interval of the test-retest variability for individuals with stable OAG is designated as such with an open triangle identifies. A location which exhibits a negative difference

in sensitivity from baseline beyond the 95% confidence interval on two successive examinations or on three successive examinations is designated by a half filled triangle identifies and a filled (black) triangle, respectively. By using the Pattern Deviation approach, the analysis corrects for the presence of cataract and identifies change in the depth and or area of focal losses (Bengtsson et al 1997a; Katz 2000; Bengtsson and Heijl 2008). The technique is based upon the SITA algorithms although the technique does enable the use of baseline fields derived by the Full Threshold algorithm. Progression, or possible progression, identified by GPA exhibits close agreement with expert clinical assessment (Arnalich-Montiel et al 2009) and detects progressive loss at an earlier stage than pointwise univariate linear regression analysis (Arnalich-Montiel et al 2009; Casas-LIera et al 2009).

1.4.5.1 Glaucoma Progression Index

The Glaucoma Progression Index (GPI) was developed to calculate the age-corrected defect depth at stimulus locations identified as significantly depressed by Pattern Deviation probability analysis (Bengtsson and Heijl 2008). The rate of progression of the GPI is calculated by linear regression analysis and is presented in terms of the change in the GPI per year.

1.5 Clinical trials

1.5.1 Ocular Hypertension Treatment Study

The Ocular Hypertension Treatment Study (OHTS) investigated the efficacy of IOP reduction in individuals with OHT. The individuals were required to have 'normal' visual fields (Johnson et al 2002). A normal field was defined according the HFA STATPAC 2 criteria for normality of the MD, PSD, SF, CPSD and GHT. In terms of any clustered locations exhibiting abnormality by Total and Pattern Deviations probability analysis that were indicative of early glaucomatous visual field loss. All

available topical hypotensive treatments were permitted (Gordon and Kass 1999). The study showed that the probability of developing reproducible visual field defect or ONH deterioration was 4.4% in the treated group and 9.5% in the untreated group (Gordon et al 2002; Kass et al 2002).

1.5.2 Collaborative Initial Glaucoma Treatment Study

The Collaborative Initial Glaucoma Treatment Study (CIGTS) randomized individuals with newly diagnosed OAG to medical versus surgical treatment (i.e. trabeculectomy) (Lichter et al 2001). On average, the IOP was lowered by 48% and 35% in the surgical and medical group, respectively. However, the greater IOP reduction in the surgically treated group did not result in better preservation of the visual field. Paradoxically, the surgical group exhibited visual field score which was 0.36 units worse than that of the medically treated group ($p=0.003$).

The visual field determined using HFA Program 24-2 was evaluated in terms of the extent and depth of a defect delineated by the Total Deviation probability map (Musch et al 1999). A scoring system, adapted from the AGIS study (Section 1.5.3), scored all stimulus locations exhibiting a probability level of $p \leq 0.05\%$. A location surrounded by two or more locations exhibiting abnormality by Total Deviation analysis was scored as being between one and four depending upon the depth of the given defect an upon that of each of the two or several neighbouring locations, then a weighting scoring system was applicated (i. e. between 1 and 4 points) which took into consideration the depth of the given defect and the two most defective neighbouring points. The scores for all 52 locations were summed resulting in a value between 0 and 208. This sum was scaled (i. e. by dividing it by 10.4) to give a final score of between 0 (no defect) and 20 (all locations showing a defect at the

$p<0.005$ level). An increase in the baseline score by ≥3 at each of three follow-up examinations was defined as progression (Musch et al 1999; Vesti et al 2003).

1.5.3 Advanced Glaucoma Intervention Study

The Advanced Glaucoma Intervention Study (AGIS) was a randomized controlled trial which evaluated the clinical course of medically uncontrollable OAG using two surgical treatment sequences, namely: laser trabeculoplasty, trabeculectomy and trabeculectomy (ATT); or trabeculectomy, argon laser trabeculoplasty, and trabeculectomy (TAT). In terms of visual field outcome, the TAT sequence was better for white individuals than for African Americans (AGIS 1998).

Visual field loss was scored between 0 (i.e. no defect) and 20 (i.e. end stage visual field loss) based upon the defect depth by Total Deviation analysis with the field being divided into three sectors: nasal, superior and inferior. A location was considered to be abnormal if the defect depth was between 5 and 9dB depending upon the eccentricity of the given location. A nasal defect was defined as three or more contiguous locations, that could cross the horizontal midline, exhibiting abnormality. A nasal step was defined as one or more contiguous locations in the superior or inferior nasal area exhibiting abnormality in the absence of locations exhibiting abnormality in the opposite nasal region. A nasal defect or a nasal step were each scored as 1. If the defect depth was ≥12dB in more than half of the locations in the nasal sector (i.e. ≥4 locations), the assigned score was 2. The superior and inferior hemifields were scored separately. The number of groups of three or more contiguous locations exhibiting abnormality within these sectors was summed. A score of 1, 2, 3, or 4 was added for a total of 3 to 5 locations, 6 to 12 locations, 13 to 20 locations and more than 20 locations, respectively. A score of 1,

2, 3, 4 or 5 was added if at least half of the locations exhibited defect depths of ≥12, ≥16, ≥20, ≥24 or ≥28dB, respectively. A maximum score of 9 could be assigned to each hemifield and a maximum score of 2 to the nasal area. Progression was defined as an increase in the score by 4 or more at each of three consecutive follow-up examinations (AGIS 1994; 1998; Vesti et al 2003).

1.5.4 Early Manifest Glaucoma Trial

The Early Manifest Glaucoma Trial (EMGT) monitored individuals with early glaucoma (Leske et al 1999). The individuals were separated in a group who were treated with argon laser trabeculoplasty plus betaxolol and in a group without immediate treatment. The rate of progression was by 45% in the treated and by 62% in the untreated group, respectively (Leske et al 2003). The reducing of the IOP by approximately 20% decreased the risk of worsening in glaucoma by 50%.

The criteria for visual field loss progression in the EMGT were based on Glaucoma Change Probability maps (Morgan et al 1991; Heijl et al 1990a; Heijl et al 1990b) which use a mathematical model of random threshold variability in the fields of individuals with glaucomatous visual field loss. In this model the defect depth, the stimulus location and the general severity of the visual field loss is weighted. Every examination location from a follow-up field is compared to that from the same examination location derived from that of two averaged baseline fields. Visual field progression is identified when in at least in three follow-up visual fields three or more examination locations in any area changed more than would be expected due to normal variability ($p<5\%$).

Visual field progression was defined in terms of the linear regression of MD against time to follow-up (i.e. dB loss per year) and in terms of the Glaucoma Change Probability analysis (Section 1.4.4) (Heijl et al 2009).

The EMGT and CIGTS methods identify rates of progression that are twice that identified by the AGIS method (Katz et al 1999). Nevertheless, EMGT and CIGTS methods did not identify the same individuals as exhibiting progressive loss.

1.6 Alternative types of perimetry

Considerable progress has been made in determining the properties of the various types of retinal ganglion cells (Lennie 1980; de Monasterio et al 1985; Shapley and Perry 1986; Livingstone and Hubel 1987; 1988; Shapley 1990; Curcio et al 1991; Dacey 1993a,b; Dacey and Lee 1994; Hendry and Yoshioka 1994; Calkins 2001; Carcieri et al 2003; Koch et al 2004; Famiglietti 2005; Sagdullaev and McCall 2005; Trong and Rieke 2008; Szmajda et al 2008; Isayama et al 2009; van Wyk et al 2009). As a consequence, various perimetric techniques have been developed for the detection and assessment of OAG which are based upon the physiology of the ganglion cells. Some of these newer methods are described in Section 1.6.1 to 1.6.4, below, whilst those of SWAP and Pulsar perimetry which form the topic of this thesis are described in detail later (Chapter 3 and 4).

1.6.1 Frequency-doubling Technology perimetry (FDT, Matrix)

The stimulus for the first commercially available FDT perimeter comprised a low spatial frequency sinusoidal grating (0.25 cycle per degree) presented at a high temporal frequency counterphased flicker (25Hz). Under such stimulus conditions, the grating appears to exhibit twice the spatial frequency (Kelly 1981; Maddess and

Henry 1992; Maddess et al 1995). The frequency-doubling is produced by a nonlinear response to contrast which is thought to be mediated by the M_y cells (Maddess and Henry 1992; Maddess et al 1995). The M_y cells are a subset of the parasol ganglion cells which project to the magnocellular layers of the lateral geniculate nucleus and form the magnocellular pathway and, as a consequence, are also known as M cells. The M cells are considered to underlie the processing of motion, of flicker perception, of low spatial frequencies and of high temporal frequencies (Livingstone and Hubel 1987; 1988). Given the physiology associated with processing of the FDT stimulus, early visual field loss should be more noticeable with FDT than with SAP either on the basis that OAG selectively damages the large diameter axons (M cells), (Quigley et al 1987; 1988; Glovinsky et al 1991; Kerrigan-Baumrind et al 2000) or on the basis of the minimal redundancy of the M_y cells, or a combination of both.

With the commercially available FDT, two full threshold tests, C-20 and N-30, and two suprathreshold tests, C-20-1 and C-20-5, are available. The stimulus subtends 10° by 10°. Program C-20 comprises 17 stimulus locations, namely four in each quadrant and a foveal stimulus. Program N-30 incorporates two additional stimulus locations between 20° and 30° eccentricity, nasally, above and below the horizontal midline. The dynamic range of the stimuli extends from 0dB to 33.1dB. A modified binary search (MOBS) staircase system is used to estimate the threshold (Tyrell and Owens 1988; Johnson and Samuels 1997).

The two screening procedures, C-20-1 and C-20-5 are quite similar to each other, except that the stimuli initially presented are at the 1% probability level for the C-

20-1 strategy and at the 5% level for the C-20-5 strategy (i.e. a stimulus that 99% and 95%, respectively, of the normal population are able to detect).

In general, FDT is a very useful and efficient tool for detecting visual field loss resulting from OAG and from neuro-ophthalmological disease (Johnson and Samuels 1997, Sponsel et al 1998, Cello et al 2000; Iester 2000; Trible et al 2000; Thomas et al 2001; Wadood et al 2002).

The second generation FDT perimeter, the Matrix, was introduced in 2003. The dynamic range of the Matrix is compatible with that of the original FDT perimeter (Anderson et al 2005). The Matrix perimeter includes two screening tests, N-30 Screening and 24-2 Screening. The N-30 Screening test uses 19 stimuli which subtend 8-9° by 9-10° and one circular 10° stimulus for the macular region. The 24-2 screening program uses 55 stimuli which subtend 5° by 5° and one circular stimulus 5° in diameter for the macular region. The stimulus for the N-30 Screening test comprises a 0.25 cycles per degree sine wave grating which is counterphased at 25Hz and for the 24-2 Screening test it comprises a 0.5 cycles per degree grating counterphased at 18Hz. The N-30 test of the Matrix perimeter thus corresponds exactly to that of the original FDT perimeter and uses the same and normative database. The examination duration is generally under one minute for the N-30 Screening test and approximately 1.5 minutes for the 24-2 Screening test (Yudcovitch 2006).

The threshold test strategies 24-2 and 30-2 used by Matrix are analogous to Programs 24-2 and 30-2 of the HFA II. The stimulus locations differ only in that the

Matrix has a 3° separation along the vertical meridian and 1° separation along the horizontal meridian. The 3° separation either side of the vertical meridian permits a better visualization of post-chiasmal neurological based field loss, whereas the 1° sparing either side of the horizontal meridian allows a better definition of glaucomatous field loss.

Threshold is determined using the ZEST (Zippy Estimation of Sequential Threshold) algorithm (Vingrys and Pianta 1999; Turpin et al 2002; 2003; McKendrick and Turpin 2005) which is similar to SITA in that it utilises a Bayesian approach to the estimation of threshold. Matrix provides a more detailed description of glaucomatous field loss compared to the FDT although the examination duration is approximately 30% longer (Brusini et al 2006).

FDT perimetry is capable of the longitudinal monitoring of field loss (Johnson et al 1999; McKendrick and Turpin 2005). The technique exhibits a shorter examination duration compared to SAP (Patel et al 2007) and lower within-test variability (Yudcovitch 2006).

A learning effect is present for Frequency-Doubling Technology with the Matrix perimeter in those naïve to SAP (Hong et al 2007; Pierre-Filho et al 2009) and in those experienced in SAP (Centofanti et al 2008). For those naïve to SAP, the MD improved from the first examination to the second and third examinations by approximately 2.8dB for individuals with OAG (Hong et al 2007) and by between 1.7dB and 4.1dB for normal individuals (Hong et al 2007; Pierre-Filho et al 2009).

The test-retest variability of Matrix perimetry increases with increase in defect depth (Hutchinson et al 2004).

The 24-2 threshold test of the Matrix perimeter yields similar outcomes to that of SAP for the detection of glaucomatous field loss (Spry et al 2005b; Burgansky-Eliash et al 2005; Kimura et al 2005; Burgansky-Eliash et al 2007; Zarkovic et al 2007; Bozkurt et al 2008), in resolved optic neuritis (Sakai et al 2007), in optic nerve and chiasmal lesions (Huang et al 2008) and in Type 1 diabetes (Oddone et al 2008). However, compared with SAP, the technique may miss (Clement et al 2009) or may be superior (Racette et al 2008) for the detection of early visual field loss.

1.6.2 Flicker perimetry

There are three different types of flicker stimuli that can be used for the investigation of visual function: Critical Flicker Fusion (CFF) perimetry, Temporal Modulation Perimetry (TMP) and luminance pedestal flicker perimetry. Flicker perimetry is based upon the concept that a rapidly flickering stimulus is mediated by magnocellular mechanisms (M-cell) (Quigley et al 1987; 1988; Glovinsky et al 1991; Kerrigan-Baumrind et al 2000).

CFF perimetry determines the highest flicker frequency that can be distinguished from a uniform steady stimulus of high (near 100%) contrast. The technique is available on the Octopus 300 and 900 series perimeters. A reduced CFF in individuals with OAG and in the fellow eye of individuals with unilateral OAG was initially shown by Tyler (1981). Since then a number of studies have suggested that the technique is superior to SAP for the detection and evaluation of the extent of

glaucomatous field loss (Lachenmayr et al 1991a,b; 1992a,b,c; Lachenmayr 1994). In addition, CFF thresholds are less affected by age compared with SAP and the stimulus is more robust to optical defocus and image degradation arising from cataract (Lachenmayr et al 1991a,b; 1992a). However, the technique exhibits a reduced dynamic range and increased within- and between-examination variability in normal individuals compared to SAP.

Contrast modulation flicker uses a stimulus that is of equal luminance to the background. The contrast of the stimulus is modulated temporally at a given frequency and the amplitude of flicker modulation needed for detection of the stimulus is determined. The optimum temporal frequencies for the detection of glaucomatous damage seemingly range between 2 and 16Hz Casson and Johnson 1992; Casson et al 1993a; Yoshiyama and Johnson 1997).

Luminance pedestal flicker utilises a flickering stimulus which is superimposed upon a pedestal, i.e. a luminance increment, of uniform luminance and determines the amount of flicker that is needed to distinguish the flicker from the pedestal (Austin et al 1994; Anderson and Vingrys 2000; 2002).

1.6.3 Motion perimetry

The concept for the use of Motion perimetry in the investigation of glaucomatous damage is based upon the concept that motion sensitivity is mediated by M-cell mechanisms (Lennie 1980; Livingstone and Hubel 1987; 1988; Shapley 1990).

Various different methods of Motion perimetry have been described. One method involves the detection of the direction of a single dot or line stimulus (Fitzke and Poinoosawmy1987; Johnson et al 1994b; Wang et al 1996; Bosworth et al 1998, Westcott et al 1998, Shabana et al 2003). Individuals with OAG or with OHT exhibit elevated motion-displacement thresholds at locations which are normal by SAP (Wall et al 1997a; Bosworth et al 1998).

A second method utilises random dot motion coherence perimetry whereby the direction of movement of a subgroup of dots is determined from a background of dots each moving in random directions. The threshold is designated in terms of the percentage of coherent dots. Good agreement is present between random dot motion coherence perimetry and SAP (Wall and Ketoff 1995; Bosworth et al 1997).

1.6.4 High-pass Resolution Perimetry

High-pass Resolution Perimetry (HRP) utilises a series of 'ring' targets which are 'high-pass' spatial frequency filtered and comprise a light circular centre and a dark annular surround. The ring stimuli have 14 different sizes in increments of 0.1 log unit (1dB) steps. Therefore the perimeter has an operating range of 14dB. The luminance of the dark surround is $15cdm^{-2}$ and of the centre, $25cdm^{-2}$. The background luminance is $20cdm^{-2}$. The stimulus size is varied using an up-down staircase of variable step sizes. The concept of HRP is that it should correspond to the centre-surrounded arrangement of retinal ganglion receptive fields (Frisen 1986; 1987a,b; Frisen and Nikolajeff 1993).

It is likely that HRP primarily reflects the function of the P cells (Lennie 1980; Livingstone and Hubel 1987; 1988; Shapley 1990) as is the case for SAP. The representation of the P cells in the central retina is much greater than in the periphery. Contrary to SAP, HRP determines sensitivity by varying the size and not by the luminance intensity of the stimulus.

The HRP threshold is correlated with retinal ganglion cell density as a function of eccentricity and of age (Frisen 1988; 1993). The stimulus distribution of the HRP is thought to correspond with the arrangement of the ganglion cells and therefore HRP may be superior to SAP in case of detection of visual field defects (Frisen 1986; 1987b). However, such a concept suggests that HRP thresholds are sampling-limited. This latter suggestion has been refuted (Ennis and Johnson 2002) on the basis that the true level of resolution acuity in the periphery is probably underestimated as a result of the proportionately higher contrast in the periphery. Therefore, HRP thresholds are unlikely to be a direct measure of the underlying ganglion cell density.

Some authors have reported that the HRP performs as well as, or better than, SAP (Frisen 1993; Chauhan et al 1993c,d; 1999; Graham and Drance 1995; Martinez et al 1995; Meyer and Funk 1995; Birt et al 1998) whereas others have found that HRP performs less well (Lachenmayr et al 1991a; Sample et al 1992a). The HRP exhibits less variability at visual field locations with reduced sensitivity (Chauhan and House 1991; Wall et al 1991) than does SAP and this should enable the earlier determination of progressive visual field loss than with SAP (Chauhan et al 1993d; 1999). HRP has been shown to correlate with RNFL thickness (Airaksinen et al

1990; Shirakashi et al 1997; 1999) and the neuro-retinal rim area (Tomita et al 1993) in some studies but not in others (Chauhan et al 1993a).

1.6.5 Short-wavelength Automated Perimetry

Short-wavelength Automated Perimetry (SWAP) will be discussed in Chapter 3.

1.6.6 Pulsar perimetry

Pulsar perimetry will be discussed in Chapters 4 and 5.

1.7 Imaging techniques of the optic nerve and nerve fibre layer

The assessment of the ONH and of the RNFL is very important in the detection and management of OAG. An objective evaluation of morphological damage is possible due to the advent of digital imaging technology which enables a three-dimensional digital reconstruction of the retina and of the ONH. Three principal techniques are currently available, namely Optical Coherence Tomography (OCT), Scanning Laser Polarimetry (SLP) and Scanning Laser Tomography (SLT). SLT with the Heidelberg Retina Tomograph (HRT) is the technique which was used in this thesis for the assessment of structure (Chapters 3 and 4) and is therefore discussed, in some detail, below.

1.7.1 Heidelberg Retina Tomography (HRT I, HRT II, HRT III)

The first digital imaging system developed for the eye was the Heidelberg Retina Tomograph. The technology of the HRT is based upon confocal imaging. A laser source (675nm) is focused on a single point of the object and the light reflected from the object is focused through a confocal aperture onto a detector that is conjugate to the focal plane. The aperture eliminates light reflected or scattered from adjacent

regions of the object (Bartsch et al 1989; Kruse et al 1989; Zinser et al 1989) and ensures that only light reflected from the structure at the focal plane is registered by the detector. Oscillating mirrors deflect the laser beam periodically in the x- and y-directions to acquire an image/ section in two dimensions. Each section consists of 256 x 256 pixels with the HRT I and 384 x 384 pixels with the HRT II and HRT III, respectively. The transverse field of view with the HRT I is adjustable to 10° x 10°, 15° x 15° or 20° x 20° but is 15° x 15° with the HRT II and HRT III. A three-dimensional image is achieved by adjusting the position of the focal plane (i.e. along the z-axis) and by superimposition of the resultant further sections. A series of between 16 and 64 (32 for the HRT I) consecutive and equidistant two-dimensional optical sections through the optic nerve head are generated by the HRT II and the HRT III. The total longitudinal field of view (scan depth) extends from 0.5 to 4.0mm (adjustable) with the HRT I and from 1.0 to 4.0mm with the HRT II (automatic). The spatial resolution is approximately 10μm per pixel.

A minimum of three scan acquisitions should be generated to compute a mean topography image. The software of the HRT II provides 22 stereo-metric parameters. The newer HRT III differentiates itself from the other earlier models with an advanced glaucoma analysis including the Glaucoma Probability Score (GPS), the Topographic Change Analysis (TCA), the active image quality control, ethnic databases of normative values, adjustments for variations in optic disc size, and asymmetry analysis.

The variable, which separates the cup and the neuroretinal rim, is called the 'Reference Plane' (RP) and almost all stereo-metric parameters are dependent on its

position. A fixed offset reference plane of 320μm below the Mean Retinal Height (MRH), the so called 'Standard Reference Plane' (SRP) was originally adopted in the standard HRT software. The MRH was determined for a of 6° sector in the superior temporal papillomacular bundle since the latter is considered to be relatively stable in OAG. However, such an approach has been contested (Greenfield et al 2003). The SRP is now defined at 50μm below the ONH margin (Scheuerle and Schmidt 2004) to be sure that the automatic reference level determination remains below the OHN margin. This approach overcomes the problem of the intra-individual variability in the ONH topography which limits the accuracy of the fixed offset RP approach. An alternative RP has been proposed, the 320 RP, which lies 320μm posterior to the reference ring which is situated in the image periphery, and which seemingly results in less variability in the delineation of the rim area (Poli et al 2008). A novel approach for the identification of progressive damage has been proposed which utilises the SRP at baseline and the 320 RP at follow-up on the basis that the latter is less prone to the glaucomatous process (Asaoka et al 2009).

The retinal surface height profile along the contour line is independent from the RP. The height profile always starts temporally at 0°. The nerve fibre bundles at 90° and 270° in the normal eye typically generate the so called 'double hump' aspect due to their increased thickness in these regions (Burk et al 1990; Dichtl et al 2004). The double hump profile gives rise to two quantitative parameters: the 'Height Variation Contour' (HVC), which is the difference between the most elevated and most depressed point on the contour line, and the 'Mean Retinal Nerve Fiber Layer thickness', which is the mean height difference between the SRP and the height profile along the contour line. In relation to the MRH and the SRP, the double hump can be used as a quantitative criterion in the evaluation of the RNFL. In case of

advanced OAG, the contour line is often situated below the MRH, whereas in generalized depressions of the retinal surface due to global atrophy of the RNFL and low SRP values, even in glaucomatous damage, one or two polar peaks can reach the MRH (Adams et al 1991; Scheuerle et al 2001).

Mikelberg's Discriminant function (Mikelberg et al 1995) (FSM) utilises the 'Cup Shape Measure' (CSM), the 'Rim Volume' (RV), the HVC and the patient's age. ($F \geq 0$ means that the optic disc will be considered as 'normal' and $F < 0$ indicates OAG). The FSM classification is dependent on a RP and, using the SRP, a sensitivity of 89% and a specificity of 84% have been achieved (Mikelberg et al 1995).

The Burk Discriminant function (RB) (Burk et al 1990; 1991) is independent of the RP but uses the drawn contour line (Burk et al 1998) and incorporates the 'Contour Line Mean Height' (CLM) in the temporal quadrant of the optic disc, which is the CLM difference between the temporal superior octant and the temporal quadrant, and the CSM in the temporal superior octant.

Nevertheless, it has been suggested that greatest diagnostic precision for OAG can be achieved with the three parameters: RNFL cross sectional area, CSM and the global Cup-Disc Area Ratio (CDAR) (Uchida et al 1996). However, others have argued that these parameters are related to disc size (Iester et al 1997a; Bathija et al 1998) thereby confounding the diagnosis and have advocated the use of the HVC, CSM and RV (Iester et al 1997c), the HVC, RNFL thickness, the CSM and the 'Rim

Area' (RA) (Bathija et al 1998) or the Log (RA) and the CDAR (Wollstein et al 1998) (Table 1.1).

A different approach was that of the 'Moorfields Regression Analysis' (MRA) (Wollstein et al 1998; 2000). The technique utilises the 95%, 99% and 99.9% confidence limits of the normal rim area at each of six sectors. The original database for the MRA yielded a specificity 96%% and a sensitivity 84% (Wollstein et al 2000) and a sensitivity of 86% at 100% specificity (Deghislage et al 2008) and a sensitivity of 77% and a specificity of 67% with the larger database of the HRT III (Oddone et al 2008).

The 'Glaucoma Probability Score' (GPS) is a classification system for the HRT III which is based upon the steepness of the slope of the cup and of the cup size at each of the six sectors, and upon three additional parameters, cup depth, horizontal RNFL curve and vertical RNFL curve (representing five in totals) for all six sectors, combined. The GPS is given as the magnitude of the probability level, itself, and as a descriptor 'Within Normal Limits', 'Borderline', and 'Outside Normal Limits'. The GPS exhibits a sensitivity of 80% and a specificity of 57% compared to 77% and 67% respectively with the MRA (Oddone et al 2008). The GPS was less specific and more influenced by ONH size than the MRA. However, the CSM and the RB provided the best diagnostic precision. Interestingly, however, the diagnostic precision is similar to that of the Mikelberg and Bathija discriminate functions (Iester 2008). The reproducibility of the GPS, assessed in terms of the interclass correlation coefficient, is almost perfect for normal individuals and ranged from perfect to substantial in OAG (0.922 to 0.705) (Taibbi et al 2009).

Further, all the HRT measurements depend upon the accuracy of the manually drawn contour line. The accuracy of the contour line can be markedly improved when it is drawn in conjunction with the viewing of a convention image of the ONH (Iester et al 2001). A summary of the different automated classification procedures is shown in Table 1.1.

Reference	Parameters used	Sensitivity (%)	Specificity (%)	Normal eyes (n)	Glaucoma eyes (n)	VF: average MD value
(Mikelberg et al 1995)	HVC, CSM, RV	87.0	84.4	45	46	-5.5dB
(Iester et al 1997)	HVC, CSM, RV	All eyes: 74.2 DA: <2mm^2, 64.7; 2-3mm^2, 78.7; >3mm^2, 83.3	All eyes: 88.3 DA: <2mm^2, 83.3; 2-3mm^2, 89.7; >3mm^2, 88.9	60	93	-8.3dB
(Uchida et al 1998)	HVC, CSM, RV	80	83	0	30	-3.7dB
(Burk et al 1998)	CLM (TSO, TQ, TIO), CSM	74.1	85.9	78	58	-15.8dB
(Bathija et al 1998)	HVC, RNFLT, CSM, RA	All eyes: 78 DA: <2mm^2, 71.4;2-3mm^2, 94.4	All eyes: 88 DA: <2mm^2, 92.6; 2-3mm^2, 81.8	49	50	>-10dB
(Wollstein et al 1998)	Log (RA): CDAR	84.3 74.5	96.3 97.5	80	51	-3.6dB

DA: Disc Area
CA: Cup Area
RA: Rim Area
CV: Cup Volume
CDAR: Cup-Disc Area Ratio
CSM: Cup Shape Measure
HVC: Height Variation Contour
RNFLT: Retinal Nerve Fiber Layer Thickness
CLM: Contour Line Mean Height
TSO: Temporal Superior Octant
TQ: Temporal Quadrant
TIO: Temporal Inferior Octant

Table 1.1 A summary of the different automated classification procedures.

Scanning laser tomography is also used for the identification of progressive damage to the ONH. Two different methods are used for the identification of progressive damage with the HRT. Firstly, the change in the stereo-metric parameters between the given examinations can be quantified. Secondly, the differences in the local

height measurements between the two examinations can be calculated. The first method allows a quantitative evaluation of change, whereas the second method shows a better localization of change within the image. The former also enables the identification of progressive damage in any number and combination of parameters. With the latter approach, if the difference in the local height measurements (pixel) of two images is greater than the standard deviation calculated for each corresponding pixel, then the change can be displayed in a colour-coded map. Deteriorating regions are displayed in red and improving regions are displayed in green. No reference plane or contour line is needed with this method.

To enhance the significance of a local height change, a change probability map analysis was developed (Chauhan 1996; 2000). The 384x384-pixel array of topographic height values obtained with each image from the HRT II (HRT I 256x256) is divided into an array of 96x96 (HRT I 64x64) superpixels, where each superpixel contains 16 (i.e. 4x4) pixels. An analysis of variance (ANOVA) compares each superpixel with the three baseline and the three follow-up images. This means that, for each superpixel, there are 48 baseline and 48 follow-up height measurements. The reproducibility of local height measurements at each location in a mean topography image is approximately 20μm both in normal and in glaucomatous eyes, (Kruse et al 1989; Weinreb et al 1993; Janknecht and Funk 1994; Rohrschneider et al 1994) and the Coefficients of Variation (CoV) of the stereometric parameters are about 5% (Mikelberg et al 1993; Rohrschneider et al 1994).

CHAPTER 2

RATIONALE AND DESCRIPTION OF THE RESEARCH

2.1 Previous work

The thesis was a continuation of the work previously undertaken by members of the Group initially at Aston University, Birmingham, and, latterly, at Cardiff University, Cardiff, which is concerned with sources of variability associated with SAP and with SWAP.

The group had investigated the effect on SAP of intra-ocular light scatter arising from cataract (Wood et al 1987a; 1989; Dengler-Harles et al 1990), the perimetric learning effect (Wood et al 1987b; Wild et al 1989; 1991; Searle et al 1991), the perimetric fatigue effect (Hudson et al 1994), stato-kinetic dissociation (Hudson and Wild 1992), threshold estimation (Flanagan et al 1993a; 1993b) and the identification of visual field progression (Wild et al 1993; 1997). In its studies of SWAP, the group had originally shown that the between-subject normal variability at each stimulus was greater for SWAP than that for SAP (Wild et al 1995; Wild et al 1998) even when corrected for ocular media absorption (OMA) and that, as a result, the confidence limits for normality for SWAP were wider than those for SAP. In addition, they had also shown that both the Short-term fluctuation (SF) (Wild et al 1998) and the Long-term fluctuation (LF) (Hutchings et al 2001) was greater in normal individuals and in patients with OAG, respectively, compared to that for SAP. The group had identified further sources of variability namely, variations in macular pigment absorption (Wild and Hudson 1995), variations in intraocular light scatter arising from cataract (Moss and Wild 1994; Moss et al 1995), variations in the efficiency between threshold algorithms (Wild et al 1998) and the presence of a

learning effect in normal individuals (Wild and Moss 1996) and in individuals with OAG (Wild et al 2006).

2.2 Rationale

Countless papers have compared the efficiency of different algorithms for the estimate of threshold. Unfortunately, all most all the studies are cross-sectional in design. The majority of the earlier studies did not consider the impact of the perimetric learning effect on the outcome of the results (the expected improvement in performance arising from successive examinations) whilst more recent studies assume that participants are fully experienced in the requirements of automated perimetry.

The start of this thesis fortuitously coincided with the launch of SITA SWAP. The application of the SITA theory to SWAP had been considered essential in order to reduce both the excessive examination time and the increased between-subject normal variability, relative to SAP, arising from the Full Threshold and FASTPAC algorithms for SWAP. The study of the SITA SWAP algorithm represented a natural follow-on of the work already undertaken by the Group in relation to the Full Threshold and FASTPAC algorithms for SWAP. Following extensive discussions with Carl Zeiss Meditec, a first copy of the commercial version of SITA SWAP was made available to the author at Castelberg Optometry. The latter was the first optometric practice in Europe to be supplied with this algorithm. The SITA SWAP algorithm is usually undertaken with Program 24-2 which examines 54 locations out to a maximum of 27 degrees eccentricity. The aim of the first part of the thesis, therefore, was to determine the performance of the SITA SWAP algorithm in

normal individuals, in individuals with OAG and in individuals with OHT relative to SAP.

Approximately one year after the launch of the SITA SWAP algorithm, a prototype version of a new type of perimetry, Pulsar perimetry, was introduced. The stimulus parameters of the Pulsar are claimed to stimulate, predominantly, the magnocellular pathway. The Pulsar perimeter is thus similar in concept to the Frequency-Doubling Technology in this respect. The stimulus for the Pulsar perimeter comprises a 5 degrees diameter circular wave presented for a duration of 500msec, isoluminant to the background, and temporally modulated at 30Hz. The spatial frequency of the circular stimulus varies in 35 steps from 0.5 cycles/ degree to 6.3 cycles/ degree. The corresponding variation in contrast ranges between 6% and 100%. Pulsar perimetry is usually undertaken with the TOP algorithm and Program CP-T30W which examines 66 stimulus locations out to a maximum eccentricity of 30 degrees. The aim of the second part of the thesis, therefore, was to determine the performance of Pulsar perimetry in normal individuals, in individuals with OAG and in individuals with OHT.

Chapter 3 describes the prospective longitudinal observational study designed to determine the performance of the SITA SWAP algorithm relative to the SITA Standard algorithm and SITA Fast algorithms in normal individuals naïve to perimetry, in individuals with OHT and in individuals with OAG both experienced in SAP but naïve to SWAP. The performance was defined in terms of several aspects. Firstly, the learning effect for SITA SWAP. Secondly, the within-visit between-algorithm and the within-algorithm between-visit differences in sensitivity

for the SITA SWAP algorithm relative to the SITA Standard, SITA Fast algorithms of SAP. Thirdly, the diagnostic capability of SITA SWAP relative to the SITA Standard and SITA Fast algorithms of SAP. Fourthly, the structure (as assessed by the Heidelberg Retina Tomograph) function relationship for SITA SWAP and for SITA Standard.

Chapter 4 describes the prospective longitudinal observational study designed to determine the performance of the Pulsar perimeter relative to the SITA Standard algorithm in normal individuals naïve to perimetry, in individuals with OHT and in individuals with OAG both experienced in SAP. The design of the study was similar to that described in Chapter 3 and determined four aspects. Firstly, the learning effect for Pulsar perimetry. Secondly, the within-visit between-algorithm and the within-algorithm between-visit differences in sensitivity for Pulsar perimetry relative to the SITA Standard algorithm. Thirdly, the diagnostic capability of Pulsar perimetry relative to the SITA Standard algorithm. Fourthly, the structure (as assessed by the Heidelberg Retina Tomograph) function relationship for Pulsar perimetry and for the SITA Standard algorithm.

Chapter 5 describes the effect of optical defocus on the Pulsar stimulus. The effect of optical defocus has been described for FDT (Anderson and Johnson 2003) on detection acuity and resolution acuity in the periphery (Wang et al 1997) and on detection thresholds in the fovea and periphery (Anderson et al 2001).

2.3 The performance of the SITA SWAP algorithm

2.3.1 The learning effect

A number of studies have investigated the learning effect for SAP (Wood et al 1987b; Wild et al 1989; Heijl et al 1989c; Kulze et al 1990; Werner et al 1990; Searle et al 1991; Wild et al 1991; Heijl and Bengtsson 1996). The learning effect describes the increase in the magnitude of the differential light sensitivity with repeated examination. In general, the learning effect for SAP is present during the examination of the first eye at the first visit, is transferred from the first to the second eye at the first visit and occurs from the first to the second and from the second to the third visits. It is greater in the peripheral annulus of the central field than in the more central annuli and is greater for intermediate values of sensitivity than for normal values (Wood et al 1987b; Heijl at al 1989b; Searle et al 1991). The lack of experience in perimetry can therefore mimic the presence of abnormality particularly during the initial examinations.

The learning effect has also been observed for FDT (Iester et al 2000; Horani et al 2002; Heeg et al 2003; Contestabile et al 2007; Hong et al 2007), for CFF thresholds (Seitz et al 2006; Bernardi et al 2007) and for HRP (Drance et al 1989).

The characteristics of the learning effect for SWAP as measured with the Full Threshold algorithm in normal individuals, and in individuals with OHT, who are naïve to SAP are similar to that for SAP but the effect has been found to last longer than for SAP i.e. to be still present at the third and even the fourth examinations. Clearly, such a finding is clinically unacceptable. A fatigue effect is present for SAP and, during the initial examinations, acts as an opposing vector to the learning effect (Hudson et al 1994). The fatigue effect describes the decline in the differential light

sensitivity as the examination duration increases. The effect increases with increase in age and is greater for the second eye compared to the first eye at any given examination. Although the extent of the fatigue has not been quantified for SWAP, it can be hypothesised that the shorter duration of the SITA SWAP algorithm compared to the Full Threshold algorithm will result in a reduction in the fatigue effect and a consequent increase in the magnitude of the learning effect for the SITA SWAP algorithm.

There are numerous potential experimental designs for the study of the perimetric learning effect. Such designs can include repeated perimetry after an interval of minutes, of hours, of days, of weeks or of months. One design, namely repeated perimetry at weekly intervals over a period of five weeks was utilized by Heijl and Bengtsson (1996) for SAP. This design has subsequently been adopted by Wild and Moss (1996), Rossetti and colleagues (2006) and Wild and colleagues (2006) for SWAP Full Threshold. At one session within a visit, individuals underwent examination with the SITA standard algorithm. At a second session within the same visit, individuals underwent examination with the SITA Fast and SITA SWAP algorithms. The order of sessions and the order of examination with the SITA Fast and SITA SWAP algorithms within the session were both randomized between individuals at each of the subsequent visits. The analysis of the learning effect is generally only considered in terms of any improvement in the visual field indices MD and PSD and any reduction in the examination duration, within- and between-eyes, and between groups. In addition to this latter approach, additional analyses were undertaken in this thesis, within- and between-eyes and between groups, of the alteration in sensitivity at each stimulus location, over the five visits, in terms of the central and peripheral mean sensitivities, in terms of the absolute value of sensitivity

and in terms of the Total and of the Pattern Deviation probability values, respectively. The analyses showed clear evidence for a learning effect which was evident for all three algorithms across all three groups and was most pronounced for the SITA SWAP algorithm.

2.3.2 The within-examination, between-individual, between-algorithm variability

The confidence limits for normality at each individual stimulus location are determined from the within-examination, between-individual variability in normal individuals. Such variability increases with increase in eccentricity (Greve 1973; Parrish et al 1984; Lewis et al 1986; Heijl et al 1987a) and with increasing age (Katz and Sommer 1987) and is greater for SWAP than for SAP for both the Full Threshold and the FASTPAC algorithms (Wild et al 1998). However, the variability is similar for the SWAP Full Threshold algorithm and the SWAP FASTPAC algorithm. The increased within-examination between-individual variability and thus the increased confidence intervals, for the older SWAP algorithms compared to those for SAP limit the utility of SWAP, at least for the two older algorithms, in that the defect depth for SWAP has to be greater than that for SAP to achieve statistical abnormality. In SAP, the variability for the SITA Standard algorithm is 31% smaller compared to the corresponding Full Threshold and FASTPAC algorithms, whilst the SITA Fast algorithm exhibits a 41% reduction compared to the FASTPAC algorithm (Bengtsson and Heijl 1999b). In SWAP, the SITA SWAP algorithm exhibits a 22% reduction in variability compared to the Full Threshold algorithms (Bengtsson and Heijl 2003). However, and most importantly, the magnitude of the within-examination, between-individual normal variability for SITA SWAP compared to that for the SITA Standard algorithm is unknown. It was hypothesised that, although such variability is reduced for the SITA SWAP algorithm compared to the SWAP

Full Threshold algorithm, it would still be greater than the reduction in variability of both the SITA Standard and the SITA Fast algorithms compared to the Full Threshold and FASTPAC algorithms. If so, and despite the advent of the state-of-the-art algorithms for both SAP and SWAP, the defect depth for SWAP would, once again, have to be greater than that for the corresponding SAP algorithms (SITA Standard and Fast) to achieve statistically abnormality.

The within-examination, between-individual, variability at each stimulus location between the SITA Standard, SITA Fast and SITA SWAP algorithms were analysed for Visit 5 in terms of the visual field indices MD and PSD, in terms of the absolute value of sensitivity at each location and in terms of the Total and of the Pattern Deviation probability values at each location, respectively, for the normal individuals. In addition, a similar analysis was separately undertaken at Visit 5 for the individuals with OHT and for the individuals with OAG to determine the diagnostic capability (i.e. designation of the presence and extent of abnormality) of each of the three algorithms. The between-algorithm difference in MD and in PSD at Visit 5 was narrowest for the two SAP algorithms. Furthermore, SITA SWAP under-estimated the sensitivity derived by each SAP algorithm by approximately 5dB and overestimated the extent of apparent abnormality in the height of the visual field, relative to each SAP algorithm, in the normal individuals and in the individuals with OHT.

2.3.3 The within-algorithm, within-individual, between-visit variability (Visits 1 to 5 and Visits 4 to 5)

The time at which the emergence of either early visual field loss or of progressive visual field loss is identified by any given algorithm is dependent upon the

magnitude of the associated within- and between-examination (visit) variability. In order to designate progression of the visual field, the difference between the two given examinations must be greater than the associated variability both within- and between- the two examinations (Werner et al 1989).

Both, the Short-term (SF) (the within-algorithm, within-individual, within-examination [visit] variability) and the Long-term fluctuation (LF) (the within-algorithm, within-individual, between-examination [visit] variability) associated with the Full Threshold algorithm are greater for SWAP compared to SAP (Hutchings et al 2001). It was hypothesized that given the greater variability of SWAP, in general, compared to SAP, the SITA SWAP algorithm would exhibit greater within-algorithm, within individual, between-visit variability compared to the SITA Standard and SITA Fast algorithms, respectively, thereby limiting the utility of SITA SWAP in the identification of progressive field loss compared to the SITA algorithms.

The within-algorithm, within-individual, between-visit variability at each stimulus location for the SITA Standard, SITA Fast and SITA SWAP algorithms were separately analysed for each of the three algorithms between Visits 1 to 5 and between Visits 4 to 5 in terms of the difference in the visual field indices MD and PSD, in terms of the differences in the absolute value of sensitivity at each location and in terms of the Total and of the Pattern Deviation probability values at each location, respectively, for the normal individuals, for the individuals with OHT and for the individuals with OAG. Particularly, with SITA SWAP, the within individuals

analysis of the MD and PSD showed considerable between-individual variation in performance.

2.3.4 The structural and functional relationship

A comparison of the relationship between the magnitudes of three structural parameters derived by confocal scanning laser ophthalmoscopy (HRT II; Heidelberg Engineering, GmbH, Dossenheim, Germany) and the magnitudes of the visual field indices derived by SITA SWAP with those for SITA Standard and SITA Fast provided further evidence as to the capability of SWAP to detect more extensive glaucomatous damage than SAP. Confocal scanning laser ophthalmoscopy was used as the structural standard since it was the instrument of choice in the practice of the ophthalmologist PD Dr. med. M. Zulauf who was responsible for the clinical management of the individuals with OHT and of the individuals with OAG. Scanning laser ophthalmoscopy with the HRT was introduced in the late 1980s and is a well validated and accepted technique. Three separate diagnostic criteria were used for the HRT. The first was that of Mikelberg's discriminant function (FMS) (Mikelberg et al 1995), involving the 'Cup Shape Measure' (CSM), the 'Rim Volume' and the 'Height Variation Contour'. The second was that of Burk's discriminate function (RB) (Mikelberg et al 1995; Burk et al 1998) based upon the difference between the 'Contour Line Mean Height' (CLM) in the temporal quadrant of the optic disc, which is the CLM difference between the temporal superior octant and temporal quadrant and the CSM in the temporal superior octant. The third was that of the ratio of the rim to the disc.

The structure-function relationship for SAP has been well documented for SAP using either the Full Threshold, SITA Standard or SITA Fast algorithms and either

confocal scanning laser ophthalmoscopy (Brigatti and Caprioli 1995; Mikelberg et al 1995; Tsai et al 1995; Yamagishi et al 1997; Iester et al 1997b,c; Teesalu et al 1997b; Gardiner et al 2005; Rossi et al 2005; Shah et al 2006), optical coherence tomography (Schuman et al 1995b; Pieroth et al 1999; Kanamori et al 2003; Shah et al 2006), or nerve fibre layer polarimetry (Weinreb et al 1995, Chen et al 1998, Weinreb et al 1998). However, despite the fact that the correlations were statistically significant concerning scanning laser ophthalmoscopy, the degree of correlation was not adequate enough to allow diagnosis of glaucoma using any of these stereometric parameters alone (Mardin et al 1999). The optimum outcome of the various relationships exhibits a moderate correlation between structure and function in the region of r=0.6 (Brigatti and Caprioli 1995; Rossi et al 2005).

Studies of the relationship between structure and function for SWAP are less common and have largely been undertaken with the Full Threshold algorithm for SWAP (Teesalu et al 1997b; 1998; Rossi et al 2005; Shah et al 2006). Such studies, perhaps surprisingly, given the claimed superiority of SWAP over SAP for the detection of visual field loss in advance of that for SAP, indicate a similar modest structure function-relationship for SWAP. No studies have yet evaluated the structure-function relationship for SITA SWAP and, as a consequence, there are no studies which have compared the performance of SWAP in this respect with that of either, or both, SITA Standard and SITA Fast, on the same cohort of individuals. It can be hypothesized that, if SWAP is capable of identifying visual field loss in advance of SAP and that if SITA SWAP provides a more sensitive measure of field loss than Full Threshold or FASPAC SWAP, then the structure-function relationship for SITA SWAP should be better than that for SITA Standard and for SITA Fast. Such an outcome for SWAP might be expected to exhibit a higher correlation with a

slope in the direction of functional abnormality than the corresponding relationship for SAP. Confocal scanning laser ophthalmoscopy was again used as the structural standard. Contingency tables and Venn diagrams were plotted for the HRT parameters: Mikelberg discriminate function (Mikelberg et al 1995), Burk discriminate function (Burk et al 1998) and the rim-disc area ratio and various outcomes of the visual field: a statistically significant MD, a statistically significant PSD and a clinical evaluation by Professor Wild. The SITA SWAP algorithm exhibited the poorest specificity and a similar (but poor) sensitivity to the two SAP algorithms when considered in terms of the MD. The specificity and sensitivity of SITA SWAP was similar for all three groups.

2.4 The performance of Pulsar perimetry

The evaluation of Pulsar perimetry followed a similar approach to that for the evaluation of SITA SWAP. Three groups of individuals: normal individuals, individuals with OHT and individuals with OAG each attended for five visits each separated by one week. All the normal individuals were naïve to any form of perimetry. However, due to difficulties in the recruitment of new individuals with either OHT or OAG, the majority of the individuals with OHT and with OAG had taken part in the study of the performance of SITA SWAP. These individuals were enrolled, on average, two months after completing the SITA SWAP study. As a consequence, it can be argued that, as such, these individuals were highly trained/ experienced in both SAP and SWAP and would bias the outcome of the study in that they were not representative of the 'typical' glaucomatous patient. Alternatively, it can be argued that the outcome would represent SITA Standard and/ or Pulsar perimetry at its optimum potential (since there would be no learning effect present).

2.4.1 The learning effect

The design of the study was similar to that for the SITA SWAP study. Individuals attended for 5 separate examinations each separated by one week. At one session within the first visit individuals underwent examination with the SITA Standard algorithm. At the second session individuals underwent examination with the Pulsar algorithm. The order of examination between individuals was randomized at each session for each of the five visits. It was expected that the individuals with OHT and the individuals with OAG would not improve over the five visits for the SITA Standard algorithm given their previous experience. However, such individuals could be expected to improve over the five sessions of Pulsar perimetry. The normal individuals were naïve to any type of perimetry and could be expected to improve over the five sessions for both types of perimetry. The SITA Standard, rather than the SITA Fast algorithm was used as it is consider to be the 'gold standard' algorithm.

2.4.2 The within-examination, between-individual between-algorithm variability

The magnitude of the within-examination, between-individual, between-algorithm variability of Pulsar perimetry compared to that of the SITA Standard algorithm was unknown. The results were analyzed in a comparable manner to that described in Section 2.3.2. In general, the between-algorithm difference was widest in the individuals with OAG and was narrower in the second (left) eye examined for all diagnostic groups.

2.4.3 Within-algorithm, within-individual, between-visit variability (Visits 1 to 5 and Visits 4 to 5)

The within-algorithm, within-individual, between-visit variability (Visits 1 to 5 and Visits 4 to 5) of Pulsar perimetry compared to that of the SITA Standard algorithm

was unknown and was analyzed in a comparable manner to that described in Section 2.3.3. A somewhat surprising finding was the apparent deterioration in performance for Pulsar perimetry, compared to the SITA Standard algorithm, in both eyes of the individuals with OAG at Visit 5.

2.4.4 The structural and functional relationship

The relationships between the magnitudes of the various structural parameters derived by confocal scanning laser ophthalmoscopy and the magnitudes of the visual field indices derived by Pulsar perimetry are not known. A comparison of the relationships with those for the SITA Standard algorithm would provide further evidence as to the capability of Pulsar perimetry to detect more extensive glaucomatous damage than SAP. The outcome for Pulsar perimetry might also be expected to exhibit a higher correlation and a slope more in the direction of functional abnormality than the corresponding relationship for SAP. Confocal scanning laser ophthalmoscopy was again used as the structural standard. Contingency tables and Venn diagrams were plotted for the HRT parameters, Mikelberg discriminate function (Mikelberg et al 1995), Burk discriminate function (Burk et al 1998) and the rim-disc area ratio and the MD and PSD for SITA Standard algorithm and MD and sLV for Pulsar perimetry for the normal individuals, for the individuals with OHT and for the individuals with OAG and for all three groups together. SITA Standard and Pulsar perimetry exhibited poor sensitivity for the detection of OAG for all three definitions of visual field abnormality.

2.5 The defocus tolerance in Pulsar perimetry

Defocus attenuates the luminance of the centre of the image due to the resulting spread of the stimulus image area on the retina. It is well established that defocus adversely influences the outcome of SAP (Weinreb and Perlman 1986; Atchison 1987; Herse 1992; Park and Youn 1994; Anderson et al 2001). The Pulsar stimulus contains spatial frequencies which range from 0.5 to 6.3 cycles per degree. The influence of defocus on such spatial frequencies is unknown but, apriori, might be expected to be relatively minimal. It was therefore considered clinically important to investigate the influence of defocus on the Pulsar stimulus. However, the slopes of the degradation in the group mean MS and MD were found to be 1.5dB per dioptre of defocus both for the normal individuals and for the individuals with OAG.

2.6 Logistics

The author was enrolled for a research degree as part of the innovative joint Cardiff University and Pennsylvania College of Optometry (PCO) programme for individuals who had obtained a Masters degree in Clinical Optometry from PCO. At the end of the first year of research, the author was required to submit a First Year Continuation Report on his research, to date, and undergo a vive voce defence of the Report. Following the vive voce examination, the author was approved to continue his research towards the award of the degree of PhD.

The research was conducted under the academic supervision of Professor John Wild of Cardiff University and under the local clinical supervision of ophthalmologist PD Dr. med. Mario Zulauf of the University of Basel, Basel, Switzerland and in private practice in Chur, Switzerland. PD Dr. med. M. Zulauf is a former president of the Swiss Glaucoma Association. It was fortuitous for the author that Professor Wild

and Dr. Zulauf had been friends since when they had first met at the meeting of the International Perimetric Society in Amsterdam, The Netherlands, in 1986.

The research was undertaken in the private practice of Castelberg Optometry, Landquart, Switzerland. All three studies were approved by the appropriate Canton Ethical Committee (Ethikkommission des Kantons Graubünden, Chur, Switzerland). The original applications for the first two studies (described in Chapters 3 and 4, respectively) necessitated a resubmission, due to some minor, formal, insurance problems and questions concerning the reimbursement of the participants in each of the two studies. The delay resulting from the resubmission process was approximately one month in each case. However, the delivery of the SITA SWAP algorithm was delayed by six months and, as a result, the delay in obtaining ethical approval proved to be of no consequence. The Ethikkommission des Kantons Graubünden granted a six month extension to the SITA SWAP study without any further problems. The author used the time arising from the delay in the arrival of the SITA SWAP software to familiarize himself with the literature and to begin writing the First Year Continuation Report required by Cardiff University. The third study, described in Chapter 5, gained ethical approval from the Ethikkommission des Kantons Graubünden at the first submission.

Normal individuals were recruited from the practice of Castelberg Optometry, Landquart, Switzerland. The individuals with OHT and the individuals with OAG were recruited from the practice of PD Dr. med Zulauf in Chur, Switzerland. Prior to enrolment into a given study, an optometric examination was undertaken on each individual to ascertain suitability for entry into the study. Each individual gave

signed informed consent after an explanation of the appropriate procedures, risks and possible consequences of the study.

PD Dr. med Zulauf (MZ) provided the diagnosis for all of the normal individuals and for all individual with OHT and OAG, except of three individuals with OHT and three with OAG. The diagnosis of these six individuals was provided by two other ophthalmologists in the region.

Despite the large number of patients (approximately 10,000) attending the Castelberg optometry practice and the enthusiastic assistance from PD Dr. med. Zulauf, the recruitment of individuals with OHT and the individuals with OAG was time consuming. Many patients did not meet the strict inclusion criteria for each of the studies. General health problems, such as stroke or diabetes or, cataract often reduced the number of potential individuals available for the study. Each of the studies required five visits each separated by one week and an initial visit to determine suitability for inclusion into the given study. Due to the length and the number of visits, it was very often difficult to persuade and to motivate the normal individuals and the individuals with either OHT or OAG to participate in any one of the studies. Frequently, work commitments or the demands of private life were reasons cited for a lack of willingness to participate in the studies.

The Ethikkommission des Kantons Graubünden did not permit a monetary incentive to facilitate recruitment. To encourage participation in the SITA SWAP study, individuals were given the incentive of a pair of progressive lenses, free of charge, on completion of the six study visits. Those being recruited for either of the two

Pulsar studies were given the incentive of a pair of single vision lenses, free of charge, or (if preferred) a 50% discount on the cost of a pair of progressive lenses. All progressive lenses were provided to the author by Carl Zeiss, Switzerland, at a discount of 50%. Carl Zeiss also provided 30 pairs of single vision lenses. Where appropriate, individuals were offered reimbursement of their travel expenses. Fortunately, all individuals, once included in the given study, completed the necessary number of visits and, as a consequence there were no individuals who withdrew prior to completion of the given study.

A registered nurse, Ms. Beatrice Thöny, from Chur, Switzerland, planned and coordinated the visits of the individuals. In total, 143 individuals provided 4705 visual fields. Ms Thöny also undertook approximately 60% of the visual field examinations with the author undertaking the remainder. Thirty three percent of the individuals were examined exclusively by Ms Thöny, 17% exclusively by the author and 50% by a combination of the two perimetrists. Ms Thöny and the author were trained in the operation of the HFA by Professor Wild over a period of three days prior to the onset of the first study. In addition, the print-outs from the various algorithms and perimeters were regularly monitored by Professor Wild and PD Dr. med. Zulauf for quality control purposes. The various Analyses of Variance used in the statistical analyses also included the between-subjects factor 'perimetrist' to determine any differences between the two perimetrists. No such differences were present in any of the three studies given the available power.

Supervision by Professor Wild was provided via weekly telephone conferences, via 2-3 visits per year to Landquart and via meetings at conferences e.g. that of the

Association for Research in Vision and Ophthalmology (ARVO). The author made visits to the School of Optometry and Vision Sciences, Cardiff University 1-2 times per year. PD Dr. med. Zulauf provided invaluable and constant local support in Landquart.

Despite the time consuming nature of the recruitment phase and of the perimetric sessions, the experience of undertaking visual field examinations on such pleasant individuals will never be forgotten.

2.7 Patient data export from the HFA and Pulsar perimeters

2.7.1 Patient data export from the HFA perimeter

At the time of the study, it was possible to export certain data, such as the raw data and the general biographic data, via the serial interface of the HFA. It was not possible to retrieve the Total and Pattern Standard Deviation values and the corresponding probability levels. In order to obtain the desired data, all the visual fields were printed out and scanned with a document scanner. The scanned data were digitised in the form of images with Omnipage (Nuance Communications UK, Ltd) and Optical Character Recognition (OCR) software. The resultant images were entered into a data-base structure (Microsoft Access) using various VisualBasic.Net programmes (Microsoft) specifically coded for the study by a software engineer in Landquart, Peter Grischott. Quality control inspection of the resultant data were undertaken and any irregularities in the data arising from the OCR were corrected. The evaluation and computation of the data as well as the production of most tables and figures were realised with the help of these VisualBasic.Net programmes.

2.7.2 Patient data export from the Pulsar perimeter

The raw data from the Pulsar perimeter was exported into a Microsoft Access data-base by means of a VisualBasic.Net application. The data was then entered into an Excel table. Because the formula used to compute the Comparison probability plots in the software of the Pulsar perimeter used in the study deviated slightly from newer updated formulae, Prof. M. Gonzalez de la Rosa, Department of Ophthalmology, Hospital Universitario de Canarias, Universidad de la Laguna, Spain, provided, in Excel format, the corresponding normative database, as well as various conversion formulae. Also, in the case of the Pulsar perimeter, as with the HFA perimeter, the data were entered into a Microsoft Access data-base.

CHAPTER 3

THE PERFORMANCE OF SITA SWAP

3.1 Introduction

3.1.1 The different ganglion cells and their pathways from the retina to the lateral geniculate nucleus and beyond

Open angle glaucoma damages the axons of the retinal ganglion cells. The axons of the different kinds of human retinal ganglion cells (parasol cells, midget cells and small bistratified cells) leave the retina by way of the ONH. After traversing the ONH, the optic nerve, chiasm and optic tract, the fibres synapse in the lateral geniculate nucleus (LGN). The axons of the parasol, small bistratified and midget ganglion cells terminate in particular layers of the LGN. The two most ventral layers of the LGN, the magnocellular layers, comprise the large axons from the parasol cells which are thus also referred to as the magnocellular ganglion cells (M cells). The dorsal four layers, the parvocellular layers, consist of smaller neurons, the midget cells which are referred to as the parvocellular ganglion cells (P cells). Monkey models indicate that the number of M cells contribute approximately 10 to 15%, and the P cells approximately 80%, of the total population of retinal ganglion cells, respectively (Shapley and Perry 1986; Dacey 1993b). P cells have a low speed of transmission and are most responsive to high spatial frequencies and low temporal frequencies (Lennie 1980; Livingstone and Hubel 1987; 1988; Shapley 1990; Dacey and Petersen 1992; Ferrera et al 1994; Dacey 2000; Shabana et al 2003; Yücel et al 2003; Callaway 2005; Battista et al 2009). This implies that they are responsible for the processing of fine detail, colour information and form vision (steady stimulus presentation). The M cells, which have a fast speed of transmission, respond to high temporal frequencies and low spatial frequencies (Lennie 1980; Livingstone and Hubel 1987; 1988; Shapley 1990; Dacey and Petersen 1992;

Ferrera et al 1994; Anderson and O'Brien 1997, Shabana et al 2003; Yücel et al 2003; Callaway 2005; Battista et al 2009). Therefore, M cells are involved in the processing of rapid flicker and motion perception.

The axons from a sparsely populated retinal ganglion cell type, the small bi-stratified ganglion cells (Dacey 1993a; 1999; Dacey and Lee 1994; Martin et al 1997; Shabana et al 2003; Yücel et al 2003; Callaway 2005) lie in the interlaminar, (koniocellular), regions of the LGN and are called koniocellular ganglion cells (K cells) (Hendry and Yoshioka 1994). These ganglion cells, and their axons, are responsible for the transmission of blue-yellow colour-opponent information, i.e. that which is used in SWAP. The K cells comprise about 5-10% of the total retinal ganglion cell population (de Monasterio et al 1985; Curcio et al 1991; Dacey 1993a; Calkins 2001) and the axons are larger than those the P cells.

Evidence from histology suggests that the axons of the larger retinal ganglion cells may be preferentially damaged in early glaucoma (Quigley et al 1987; 1988, Glovinsky et al 1991; 1993; Luo et al 2001; 2009). However, this hypothesis has been questioned (Weinreb et al 1994). The M cell fibres exhibit a range of diameters and the size of any given axon type also depends upon eccentricity; some peripherally located P cells exhibit axons which are larger than those of the more centrally located M ganglion cells. An alternative hypothesis suggests that glaucomatous damage is not selective to any one ganglion cell type and the damage to subsets of retinal ganglion cells with sparse representation, such as those of the K cells, or of the M cells, is more apparent because of the minimal redundancy of these cell types (Ansari et al 2002; Spry et al 2005a). Colour perception is mediated

by the parvo- and the koniocellular pathways (Merigan and Maunsell 1993; Felius et al 1995). Contrary to the M cells (Lee and Sun 2003) which have no, or only weak, colour opponency, the P cells are characterized by colour opponency (De Valois et al 1966; Wiesel and Hubel 1966; Gouras 1968). The colour-opponent system of the parvo- and the koniocellular pathways is connected to three types of cones (photoreceptors). Two types of cones, the long-wavelength sensitive (LWS) cones and the medium-wavelength sensitive (MWS) cones form a red-green channel, whereas the third type, the short-wavelength sensitive (SWS) cones, form the blue-yellow channel. The SWS cones represent approximately 5-10% of the total number of cones in the retina (de Monasterio et al 1985; Wikler and Rakic 1990; Curcio et al 1991; Calkins 2001; Linberg et al 2001) and do not contribute to the luminance channel (Eisner and MacLeod 1980; Cavanagh et al 1987) which is the channel responsible for the processing of the stimuli used in SAP. It is assumed that, due to the apparent higher metabolic requirements (de Monasterio et al 1981), SWS cones will be more affected by hypoxia and ischaemia (Greenstein et al 1989; Yamamoto et al 1996; Cho et al 2000; Madea et al 2001), than the two other groups of cones. These findings support the hypothesis of selective damage to the SWS pathway in OAG. The distribution of the SWS cones in the retina is similar to the distribution of rod photoreceptors. The SWS cones are absent in the central fovea and peak between 1.5 degrees and 7 to 8 degrees eccentricity, after which the number declines (Martin and Grunert 1999; Volbrecht et al 2000).

3.1.2 Two-colour increment threshold technique

Stiles (1939; 1959) developed a two-colour increment threshold technique to isolate the SWS pathway. A blue stimulus is used to optimally stimulate a one-colour mechanism. The peak wavelength of this stimulus corresponds approximately to the peak response of the SWS cones. Another colour, a high luminance yellow, is used as background to help saturate the MWS and the LWS pathways and to suppress, simultaneously, the activity of the rods. This selective isolation of the SWS pathway is the principle for, and the basis of, SWAP.

3.1.3 Ideal stimulus parameters for SWAP

Before 1995, SWAP was undertaken with a variety of different stimulus characteristics depending upon the given research group (Heron et al 1988; Johnson et al 1988b; De Jong et al 1990; Sample and Weinreb 1990; 1992b; Johnson et al 1993a,b; Johnson and Marshall 1995). However, in order for SWAP to become a clinically accepted technique, it was necessary to standardize the stimulus parameters (Sample et al 1996).

The choice of stimulus parameters, by necessity, is a compromise between the maximum isolation of the SWS pathway and the available measurement range of the perimeter (the dynamic range). Also, the stimulus wavelength must be influenced, as little as possible, by absorption within the crystalline lens, particularly from age-related lens yellowing. Greater SWS pathway isolation is achieved by using a narrowband blue stimulus, originally employed by Sample and Weinreb (1990; 1992b). The narrow band blue stimulus is also less prone to shifts in the peak retinal wavelength due to ocular media absorption (Sample et al 1996); but, due to the

reduced transmission, it exhibits a decreased dynamic range (Hudson et al 1993; Moss et al 1995; Wild et al 1995).

A broadband blue stimulus which increases the dynamic range of the perimeter was used by Johnson and colleagues (Johnson et al 1993a,b;1995a) and others (Hudson et al 1993; Moss et al 1995; Wild and Moss 1996). However, the MWS pathway may be stimulated in an extensive SWS defect (Sample and Weinreb 1990).

The standardized stimulus parameters which are used in the commercially available SWAP comprise a 100cdm^{-2} yellow background (Schott OG 530 filter) and a size V narrow-band blue stimulus (Omega 440nm filter, 27nm bandwidth for the HFA, 15nm bandwidth for the Octopus) presented for a stimulus duration of 200msec. In the early studies of SWAP, the magnitude of the background luminance was equivocal. According to Yeh and colleagues (1989), the background luminance should be a minimum of 300cdm^{-2} to saturate, adequately, the rod pathway. A background luminance of 200cdm^{-2} was used by Johnson and colleagues (1988b; 1993a,b). Others, (Hudson et al 1993; Moss et al 1995; Wild and Moss 1996) used 330cdm^{-2}. Sample and Weinreb (1990) employed a background luminance of 80.9cdm^{-2} and argued that a greater level of background luminance merely increased the SWS threshold rather than the magnitude of SWS isolation.

Since minimal SWS pathway isolation is present for a stimulus size of less than Goldmann size IV (Adams et al 1991), and also because maximal SWS pathway isolation is obtained with a 2 degrees diameter stimulus (King-Smith and Carden 1976), the use of Goldmann size V (1.75 degrees) was universally accepted from the

outset. Since the temporal summation of the SWS pathway is maximal at a duration of 200msec, the latter was also used from the beginning (King-Smith and Carden 1976).

The standardized stimulus parameters ensure that the SWS pathway isolation for the HFA is approximately 1.3 log units (13dB) at fixation and approximately 0.9 log units (9dB) at 20 degrees eccentricity. The corresponding values for the Octopus perimeters are 18dB and 14dB, respectively. This degree of isolation seems to be sufficient for the examination of patients exhibiting mild loss (Demirel and Johnson 2000). With deeper defects (up to a defect depth of 12-14dB paracentrally) the response may be mediated by the MWS and LWS pathways (Felius et al 1995). The latter finding would suggest that there is no advantage to using SWAP in moderate to advanced visual field loss. However, Demirel and Johnson (2000) have also shown that isolation can be maintained even when SWAP field loss is moderate (determined as an MD of no worse than -12dB).

The higher sensitivities in the SITA SWAP algorithm compared to the older Full Threshold SWAP produce a 4dB increase in the dynamic range (Bengtsson and Heijl 2003). An increase in the dynamic range implies, of course, that deeper defects can be examined with SWAP. However, SWAP has a reduced dynamic range compared to SAP as a result of the greater luminance of the yellow background together with the reduced transmission of the blue filter. The maximum stimulus luminance for SWAP with the HFA is 65 apostilbs ($20.6cdm^{-2}$) compared to the 10000 apostilbs ($3183cdm^{-2}$) for SAP. Thus, the reduced stimulus luminance renders SWAP less suitable than SAP for moderate or advanced glaucoma.

3.1.4 The between-individual variability and the Frequency of Seeing curve for SWAP

The magnitude of sensitivity varies among individuals of the same age (Heijl et al 1987b). Age-corrected confidence limits for normality at each stimulus location are very important for the delineation of visual field loss (Heijl et al 1987b). The calculation of such confidence limits, which are used in the height (HFA Total Deviation; Octopus Comparison) and shape (HFA Pattern Deviation; Octopus Corrected Comparison) probability maps, is based upon the between-individual normal variability of the threshold estimate at each stimulus location. The between-individual variation in the normal threshold at each stimulus location is, on average, 2.7 times greater for SWAP without correction for ocular media absorption (OMA) than for SAP and 1.9 times greater after correction for OMA (Wild et al 1998).

The between-subject normal variability for SWAP is similar for the 4-2dB double crossing of threshold employed in the Full Threshold algorithm and for the single 3dB crossing of the threshold employed in the FASTPAC algorithm of the HFA (Wild et al 1998).

The increased between-individual normal variability with Full Threshold SWAP compared to SAP indicates that the reduction in sensitivity required to indicate statistical abnormality for SWAP is deeper than that for SAP and this complicates the detection of abnormality by SWAP. The age-related decline in sensitivity is the same with the SITA SWAP and Full Threshold SWAP algorithms (Bengtsson and Heijl 2003). The age-corrected normal sensitivity is approximately 4dB higher and the variance 22% lower with SITA SWAP compared to Full Threshold SWAP. The normal limits for the Total Deviation at the P<5% significance level are, on average,

14% narrower with SITA SWAP than with the Full Threshold SWAP (Bengtsson and Heijl 2003).

The effect of the increased confidence limits for normality and the difficulty in evaluating the influence of OMA on the SWS stimulus are readily apparent in the HFA STATPAC analysis program of the Full Threshold SWAP. The Total and Pattern Deviation probability analysis for the commercially available Full threshold SWAP underestimates the presence and depth of loss compared to that of SAP (Wild 2001). It seems that such underestimation is particularly common in the superior field and largely arises from the increased variability of SWAP in this region.

Slightly greater field loss with Full Threshold SWAP compared to SAP occurs either in the presence of a measured hill of vision, which is elevated above that of the age-corrected hill, or when the defect is paracentral in origin and the magnitude of the confidence limits for SWAP are similar to those of SAP (Wild 2001).

The probability of detection of a stimulus is determined from the Frequency of Seeing curve (FOS), whereby the percentage of seen responses is plotted against the log of the stimulus luminance. The curve is typically S-shaped (sigmoid) (Weber and Rau 1992). Threshold is usually defined as the stimulus luminance which has a 50% probability of detection (Anderson and Patella 1999; Doshi and Harvey 2003; Weijland et al 2004). As the luminance of the stimulus increases, the percentage of perceived stimuli tends to, but does not achieve, 100%. The slope of the FOS curve is an indication of the variability associated with the derivation of threshold (the

Short-term fluctuation). Therefore, an increasingly flatter slope indicates increasing variability.

The between-individual variability for normal individuals increases with increasing eccentricity and with increasing age and is greater for SWAP than for SAP (Wild et al 1995). One component of the increased between-individual variability for SWAP, compared to SAP, is the between-individual variation in the intraocular light scatter resulting from the increased background luminance of SWAP compared to SAP impacting upon the SWS stimulus (Moss and Wild 1994). Another source is the between-individual variation in OMA (Moss et al 1995). A further source, which only affects the paracentral region, is the between-subject variation in the density of macular pigment (Wild and Hudson 1995).

3.1.5 Short-term fluctuation and Long-term fluctuation in SWAP

The within-test variability in the threshold at any stimulus location is designated as the Short-term fluctuation (SF) (Bebié et al 1976b; Flammer et al 1984b). The between-test variability in threshold is designated as the Long-term fluctuation (LF) (Bebié et al 1976b; Flammer et al 1984b,c; Hutchings et al 2000). For SAP, the SF and LF independently increase as sensitivity declines both in the normal and in the abnormal eye (Flammer et al 1984b,c). Contrary to early studies, which suggested that the SF derived by Full Threshold SWAP in normal individuals was similar in magnitude to that for Full Threshold SAP (Sample et al 1993a), the SF for Full Threshold SWAP is, in fact, larger than that for Full Threshold SAP (Wild et al 1998; Kwon et al 1998). Estimates of the difference in magnitude between the SF for the Full Threshold SWAP and that for SAP vary from 17% (Wild et al 1998) to 55% (Kwon et al 1998). The SF for individuals with OAG is greater than that for

patients with OHT for both SAP (Flammer et al 1984b) and SWAP (Sample et al 1993a; Wild et al 1995). However, the magnitude of the SF determined by the two techniques is similar both in OAG and in OHT (Sample et al 1993a; Wild et al 1995).

The LF is greater for Full Threshold SWAP compared to that for SAP both in normal individuals and in individuals with OAG. A measure of the LF in normal individuals (which included the influence of the SF) across the central field was 107% and 41% larger for SWAP than for SAP, using the HFA and the Octopus perimeters, respectively (Kwon et al 1998). The LF was 23% greater with Full Threshold SWAP than with SAP in stable OAG (Blumenthal et al 2000). The two components of the classically defined LF, the homogeneous and heterogeneous components, are larger for Full Threshold SWAP than that for SAP by 79% and 43%, respectively, in glaucoma suspects and by 25% and 34% in OAG (Hutchings et al 2001). The increased SF and the increased LF for SWAP relative to SAP will make it more difficult to detect the presence of progressive visual field loss compared to SAP.

3.1.6 The application of SWAP in patients with OHT and OAG

In one of the earliest studies (Sample et al 1993b), SWAP was undertaken on 55 glaucoma suspects. The participants were divided, on the basis of intraocular pressure and vertical cup: disc ratio, into low-, medium-, and high-risk categories. The group mean MD and the group mean number of abnormal stimulus locations for SWAP (defined as a cluster of three or more locations, each 6dB below the normal age- and lens-density-corrected value) at the initial examination were similar for the low- and medium-risk groups, but greater for the high-risk category. However, Wild

(2001) argued that the definition of abnormality was empirical and did not consider the variability associated with the threshold estimate.

Johnson and colleagues (1995a) used the risk model of Hart and colleagues (1979) to categorise the probability of developing OAG, in each eye, of 232 patients with OHT. The prevalence of visual field loss for Full Threshold SWAP, based upon abnormality in height, increased with increase in risk category, rising to one third in the high-risk group. An almost identical study (Polo et al 2001) found that the prevalence of visual field loss for SWAP in OHT also increased with increase in risk category, rising to over 50% in the high-risk group.

A prospective 4 year follow-up study (Johnson et al 2003), perhaps not surprisingly, found a strong association between glaucomatous ONH damage at baseline and the subsequent development of a visual field defect by SAP. A higher percentage of glaucomatous ONHs were also found in the group of individuals exhibiting visual field loss to Full Threshold SWAP at baseline and in those who later developed defects to SWAP.

The areal extent of visual field loss with Full Threshold SWAP seems to be more pronounced than that with SAP in OAG. This conclusion is based upon two studies both of which used non-standardized stimulus parameters and both of which only employed small cohorts of individuals. The first study found that 9 of 16 glaucomatous eyes each exhibited results in two or more quadrants for SWAP which lay more than two standard deviations from the normal value based upon 10 age-matched normal subjects (Sample and Weinreb 1990). The other study reported that

25 of 32 eyes exhibited a wider area of loss, relative to 95% confidence limits, for SWAP, corrected for OMA, than for SAP (Johnson et al 1993b). However, abnormality in these two studies was defined in terms of a reduction in the height of the field rather than in the alteration of the shape (Wild 2001).

Due to the lack of equivalent techniques for identifying progressive loss in SWAP relative to SAP, which are based either upon the linear regression of sensitivity against time to follow-up or upon the change in sensitivity from baseline lying outside the normal random test-retest variability exhibited in stable OAG (Change Probability analysis) (Heijl et al 1989a, Bengtsson et al 1997a), the identification of progressive visual field loss with SWAP at each stimulus location is difficult.

One approach for evaluating progressive loss derived by SWAP was proposed and described (Kono et al 2000) which was based upon the cumulative defect, or Bebié, curve (Bebié et al 1989). However, others (Åsman and Olsson 1995) have criticised the cumulative defect curve on the basis that it does not deal satisfactorily with the location-dependent variation in the fluctuation associated with the threshold estimate and a similar criticism is present with the modified technique of Kono and colleagues (2000).

The claim that Full Threshold SWAP identifies progressive field loss earlier than SAP is based upon several prospective studies. Four studies involved patients with OHT and two studies involved patients with OAG. Unfortunately, four of the studies (Sample and Weinreb 1992b; Sample et al 1993b; Johnson et al 1993a,b) employed only small cohorts of individuals while the fifth (Demirel and Johnson 2001) was

based upon patients with OHT, only. Four of the studies did not utilise a formal quantitative definition of progressive loss.

The first study (Sample and Weinreb 1992b) involved 21 eyes with OAG which were examined with SAP and SWAP over a follow-up of between 6 and 26 months. Of the 21 eyes, nine worsened by greater than 0.2 log units with SWAP, but were stable with SAP. Abnormality for SWAP was defined in terms of deviations in absolute values of sensitivity relative to those of 21 normal individuals matched to the OAG group. Such a definition does not consider the variability associated with the threshold estimate (Flammer et al 1984b; Heijl et al 1987a).

The second study involved 25 eyes with OHT which were followed-up over an interval of between 13 and 37 months (Sample et al 1993b). Five eyes developed OAG over the follow-up period on the basis of a repeatable visual field defect by SWAP. Unfortunately, the criteria to define progressive field loss for SWAP were not clear and the proportion of the five eyes exhibiting abnormality in SAP perimetry was not given (Wild 2001).

The third and the fourth studies were undertaken by Johnson and colleagues (1993a,b). These studies suggested that SWAP was able to delineate the presence of visual field loss in advance of SAP by at least 3 to 4 years. However, their conclusion was only based upon a small number of patients with OHT and a small number of individuals exhibiting progressive glaucomatous loss.

The final study, which corrected the results of SWAP for OMA was undertaken by Demirel and Johnson (2001) on 500 eyes with OHT. The patients were examined annually over a five-year follow-up period. The baseline prevalence of SWAP and SAP deficits was 9.4% and 1.4% respectively. During the study, incident rates of field loss were 6.2% (1.2% per year) for SWAP and 5.9% (1.18% per year) for SAP.

The superiority of Full Threshold SWAP over SAP in delineating progressive field loss in glaucoma is by no means clear from these studies (Wild 2001). The incidence rates for glaucomatous visual field loss are similar between SWAP and SAP. The Full Threshold SWAP, with its current inherent limitations described earlier, may offer little advantage over SAP for the detection of progressive visual field loss (Caprioli 2001).

3.1.7 Crystalline lens aging and cataract in relation to SWAP

Many patients with either OAG or OHT exhibit cataract. This problem and the absorption of short-wavelength light resulting from the normal age-related yellowing of the crystalline lens poses a considerable limitation for SWAP. Cataract predominantly causes a general reduction in sensitivity for both SAP and SWAP (Moss and Wild 1994; Moss et al 1995). In general, individuals with posterior subcapsular cataract demonstrate a greater reduction in differential light sensitivity for SWAP than for SAP. This is most likely to arise from the increased background luminance of SWAP and the concomitant reduction in pupil size (Moss et al 1995). Conversely, the visual field for SAP is primarily affected by anterior cortical cataract. This can be explained by the smaller stimulus size (Goldmann size III) and the relatively lower background luminance of SAP, and the consequent larger pupil

size, which results in the peripheral anterior cortical cataract exerting a maximal effect.

After the age of approximately 60, the age-related yellowing of the crystalline lens progresses much more rapidly than previously (Werner 1982; Zeimer et al 1987; Sample et al 1988; Johnson et al 1989; Siik et al 1991; Cook et al 1994; Delori and Burns 1996) resulting in an increase in absorption of short-wavelength light. OMA exhibits large between–individual variability particularly in the older age groups (Sample et al 1988; Johnson et al 1988b; Siik et al 1991) and causes a reduction in the height of the visual field. The between–individual variation of OMA in the same age group makes the interpretation of the visual field derived by SWAP difficult.

The MS index for SWAP in normal individuals can be predicted more accurately by an index of the crystalline lens transmission, calculated by blue-green autofluorescence, than by age alone (Teesalu et al 1997a). A video-based method to measure lens density by means of a double pass reflection technique based upon the intensity of the fourth Purkinje image for different blue wavelengths has been used with SWAP (Johnson et al 1993c; Keltner and Johnson 1995; Demirel and Johnson 2001). This technique takes approximately one minute per eye and seems to be a clinically practical way to measure absorption (Johnson et al 1993c; Johnson and Marshall 1995). However, the technique is not commercially available. Another technique for measuring OMA, the scotopic threshold technique, although extensively applied in research settings (Johnson et al 1989; Sample et al 1989; Lutze and Bresnick 1991; Wild et al 1995; Johnson and Marshall 1995; Polo et al 1998) is not clinically practicable due to the long (at least 8-10 minutes) dark

adaptation time (Johnson et al 1993a). After correcting for absorption measured either by autofluorescence (Teesalu et al 1997a) or by the scotopic threshold technique (Wild et al 1998), the between-subject normal variability of the threshold derived by SWAP is markedly reduced, but is still higher than that for SAP.

3.1.8 Normal hill of vision for SWAP

In SAP, the age-related decline in sensitivity is approximately 0.8dB per decade for the Full Threshold algorithm (Heijl et al 1987a; Flanagan et al 1993b) and the magnitude of the slope steepens with increase in eccentricity. The age-decline in sensitivity for SWAP is steeper than that for SAP and lies between 1.5dB and 2.2dB for prototype stimuli (Johnson et al 1988b; Johnson and Marshall 1995) and also between 1.5dB and 2.2dB for the standardized stimuli for SWAP (Wild et al 1998). The inferior visual field for Full Threshold SWAP exhibits higher sensitivity compared to the superior field (Sample et al 1997). And this asymmetry is similar greater than that of SAP.

The reason for the greater age decline of Full Threshold SWAP compared to that of SAP is unclear. Probable explanations included: reduction in foveal cone photopigment (van Norren and van Meel 1985; Kilibride et al 1986), reduction in photoreceptor density (Gartner and Henkind 1981; Farber et al 1985), reduction in the morphology and density of the retinal ganglion cells (Dolman et al 1980; Balazsi et al 1984), and reduction in the number and morphology and density of cortical cells (Scheibel et al 1975; Devaney and Johnson 1980). The preferential damage of SWS cones by prolonged exposure to UV radiation also seems to play a likely role (Ham et al 1982). However, these changes in the SWS cone function cannot account for all of the age-related reduction in sensitivity of the SWS pathway. The most

plausible explanation is that of Johnson (1994a) who argued that the greater age-related decline in sensitivity arises from the reduced redundancy of the SWS pathway compared to other visual pathways.

3.1.9 Relationship between structural changes and SWAP

The general relationship between structural changes of the ONH and visual function loss was considered initially over 150 years ago. Various reports during the past 40 years indicate that the presence of glaucomatous visual field loss is predictable based upon the appearance of the ONH (Shutt et al 1967; Drance 1974; Read and Spaeth 1974; Drance 1975; Hitchings and Spaeth 1977; Gloster 1979; Goldberg 1981; Hitchings and Anderton 1983). Less predictable is the relationship between the location and severity of the visual field loss and the appearance of the ONH (Holmin 1982; Lewis et al 1983). Based upon the few longitudinal studies (Katz et al 1989; Zeyen et al 1992; Zeyen and Caprioli 1993; Miglior et al 1996; Kamal et al 1999; Kamal et al 2000), ONH changes usually occur prior to the occurrence of visual field loss. However, the number of patients that have been evaluated in these studies is relatively small.

Structural damage to the ONH and to the retinal nerve fiber layer (RNFL) is correlated with the magnitude of the visual field loss by SWAP. In some studies, the appearance of the ONH is documented by stereo photographs (Girkin et al 2000; Johnson et al 2002; Johnson et al 2003) and in others and also by HRT (Teesalu et al 1997b; Teesalu et al 1998; Mistlberger 2002; Rossi et al 2005; Shah et al 2006; Ferreras et al 2007). The RNFL has been evaluated using scanning laser polarimetry (GDx-VCC) (Mistlberger 2002; Bagga et al 2006; Ferreras et al 2007) and by

optical coherence tomography (OCT) (Mistlberger 2002; Mok et al 2003, Sanchez-Galeana et al 2004; Bagga et al 2006; Ferreras et al 2007).

3.1.10 Fatigue effect

The perimetric learning and fatigue effects oppose each other both within- and between-eyes during any given visit. The outcome changes from the initial examination to the follow-up examinations as the patient becomes more experienced in perimetry. The learning effect declines but the fatigue effect remains and the latter, as a consequence of the decline in the learning effect, become more obvious. The fatigue effect describes the reduction in sensitivity for SAP and occurs in normal individuals, in individuals with OAG, in individuals with OHT and in individuals with other optic neuropathies (Heijl 1977a; Johnson et al 1988a; Wild et al 1991; Hudson et al 1994). It is evident that the fatigue effect can either mimic the presence of a defect or exacerbate the appearance of existing visual field loss (Hudson et al 1994). The fatigue effect has received little attention in SWAP. The fatigue effect for SWAP is likely, at least, to be similar in magnitude to that for SAP, but may be more pronounced in the Full Threshold SWAP due to the longer examination duration relative to SAP.

3.1.11 HFA SITA Standard, SITA Fast and SITA SWAP algorithms

The Full Threshold, FASTPAC and both older SWAP algorithms all use bracketing strategies to determine the threshold and the threshold is designated as the 'last seen' stimulus (Bengtsson et al 1997b, Bengtsson and Heijl 1998a). The SITA Standard and the SITA Fast algorithms were described in Chapter 1. The SITA SWAP algorithm (Bengtsson 2003) is discussed in detail in this section.

A similar approach to that for SITA Standard and SITA Fast was adopted for the development of SITA SWAP (Bengtsson et al 1997b). A model of the age-corrected normal visual field for SWAP was derived from a database of 392 normal visual fields from ten different centres. The FOS curves from normal and glaucomatous eyes were taken into account to determine the SWAP threshold variability. The slope of the FOS curve (σ) is a measure of the variability of the threshold estimate. The slope for SWAP (σ=1.79dB) is twice as large as that for SAP (σ=0.86dB) in normal individuals and in individuals with OAG (Olsson et al 1998). A computer based simulator, which was used to develop the SITA algorithms for SAP was modified in order to create many different models of SITA SWAP (Bengtsson et al 1997b). The visual fields from 80 normal eyes and from 25 eyes with a glaucomatous ONH and corresponding visual field loss were used for the modified simulator (Bengtsson et al 1997b). The various characteristics of the response were evaluated by empirically derived SWAP FOS curves and frequencies of incorrect answers (Olsson 1991). From the calculated difference between the true threshold and the simulated fields, the accuracy of the estimate was obtained. To balance the accuracy of thresholds against the examination duration, simulations with different stimulus step sizes were performed.

As with the SITA algorithms for SAP, Bengtsson (2003) used the 'Error Related Factor' (ERF) as well to interrupt the stimulus staircase in SITA SWAP when a desired confidence in the threshold is reached. The magnitude of the ERF was adapted to optimize the accuracy of the estimate against the examination duration. She tested four different SITA SWAP versions on ten eyes twice at four separate visits with differing ERF's. Finally, the selected version of SITA SWAP was tested and compared with each of the two older SWAP strategies. In this case, ten eyes of

normal individuals and 31 eyes of individuals with OAG were studied. All stages of severities of glaucomatous field loss were represented (defined by the MD index derived with SITA Fast). All individuals underwent six examinations with SWAP at three separate visits, two examinations with the selected SITA SWAP version, and two each with the Full Threshold and FASTPAC SWAP algorithms. The test order of programs was randomized so that approximately one third of normals were first tested with each SWAP strategy. Furthermore, after the SITA SWAP session, one SITA Fast test was always administered additionally.

The mean examination duration with SITA SWAP was 3.6 minutes; with FASTPAC SWAP 7.7 minutes; and with Full Threshold SWAP 11.8 minutes (Bengtsson 2003). The threshold reproducibility did not differ between any of the three algorithms (p=0.553); the mean of the differences was 2.4dB for SITA SWAP, 2.4dB for FASTPAC SWAP and 2.3dB for Full Threshold SWAP. The MS was higher for SITA SWAP (21.6dB) compared to that with FASTPAC SWAP (17.8 dB) (p=0.026) and Full Threshold SWAP (17.3dB) (p=0.012).

The higher MS for SITA SWAP compared to the longer SWAP algorithms was partially attributable to the absence of the fatigue effect present with the Full Threshold SWAP algorithm and which decreases sensitivity by approximately 1.5dB over the duration of the examination (Gardiner et al 2006). Another reason, which accounts for a difference of approximately 1dB is that the Full Threshold algorithm defines threshold as the 'last seen stimulus' and the SITA SWAP algorithm defines threshold as the 50^{th} percentile on the FOS curve. However, the remaining discrepancy is unexplained.

The performance of the SITA SWAP in relation to the magnitude of the learning effect arising from the shorter duration of the examination; in relation to the within-algorithm, within-individual, between-visit variability (which determines the time at which the emergence of either early visual field loss or of progressive visual field loss is identified by a given algorithm relative to one or other algorithms); in relation to the within-examination, between individual, between-algorithm variability (which determines the confidence limits for normality); and in relation to the structure-function correlation, are either unknown or have received little attention.

3.2 Purpose

The aim of the study, therefore, was to determine the characteristics of SITA SWAP in the clinical environment with particular reference to SAP undertaken with the SITA Standard and SITA Fast algorithms. Four specific characteristics of SITA SWAP were to be investigated, namely, the presence, magnitude and temporal characteristics of any learning effect; the magnitude of the within-algorithm, within-individual, between-visit variability following any cessation of any learning effect; the magnitude of the within-examination, between-individual, between-algorithm variability; and the structure–function relationship.

3.3 Methods

3.3.1 Case series

The case series comprised 79 consecutively presenting individuals who met the inclusion criteria for enrolment in the study and who, during the recruitment phase, had volunteered to take part in the study. All individuals were provided with verbal and written information concerning the nature of the study, and had given written consent, in accordance with the requirements, and approval, of the Ethikkommission

des Kantons Graubünden, which is, in turn, in accordance with the tenets of the Declaration of Helsinki.

The case series consisted of three groups of individuals. One group comprised 29 normal individuals (16 females and 13 males) who were recruited from the optometric practice of the author in Landquart, Switzerland. The mean age was 54.8 years (SD=9.7; range 40-76 years). Each of the remaining two groups comprised 25 individuals. One group comprised individuals with OHT and consisted of 14 females and 11 males. The mean age was 60.0 years (SD=7.9; range 48-76 years). The other group comprised individuals with OAG and consisted of 17 females and 8 males. The mean age was 63 years (SD=8.3; range 46-73 years). Twenty-two of the 25 individuals with OHT and 22 of the 25 individuals with OAG were drawn from the ophthalmological practice of PD Dr. med. Zulauf, Chur, Switzerland. The remaining 6 individuals were drawn from the practices of three ophthalmologists within Landquart, Switzerland.

Based upon a range of differences in the visual field index MD of +/- 3.0dB (range 6.0), the SD of the differences was estimated to be approximately 1.5dB (4SD being 95% of the distribution). A sample of 26 patients therefore provided 90% power of detecting a 1.0dB difference between visits and/ or between algorithms (Wild et al 1999a,b; 2006).

The individuals were matched as closely as possible in age. The age profile across the three groups is given in Table 3.1.

As with any case series, the representative nature of the series to that within the general population can only be determined from comparisons with other case series compiled for similar studies.

Age (years)	Normal Individuals	OHT	OAG
40-49	6	1	3
50-59	15	11	3
60-69	4	6	10
70-79	4	7	9

Table 3.1 The number of individuals and distribution of age within each of the three groups.

All individuals underwent an optometric examination at baseline including visual acuity, refraction, tonometry, slit lamp biomicroscopy of the fundus and optic nerve head and wide angle non-mydriatic fundus photography. This examination was undertaken to derive the appropriate information particularly that of the refraction which was required not only for perimetry but also for the spectacles which were to be offered as an inducement to participate in the study. All individuals also had an ophthalmological examination including visual acuity, tonometry, gonioscopy, slit lamp biomicroscopy of the fundus and ONH and scanning laser ophthalmoscopy (26 of the 29 normal individuals, 24 of the 25 individuals with OHT and all 25 of the individuals with OAG) with the Heidelberg Retina Tomograph II (HRT II) (Heidelberg Engineering GmbH, Dossenheim, Germany).

In the case of those individuals with OHT or OAG, the ophthalmological examination was undertaken prior to the optometric examination and, in the case of the normal individual after the optometric examination. The interval between the two types of examination was, generally, one month.

For the optometric examination, the IOP was measured with the Pascal Dynamic Contour Tonometer (Zeimer Ophthalmic Systems AG, Port, Switzerland). For the ophthalmological examination the IOP was measured with the Goldmann applanation tonometer and central corneal thickness with the Quantel Pocket I ultrasonic pachometer (Quantel Medical SA, Clermont-Ferrand, France).

Each individual was required to exhibit in each eye a visual acuity of 7/10 or better (equivalent to 6/9 or better); a distance refractive error of ≤+/-7.0 dioptres mean sphere and ≤+/-3.0 dioptres cylinder; a normal anterior segment, and lenticular changes not greater than NC2.0, NO2.0, C1.0, or P1.0 by the Lens Opacities Classification System III (LOCS III) (Chylack et al 1993). In addition, no individual was receiving systemic medication, or manifested any systemic disease, known to affect the visual field; all had a negative family history of ocular disease or any systemic disease with potential ocular involvement.

Normal individuals were categorized on the basis of normal findings from the clinical examination and exhibited an upper limit for the IOP of ≤20mmHg.

Individuals with OHT were categorized on the basis of a central corneal thickness-corrected IOP of ≥22mmHg in both eyes on at least two occasions separated by at

least one month, or a pre-treatment IOP ≥22 mmHg under similar circumstances, in the presence of a normal disc by stereo observation and a normal visual field, considered post hoc, on the basis of the results from the study. A normal appearance of the field was defined after Morgan and colleagues (2005) according to the following guidelines: a field exhibiting complete normality by Pattern Deviation probability analysis; a field containing one non-edge location exhibiting apparent abnormality at the p<2.0% level or worse; or as a field containing up to 3 unclustered locations in any one horizontal hemifield at the p<5% level. Locations exhibiting apparent abnormality arising from the presence of obvious artefacts such as lens rim, upper lid contamination, or seed-point (i.e. those at 9°, 9° eccentricity) errors, and those locations immediately adjacent to the blind spot were not considered in the evaluation of the given field. In the case of at least two or more successive IOP measurements, the prior measurements had been taken by PD Dr. med. Zulauf and the final measurement by the author at the baseline examination.

Four of the 25 individuals with OHT were each receiving a single topical agent in each eye for IOP control (two were receiving a nonselective β-adrenergic receptor blocker, one an α-adrenergic agonist and one a carbonic anhydrase inhibitor). A fifth individual was being treated with a combination therapy of a carbonic anhydrase inhibitor and a β-adrenergic receptor blocker. All five had been treated with the given regimen for at least two months prior to entry into the study and remained on the same regimen throughout the five week period. The level of risk of the OHT in the worst eye was classified, post hoc, using the STAR II system (Scoring Tool for Assessing Risk, Pfizer Inc.) (Gordon et al 2007) which determines the level of risk on the basis of the following: the magnitude of the corneal thickness-corrected IOP; the more asymmetric disc; a thin corneal thickness; and the mean of the PSD index

obtained at the two most recent visual field examinations. The latter was derived from the SITA Standard strategy at Visits 4 and 5 (see Section 3.4.1.1.3, below).

The group with OHT comprised 4 individuals at low risk (mean 3.8%; SD=0.6), 16 individuals designated at medium risk (mean 9.7%; SD 2.6) and 5 at high risk (mean 28.4%; SD=10.6). Nineteen of the 25 individuals with OHT had previous experience of standard automated perimetry (SAP). The mean number of previous examination sessions (i.e. visits) for these 19 individuals was 4.7 (SD=3.2; range 1-12 sessions).

Individuals with OAG were categorized on the basis of an optic nerve head, viewed by stereo-observation, characteristic of the disease including generalized or focal thinning of the neuro-retinal rim, disc asymmetry, changes in the lamina cribrosa, pallor, vessel changes or disc margin haemorrhage. The Heidelberg Retina Tomograph reflectance image for the optic nerve heads of each of the 25 individuals with OAG and the values of the parameters for Disc Area, Cup Shape Measure, Height Variation Contour, Linear Cup:Disc ratio and the Mikelberg and Burk Discriminant functions are given in Figure 3.1.

Patient ID	**Right eye**	**DA (mm^2); CSM; HVC (mm); Linear cup/disc ratio; FSM; RB**	**Left eye**	**DA (mm^2); CSM; HVC (mm); Linear cup/disc ratio; FSM; RB**
1	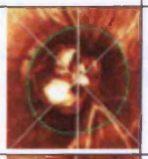	1.83; -0.14; 0.54; 0.59; -0.46; 1.70	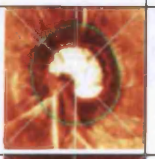	1.51; -0.24; 0.47; 0.61; 0.02; 1.67
2	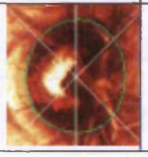	1.93; -0.13; 0.54; 0.48; 1.51; 1.69	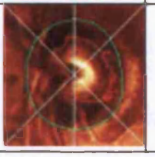	1.80; -0.11; 0.55; 0.57; -1.09; 0.44

3	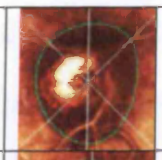	1.99; -0.13; 0.37; 0.48; 2.09; 1.39	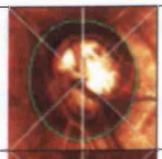	2.04; -0.11; 0.34; 0.65; 0.04; 0.48
4		2.29; 0.07; 0.27; 0.83; -3.21; -0.80	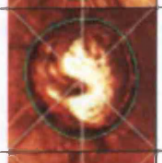	2.32; 0.03; 0.35; 0.83; -3.33; -0.67
5		1.91; 0.04; 0.43; 0.91; -5.32; -2.95	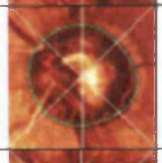	2.06; -0.05; 0.28; 0.81; -2.23; -1.69
6		1.87; -0.22; 0.39; 0.55; 2.47; 1.49	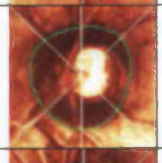	1.71; -0.22; 0.45; 0.54; 1.01; 2.04
7		1.64; -0.21; 0.35; 0.61; -0.80; 0.68	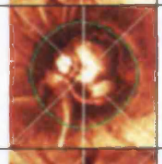	1.85; -0.17; 0.39; 0.64; -0.61; 0.46
8	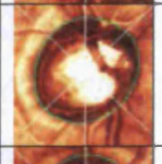	1.93; -0.02; 0.33; 0.79; -2.70; 0.22		1.84; -0.03; 0.40; 0.80; -3.19; 0.26
9	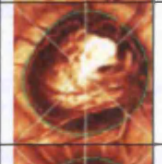	2.67; -0.01; 0.22; 0.82; -2.37; -1.01		2.73; -0.04; 0.34; 0.79; -1.23; 0.74
10	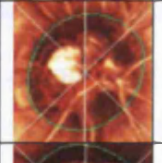	2.43; -0.22; 0.38; 0.53; 2.39; 1.62	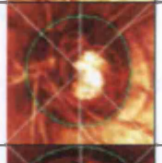	2.05; -0.19; 0.35; 0.59; 1.22; 1.49
11	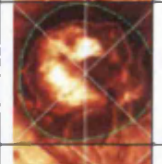	3.29; -0.08; 0.30; 0.70; -0.17; -0.54	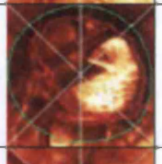	3.45; -0.03; 0.36; 0.73; -2.12; -0.28
12	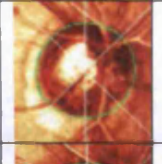	1.92; -0.14; 0.34; 0.61; -0.18; -0.23	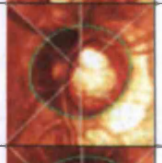	1.91; -0.19; 0.45; 0.59; 0.34; 0.89
13	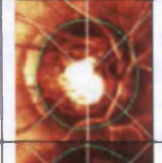	2.27; -0.09; 0.35; 0.68; -1.31; 1.54	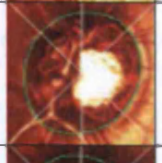	2.85; -0.10; 0.33; 0.66; -0.41; 0.44
14		2.41; -0.05; 0.27; 0.75; -2.06; 0.24		2.62; -0.09; 0.33; 0.76; -1.20; 0.76
15		2.35; 0.0; 0.21; 0.81; -2.55; -1.01	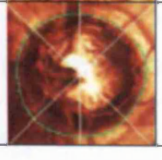	2.71; 0.01; 0.28; 0.75; -2.03; -1.18

16	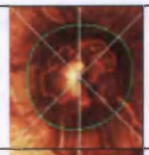	2.07; -0.14; 0.40; 0.55; 0.66; 1.75	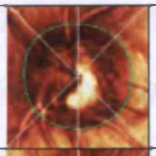	2.12; -0.11; 0.36; 0.65; 0.02; 0.81
17		1.34; -0.26; 0.27; 0.57; 1.03; 0.45		1.85; -0.11; 0.37; 0.41; 1.15; 0.86
18	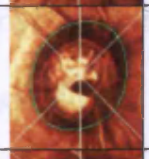	1.80; -0.04; 0.29; 0.70; -1.86; -0.17		2.22; -0.03; 0.17; 0.84; -2.11; -0.97
19	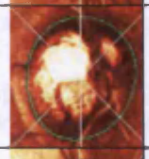	2.84; -0.02; 0.53; 0.63; -0.67; 1.24	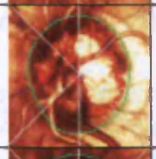	2.55; -0.07; 0.45; 0.56; -0.22; 0.34
20	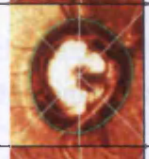	2.18; -0.02; 0.27; 0.74; -2.23; -0.34	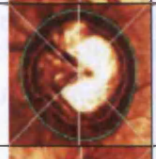	2.76; 0.06; 0.24; 0.80; -3.30; -0.71
21	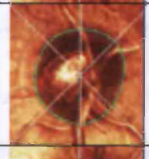	1.61; -0.32; 0.33; 0.48; 2.74; 1.21	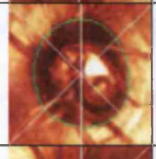	1.92; -0.16; 0.35; 0.56; 0.49; 1.13
22		1.62; -0.15; 1.05; 0.63; -2.27; 3.99	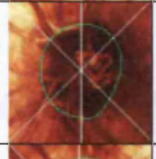	1.33; -0.23; 0.61; 0.32; 1.27; 2.74
23	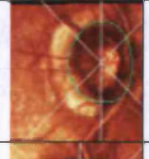	1.01; -0.12; 0.50; 0.19; -1.79; 0.92	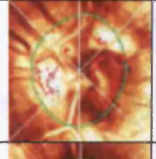	2.12; -0.23; 0.24; 0.49; 0.88; -0.04
24	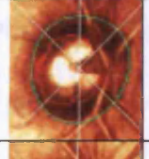	2.06; -0.09; 0.42; 0.65; -0.22; 1.21		2.18; -0.13; 0.36; 0.70; -0.74; 0.29
25		1.92; -0.07; 0.23; 0.60; -0.55; -0.92		1.69; -0.15; 0.53; 0.55, -0.69; 0.54

Figure 3.1 The Heidelberg Retina Tomograph reflectance images for the ONHs of the 25 individuals with open angle glaucoma. (DA: Disc Area; CSM: Cup Shape Measure; HVC: Height Variation Contour FSM: Mikelberg Discriminant function; RB: Burk Discriminant function).

Seventeen individuals were receiving a single topical agent in each eye for control of IOP (three were receiving a non-selective β-receptor blocker, two an α-adrenergic agonist, eleven a prostaglandin analogue and one a prostaglandin analogue/ β-

receptor blocker combination). Two individuals required two topical agents for IOP control (one a combination of a β-adrenergic receptor blocker/ carbonic anhydrase inhibitor and an α-adrenergic receptor agonist and one a combination of a β-receptor blocker and a prostaglandin analogue). One individual had previously undergone bilateral trabeculectomy and was receiving a systemic β-receptor blocker. One individual required a systemic β-receptor blocker. Four individuals were not receiving any therapy for their glaucoma (Three individuals had previously been considered to be OHTs and were re-categorised, post hoc, as OAG on the basis of the visual field examinations conducted as part of the study. The fourth individual exhibited low tension glaucoma). In those cases where the appearance of the ONH was in doubt, the diagnosis of OAG or OHT was also based, post hoc, upon the appearance of the visual field derived during the study. Glaucomatous visual field loss was defined after Morgan et colleagues (2005) according to the following guidelines: a minimum of one location in the paracentral or nasal step regions corresponding to Sectors 1 or 2, or to the inferior three locations in Sector 3 of the Glaucoma Hemifield Test exhibiting repeatable abnormality at the $p<0.5\%$ level by Pattern Deviation probability analysis; or as two or more locations situated in a cluster exhibiting repeatable abnormality at the $p<2.0\%$ level, or lower, by Pattern Deviation probability analysis excluding any location in the cluster that was situated in the opposite horizontal hemifield.

The severity of the visual field loss for the individuals with OAG was graded, post hoc, on the appearance of the eye with the more severe loss recorded with the SITA Standard algorithm at the last visit of the study protocol. The staging system was that of Hodapp and associates (1993), modified by Litwak (2001) for the SITA algorithms, which classifies field loss in terms of the number and severity of the

Pattern Deviation probability levels at each location and in terms of the defect depth at the four central locations adjacent to fixation. The use of the MD index was omitted from the classification system in order to emphasize the spatial component in the grading of the field loss (Åsman et al 2004). Five of the 25 individuals exhibited a normal visual field, 15 exhibited mild loss, 4 moderate losses and one severe loss.

Four of the 29 normal individuals, two of the 25 individuals with OHT and five of the 25 individuals with OAG were receiving artificial tears because of minor dry eye problems.

3.3.2 Examination protocols

In addition to the baseline visit, each individual attended for five further visits. Each of these five visits was separated by one week and was divided into two sessions. At one session, each eye was examined with Program 24-2 of the Humphrey Field Analyzer 745i (HFA; Carl Zeiss Meditech Inc., Dublin, CA) using the SITA Standard algorithm. At the other session, each eye was examined with Program 24-2 and the SITA SWAP and SITA Fast algorithms using the same perimeter. The order of the sessions and the order of the algorithms within the sessions were randomized within individuals and varied over each of the five visits. The visual field of the right eye was always examined before that of the left eye.

Each individual wore, in the form of full-aperture trial lenses, the appropriate refractive correction, when necessary, for the viewing distance of the perimeter bowl. Each eye underwent an adaptation time of not less than three minutes to the

bowl luminance of the perimeter prior to examination with the SITA SWAP algorithm in order to ensure adequate saturation of the MWS and LWS pathways. The corresponding adaptation time for the SITA Standard and SITA Fast algorithms was approximately one minute. The non-examined eye was occluded with an opaque patch.

In addition to the standard Heijl-Krakau technique and to the gaze tracker, fixation was monitored continuously via the video monitor of the HFA. The influence of any fatigue effect was reduced by providing a rest period of approximately one minute-halfway through the examination of each eye and a five-minute rest period between the examinations of each eye within a given session. During such rest periods the individual remained adapted to the perimeter bowl. A rest period of approximately 30 minutes was given between sessions. Each patient received the same instructions throughout each examination at each visit.

Two perimetrists performed the perimetry, Mrs Beatrice Thöny, the practice nurse, and the author. The number of individuals in each group assigned to each perimetrist and to a combination of the two perimetrists is given in Table 3.2.

	Normal	**OHT**	**OAG**
CAC and BT	14	15	13
BT, only	14	5	6
CAC, only	1	5	6

Table 3.2 The number of individuals in each group assigned to each perimetrist and to a combination of the two perimetrists.

3.3.3 Analysis

The stimulus locations above and below the physiological blind spot were discarded from the analysis.

3.3.3.1 The learning effect

3.3.3.1.1 Visual field indices

The analysis of the learning effect was undertaken in terms of the magnitudes of the conventional visual field indices Mean Sensitivity (MS), Mean Deviation (MD) and Pattern Standard Deviation (PSD) within- and between-eyes and between groups, over the five visits. A separate ANOVA was undertaken for each index. Age, diagnostic group, number of previous examinations with SAP, and the examining perimetrist were considered as between-subject factors. Visit, eye and algorithm were considered as within-subject factors. The examination duration was also analyzed in a similar manner.

3.3.3.1.2 Peripheral mean sensitivity and central mean sensitivity

The analysis of the learning effect was also undertaken in terms of the magnitudes of the proportionate change in the in the peripheral (PMS) and central mean sensitivities (CMS) over the five visits using ANOVA in an identical manner to that used for the absolute change in each conventional index.

The 22 stimulus locations within the central annulus out to 15 degrees eccentricity horizontally and 15 degrees vertically were designated as those locations from which the CMS was calculated (Table 3.8). The remaining 30 locations in the peripheral annulus beyond these eccentricities were designated as those locations from which the PMS was calculated.

3.3.3.1.3 The within-individual within-algorithm between-visit (Visits 1 and 5) difference in sensitivity

The within-individual within-algorithm between-visit difference in sensitivity across each stimulus location was expressed as the distribution of the difference in sensitivity at each location between Visits 1 and 5 as a function of the sensitivity at the corresponding stimulus location recorded at Visit 1.

The within-individual within-algorithm between-visit difference in sensitivity across each stimulus location was also expressed as the distribution of the difference in the magnitudes of the Total Deviation and Pattern Deviation probability levels, respectively, between Visits 1 and 5 and illustrated in terms of contingency tables.

3.3.3.2 The within-individual within-algorithm between-visit (Visits 4 and 5) variability

Three separate analyses were used to determine the within-individual within-algorithm between-examination variability at Visits 4 and 5 based upon the assumption that the learning effect had plateaued by Visit 4. The first sub-analysis calculated the difference in each of the visual field indices, MD and PSD between Visits 4 and 5 for each of the three groups and for all three groups, combined, in terms of the average of the two indices. Such an approach overcomes the limitations associated with the use of correlation analysis (Bland and Altman 1986) and has been widely used in clinical vision science research. The second sub-analysis determined the difference in sensitivity at each stimulus location across all individuals in the three groups and compared the difference in terms of the magnitude of the sensitivity at the corresponding stimulus location recorded at the fourth visit. The third sub-analysis compared the magnitudes of the Total Deviation (TD) and of the Pattern Deviation (PD) probability values at each stimulus location

in each algorithm between Visits 4 and 5 across all individuals in the three groups. The magnitudes were illustrated in terms of contingency tables.

3.3.3.3 The between-individual within-visit (Visit 5) between-algorithm variability

The between-individual within-visit between-algorithm variability at Visit 5 was analysed in four separate ways. The first sub-analysis illustrated the between-algorithm differences in the MD and in the PSD indices, respectively, between each pair of algorithms at Visit 5 across the three groups in terms of the average of the two indices. Such an approach again overcomes the limitations associated with the use of correlation analysis (Bland and Altman 1986).

The second sub-analysis determined the difference in sensitivity between each pair of algorithms at Visit 5 for each stimulus location across all patients in the three groups and compared the respective difference in terms of the magnitude of the sensitivity at the corresponding stimulus location recorded with the comparison algorithm of the given pair. Such an approach has been utilized previously (Heijl et al 1989b; Wild et al 1999a,b).

The third sub-analysis compared the magnitudes of the Total Deviation (TD) and of the Pattern Deviation (PD) probability values, respectively, at each stimulus location across all patients in the three groups between each pair of algorithms at Visit 5.

The fourth sub-analysis compared the between-individual variability at each stimulus location in the normal individuals for each algorithm in terms of the Coefficient of Variation (CoV) (the standard deviation divided by the mean). Such

an analysis would provide some indication of the difference in the magnitude of the confidence limits at each location between the two algorithms.

3.3.3.4 The structure-function relationship

The relationships between the magnitudes of the Mikelberg discriminate function (FSM), the Burk discriminate function (RB) and the rim-disc ratio, derived by confocal scanning laser ophthalmoscopy (HRT II), were compared with the magnitudes of the probability levels of MD and PSD visual field indices derived by SITA Standard, SITA Fast and SITA SWAP, respectively, at Visit 5 for the right and the left eyes and for each diagnostic group and were illustrated in terms of contingency tables and Venn diagrams.

3.4 Results

Remarkably, the incorrect responses to the false-positive catch trials lay outside the normal range of 20% in only 11 of the 2370 visual field examinations involving all three algorithms. Of these 11 examinations, 4 examinations (4 individuals) yielded incorrect responses between 20% and 23%, six examinations (six individuals) between 25% and 31% incorrect responses and one examination 43% incorrect responses. Perhaps even more remarkably, only one examination resulted in more than 33% incorrect responses to the false-negative catch trials, namely 45%. Five of the visual fields were flagged as 'N/A' indicating that the false-negative catch trials could not be implemented due to the advanced nature of the field loss. A total of 185 fields (from 41 individuals) exhibited more than 20% fixation losses with the Heijl-Krakau technique and of these, 90 with more than 30% fixation losses. Of the 185 fields, only one was recorded with the SITA SWAP algorithm despite the use of the larger stimulus, size V.

All visual fields were included in the analysis irrespective of the magnitude of the incorrect responses to the various catch trials. Indeed, the use of a cut-off of 33% for the incorrect responses to the false-negative catch trials and for the number of false-positive responses increases the number of usable fields with minimal effect on the sensitivity or specificity of the examination (Bickler-Bluth et al 1989; Birt et al 1997).

3.4.1 The learning effect

3.4.1.1 Visual field indices

3.4.1.1.1 Mean Sensitivity

The group mean MS (SD) at each of the five visits for each eye of the individuals in each of the three groups, as a function of algorithm is shown in Table 3.3.

Algorithm	Visit 1		Visit 2		Visit 3		Visit 4		Visit 5	
	RE	LE	RE	LE	RE	LE	RE	LE	RE	LE
SITA Standard	30.51 (1.21)	30.30 (1.40)	30.87 (1.25)	30.38 (1.65)	31.12 (1.21)	30.70 (1.45)	31.16 (1.23)	30.71 (1.34)	31.08 (1.64)	30.80 (1.98)
SITA Fast	30.60 (1.19)	30.33 (1.33)	30.87 (0.90)	30.71 (1.18)	31.05 (1.09)	30.67 (1.32)	30.89 (1.31)	30.82 (1.43)	31.15 (1.08)	30.84 (1.28)
SITA SWAP	25.34 (3.75)	25.48 (3.62)	26.10 (3.50)	25.78 (3.80)	26.25 (3.46)	25.96 (3.76)	26.18 (3.45)	25.82 (3.72)	26.70 (3.12)	26.27 (3.39)
SITA Standard	30.37 (1.10)	30.27 (1.31)	30.85 (1.23)	30.53 (1.14)	30.94 (1.10)	30.50 (1.15)	30.97 (1.20)	30.49 (1.60)	31.01 (1.14)	30.58 (1.13)
SITA Fast	30.53 (1.07)	30.28 (1.32)	30.81 (1.08)	30.61 (1.35)	30.74 (1.10)	30.73 (1.12)	30.10 (1.15)	30.67 (1.16)	30.95 (1.30)	30.61 (1.31)
SITA SWAP	24.53 (3.53)	25.30 (3.42)	25.84 (3.09)	25.89 (3.22)	26.14 (2.71)	26.34 (2.89)	26.05 (2.22)	26.00 (2.73)	26.15 (2.68)	26.08 (2.83)
SITA Standard	28.12 (5.22)	28.36 (2.87)	28.65 (4.39)	28.74 (2.07)	28.80 (4.51)	29.12 (2.34)	28.97 (4.21)	29.17 (2.11)	28.86 (4.16)	29.10 (2.05)
SITA Fast	28.63 (4.34)	28.71 (2.36)	28.81 (4.34)	29.00 (2.27)	28.95 (4.50)	29.35 (2.08)	29.04 (4.12)	29.40 (2.02)	29.49 (3.71)	29.32 (1.89)
SITA SWAP	22.83 (5.25)	22.97 (4.67)	23.40 (5.06)	23.66 (3.81)	23.90 (4.86)	24.26 (3.66)	24.50 (4.94)	24.63 (3.29)	24.30 (4.79)	24.62 (3.48)

Table 3.3 The group mean MS (SD) at each of the five visits for each eye as a function of the algorithm for the normal individuals (no shading), the individuals with OHT (light shading), and the individuals with OAG (dark shading).

The group mean MS (SE) for each eye at each visit for each of the three algorithms is also shown graphically in Figures 3.2a to 3.2c for each of the three groups.

From the ANOVA, overall, the MS became less positive (i.e. worsened) with increase in age (p=0.003). The magnitude of the MS was independent of the influence of the perimetrist (p=0.332) of the extent of the previous experience of perimetry (p=0.567) and of the order of the three algorithms within the examination

(p=0.879). It was similar between the two eyes (p=0.207). The magnitude of the MS varied across the three algorithms (p<0.001) but the extent of this variation was similar across the three groups (p=0.373). As would be expected, the MS varied between the three diagnostic groups (p=0.006) being least for the individuals with OAG.

The magnitude of the MS improved over the five visits (p<0.001). The difference in the improvement between the three algorithms did not reach statistical significance (p=0.073) and was similar between the three groups (p=0.443). On average, the MS for SITA Standard improved by 0.54dB for the normal individuals, by 0.47dB for those with OHT, and by 0.74dB for those with OAG. The corresponding improvement across the three groups for SITA Fast was 0.53dB, 0.38dB, and 0.74dB, respectively, and for SITA SWAP 1.08dB, 1.2dB, and 1.56dB.

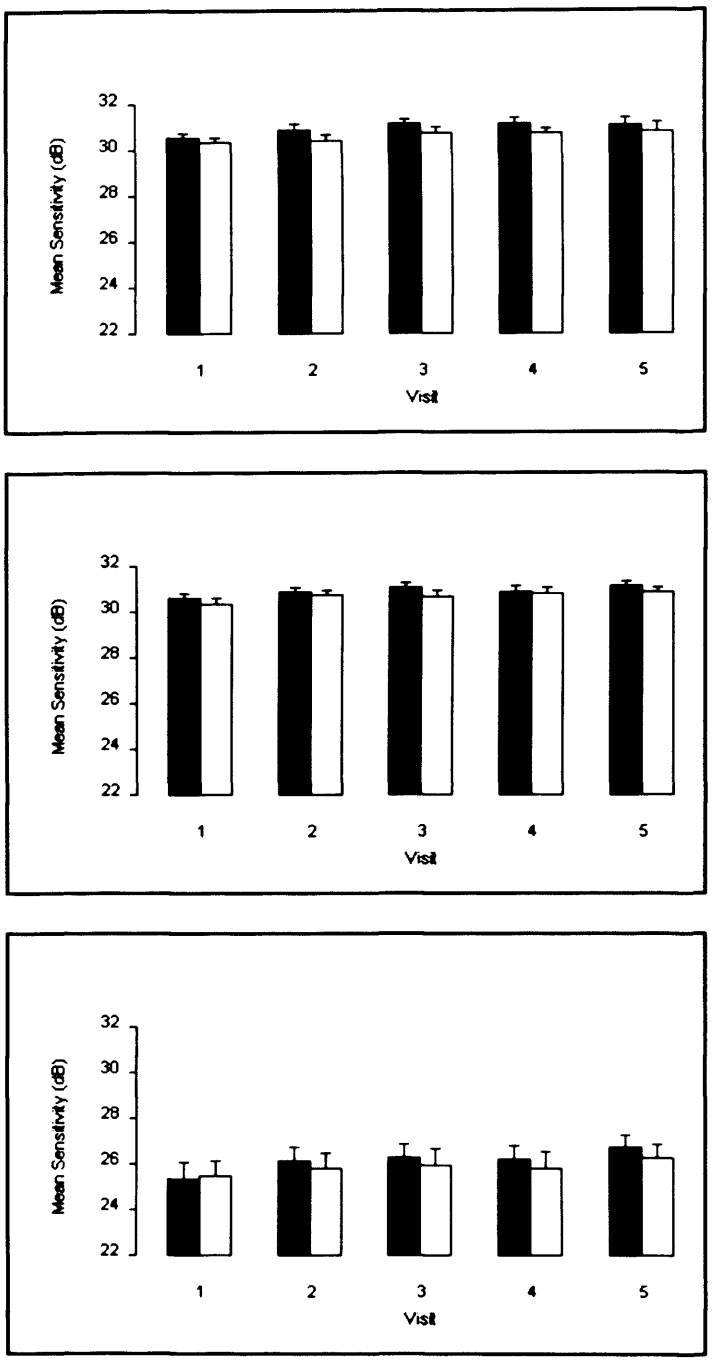

Figure 3.2a The group mean MS (SE) at each of the five visits for each eye as a function of the algorithm for the normal individuals: right eye dark bars; left eye, open bars. Top: SITA Standard. Middle: SITA Fast. Bottom: SITA SWAP.

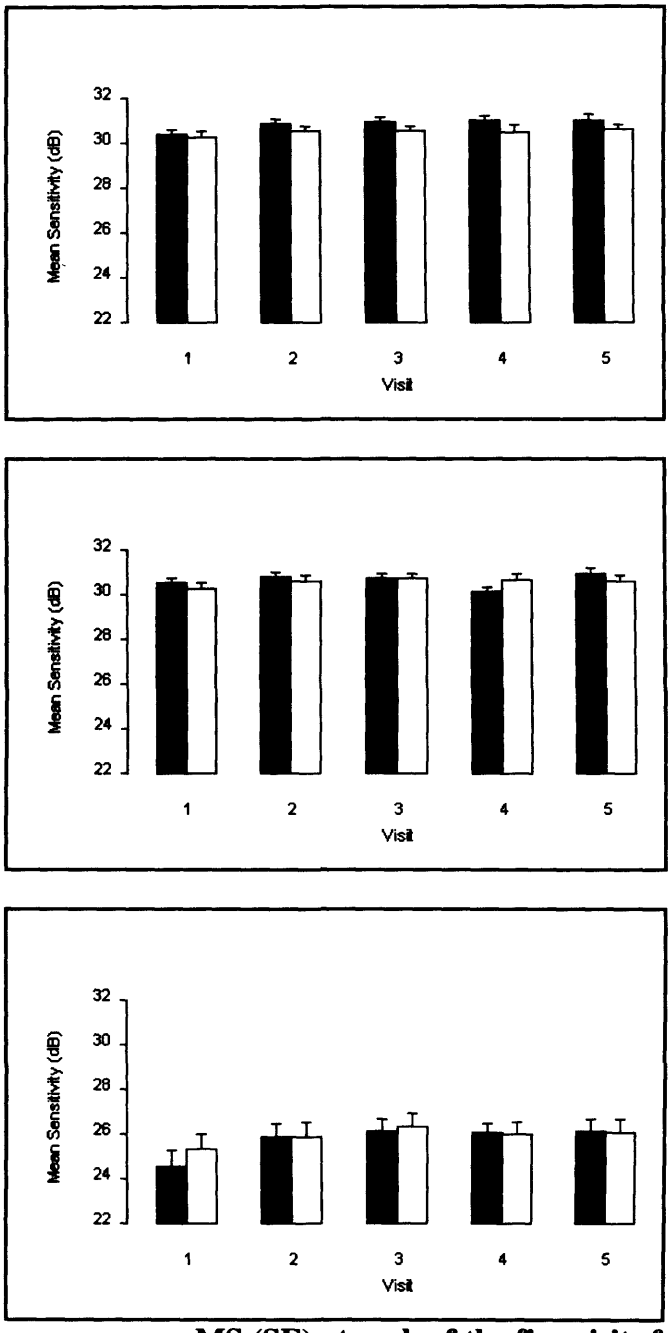

Figure 3.2b The group mean MS (SE) at each of the five visits for each eye as a function of the algorithm for the individuals with OHT: right eye dark bars; left eye, open bars. Top: SITA Standard. Middle: SITA Fast. Bottom: SITA SWAP.

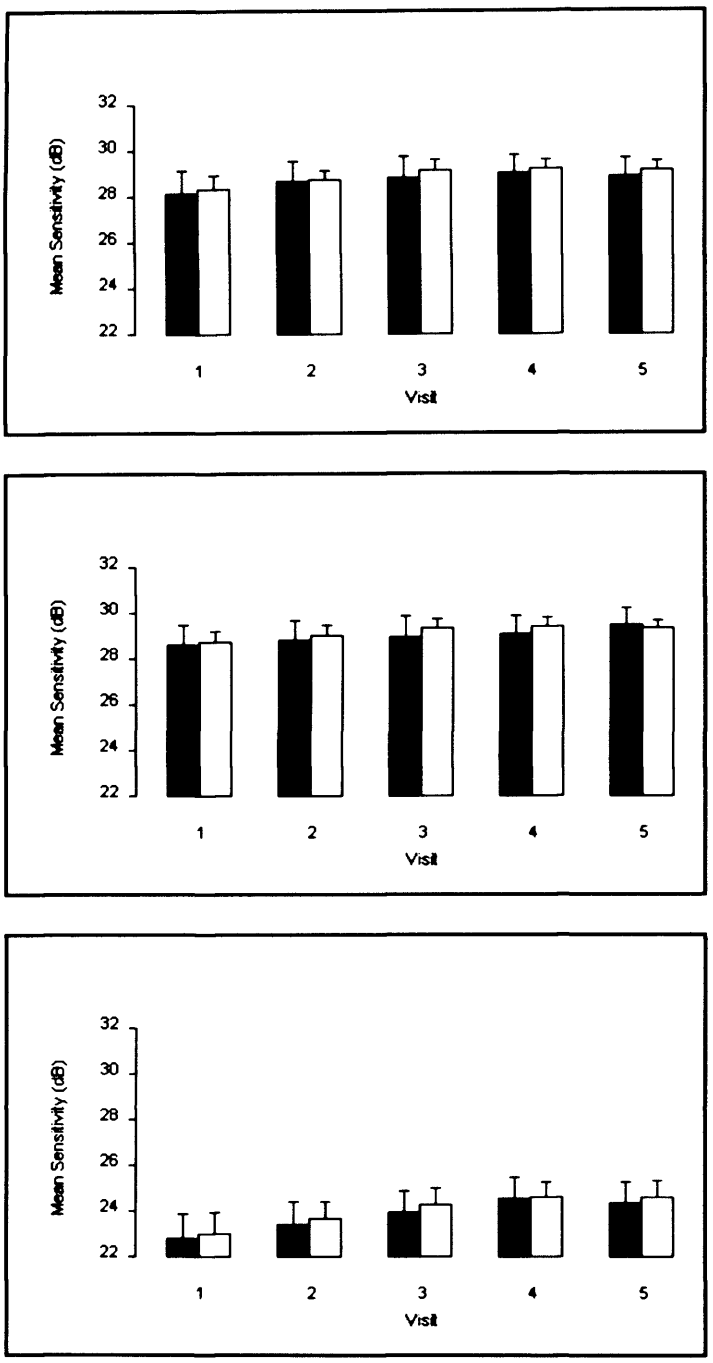

Figure 3.2c The group mean MS (SE) at each of the five visits for each eye as a function of the algorithm for the individuals with OAG: right eye dark bars; left eye, open bars. Top: SITA Standard. Middle: SITA Fast. Bottom: SITA SWAP.

The decline in Mean Sensitivity (MS) for the normal individuals, at each visit, with increase in age for each eye for each of the three algorithms is shown in Table 3.4.

Visits	SITA Standard		SITA Fast		SITA SWAP	
	RE	LE	RE	LE	RE	LE
1	-0.0369 0.0860	-0.0652 0.2012	-0.0509 0.1678	-0.0501 0.1305	-0.2653 0.4326	-0.2437 0.4180
2	-0.0620 0.2282	-0.0820 0.2282	-0.0520 0.3060	-0.0636 0.2682	-0.2341 0.4138	-0.2560 0.4187
3	-0.0683 0.2941	-0.0928 0.3788	-0.0577 0.2614	-0.0680 0.2465	-0.2548 0.5006	-0.2697 0.4762
4	-0.0683 0.3519	-0.0866 0.3882	-0.0788 0.3351	-0.0908 0.3714	-0.2256 0.3946	-0.2613 0.4568
5	-0.0907 0.2841	-0.1296 0.3737	-0.0792 0.4956	-0.0909 0.4676	-0.2023 0.3737	-0.2464 0.4869

Table 3.4 The decline in group mean MS for the normal individuals with increase in age (dB per year). The lower value indicates the Coefficient of Determination (R^2).

The declines in MS, recorded at Visit 5 for the SITA Standard algorithm were -0.0907dB for the right and -0.1296dB for the left eye, -0.0792dB for the right and -0.0909dB for the left eye for the SITA Fast algorithm and -0.2023dB for the right and -0.2464dB for the left eye for the SITA SWAP algorithm per year. The decline in MS using the SITA SWAP algorithm was approximately 2 to 2.5 times greater than using the other two algorithms.

The decline in the group mean sensitivity, at Visit 5, with increase in age at each stimulus location for each eye, for each of the three algorithms is shown in Figure 3.3a to Figure 3.3f. The stimulus grid for the left eye is converted to right eye format

to aid between-eye comparisons. The lower value indicates the Coefficient of Determination (R^2).

		-0.0840 0.0309	-0.0999 0.0616	-0.1145 0.1341	-0.2061 0.3309		
	0.0127 0.0016	-0.0468 0.0506	-0.0887 0.1268	-0.0942 0.2323	-0.0921 0.1955	-0.1448 0.2142	
-0.1556 0.1696	-0.0807 0.1704	-0.0786 0.1298	-0.0635 0.1314	-0.0897 0.2784	-0.0429 0.0709	-0.0751 0.1224	-0.1634 0.3474
-0.1953 0.2371	-0.1217 0.1617	-0.0818 0.1636	-0.0305 0.0471	-0.0730 0.1874	-0.0474 0.1270	-0.0867 0.3387	-0.1503 0.2991
-0.1288 0.1222	-0.1624 0.2699	-0.0723 0.1427	-0.0535 0.1273	-0.0447 0.1527	-0.0474 0.1270	-0.0957 0.3552	-0.0991 0.2372
-0.1449 0.1922	-0.0797 0.1931	-0.0592 0.1104	-0.0290 0.0299	-0.0650 0.1978	-0.0618 0.1216	-0.0406 0.0450	-0.1140 0.2494
	-0.0787 0.0896	-0.0572 0.1194	-0.0902 0.2000	-0.0837 0.1875	-0.0498 0.0908	-0.0763 0.1439	
		-0.1425 0.3288	-0.1425 0.2753	-0.1209 0.1924	-0.0887 0.1702		

Figure 3.3a The decline in the group mean sensitivity at each stimulus location with increase in age for the right eye of the normal individuals (dB per year), at Visit 5, for the SITA Standard algorithm. The lower value indicates the Coefficient of Determination (R^2).

> -0.10	> -0.15	> -0.20	> -0.25	> -0.30	> -0.35

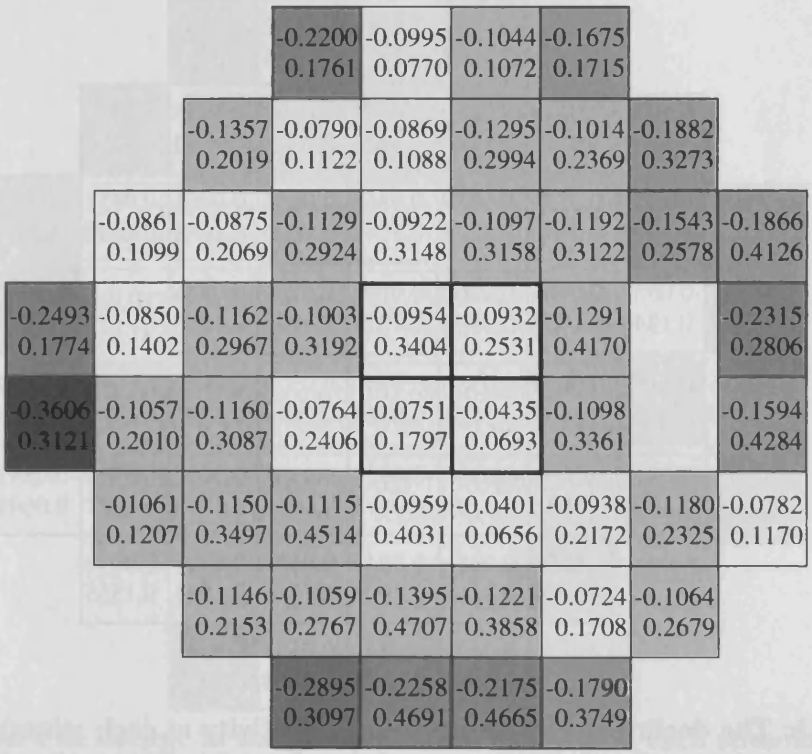

Figure 3.3b The decline in the group mean sensitivity at each stimulus location with increase in age for the left eye of the normal individuals (dB per year), at Visit 5, for the SITA Standard algorithm displayed in right eye format to aid between-eye comparisons. The lower value indicates the Coefficient of Determination (R^2).

			-0.1337 0.2909	-0.0567 0.1055	-0.0622 0.1364	-0.1607 0.2532		
		-0.0351 0.0177	-0.0812 0.2900	-0.0843 0.3121	-0.0929 0.3125	-0.0935 0.2662	-0.1536 0.3292	
	-0.1448 0.3473	-0.0793 0.2196	-0.0859 0.3228	-0.0865 0.3049	-0.0558 0.2026	-0.0461 0.1088	-0.0851 0.2496	-0.1027 0.2484
-0.2342 0.2384	-0.0532 0.1245	-0.0461 0.1030	-0.0260 0.0495	-0.0594 0.2324	-0.0769 0.3729	-0.0735 0.4263		-0.1680 0.3647
-0.0836 0.1380	-0.1183 0.2069	-0.0424 0.2169	-0.0380 0.1521	-0.0341 0.0765	-0.0574 0.2649	-0.0982 0.3251		-0.0567 0.1126
	-0.0848 0.1535	-0.0042 0.4045	-0.0396 0.1196	-0.0328 0.0578	-0.0303 0.0811	-0.0652 0.1543	-0.0410 0.0621	-0.0547 0.0691
		-0.1260 0.3911	-0.0856 0.3165	-0.0647 0.2909	-0.0557 0.1716	-0.0397 0.1064	-0.0978 0.1555	
			-0.0497 0.0684	-0.0369 0.0594	-0.0572 0.1361	-0.1546 0.5323		

Figure 3.3c The decline in the group mean sensitivity at each stimulus location with increase in age for the right eye of the normal individuals, at Visit 5 (dB per year), for the SITA Fast algorithm. The lower value indicates the Coefficient of Determination (R^2).

> -0.10	> -0.15	> -0.20	> -0.25	> -0.30	> -0.35

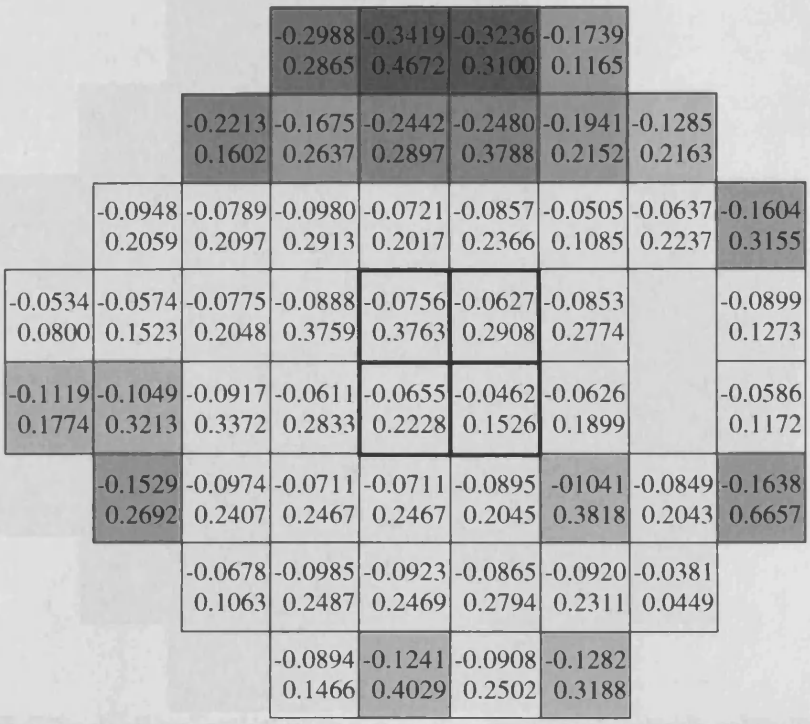

Figure 3.3d The decline in the group mean sensitivity at each stimulus location with increase in age for the left eye of the normal individuals, at Visit 5 (dB per year), for the SITA Fast algorithm displayed in right eye format to aid between-eye comparisons. The lower value indicates the Coefficient of Determination (R^2).

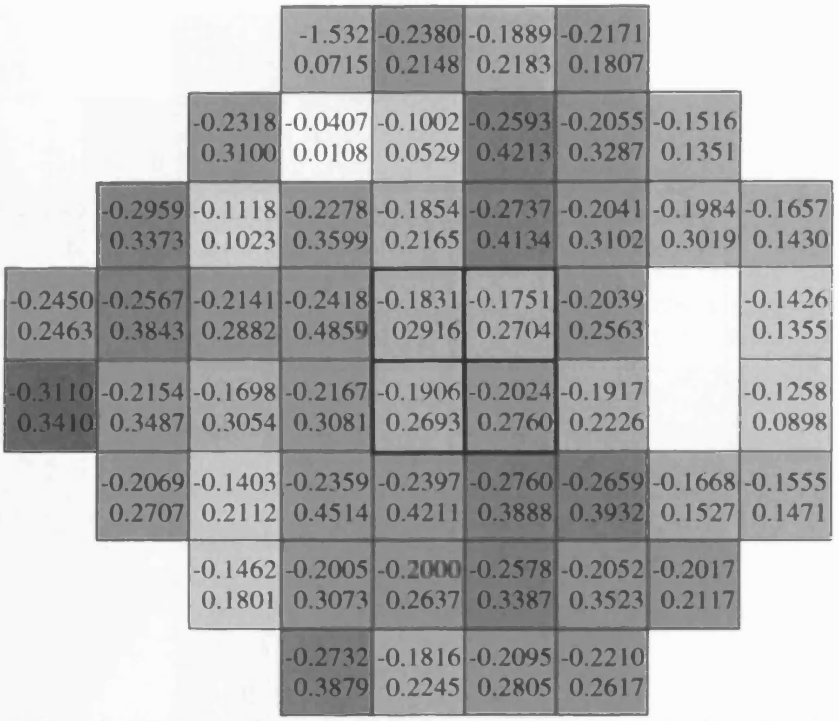

Figure 3.3e The decline in the group mean sensitivity at each stimulus location with increase in age for the right eye of the normal individuals (dB per year), at Visit 5, for the SITA SWAP algorithm. The lower value indicates the Coefficient of Determination (R^2).

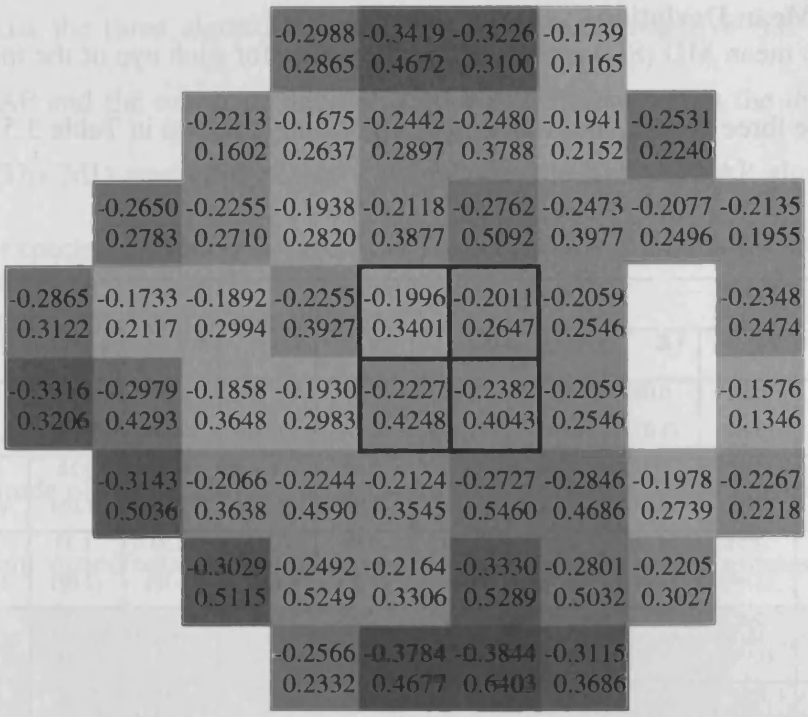

Figure 3.3f The decline in the group mean sensitivity at each stimulus location with increase in age for the left eye of the normal individuals (dB per year), at Visit 5, for the SITA SWAP algorithm displayed in right eye format to aid between-eye comparisons. The lower value indicates the Coefficient of Determination (R^2).

> -0.10	> -0.15	> -0.20	> -0.25	> -0.30	> -0.35

The decline in group mean sensitivity at each location in general increased with in eccentricity and this increase was greater in the left eye (second eye examined) than in the right eye and was greater for SWAP than for SAP.

3.4.1.1.2 Mean Deviation

The group mean MD (SD) at each of the five visits for each eye of the individuals in each of the three groups, as a function of algorithm is shown in Table 3.5.

Algorithm	Visit 1		Visit 2		Visit 3		Visit 4		Visit 5	
	RE	LE	RE	LE	RE	LE	RE	LE	RE	LE
SITA Standard	0.88 (0.99)	0.08 (1.07)	0.63 (0.96)	0.11 (1.29)	0.63 (0.99)	0.11 (1.06)	0.88 (0.99)	0.42 (0.97)	0.72 (1.13)	0.43 (1.33)
SITA Fast	0.02 (1.03)	-0.19 (1.13)	0.29 (0.74)	0.16 (0.93)	0.49 (0.85)	0.14 (1.07)	0.36 (1.00)	0.28 (1.05)	0.59 (0.73)	0.27 (0.94)
SITA SWAP	-1.78 (2.94)	-1.61 (2.79)	-1.02 (2.78)	-1.31 (2.99)	-0.84 (2.63)	-1.13 (2.91)	-0.93 (2.70)	-1.27 (2.89)	-0.43 (2.54)	-0.85 (2.55)
SITA Standard	0.42 (1.06)	0.32 (1.17)	0.85 (1.16)	0.57 (1.00)	1.00 (1.56)	0.55 (1.00)	1.01 (1.11)	0.59 (1.30)	1.06 (1.10)	0.64 (1.00)
SITA Fast	0.28 (1.02)	0.07 (1.16)	0.55 (1.02)	0.39 (1.24)	0.48 (1.14)	0.52 (1.00)	0.71 (1.14)	0.45 (1.01)	0.71 (1.30)	0.37 (1.29)
SITA SWAP	-1.90 (3.21)	-1.03 (2.91)	-0.53 (2.64)	-0.45 (2.79)	-0.25 (0.55)	-0.01 (2.52)	-0.32 (1.99)	-0.36 (2.34)	-0.21 (2.31)	-0.32 (2.39)
SITA Standard	-1.42 (4.90)	-1.20 (2.33)	-1.03 (4.16)	-0.95 (1.67)	-0.90 (4.29)	-0.56 (1.88)	-0.75 (3.99)	-0.53 (1.74)	-0.18 (4.01)	-0.60 (1.70)
SITA Fast	-1.41 (4.21)	-1.27 (2.04)	-1.22 (4.24)	-0.96 (1.85)	-1.06 (4.47)	-0.66 (1.69)	-0.97 (4.01)	-0.59 (1.64)	-0.53 (3.61)	-0.65 (1.53)
SITA SWAP	-3.15 (4.80)	-2.92 (3.94)	-2.48 (4.59)	-2.16 (3.02)	-1.97 (4.33)	-1.63 (2.93)	-1.40 (4.44)	-1.22 (2.93)	-1.58 (4.37)	-1.27 (2.75)

Table 3.5 The group mean MD (SD) at each of the five visits for each eye as a function of the algorithm for the normal individuals (no shading), the individuals with OHT (light shading), the individuals with OAG (dark shading).

The group mean MD (SE) for each eye at each visit for each of the three algorithms is also shown graphically in Figures 3.4a to 3.4c for each of the three groups.

The ANOVA indicates, overall, the MD became more negative (i.e. worsened) with increase in age (p=0.003). The magnitude of the MD was independent of the influence of the perimetrist (p=0.332) of the extent of the previous experience of perimetry (p=0.567) and of the order of the three algorithms within the examination (p=0.509). It was similar between the two eyes (p=0.322). The magnitude of the MD

varied across the three algorithms ($p<0.001$) being most negative (i.e. worst) for SITA SWAP and the extent of this variation was different across the three groups ($p=0.049$).The MD was most negative (worst) for the SITA SWAP algorithm. As would be expected, it varied between the three diagnostic groups ($p<0.001$) being most negative for the individuals with OAG.

The magnitude of the MD improved over the five visits ($p<0.001$). The extent of the improvement varied between the three algorithms ($p=0.016$) being greatest for SITA SWAP. The extent of the improvement over the five visits was similar between the three groups ($p=0.402$). On average, the MD for SITA Standard improved by 0.25dB for the normal individuals, by 0.48dB for those with OHT, and by 0.92dB for those with OAG. The corresponding improvement across the three groups for SITA Fast was 0.49dB, 0.37dB, and 0.67dB, respectively, and for SITA SWAP 1.06dB, 1.20dB, and 1.61dB.

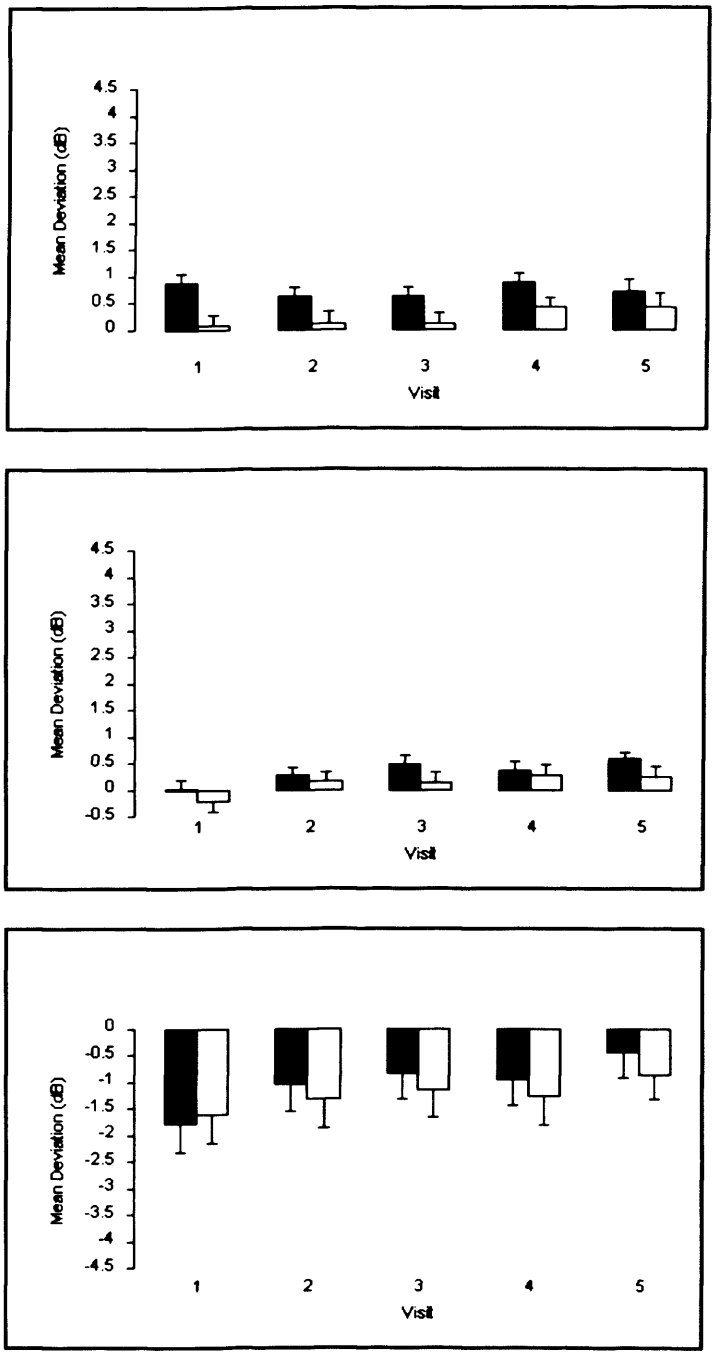

Figure 3.4a The group mean MD (SE) at each of the five visits for each eye as a function of the algorithm for the normal individuals: right eye dark bars; left eye, open bars. Top: SITA Standard. Middle: SITA Fast. Bottom: SITA SWAP.

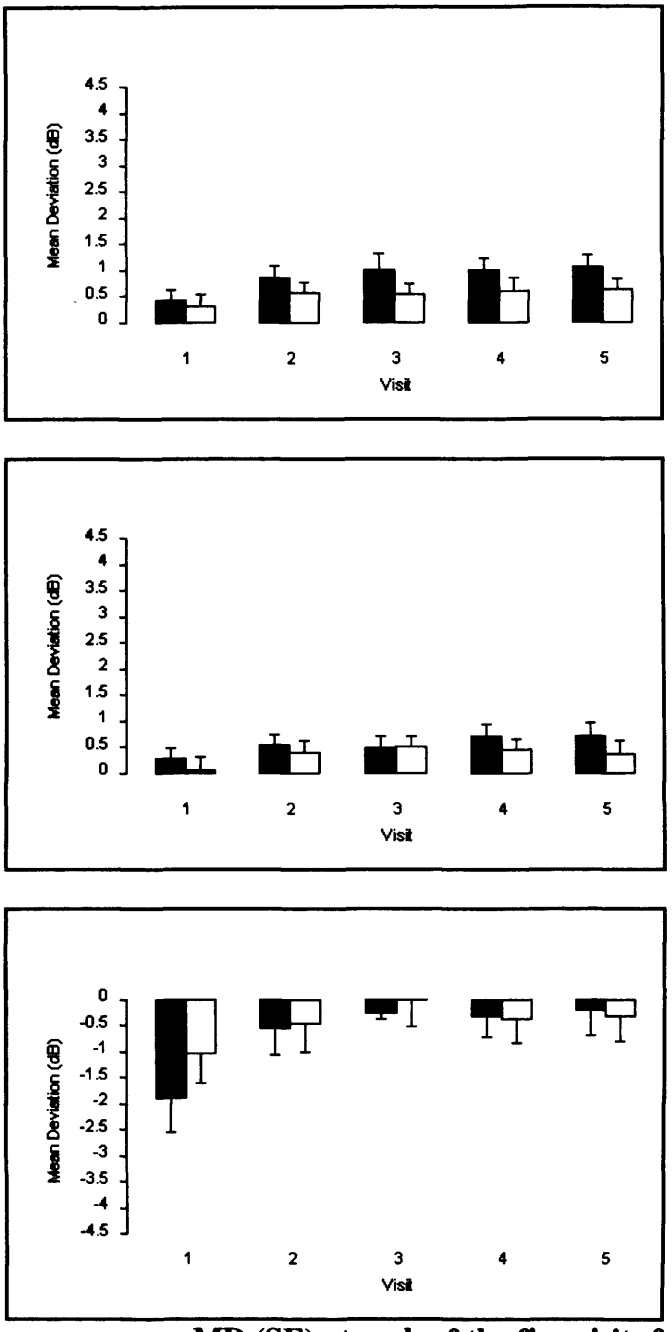

Figure 3.4b The group mean MD (SE) at each of the five visits for each eye as a function of the algorithm for the individuals with OHT: right eye dark bars; left eye, open bars. Top: SITA Standard. Middle: SITA Fast. Bottom: SITA SWAP.

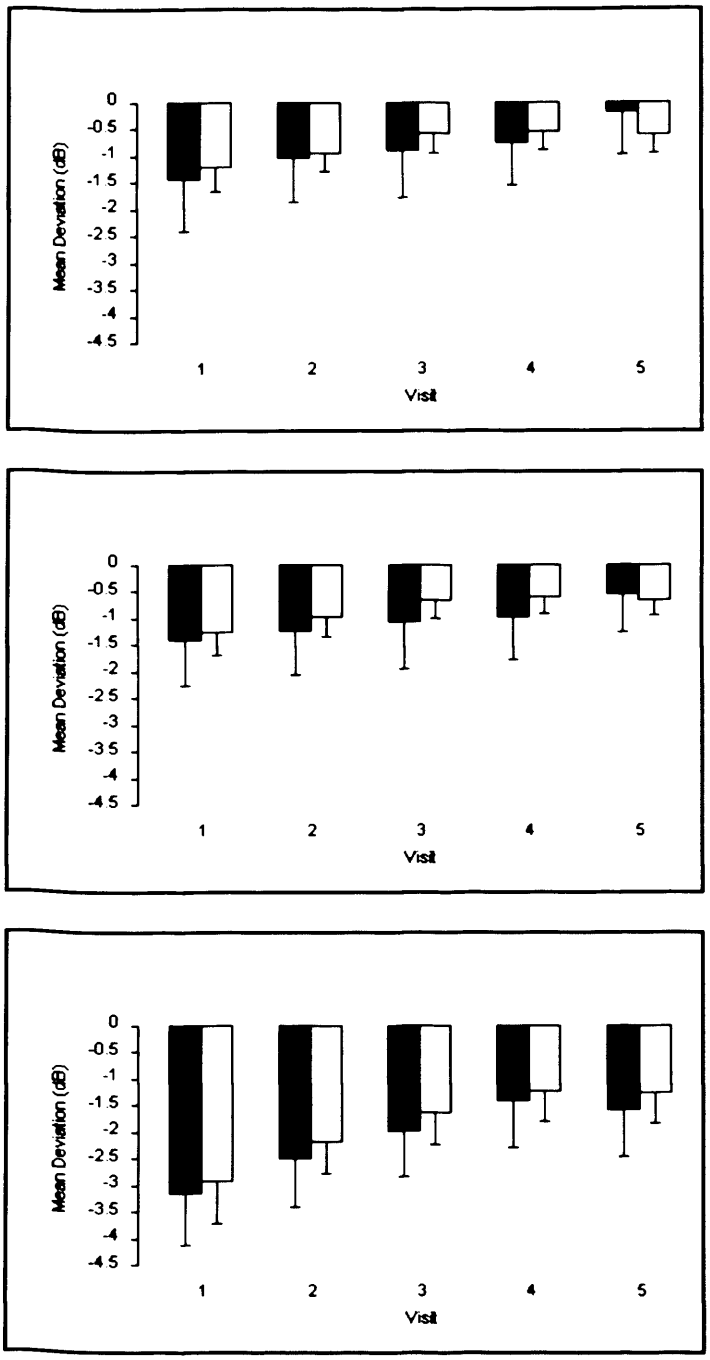

Figure 3.4c The group mean MD (SE) at each of the five visits for each eye as a function of the algorithm for the individuals with OAG: right eye dark bars; left eye, open bars. Top: SITA Standard. Middle: SITA Fast. Bottom: SITA SWAP.

3.4.1.1.3 Pattern Standard Deviation

The group mean PSD (SD) at each of the five visits for each eye of the individuals in each of the three groups, as a function of algorithm is shown in Table 3.6.

Algorithm	Visit 1		Visit 2		Visit 3		Visit 4		Visit 5	
	RE	LE	RE	LE	RE	LE	RE	LE	RE	LE
SITA Standard	1.58 (0.46)	1.54 (0.49)	1.48 (0.56)	1.58 (0.30)	1.48 (0.32)	1.58 (0.45)	1.39 (0.30)	1.42 (0.45)	1.50 (0.58)	1.55 (0.80)
SITA Fast	1.51 (0.51)	1.42 (0.48)	1.30 (0.21)	1.43 (0.46)	1.35 (0.35)	1.40 (0.42)	1.38 (0.30)	1.41 (0.46)	1.34 (0.33)	1.37 (0.30)
SITA SWAP	2.88 (0.89)	2.75 (0.84)	2.47 (0.49)	2.60 (0.52)	2.40 (0.52)	2.46 (0.63)	2.42 (0.46)	2.54 (0.66)	2.31 (0.43)	2.38 (0.52)
SITA Standard	1.58 (0.36)	1.80 (0.76)	1.60 (0.56)	1.82 (0.85)	1.66 (0.38)	1.70 (0.69)	1.46 (0.23)	1.70 (1.74)	1.57 (0.24)	1.64 (0.69)
SITA Fast	1.40 (0.24)	1.69 (0.79)	1.36 (0.19)	1.55 (0.56)	1.48 (0.32)	1.64 (0.77)	1.35 (0.22)	1.50 (0.83)	1.40 (0.34)	1.76 (1.29)
SITA SWAP	3.00 (0.80)	2.89 (1.03)	2.55 (2.64)	2.89 (0.72)	2.59 (0.55)	2.64 (0.98)	2.55 (0.46)	2.55 (0.63)	2.48 (0.61)	2.56 (0.64)
SITA Standard	2.33 (1.95)	2.48 (1.73)	2.41 (2.20)	2.18 (1.37)	2.52 (2.56)	2.01 (1.05)	2.34 (2.14)	1.93 (0.88)	2.24 (2.19)	1.95 (1.07)
SITA Fast	2.17 (2.28)	2.07 (1.52)	2.25 (2.14)	1.99 (1.44)	2.21 (2.22)	1.99 (1.26)	2.22 (2.42)	1.68 (0.65)	2.00 (2.26)	1.96 (0.85)
SITA SWAP	3.50 (1.34)	3.54 (1.79)	3.22 (1.38)	3.23 (1.23)	3.17 (1.33)	3.16 (1.12)	3.09 (1.47)	2.81 (0.62)	3.04 (1.39)	2.94 (1.09)

Table 3.6 The group mean PSD (SD) at each of the five visits for each eye as a function of the algorithm for the normal individuals (no shading), the individuals with OHT (light shading), the individuals with OAG (dark shading).

The group mean (SE) PSD for each eye at each visit for each of the three algorithms is also shown graphically in Figures 3.5a to 3.5c for each of the three groups.

The ANOVA showed that, overall, the PSD was independent of the extent of the previous experience of perimetry (p=0.567) and of the order of the three algorithms within the examination (p=0.491). It was similar between the two eyes (p=0.684). The magnitude of the PSD varied across the three algorithms being largest (worst)

for SITA SWAP ($p<0.001$) and the extent of this variation between the three algorithms was similar across the three groups ($p=0.902$). As would be expected, it varied between the three diagnostic groups ($p<0.003$) being largest (worst) for the individuals with OAG.

The magnitude of the PSD, overall, improved over the five visits ($p<0.001$). The extent of the improvement was similar between the three algorithms ($p=0.076$). The extent of the improvement in the PSD over the five visits was similar between the three groups ($p=0.659$). On average, the PSD for SITA Standard reduced by 0.05dB for the normal individuals, by 0.09dB for those with OHT, and by 0.31dB for those with OAG. The corresponding reduction across the three groups for SITA Fast was 0.11dB, -0.05dB, and 0.14dB, respectively, and for SITA SWAP 0.47dB, 0.43dB, and 0.53dB.

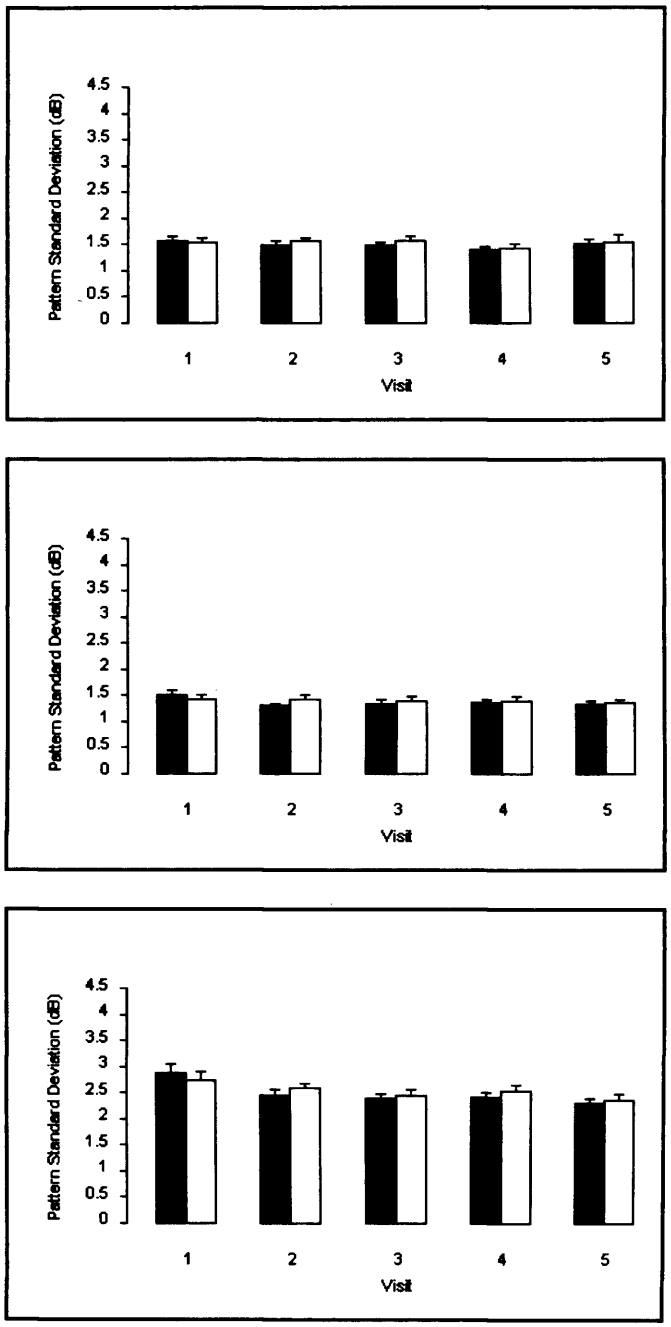

Figure 3.5a The group mean PSD (SE) at each of the five visits for each eye as a function of the algorithm for the normal individuals: right eye dark bars; left eye, open bars. Top: SITA Standard. Middle: SITA Fast. Bottom: SITA SWAP.

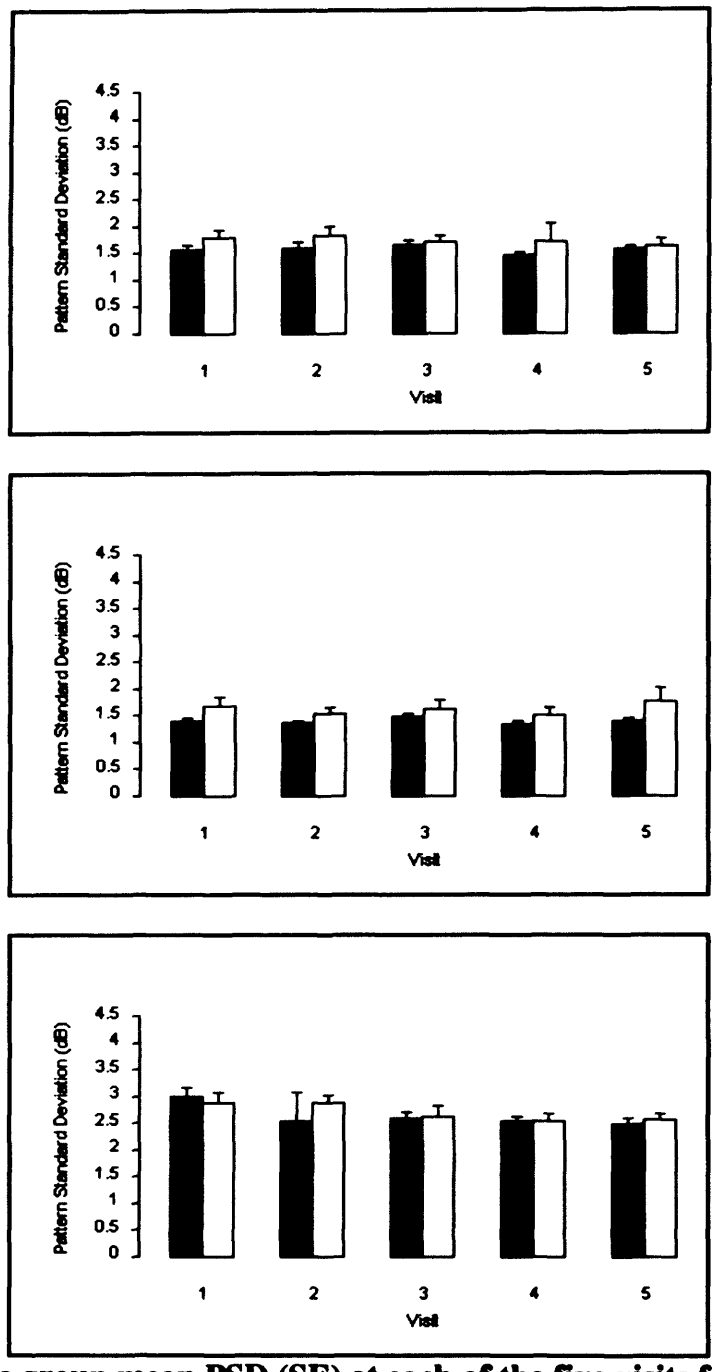

Figure 3.5b The group mean PSD (SE) at each of the five visits for each eye as a function of the algorithm for the individuals with OHT: right eye dark bars; left eye, open bars. Top: SITA Standard. Middle: SITA Fast. Bottom: SITA SWAP.

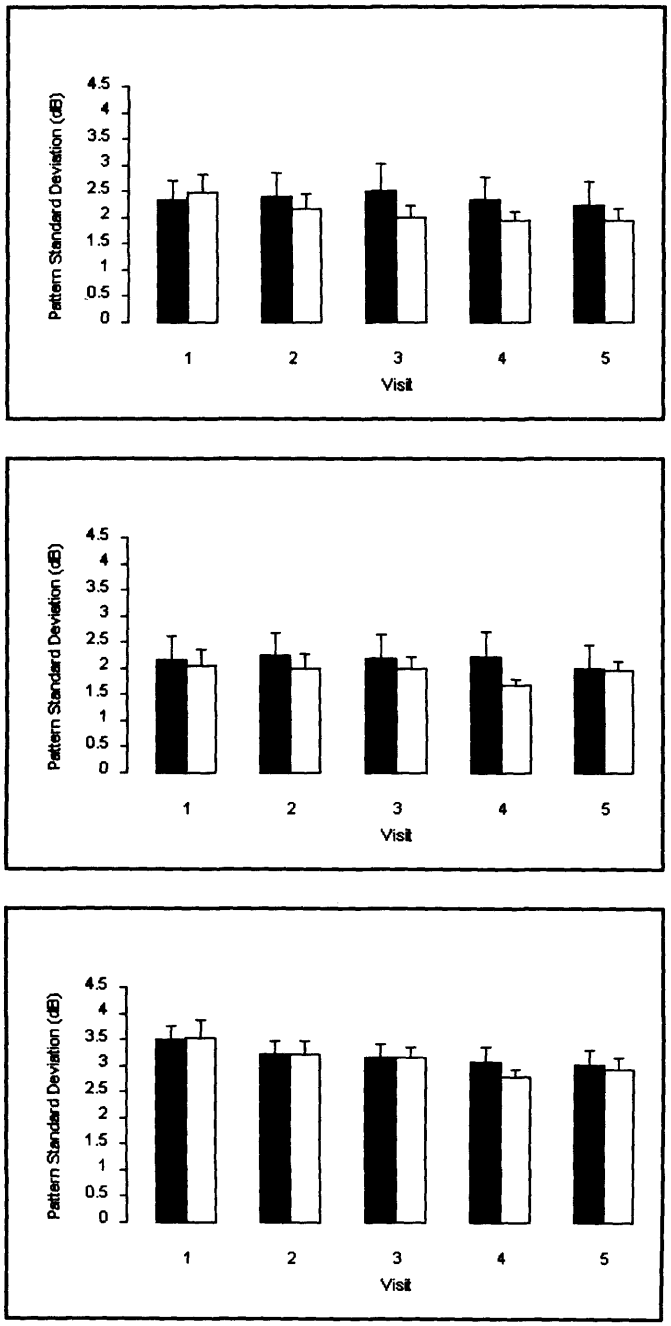

Figure 3.5c The group mean PSD (SE) at each of the five visits for each eye as a function of the algorithm for the individuals with OAG: right eye dark bars; left eye, open bars. Top: SITA Standard. Middle: SITA Fast. Bottom: SITA SWAP.

3.4.1.1.4 Examination duration

The group mean examination duration (SD) (seconds) at each of the five visits for each eye of the individuals in each of the three groups, as a function of algorithm is shown in Table 3.7.

Algorithm	Visit 1		Visit 2		Visit 3		Visit 4		Visit 5	
	RE	LE	RE	LE	RE	LE	RE	LE	RE	LE
SITA Standard	280 (30)	286 (31)	273 (24)	282 (35)	268 (23)	274 (50)	270 (23)	275 (26)	268 (32)	276 (36)
SITA Fast	173 (19)	172 (24)	163 (16)	166 (17)	160 (16)	165 (16)	166 (18)	163 (16)	160 (14)	161 (15)
SITA SWAP	208 (26)	202 (26)	198 (21)	201 (24)	197 (23)	198 (25)	193 (19)	193 (23)	188 (18)	188 (19)
SITA Standard	287 (33)	288 (37)	276 (26)	283 (35)	277 (22)	272 (19)	274 (30)	272 (27)	269 (33)	280 (31)
SITA Fast	170 (21)	177 (19)	165 (18)	172 (21)	170 (19)	171 (28)	166 (19)	171 (25)	166 (22)	169 (34)
SITA SWAP	220 (44)	205 (30)	198 (29)	201 (37)	196 (23)	197 (33)	196 (22)	197 (24)	196 (29)	197 (31)
SITA Standard	319 (76)	317 (59)	302 (40)	304 (40)	295 (51)	298 (40)	300 (51)	304 (40)	293 (38)	304 (35)
SITA Fast	194 (45)	186 (26)	182 (33)	183 (24)	182 (35)	176 (24)	182 (28)	176 (19)	174 (30)	173 (20)
SITA SWAP	244 (62)	222 (43)	220 (39)	219 (39)	210 (33)	211 (35)	209 (35)	202 (27)	204 (40)	202 (30)

Table 3.7 The group mean examination duration (SD) (seconds) at each of the five visits for each eye as a function of the algorithm for the normal individuals (no shading), the individuals with OHT (light shading), the individuals with OAG (dark shading).

The group mean examination duration for each eye at each visit for each of the three algorithms is also shown graphically in Figures 3.6a to 3.6c for each of the three groups.

The ANOVA showed that the examination duration was similar between the two eyes (p=0.487). The magnitude of the examination duration was independent of the influence of the extent of the previous experience of perimetry (p=0.567). It varied

depending upon the order of the three algorithms within the examination ($p=0.010$) (i.e. was longer with the first algorithm) but the effect on the examination duration of the order of the algorithms was similar across the three groups ($p=0.249$) and similar across each algorithm ($p=0.081$). The magnitude of the examination duration varied across the three algorithms ($p<0.001$) being longest for the SITA Standard algorithm. As would be expected, it also varied across the three groups ($p<0.001$) being longest for those with OAG. The magnitude of the difference between the three algorithms became more apparent across the three groups ($p=0.001$).

The magnitude of the examination duration reduced over the five visits ($p<0.001$). The extent of this reduction was similar between the three algorithms ($p=0.173$) but differed across the three groups ($p=0.002$). On average, the examination duration for SITA Standard becomes shorter by 11 seconds for the normal individuals, by 13 seconds for those with OHT, and by 19.5 seconds for those with OAG. The corresponding reduction in the examination duration across the three groups for SITA Fast was 12 seconds, 6 seconds and 16.5 seconds, respectively, and for SITA SWAP 17 seconds, 16 seconds, and 30 seconds.

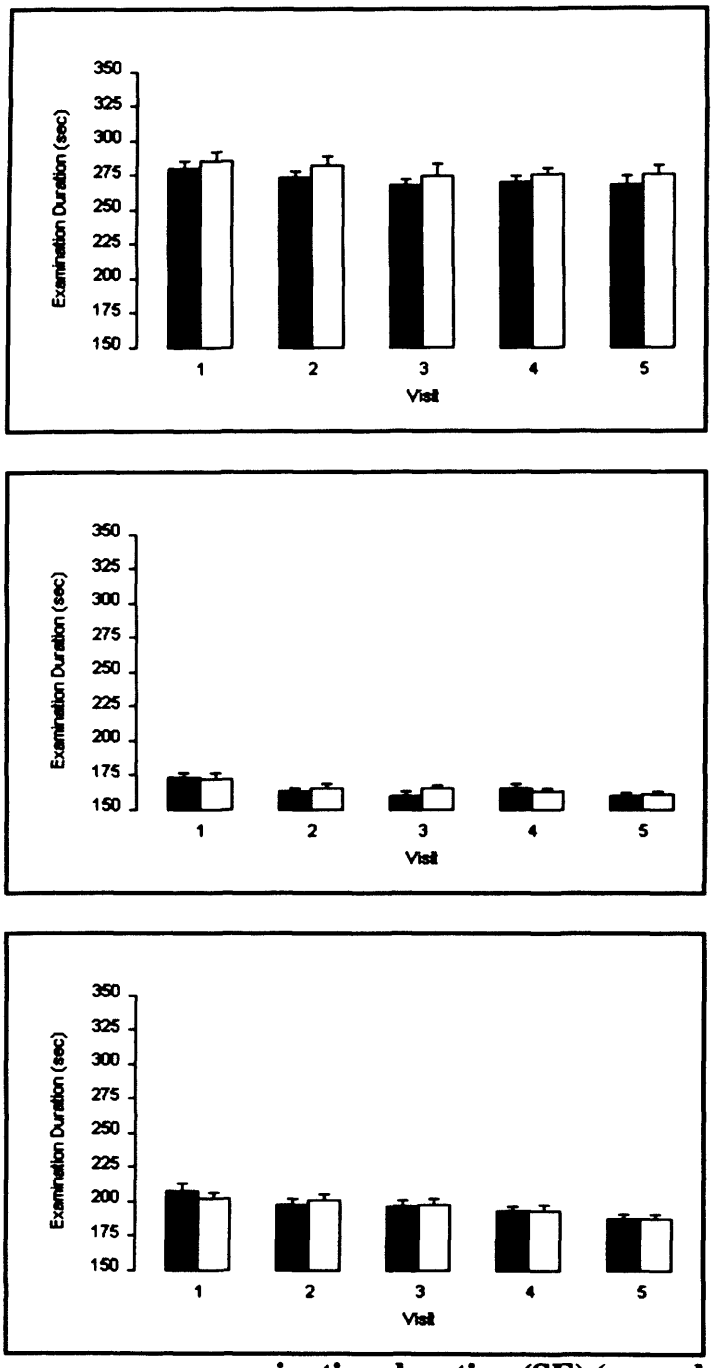

Figure 3.6a The group mean examination duration (SE) (seconds) at each of the five visits for each eye as a function of the algorithm for the normal individuals: right eye dark bars; left eye, open bars. Top: SITA Standard. Middle: SITA Fast. Bottom: SITA SWAP.

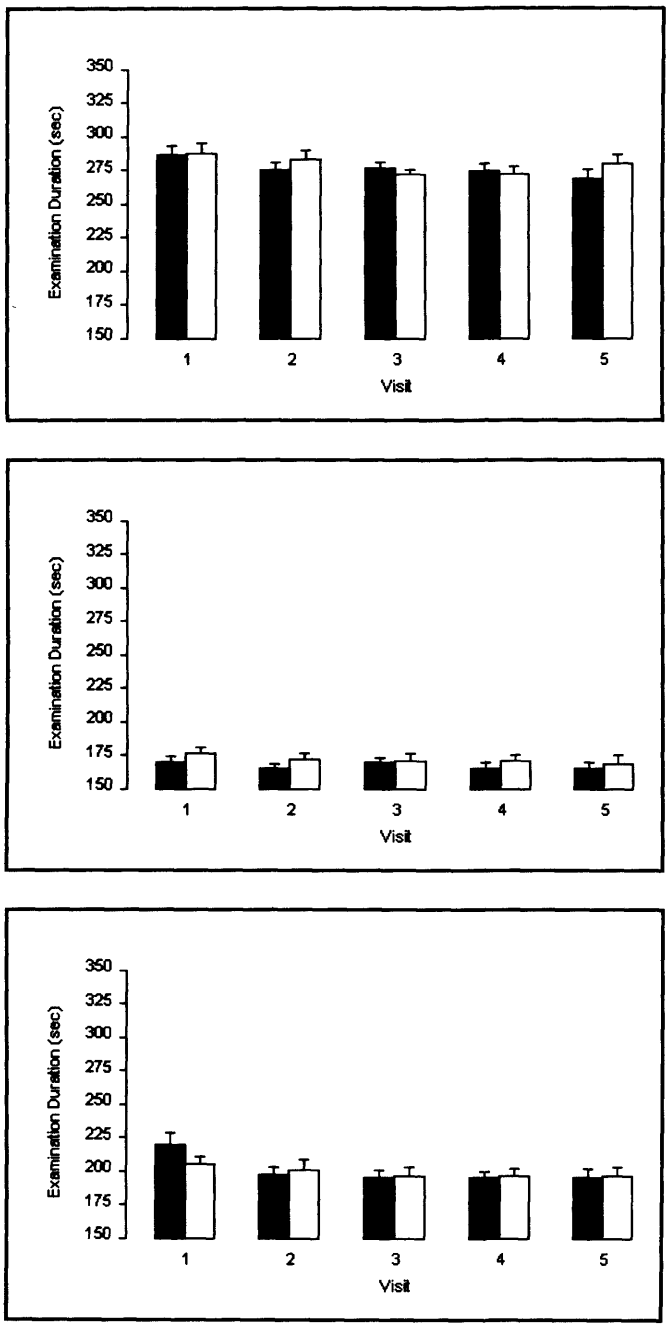

Figure 3.6b The group mean examination duration (SE) (seconds) at each of the five visits for each eye as a function of the algorithm for the individuals with OHT: right eye dark bars; left eye, open bars. Top: SITA Standard. Middle: SITA Fast. Bottom: SITA SWAP.

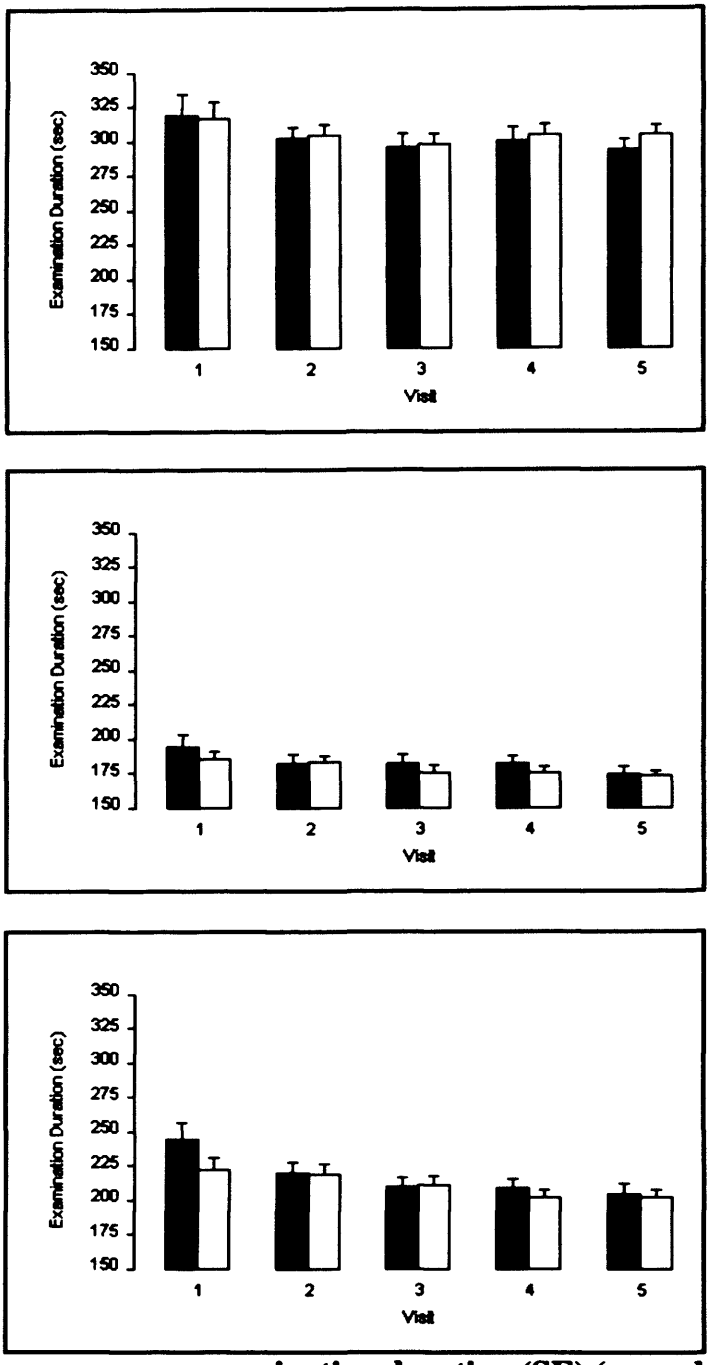

Figure 3.6c The group mean examination duration (SE) (seconds) at each of the five visits for each eye as a function of the algorithm for the individuals with OAG: right eye dark bars; left eye, open bars. Top: SITA Standard. Middle: SITA Fast. Bottom: SITA SWAP.

3.4.1.1.5 Ratio of the peripheral mean sensitivity to the central mean sensitivity

The group mean (SD) ratio of the peripheral mean sensitivity (PMS) to the central mean sensitivity (CMS) at each of the five visits for each eye of the individuals in each of the three groups, as a function of algorithm is shown in Table 3.8.

Algorithm	Visit 1		Visit 2		Visit 3		Visit 4		Visit 5	
	RE	LE	RE	LE	RE	LE	RE	LE	RE	LE
SITA Standard	0.93 (0.03)	0.92 (0.03)	0.93 (0.03)	0.93 (0.04)	0.93 (0.03)	0.93 (0.03)	0.93 (0.02)	0.93 (0.02)	0.93 (0.03)	0.93 (0.05)
SITA Fast	0.93 (0.03)	0.93 (0.03)	0.94 (0.02)	0.94 (0.02)	0.93 (0.02)	0.93 (0.02)	0.93 (0.03)	0.93 (0.03)	0.93 (0.02)	0.93 (0.02)
SITA SWAP	0.89 (0.05)	0.88 (0.06)	0.88 (0.05)	0.88 (0.05)	0.88 (0.05)	0.88 (0.05)	0.89 (0.06)	0.88 (0.05)	0.89 (0.04)	0.88 (0.05)
SITA Standard	0.93 (0.03)	0.92 (0.03)	0.94 (0.02)	0.93 (0.03)	0.93 (0.02)	0.93 (0.02)	0.93 (0.02)	0.92 (0.06)	0.93 (0.02)	0.93 (0.02)
SITA Fast	0.94 (0.02)	0.93 (0.03)	0.94 (0.02)	0.93 (0.02)	0.94 (0.03)	0.93 (0.03)	0.94 (0.02)	0.93 (0.02)	0.93 (0.02)	0.93 (0.02)
SITA SWAP	0.89 (0.05)	0.86 (0.09)	0.88 (0.06)	0.88 (0.05)	0.89 (0.06)	0.88 (0.06)	0.89 (0.05)	0.88 (0.05)	0.90 (0.04)	0.89 (0.05)
SITA Standard	0.92 (0.05)	0.90 (0.06)	0.92 (0.05)	0.91 (0.04)	0.93 (0.07)	0.92 (0.04)	0.93 (0.03)	0.92 (0.03)	0.93 (0.04)	0.92 (0.03)
SITA Fast	0.93 (0.03)	0.91 (0.05)	0.93 (0.03)	0.91 (0.05)	0.94 (0.05)	0.92 (0.03)	0.94 (0.05	0.93 (0.03)	0.94 (0.03	0.92 (0.04)
SITA SWAP	0.91 (0.14	0.86 (0.08)	0.89 (0.06)	0.86 (0.07)	0.89 (0.07)	0.87 (0.06)	0.89 (0.06)	0.88 (0.06)	0.89 (0.06)	0.88 (0.07)

Table 3.8 The group mean (SD) ratio of the PMS to the CMS at each of the five visits for each eye as a function of the three algorithms for the normal individuals (no shading), the individuals with OHT (light shading), the individuals with OAG (dark shading).

The group mean ratio of the PMS to the CMS and the ratio of the standard deviation (SD) for each eye at each visit for each of the three algorithms is also shown graphically in Figures 3.7a to 3.7c for each of the three groups.

The ANOVA showed that, overall, the ratio differed between the three algorithms but was independent of the order of algorithm within the examination (p=0.126). Surprisingly, it differed between the two eyes (p=0.322) being greater for the left

(second examined) eye but this effect was similar across the three algorithms ($p=0.359$).

The alteration in the ratio over the five visits just failed to achieve statistical significance ($p<0.055$).

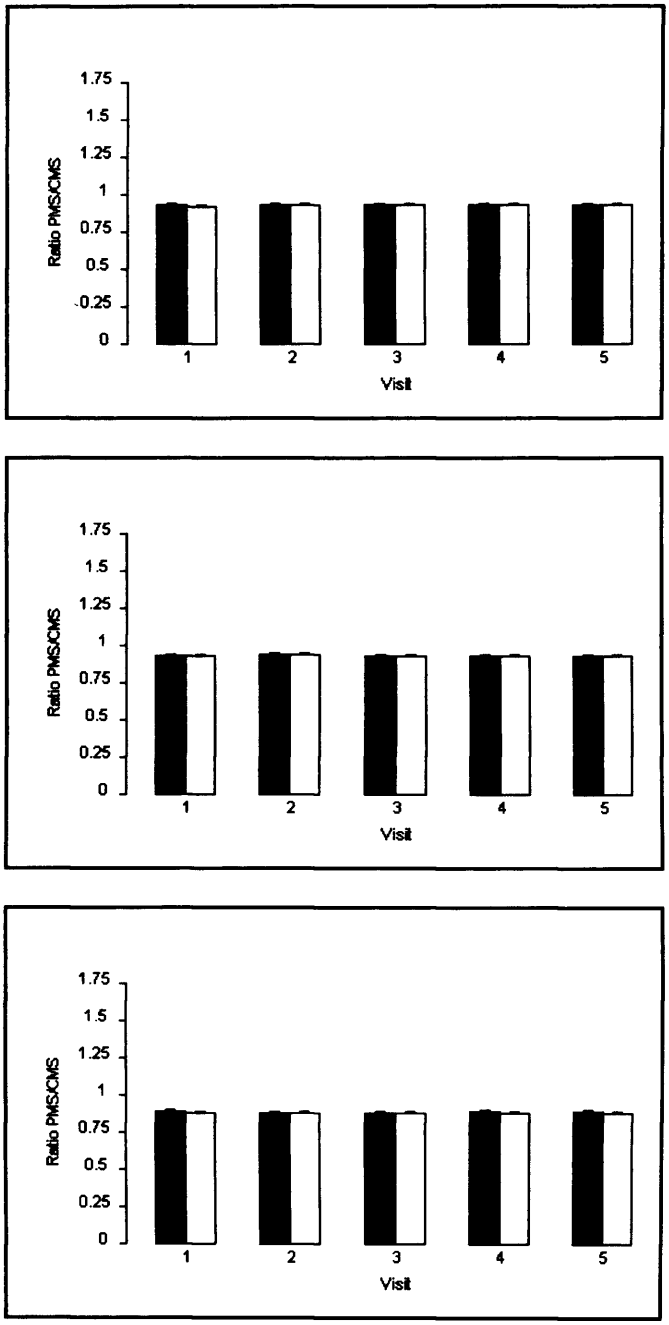

Figure 3.7a The group mean (SE) ratio PMS/CMS at each of the five visits for each eye as a function of the algorithm for the normal individuals: right eye, dark bars; left eye, open bars. Top: SITA Standard. Middle: SITA Fast. Bottom: SITA SWAP.

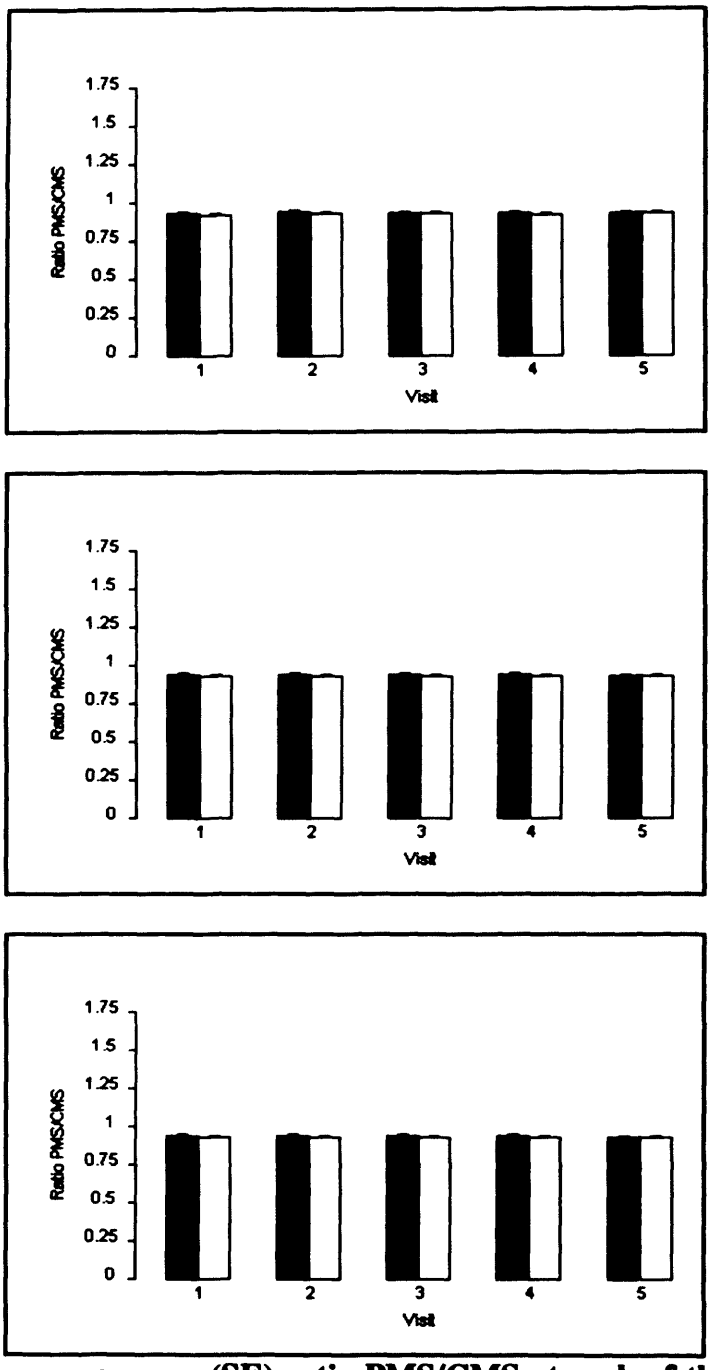

Figure 3.7b The group mean (SE) ratio PMS/CMS at each of the five visits for each eye as a function of the algorithm for the individuals with OHT: right eye, dark bars; left eye, open bars. Top: SITA Standard. Middle: SITA Fast. Bottom: SITA SWAP.

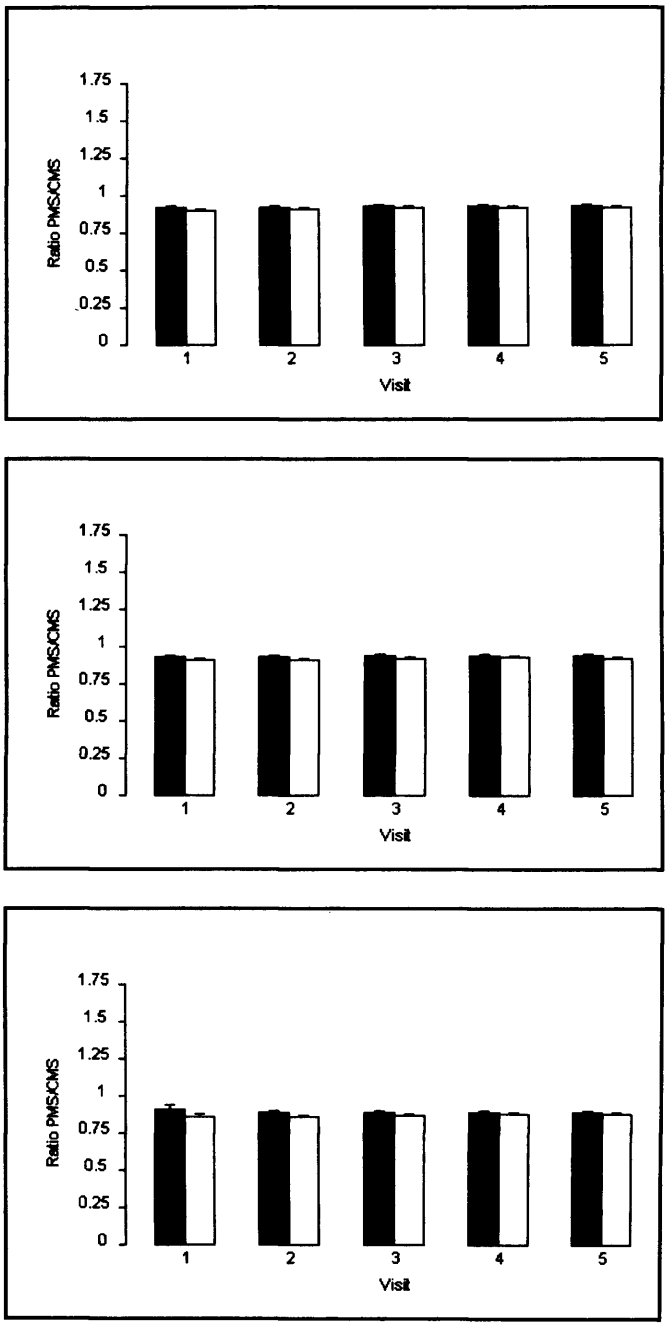

Figure 3.7c The group mean (SE) ratio PMS/CMS at each of the five visits for each eye as a function of the algorithm for the individuals with OAG: right eye, dark bars; left eye, open bars. Top: SITA Standard. Middle: SITA Fast. Bottom: SITA SWAP.

3.4.1.2 The within individual within-algorithm between-visit (Visits 1 and 5) difference (improvement) in sensitivity

The within individual within-algorithm differences in the MD index between Visits 1 and 5 for each of the three algorithms, for each of the three groups of individuals and for the three groups, combined, are summarised in Table 3.9 and are illustrated in Figures 3.8a to 3.8d. The mean of the differences was greater for SITA SWAP in each eye for each of the three groups compared to that for either SAP algorithm indicating a differential overall improvement in sensitivity/ learning effect for SWAP between Visits 1 and 5. This differential learning effect for SWAP was substantially greater for the right eye.

Algorithm	Eye	Normal	OHT	OAG	All groups
SITA Standard	RE	4.91 dB	2.62 dB	4.49 dB	4.14 dB
	LE	4.17 dB	3.78 dB	4.86 dB	4.26 dB
SITA Fast	RE	3.91 dB	3.42 dB	4.10 dB	3.84 dB
	LE	4.30 dB	3.38 dB	4.46 dB	4.06 dB
SITA SWAP	RE	5.25 dB	6.76 dB	6.30 dB	6.04 dB
	LE	5.19 dB	5.22 dB	9.76 dB	7.09 dB

Table 3.9 The within-individual within-algorithm difference in the MD between Visits 1 and 5 expressed as the range of the limits of agreement (defined as the mean of the differences +/- 1.96SD) for the three algorithms for each eye of the three groups of individuals and for the three groups, combined.

The range of the limits of agreement for the difference in MD for the SITA Standard algorithm between the two visits was similar to, or possibly slightly wider than, that for the SITA Fast algorithm. The range for the SITA SWAP algorithm was substantially wider than for either SAP algorithm for each of the three diagnostic groups.

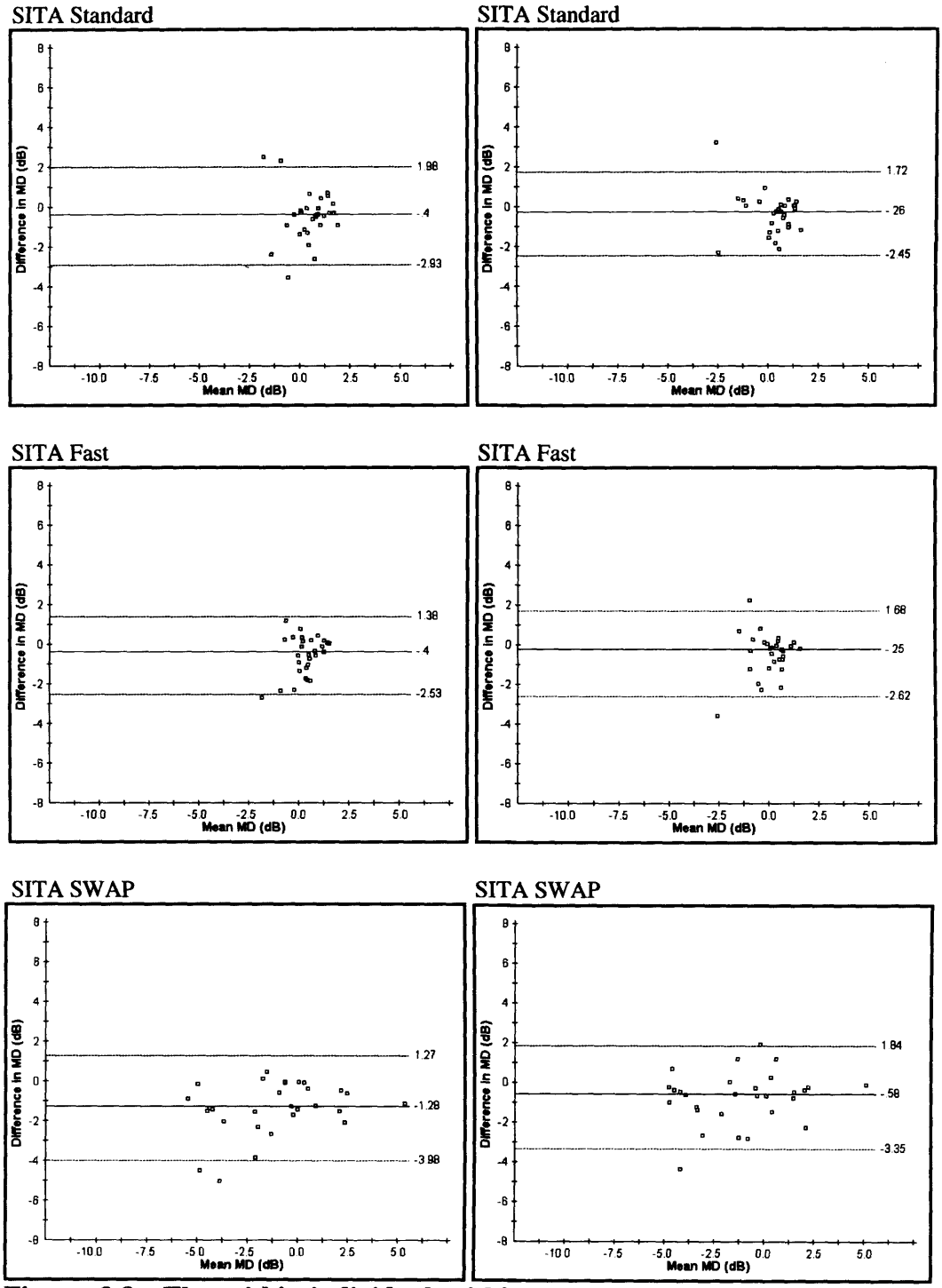

Figure 3.8a The within-individual within-algorithm difference in the MD between Visits 1 and 5 against the mean of the two MDs for the right eye (left column) and for the left eye (right column) for the normal individuals. Top: SITA Standard. Middle: SITA Fast. Bottom: SITA SWAP. The solid line indicates the mean of the differences and the upper and lower dotted lines the mean of the differences +/- 1.96SD, respectively.

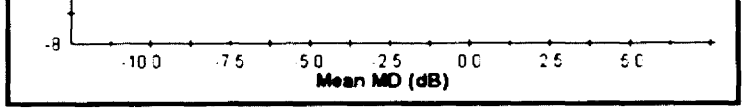

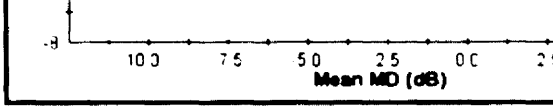

SITA Fast

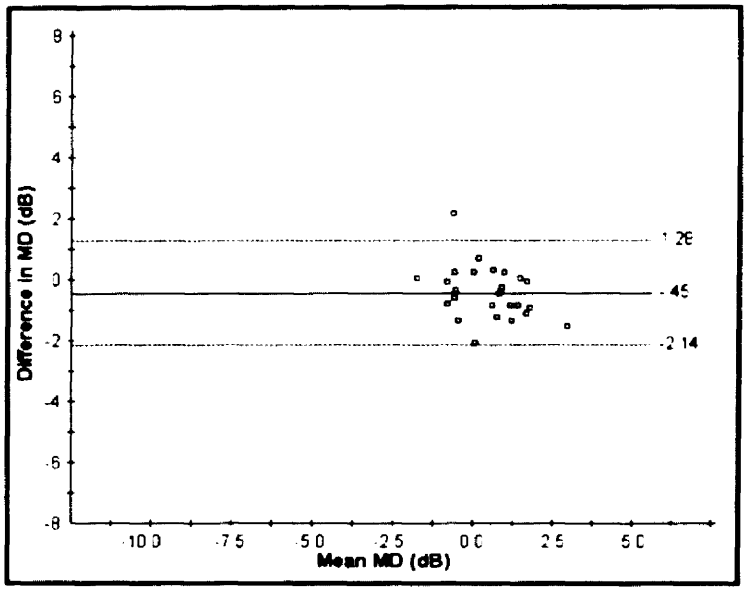

SITA Fast

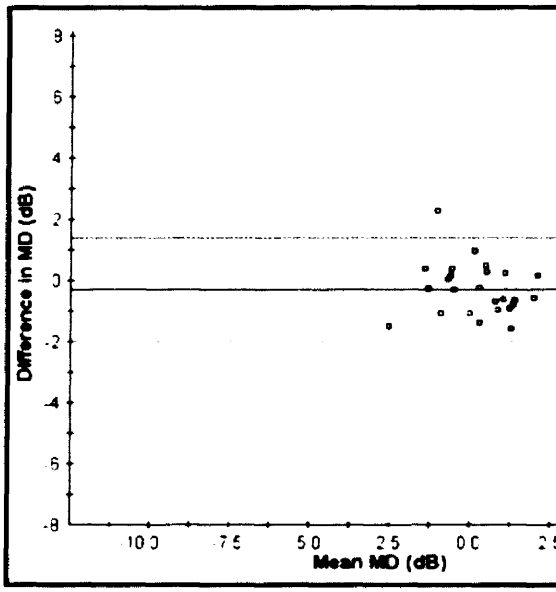

SITA SWAP

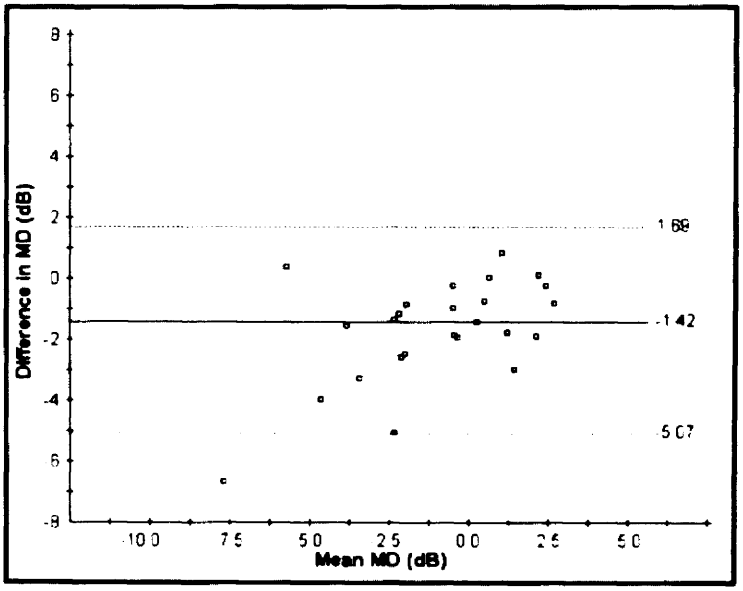

SITA SWAP

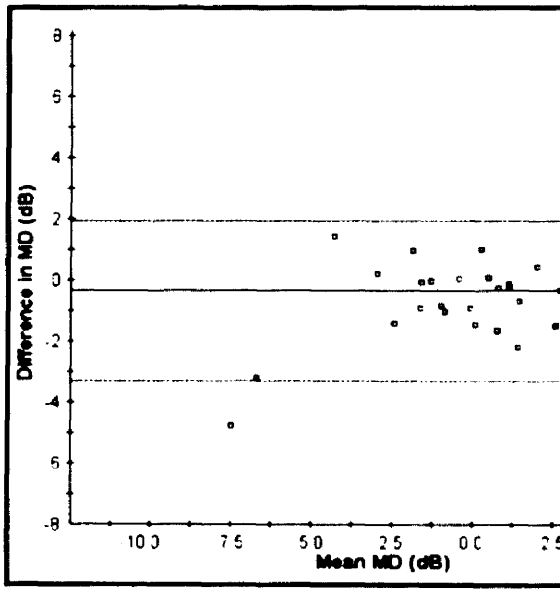

Figure 3.8b The within-individual within-algorithm difference in between Visits 1 and 5 against the mean of the two MDs for the righ column) and for the left eye (right column) for the individuals w Top: SITA Standard. Middle: SITA Fast. Bottom: SITA SWAP. line indicates the mean of the differences and the upper and low lines the mean of the differences +/- 1.96SD, respectively.

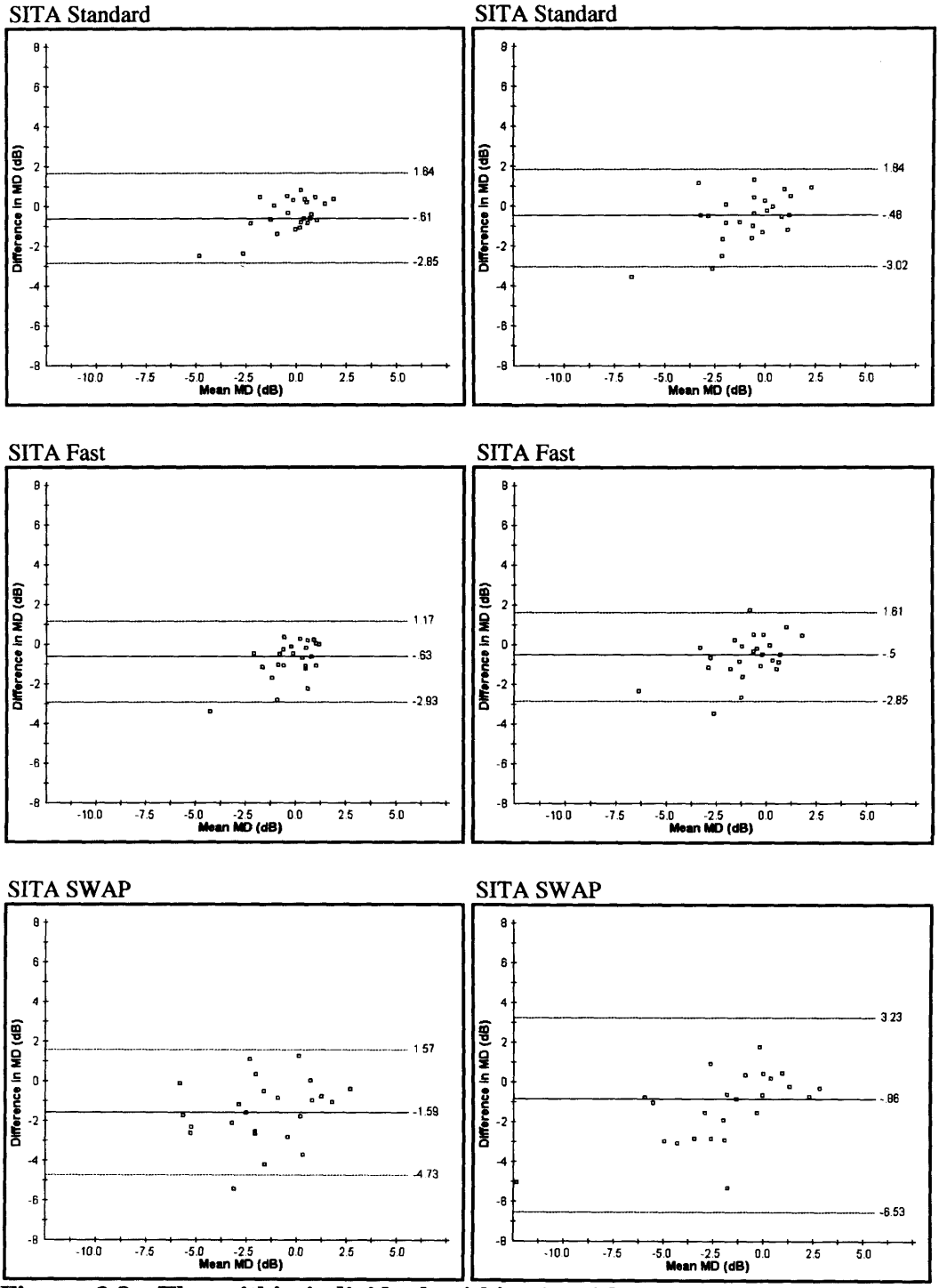

Figure 3.8c The within-individual within-algorithm difference in the MD between Visits 1 and 5 against the mean of the two MDs for the right eye (left column) and for the left eye (right column) for the individuals with OAG. Top: SITA Standard. Middle: SITA Fast. Bottom: SITA SWAP. The solid line indicates the mean of the differences and the upper and lower dotted lines the mean of the differences +/- 1.96SD, respectively.

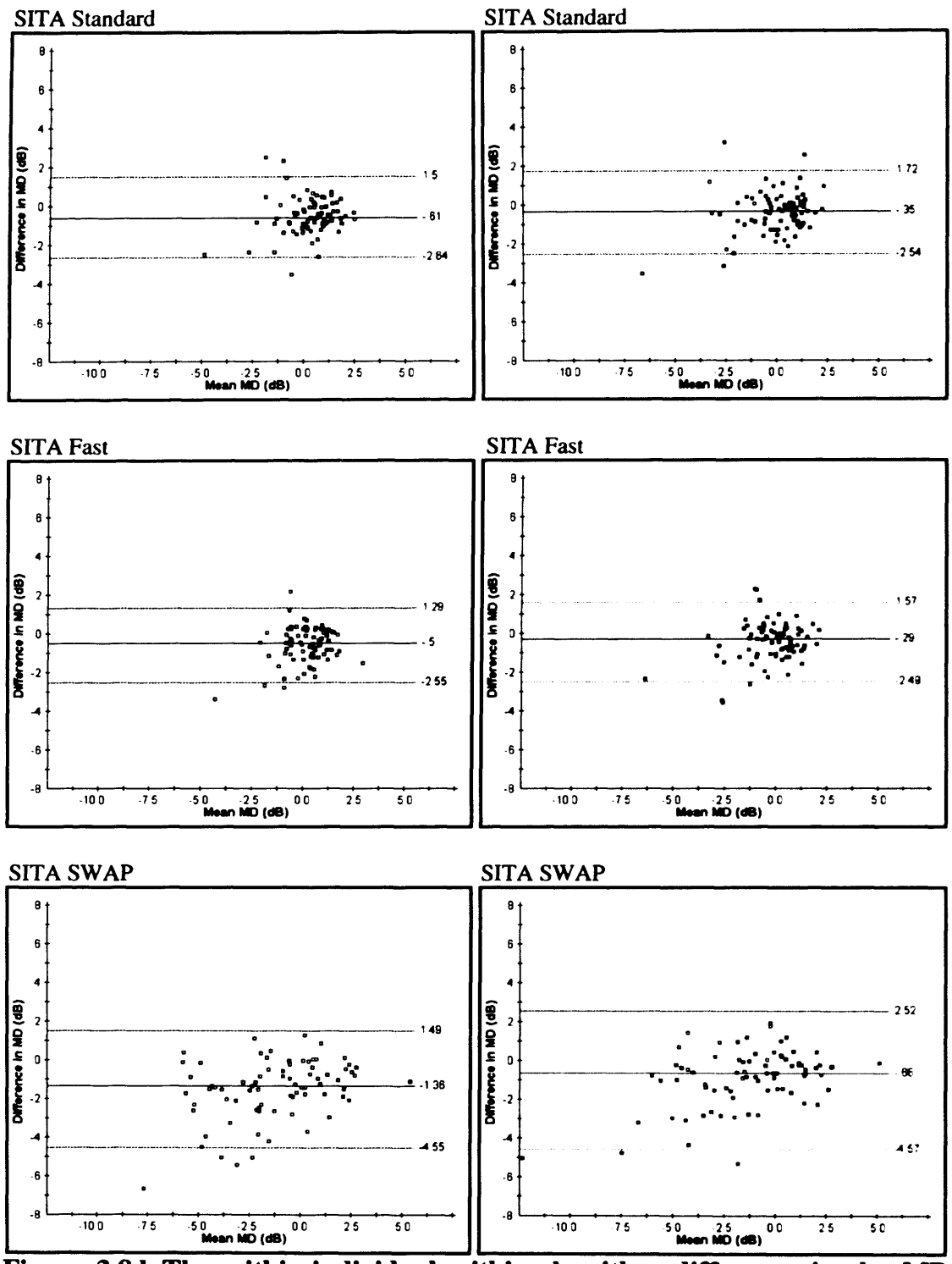

Figure 3.8d The within-individual within-algorithm difference in the MD between Visits 1 and 5 against the mean of the two MDs for the right eye (left column) and for the left eye (right column) for the three groups, combined. Top: SITA Standard. Middle: SITA Fast. Bottom: SITA SWAP. The solid line indicates the mean of the differences and the upper and lower dotted lines the mean of the differences +/- 1.96SD, respectively.

The within-algorithm differences in the PSD index between Visits 1 and 5 for each of the three algorithms, for each of the three groups of individuals and for the three groups, combined, are summarised in Table 3.10 and are illustrated in Figures 3.9a to 3.9d. The mean of the differences approximated to zero for each algorithm for each group indicating no improvement in localised/ focal abnormality between Visits 1 and 5. This would, of course, be expected in the normal individuals and in the group with OHT, but might not have been expected in the group with glaucoma.

Algorithm	Eye	Normal	OHT	OAG	All groups
SITA Standard	RE	2.07 dB	1.37 dB	4.01 dB	2.66 dB
	LE	2.64 dB	2.46 dB	4.77 dB	3.50 dB
SITA Fast	RE	2.12 dB	1.18 dB	3.14 dB	2.30 dB
	LE	1.76 dB	3.24 dB	5.71 dB	3.82 dB
SITA SWAP	RE	2.96 dB	2.08 dB	4.43 dB	3.25 dB
	LE	2.45 dB	2.38 dB	4.18 dB	3.07 dB

Table 3.10 The within-individual within-algorithm difference in the PSD between Visits 1 and 5 expressed as the range of the limits of agreement (defined as the mean of the differences +/- 1.96SD) for the three algorithms for each eye of the three groups of individuals and for the three groups, combined.

The range of the limits of agreement for the difference in PSD was wider for the SITA Fast algorithm compared to the SITA Standard algorithm for the individuals with OHT and for the individuals with OAG. However, for the normal group, who had been naïve to any form of perimetry, the range was wider for the SITA Standard algorithm compared to the SITA Fast algorithm. The range for the SITA SWAP algorithm was substantially wider than for either SAP algorithm for each of the three diagnostic groups.

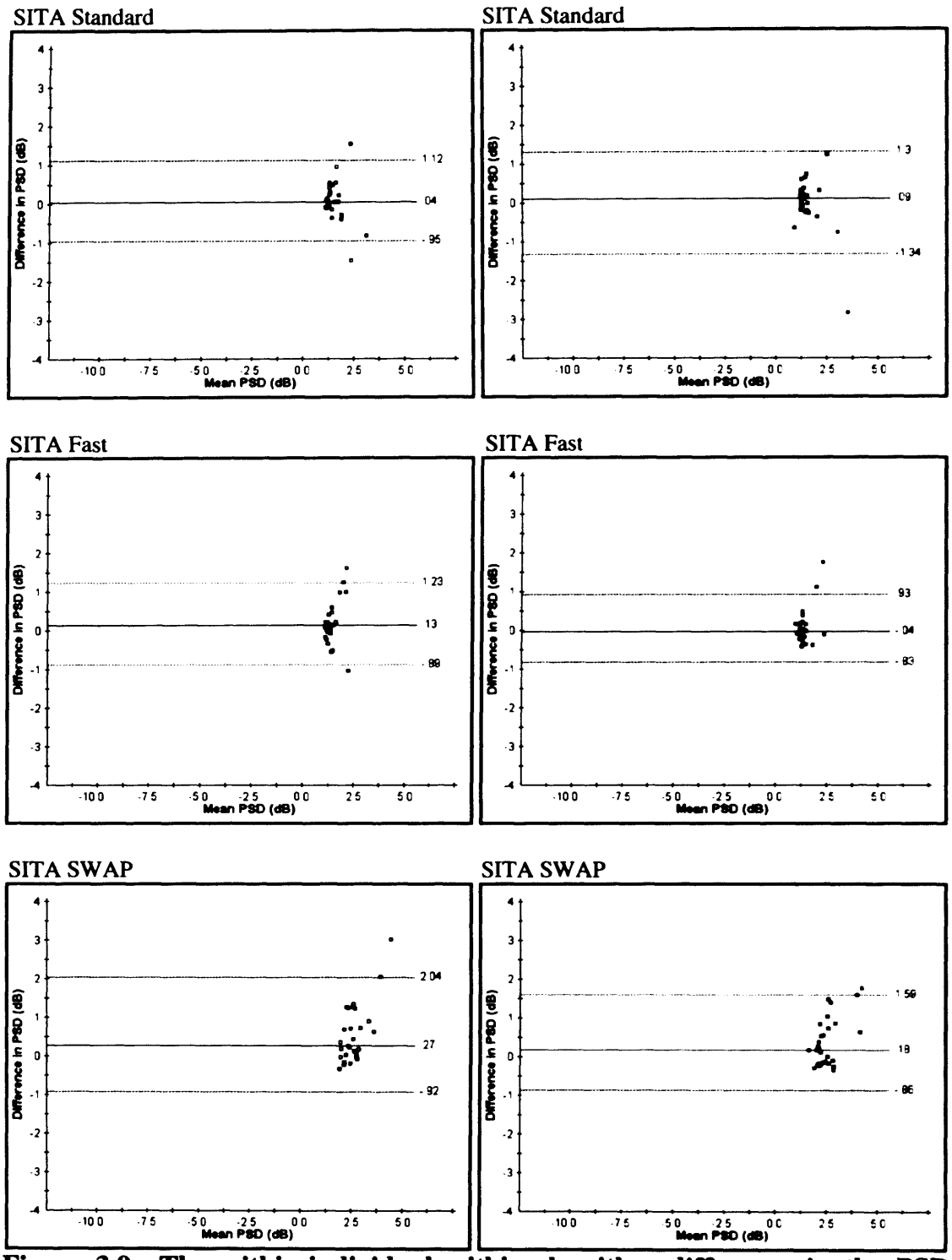

Figure 3.9a The within-individual within-algorithm difference in the PSD between Visits 1 and 5 against the mean of the two PSDs for the right eye (left column) and for the left eye (right column) for the normal individuals. Top: SITA Standard. Middle: SITA Fast. Bottom: SITA SWAP. The solid line indicates the mean of the differences and the upper and lower dotted lines the mean of the differences +/- 1.96SD, respectively.

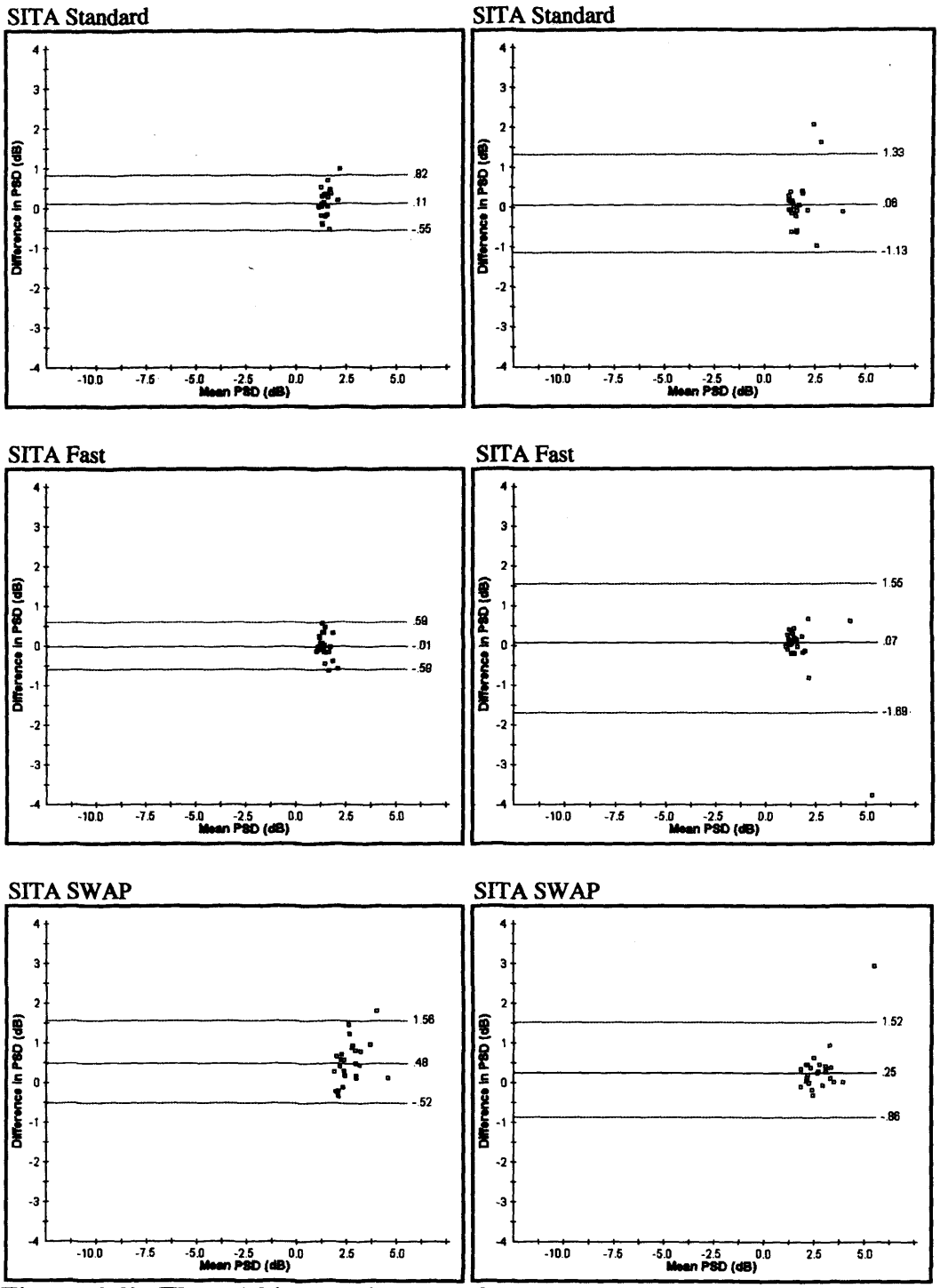

Figure 3.9b The within-individual within-algorithm difference in the PSD between Visits 1 and 5 against the mean of the two PSDs for the right eye (left column) and for the left eye (right column) for the individuals with OHT. Top: SITA Standard. Middle: SITA Fast. Bottom: SITA SWAP. The solid line indicates the mean of the differences and the upper and lower dotted lines the mean of the differences +/- 1.96SD, respectively.

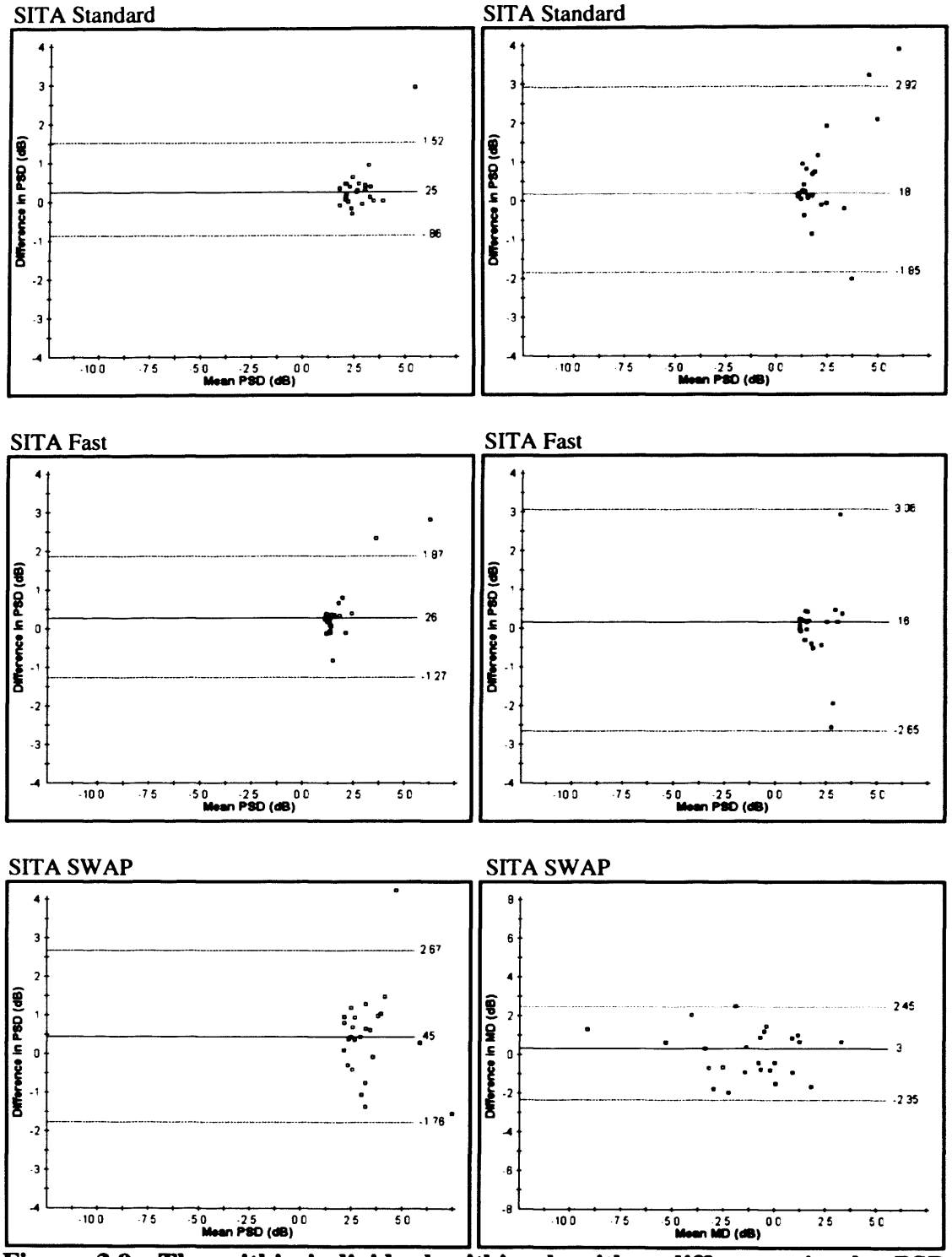

Figure 3.9c The within-individual within-algorithm difference in the PSD between Visits 1 and 5 against the mean of the two PSDs for the right eye (left column) and for the left eye (right column) for the individuals with OAG. Top: SITA Standard. Middle: SITA Fast. Bottom: SITA SWAP. The solid line indicates the mean of the differences and the upper and lower dotted lines the mean of the differences +/- 1.96SD, respectively.

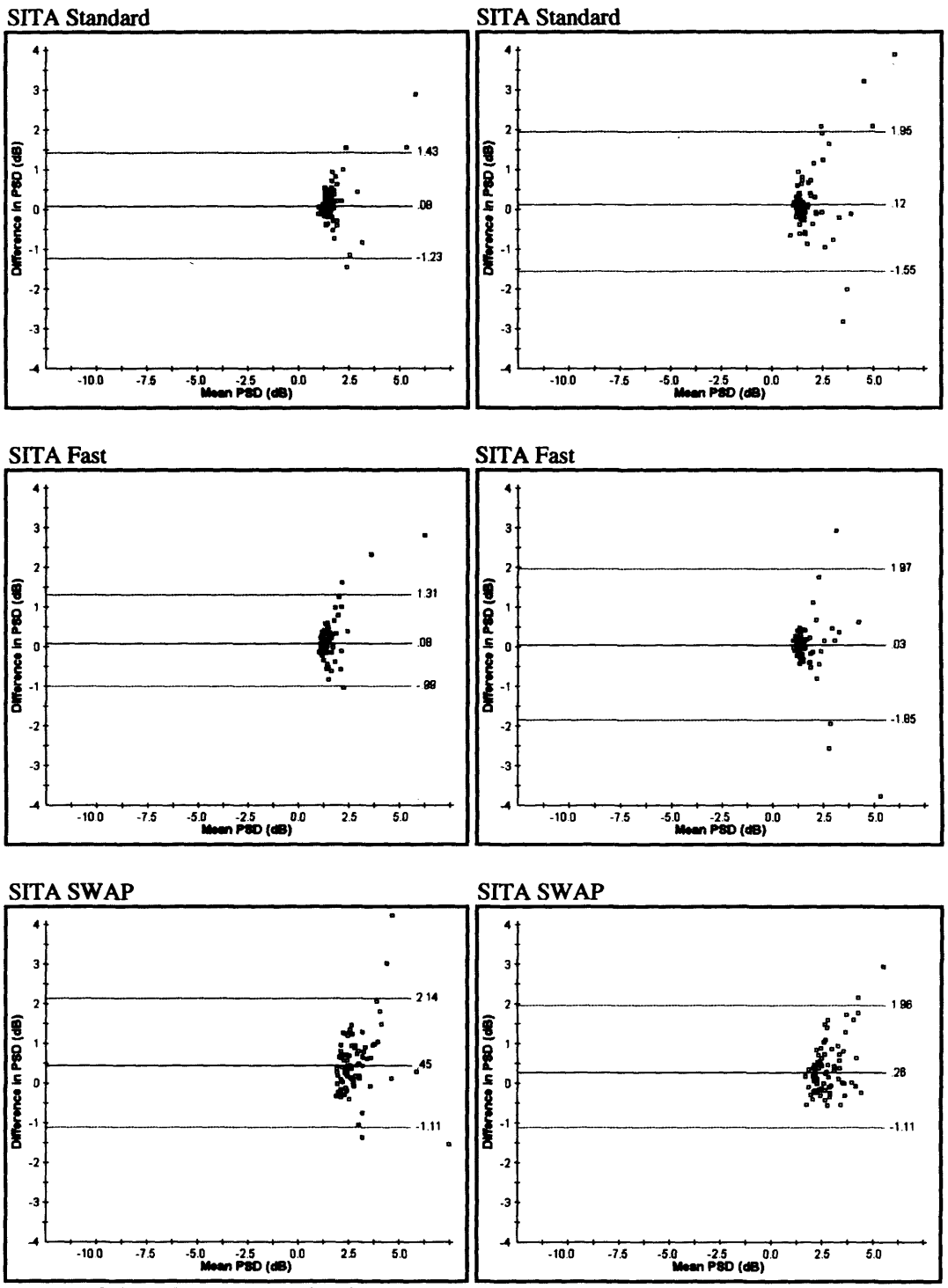

Figure 3.9d The within-individual within-algorithm difference in the PSD between Visits 1 and 5 against the mean of the two PSDs for the right eye (left column) and for the left eye (right column) for the three groups, combined. Top: SITA Standard. Middle: SITA Fast. Bottom: SITA SWAP. The solid line indicates the mean of the differences and the upper and lower dotted lines the mean of the differences +/- 1.96SD, respectively.

The within-individual within-algorithm between-visit difference in sensitivity across each stimulus location expressed as the 10^{th}, 50^{th} and 90^{th} percentiles of the distribution of the difference in sensitivity at each location between Visits 1 and 5 as a function of the sensitivity at the corresponding stimulus location recorded at Visit 5 is shown in Figures 3.10a to 3.10d for each eye of each of the three groups and for all three groups, combined. In this format, a positive slope for the 50^{th} percentile indicates an improvement in sensitivity.

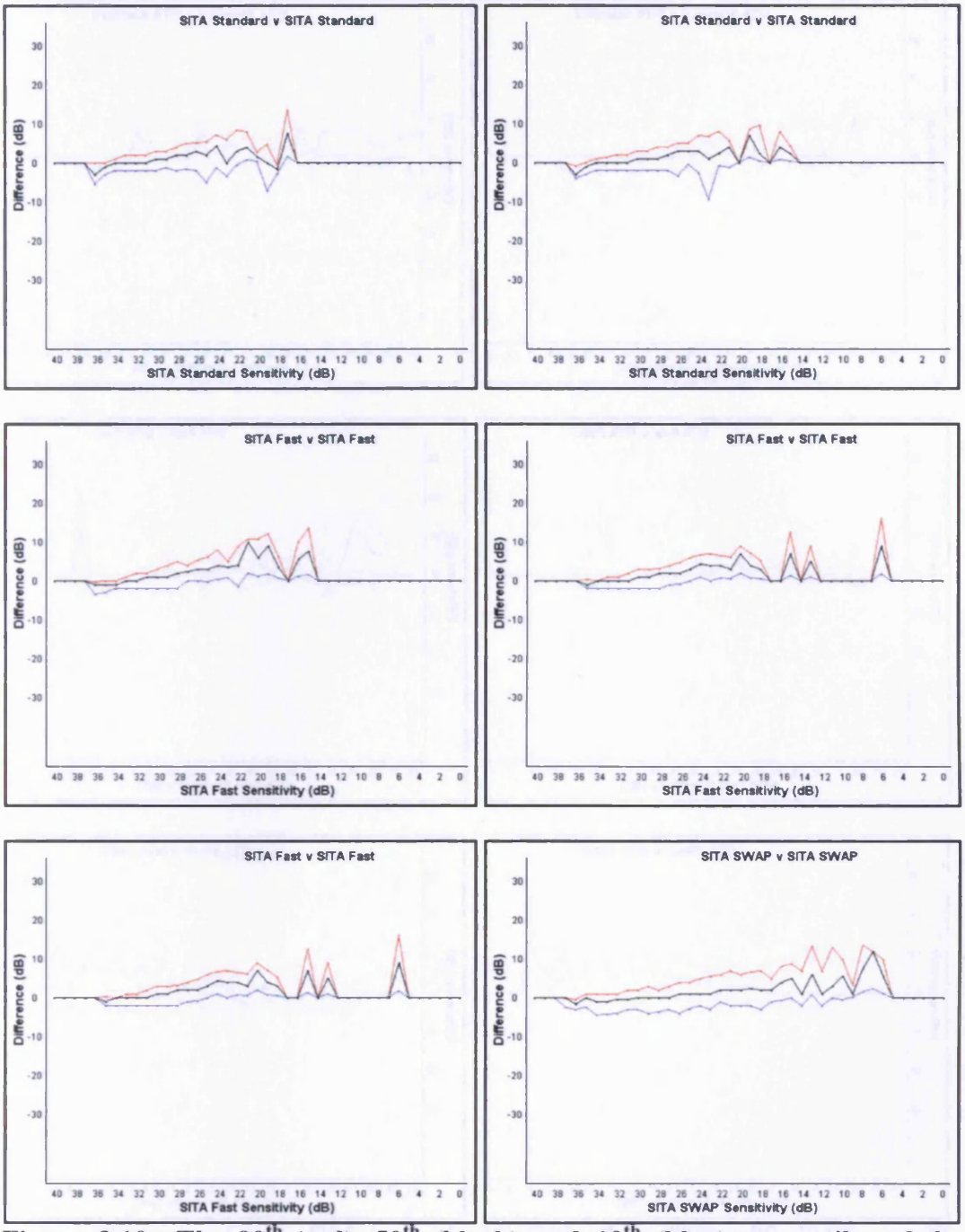

Figure 3.10a The 90th (red), 50th (black) and 10th (blue) percentiles of the distribution of the within-individual within-algorithm between-visit difference in sensitivity across all stimulus locations for the normal individuals between Visits 5 and 1 as a function of the sensitivity at the corresponding stimulus location recorded at Visit 1: right eye, left column; left eye, right column. Top: SITA Standard. Middle: SITA Fast. Bottom: SITA SWAP.

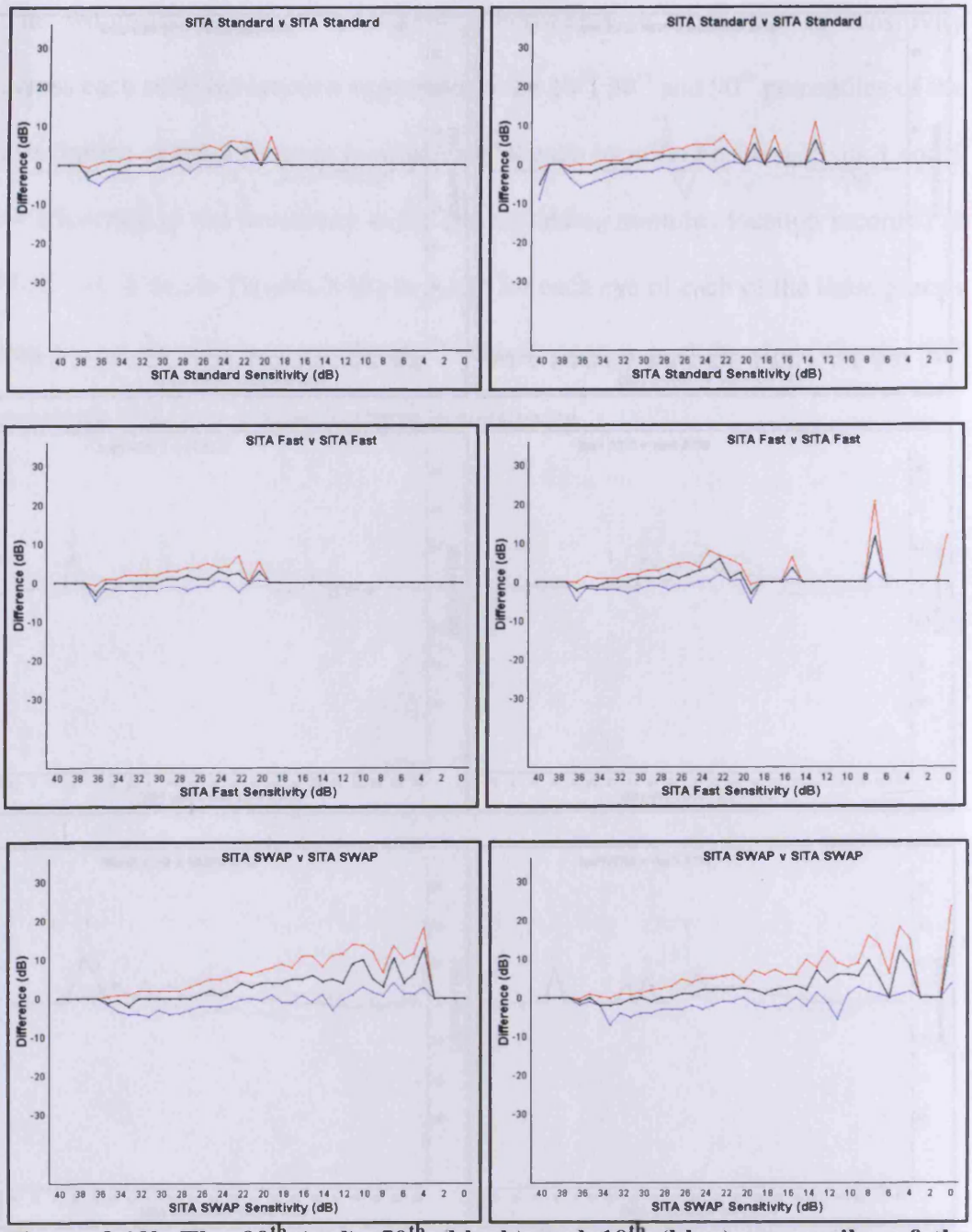

Figure 3.10b The 90th (red), 50th (black) and 10th (blue) percentiles of the distribution of the within-individual within-algorithm between-visit difference in sensitivity across all stimulus locations for the individuals with OHT between Visits 5 and 1 as a function of the sensitivity at the corresponding stimulus location recorded at Visit 1: right eye, left column; left eye, right column. Top: SITA Standard. Middle: SITA Fast. Bottom: SITA SWAP.

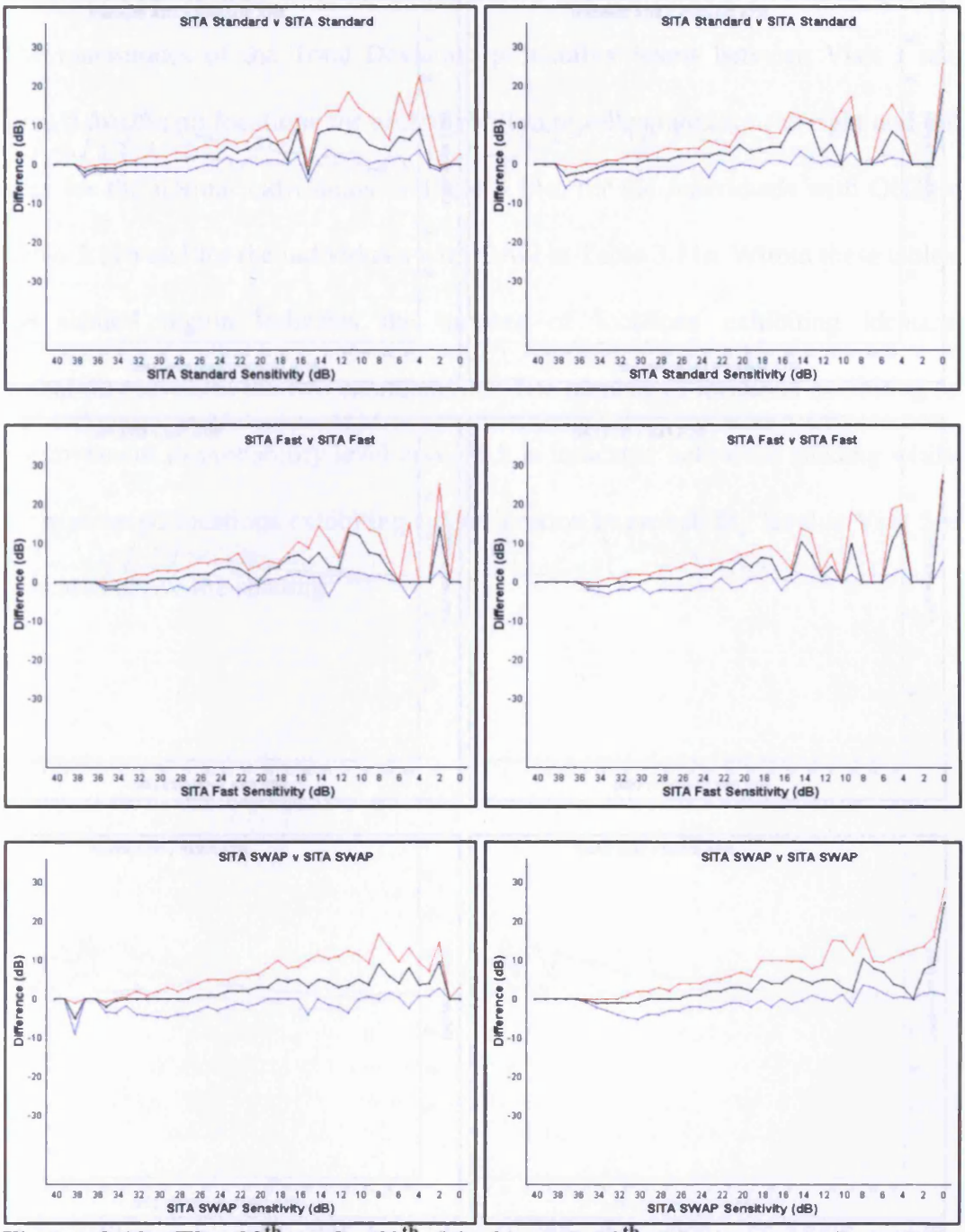

Figure 3.10c The 90th (red), 50th (black) and 10th (blue) percentiles of the distribution of the within-individual within-algorithm between-visit difference in sensitivity across all stimulus locations for the individuals with OAG between Visits 5 and 1 as a function of the sensitivity at the corresponding stimulus location recorded at Visit 1: right eye, left column; left eye, right column. Top: SITA Standard. Middle: SITA Fast. Bottom: SITA SWAP.

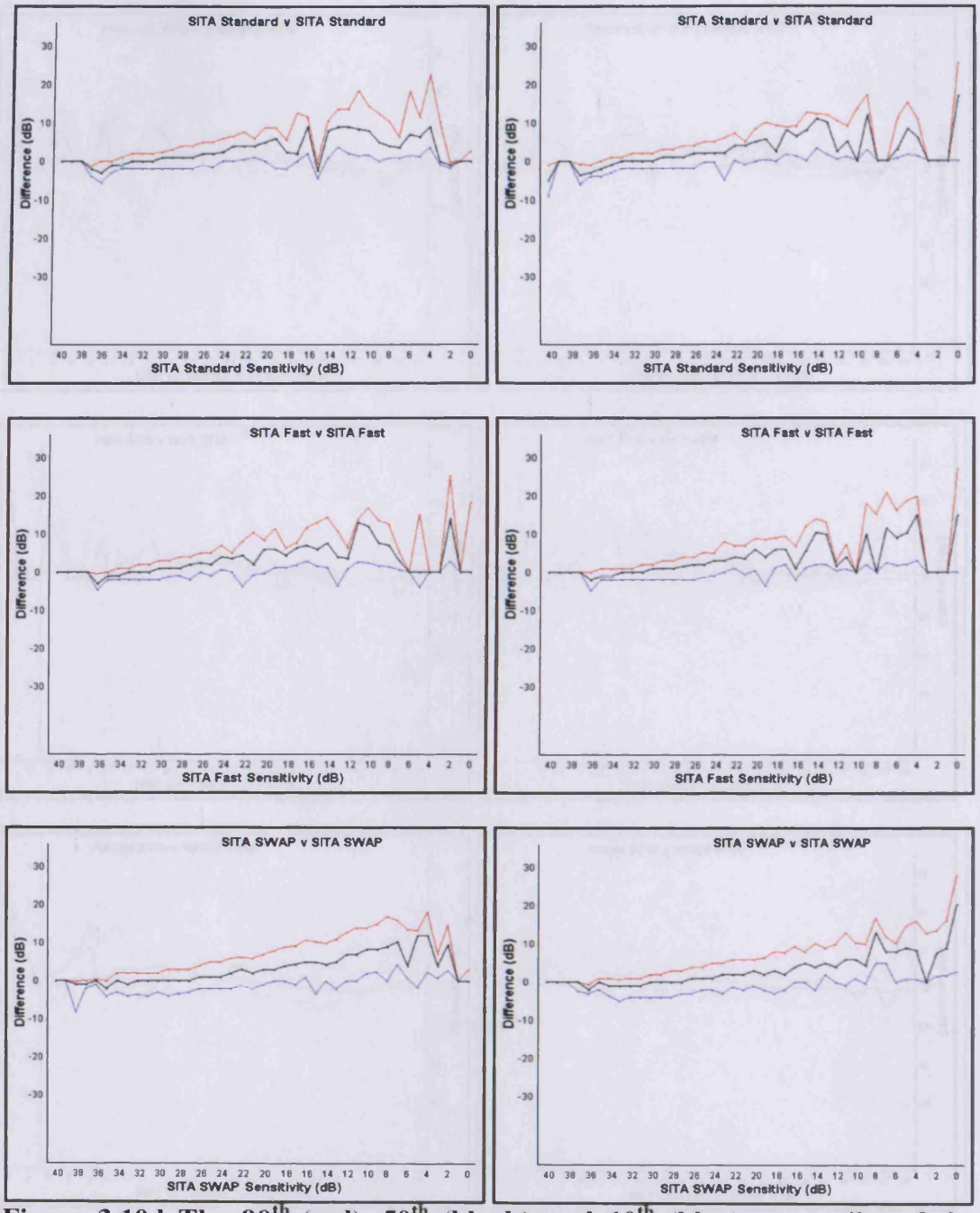

Figure 3.10d The 90th (red), 50th (black) and 10th (blue) percentiles of the distribution of the within-individual within-algorithm between-visit difference in sensitivity across all stimulus locations for the individuals in all three groups between Visits 5 and 1 as a function of the sensitivity at the corresponding stimulus location recorded at Visit 1: right eye, left column; left eye, right column. Top: SITA Standard. Middle: SITA Fast. Bottom: SITA SWAP.

The magnitudes of the Total Deviation probability levels between Visit 1 and Visit 5, across all locations for each algorithm are illustrated for the right and left eyes for the normal individuals in Table 3.11a, for the individuals with OHT in Table 3.11b and for the individuals with OAG in Table 3.11c. Within these tables, the shaded region indicates the number of locations exhibiting identical probability levels at the two examinations. The number of locations exhibiting an improvement in probability level at Visit 5 is indicated below the shading whilst the number of locations exhibiting a deterioration in probability level at Visit 5 is indicated above the shading.

SITA Standard

SITA Standard	NS	<5%	<2%	<1%	<0,5%
NS	1383	30	9	5	5
<5%	42	0	1	0	2
<2%	9	1	1	1	1
<1%	8	0	0	0	2
<0,5%	7	0	0	1	0

SITA Standard

SITA Standard	NS	<5%	<2%	<1%	<0,5%
NS	1362	30	10	8	6
<5%	44	6	3	0	1
<2%	11	2	0	0	2
<1%	9	5	2	1	0
<0,5%	4	0	0	0	2

SITA Fast

SITA Fast	NS	<5%	<2%	<1%	<0,5%
NS	1408	16	3	1	2
<5%	36	1	0	1	0
<2%	12	1	2	0	0
<1%	18	0	0	0	0
<0,5%	7	0	0	0	0

SITA Fast

SITA Fast	NS	<5%	<2%	<1%	<0,5%
NS	1351	34	5	7	2
<5%	55	6	2	2	0
<2%	24	0	0	0	0
<1%	10	3	0	0	0
<0,5%	5	2	0	0	0

SITA SWAP

SITA SWAP	NS	<5%	<2%	<1%	<0,5%
NS	1250	31	7	0	0
<5%	113	11	2	2	1
<2%	34	4	1	1	0
<1%	16	2	1	0	0
<0,5%	21	4	4	2	1

SITA SWAP

SITA SWAP	NS	<5%	<2%	<1%	<0,5%
NS	1251	53	7	2	0
<5%	83	18	4	1	1
<2%	38	10	3	0	0
<1%	15	4	1	2	1
<0,5%	8	5	0	1	0

Table 3.11a The magnitudes of the Total Deviation probability levels between Visit 1 (ordinate) and Visit 5 (abscissa), across all locations for the normal individuals for the right eye (left column) and left eye (right column). Top: SITA Standard. Middle: SITA Fast. Bottom: SITA SWAP. The shading indicates the number of locations exhibiting identical probability levels at the two examinations. The number of locations exhibiting an improvement in probability level at Visit 5 is indicated below the shading. The number of locations exhibiting a deterioration in probability level at Visit 5 is indicated above the shading.

As would be expected, the extent of the improvement in the Total Deviation probability level for the normal individuals with the SITA Standard algorithm between Visit 1 and Visit 5 (Table 3.11a) was relatively small in each eye, (right eye, 68 locations exhibiting an improvement, 56 locations exhibiting a deterioration [a 1.2 fold overall improvement]; left eye, 77 locations exhibiting an improvement,

60 locations exhibiting a deterioration [a 1.3 fold overall improvement]) i.e. a normal visual field remains a normal visual field. However, a greater improvement was present for the SITA Fast algorithm particularly in the right eye between the two visits (right eye, 74 locations exhibiting an improvement, 23 locations exhibiting a deterioration [a 3.2 fold overall improvement]; left eye, 99 locations exhibiting an improvement, 52 locations an exhibiting deterioration [a 1.9 fold overall improvement]). The SITA SWAP algorithm exhibited an even larger improvement between the two visits and this improvement was greater for the right eye compared to that of the left eye (right eye, 201 locations exhibiting an improvement, 44 locations exhibiting a deterioration [a 4.6 fold overall improvement]; left eye, 165 locations exhibiting an improvement, 69 locations exhibiting a deterioration [a 2.4 fold overall improvement]). The majority of the locations, for each of the three algorithms, which exhibited a change in probability level between the two visits, exhibited either an improvement from the 5% probability level to normal or a deterioration from normal to the 5% probability level.

SITA Standard

SITA Standard	NS	<5%	<2%	<1%	<0,5%
NS	1231	15	0	0	0
<5%	36	4	0	0	0
<2%	9	0	1	0	0
<1%	1	2	0	0	0
<0,5%	1	0	0	0	0

SITA Standard

SITA Standard	NS	<5%	<2%	<1%	<0,5%
NS	1195	22	5	2	3
<5%	39	6	0	0	0
<2%	14	0	1	0	0
<1%	8	0	0	1	1
<0,5%	1	1	0	0	1

SITA Fast

SITA Fast	NS	<5%	<2%	<1%	<0,5%
NS	1203	16	7	5	2
<5%	39	9	1	1	0
<2%	11	1	3	0	0
<1%	1	1	0	0	0
<0,5%	0	0	0	0	0

SITA Fast

SITA Fast	NS	<5%	<2%	<1%	<0,5%
NS	1168	28	7	6	3
<5%	45	10	3	0	0
<2%	6	1	2	1	1
<1%	13	1	0	0	0
<0,5%	2	0	1	1	1

SITA SWAP

SITA SWAP	NS	<5%	<2%	<1%	<0,5%
NS	1065	14	6	0	2
<5%	95	6	1	3	1
<2%	43	5	1	0	1
<1%	19	3	3	0	1
<0,5%	20	5	3	2	1

SITA SWAP

SITA SWAP	NS	<5%	<2%	<1%	<0,5%
NS	1143	23	5	2	2
<5%	36	12	1	0	0
<2%	15	6	4	1	0
<1%	5	6	1	0	0
<0,5%	15	10	9	0	4

Table 3.11b The magnitudes of the Total Deviation probability levels between Visit 1 (ordinate) and Visit 5 (abscissa), across all locations for the individuals with OHT for the right eye (left column) and left eye (right column). Top: SITA Standard. Middle: SITA Fast. Bottom: SITA SWAP. The shading indicates the number of locations exhibiting identical probability levels at the two examinations. The number of locations exhibiting an improvement in probability level at Visit 5 is indicated below the shading. The number of locations exhibiting a deterioration in probability level at Visit 5 is indicated above the shading.

The extent of the improvement in the Total Deviation probability level between Visit 1 and Visit 5 for the individuals with OHT (Table 3.11b) was different with SITA Standard to that for the normal individuals but similar with SITA Fast. (For the SITA Standard algorithm, 49 locations in the right eye exhibited an improvement and 15 locations exhibited a deterioration [a 3.3 fold overall

improvement]; 63 locations in the left eye exhibited an improvement and 33 locations exhibited a deterioration [a 1.9 fold overall improvement]. For the SITA Fast algorithm, 53 locations in the right eye exhibited an improvement and 32 locations exhibited a deterioration [a 1.7 fold overall improvement]; 70 locations in the left eye exhibited improvement and 49 locations exhibited deterioration [a 1.4 fold overall improvement]). However, the extent of the improvement for the SITA SWAP algorithm was appreciably greater than that for SAP and was greater for the right eye compared to that of the left eye i.e. the first eye examined (right eye, 198 locations exhibited an improvement and 29 locations exhibited a deterioration [a 6.8 fold overall improvement]; left eye, 103 locations exhibited an improvement and 34 locations exhibited a deterioration [a 3.0 fold overall improvement]). As with the normal individuals, the majority of the locations, for each of the three algorithms, which exhibited a change in probability level between the two visits exhibited either an improvement from the 5% probability level to normal or a deterioration from normal to the 5% probability level.

SITA Standard

SITA Standard	NS	<5%	<2%	<1%	<0,5%
NS	1081	24	7	3	2
<5%	48	6	2	0	0
<2%	17	6	2	1	3
<1%	6	2	3	1	1
<0,5%	9	3	6	9	58

SITA Standard

SITA Standard	NS	<5%	<2%	<1%	<0,5%
NS	1008	31	5	8	1
<5%	66	14	5	3	2
<2%	29	9	3	4	2
<1%	18	9	3	7	4
<0,5%	20	4	7	8	30

SITA Fast

SITA Fast	NS	<5%	<2%	<1%	<0,5%
NS	1074	29	6	0	1
<5%	67	4	1	1	2
<2%	19	2	1	1	0
<1%	10	5	5	5	5
<0,5%	11	5	2	11	33

SITA Fast

SITA Fast	NS	<5%	<2%	<1%	<0,5%
NS	990	38	9	7	4
<5%	68	12	9	7	1
<2%	36	7	9	5	2
<1%	17	6	13	11	3
<0,5%	12	5	5	16	8

SITA SWAP

SITA SWAP	NS	<5%	<2%	<1%	<0,5%
NS	1001	33	6	3	1
<5%	81	16	2	1	1
<2%	34	6	1	0	3
<1%	12	5	2	2	1
<0,5%	23	8	5	6	47

SITA SWAP

SITA SWAP	NS	<5%	<2%	<1%	<0,5%
NS	1008	26	5	3	2
<5%	78	13	4	2	3
<2%	30	5	3	0	0
<1%	17	5	5	1	1
<0,5%	41	11	9	10	18

Table 3.11c The magnitudes of the Total Deviation probability levels between Visit 1 (ordinate) and Visit 5 (abscissa), across all locations for the individuals with OAG for the right eye (left column) and left eye (right column). Top: SITA Standard. Middle: SITA Fast. Bottom: SITA SWAP. The shading indicates the number of locations exhibiting identical probability levels at the two examinations. The number of locations exhibiting an improvement in probability level at Visit 5 is indicated below the shading. The number of locations exhibiting a deterioration in probability level at Visit 5 is indicated above the shading.

The extent of the improvement in the Total Deviation probability level between Visit 1 and Visit 5 for the individuals with OAG (Table 3.11c) was different to that both of the normal individuals and of the individuals with OHT. (For the SITA Standard Algorithm, 109 locations in the right eye exhibited an improvement and 43 locations exhibited a deterioration [a 2.5 fold overall improvement] and 173

locations in the left eye exhibited an improvement and 65 locations exhibited a deterioration [a 2.7 fold overall improvement]. For the SITA Fast algorithm, 137 locations in the right eye exhibited an improvement and 46 locations exhibited a deterioration [a 3.0 fold overall improvement] and 185 locations in the left eye exhibited an improvement and 85 locations exhibited a deterioration [a 2.2 fold overall improvement]). For SWAP, the effect was greater for the left eye (i.e. the second eye examined). For the right eye, 182 locations exhibited an improvement and 51 locations exhibited a deterioration [a 3.6 fold overall improvement]. For the left eye, 211 locations exhibited an improvement and 46 locations exhibited a deterioration [a 4.6 fold overall improvement]). Once again, the majority of the locations, for each of the three algorithms, which exhibited a change in probability level between the two visits exhibited either an improvement from the 5% probability level to normal or a deterioration from normal to the 5% probability level.

The between-visit difference (between Visits 1 and 5) for each algorithm for each group is summarized in Table 3.12 for both the Total Deviation and the Pattern Deviation probability levels.

Algorithm	Eye	Normal	OHT	OAG
SITA Standard	RE	1.2 / 1.0	3.3 / 1.7	2.5 / 1.4
	LE	1.3 / 1.2	1.9 / 1.0	2.7 / 1.8
SITA Fast	RE	3.2 / 1.7	1.7 / 1.1	3.0 / 1.5
	LE	1.9 / 1.2	1.4 / 1.3	2.2 / 1.4
SITA SWAP	RE	4.6 / 2.5	6.8 / 2.1	3.6 / 1.5
	LE	2.4 / 1.6	3.0 / 1.6	4.6 / 1.9

Table 3.12 The summary of the between-visit difference (Visits 1 and 5) expressed in terms of the ratio of the difference in the number of stimulus locations exhibiting an abnormal Total Deviation (Tables 3.11a to 3.11c) and Pattern Deviation probability level (Tables 3.13a to 3.13c) for each algorithm and for each group. The value before the oblique is the overall incremental change in the Total Deviation probability levels. The value after the oblique is the overall incremental change in the Pattern Deviation probability levels. (A positive value indicates an improvement i.e. a reduction in the number of stimulus locations exhibiting a significant, and/ or a less significant, probability level relative to Visit 1 and a negative value indicates a deterioration i.e. an increase in the number of stimulus locations exhibiting a significant and/ or more significant probability level relative to Visit 1).

The magnitudes of the Pattern Deviation probability levels between Visit 1 and Visit 5, across all locations for each algorithm are illustrated for the right and left eyes for the normal individuals in Table 3.13a for the individuals with OHT in Table 3.13b and for the individuals with OAG in Table 3.13c. Once again, the shaded regions indicate the number of locations exhibiting identical probability levels at the two examinations. The number of locations exhibiting an improvement in probability level at Visit 5 is indicated below the shading whilst the number of locations exhibiting a deterioration in probability level at Visit 5 is indicated above the shading.

SITA Standard

SITA Standard	NS	<5%	<2%	<1%	<0,5%
NS	1298	54	20	10	3
<5%	57	8	1	0	4
<2%	22	1	0	1	1
<1%	9	2	1	3	2
<0,5%	7	0	0	1	3

SITA Standard

SITA Standard	NS	<5%	<2%	<1%	<0,5%
NS	1305	49	19	6	7
<5%	56	2	3	2	1
<2%	26	6	2	0	3
<1%	10	1	0	1	0
<0,5%	3	0	2	2	2

SITA Fast

SITA Fast	NS	<5%	<2%	<1%	<0,5%
NS	1294	52	12	6	2
<5%	68	8	0	2	0
<2%	24	5	2	1	0
<1%	21	2	0	0	1
<0,5%	10	0	0	0	0

SITA Fast

SITA Fast	NS	<5%	<2%	<1%	<0,5%
NS	1284	62	17	10	3
<5%	67	10	4	2	0
<2%	23	5	0	0	1
<1%	11	5	0	0	0
<0,5%	3	1	0	0	0

SITA SWAP

SITA SWAP	NS	<5%	<2%	<1%	<0,5%
NS	1310	29	8	2	4
<5%	56	7	6	0	2
<2%	35	3	1	0	2
<1%	12	0	0	0	1
<0,5%	18	5	2	3	2

SITA SWAP

SITA SWAP	NS	<5%	<2%	<1%	<0,5%
NS	1293	42	15	8	3
<5%	52	9	3	1	1
<2%	23	4	2	2	0
<1%	16	2	0	1	1
<0,5%	18	5	2	2	3

Table 3.13a The magnitudes of the Pattern Deviation probability levels between Visit 1 (ordinate) and Visit 5 (abscissa), across all locations for the normal individuals for the right eye (left column) and left eye (right column). Top: SITA Standard. Middle: SITA Fast. Bottom: SITA SWAP. The shading indicates the number of locations exhibiting identical probability levels at the two examinations. The number of locations exhibiting an improvement in probability level at Visit 5 is indicated below the shading. The number of locations exhibiting a deterioration in probability level at Visit 5 is indicated above the shading.

The extent of the improvement in the Pattern Deviation probability level between Visit 1 and Visit 5 for the normal individuals (Table 3.13a) was relatively small for both SAP algorithms. (The number of locations exhibiting an improvement in probability level with the SITA Standard algorithm for the right eye was 100, and the number exhibiting a deterioration was 96, [no overall improvement] and in the

left eye 106 and 90, respectively [a 1.2 fold overall improvement]. For SITA Fast, the improvement occurred at 130 locations and the deterioration at 76 locations for the right eye, [a 1.7 fold overall improvement] and for the left eye 115 and 99 locations, respectively [a 1.2 fold overall improvement]. An improvement for SITA SWAP in the right eye occurred at 134 locations and a deterioration at 54 locations [a 2.5 fold overall improvement]. For the left eye, 124 locations in the left eye exhibited an improvement and 76 exhibited a deterioration [a 1.6 fold overall improvement]). These improvements were less than those for the improvement in the Total Deviation probability level. Again, the majority of the locations, for each of the three algorithms, which exhibited a change in probability level between the two visits, exhibited either an improvement from the 5% probability level to normal or a deterioration from normal to the 5% probability level.

SITA Standard

SITA Standard	NS	<5%	<2%	<1%	<0,5%
NS	1096	55	7	4	0
<5%	69	6	1	2	1
<2%	21	6	1	1	0
<1%	16	1	1	2	0
<0,5%	7	2	0	1	0

SITA Standard

SITA Standard	NS	<5%	<2%	<1%	<0,5%
NS	1094	58	13	8	7
<5%	52	7	6	5	1
<2%	20	5	2	0	0
<1%	12	1	1	1	0
<0,5%	3	0	0	2	2

SITA Fast

SITA Fast	NS	<5%	<2%	<1%	<0,5%
NS	1092	62	12	4	6
<5%	60	10	5	2	0
<2%	27	3	2	3	0
<1%	6	3	1	0	0
<0,5%	1	0	0	0	1

SITA Fast

SITA Fast	NS	<5%	<2%	<1%	<0,5%
NS	1078	47	16	10	4
<5%	75	16	2	4	0
<2%	17	1	1	2	1
<1%	17	1	0	0	1
<0,5%	2	2	1	0	2

SITA SWAP

SITA SWAP	NS	<5%	<2%	<1%	<0,5%
NS	1053	44	13	3	4
<5%	60	11	5	1	2
<2%	35	3	1	1	0
<1%	20	3	1	3	1
<0,5%	27	5	1	1	2

SITA SWAP

SITA SWAP	NS	<5%	<2%	<1%	<0,5%
NS	1084	45	12	4	5
<5%	59	13	4	0	2
<2%	16	4	0	1	1
<1%	10	3	2	0	0
<0,5%	20	4	1	2	8

Table 3.13b The magnitudes of the Pattern Deviation probability levels between Visit 1 (ordinate) and Visit 5 (abscissa), across all locations for the individuals with OHT for the right eye (left column) and left eye (right column). Top: SITA Standard. Middle: SITA Fast. Bottom: SITA SWAP. The shading indicates the number of locations exhibiting identical probability levels at the two examinations. The number of locations exhibiting an improvement in probability level at Visit 5 is indicated below the shading. The number of locations exhibiting a deterioration in probability level at Visit 5 is indicated above the shading.

The extent of the improvement in the Pattern Deviation probability level between Visit 1 and Visit 5 for the individuals with OHT (Table 3.13b) was relatively small for all three algorithms. (The number of locations exhibiting an improvement in probability level with the SITA Standard algorithm for the right eye was 124, and the number exhibiting a deterioration was 71, [a 1.7 fold overall improvement] and

for the left eye 96 and 98, respectively [no overall improvement]. For SITA Fast, the improvement occurred at 101 locations and a deterioration at 94 locations for the right eye, [a 1.1 fold overall improvement]. The corresponding results for the left eye were 116 and 87 locations, respectively [a 1.3 fold overall improvement]. An improvement for SITA SWAP in the right eye occurred at 156 locations and a deterioration at 74 locations [a 2.1 fold overall improvement]. For the left eye, 121 locations in the left eye exhibited an improvement and 74 exhibited a deterioration [a 1.6 fold overall improvement]). These improvements were less than those for the improvement in the Total Deviation probability level. Again, the majority of the locations, for each of the three algorithms, which exhibited a change in probability level between the two visits, exhibited either an improvement from the 5% probability level to normal or a deterioration from normal to the 5% probability level.

SITA Standard	NS	<5%	<2%	<1%	<0,5%
NS	1038	44	12	9	6
<5%	55	6	2	1	1
<2%	27	4	1	2	7
<1%	15	1	4	3	6
<0,5%	6	2	3	5	40

SITA Standard	NS	<5%	<2%	<1%	<0,5%
NS	1032	41	6	5	8
<5%	62	11	9	4	0
<2%	24	2	1	1	5
<1%	14	5	1	4	3
<0,5%	26	7	1	6	22

SITA Fast	NS	<5%	<2%	<1%	<0,5%
NS	1027	54	18	6	3
<5%	63	6	5	2	1
<2%	20	5	1	1	0
<1%	20	2	5	0	2
<0,5%	18	3	1	5	32

SITA Fast	NS	<5%	<2%	<1%	<0,5%
NS	983	60	16	10	12
<5%	71	7	4	5	2
<2%	29	3	4	3	2
<1%	25	6	8	10	6
<0,5%	5	6	6	8	9

SITA SWAP	NS	<5%	<2%	<1%	<0,5%
NS	971	62	16	9	13
<5%	73	10	2	6	1
<2%	34	2	1	0	3
<1%	13	1	2	1	1
<0,5%	33	12	4	1	29

SITA SWAP	NS	<5%	<2%	<1%	<0,5%
NS	1005	46	13	7	11
<5%	76	13	1	2	5
<2%	22	8	0	5	4
<1%	20	1	0	1	1
<0,5%	33	5	9	2	10

Table 3.13c The magnitudes of the Pattern Deviation probability levels between Visit 1 (ordinate) and Visit 5 (abscissa), across all locations for the individuals with OAG for the right eye (left column) and left eye (right column). Top: SITA Standard. Middle: SITA Fast. Bottom: SITA SWAP. The shading indicates the number of locations exhibiting identical probability levels at the two examinations. The number of locations exhibiting an improvement in probability level at Visit 5 is indicated below the shading. The number of locations exhibiting a deterioration in probability level at Visit 5 is indicated above the shading.

For the individuals with OAG, the extent of the improvement in the Pattern Deviation probability level between Visit 1 and Visit 5 (Table 3.12c) was, in general, similar for all algorithms. (For the SITA Standard algorithm, 122 locations in the right eye exhibited an improvement and 90 locations exhibited a deterioration [a 1.4 fold overall improvement]; 148 locations in the left eye exhibited an

improvement and 82 locations exhibited a deterioration [a 1.8 fold overall improvement]. For the SITA Fast algorithm, 142 locations in the right eye exhibited an improvement and 92 locations exhibited a deterioration [a 1.5 fold overall improvement]; 167 locations in the left eye exhibited an improvement and 120 locations exhibited deterioration [a 1.4 fold overall improvement]. The extent of the improvement for the SITA SWAP algorithm was slightly greater for the left eye than that for the right (right eye, 175 locations exhibited an improvement and 113 locations exhibited a deterioration [a 1.5 fold overall improvement]: left eye, 176 locations exhibited an improvement and 95 locations exhibited a deterioration [a 1.9 fold overall improvement]). As it was the case with the Total Deviation probability level, the majority of the locations, for each of the three algorithms, which exhibited a change in probability level between the two visits exhibited either an improvement from the 5% probability level to normal or a deterioration from normal to the 5% probability level.

3.4.2 The within-individual within-algorithm between-visit (Visits 4 and 5) variability

The within-algorithm differences in the MD index between Visits 4 and 5 for each of the three algorithms, for each of the three groups of individuals and for the three groups, combined, are summarised in Table 3.14 and are illustrated in Figures 3.11a to 3.11d. The mean of the differences approximated to zero for each algorithm in each group indicating very little, if any, improvement in sensitivity/ learning effect between Visits 4 and 5.

Algorithm	Eye	Normal	OHT	OAG	All groups
SITA Standard	RE	3.61dB	1.88 dB	2.20 dB	2.72 dB
	LE	3.67 dB	3.57 dB	2.36 dB	3.23 dB
SITA Fast	RE	2.66 dB	3.27 dB	3.78 dB	3.27 dB
	LE	2.47 dB	3.37 dB	2.75 dB	2.83 dB
SITA SWAP	RE	4.54 dB	5.05 dB	3.42 dB	4.48 dB
	LE	3.88 dB	4.80 dB	4.80 dB	4.50 dB

Table 3.14 The within-individual within-algorithm differences in the MD between Visits 4 and 5 expressed as the range of the limits of agreement (defined as the mean of the differences +/- 1.96SD) for the three algorithms for each eye of the three groups of individuals and for the three groups, combined.

The range of the limits of agreement for the difference in MD was wider for the SITA Fast algorithm compared to the SITA Standard algorithm for the individuals with OHT and for the individuals with OAG. However, for the normal group who were naïve to any form of perimetry, the range was wider for the SITA Standard algorithm compared to the SITA Fast algorithm. The range for the SITA SWAP algorithm was substantially wider than for either SAP algorithm for each of the three diagnostic groups.

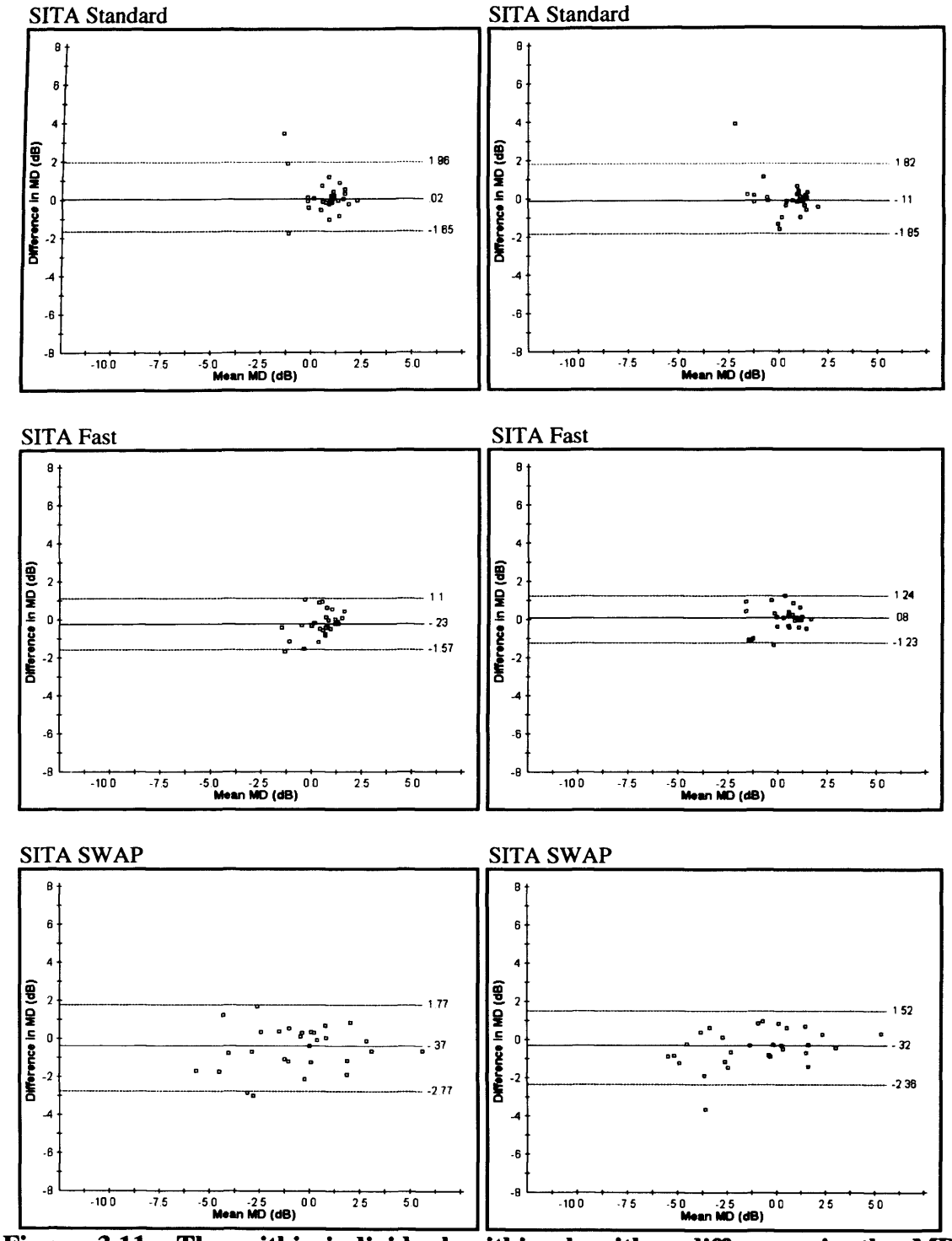

Figure 3.11a The within-individual within-algorithm difference in the MD between Visits 4 and 5 against the mean of the two MDs for the right eye (left column) and for the left eye (right column) for the normal individuals. Top: SITA Standard. Middle: SITA Fast. Bottom: SITA SWAP. The solid line indicates the mean of the differences and the upper and lower dotted lines the mean of the differences +/- 1.96SD, respectively.

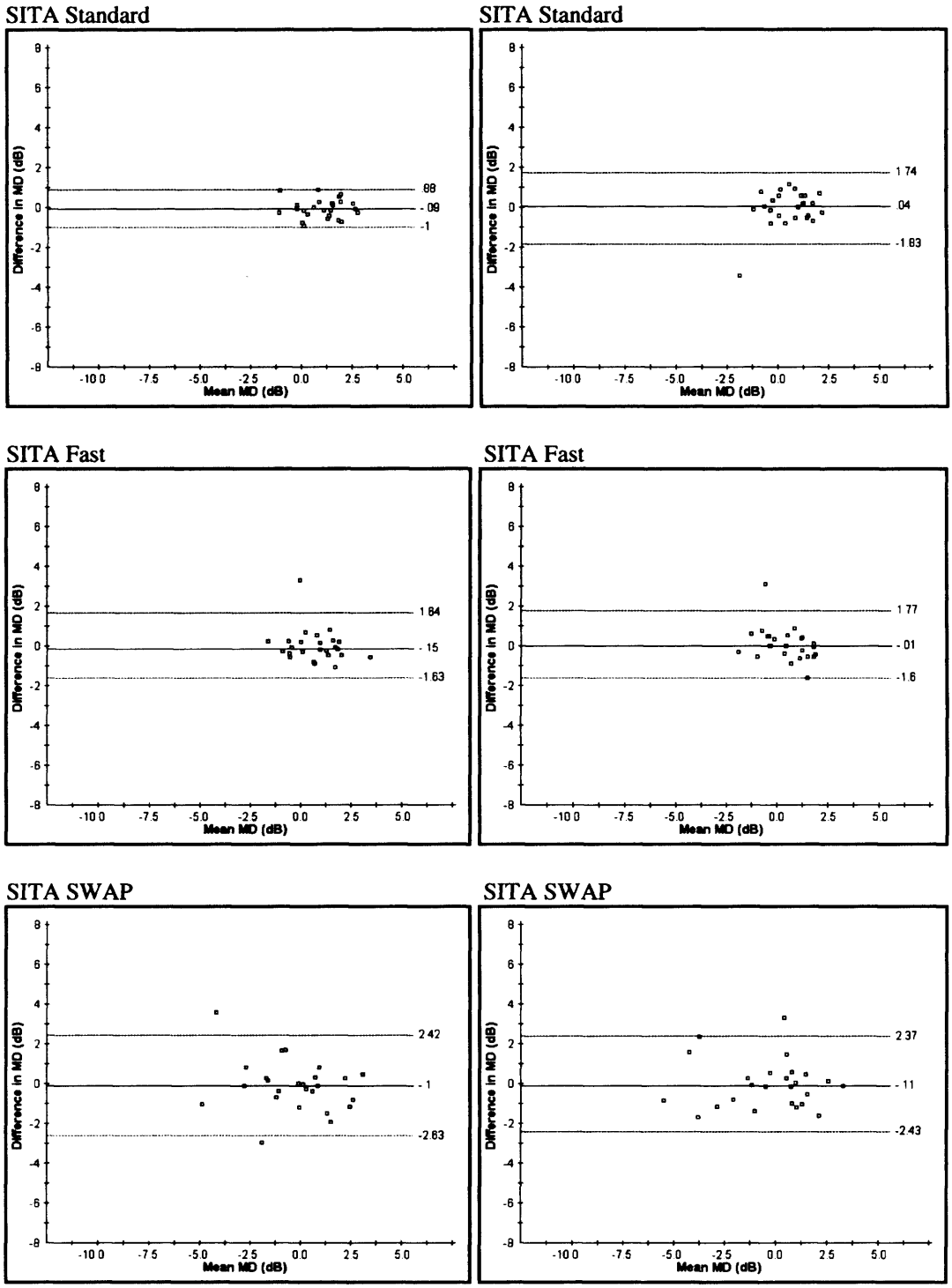

Figure 3.11b The within-individual within-algorithm difference in the MD between Visits 4 and 5 against the mean of the two MDs for the right eye (left column) and for the left eye (right column) for the individuals with OHT. Top: SITA Standard. Middle: SITA Fast. Bottom: SITA SWAP. The solid line indicates the mean of the differences and the upper and lower dotted lines the mean of the differences +/- 1.96SD, respectively.

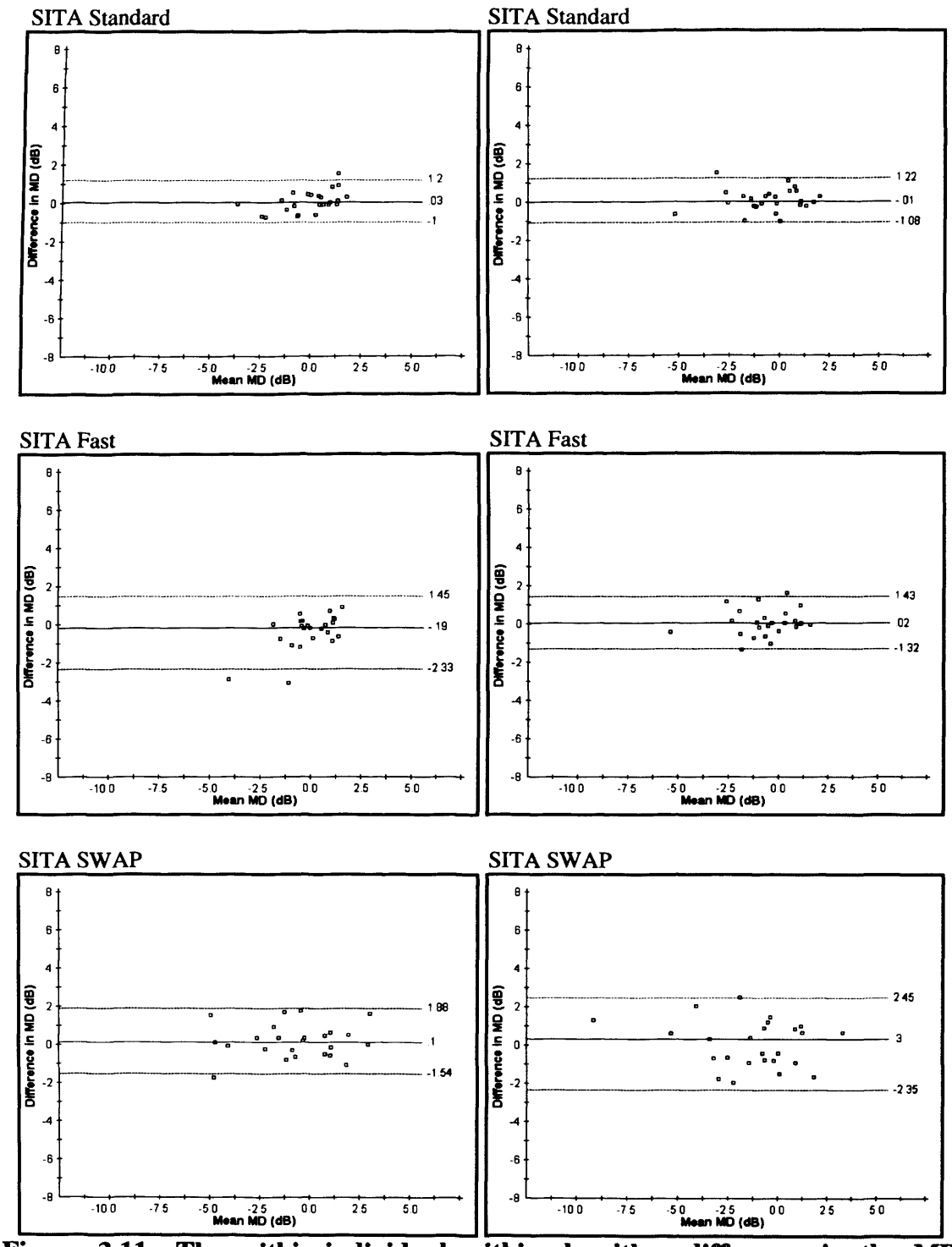

Figure 3.11c The within-individual within-algorithm difference in the MD between Visits 4 and 5 against the mean of the two MDs for the right eye (left column) and for the left eye (right column) for the individuals with OAG. Top: SITA Standard. Middle: SITA Fast. Bottom: SITA SWAP. The solid line indicates the mean of the differences and the upper and lower dotted lines the mean of the differences +/- 1.96SD, respectively.

groups, combined, are summarised in Table 3.15 and are illustrated in Figures 3.12a to 3.12d. The mean of the differences approximated to zero in each eye for each algorithm in each group indicating very little, if any, improvement in sensitivity/ learning effect between Visits 4 and 5.

Algorithm	Eye	Normal	OHT	OAG	All groups
SITA Standard	RE	2.06 dB	1.03 dB	1.89 dB	1.75 dB
	LE	2.71 dB	6.59 dB	1.42 dB	4.11 dB
SITA Fast	RE	1.19 dB	1.21 dB	2.53 dB	1.80 dB
	LE	1.10 dB	5.03 dB	3.04 dB	3.37 dB
SITA SWAP	RE	1.66 dB	1.72 dB	2.71 dB	2.04 dB
	LE	1.31 dB	1.83 dB	3.52 dB	2.38 dB

Table 3.15 The within-individual within-algorithm differences in the PSD between Visits 4 and 5 expressed as the range of the limits of agreement (defined as the mean of the differences +/- 1.96SD) for the three algorithms for each eye for each of the three groups of individuals and for the three groups, combined.

The range of the limits of agreement for the difference in PSD was wider for the SITA Fast algorithm compared to the SITA Standard algorithm for the individuals with OHT and for the individuals with OAG. However, for the normal group who were naïve to any form of perimetry, the range was wider for the SITA Standard algorithm compared to the SITA Fast algorithm. The range for the SITA SWAP algorithm was substantially wider than for either SAP algorithm for each of the three diagnostic groups.

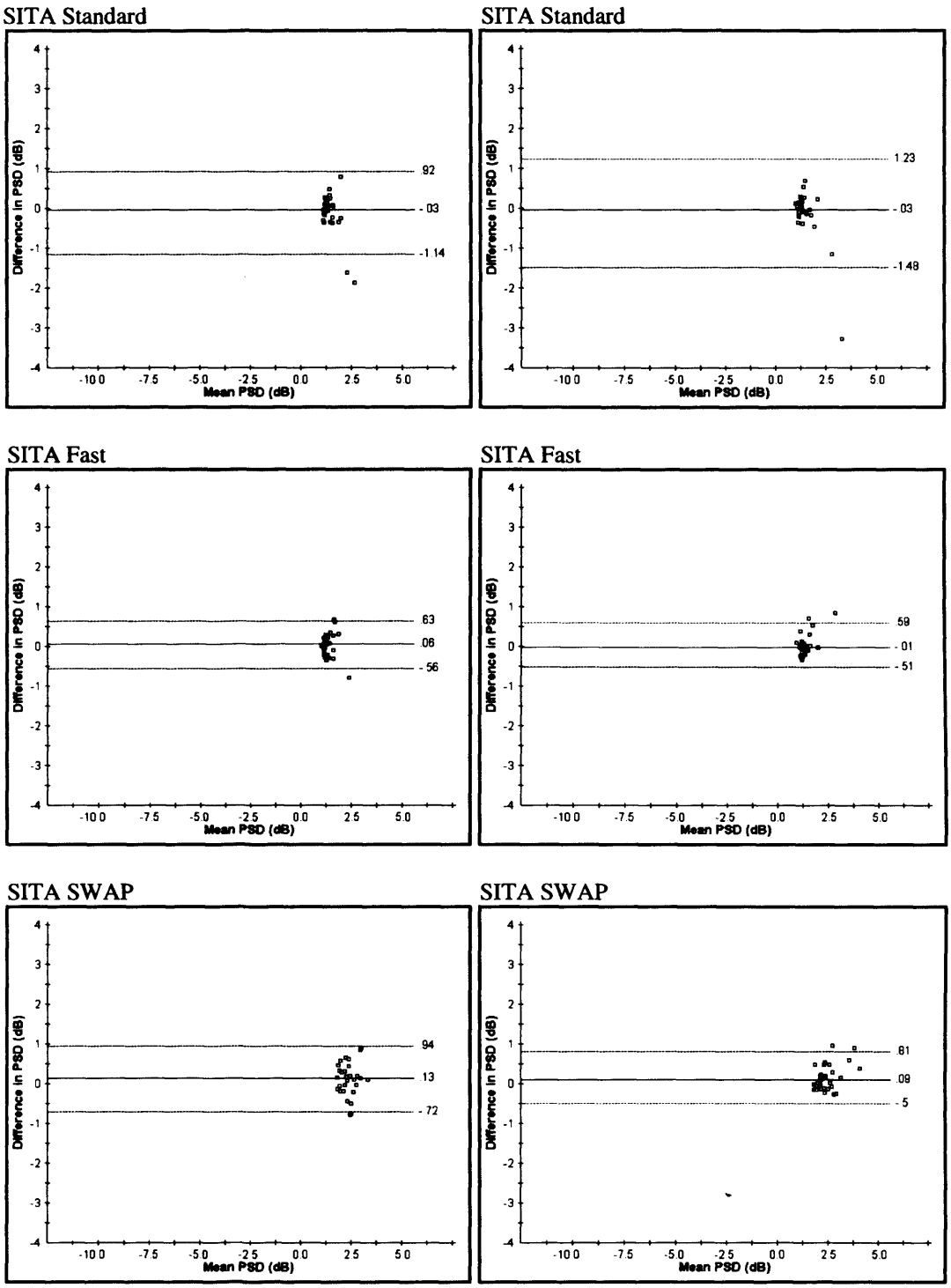

Figure 3.12a The within-individual within-algorithm difference in the PSD between Visits 4 and 5 against the mean of the two PSDs for the right eye (left column) and for the left eye (right column) for the normal individuals. Top: SITA Standard. Middle: SITA Fast. Bottom: SITA SWAP. The solid line indicates the mean of the differences and the upper and lower dotted lines the mean of the differences +/- 1.96SD, respectively.

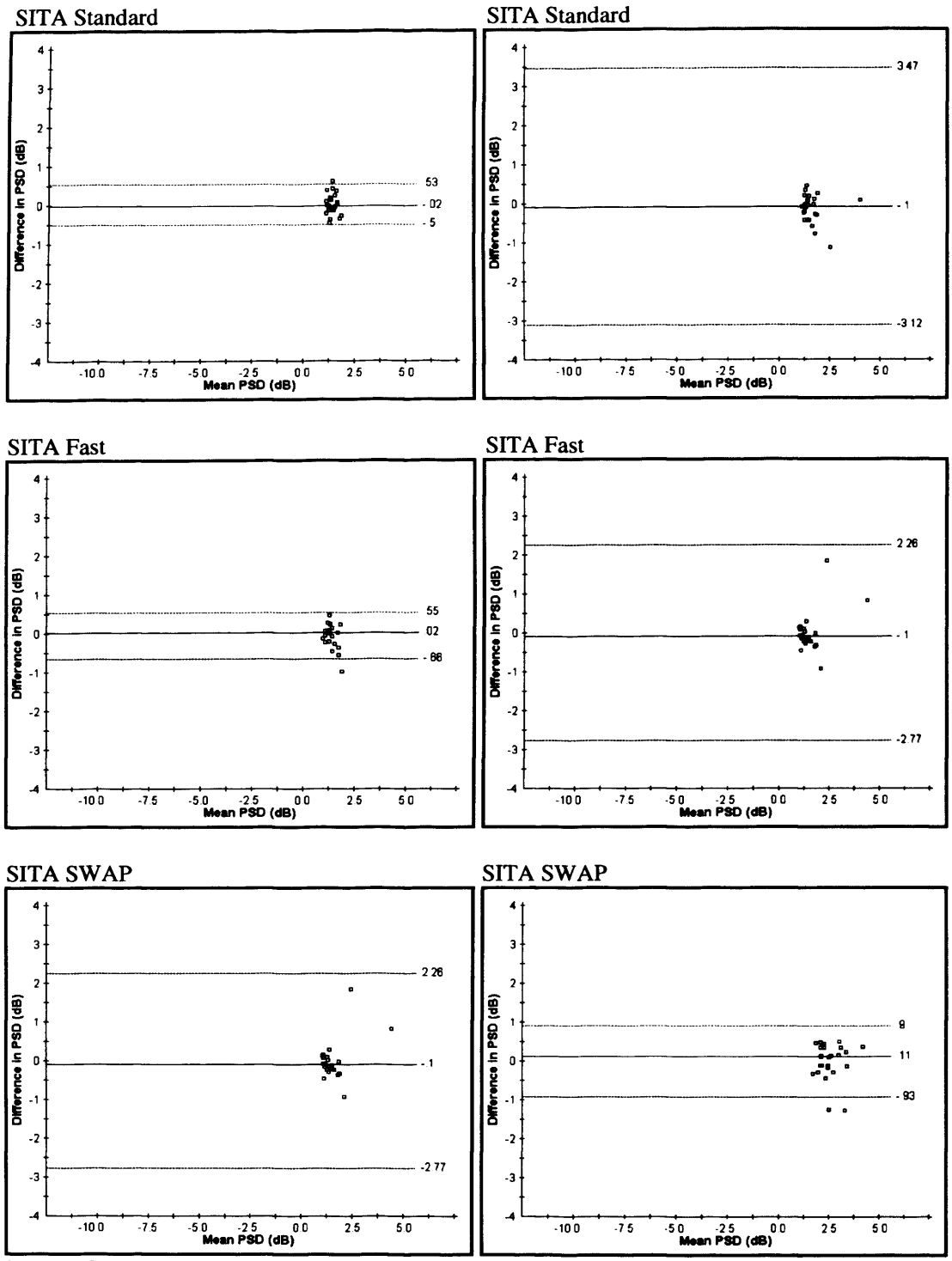

Figure 3.12b The within-individual within-algorithm difference in the PSD between Visits 4 and 5 against the mean of the two PSDs for the right eye (left column) and for the left eye (right column) for the individuals with OHT. Top: SITA Standard. Middle: SITA Fast. Bottom: SITA SWAP. The solid line indicates the mean of the differences and the upper and lower dotted lines the mean of the differences +/- 1.96SD, respectively.

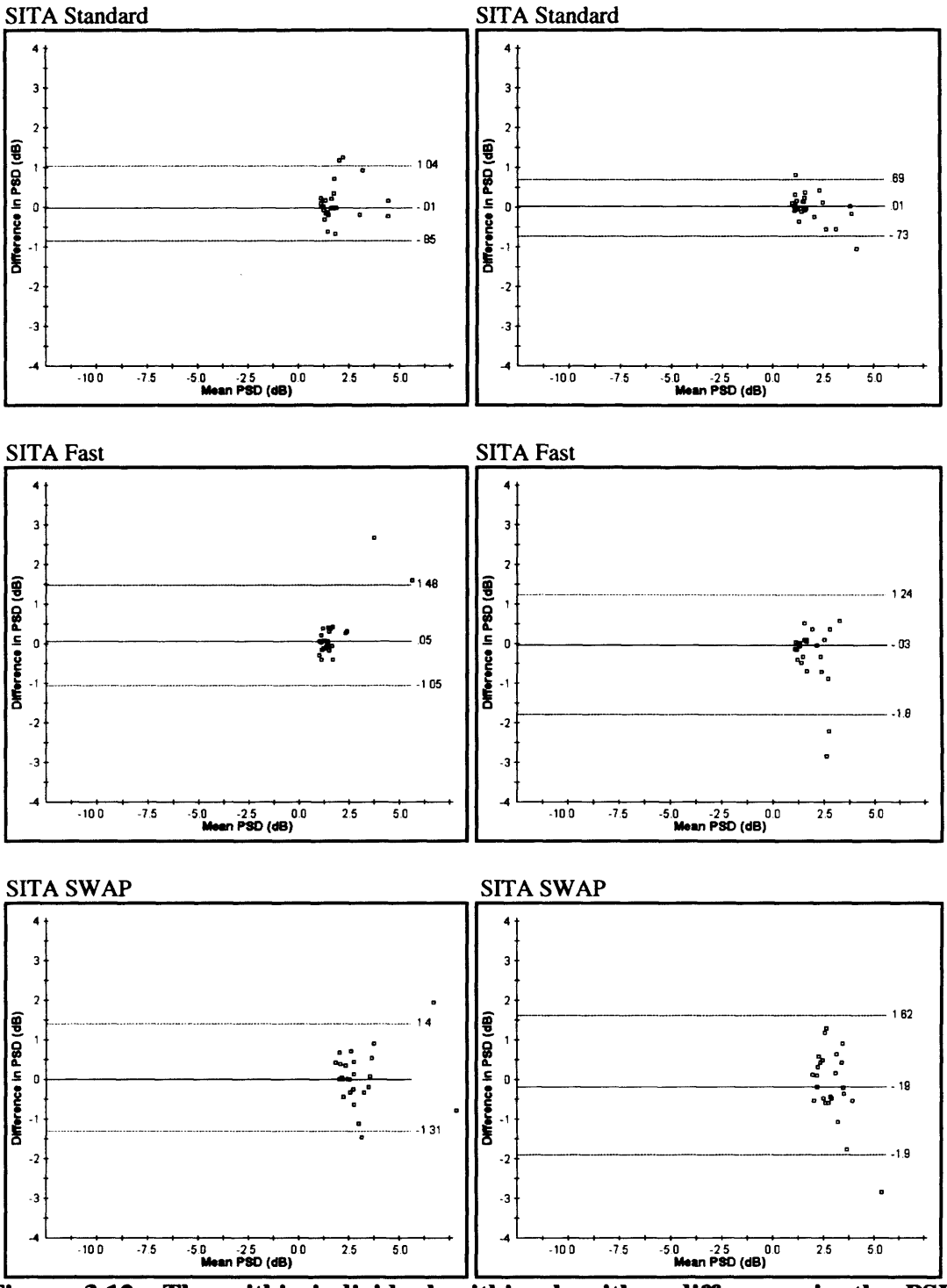

Figure 3.12c The within-individual within-algorithm difference in the PSD between Visits 4 and 5 against the mean of the two PSDs for the right eye (left column) and for the left eye (right column) for the individuals with OAG. Top: SITA Standard. Middle: SITA Fast. Bottom: SITA SWAP. The solid line indicates the mean of the differences and the upper and lower dotted lines the mean of the differences +/- 1.96SD, respectively.

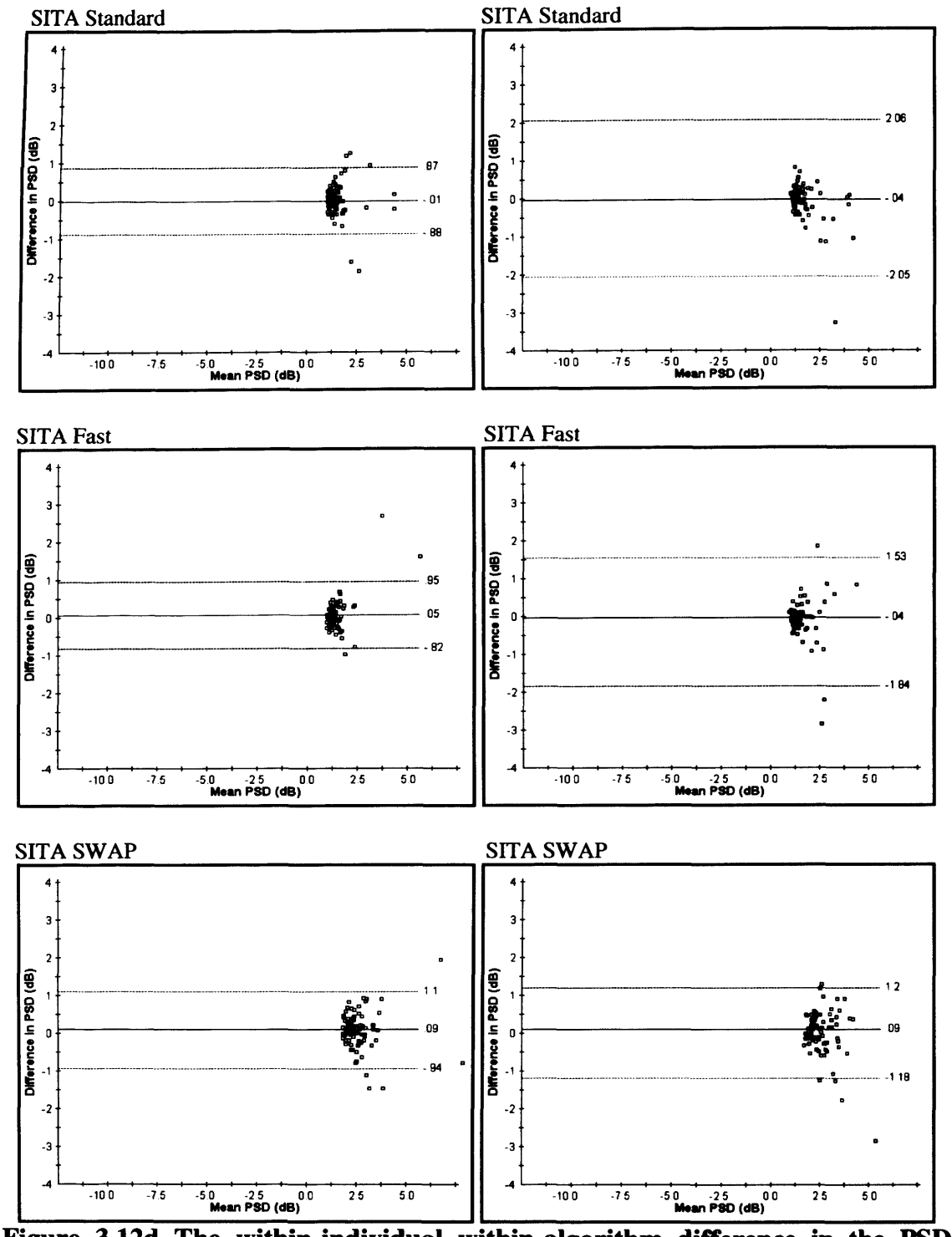

Figure 3.12d The within-individual within-algorithm difference in the PSD between Visits 4 and 5 against the mean of the two PSDs for the right eye (left column) and for the left eye (right column) for the three groups, combined. Top: SITA Standard. Middle: SITA Fast. Bottom: SITA SWAP. The solid line indicates the mean of the differences and the upper and lower dotted lines the mean of the differences +/- 1.96SD, respectively.

The within-individual within-algorithm between-visit difference in sensitivity across each stimulus location expressed as the distribution of the difference in sensitivity at

each location between Visits 4 and 5 as a function of the sensitivity at the corresponding stimulus location recorded at Visit 4 is shown in Figures 3.13a to 3.13d for each eye of each of the three groups. In this format, a positive slope for the percentiles indicates an improvement in sensitivity.

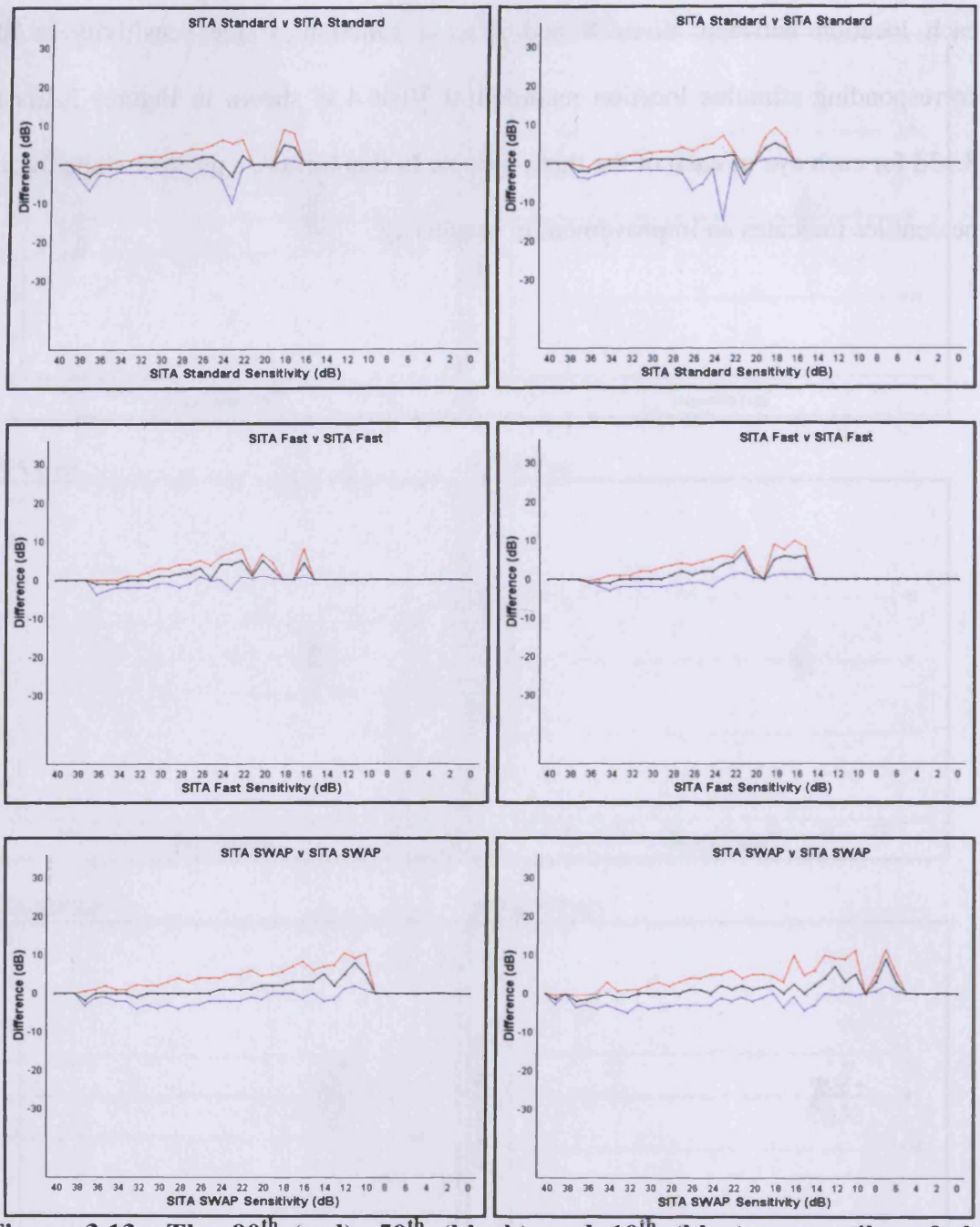

Figure 3.13a The 90th (red), 50th (black) and 10th (blue) percentiles of the distribution of the within-individual within-algorithm between-visit difference in sensitivity across all stimulus locations for the normal individuals between Visit 4 and 5 as a function of the sensitivity at the corresponding stimulus location recorded at Visit 4: right eye, left column; left eye, right column. Top: SITA Standard. Middle: SITA Fast. Bottom: SITA SWAP.

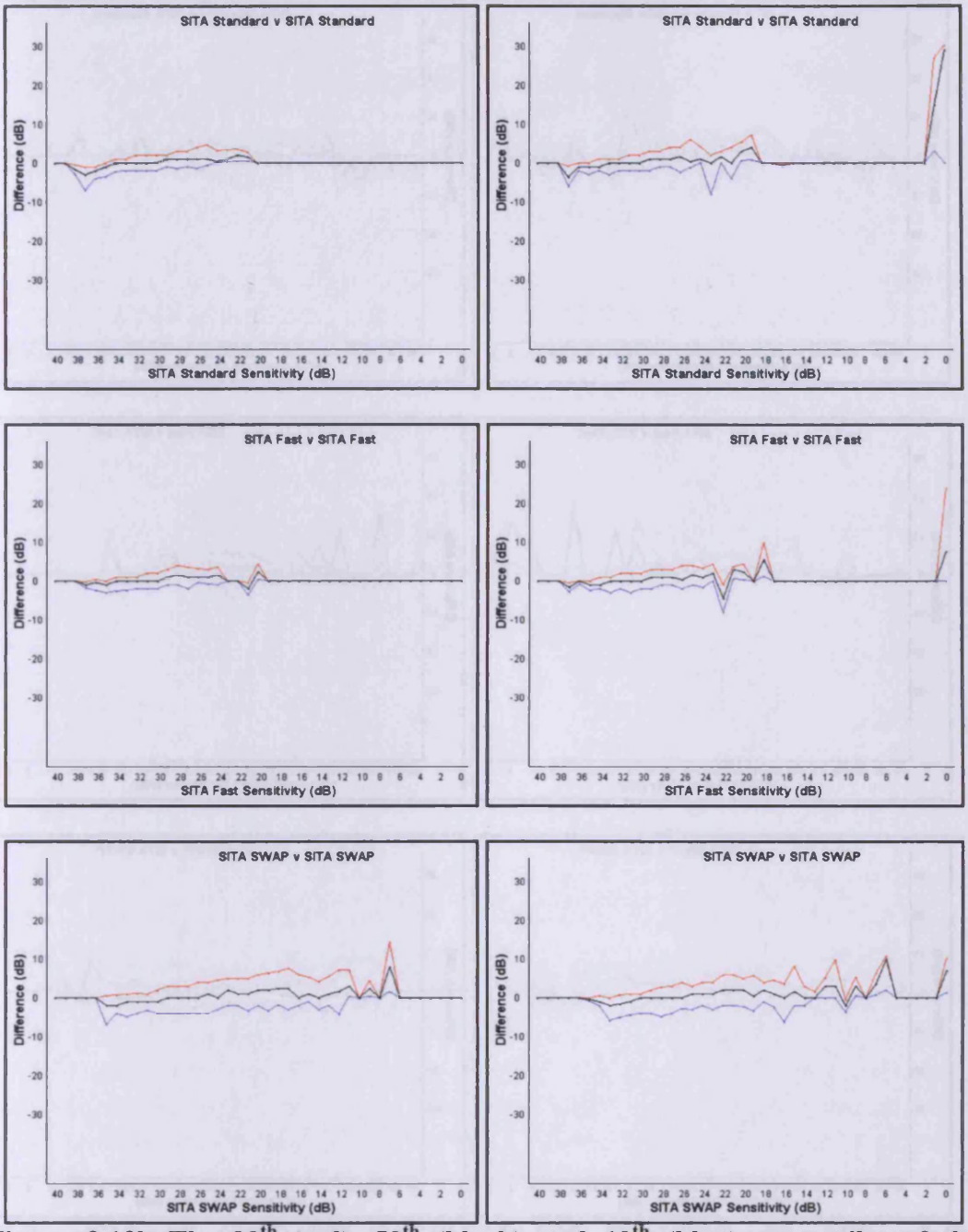

Figure 3.13b The 90th (red), 50th (black) and 10th (blue) percentiles of the distribution of the within-individual within-algorithm between-visit difference in sensitivity across all stimulus locations for the individuals with OHT between Visit 4 and 5 as a function of the sensitivity at the corresponding stimulus location recorded at Visit 4: right eye, left column; left eye, right column. Top: SITA Standard. Middle: SITA Fast. Bottom: SITA SWAP.

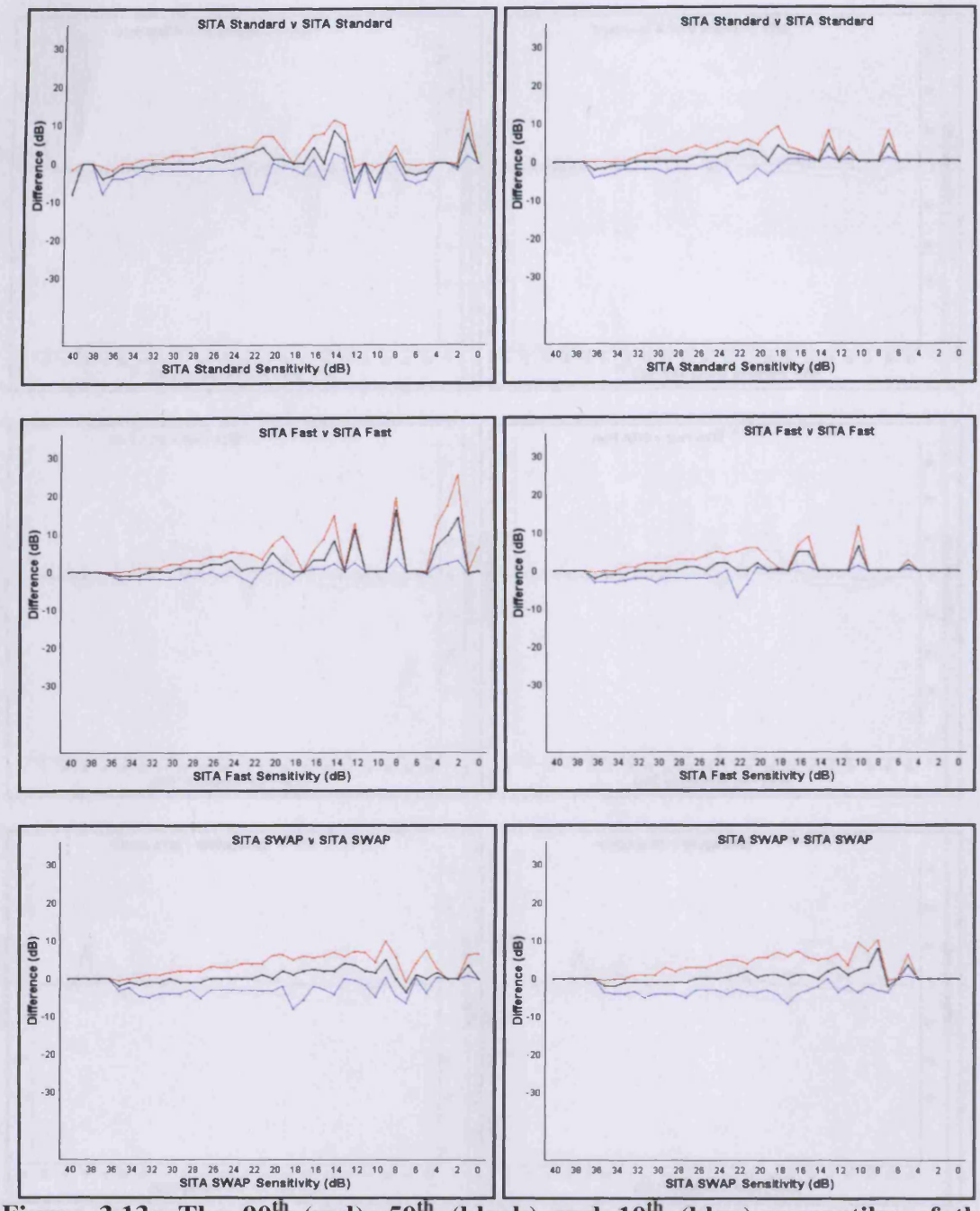

Figure 3.13c The 90th (red), 50th (black) and 10th (blue) percentiles of the distribution of the within-individual within-algorithm between-visit difference in sensitivity across all stimulus locations for the individuals with OAG between Visit 4 and 5 as a function of the sensitivity at the corresponding stimulus location recorded at Visit 4: right eye, left column; left eye, right column. Top: SITA Standard. Middle: SITA Fast. Bottom: SITA SWAP.

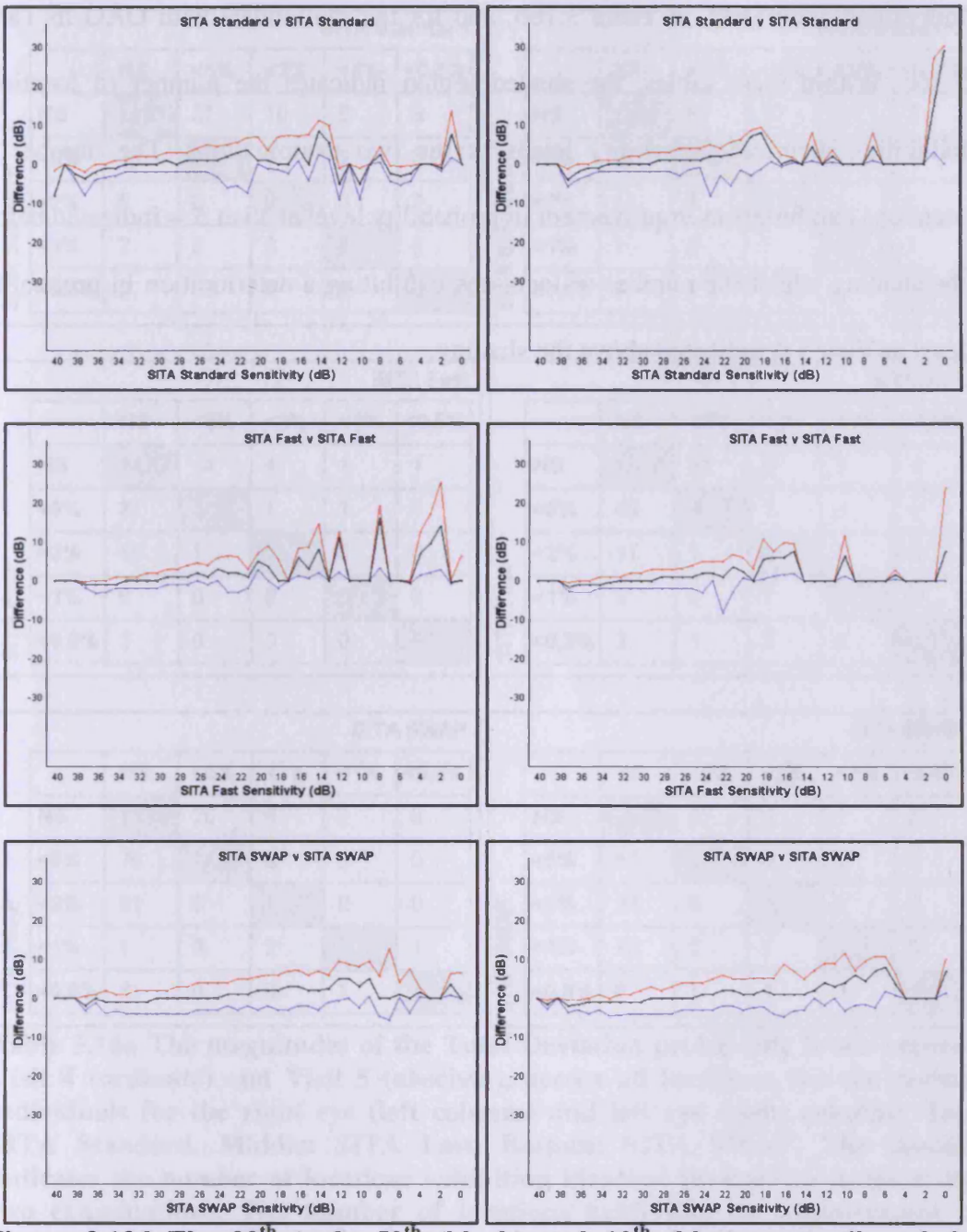

Figure 3.13d The 90th (red), 50th (black) and 10th (blue) percentiles of the distribution of the within-individual within-algorithm between-visit difference in sensitivity across all stimulus locations for the individuals in all three groups, combined, between Visit 4 and 5 as a function of the sensitivity at the corresponding stimulus location recorded at Visit 4: right eye, left column; left eye, right column. Top: SITA Standard. Middle: SITA Fast. Bottom: SITA SWAP.

The magnitudes of the differences between the Total Deviation probability levels at Visit 4 and at Visit 5, across all locations, for each algorithm are illustrated for the right and for the left eyes for the normal individuals in Table 3.16a for the

individuals with OHT in Table 3.16b, and for the individuals with OAG in Table 3.16c. Within these tables, the shaded region indicates the number of locations exhibiting identical probability levels at the two examinations. The number of locations exhibiting an improvement in probability level at Visit 5 is indicated below the shading whilst the number of locations exhibiting a deterioration in probability level at Visit 5 is indicated above the shading.

SITA Standard

SITA Standard	NS	<5%	<2%	<1%	<0,5%
NS	1425	31	10	5	8
<5%	15	0	1	2	2
<2%	5	0	0	0	0
<1%	2	0	0	0	0
<0,5%	2	0	0	0	0

SITA Standard

SITA Standard	NS	<5%	<2%	<1%	<0,5%
NS	1389	34	13	8	7
<5%	26	9	2	0	4
<2%	11	0	0	1	0
<1%	3	0	0	0	0
<0,5%	1	0	0	0	0

SITA Fast

SITA Fast	NS	<5%	<2%	<1%	<0,5%
NS	1426	14	4	1	1
<5%	31	3	1	1	1
<2%	15	1	0	0	0
<1%	6	0	0	0	0
<0,5%	3	0	0	0	0

SITA Fast

SITA Fast	NS	<5%	<2%	<1%	<0,5%
NS	1377	37	5	2	1
<5%	45	5	1	3	1
<2%	11	1	0	3	0
<1%	9	1	1	1	0
<0,5%	3	1	0	0	0

SITA SWAP

SITA SWAP	NS	<5%	<2%	<1%	<0,5%
NS	1339	26	9	2	0
<5%	70	14	3	2	0
<2%	21	9	1	0	0
<1%	1	3	2	0	1
<0,5%	3	0	0	1	1

SITA SWAP

SITA SWAP	NS	<5%	<2%	<1%	<0,5%
NS	1280	57	9	1	0
<5%	67	24	4	1	1
<2%	20	6	0	1	0
<1%	12	2	1	0	0
<0,5%	6	1	1	3	1

Table 3.16a The magnitudes of the Total Deviation probability levels between Visit 4 (ordinate) and Visit 5 (abscissa), across all locations, for the normal individuals for the right eye (left column) and left eye (right column). Top: SITA Standard. Middle: SITA Fast. Bottom: SITA SWAP. The shading indicates the number of locations exhibiting identical probability levels at the two examinations. The number of locations exhibiting an improvement in probability level at Visit 5 is indicated below the shading. The number of locations exhibiting a deterioration in probability level at Visit 5 is indicated above the shading.

The normal individuals exhibited a net overall reduction in the Total Deviation probability level for the STIA Standard algorithm between Visit 4 and Visit 5 (Table 3.16a) (right eye, 24 locations exhibited an improvement and 59 locations exhibited a deterioration [a 2.5 fold overall reduction]; left eye, 41 locations exhibited an improvement and 69 locations exhibiting a deterioration [a 1.7 fold overall

reduction]). However, an improvement was present for the SITA Fast algorithm particularly in the right eye between the two visits (right eye, 56 locations exhibited an improvement, 23 locations exhibiting a deterioration [a 2.4 fold overall improvement]; left eye, 72 locations exhibited an improvement, 53 locations exhibited deterioration [a 1.4 fold overall improvement]). The SITA SWAP algorithm exhibited a similar improvement between the two visits to the SITA Fast algorithm in each eye (right eye, 110 locations exhibiting an improvement, 43 locations exhibiting a deterioration [a 2.6 fold overall improvement]; left eye, 119 locations exhibiting an improvement, 74 locations exhibiting a deterioration [a 1.6 fold overall improvement]). The majority of the locations, for each of the three algorithms, which exhibited a change in probability level between the two visits, exhibited either an improvement from the 5% probability level to normal or a deterioration from normal to the 5% probability level.

SITA Standard

SITA Standard	NS	<5%	<2%	<1%	<0,5%
NS	1269	14	1	0	0
<5%	9	4	0	0	0
<2%	0	1	0	0	0
<1%	0	2	0	0	0
<0,5%	0	0	0	0	0

SITA Standard

SITA Standard	NS	<5%	<2%	<1%	<0,5%
NS	1224	28	5	3	3
<5%	21	1	0	0	0
<2%	2	0	1	0	0
<1%	1	0	0	0	0
<0,5%	9	0	0	0	2

SITA Fast

SITA Fast	NS	<5%	<2%	<1%	<0,5%
NS	1225	20	6	4	2
<5%	22	8	2	1	0
<2%	7	0	3	1	0
<1%	0	1	0	0	0
<0,5%	0	0	0	0	0

SITA Fast

SITA Fast	NS	<5%	<2%	<1%	<0,5%
NS	1202	30	10	6	3
<5%	25	8	3	0	1
<2%	3	1	0	1	0
<1%	3	1	0	0	0
<0,5%	1	0	0	1	1

SITA SWAP

SITA SWAP	NS	<5%	<2%	<1%	<0,5%
NS	1188	22	5	2	4
<5%	38	10	4	1	2
<2%	5	1	4	1	0
<1%	1	0	0	1	0
<0,5%	0	0	1	0	0

SITA SWAP

SITA SWAP	NS	<5%	<2%	<1%	<0,5%
NS	1177	32	8	1	2
<5%	23	17	7	2	2
<2%	9	6	3	0	0
<1%	1	1	1	0	0
<0,5%	4	1	1	0	2

Table 3.16b The magnitudes of the Total Deviation probability levels between Visit 4 (ordinate) and Visit 5 (abscissa), across all locations for the individuals with OHT for the right eye (left column) and left eye (right column). Top: SITA Standard. Middle: SITA Fast. Bottom: SITA SWAP. The shading indicates the number of locations exhibiting identical probability levels at the two examinations. The number of locations exhibiting an improvement in probability level at Visit 5 is indicated below the shading. The number of locations exhibiting a deterioration in probability level at Visit 5 is indicated above the shading.

The individuals with OHT exhibited little alteration in the Total Deviation probability level for the STIA Standard algorithm between Visit 4 and Visit 5 (Table 3.16b) (right eye, 12 locations exhibited an improvement and 15 locations exhibited a deterioration; left eye, 33 locations exhibited an improvement and 39 locations exhibiting a deterioration [a 1.3 fold overall reduction]). A reduction was also

exhibited for the SITA Fast algorithm in each eye between the two visits (right eye, 30 locations exhibited an improvement, 36 locations exhibiting a deterioration [a 1.2 fold overall reduction]; left eye, 35 locations exhibited an improvement, 54 locations exhibited deterioration [a 1.5 fold overall reduction]). The SITA SWAP algorithm exhibited similar levels in each eye between the two visits (right eye, 46 locations exhibiting an improvement, 41 locations exhibiting a deterioration [a 1.1 fold overall improvement]; left eye, 47 locations exhibiting an improvement, 54 locations exhibiting a deterioration [a 1.1 fold overall reduction]). The majority of the locations, for each of the three algorithms, which exhibited a change in probability level between the two visits, exhibited either an improvement from the 5% probability level to normal or a deterioration from normal to the 5% probability level.

SITA Standard

SITA Standard	NS	<5%	<2%	<1%	<0,5%
NS	1112	21	8	3	2
<5%	27	13	4	2	3
<2%	9	0	2	1	4
<1%	7	4	1	2	1
<0,5%	6	3	5	6	54

SITA Standard

SITA Standard	NS	<5%	<2%	<1%	<0,5%
NS	1084	35	11	12	7
<5%	43	12	5	5	2
<2%	17	8	3	4	2
<1%	12	8	3	3	10
<0,5%	5	4	1	6	18

SITA Fast

SITA Fast	NS	<5%	<2%	<1%	<0,5%
NS	1115	21	4	2	0
<5%	36	11	2	1	1
<2%	14	4	3	1	0
<1%	6	6	5	9	2
<0,5%	10	3	1	5	38

SITA Fast

SITA Fast	NS	<5%	<2%	<1%	<0,5%
NS	1037	43	14	11	3
<5%	51	11	8	6	4
<2%	16	9	14	7	2
<1%	17	3	5	20	6
<0,5%	2	2	4	2	3

SITA SWAP

SITA SWAP	NS	<5%	<2%	<1%	<0,5%
NS	1109	43	10	4	2
<5%	29	11	3	1	2
<2%	8	5	2	1	2
<1%	3	2	0	2	0
<0,5%	2	7	1	4	47

SITA SWAP

SITA SWAP	NS	<5%	<2%	<1%	<0,5%
NS	1104	44	15	7	7
<5%	51	7	4	3	1
<2%	12	4	5	1	6
<1%	3	3	0	3	2
<0,5%	4	2	2	2	8

Table 3.16c The magnitudes of the Total Deviation probability levels between Visit 4 (ordinate) and Visit 5 (abscissa), across all locations for the individuals with OAG for the right eye (left column) and left eye (right column). Top: SITA Standard. Middle: SITA Fast. Bottom: SITA SWAP. The shading indicates the number of locations exhibiting identical probability levels at the two examinations. The number of locations exhibiting an improvement in probability level at Visit 5 is indicated below the shading. The number of locations exhibiting a deterioration in probability level at Visit 5 is indicated above the shading.

The individuals with OAG, in general, exhibited little improvement in the Total Deviation probability level for both SAP algorithms between Visit 4 and Visit 5 (Table 3.16c). (For the SITA Standard algorithm in the right eye, 68 locations exhibited an improvement and 49 locations a deterioration [a 1.4 fold overall

improvement]; in the left eye, 107 locations exhibited an improvement and 93 locations exhibited a deterioration [a 1.2 fold overall improvement]). An improvement was also exhibited for the SITA Fast algorithm in each eye between the two visits. (For the right eye, 90 locations exhibited an improvement and 34 a deterioration [a 2.6 fold overall improvement]; for the left eye, 111 locations exhibited an improvement and 104 locations a deterioration [a 1.1 fold overall improvement]. The SITA SWAP algorithm exhibited little deterioration in the Total deviation probability levels in each eye between the two visits, namely, for the right eye, 61 locations exhibited an improvement and 68 locations exhibited a deterioration [a 1.1 fold overall deterioration]; for the left eye, 83 locations exhibited an improvement and 90 locations exhibited a deterioration [a 1.1 fold overall deterioration]). The majority of the locations, for each of the three algorithms, which exhibited a change in probability level between the two visits, exhibited either an improvement from the 5% probability level to normal or a deterioration from normal to the 5% probability level.

The between-visit difference (between Visits 4 and 5) for each algorithm for each group is summarized in Table 3.17 for both the Total Deviation and the Pattern Deviation probability levels.

Algorithm	Eye	Normal	OHT	OAG
SITA Standard	RE	-2.5 /-1.6	-1.3 / 1.1	1.4 / 1.3
	LE	-1.7 /-1.4	-1.2 /-1.4	1.2 / 1.2
SITA Fast	RE	2.4 / 1.4	-1.2 /-1.1	2.6 / 1.2
	LE	1.4 / 1.0	-1.5 /-1.2	1.1 / 1.0
SITA SWAP	RE	2.6 / 1.1	1.1 / 1.0	-1.1 / -1.1
	LE	1.6 / 1.2	-1.1 / -1.1	-1.1 / 1.2

Table 3.17 The summary of the between-visit difference (Visits 4 and 5) expressed in terms of the ratio of the difference in the number of stimulus locations exhibiting an abnormal Total Deviation (Tables 3.16a to 3.16d) and Pattern Deviation probability level (Tables 3.18a to 3.18d) for each algorithm and for each group. The value before the oblique is the overall incremental change in the Total Deviation probability levels. The value after the oblique is the overall incremental change in the Pattern Deviation probability levels. (A positive value indicates an improvement i.e. a reduction in the number of stimulus locations exhibiting a significant, and/ or a less significant, probability level relative to Visit 4 and a negative value indicates a deterioration i.e. an increase in the number of stimulus locations exhibiting a significant and/ or more significant probability level relative to Visit 4).

The magnitudes of the differences between the Pattern Deviation probability levels at Visit 4 and at Visit 5, across all locations, for each algorithm are illustrated for the right and for the left eyes for the normal individuals in Table 3.18a for the individuals with OHT in Table 3.18b, and for the individuals with OAG in Table 3.18c. Within these tables, the shaded region indicates the number of locations exhibiting identical probability levels at the two examinations. The number of locations exhibiting an improvement in probability level at Visit 5 is indicated below the shading whilst the number of locations exhibiting deterioration in probability level at Visit 5 is indicated above the shading.

SITA Standard

SITA Standard	NS	<5%	<2%	<1%	<0,5%
NS	1328	57	20	11	10
<5%	46	6	2	2	1
<2%	10	1	0	2	2
<1%	6	1	0	0	0
<0,5%	3	0	0	0	0

SITA Standard

SITA Standard	NS	<5%	<2%	<1%	<0,5%
NS	1331	53	20	8	5
<5%	44	3	4	2	4
<2%	15	1	2	1	2
<1%	7	1	0	0	2
<0,5%	3	0	0	0	0

SITA Fast

SITA Fast	NS	<5%	<2%	<1%	<0,5%
NS	1312	50	10	9	2
<5%	75	13	4	0	1
<2%	19	1	0	0	0
<1%	9	1	0	0	0
<0,5%	2	0	0	0	0

SITA Fast

SITA Fast	NS	<5%	<2%	<1%	<0,5%
NS	1296	69	17	7	2
<5%	63	7	0	1	1
<2%	18	1	0	3	1
<1%	9	5	3	1	0
<0,5%	2	1	1	0	0

SITA SWAP

SITA SWAP	NS	<5%	<2%	<1%	<0,5%
NS	1368	34	13	2	4
<5%	34	7	3	1	0
<2%	18	3	1	1	2
<1%	6	0	0	0	3
<0,5%	5	0	0	1	2

SITA SWAP

SITA SWAP	NS	<5%	<2%	<1%	<0,5%
NS	1319	46	13	8	3
<5%	51	7	4	4	1
<2%	13	4	4	1	0
<1%	10	3	0	0	0
<0,5%	9	2	1	1	4

Table 3.18a The magnitudes of the Pattern Deviation probability levels between Visit 4 (ordinate) and Visit 5 (abscissa), across all locations for the normal individuals for the right eye (left column) and left eye (right column). Top: SITA Standard. Middle: SITA Fast. Bottom: SITA SWAP. The shading indicates the number of locations exhibiting identical probability levels at the two examinations. The number of locations exhibiting an improvement in probability level at Visit 5 is indicated below the shading. The number of locations exhibiting deterioration in probability level at Visit 5 is indicated above the shading.

The extent of the improvement and/ or deterioration in the Pattern Deviation probability levels between Visit 4 and Visit 5 for the normal individuals (Table 3.18a) was relatively small for both SAP algorithms. (The number of locations exhibiting an improvement in probability levels with the SITA Standard algorithm for the right eye was 67, and the number exhibiting a deterioration was 107, [a 1.6

fold overall deterioration] and for the left eye 71 and 101 locations, respectively [a 1.4 fold overall deterioration]. For SITA Fast, the improvement occurred at 107 locations and the deterioration at 76 locations for the right eye, [a 1.4 fold overall improvement] and for the left eye at 103 and 101 locations, respectively [no overall improvement]. An improvement with SITA SWAP for the right eye occurred at 67 locations and a deterioration at 63 locations [a 1.1 fold overall improvement]. For the left eye, 94 locations exhibited an improvement and 80 exhibited a deterioration [a 1.2 fold overall improvement]). These improvements and/ or deteriorations were fewer, in general, than those of the Total Deviation probability levels. Again, the majority of the locations, for each of the three algorithms, which exhibited a change in probability levels between the two visits, exhibited either an improvement from the 5% probability level to normal or a deterioration from normal to the 5% probability level.

SITA Standard	NS	<5%	<2%	<1%	<0,5%
NS	1133	53	5	5	1
<5%	63	13	4	1	0
<2%	11	3	1	3	0
<1%	2	1	0	0	0
<0,5%	0	0	0	1	0

SITA Standard	NS	<5%	<2%	<1%	<0,5%
NS	1116	59	14	12	6
<5%	37	8	2	2	2
<2%	15	3	4	1	0
<1%	3	1	2	1	0
<0,5%	10	0	0	0	2

SITA Fast	NS	<5%	<2%	<1%	<0,5%
NS	1112	64	11	5	6
<5%	57	8	4	2	0
<2%	11	4	3	1	0
<1%	6	2	2	1	1
<0,5%	0	0	0	0	0

SITA Fast	NS	<5%	<2%	<1%	<0,5%
NS	1119	54	17	15	4
<5%	48	5	3	1	1
<2%	17	5	0	0	1
<1%	3	3	0	0	0
<0,5%	2	0	0	0	2

SITA SWAP	NS	<5%	<2%	<1%	<0,5%
NS	1125	46	15	4	5
<5%	50	14	2	1	1
<2%	15	3	2	2	0
<1%	2	1	1	1	0
<0,5%	3	2	1	1	3

SITA SWAP	NS	<5%	<2%	<1%	<0,5%
NS	1124	48	11	4	10
<5%	43	13	3	0	2
<2%	11	3	3	2	2
<1%	5	2	0	0	0
<0,5%	6	3	2	1	2

Table 3.18b The magnitudes of the Pattern Deviation probability levels between Visit 4 (ordinate) and Visit 5 (abscissa), across all locations for the individuals with OHT for the right eye (left column) and left eye (right column). Top: SITA Standard. Middle: SITA Fast. Bottom: SITA SWAP. The shading indicates the number of locations exhibiting identical probability levels at the two examinations. The number of locations exhibiting an improvement in probability level at Visit 5 is indicated below the shading. The number of locations exhibiting a deterioration in probability level at Visit 5 is indicated above the shading.

For the individuals with OHT, the extent of the improvement and/ or deterioration in the Pattern Deviation probability level between Visit 4 and Visit 5 (Table 3.18b) was relatively modest for both SAP algorithms. (With the SITA Standard algorithm, 81 locations for the right eye exhibited an improvement and 72 locations exhibited a deterioration [a 1.1 fold overall improvement]; 71 locations for the left eye exhibited

an improvement and 98 locations exhibited a deterioration [a 1.4 fold overall deterioration]. With the SITA Fast algorithm, 82 locations for the right eye exhibited an improvement and 94 locations exhibited a deterioration [a 1.1 fold overall deterioration]; 78 locations for the left eye exhibited an improvement and 96 locations exhibited a deterioration [a 1.2 fold overall deterioration]. The extent of the improvement and/ or deterioration with the SITA SWAP algorithm was similar for the right compared to that for the left eyes; namely, for the right eye, 79 locations exhibited an improvement and 76 locations exhibited a deterioration [no overall improvement] and for the left eye, 76 locations exhibited an improvement and 82 locations exhibited a deterioration [a 1.1 fold overall deterioration]). As was the case with the Total Deviation probability levels, the majority of the locations, for each of the three algorithms, which exhibited a change in probability levels between the two visits, exhibited either an improvement from the 5% probability level to normal or a deterioration from normal to the 5% probability level.

SITA Standard

SITA Standard	NS	<5%	<2%	<1%	<0,5%
NS	1051	39	14	10	6
<5%	43	8	1	3	6
<2%	13	4	3	1	3
<1%	18	4	2	2	3
<0,5%	16	2	2	4	42

SITA Standard

SITA Standard	NS	<5%	<2%	<1%	<0,5%
NS	1062	46	8	7	7
<5%	51	6	3	7	10
<2%	19	4	1	4	4
<1%	17	5	3	0	6
<0,5%	9	5	3	2	11

SITA Fast

SITA Fast	NS	<5%	<2%	<1%	<0,5%
NS	1058	53	15	4	1
<5%	51	7	7	4	2
<2%	16	5	3	0	1
<1%	14	2	2	4	0
<0,5%	9	3	3	2	34

SITA Fast

SITA Fast	NS	<5%	<2%	<1%	<0,5%
NS	1018	58	15	10	8
<5%	59	7	7	8	5
<2%	22	9	7	4	4
<1%	12	4	4	9	6
<0,5%	2	4	5	5	8

SITA SWAP

SITA SWAP	NS	<5%	<2%	<1%	<0,5%
NS	1047	56	16	9	12
<5%	47	17	4	2	4
<2%	17	1	1	2	1
<1%	8	5	3	2	4
<0,5%	5	8	1	2	26

SITA SWAP

SITA SWAP	NS	<5%	<2%	<1%	<0,5%
NS	1048	53	10	10	15
<5%	67	8	5	3	4
<2%	21	5	3	3	4
<1%	12	2	2	1	1
<0,5%	8	5	3	0	7

Table 3.18c The magnitudes of the Pattern Deviation probability levels between Visit 4 (ordinate) and Visit 5 (abscissa), across all locations for the individuals with OAG for the right eye (left column) and left eye (right column). Top: SITA Standard. Middle: SITA Fast. Bottom: SITA SWAP. The shading indicates the number of locations exhibiting identical probability levels at the two examinations. The number of locations exhibiting an improvement in probability level at Visit 5 is indicated below the shading. The number of locations exhibiting a deterioration in probability level at Visit 5 is indicated above the shading.

For the individuals with OAG, the extent of the improvement and/ or deterioration in the Pattern Deviation probability levels between Visit 4 and Visit 5 (Table 3.18c) was, in general, similar for all algorithms. (With the SITA Standard algorithm, 108 locations for the right eye exhibited an improvement and 86 locations exhibited a deterioration [a 1.3 fold overall improvement]; 118 locations for the left eye

exhibited an improvement and 102 locations exhibited a deterioration [a 1.2 fold overall improvement]. With the SITA Fast algorithm, 107 locations for the right eye exhibited an improvement and 87 locations exhibited a deterioration [a 1.2 fold overall improvement]; 126 locations for the left eye exhibited an improvement and 125 locations exhibited a deterioration [no overall improvement]. The extent of the improvement and/ or deterioration with the SITA SWAP algorithm was similar for the right and for the left eye, namely, for the right eye, 97 locations exhibited an improvement and 110 locations exhibited a deterioration [a 1.1 fold overall deterioration]; for the left eye, 125 locations exhibited an improvement and 108 locations exhibited a deterioration [a 1.2 fold overall improvement]). As it was the case with the Total Deviation probability levels, the majority of the locations, for each of the three algorithms, which exhibited a change in probability levels between the two visits, exhibited either an improvement from the 5% probability level to normal or a deterioration from normal to the 5% probability level.

3.4.3 The within-visit (Visit 5) between-algorithm difference in sensitivity

The various between-algorithm differences in the MD at Visit 5 are summarised in Table 3.19 and are illustrated in Figure 3.14a for the normal individuals, for the individuals with OHT in Figure 3.14b, for the individuals with OAG in Figure 3.14c, and for all individuals, combined, in Figure 3.14d.

Algorithm	Eye	Normal	OHT	OAG	All groups
SITA Standard v SITA Fast	**RE**	3.38 dB	3.19 dB	2.79 dB	3.28 dB
	LE	2.52 dB	3.25 dB	2.05 dB	2.63 dB
SITA Standard v SITA SWAP	**RE**	10.03 dB	7.39 dB	7.66 dB	8.47 dB
	LE	8.36 dB	7.58 dB	8.45 dB	8.11 dB
SITA Fast v SITA SWAP	**RE**	9.32 dB	7.22 dB	7.86 dB	8.14 dB
	LE	8.56 dB	7.07 dB	8.43 dB	8.02 dB

Table 3.19 The between-algorithm differences in the MD at Visit 5 expressed as the range of the limits of agreement (defined as the mean of the differences +/- 1.96SD) for the three algorithms for each eye of the three groups of individuals and for the three groups, combined.

The range of the limits of agreement of the difference in the MD was smallest, in all three diagnostic groups, for the comparison between the SITA Standard and SITA Fast algorithms. The range of the differences was substantially wider for SITA SWAP when compared to either algorithm for SAP across each of the diagnostic groups.

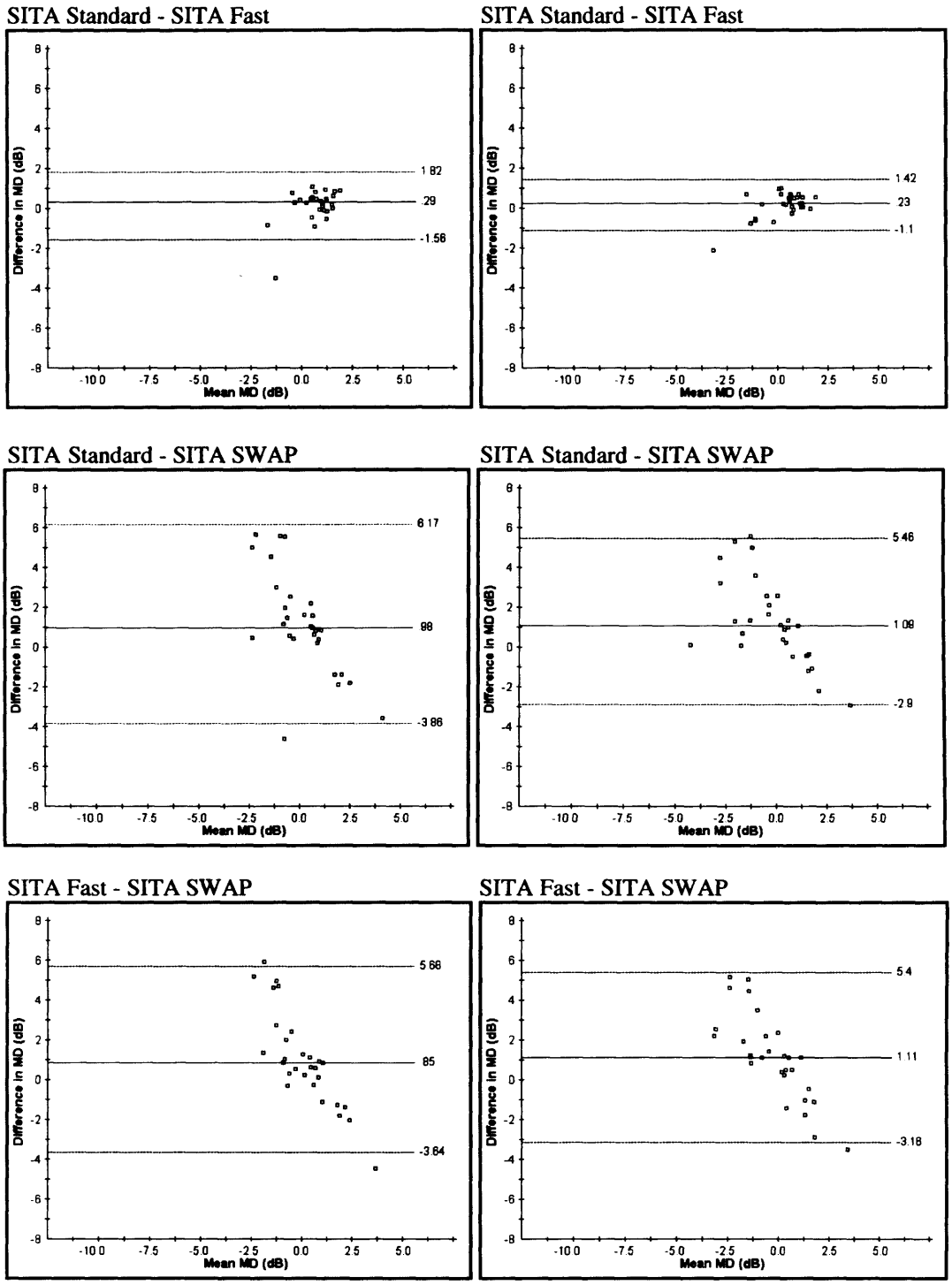

Figure 3.14a The within-individual between-algorithm difference in the MD at Visit 5 against the mean of the two MDs for the right eye (left column) and for the left eye (right column) for the normal individuals. Top: SITA Standard v SITA Fast. Middle: SITA Standard v SITA SWAP. Bottom: SITA Fast v SITA SWAP. The solid line indicates the mean of the differences and the upper and lower dotted lines the mean of the differences +/- 1.96SD, respectively.

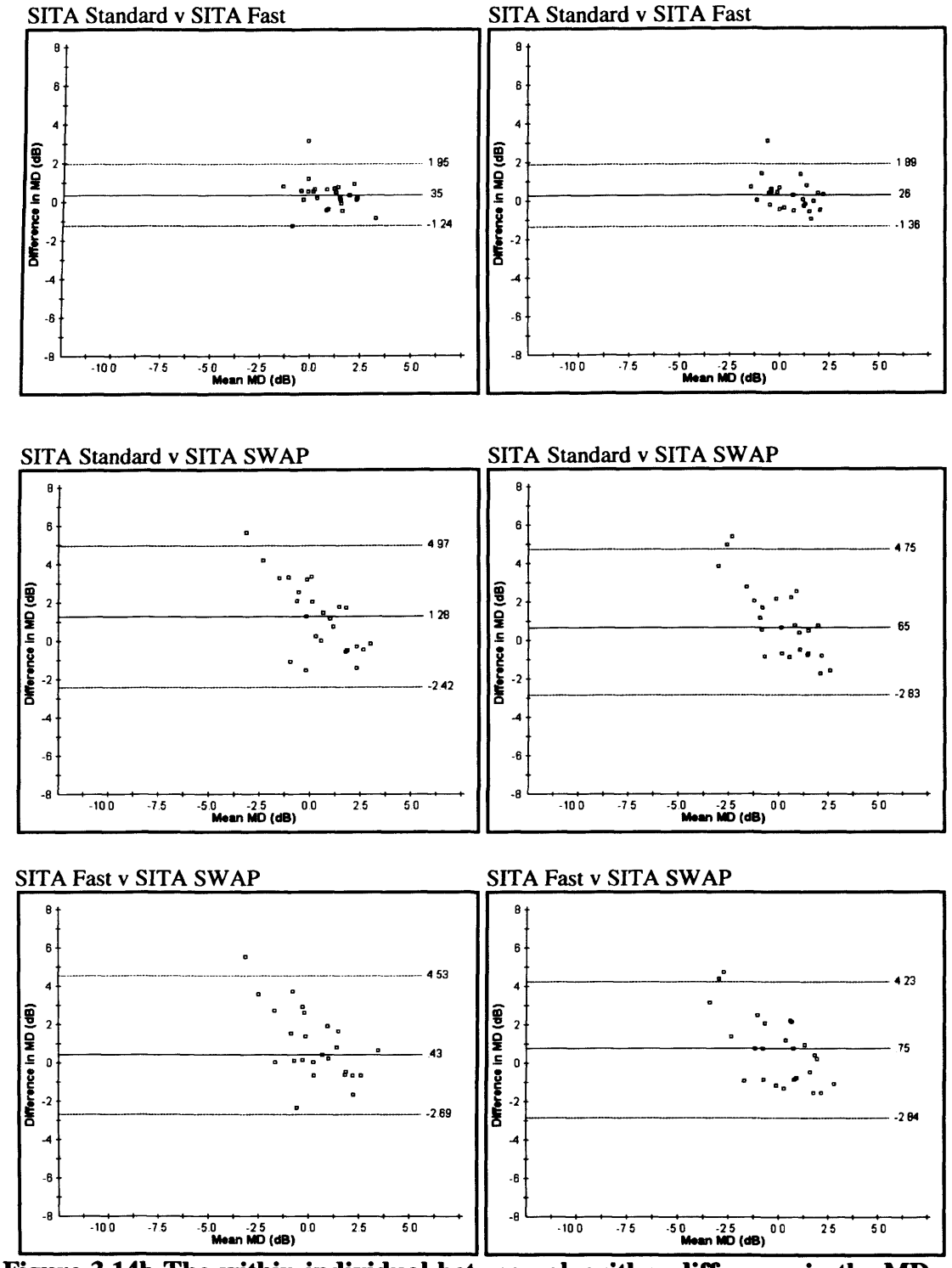

Figure 3.14b The within-individual between-algorithm difference in the MD at Visit 5 against the mean of the two MDs for the right eye (left column) and for the left eye (right column) for the individuals with OHT. Top: SITA Standard v SITA Fast. Middle: SITA Standard v SITA SWAP. Bottom: SITA Fast v SITA SWAP. The solid line indicates the mean of the differences and the upper and lower dotted lines the mean of the differences +/- 1.96SD, respectively.

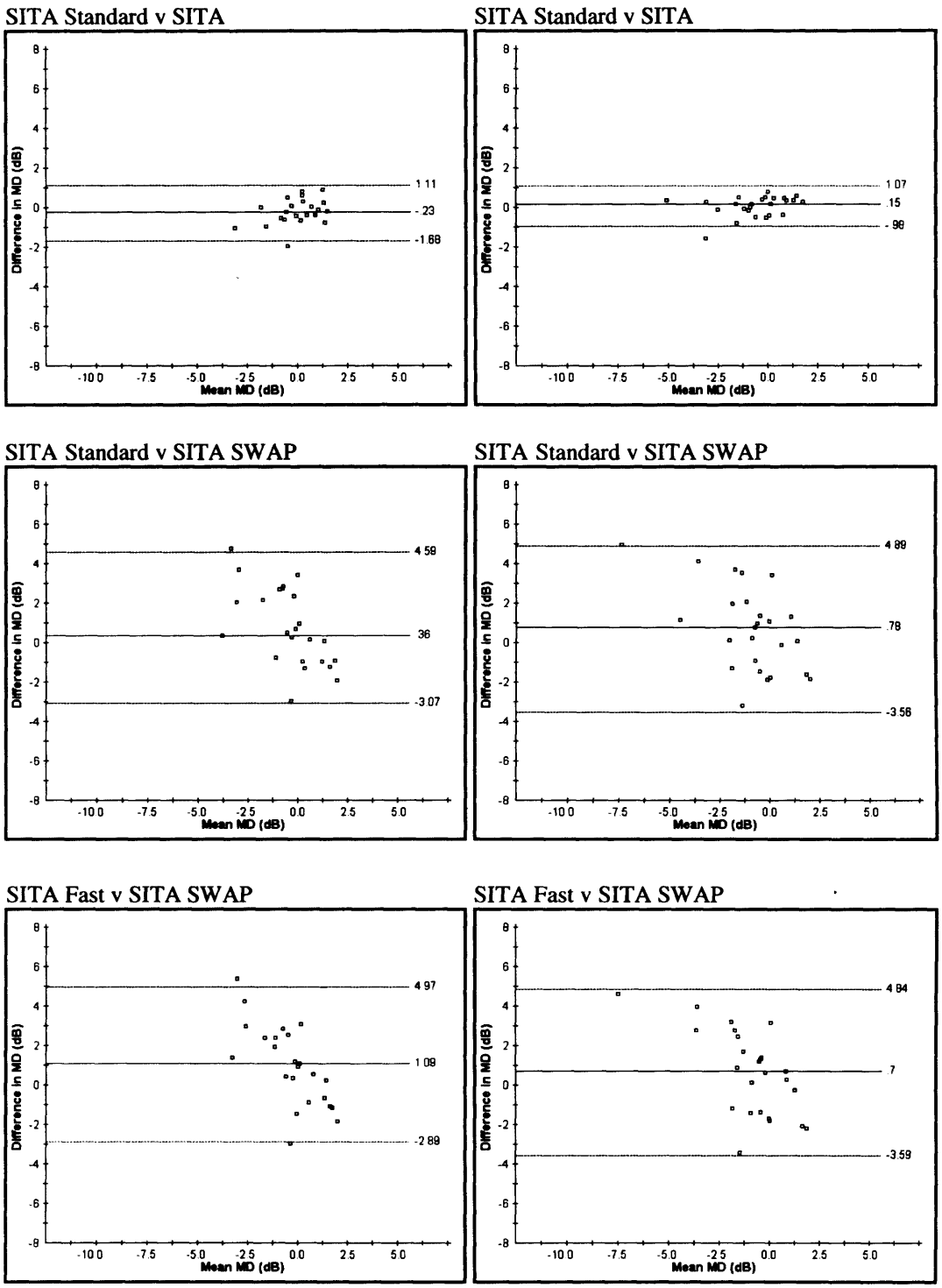

Figure 3.14c The within-individual between-algorithm difference in the MD at Visit 5 against the mean of the two MDs for the right eye (left column) and for the left eye (right column) for the individuals with OAG. Top: SITA Standard v SITA Fast. Middle: SITA Standard v SITA SWAP. Bottom: SITA Fast v SITA SWAP. The solid line indicates the mean of the differences and the upper and lower dotted lines the mean of the differences +/- 1.96SD, respectively.

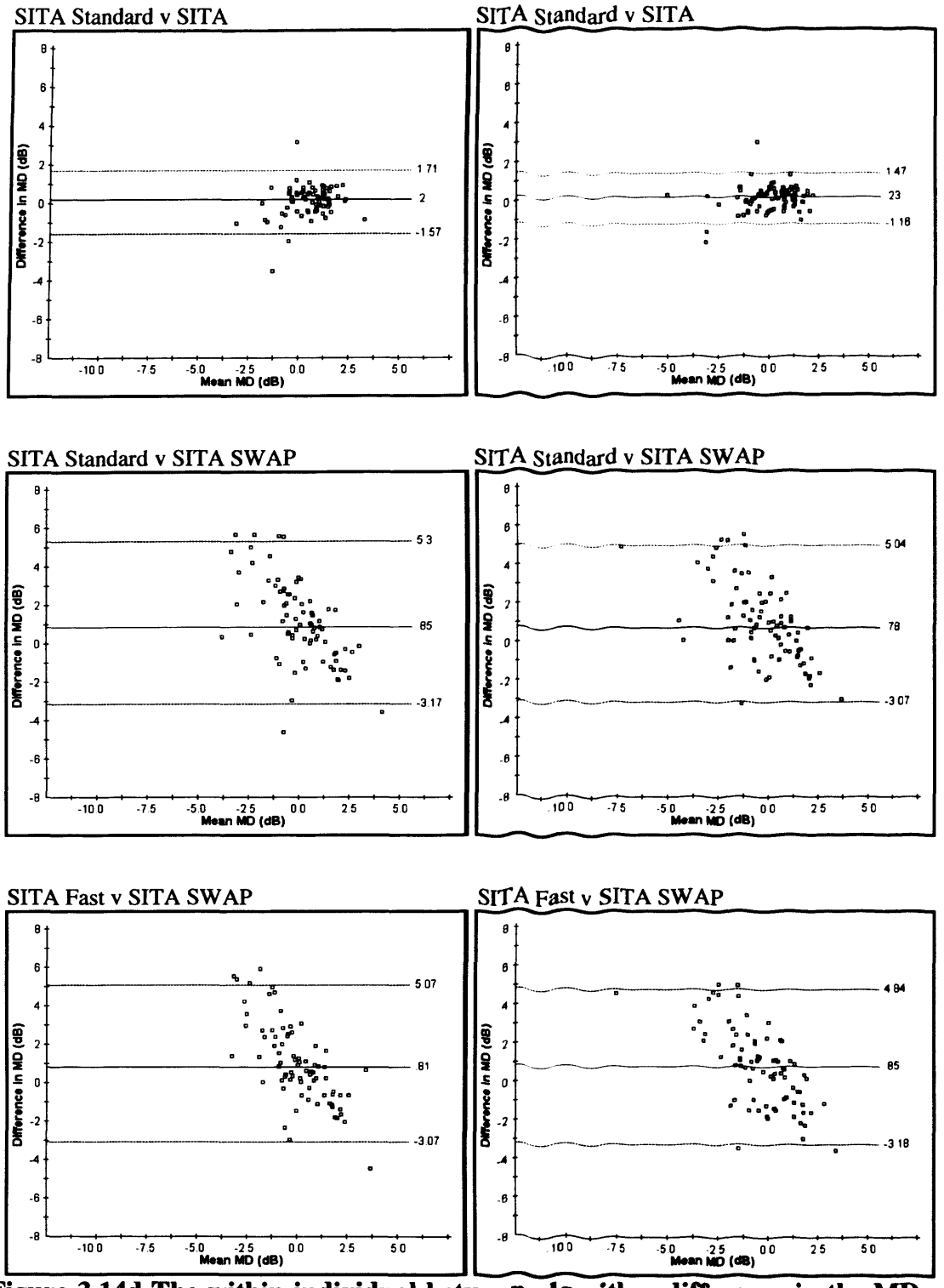

Figure 3.14d The within-individual between-algorithm difference in the MD at Visit 5 against the mean of the two MDs for the right eye (left column) and for the left eye (right column) for the three groups, combined. Top: SITA Standard v SITA Fast. Middle: SITA Standard v SITA SWAP. Bottom: SITA Fast v SITA SWAP. The solid line indicates the mean of the differences and the upper and lower dotted lines the mean of the differences +/- 1.96SD, respectively.

The various between-algorithm differences in the PSD at Visit 5 are summarised in Table 3.20 and are illustrated in Figure 3.15a for the normal individuals, for the individuals with OHT in Figure 3.15b, for the individuals with OAG in Figure 3.15c, and for all individuals, combined, in Figure 3.15d.

Algorithm	Eye	Normal	OHT	OAG	All groups
SITA Standard	**RE**	1.60 dB	1.69 dB	2.10 dB	2.80 dB
v SITA Fast	**LE**	2.58 dB	4.75 dB	3.43 dB	3.63 dB
SITA Standard	**RE**	2.90 dB	2.55 dB	4.40 dB	3.34 dB
v SITA SWAP	**LE**	3.19 dB	2.44 dB	3.50 dB	3.05 dB
SITA Fast	**RE**	2.52 dB	2.52 dB	4.48 dB	3.13 dB
v SITA SWAP	**LE**	4.60 dB	4.60 dB	4.15 dB	3.62 dB

Table 3.20 The between-algorithm differences in the PSD at Visit 5 expressed as the range of the limits of agreement (defined as the mean of the differences +/- 1.96SD) for the three algorithms for each eye of the three groups of individuals and for the three groups, combined.

The range of the limits of agreement for the difference in the PSD was wider for the algorithm comparisons involving SWAP. The range for the PSD tended to be larger for the second eye examined, in all three diagnostic groups for all three algorithms.

SITA Standard v SITA Fast

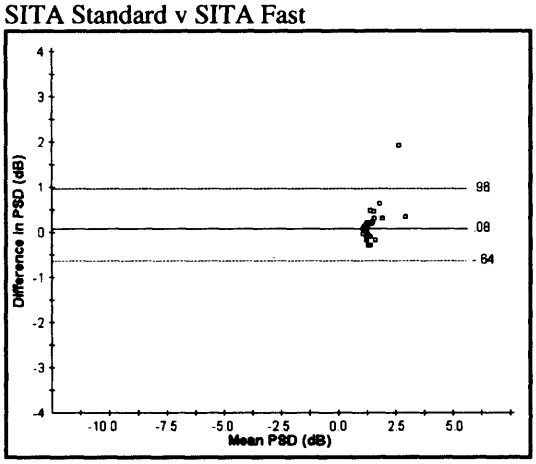

SITA Standard v SITA Fast

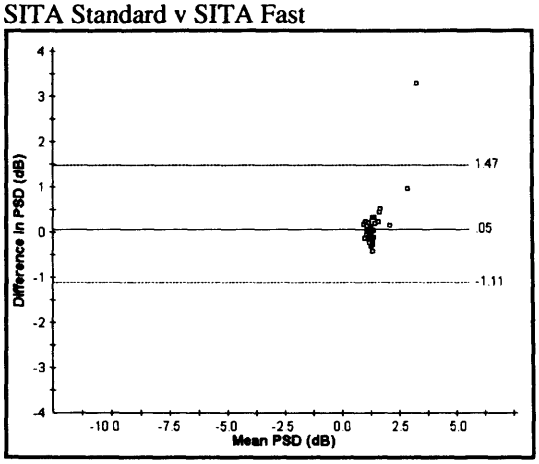

SITA Standard v SITA SWAP

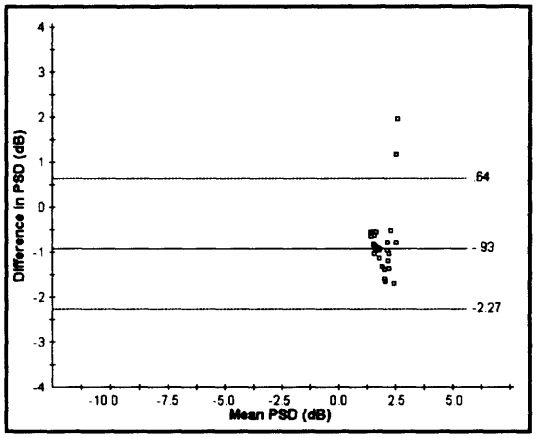

SITA Standard v SITA SWAP

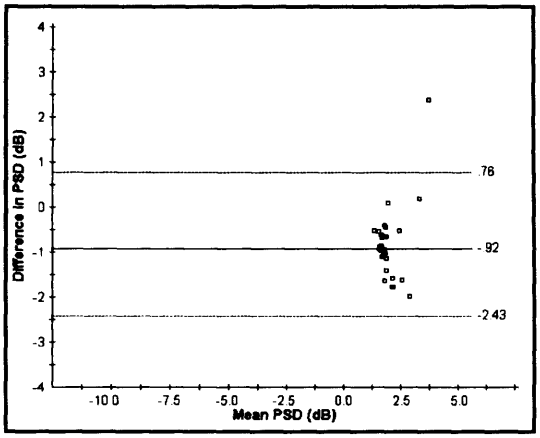

SITA Fast v SITA SWAP

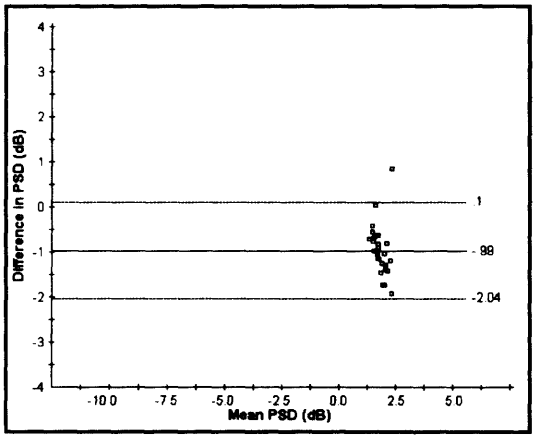

SITA Fast v SITA SWAP

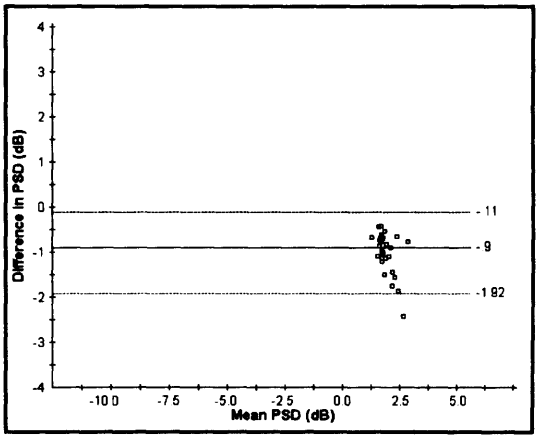

Figure 3.15a The within-individual between-algorithm difference in the PSD at Visit 5 against the mean of the two PSDs for the right eye (left column) and for the left eye (right column) for the normal individuals. Top: SITA Standard v SITA Fast. Middle: SITA Standard v SITA SWAP. Bottom: SITA Fast v SITA SWAP. The solid line indicates the mean of the differences and the upper and lower dotted lines the mean of the differences +/- 1.96SD, respectively.

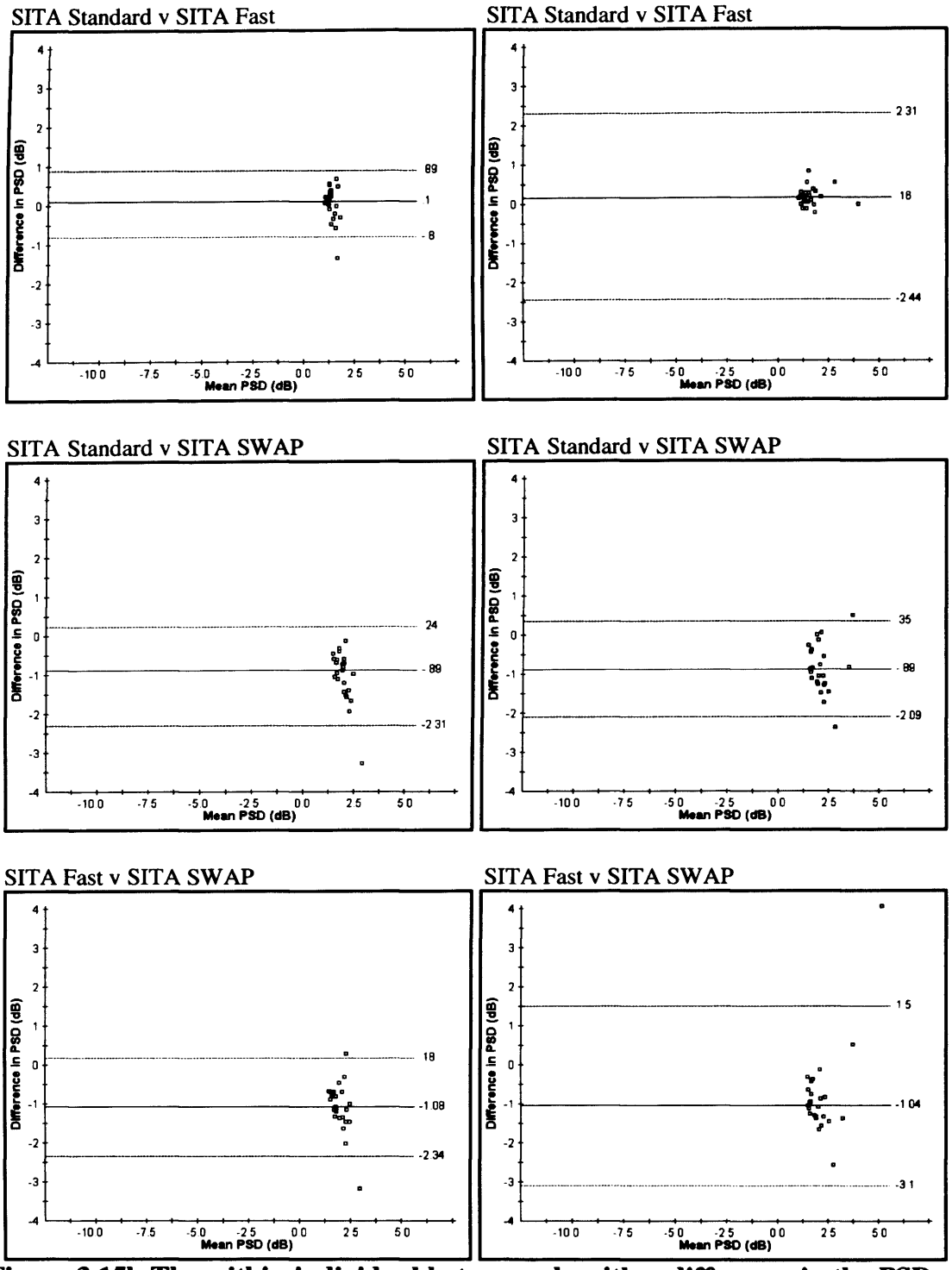

Figure 3.15b The within-individual between-algorithm difference in the PSD at Visit 5 against the mean of two PSDs for the right eye (left column) and for the left eye (right column) for the individuals with OHT. Top: SITA Standard v SITA Fast. Middle: SITA Standard v SITA SWAP. Bottom: SITA Fast v SITA SWAP. The solid line indicates the mean of the differences and the upper and lower dotted lines the mean of the differences +/- 1.96SD, respectively.

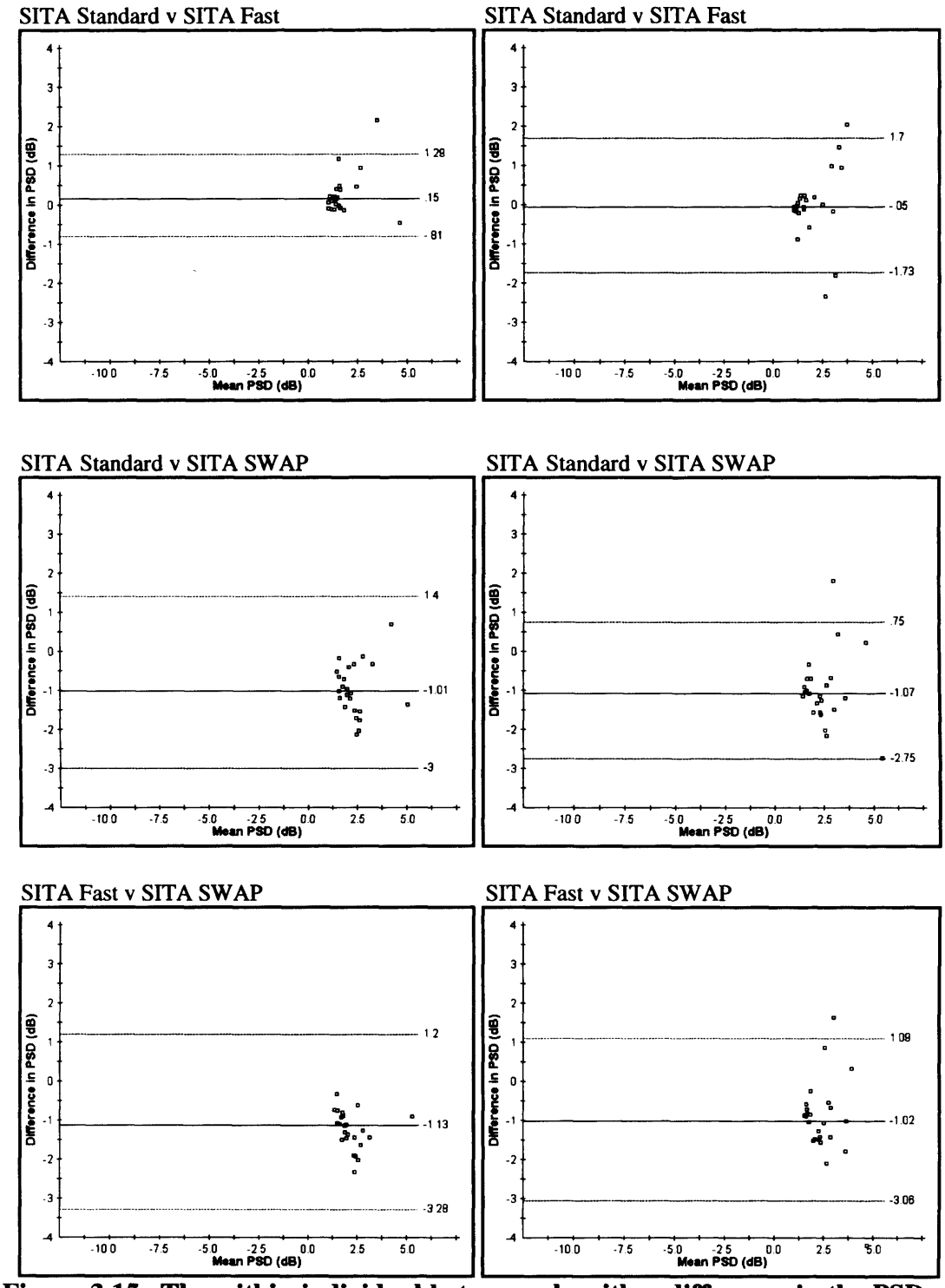

Figure 3.15c The within-individual between-algorithm difference in the PSD at Visit 5 against the mean of two PSDs for the right eye (left column) and for the left eye (right column) for the individuals with OAG. Top: SITA Standard v SITA Fast. Middle: SITA Standard v SITA SWAP. Bottom: SITA Fast v SITA SWAP. The solid line indicates the mean of the differences and the upper and lower dotted lines the mean of the differences +/- 1.96SD, respectively.

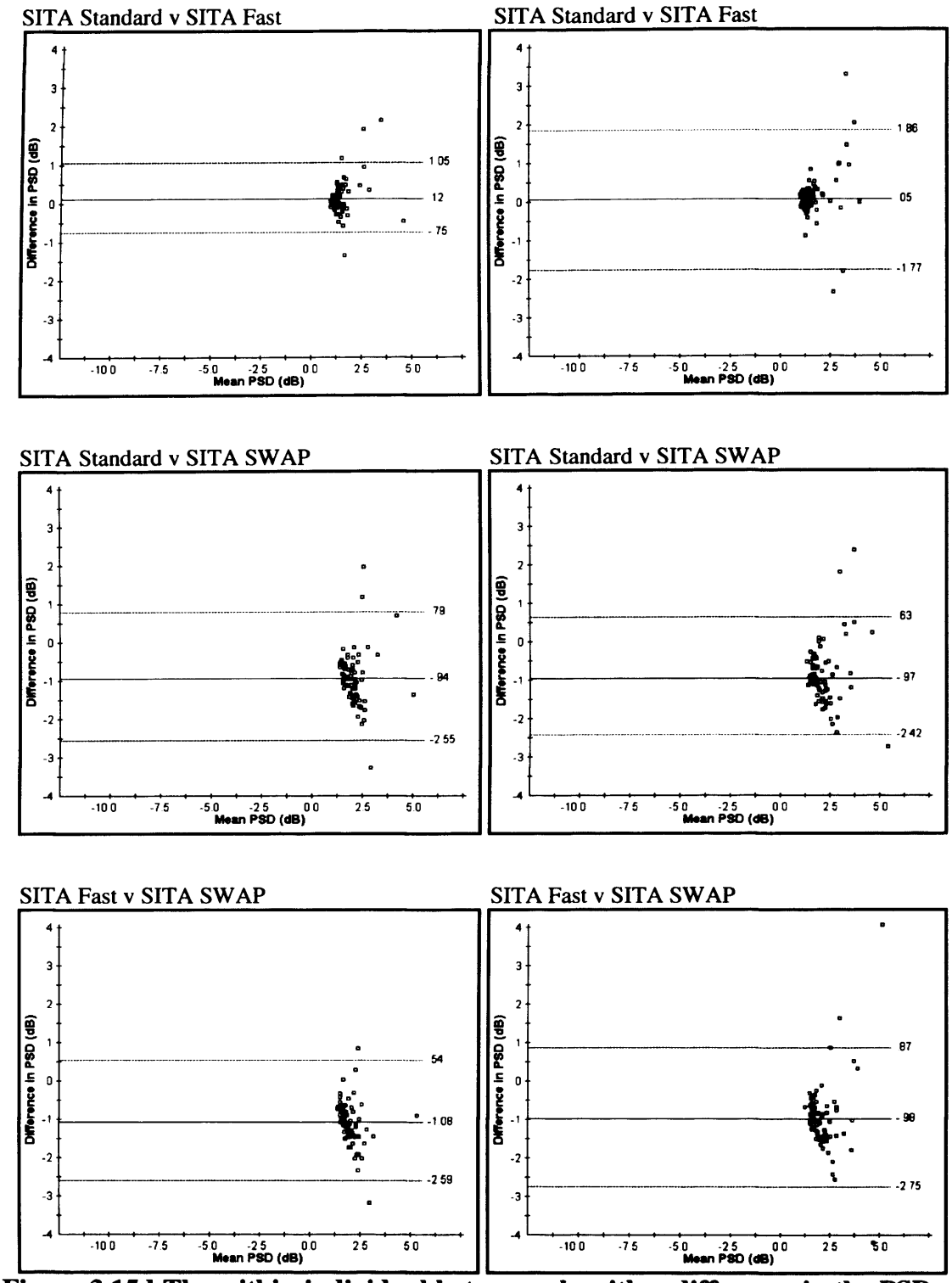

Figure 3.15d The within-individual between-algorithm difference in the PSD at Visit 5 against the mean of two PSDs for the right eye (left column) and for the left eye (right column) for the three groups, combined. Top: SITA Standard v SITA Fast. Middle: SITA Standard v SITA SWAP. Bottom: SITA Fast v SITA SWAP. The solid line indicates the mean of the differences and the upper and lower dotted lines the mean of the differences +/- 1.96SD, respectively.

The 90^{th}, 50^{th} and 10^{th} percentiles of the distribution of the differences in sensitivity between respective algorithms across all stimulus locations at Visit 5 as a function of the sensitivity at the corresponding stimulus location is shown in Figure 3.16a for the normal individuals, in Figure 3.16b for the individuals with OHT in Figure 3.16c for the individuals with OAG and in Figure 3.16d for the individuals from all the three groups, combined.

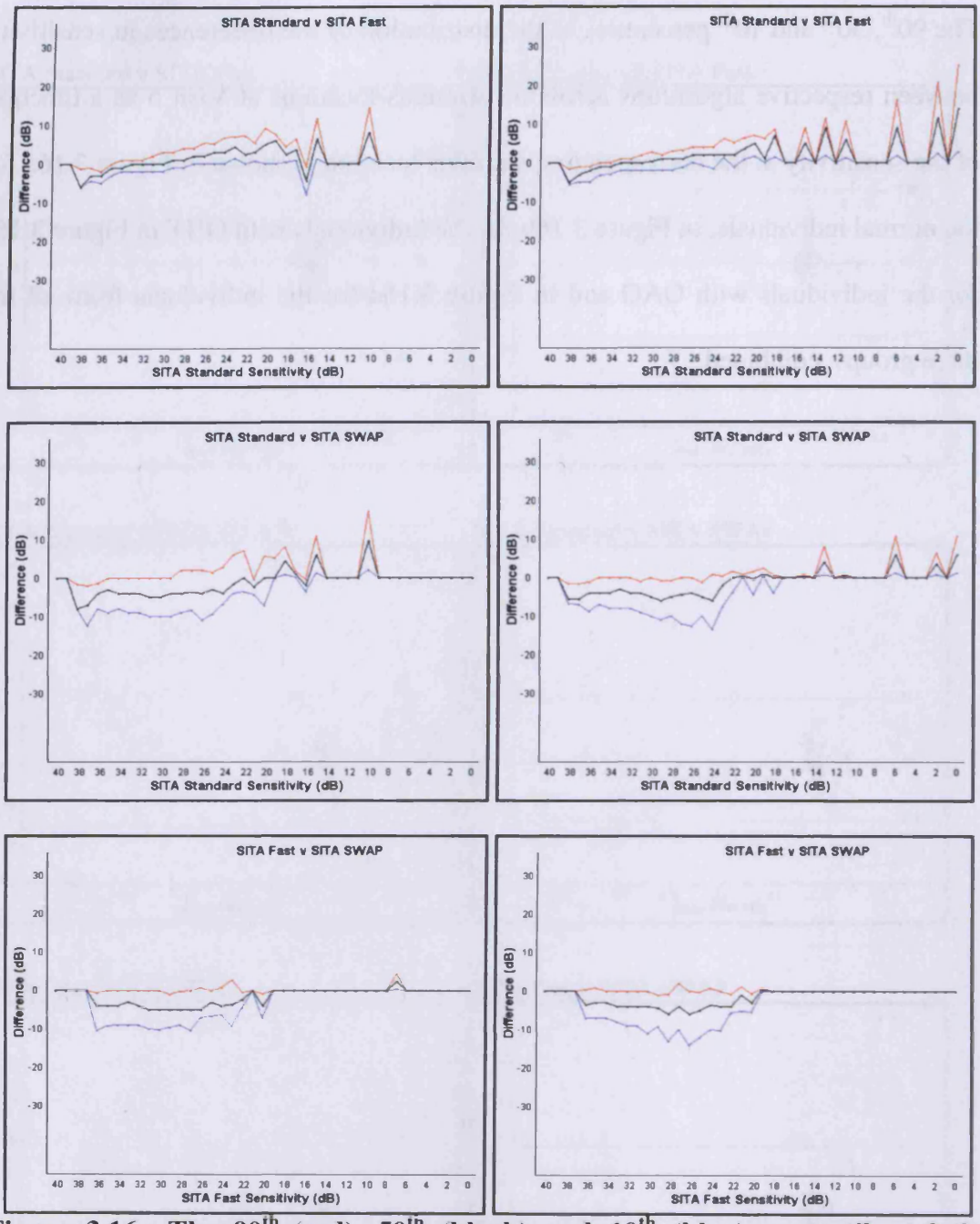

Figure 3.16a The 90th (red), 50th (black) and 10th (blue) percentiles of the distribution of the within-individual between-algorithm difference in sensitivity across all stimulus locations at Visit 5 for the normal individuals as a function of the sensitivity at the corresponding stimulus location expressed as the first algorithm minus the comparative algorithm: right eye, left column; left eye, right column. Top: SITA Standard v SITA Fast. Middle: SITA Standard v SITA SWAP. Bottom: SITA Fast v SITA SWAP.

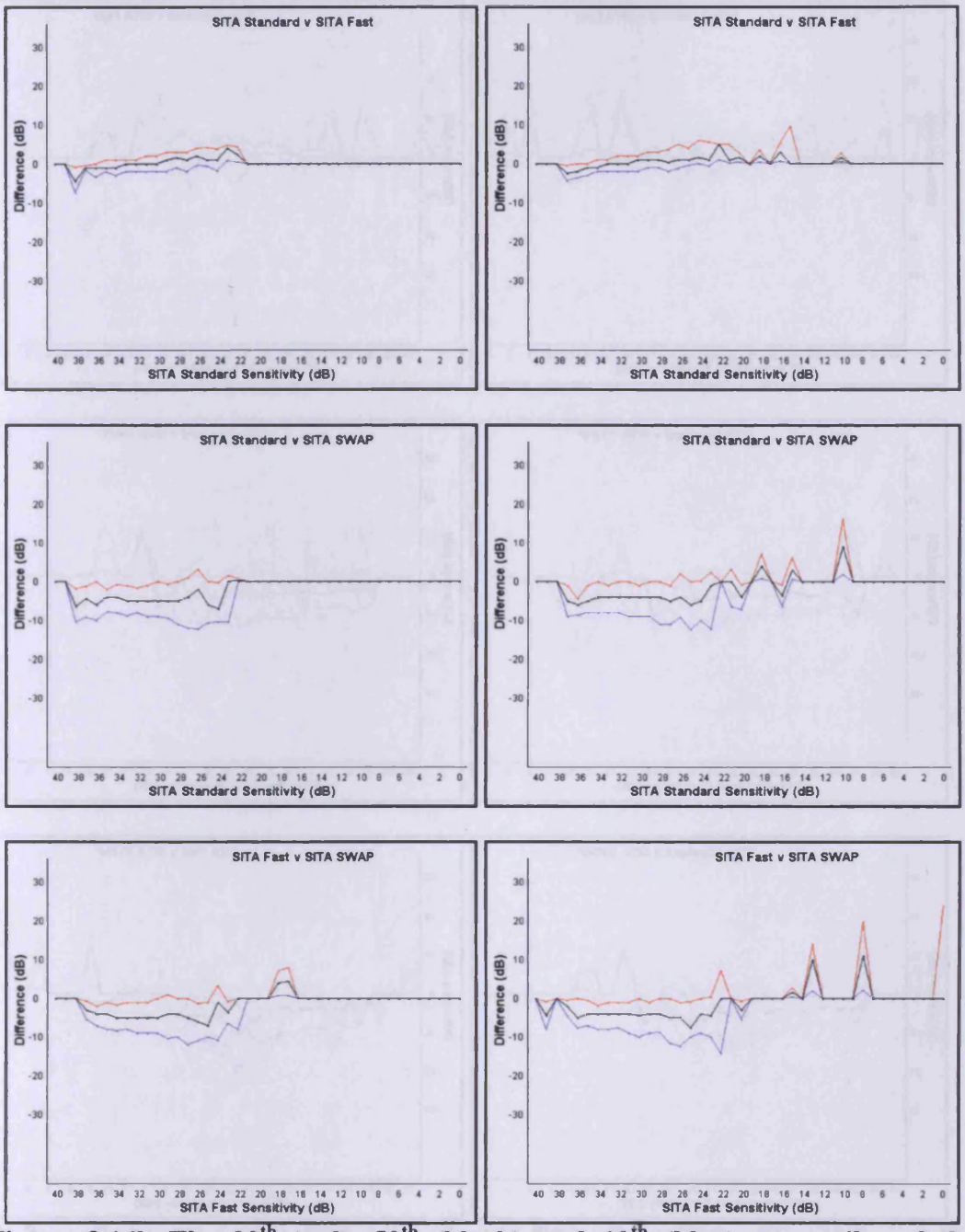

Figure 3.16b The 90th (red), 50th (black) and 10th (blue) percentiles of the distribution of the within-individual between-algorithm difference in sensitivity across all stimulus locations at Visit 5 for the individuals with OHT as a function of the sensitivity at the corresponding stimulus location expressed as the first algorithm minus the comparative algorithm: right eye, left column; left eye, right column. Top: SITA Standard v SITA Fast. Middle: SITA Standard v SITA SWAP. Bottom: SITA Fast v SITA SWAP.

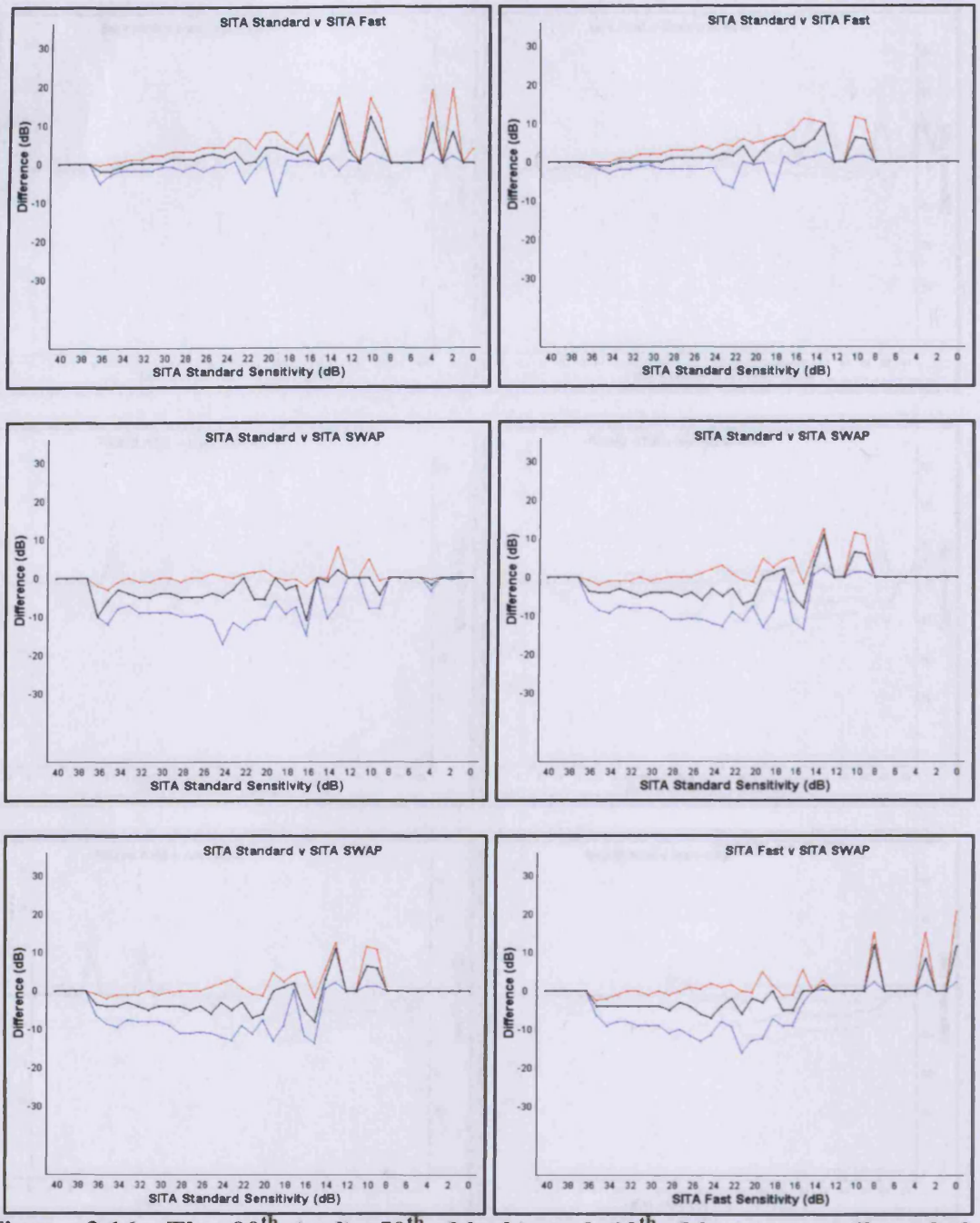

Figure 3.16c The 90th (red), 50th (black) and 10th (blue) percentiles of the distribution of the within-individual between-algorithm difference in sensitivity across all stimulus locations at Visit 5 for the individuals with OAG as a function of the sensitivity at the corresponding stimulus location expressed as the first algorithm minus the comparative algorithm: right eye, left column; left eye, right column. Top: SITA Standard v SITA Fast. Middle: SITA Standard v SITA SWAP. Bottom: SITA Fast v SITA SWAP.

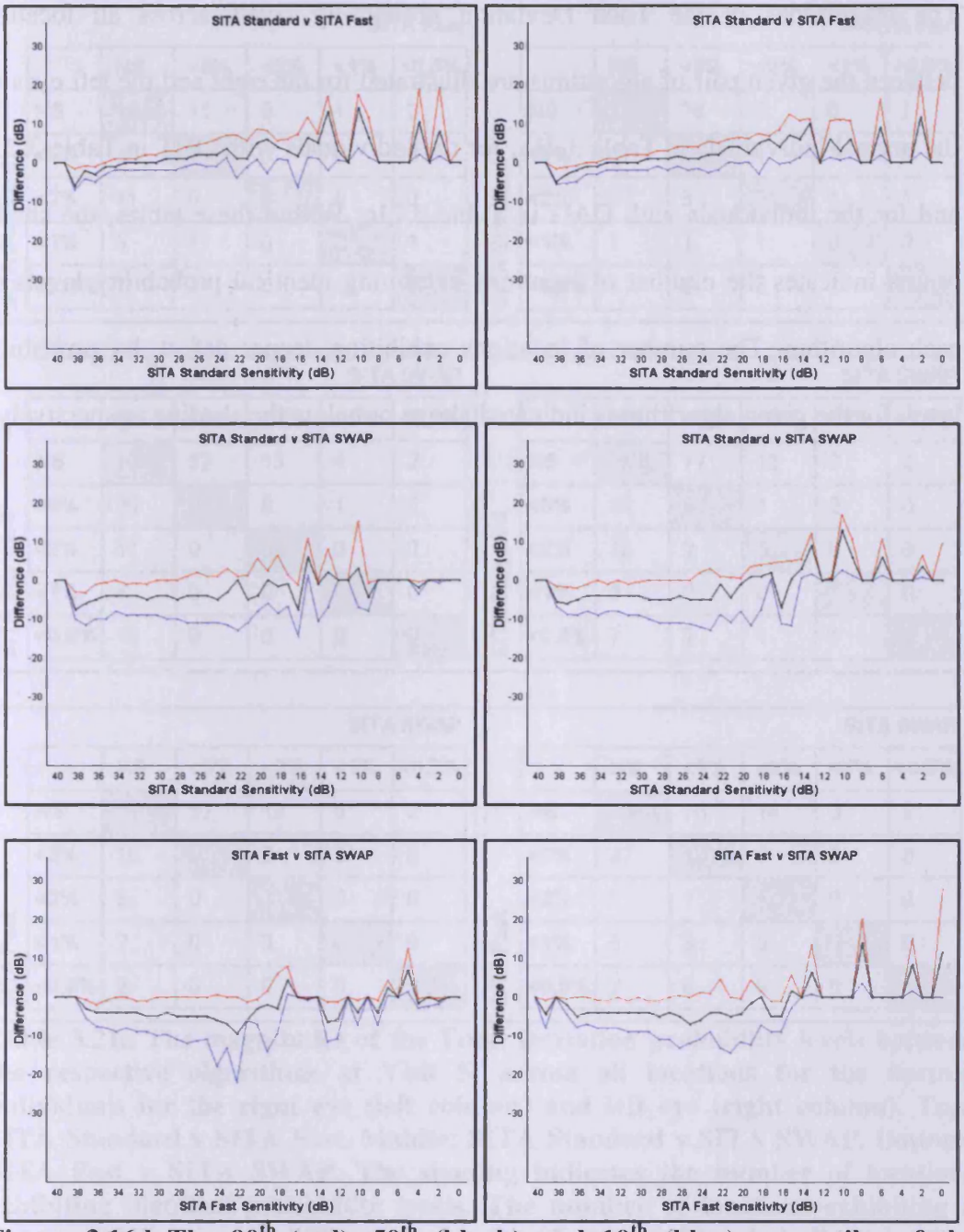

Figure 3.16d The 90th (red), 50th (black) and 10th (blue) percentiles of the distribution of the within-individual between-algorithm difference in sensitivity across all stimulus locations at Visit 5 for the individuals in all three groups as a function of the sensitivity at the corresponding stimulus location expressed as the first algorithm minus the comparative algorithm: right eye, left column; left eye, right column. Top: SITA Standard v SITA Fast. Middle: SITA Standard v SITA SWAP. Bottom: SITA Fast v SITA SWAP.

The magnitudes of the Total Deviation probability levels across all locations between the given pair of algorithms are illustrated for the right and the left eyes for the normal individuals in Table 3.21a, for the individuals with OHT in Table 3.21b, and for the individuals with OAG in Table 3.21c. Within these tables, the shaded region indicates the number of locations exhibiting identical probability levels for each algorithm. The number of locations exhibiting deeper defect, by probability level, for the given algorithm is indicated above or below the shading, respectively.

SITA Standard / SITA Fast

	NS	<5%	<2%	<1%	<0,5%
NS	1428	15	5	1	0
<5%	30	1	0	0	0
<2%	11	0	0	0	0
<1%	5	1	0	0	1
<0,5%	7	1	0	1	1

SITA Standard / SITA Fast

	NS	<5%	<2%	<1%	<0,5%
NS	1392	28	3	6	1
<5%	31	10	1	1	0
<2%	10	3	0	1	1
<1%	7	1	1	0	0
<0,5%	5	3	2	1	0

SITA Standard / SITA SWAP

	NS	<5%	<2%	<1%	<0,5%
NS	1378	52	15	4	2
<5%	30	0	0	1	0
<2%	11	0	0	0	0
<1%	7	0	0	0	0
<0,5%	10	0	0	0	0

SITA Standard / SITA SWAP

	NS	<5%	<2%	<1%	<0,5%
NS	1336	77	13	2	2
<5%	31	9	1	2	0
<2%	13	2	0	0	0
<1%	8	0	0	1	0
<0,5%	7	2	1	1	0

SITA Fast / SITA SWAP

	NS	<5%	<2%	<1%	<0,5%
NS	1407	52	15	5	2
<5%	18	0	0	0	0
<2%	5	0	0	0	0
<1%	2	0	0	0	0
<0,5%	2	0	0	0	0

SITA Fast / SITA SWAP

	NS	<5%	<2%	<1%	<0,5%
NS	1350	76	14	3	2
<5%	32	10	0	3	0
<2%	5	1	1	0	0
<1%	6	3	0	0	0
<0,5%	2	0	0	0	0

Table 3.21a The magnitudes of the Total Deviation probability levels between the respective algorithms at Visit 5, across all locations for the normal individuals for the right eye (left column) and left eye (right column). Top: SITA Standard v SITA Fast. Middle: SITA Standard v SITA SWAP. Bottom: SITA Fast v SITA SWAP. The shading indicates the number of locations exhibiting identical probability levels. The number of locations exhibiting a deeper defect, by probability level, for the given algorithm is indicated either above or below the shading, respectively.

SITA Standard \ SITA Fast	NS	<5%	<2%	<1%	<0,5%
NS	1239	21	10	6	2
<5%	15	5	1	0	0
<2%	0	1	0	0	0
<1%	0	0	0	0	0
<0,5%	0	0	0	0	0

SITA Standard \ SITA Fast	NS	<5%	<2%	<1%	<0,5%
NS	1204	36	10	4	3
<5%	22	3	2	2	0
<2%	4	0	1	1	0
<1%	2	1	0	0	0
<0,5%	2	0	0	1	2

SITA Standard \ SITA SWAP	NS	<5%	<2%	<1%	<0,5%
NS	1222	33	12	5	6
<5%	19	0	2	0	0
<2%	1	0	0	0	0
<1%	0	0	0	0	0
<0,5%	0	0	0	0	0

SITA Standard \ SITA SWAP	NS	<5%	<2%	<1%	<0,5%
NS	1179	54	18	3	3
<5%	25	2	1	0	1
<2%	5	1	0	0	0
<1%	3	0	0	0	0
<0,5%	2	0	1	0	2

SITA Fast \ SITA SWAP	NS	<5%	<2%	<1%	<0,5%
NS	1203	29	12	5	5
<5%	21	4	1	0	1
<2%	10	0	1	0	0
<1%	6	0	0	0	0
<0,5%	2	0	0	0	0

SITA Fast \ SITA SWAP	NS	<5%	<2%	<1%	<0,5%
NS	1164	47	17	2	4
<5%	31	6	3	0	0
<2%	8	4	0	1	0
<1%	7	0	0	0	1
<0,5%	4	0	0	0	1

Table 3.21b The magnitudes of the Total Deviation probability levels between the respective algorithms at Visit 5, across all locations for the individuals with OHT for the right eye (left column) and left eye (right column). Top: SITA Standard v SITA Fast. Middle: SITA Standard v SITA SWAP. Bottom: SITA Fast v SITA SWAP. The shading indicates the number of locations exhibiting identical probability levels. The number of locations exhibiting a deeper defect, by probability level, for the given algorithm is indicated either above or below the shading, respectively.

SITA Fast

SITA Standard	NS	<5%	<2%	<1%	<0,5%
NS	1125	28	6	1	1
<5%	32	6	3	0	0
<2%	10	5	1	1	3
<1%	6	3	1	3	1
<0,5%	8	3	4	13	36

SITA Fast

SITA Standard	NS	<5%	<2%	<1%	<0,5%
NS	1082	42	20	12	5
<5%	41	11	9	6	0
<2%	9	5	5	3	1
<1%	5	7	5	8	5
<0,5%	6	3	6	17	7

SITA SWAP

SITA Standard	NS	<5%	<2%	<1%	<0,5%
NS	1085	46	15	9	6
<5%	36	6	0	0	0
<2%	14	6	0	0	0
<1%	5	4	1	1	3
<0,5%	11	7	0	2	44

SITA SWAP

SITA Standard	NS	<5%	<2%	<1%	<0,5%
NS	1085	47	14	8	7
<5%	57	5	3	2	0
<2%	13	3	3	1	3
<1%	23	2	2	1	2
<0,5%	16	3	4	4	12

SITA SWAP

SITA Fast	NS	<5%	<2%	<1%	<0,5%
NS	1089	54	13	8	7
<5%	36	4	2	1	2
<2%	8	3	0	2	2
<1%	5	2	1	0	10
<0,5%	3	5	0	1	32

SITA SWAP

SITA Fast	NS	<5%	<2%	<1%	<0,5%
NS	1054	40	16	5	8
<5%	57	3	2	5	1
<2%	26	10	4	2	3
<1%	28	5	2	2	9
<0,5%	9	2	2	2	3

Table 3.21c The magnitudes of the Total Deviation probability levels between the respective algorithms at Visit 5, across all locations for the individuals with OAG for the right eye (left column) and left eye (right column). Top: SITA Standard v SITA Fast. Middle: SITA Standard v SITA SWAP. Bottom: SITA Fast v SITA SWAP. The shading indicates the number of locations exhibiting identical probability levels. The number of locations exhibiting a deeper defect, by probability level, for the given algorithm is indicated either above or below the shading, respectively.

For the normal individuals (Table 3.21a), the SITA Standard algorithm tended to overestimate the presence of visual field loss compared to the SITA Fast algorithm by 2.5 fold for the right eye and by 1.5 fold for the left eye. The SITA SWAP algorithm overestimated the presence of visual field loss compared to the SITA Standard algorithm by 1.3 fold for the right eye and by 1.5 fold for the left eye and compared to the SITA Fast algorithm by 2.7 fold and 2.0 fold, respectively.

The number of locations exhibiting apparent abnormality by Total Deviation probability analysis was lower for the individuals with OHT (Table 3.21b) than for the normal individuals. Given these smaller numbers, the SITA Fast algorithm tended to overestimate the presence of visual field loss compared to the SITA Standard algorithm by 2.5 fold for the right eye and by 1.8 fold for the left eye. However, the SITA SWAP algorithm overestimated the presence of visual field loss compared to the SITA Standard algorithm by 2.9 fold for the right eye and by 2.2 fold for the left eye and compared to the SITA Fast algorithm by 1.4 fold and 1.4 fold, respectively.

For the individuals with OAG (Table 3.21c), the SITA Standard algorithm yielded more extensive visual field loss compared to the SITA Fast algorithm. However, this only occurred in the field of the right eye by 1.9 fold. The field of the left eye exhibited parity between the two algorithms. The relationship between the two SAP algorithms and SWAP was less clear. The SITA SWAP algorithm overestimated the presence of visual field loss compared to the SITA Standard algorithm by 1.1 fold for the right eye and by 1.5 fold for the left eye. Compared to the SITA Fast algorithm, SITA SWAP algorithm underestimated the presence of visual field loss

by 1.6 fold for the right eye and overestimated the presence of visual field loss by1.6 fold for the left eye.

The between-algorithm performance in terms of the difference in the Total and in the Pattern Deviation probability level is summarized in Table 3.22.

Algorithm	Eye	Normal	OHT	OAG
SITA Standard	**RE**	2.5 / 1.3	-2.5 /-1.3	1.9 / 1.3
v SITA Fast	**LE**	1.5 / -1.1	-1.8 / 1.1	1.0 /-1.4
SITA Standard	**RE**	-1.3 /1.5	-2.9 /-1.2	1.1 / 1.0
v SITA SWAP	**LE**	-1.5 / 1.0	-2.2 / 1.1	1.5 / 1.0
SITA Fast	**RE**	-2.7 / 1.2	-1.4 / 1.1	-1.6 /-1.2
v SITA SWAP	**LE**	-2.0 / 1.1	-1.4 / 1.0	1.6 / 1.3

Table 3.22 The summary of the between-algorithm performance (Visits 5) expressed in terms of the ratio of the difference in the number of stimulus locations exhibiting an abnormal Total Deviation (Tables 3.21a to 3.21c) and Pattern Deviation probability level (Tables 3.23a to 3.23c) for each group. The value before the oblique is the overall incremental difference in the Total Deviation probability levels. The value after the oblique is the overall incremental difference in the Pattern Deviation probability levels. (A positive value indicates less field loss i.e. a fewer number of stimulus locations exhibiting a significant, and/ or a less significant, probability level relative to first algorithm and a negative value indicates more field loss i.e. a greater number of stimulus locations exhibiting a significant, and/ or a less significant, probability level relative to first algorithm).

The magnitudes of the Pattern Deviation probability levels across all locations between the given pair of algorithms are illustrated for the right and left eyes for the normal individuals in Table 3.23a, for the individuals with OHT in Table 3.23b and for the individuals with OAG in Table 3.23c. As with the corresponding tables for the Total Deviation probability levels, the shaded region indicates the number of locations exhibiting identical probability levels for each algorithm. The number of

locations exhibiting deeper defect, by probability level, for the given algorithm is indicated above or below the shading, respectively.

SITA Standard / SITA Fast

	NS	<5%	<2%	<1%	<0,5%
NS	1323	52	10	8	0
<5%	55	8	3	1	0
<2%	20	1	1	0	0
<1%	11	3	0	0	1
<0,5%	8	3	0	0	2

SITA Standard / SITA Fast

	NS	<5%	<2%	<1%	<0,5%
NS	1309	64	18	8	1
<5%	44	10	1	3	0
<2%	21	4	0	1	0
<1%	6	2	1	0	2
<0,5%	8	3	1	0	1

SITA Standard / SITA SWAP

	NS	<5%	<2%	<1%	<0,5%
NS	1318	43	16	5	11
<5%	64	0	1	0	0
<2%	22	0	0	0	0
<1%	14	1	0	0	0
<0,5%	13	0	0	0	0

SITA Standard / SITA SWAP

	NS	<5%	<2%	<1%	<0,5%
NS	1312	54	19	10	5
<5%	49	3	2	2	2
<2%	22	3	0	1	0
<1%	10	1	0	0	0
<0,5%	9	1	1	1	1

SITA Fast / SITA SWAP

	NS	<5%	<2%	<1%	<0,5%
NS	1350	40	14	4	9
<5%	58	3	2	1	1
<2%	14	0	0	0	0
<1%	6	1	1	0	1
<0,5%	3	0	0	0	0

SITA Fast / SITA SWAP

	NS	<5%	<2%	<1%	<0,5%
NS	1304	49	17	12	6
<5%	68	8	4	2	1
<2%	18	1	1	0	1
<1%	10	2	0	0	0
<0,5%	2	2	0	0	0

Table 3.23a The magnitudes of the Pattern Deviation probability levels between the respective algorithms at Visit 5, across all locations for the normal individuals for the right eye (left column) and left eye (right column). Top: SITA Standard v SITA Fast. Middle: SITA Standard v SITA SWAP. Bottom: SITA Fast v SITA SWAP. The shading indicates the number of locations exhibiting identical probability levels. The number of locations exhibiting a deeper defect, by probability level, for the given algorithm is indicated either above or below the shading, respectively.

SITA Fast

SITA Standard	NS	<5%	<2%	<1%	<0,5%
NS	1122	59	15	7	6
<5%	54	10	4	1	1
<2%	6	4	0	0	0
<1%	3	5	1	1	0
<0,5%	1	0	0	0	0

SITA Fast

SITA Standard	NS	<5%	<2%	<1%	<0,5%
NS	1103	53	13	8	4
<5%	57	7	3	4	0
<2%	12	4	4	2	0
<1%	11	2	0	2	1
<0,5%	6	1	0	0	3

SITA SWAP

SITA Standard	NS	<5%	<2%	<1%	<0,5%
NS	1120	55	18	7	9
<5%	57	9	3	1	0
<2%	8	2	0	0	0
<1%	9	0	0	1	0
<0,5%	1	0	0	0	0

SITA SWAP

SITA Standard	NS	<5%	<2%	<1%	<0,5%
NS	1098	49	16	7	11
<5%	56	11	3	0	1
<2%	18	4	0	0	0
<1%	12	2	0	0	2
<0,5%	5	3	0	0	2

SITA SWAP

SITA Fast	NS	<5%	<2%	<1%	<0,5%
NS	1108	49	17	6	8
<5%	60	12	3	3	0
<2%	14	4	1	0	1
<1%	8	1	0	0	0
<0,5%	7	0	0	0	0

SITA SWAP

SITA Fast	NS	<5%	<2%	<1%	<0,5%
NS	1099	56	14	6	14
<5%	54	9	3	1	0
<2%	17	1	2	0	0
<1%	13	3	0	0	0
<0,5%	6	0	0	0	1

Table 3.23b The magnitudes of the Pattern Deviation probability levels between the respective algorithms at Visit 5, across all locations for the individuals with OHT for the right eye (left column) and left eye (right column). Top: SITA Standard v SITA Fast. Middle: SITA Standard v SITA SWAP. Bottom: SITA Fast v SITA SWAP. The shading indicates the number of locations exhibiting identical probability levels. The number of locations exhibiting a deeper defect, by probability level, for the given algorithm is indicated either above or below the shading, respectively.

SITA Standard \ SITA Fast	NS	<5%	<2%	<1%	<0,5%
NS	1068	51	17	4	1
<5%	45	8	4	1	1
<2%	15	3	3	0	1
<1%	10	4	3	2	1
<0,5%	10	6	3	7	34

SITA Standard \ SITA Fast	NS	<5%	<2%	<1%	<0,5%
NS	1054	57	22	15	10
<5%	43	9	5	7	2
<2%	3	7	2	3	3
<1%	8	3	3	2	4
<0,5%	5	6	6	9	12

SITA Standard \ SITA SWAP	NS	<5%	<2%	<1%	<0,5%
NS	1033	66	15	13	14
<5%	49	8	2	0	0
<2%	16	1	3	1	1
<1%	9	3	3	2	3
<0,5%	17	11	2	1	29

SITA Standard \ SITA SWAP	NS	<5%	<2%	<1%	<0,5%
NS	1057	59	15	11	16
<5%	51	6	1	3	5
<2%	13	3	0	2	0
<1%	15	2	3	0	0
<0,5%	20	3	4	1	10

SITA Fast \ SITA SWAP	NS	<5%	<2%	<1%	<0,5%
NS	1038	62	17	13	18
<5%	52	8	5	3	2
<2%	21	7	1	1	0
<1%	8	3	1	0	2
<0,5%	5	7	1	0	25

SITA Fast \ SITA SWAP	NS	<5%	<2%	<1%	<0,5%
NS	1020	55	12	12	14
<5%	65	8	4	2	3
<2%	27	3	4	0	4
<1%	24	4	0	1	7
<0,5%	20	3	3	2	3

Table 3.23c The magnitudes of the Pattern Deviation probability levels between the respective algorithms at Visit 5, across all locations for the individuals with OAG for the right eye (left column) and left eye (right column). Top: SITA Standard v SITA Fast. Middle: SITA Standard v SITA SWAP. Bottom: SITA Fast v SITA SWAP. The shading indicates the number of locations exhibiting identical probability levels. The number of locations exhibiting a deeper defect, by probability level, for the given algorithm is indicated either above or below the shading, respectively.

In general, in terms of the Pattern Deviation probability analysis, each algorithm exhibits broadly similar results in each of the diagnostic groups. For the normal individuals (Table 3.23a), the SITA Standard algorithm tended to overestimate the presence of visual field loss compared to the SITA Fast algorithm by 1.3 fold for the right eye and underestimate by 1.1 fold for the left eye. The SITA Standard algorithm overestimated the presence of visual field loss compared to the SITA

SWAP algorithm by 1.5 fold for the right eye and these algorithms exhibited parity for the left eye. The SITA Fast algorithm compared to the SITA SWAP algorithm tended to overestimate slightly the presence of visual field loss, namely, by 1.2 fold for the right eye and by 1.1 fold for the left eye.

For the individuals with OHT (Table 3.23b), the SITA Fast algorithm slightly overestimated the presence of visual field loss compared to the SITA Standard algorithm by 1.3 fold for the right eye and underestimated the presence of visual field loss by 1.1 fold for the left eye. The SITA SWAP algorithm overestimated the presence of visual field loss compared to the SITA Standard algorithm by 1.2 fold for the right eye and underestimated the presence of visual field loss by 1.1 fold for the left eye. The SITA Fast algorithm also underestimated the presence of visual field loss by 1.1 fold for the right and exhibited parity for the left eye.

For the individuals with OAG (Table 3.23c), the SITA Standard algorithm yielded similar extensive visual field loss compared to the SITA Fast algorithm, namely by 1.3 fold for the right eye and by 1.4 fold for the left eye. The SITA SWAP algorithm demonstrated parity for the right and the left eye to the SITA Standard algorithm. The SITA SWAP algorithm, compared with the SITA Fast algorithm overestimated the presence of visual field loss by 1.2 fold for the right eye and underestimated the presence of visual field loss by1.3 fold for the left eye.

The extent of the within-algorithm between-individual variability at each stimulus location for the normal individuals provides some indication of the confidence intervals for normality for the given algorithm. The Coefficient of Variation (CoV),

i.e. the standard deviation divided by the mean, at each stimulus location for each of the three algorithms at Visit 1 and at Visit 5 for each eye is given in Figures 3.17a to 3.17l and the ratio of the CoV between the three algorithm at Visit 1 and Visit 5 in Figures 3.18a to 3.18l. The use of the CoV overcomes the difference in the dynamic ranges, i.e. the dB scales, between SAP and SWAP.

		10.11	10.48	9.19	12.63		
	8.75	8.75	5.95	5.38	6.39	6.71	
8.09	5.66	5.37	4.13	5.72	4.58	8.81	6.57
9.60	7.07	4.73	2.87	4.55	4.64	5.02	6.02
9.42	6.37	4.40	3.94	3.79	3.35	3.54	6.27
8.78	5.72	4.26	3.54	4.78	6.41	7.18	9.40
	8.46	5.67	4.52	9.69	5.89	8.30	
		7.85	7.12	7.56	7.97		

Figure 3.17a The CoV (the SD divided by the mean) expressed as a percentage for the right eye of the normal individuals at each stimulus location for the SITA Standard algorithm at Visit 1.

> 10	> 14	> 18	> 22	> 26	> 30

		10.33	12.00	14.28	14.03		
	8.63	8.38	8.36	7.97	5.99	8.12	
7.87	6.76	5.23	5.07	5.51	5.23	6.99	10.60
9.87	8.60	4.92	3.91	3.43	2.97	4.55	9.36
10.36	6.54	4.87	4.05	3.25	3.70	5.91	6.43
8.40	5.14	4.09	3.13	4.18	5.13	7.28	7.50
	7.28	4.94	4.44	5.34	5.56	10.67	
		7.83	9.53	8.12	8.59		

Figure 3.17b The CoV (the SD divided by the mean) expressed as a percentage for the left eye of the normal individuals at each stimulus location for the SITA Standard algorithm at Visit 1. The figure is represented in right eye format.

		6.87	7.44	9.89	12.02		
	9.40	6.68	6.47	5.63	6.15	7.62	
12.64	7.52	7.30	5.55	5.29	5.96	5.71	6.51
9.39	5.66	4.91	4.05	3.65	4.98	5.40	5.47
10.86	5.28	3.47	3.58	4.17	3.25	3.04	7.05
	4.86	4.65	10.68	5.98	5.22	6.85	5.79	7.22
	8.82	4.22	4.52	3.92	4.29	6.13	
		6.87	5.66	5.16	7.86		

Figure 3.17c The CoV (the SD divided by the mean) expressed as a percentage for the right eye of the normal individuals at each stimulus location for the SITA Fast algorithm at Visit 1.

> 10	> 14	> 18	> 22	> 26	> 30

		8.91	12.20	17.40	13.57		
	6.57	6.38	6.40	8.47	6.76	10.50	
11.18	5.02	4.57	4.58	5.91	6.84	7.37	6.09
9.74	5.98	4.29	3.88	3.70	3.94	5.35	8.46
10.77	5.04	4.18	4.55	3.49	3.03	4.40	7.11
	8.45	4.75	4.81	3.43	3.60	4.45	8.18	8.83
	5.24	4.61	4.30	4.80	4.49	8.78	
		6.58	6.39	5.93	5.66		

Figure 3.17d The CoV (the SD divided by the mean) expressed as a percentage for the left eye of the normal individuals at each stimulus location for the SITA Fast algorithm at Visit 1. The figure is represented in right eye format.

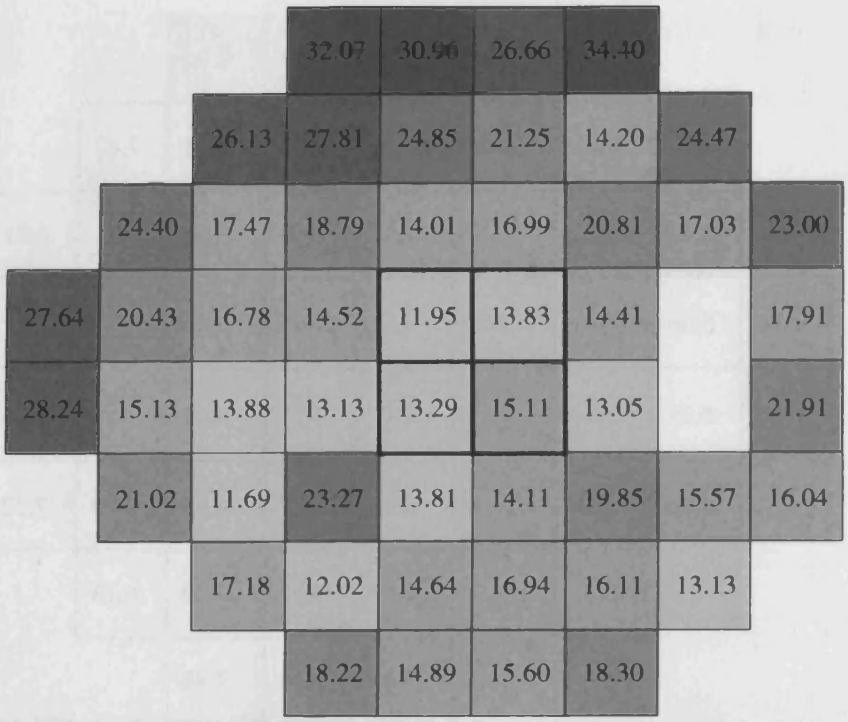

Figure 3.17e The CoV (the SD divided by the mean) expressed as a percentage for the right eye of the normal individuals at each stimulus location for the SITA SWAP algorithm at Visit 1.

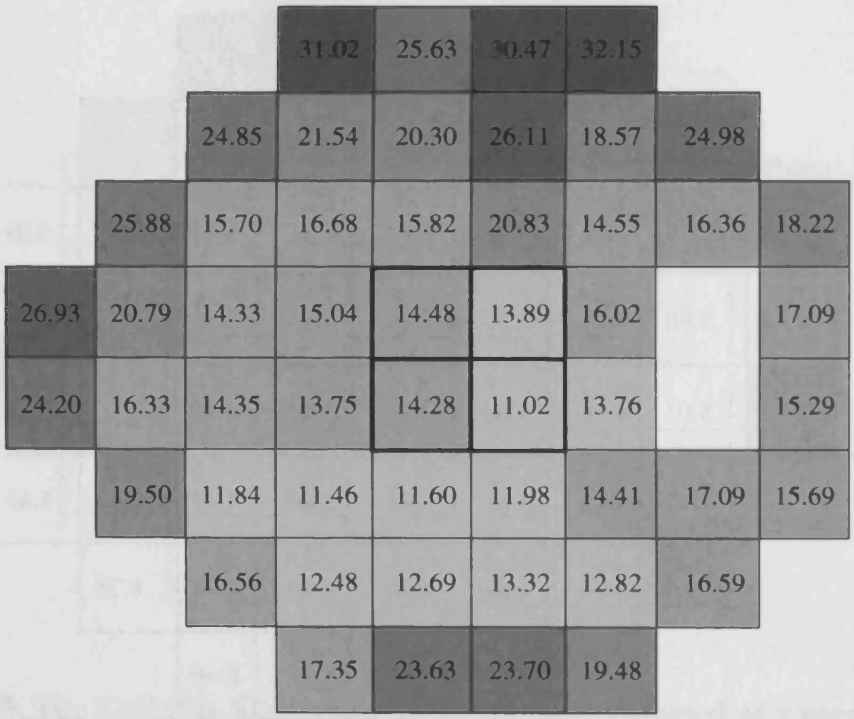

Figure 3.17f The CoV (the SD divided by the mean) expressed as a percentage for the left eye of the normal individuals at each stimulus location for the SITA SWAP algorithm at Visit 1. The figure is represented in right eye format.

		16.43	13.57	10.75	12.30		
	10.28	6.63	8.01	6.28	6.63	10.20	
12.30	6.06	6.56	5.24	5.21	4.98	6.75	8.85
13.68	9.69	6.06	4.08	4.78	3.84	4.46	8.66
12.39	9.76	5.61	4.33	2.93	3.23	4.69	6.31
10.71	5.52	5.16	4.92	4.29	5.25	5.79	7.17
	8.12	5.03	6.14	5.83	5.01	6.16	
		7.89	8.67	6.64	6.63		

Figure 3.17g The CoV (the SD divided by the mean) expressed as a percentage for the right eye of the normal individuals at each stimulus location for the SITA Standard algorithm at Visit 5.

> 10	> 14	> 18	> 22	> 26	> 30

		18.52	12.53	11.45	14.31		
	10.32	7.81	8.74	7.92	6.85	11.13	
8.67	6.21	6.60	5.14	6.12	6.89	9.97	9.70
20.82	7.39	6.77	5.48	4.85	5.51	6.15	14.28
22.69	7.61	6.40	4.67	5.24	4.84	5.83	7.76
9.92	6.08	5.06	4.60	4.78	6.22	7.73	7.42
	7.97	6.52	6.50	6.27	5.59	6.42	
		17.56	10.87	10.41	9.53		

Figure 3.17h The CoV (the SD divided by the mean) expressed as a percentage for the left eye of the normal individuals at each stimulus location for the SITA Standard algorithm at Visit 5. The figure is represented in right eye format.

		8.21	5.80	5.73	10.94		
	8.43	4.69	4.73	5.30	5.92	8.64	
7.96	5.24	4.61	4.72	3.76	4.29	5.35	6.59
16.33	4.81	4.30	3.43	3.54	3.62	3.30	8.71
7.47	8.17	2.66	2.81	3.51	3.18	5.05	5.23
	6.82	4.46	3.34	3.99	3.14	4.91	5.08	6.50
	6.17	4.73	3.65	4.06	3.69	7.59	
		5.98	4.77	4.83	6.61		

Figure 3.17i The CoV (the SD divided by the mean) expressed as a percentage for the right eye of the normal individuals at each stimulus location for the SITA Fast algorithm at Visit 5.

> 10	> 14	> 18	> 22	> 26	> 30

		9.82	8.02	9.24	11.03		
	8.62	7.01	6.25	6.99	6.83	9.11	
6.83	5.38	5.54	4.84	5.34	4.77	4.31	9.33
6.25	4.72	5.19	4.26	3.53	3.39	4.85	7.89
8.84	5.86	4.69	3.33	3.95	3.38	4.28	5.30
	9.41	6.16	4.69	4.25	5.85	5.04	5.73	6.29
	6.46	6.12	5.72	5.04	5.89	5.53	
		7.63	6.34	5.73	7.15		

Figure 3.17j The CoV (the SD divided by the mean) expressed as a percentage for the left eye of the normal individuals at each stimulus location for the SITA Fast algorithm at Visit 5. The figure is represented in right eye format.

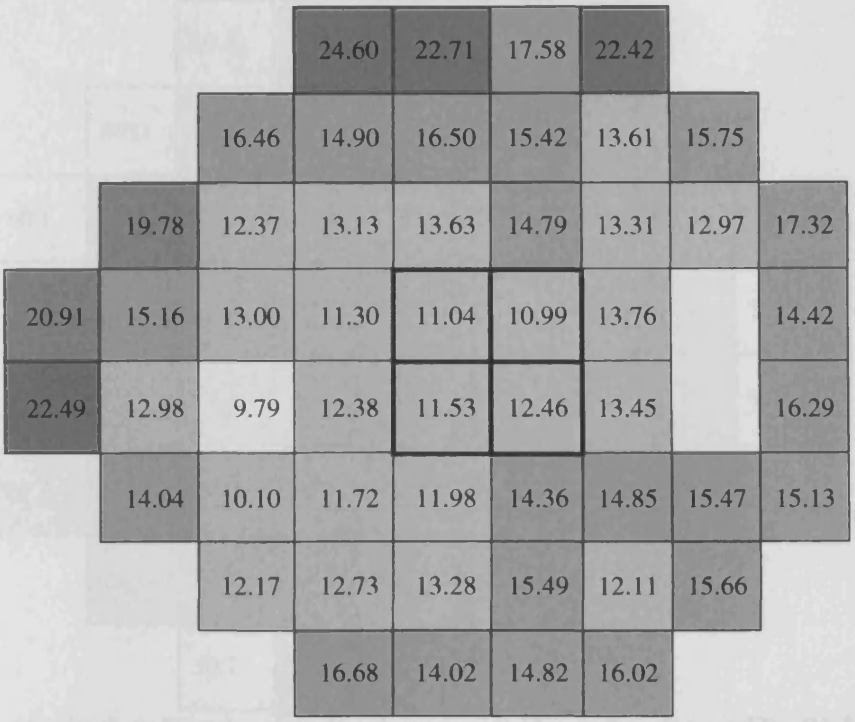

Figure 3.17k The CoV (the SD divided by the mean) expressed as a percentage for the right eye of the normal individuals at each stimulus location for the SITA SWAP algorithm at Visit 5.

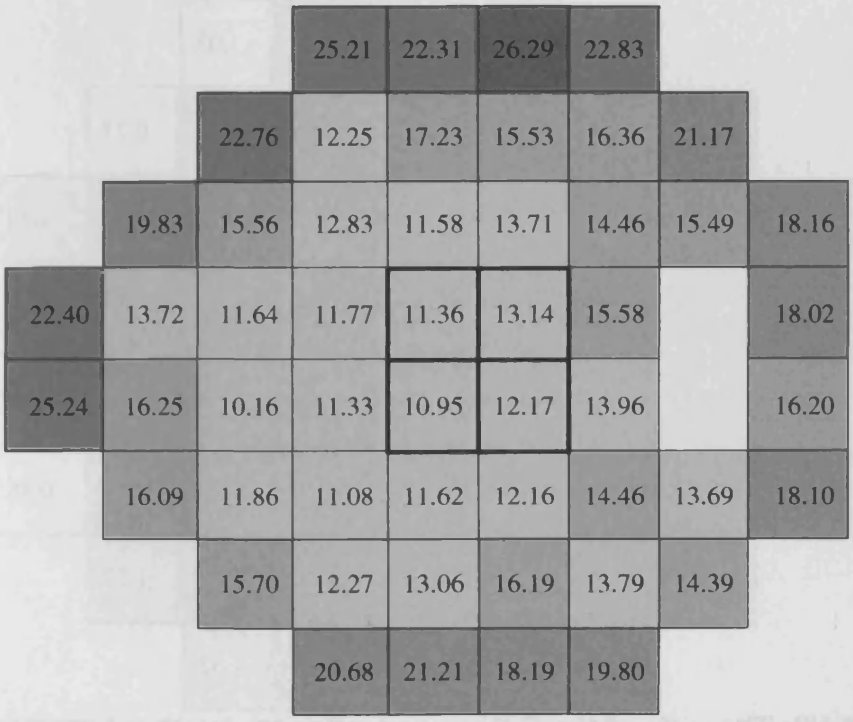

Figure 3.17l The CoV (the SD divided by the mean) expressed as a percentage for the left eye of the normal individuals at each stimulus location for the SITA SWAP algorithm at Visit 5. The figure is represented in right eye format.

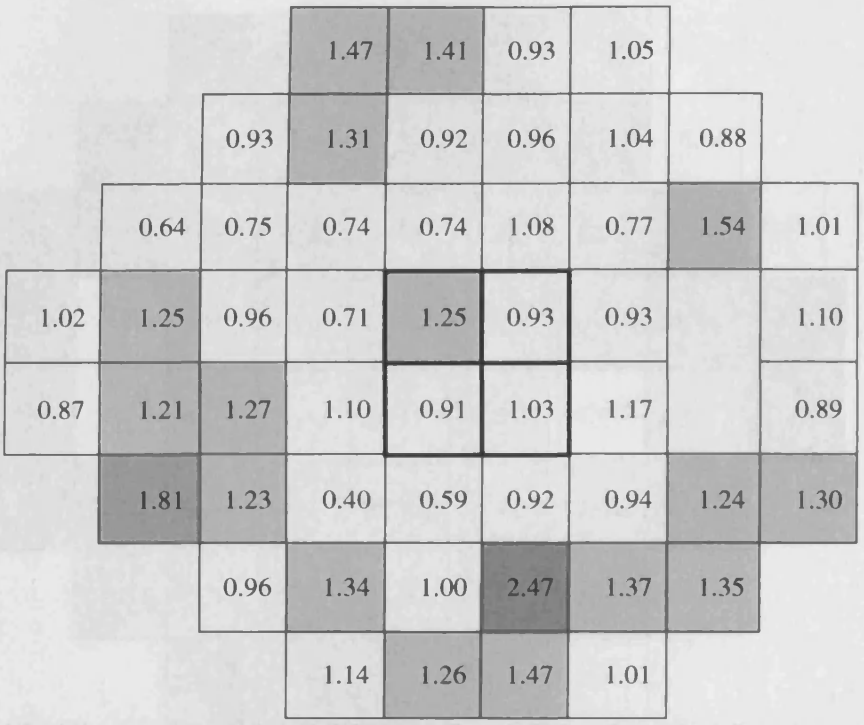

Figure 3.18a The ratio of the CoV at each stimulus location between the SITA Standard and the SITA Fast algorithms at Visit 1 for the right eye of the normal individuals.

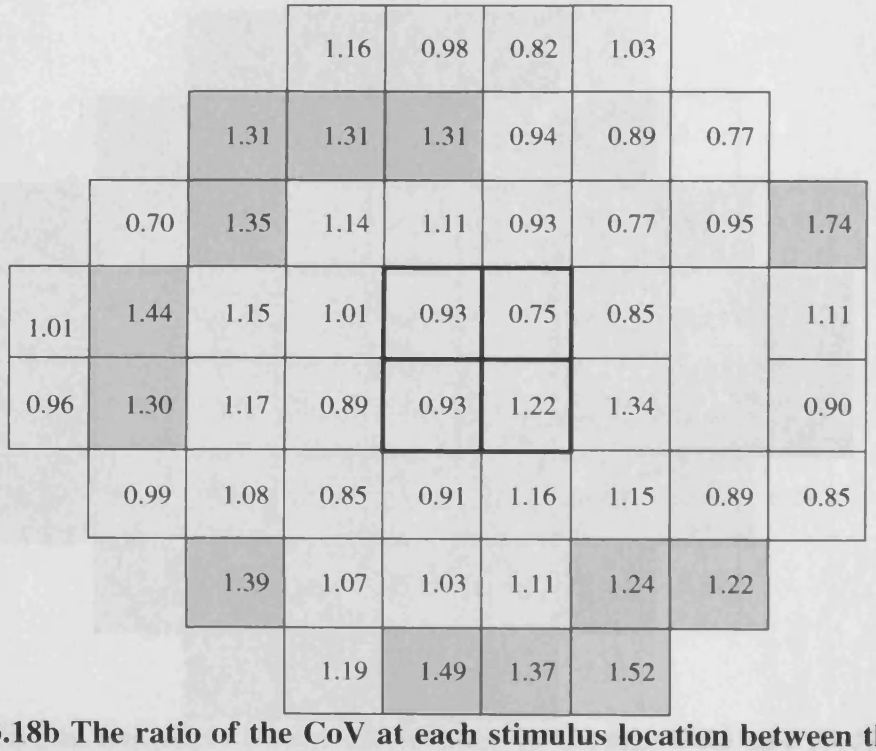

Figure 3.18b The ratio of the CoV at each stimulus location between the SITA Standard and the SITA Fast algorithms at Visit 1 for the left eye of the normal individuals. The figure is represented in right eye format.

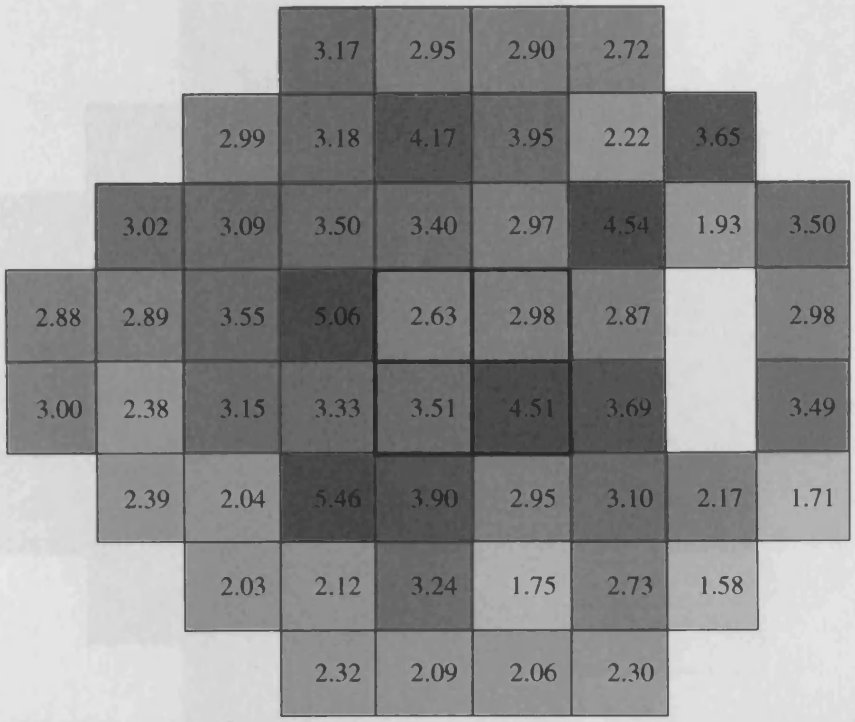

Figure 3.18c The ratio of the CoV at each stimulus location between the SITA SWAP and the SITA Standard algorithms at Visit 1 for the right eye of the normal individuals.

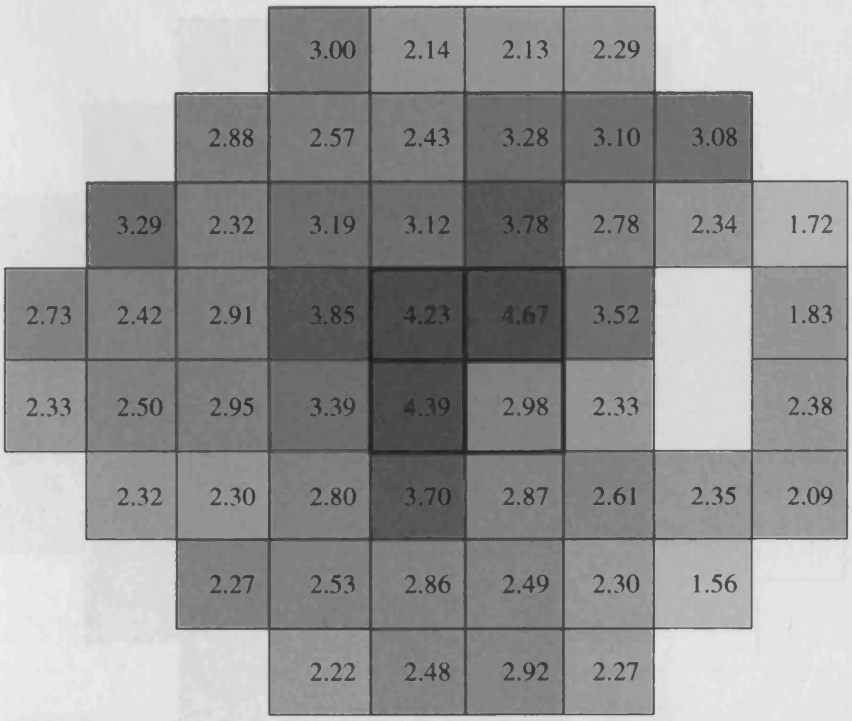

Figure 3.18d The ratio of the CoV at each stimulus location between the SITA SWAP and the SITA Standard algorithms at Visit 1 for the left eye of the normal individuals. The figure is represented in right eye format.

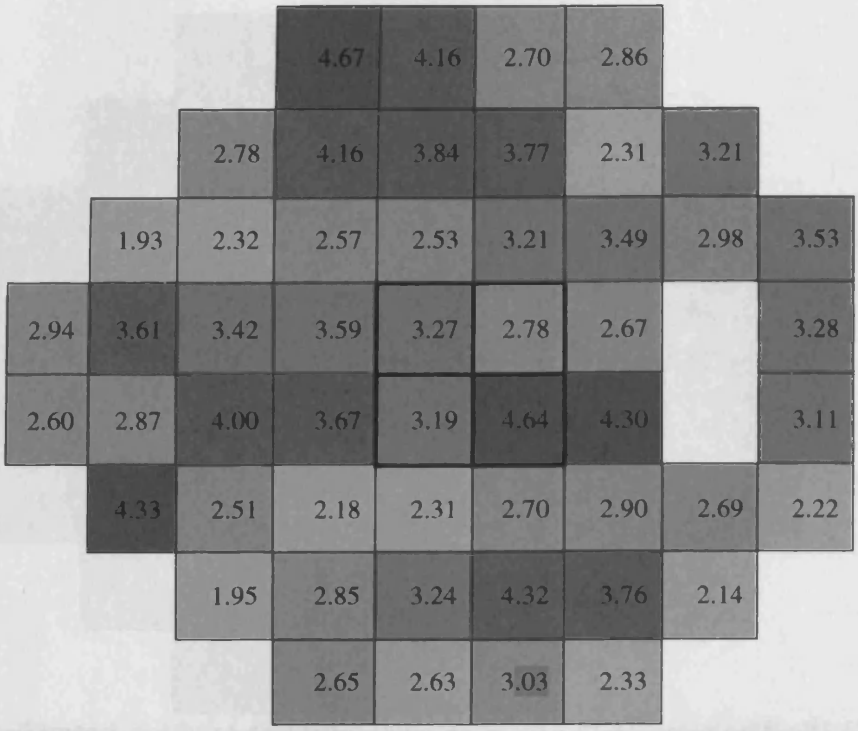

Figure 3.18e The ratio of the CoV at each stimulus location between the SITA SWAP and the SITA Fast algorithms at Visit 1 for the right eye of the normal individuals.

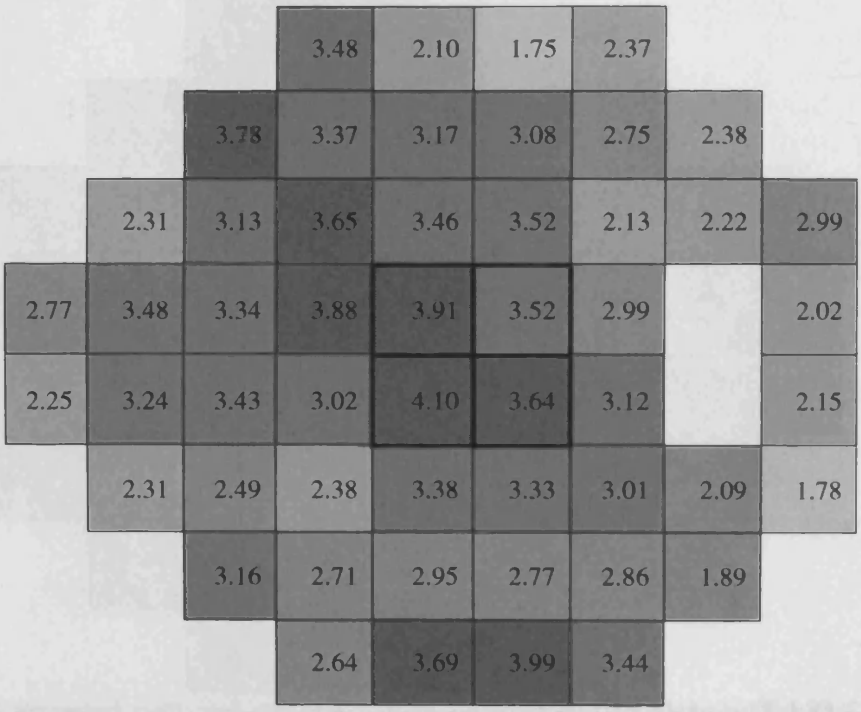

Figure 3.18f The ratio of the CoV at each stimulus location between the SITA SWAP and the SITA Fast algorithms at Visit 1 for the left eye of the normal individuals. The figure is represented in right eye format.

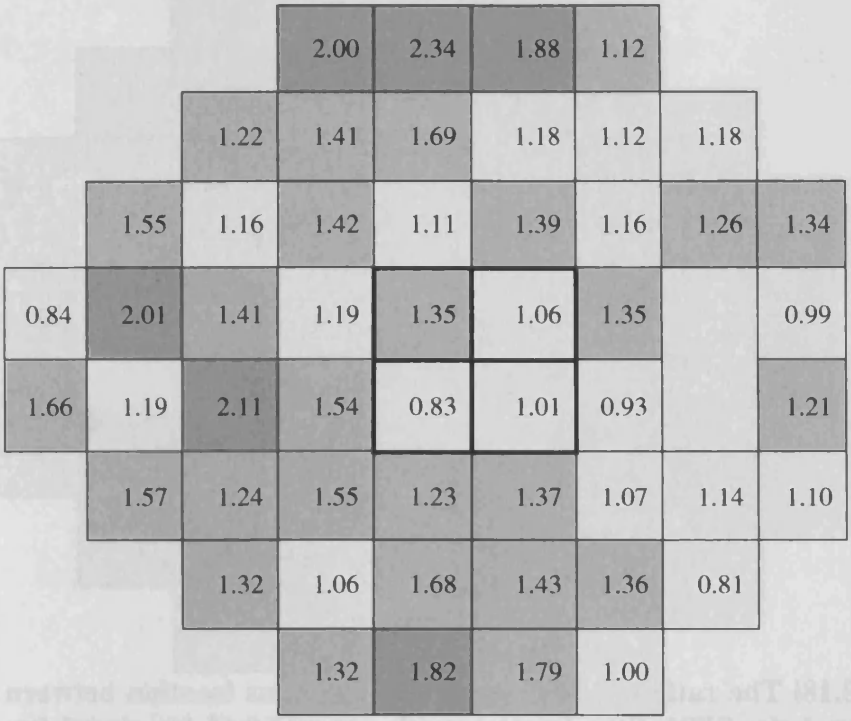

Figure 3.18g The ratio of the CoV at each stimulus location between the SITA Standard and the SITA Fast algorithms at Visit 5 for the right eye of the normal individuals.

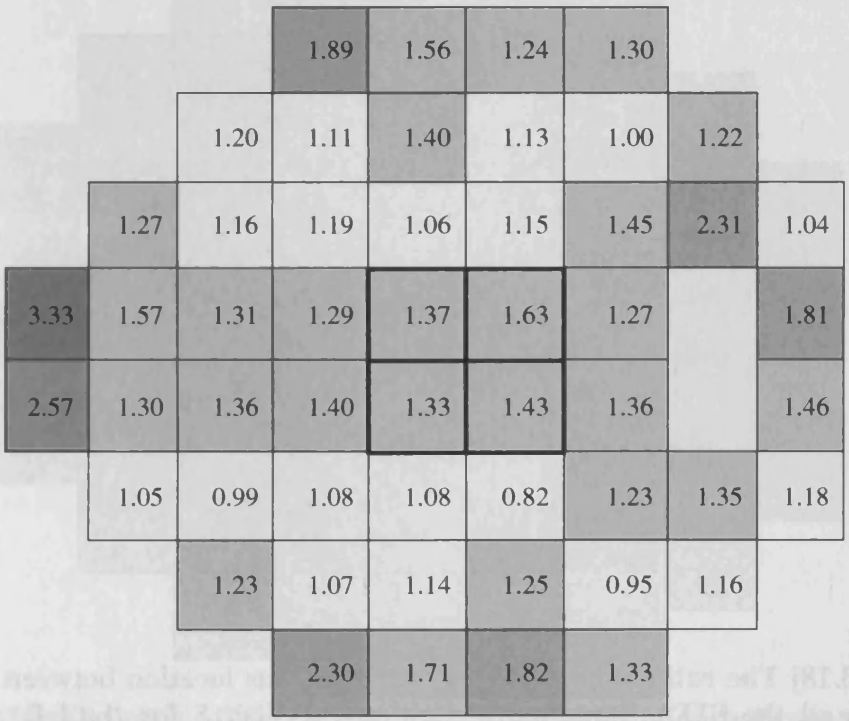

Figure 3.18h The ratio of the CoV at each stimulus location between the SITA Standard and the SITA Fast algorithms at Visit 5 for the left eye of the normal individuals. The figure is represented in right eye format.

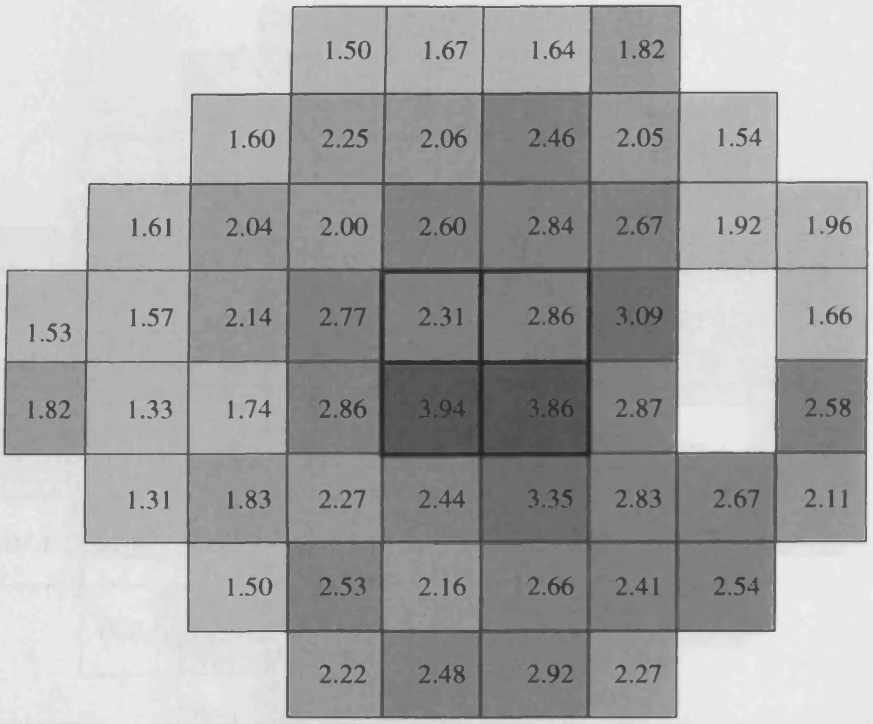

Figure 3.18i The ratio of the CoV at each stimulus location between the SITA SWAP and the SITA Standard algorithms at Visit 5 for the right eye of the normal individuals.

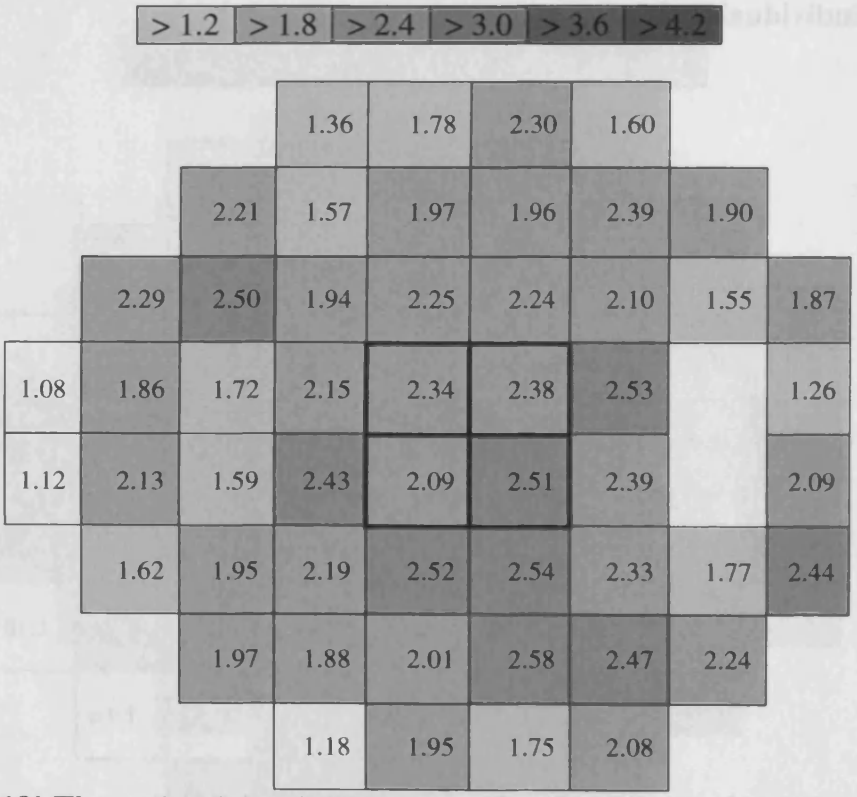

Figure 3.18j The ratio of the CoV at each stimulus location between the SITA SWAP and the SITA Standard algorithms at Visit 5 for the left eye of the normal individuals. The figure is represented in right eye format.

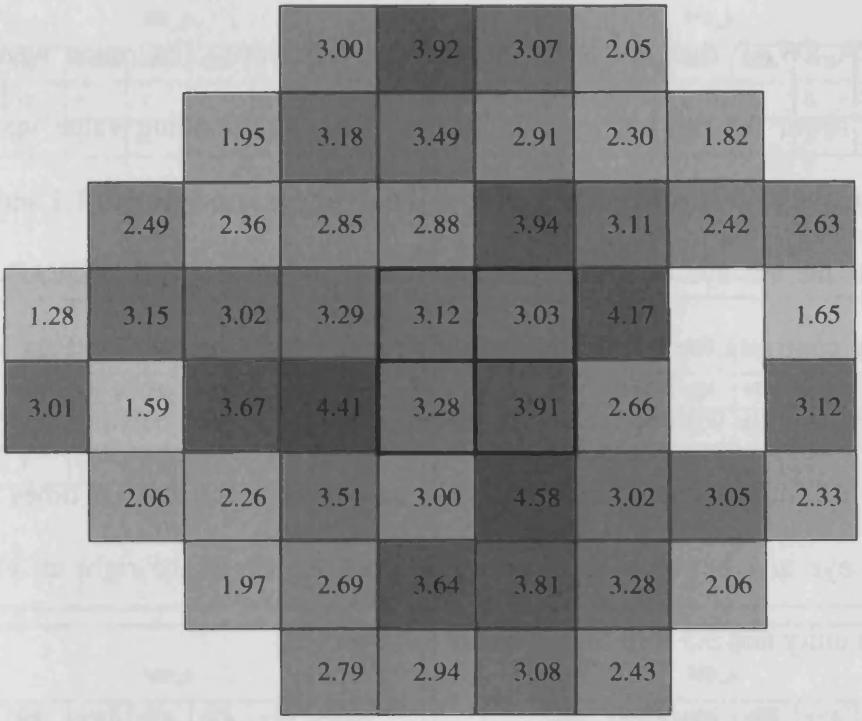

Figure 3.18k The ratio of the CoV at each stimulus location between the SITA SWAP and the SITA Fast algorithms at Visit 5 for the right eye of the normal individuals.

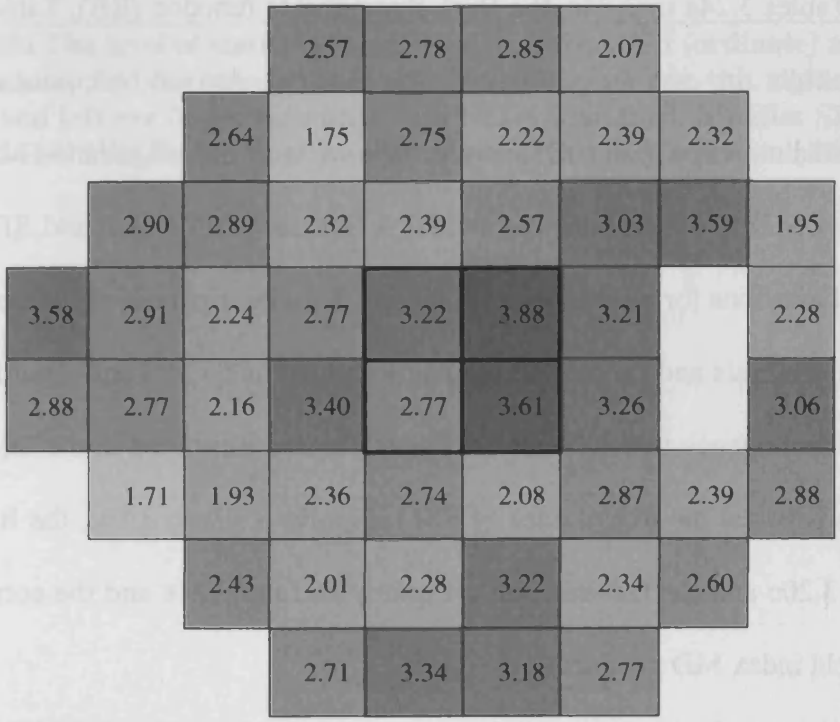

Figure 3.18l The ratio of the CoV at each stimulus location between the SITA SWAP and the SITA Fast algorithms at Visit 5 for the left eye of the normal individuals. The figure is represented in right eye format.

At Visit 1 the CoV for SWAP was between approximately 1.75 and 4.5 times larger for SITA SWAP than for SITA Standard in each eye. The ratios were possibly slightly lower for the left eye. At Visit 5, the corresponding value was between approximately 1.3 and 4 times higher for the right eye and between 1.1 and 2.5 times higher in the left eye. A similar trend was present between SITA SWAP and SITA Fast. In contrast, the ratios between SITA Standard and SITA Fast at Visit 1 increased slightly with increasing in eccentricity and ranged between approximately 0.4 and 2.5 times higher for the right eye and between 0.8 and 1.7 times higher for the left eye and between unity and 2.4 times higher in the right at Visit 5 and between unity and 3.3 fold higher in the left eye.

3.4.4 The structure-function relationship

The relationship between the magnitudes of the Mikelberg discriminate function (FSM), Tables 3.24a to 3.24c, the Burk discriminate function (RB), Tables 3.25a to 3.25c, and the rim-disc ratio, Tables 3.26a to 3.26c, derived by confocal scanning laser ophthalmoscopy (HRT II) were compared with the magnitudes of the visual field index MD (p values) derived by SITA Standard, SITA Fast and SITA SWAP across all locations for each algorithm at Visit 5 for the right and the left eyes for the normal individuals and for the individuals with OHT and OAG and are illustrated in terms of contingency tables. This relationship is also illustrated in the form of Venn diagrams between the magnitudes of FSM, Figures 3.19a to 3.19c, the RB, Figures 3.20a to 3.20c and the rim-disc ratio, Figures 3.21a to 3.21c and the corresponding visual field index MD p values.

MD_p

FSM	NS	<10%	<5%	<2%	<1%	<0,5%
NS	18	0	1	1	0	0
-	6	0	0	0	0	0

MD_p

FSM	NS	<10%	<5%	<2%	<1%	<0,5%
NS	16	0	0	0	0	1
-	9	0	0	0	0	0

MD_p

FSM	NS	<10%	<5%	<2%	<1%	<0,5%
NS	20	0	0	0	0	0
-	6	0	0	0	0	0

MD_p

FSM	NS	<10%	<5%	<2%	<1%	<0,5%
NS	15	1	1	0	0	0
-	9	0	0	0	0	0

MD_p

FSM	NS	<10%	<5%	<2%	<1%	<0,5%
NS	16	3	1	0	0	0
-	6	0	0	0	0	0

MD_p

FSM	NS	<10%	<5%	<2%	<1%	<0,5%
NS	12	4	1	0	0	0
-	8	0	1	0	0	0

Table 3.24a The level of statistical significance of the FSM (ordinate) and of the MD (abscissa) for the normal individuals at Visit 5 for the right eye (left column) and left eye (right column). Top: SITA Standard. Middle: SITA Fast. Bottom: SITA SWAP. The '-' sign indicates a statistically abnormal FSM.

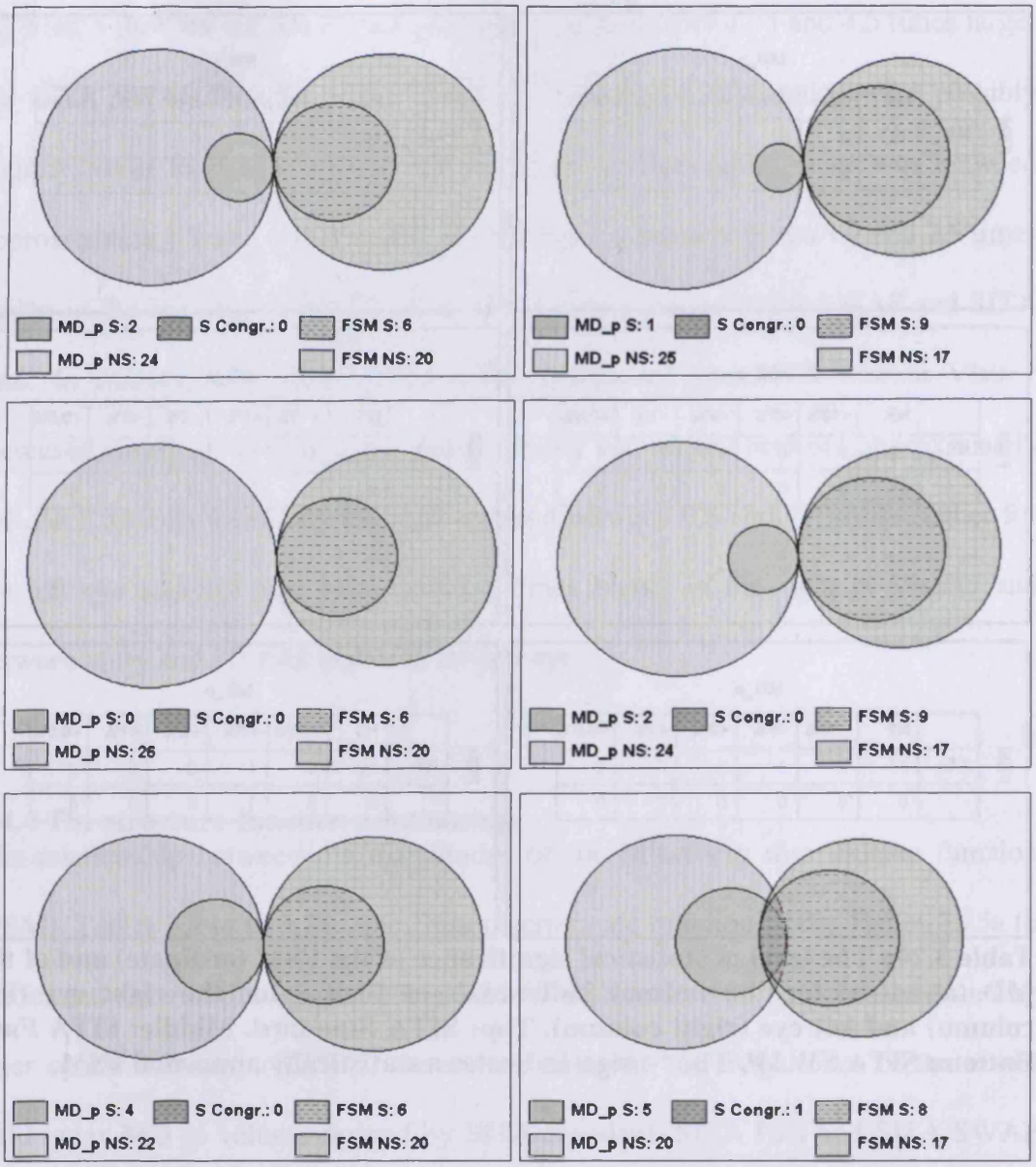

Figure 3.19a Venn diagrams, drawn to scale, illustrating the relationship between the presence (S) or absence of statistical significance (NS) associated with the respective values of FSM and MD for the normal individuals at Visit 5 for the right eye (left column) and left eye (right column). Top: SITA Standard. Middle: SITA Fast. Bottom: SITA SWAP. The number of individuals in whom both measures indicate statistically significant abnormality (S Congr[uence]) is indicated by the overlap and size of the respective two circles.

MD_p

FSM	NS	<10%	<5%	<2%	<1%	<0,5%
NS	20	0	0	0	0	0
-	4	0	0	0	0	0

MD_p

FSM	NS	<10%	<5%	<2%	<1%	<0,5%
NS	19	0	0	0	0	0
-	5	0	0	0	0	0

MD_p

FSM	NS	<10%	<5%	<2%	<1%	<0,5%
NS	19	1	0	0	0	0
-	4	0	0	0	0	0

MD_p

FSM	NS	<10%	<5%	<2%	<1%	<0,5%
NS	17	2	0	0	0	0
-	5	0	0	0	0	0

MD_p

FSM	NS	<10%	<5%	<2%	<1%	<0,5%
NS	17	2	1	0	0	0
-	4	0	0	0	0	0

MD_p

FSM	NS	<10%	<5%	<2%	<1%	<0,5%
NS	15	1	3	0	0	0
-	5	0	0	0	0	0

Table 3.24b The level of statistical significance of the FSM (ordinate) and of the MD (abscissa) for the individuals with OHT at Visit 5 for the right eye (left column) and left eye (right column). Top: SITA Standard. Middle: SITA Fast. Bottom: SITA SWAP. The '-'sign indicates a statistically abnormal FSM.

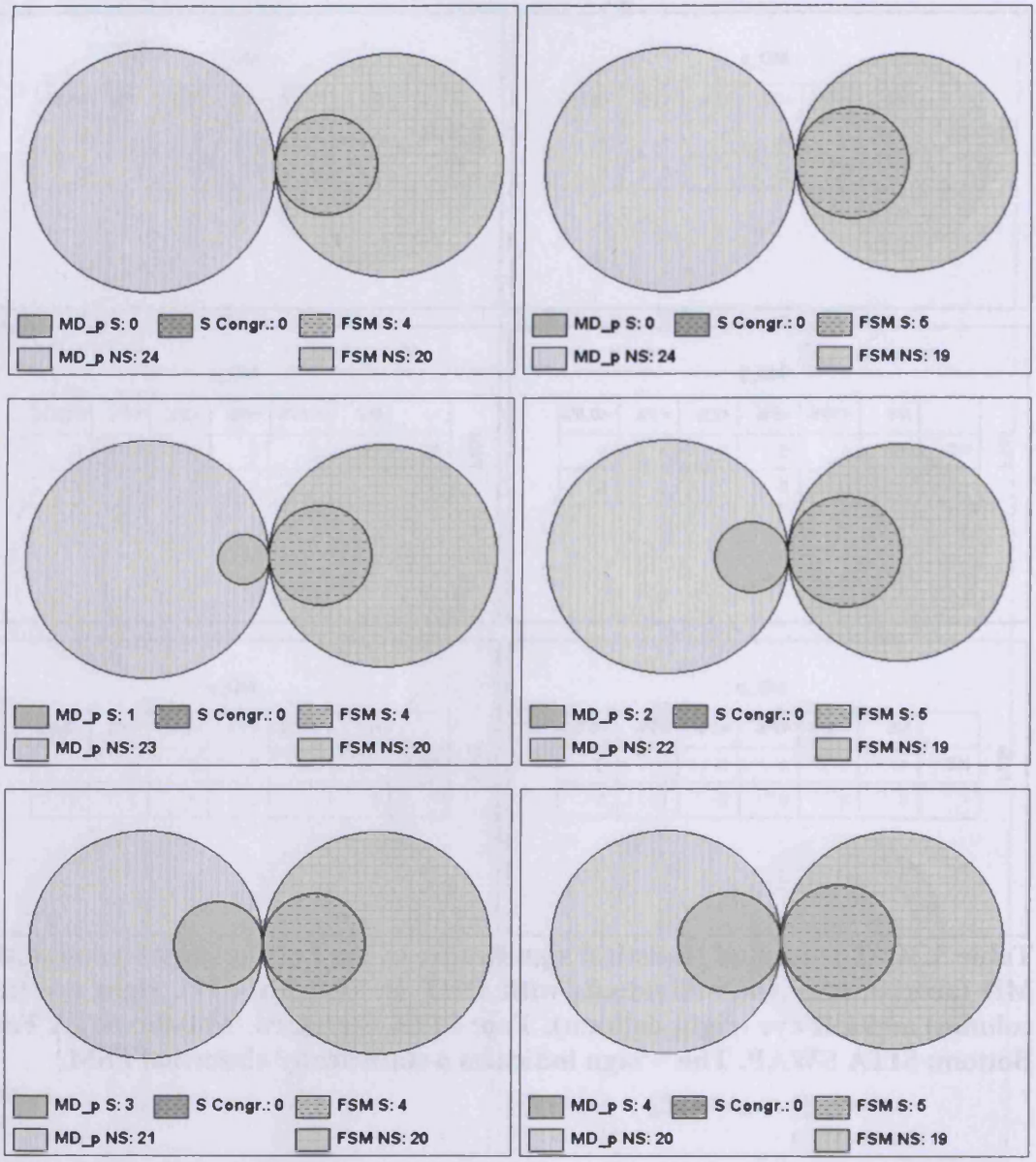

Figure 3.19b Venn diagrams, drawn to scale, illustrating the relationship between the presence (S) or absence of statistical significance (NS) associated with the respective values of FSM and MD for the individuals with OHT at Visit 5 for the right eye (left column) and left eye (right column). Top: SITA Standard. Middle: SITA Fast. Bottom: SITA SWAP. The number of individuals in whom both measures indicate statistically significant abnormality (S Congr[uence]) is indicated by the overlap and size of the respective two circles.

MD_p

FSM	NS	<10%	<5%	<2%	<1%	<0,5%
NS	8	0	0	0	0	0
-	13	2	0	0	1	1

MD_p

FSM	NS	<10%	<5%	<2%	<1%	<0,5%
NS	7	1	1	0	0	0
-	13	0	0	1	1	1

MD_p

FSM	NS	<10%	<5%	<2%	<1%	<0,5%
NS	8	0	0	0	0	0
-	14	1	0	1	0	1

MD_p

FSM	NS	<10%	<5%	<2%	<1%	<0,5%
NS	7	1	1	0	0	0
-	12	1	1	0	2	0

MD_p

FSM	NS	<10%	<5%	<2%	<1%	<0,5%
NS	7	0	1	0	0	0
-	13	2	1	0	0	1

MD_p

FSM	NS	<10%	<5%	<2%	<1%	<0,5%
NS	7	1	1	0	0	0
-	13	1	1	0	0	1

Table 3.24c The level of statistical significance of the FSM (ordinate) and of the MD (abscissa) for the individuals with OAG at Visit 5 for the right eye (left column) and left eye (right column). Top: SITA Standard. Middle: SITA Fast. Bottom: SITA SWAP. The '-'sign indicates a statistically abnormal FSM.

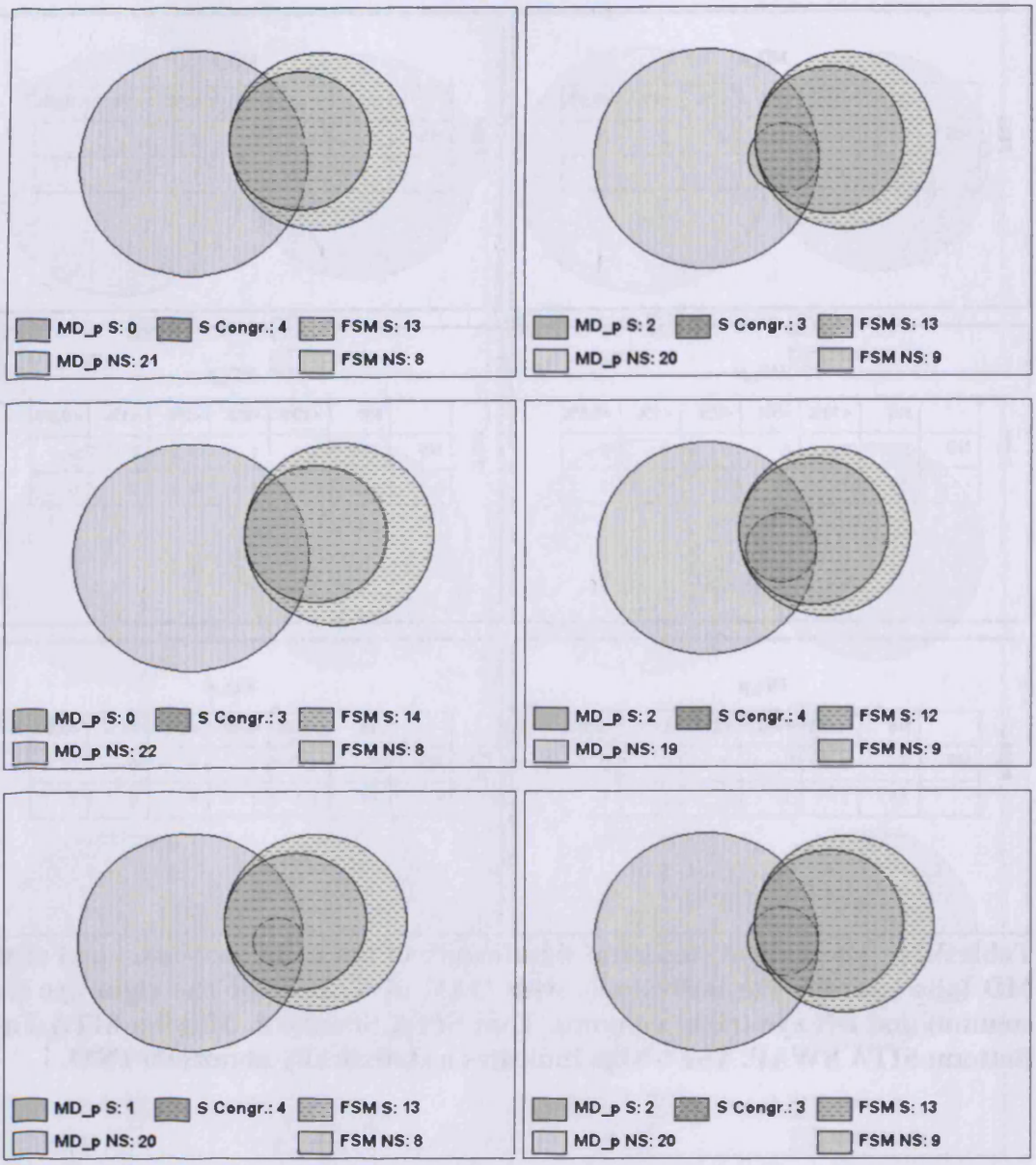

Figure 3.19c Venn diagrams, drawn to scale, illustrating the relationship between the presence (S) or absence of statistical significance (NS) associated with the respective values of FSM and MD for the individuals with OAG at Visit 5 for the right eye (left column) and left eye (right column). Top: SITA Standard. Middle: SITA Fast. Bottom: SITA SWAP. The number of individuals in whom both measures indicate statistically significant abnormality (S Congr[uence]) is indicated by the overlap and size of the respective two circles.

MD_p

RB	NS	<10%	<5%	<2%	<1%	<0,5%
NS	22	0	1	1	0	0
-	2	0	0	0	0	0

MD_p

RB	NS	<10%	<5%	<2%	<1%	<0,5%
NS	23	0	0	0	0	1
-	2	0	0	0	0	0

MD_p

RB	NS	<10%	<5%	<2%	<1%	<0,5%
NS	24	0	0	0	0	0
-	2	0	0	0	0	0

MD_p

RB	NS	<10%	<5%	<2%	<1%	<0,5%
NS	22	1	1	0	0	0
-	2	0	0	0	0	0

MD_p

RB	NS	<10%	<5%	<2%	<1%	<0,5%
NS	20	3	1	0	0	0
-	2	0	0	0	0	0

MD_p

RB	NS	<10%	<5%	<2%	<1%	<0,5%
NS	18	4	2	0	0	0
-	2	0	0	0	0	0

Table 3.25a The level of statistical significance of the RB (ordinate) and of the MD (abscissa) for the normal individuals at Visit 5 for the right eye (left column) and left eye (right column). Top: SITA Standard. Middle: SITA Fast. Bottom: SITA SWAP. The '-' sign indicates a statistically abnormal RB.

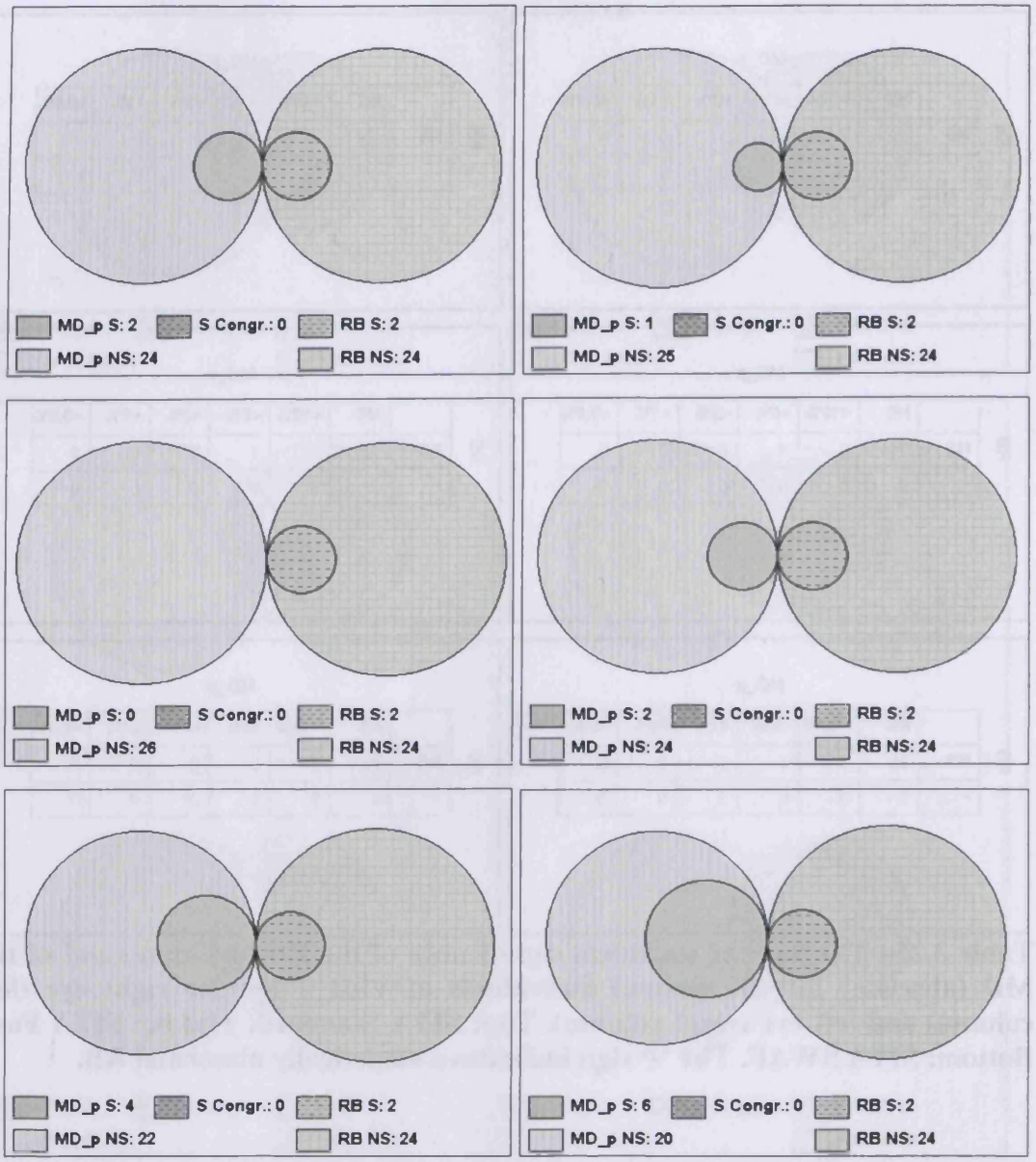

Figure 3.20a Venn diagrams, drawn to scale, illustrating the relationship between the presence (S) or absence of statistical significance (NS) associated with the respective values of RB and MD for the normal individuals at Visit 5 for the right eye (left column) and left eye (right column). Top: SITA Standard. Middle: SITA Fast. Bottom: SITA SWAP. The number of individuals in whom both measures indicate statistically significant abnormality (S Congr[uence]) is indicated by the overlap and size of the respective two circles.

MD_p

RB	NS	<10%	<5%	<2%	<1%	<0,5%
NS	24	0	0	0	0	0
-	0	0	0	0	0	0

MD_p

RB	NS	<10%	<5%	<2%	<1%	<0,5%
NS	24	0	0	0	0	0
-	0	0	0	0	0	0

MD_p

RB	NS	<10%	<5%	<2%	<1%	<0,5%
NS	23	1	0	0	0	0
-	0	0	0	0	0	0

MD_p

RB	NS	<10%	<5%	<2%	<1%	<0,5%
NS	22	2	0	0	0	0
-	0	0	0	0	0	0

MD_p

RB	NS	<10%	<5%	<2%	<1%	<0,5%
NS	21	2	1	0	0	0
-	0	0	0	0	0	0

MD_p

RB	NS	<10%	<5%	<2%	<1%	<0,5%
NS	20	1	3	0	0	0
-	0	0	0	0	0	0

Table 3.25b The level of statistical significance of the RB (ordinate) and of the MD (abscissa) for the individuals with OHT at Visit 5 for the right eye (left column) and left eye (right column). Top: SITA Standard. Middle: SITA Fast. Bottom: SITA SWAP. The '-'sign indicates a statistically abnormal RB.

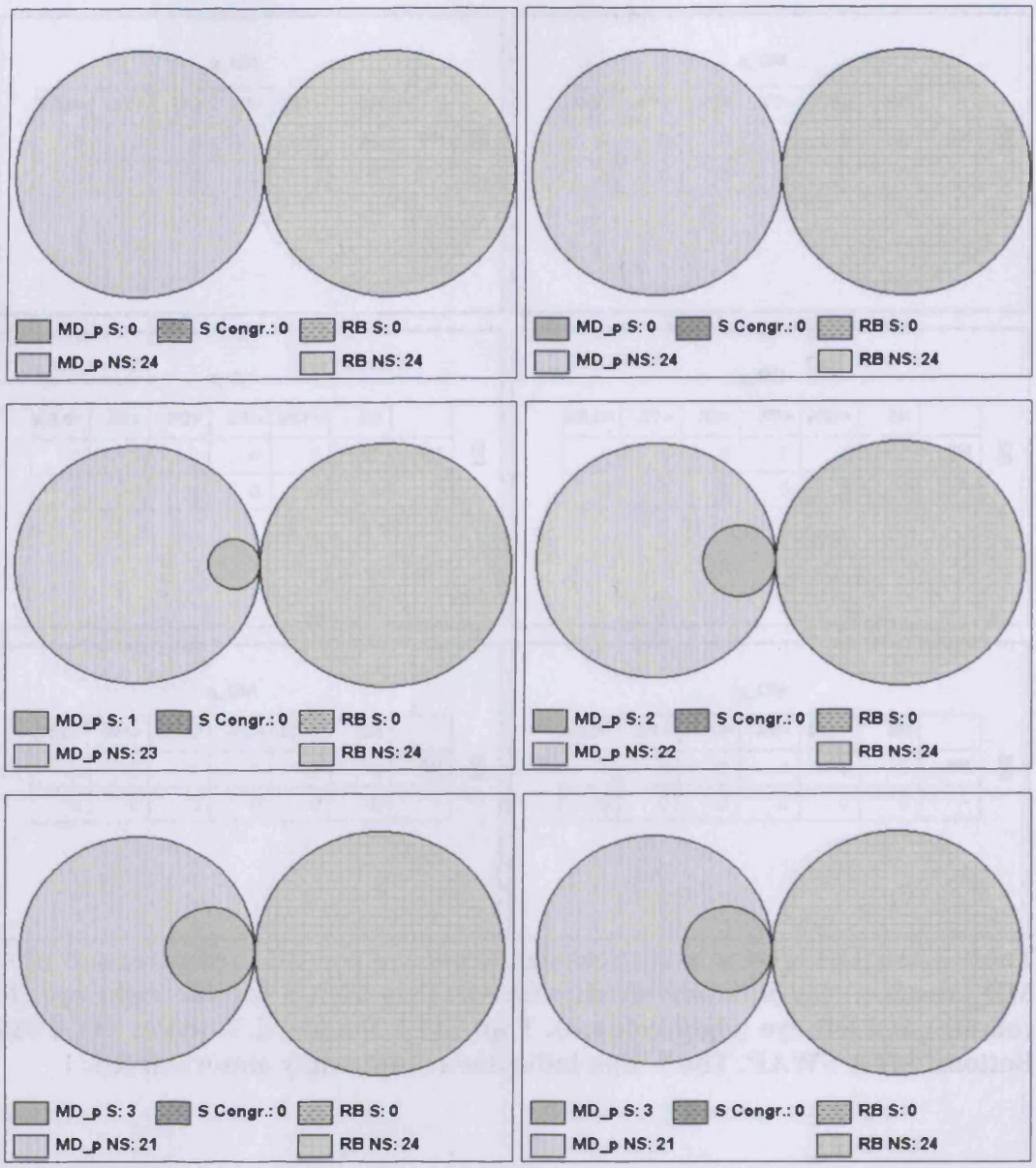

Figure 3.20b Venn diagrams, drawn to scale, illustrating the relationship between the presence (S) or absence of statistical significance (NS) associated with the respective values of RB and MD for the individuals with OHT at Visit 5 for the right eye (left column) and left eye (right column). Top: SITA Standard. Middle: SITA Fast. Bottom: SITA SWAP. The number of individuals in whom both measures indicate statistically significant abnormality (S Congr[uence]) is indicated by the overlap and size of the respective two circles.

MD_p

RB	NS	<10%	<5%	<2%	<1%	<0,5%
NS	16	0	0	0	0	1
-	5	0	0	1	1	1

MD_p

RB	NS	<10%	<5%	<2%	<1%	<0,5%
NS	16	1	0	0	0	0
-	4	0	1	1	1	1

MD_p

RB	NS	<10%	<5%	<2%	<1%	<0,5%
NS	16	0	0	1	0	0
-	6	1	0	0	0	1

MD_p

RB	NS	<10%	<5%	<2%	<1%	<0,5%
NS	15	2	0	0	0	0
-	4	0	2	0	2	0

MD_p

RB	NS	<10%	<5%	<2%	<1%	<0,5%
NS	14	1	2	0	0	0
-	6	1	0	0	0	1

MD_p

RB	NS	<10%	<5%	<2%	<1%	<0,5%
NS	14	2	1	0	0	0
-	6	0	1	0	0	1

Table 3.25c The level of statistical significance of the RB (ordinate) and of the MD (abscissa) for the individuals with OAG at Visit 5 for the right eye (left column) and left eye (right column). Top: SITA Standard. Middle: SITA Fast. Bottom: SITA SWAP. The '-'sign indicates a statistically abnormal RB.

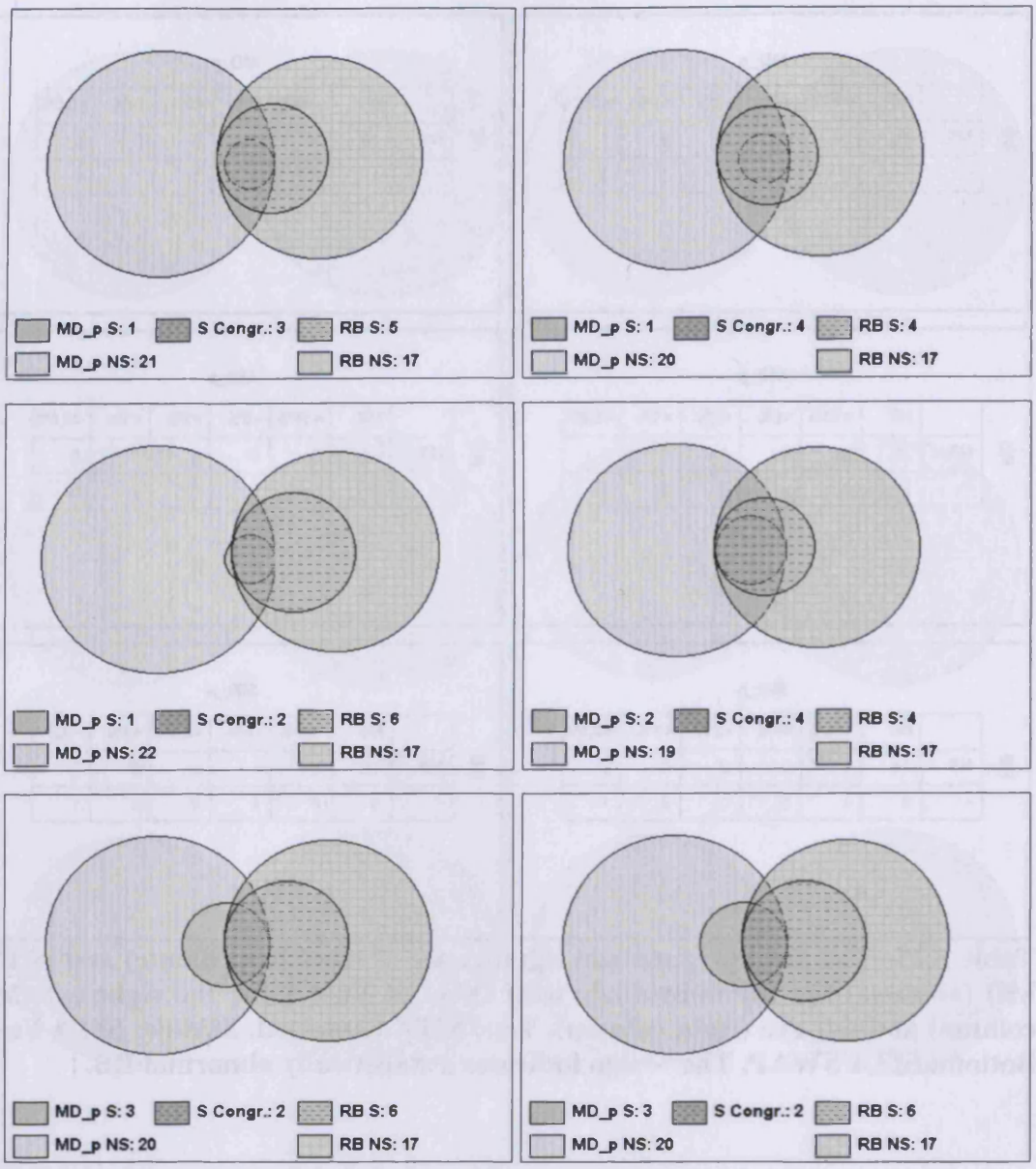

Figure 3.20c Venn diagrams, drawn to scale, illustrating the relationship between the presence (S) or absence of statistical significance (NS) associated with the respective values of RB and MD for the individuals with OAG at Visit 5 for the right eye (left column) and left eye (right column). Top: SITA Standard. Middle: SITA Fast. Bottom: SITA SWAP. The number of individuals in whom both measures indicate statistically significant abnormality (S Congr[uence]) is indicated by the overlap and size of the respective two circles.

MD_p

rim area / disc area * 100

	NS	<10%	<5%	<2%	<1%	<0,5%
NS	23	0	1	1	0	0
<5%	0	0	0	0	0	0
<1%	1	0	0	0	0	0
<0.1%	0	0	0	0	0	0

MD_p

rim area / disc area * 100

	NS	<10%	<5%	<2%	<1%	<0,5%
NS	24	0	0	0	0	1
<5%	0	0	0	0	0	0
<1%	1	0	0	0	0	0
<0.1%	0	0	0	0	0	0

MD_p

rim area / disc area * 100

	NS	<10%	<5%	<2%	<1%	<0,5%
NS	25	0	0	0	0	0
<5%	0	0	0	0	0	0
<1%	1	0	0	0	0	0
<0.1%	0	0	0	0	0	0

MD_p

rim area / disc area * 100

	NS	<10%	<5%	<2%	<1%	<0,5%
NS	23	1	1	0	0	0
<5%	0	0	0	0	0	0
<1%	1	0	0	0	0	0
<0.1%	0	0	0	0	0	0

MD_p

rim area / disc area * 100

	NS	<10%	<5%	<2%	<1%	<0,5%
NS	21	3	1	0	0	0
<5%	0	0	0	0	0	0
<1%	1	0	0	0	0	0
<0.1%	0	0	0	0	0	0

MD_p

rim area / disc area * 100

	NS	<10%	<5%	<2%	<1%	<0,5%
NS	19	4	2	0	0	0
<5%	0	0	0	0	0	0
<1%	1	0	0	0	0	0
<0.1%	0	0	0	0	0	0

Table 3.26a The level of statistical significance of the rim-disc ratio (ordinate) and of the MD (abscissa) for the normal individuals at Visit 5 for the right eye (left column) and left eye (right column). Top: SITA Standard. Middle: SITA Fast. Bottom: SITA SWAP.

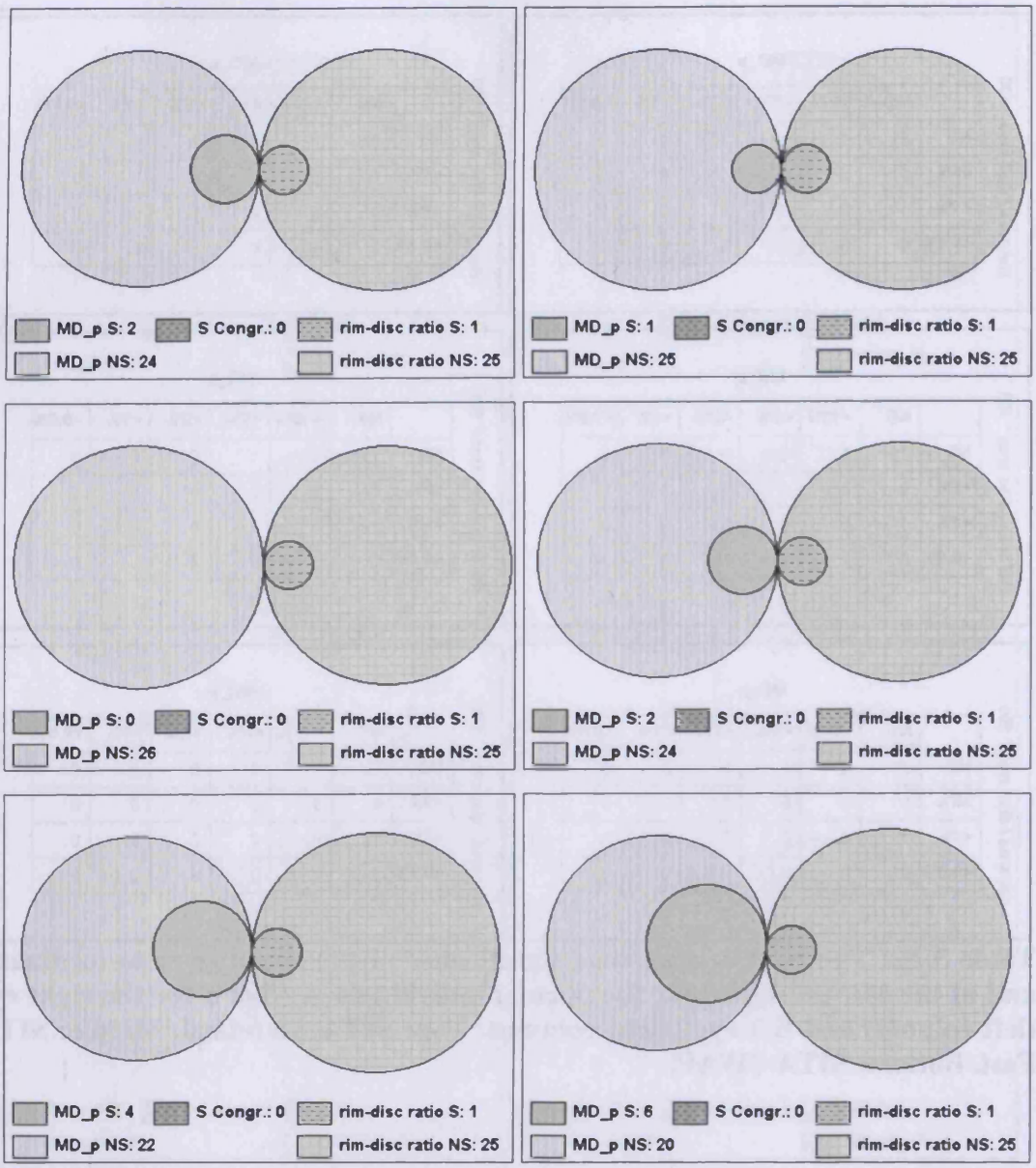

Figure 3.21a Venn diagrams, drawn to scale, illustrating the relationship between the presence (S) or absence of statistical significance (NS) associated with the respective values of the rim-disc ratio and MD for the normal individuals at Visit 5 for the right eye (left column) and left eye (right column). Top: SITA Standard. Middle: SITA Fast. Bottom: SITA SWAP. The number of individuals in whom both measures indicate statistically significant abnormality (S Congr[uence]) is indicated by the overlap and size of the respective two circles.

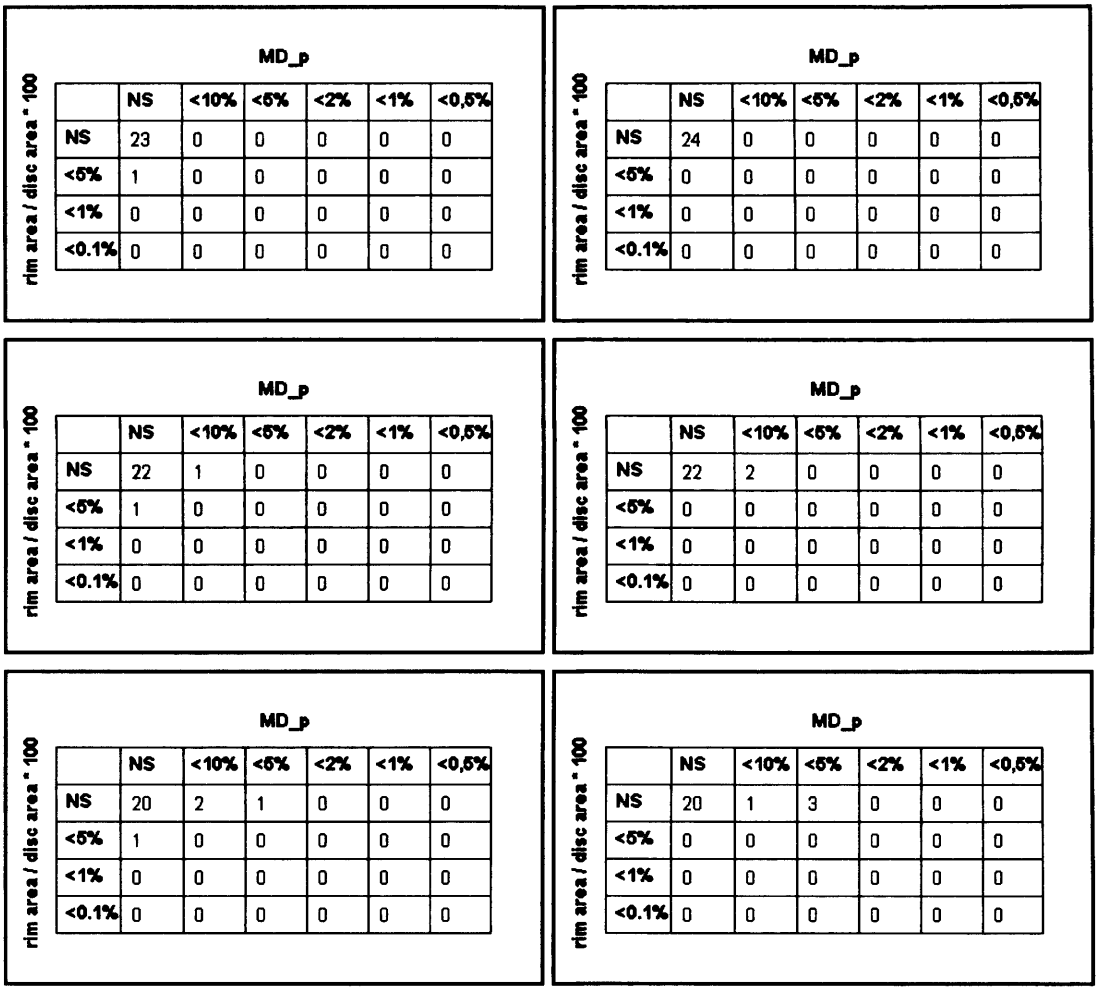

MD_p

rim area / disc area * 100

	NS	<10%	<5%	<2%	<1%	<0,5%
NS	23	0	0	0	0	0
<5%	1	0	0	0	0	0
<1%	0	0	0	0	0	0
<0.1%	0	0	0	0	0	0

MD_p

rim area / disc area * 100

	NS	<10%	<5%	<2%	<1%	<0,5%
NS	24	0	0	0	0	0
<5%	0	0	0	0	0	0
<1%	0	0	0	0	0	0
<0.1%	0	0	0	0	0	0

MD_p

rim area / disc area * 100

	NS	<10%	<5%	<2%	<1%	<0,5%
NS	22	1	0	0	0	0
<5%	1	0	0	0	0	0
<1%	0	0	0	0	0	0
<0.1%	0	0	0	0	0	0

MD_p

rim area / disc area * 100

	NS	<10%	<5%	<2%	<1%	<0,5%
NS	22	2	0	0	0	0
<5%	0	0	0	0	0	0
<1%	0	0	0	0	0	0
<0.1%	0	0	0	0	0	0

MD_p

rim area / disc area * 100

	NS	<10%	<5%	<2%	<1%	<0,5%
NS	20	2	1	0	0	0
<5%	1	0	0	0	0	0
<1%	0	0	0	0	0	0
<0.1%	0	0	0	0	0	0

MD_p

rim area / disc area * 100

	NS	<10%	<5%	<2%	<1%	<0,5%
NS	20	1	3	0	0	0
<5%	0	0	0	0	0	0
<1%	0	0	0	0	0	0
<0.1%	0	0	0	0	0	0

Table 3.26b The level of statistical significance of the rim-disc ratio (ordinate) and of the MD (abscissa) for the individuals with OHT at Visit 5 for the right eye (left column) and left eye (right column). Top: SITA Standard. Middle: SITA Fast. Bottom: SITA SWAP.

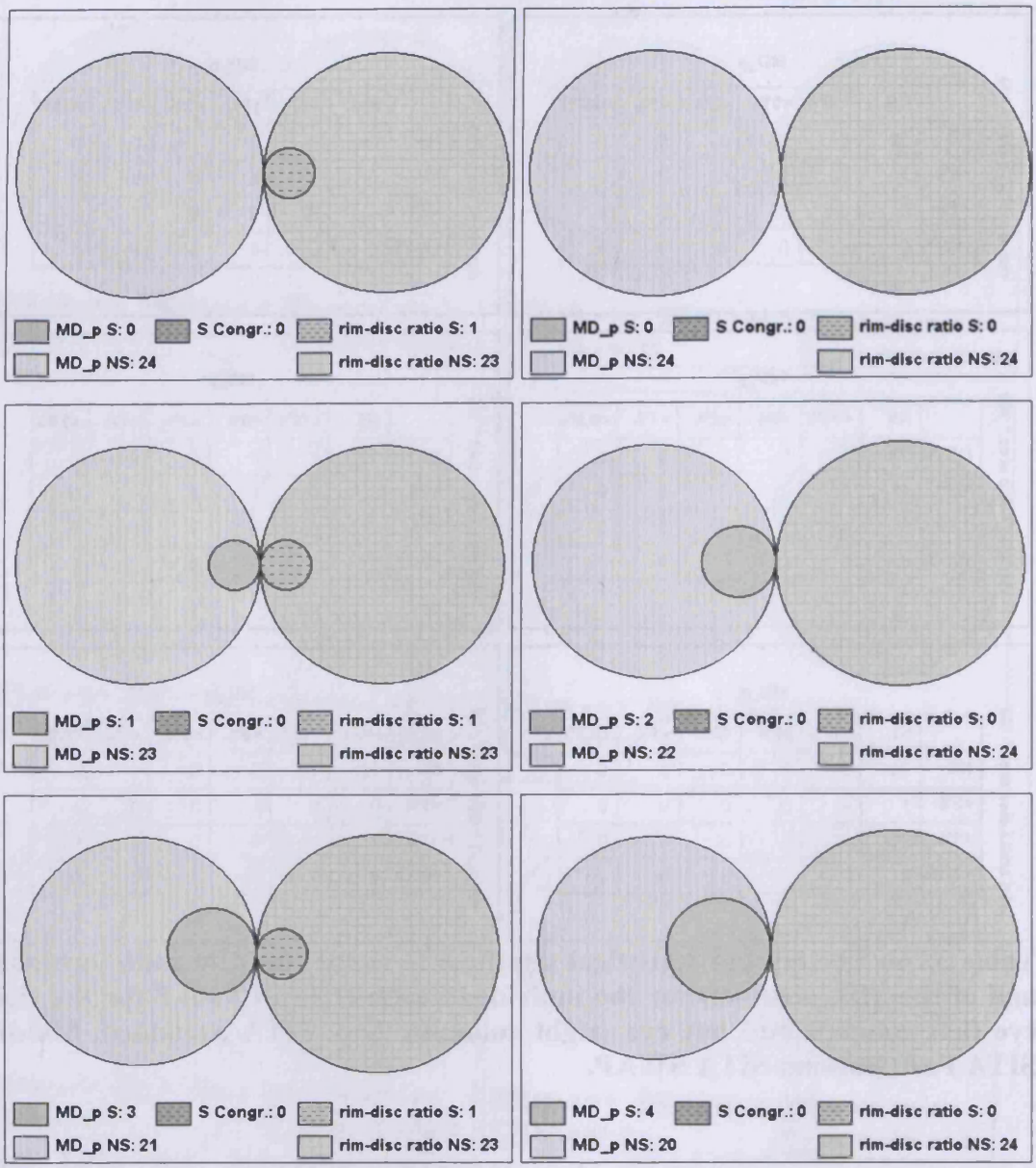

Figure 3.21b Venn diagrams, drawn to scale, illustrating the relationship between the presence (S) or absence of statistical significance (NS) associated with the respective values of the rim-disc ratio and MD for the individuals with OHT at Visit 5 for the right eye (left column) and left eye (right column). Top: SITA Standard. Middle: SITA Fast. Bottom: SITA SWAP. The number of individuals in whom both measures indicate statistically significant abnormality (S Congr[uence]) is indicated by the overlap and size of the respective two circles.

MD_p

rim area / disc area * 100	NS	<10%	<5%	<2%	<1%	<0,5%
NS	16	0	0	0	1	0
<5%	1	0	0	0	0	0
<1%	2	0	0	0	0	0
<0.1%	2	2	0	0	0	1

MD_p

rim area / disc area * 100	NS	<10%	<5%	<2%	<1%	<0,5%
NS	13	1	1	0	0	0
<5%	2	0	0	0	0	0
<1%	0	1	1	0	0	0
<0.1%	5	0	0	0	0	1

MD_p

rim area / disc area * 100	NS	<10%	<5%	<2%	<1%	<0,5%
NS	16	0	0	1	0	0
<5%	1	0	0	0	0	0
<1%	2	0	0	0	0	0
<0.1%	3	1	0	0	0	1

MD_p

rim area / disc area * 100	NS	<10%	<5%	<2%	<1%	<0,5%
NS	12	2	1	0	0	0
<5%	2	0	0	0	0	0
<1%	1	0	1	0	0	0
<0.1%	4	0	0	0	2	0

MD_p

rim area / disc area * 100	NS	<10%	<5%	<2%	<1%	<0,5%
NS	14	1	2	0	0	0
<5%	1	0	0	0	0	0
<1%	2	0	0	0	0	0
<0.1%	3	1	0	0	0	1

MD_p

rim area / disc area * 100	NS	<10%	<5%	<2%	<1%	<0,5%
NS	13	1	1	0	0	0
<5%	2	0	0	0	0	0
<1%	0	1	1	0	0	0
<0.1%	5	0	0	0	0	1

Table 3.26c The level of statistical significance of the rim-disc ratio (ordinate) and of the MD (abscissa) for the individuals with OAG at Visit 5 for the right eye (left column) and left eye (right column). Top: SITA Standard. Middle: SITA Fast. Bottom: SITA SWAP.

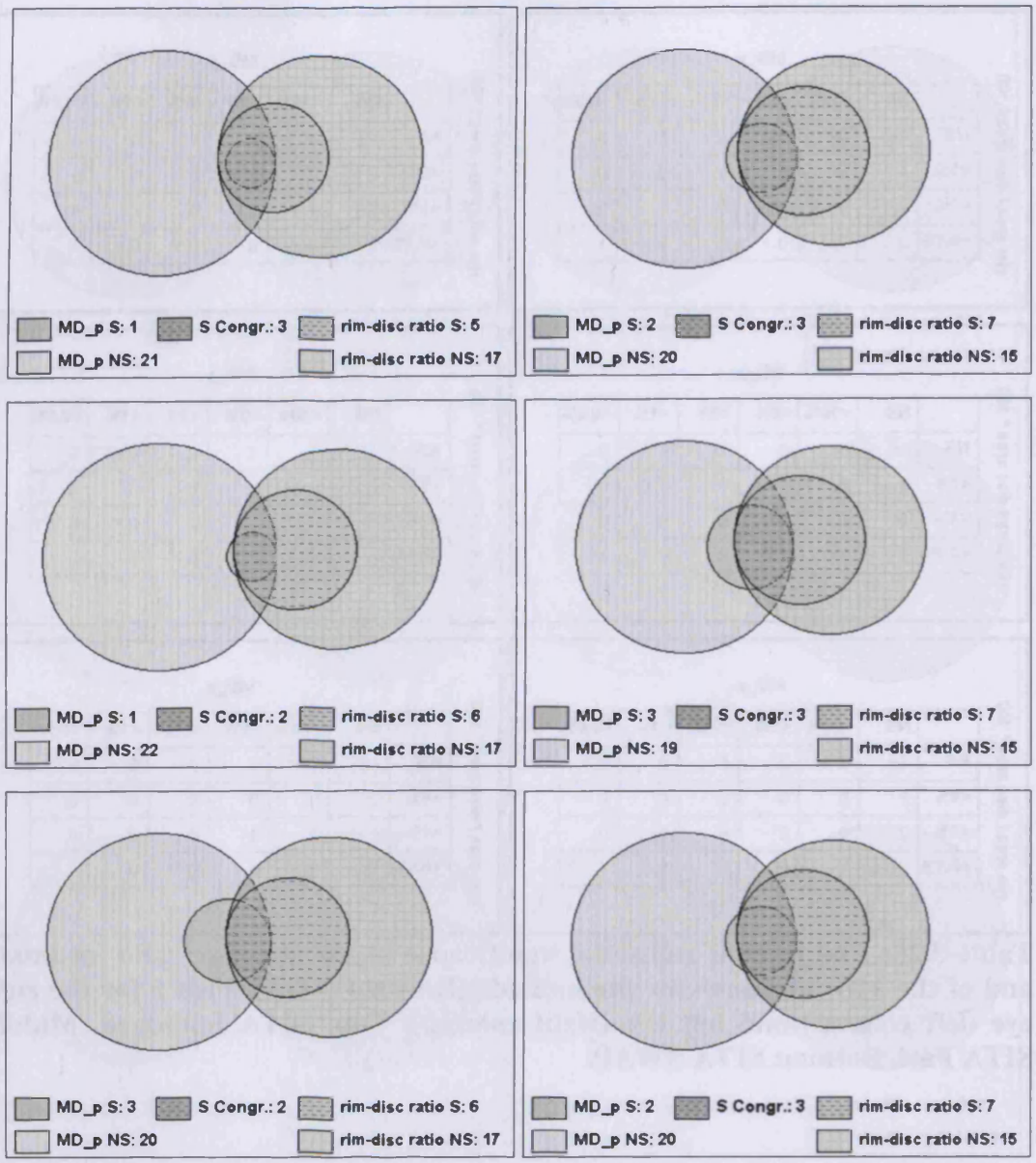

Figure 3.21c Venn diagrams, drawn to scale, illustrating the relationship between the presence (S) or absence of statistical significance (NS) associated with the respective values of the rim-disc ratio and MD for the individuals with OAG at Visit 5 for the right eye (left column) and left eye (right column). Top: SITA Standard. Middle: SITA Fast. Bottom: SITA SWAP. The number of individuals in whom both measures indicate statistically significant abnormality (S Congr[uence]) is indicated by the overlap and size of the respective two circles.

The relationship between the magnitudes of the Mikelberg discriminate function (FSM), Tables 3.27a to 3.27c, the Burk discriminate function (RB), Tables 3.28a to 3.28c, and the rim-disc ratio, Tables 3.29a to 3.29c, derived by confocal scanning laser ophthalmoscopy (HRT II) were compared with the magnitudes of the visual field index PSD (p values) derived by SITA Standard, SITA Fast and SITA SWAP across all locations for each algorithm at Visit 5 for the right and the left eyes for the normal individuals and for the individuals with OHT and OAG and are illustrated in terms of contingency tables. This relationship is also illustrated in form of Venn diagrams between the magnitudes of FSM, Figures 3.22a to 3.22c, the RB, Figures 3.23a to 3.23c and the rim-disc ratio, Figures 3.24a to 3.24c and the corresponding visual field index PSD (p values).

PSD_p

FSM	NS	<10%	<5%	<2%	<1%	<0,5%
NS	16	0	2	1	0	1
-	6	0	0	0	0	0

PSD_p

FSM	NS	<10%	<5%	<2%	<1%	<0,5%
NS	13	1	1	0	1	1
-	8	1	0	0	0	0

PSD_p

FSM	NS	<10%	<5%	<2%	<1%	<0,5%
NS	17	2	0	1	0	0
-	6	0	0	0	0	0

PSD_p

FSM	NS	<10%	<5%	<2%	<1%	<0,5%
NS	14	1	1	1	0	0
-	9	0	0	0	0	0

PSD_p

FSM	NS	<10%	<5%	<2%	<1%	<0,5%
NS	20	0	0	0	0	0
-	5	1	0	0	0	0

PSD_p

FSM	NS	<10%	<5%	<2%	<1%	<0,5%
NS	14	2	1	0	0	0
-	9	0	0	0	0	0

Table 3.27a The level of statistical significance of the FSM (ordinate) and of the PSD (abscissa) for the normal individuals at Visit 5 for the right eye (left column) and left eye (right column). Top: SITA Standard. Middle: SITA Fast. Bottom: SITA SWAP. The '-' sign indicates a statistically abnormal FSM.

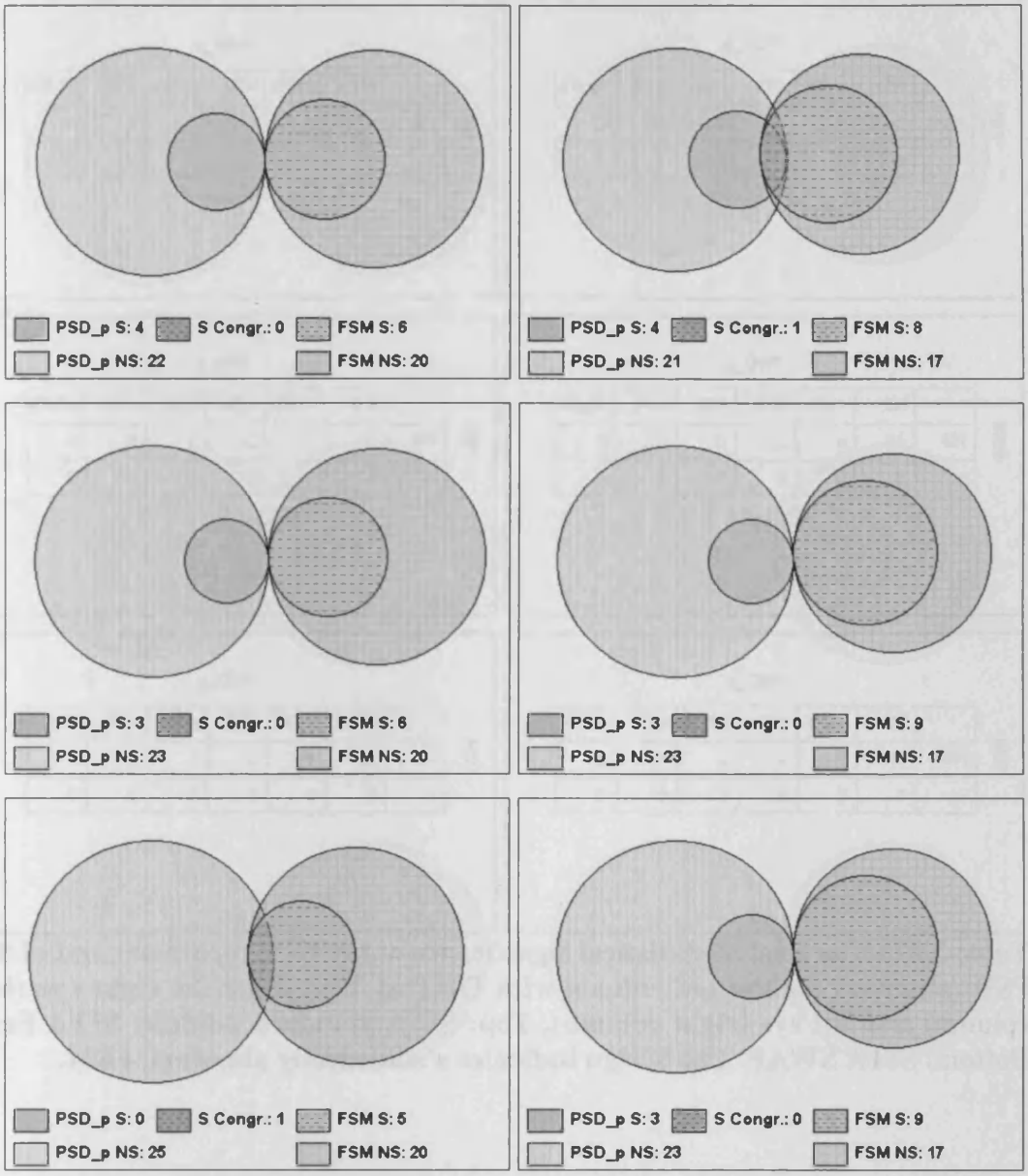

Figure 3.22a Venn diagrams, drawn to scale, illustrating the relationship between the presence (S) or absence of statistical significance (NS) associated with the respective values of FSM and PSD for the normal individuals at Visit 5 for the right eye (left column) and left eye (right column). Top: SITA Standard. Middle: SITA Fast. Bottom: SITA SWAP. The number of individuals in whom both measures indicate statistically significant abnormality (S Congr[uence]) is indicated by the overlap and size of the respective two circles.

PSD_p

FSM	NS	<10%	<5%	<2%	<1%	<0,5%
NS	18	1	1	0	0	0
-	4	0	0	0	0	0

PSD_p

FSM	NS	<10%	<5%	<2%	<1%	<0,5%
NS	12	3	2	1	0	1
-	5	0	0	0	0	0

PSD_p

FSM	NS	<10%	<5%	<2%	<1%	<0,5%
NS	14	4	2	0	0	0
-	4	0	0	0	0	0

PSD_p

FSM	NS	<10%	<5%	<2%	<1%	<0,5%
NS	13	2	2	1	0	1
-	5	0	0	0	0	0

PSD_p

FSM	NS	<10%	<5%	<2%	<1%	<0,5%
NS	17	2	0	0	1	0
-	4	0	0	0	0	0

PSD_p

FSM	NS	<10%	<5%	<2%	<1%	<0,5%
NS	15	1	2	1	0	0
-	5	0	0	0	0	0

Table 3.27b The level of statistical significance of the FSM (ordinate) and of the PSD (abscissa) for the individuals with OHT at Visit 5 for the right eye (left column) and left eye (right column). Top: SITA Standard. Middle: SITA Fast. Bottom: SITA SWAP. The '-'sign indicates a statistically abnormal FSM.

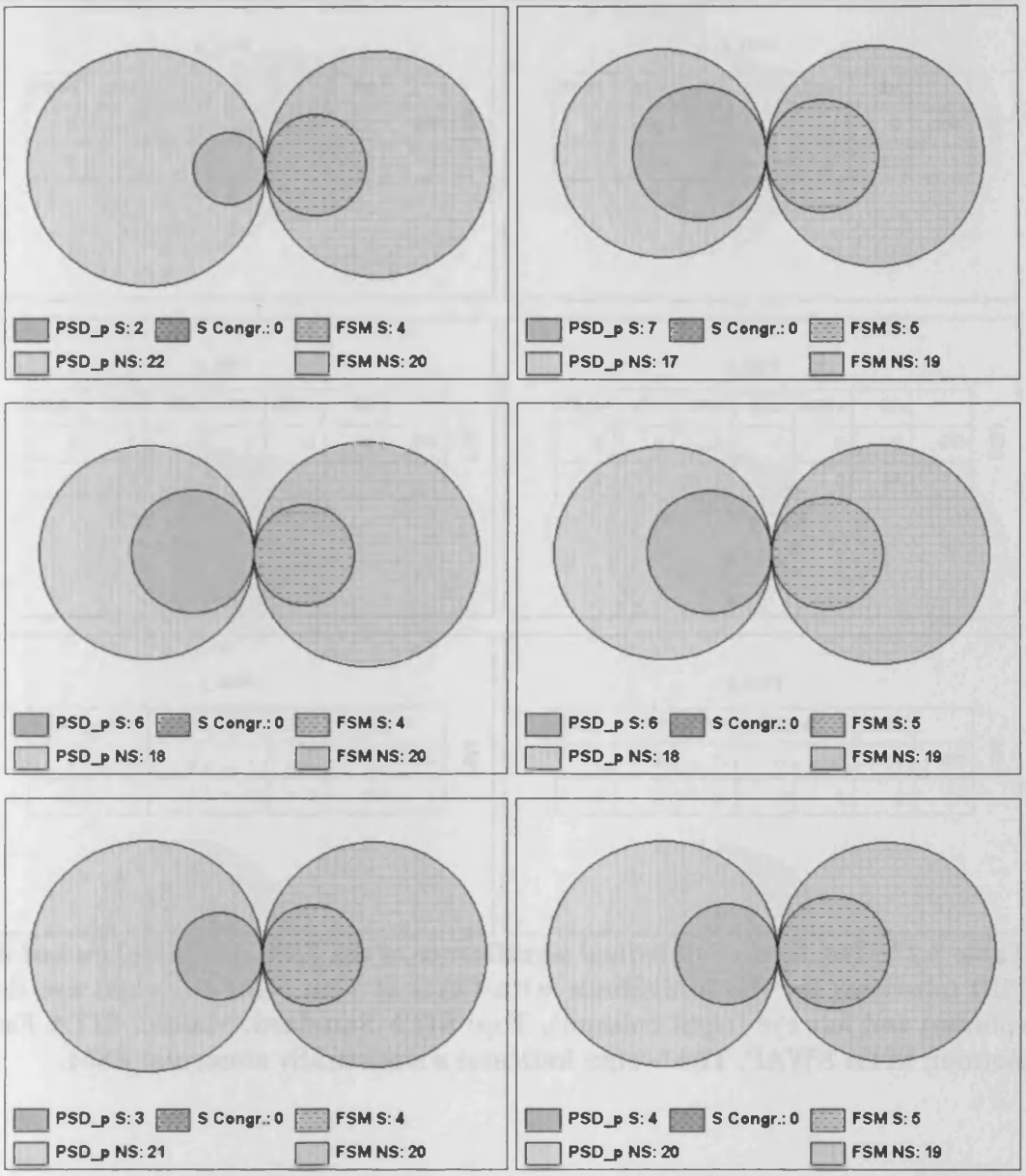

Figure 3.22b Venn diagrams, drawn to scale, illustrating the relationship between the presence (S) or absence of statistical significance (NS) associated with the respective values of FSM and PSD for the individuals with OHT at Visit 5 for the right eye (left column) and left eye (right column). Top: SITA Standard. Middle: SITA Fast. Bottom: SITA SWAP. The number of individuals in whom both measures indicate statistically significant abnormality (S Congr[uence]) is indicated by the overlap and size of the respective two circles.

PSD_p

FSM	NS	<10%	<5%	<2%	<1%	<0,5%
NS	5	2	1	0	0	0
-	12	0	0	2	0	3

PSD_p

FSM	NS	<10%	<5%	<2%	<1%	<0,5%
NS	8	0	0	1	0	0
-	9	0	2	1	1	3

PSD_p

FSM	NS	<10%	<5%	<2%	<1%	<0,5%
NS	8	0	0	0	0	0
-	10	1	3	1	0	2

PSD_p

FSM	NS	<10%	<5%	<2%	<1%	<0,5%
NS	6	0	1	1	0	1
-	8	1	1	4	1	1

PSD_p

FSM	NS	<10%	<5%	<2%	<1%	<0,5%
NS	7	1	0	0	0	0
-	8	2	5	0	0	2

PSD_p

FSM	NS	<10%	<5%	<2%	<1%	<0,5%
NS	6	2	1	0	0	0
-	8	3	2	1	1	1

Table 3.27c The level of statistical significance of the FSM (ordinate) and of the PSD (abscissa) for the individuals with OAG at Visit 5 for the right eye (left column) and left eye (right column). Top: SITA Standard. Middle: SITA Fast. Bottom: SITA SWAP. The '-'sign indicates a statistically abnormal FSM.

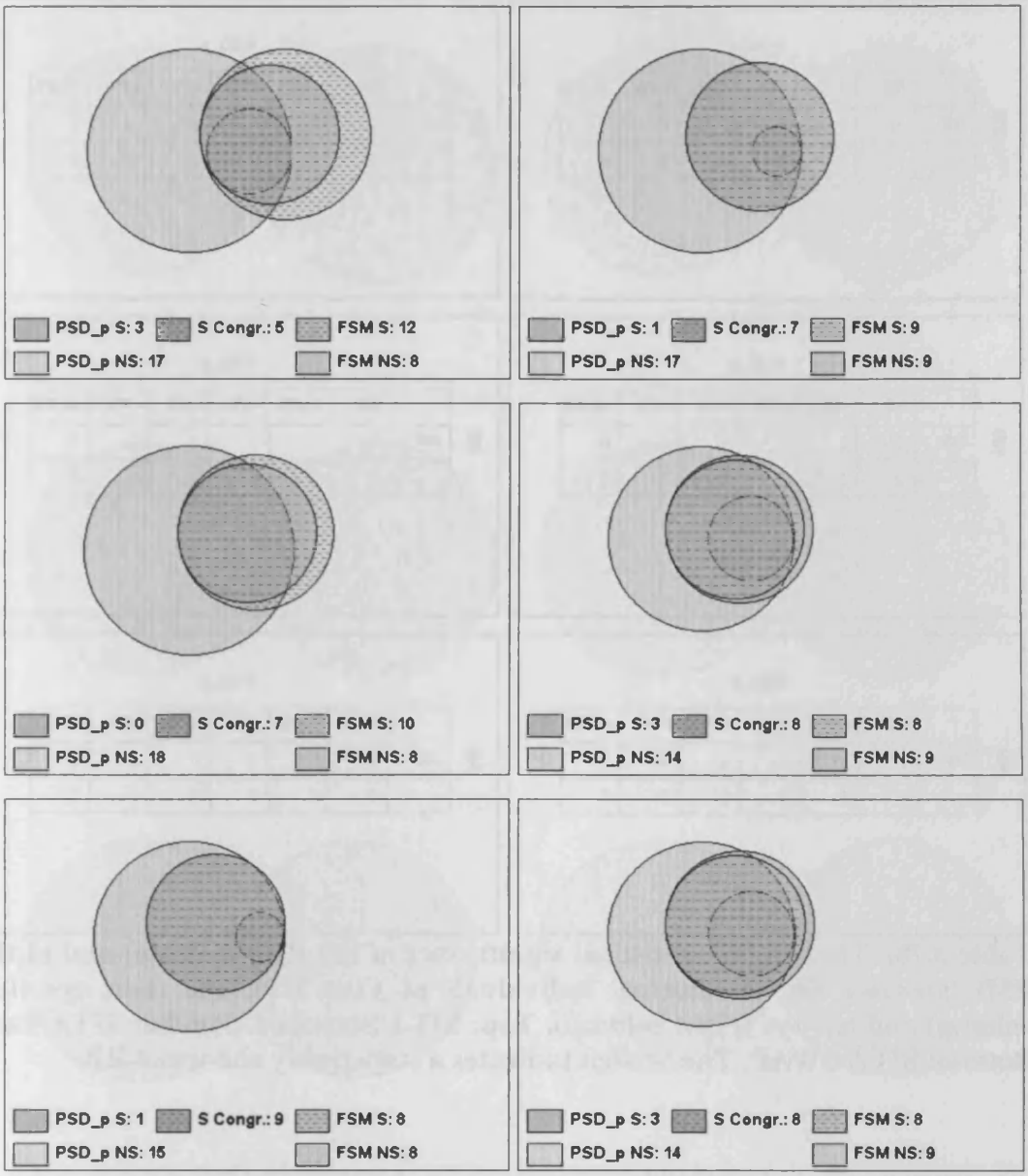

Figure 3.22c Venn diagrams, drawn to scale, illustrating the relationship between the presence (S) or absence of statistical significance (NS) associated with the respective values of FSM and PSD for the individuals with OAG at Visit 5 for the right eye (left column) and left eye (right column). Top: SITA Standard. Middle: SITA Fast. Bottom: SITA SWAP. The number of individuals in whom both measures indicate statistically significant abnormality (S Congr[uence]) is indicated by the overlap and size of the respective two circles.

PSD_p

RB	NS	<10%	<5%	<2%	<1%	<0,5%
NS	20	0	2	1	0	1
-	2	0	0	0	0	0

PSD_p

RB	NS	<10%	<5%	<2%	<1%	<0,5%
NS	19	2	1	0	1	1
-	2	0	0	0	0	0

PSD_p

RB	NS	<10%	<5%	<2%	<1%	<0,5%
NS	21	2	0	1	0	0
-	2	0	0	0	0	0

PSD_p

RB	NS	<10%	<5%	<2%	<1%	<0,5%
NS	21	1	1	1	0	0
-	2	0	0	0	0	0

PSD_p

RB	NS	<10%	<5%	<2%	<1%	<0,5%
NS	24	0	0	0	0	0
-	1	1	0	0	0	0

PSD_p

RB	NS	<10%	<5%	<2%	<1%	<0,5%
NS	21	2	1	0	0	0
-	2	0	0	0	0	0

Table 3.28a The level of statistical significance of the RB (ordinate) and of the PSD (abscissa) for the normal individuals at Visit 5 for the right eye (left column) and left eye (right column). Top: SITA Standard. Middle: SITA Fast. Bottom: SITA SWAP. The '-' sign indicates a statistically abnormal RB.

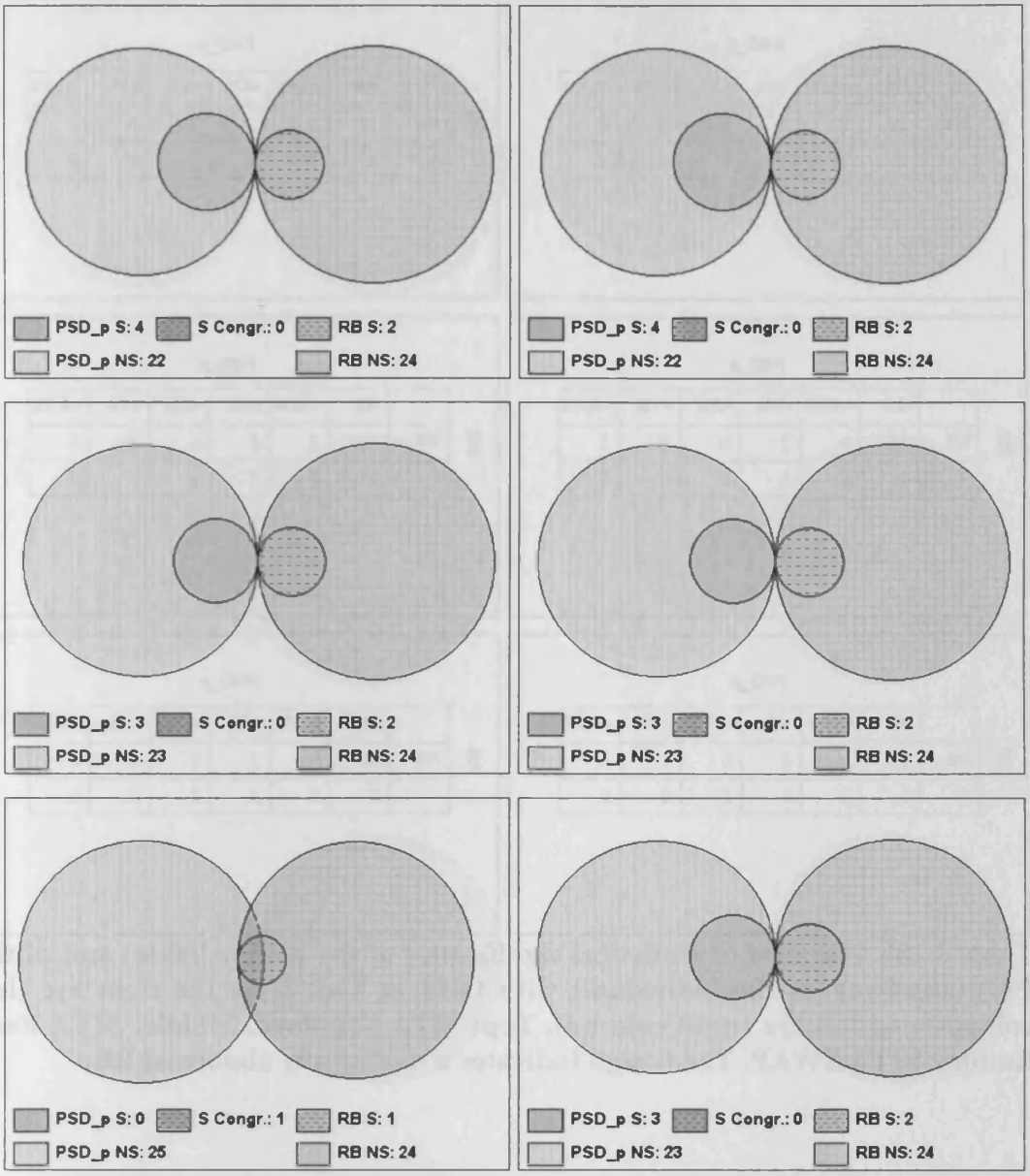

Figure 3.23a Venn diagrams, drawn to scale, illustrating the relationship between the presence (S) or absence of statistical significance (NS) associated with the respective values of RB and PSD for the individuals with OAG at Visit 5 for the right eye (left column) and left eye (right column). Top: SITA Standard. Middle: SITA Fast. Bottom: SITA SWAP. The number of individuals in whom both measures indicate statistically significant abnormality (S Congr[uence]) is indicated by the overlap and size of the respective two circles.

PSD_p

RB	NS	<10%	<5%	<2%	<1%	<0,5%
NS	22	1	1	0	0	0
-	0	0	0	0	0	0

PSD_p

RB	NS	<10%	<5%	<2%	<1%	<0,5%
NS	17	3	2	1	0	1
-	0	0	0	0	0	0

PSD_p

RB	NS	<10%	<5%	<2%	<1%	<0,5%
NS	18	4	2	0	0	0
-	0	0	0	0	0	0

PSD_p

RB	NS	<10%	<5%	<2%	<1%	<0,5%
NS	18	2	2	1	0	1
-	0	0	0	0	0	0

PSD_p

RB	NS	<10%	<5%	<2%	<1%	<0,5%
NS	21	2	0	0	1	0
-	0	0	0	0	0	0

PSD_p

RB	NS	<10%	<5%	<2%	<1%	<0,5%
NS	20	1	2	1	0	0
-	0	0	0	0	0	0

Table 3.28b The level of statistical significance of the RB (ordinate) and of the PSD (abscissa) for the individuals with OHT at Visit 5 for the right eye (left column) and left eye (right column). Top: SITA Standard. Middle: SITA Fast. Bottom: SITA SWAP. The '-'sign indicates a statistically abnormal RB.

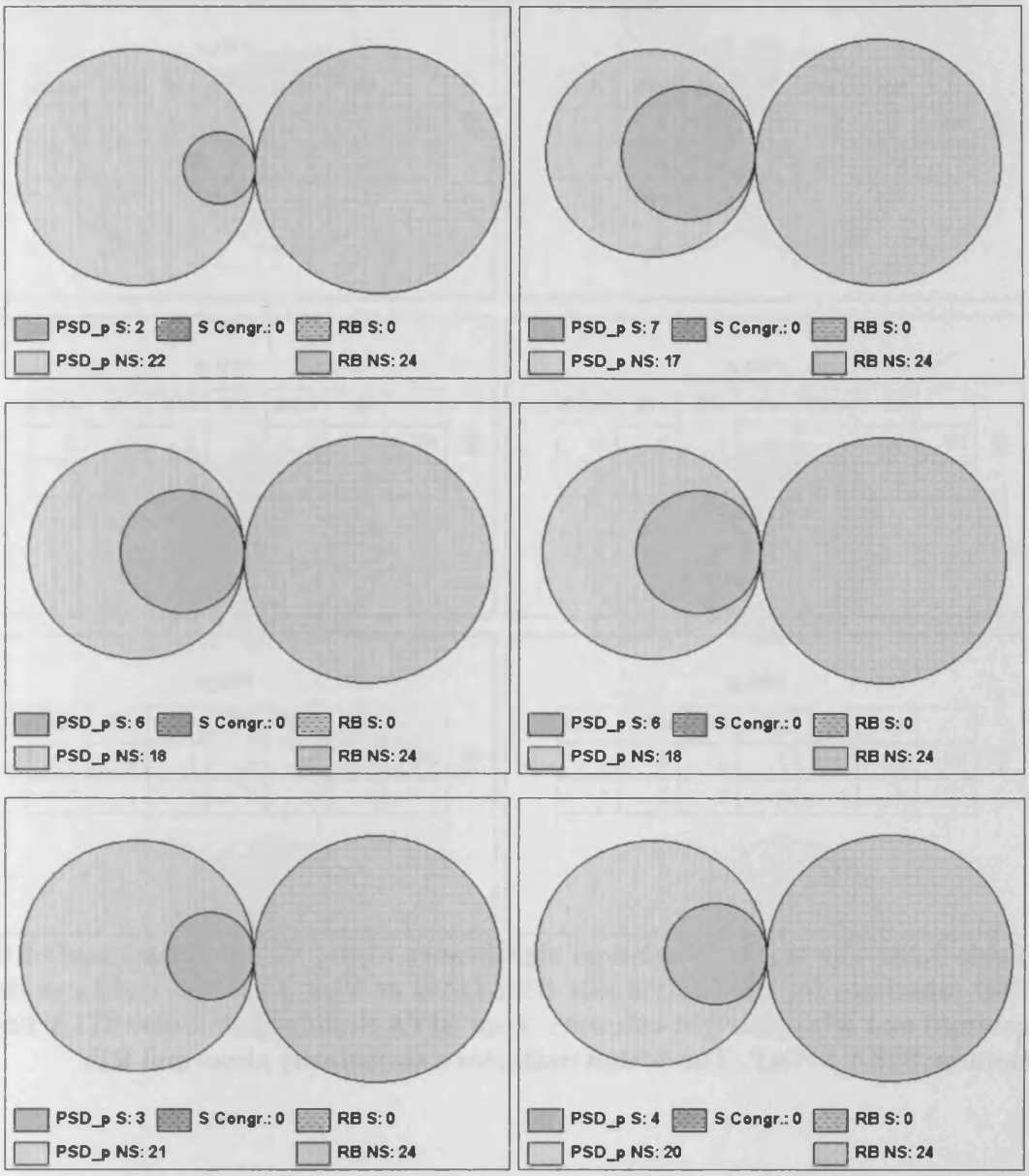

Figure 3.23b Venn diagrams, drawn to scale, illustrating the relationship between the presence (S) or absence of statistical significance (NS) associated with the respective values of RB and PSD for the individuals with OHT at Visit 5 for the right eye (left column) and left eye (right column). Top: SITA Standard. Middle: SITA Fast. Bottom: SITA SWAP. The number of individuals in whom both measures indicate statistically significant abnormality (S Congr[uence]) is indicated by the overlap and size of the respective two circles.

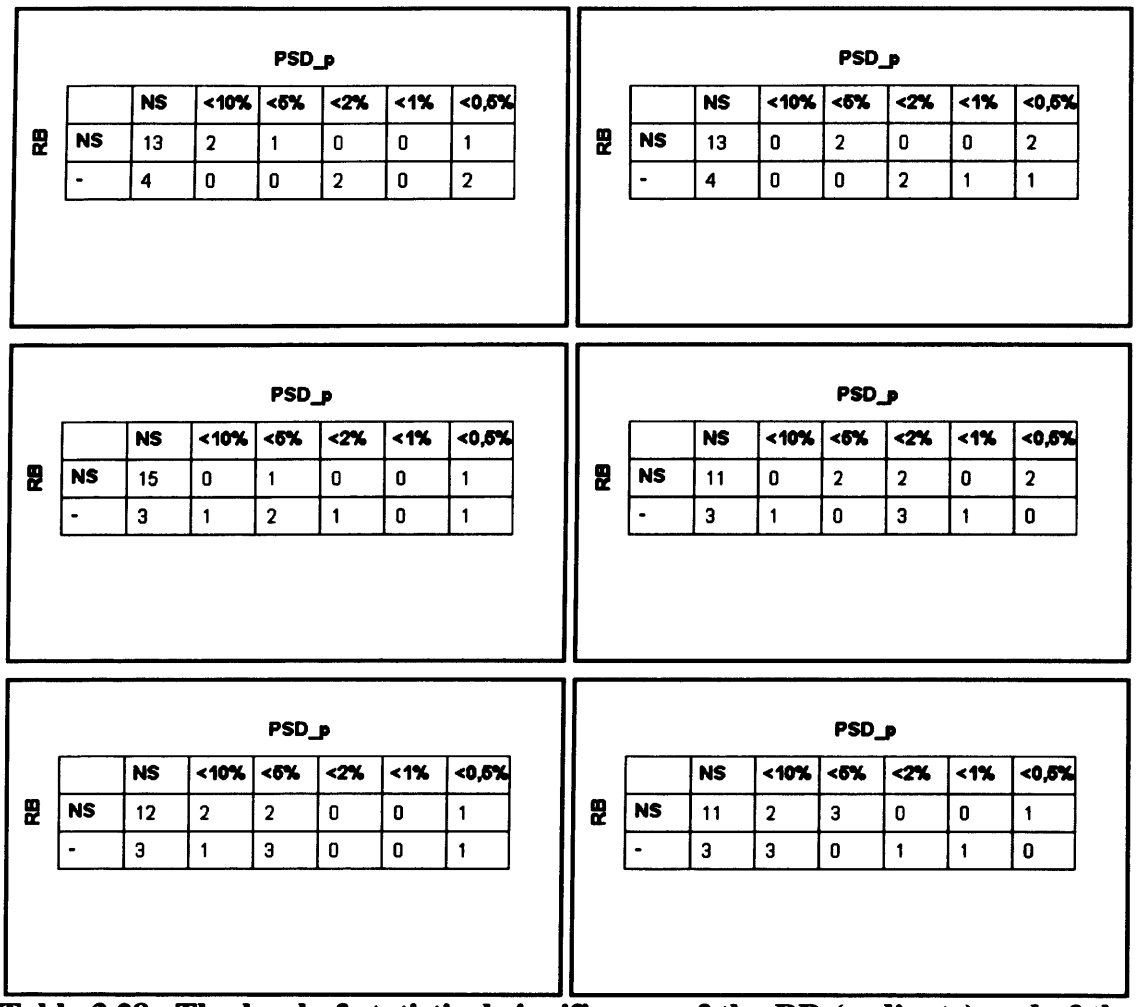

PSD_p

RB	NS	<10%	<5%	<2%	<1%	<0,5%
NS	13	2	1	0	0	1
-	4	0	0	2	0	2

PSD_p

RB	NS	<10%	<5%	<2%	<1%	<0,5%
NS	13	0	2	0	0	2
-	4	0	0	2	1	1

PSD_p

RB	NS	<10%	<5%	<2%	<1%	<0,5%
NS	15	0	1	0	0	1
-	3	1	2	1	0	1

PSD_p

RB	NS	<10%	<5%	<2%	<1%	<0,5%
NS	11	0	2	2	0	2
-	3	1	0	3	1	0

PSD_p

RB	NS	<10%	<5%	<2%	<1%	<0,5%
NS	12	2	2	0	0	1
-	3	1	3	0	0	1

PSD_p

RB	NS	<10%	<5%	<2%	<1%	<0,5%
NS	11	2	3	0	0	1
-	3	3	0	1	1	0

Table 3.28c The level of statistical significance of the RB (ordinate) and of the PSD (abscissa) for the individuals with OAG at Visit 5 for the right eye (left column) and left eye (right column). Top: SITA Standard. Middle: SITA Fast. Bottom: SITA SWAP. The '-'sign indicates a statistically abnormal RB.

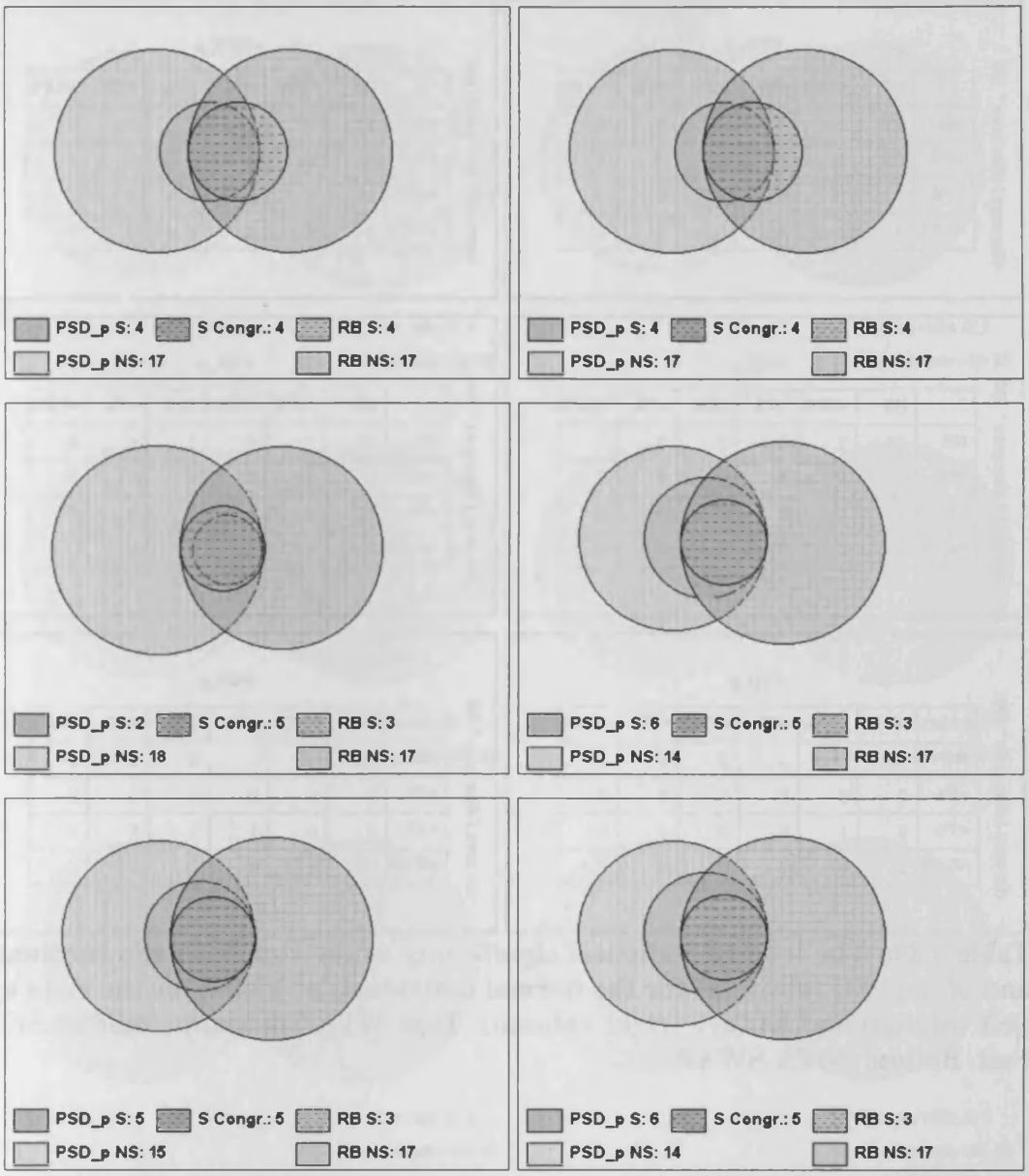

Figure 3.23c Venn diagrams, drawn to scale, illustrating the relationship between the presence (S) or absence of statistical significance (NS) associated with the respective values of RB and PSD for the individuals with OAG at Visit 5 for the right eye (left column) and left eye (right column). Top: SITA Standard. Middle: SITA Fast. Bottom: SITA SWAP. The number of individuals in whom both measures indicate statistically significant abnormality (S Congr[uence]) is indicated by the overlap and size of the respective two circles.

PSD_p

rim area / disc area * 100

	NS	<10%	<5%	<2%	<1%	<0,5%
NS	21	0	2	1	0	1
<5%	0	0	0	0	0	0
<1%	1	0	0	0	0	0
<0.1%	0	0	0	0	0	0

PSD_p

rim area / disc area * 100

	NS	<10%	<5%	<2%	<1%	<0,5%
NS	21	1	1	0	1	1
<5%	0	0	0	0	0	0
<1%	0	1	0	0	0	0
<0.1%	0	0	0	0	0	0

PSD_p

rim area / disc area * 100

	NS	<10%	<5%	<2%	<1%	<0,5%
NS	22	2	0	1	0	0
<5%	0	0	0	0	0	0
<1%	1	0	0	0	0	0
<0.1%	0	0	0	0	0	0

PSD_p

rim area / disc area * 100

	NS	<10%	<5%	<2%	<1%	<0,5%
NS	22	1	1	1	0	0
<5%	0	0	0	0	0	0
<1%	1	0	0	0	0	0
<0.1%	0	0	0	0	0	0

PSD_p

rim area / disc area * 100

	NS	<10%	<5%	<2%	<1%	<0,5%
NS	25	0	0	0	0	0
<5%	0	0	0	0	0	0
<1%	0	1	0	0	0	0
<0.1%	0	0	0	0	0	0

PSD_p

rim area / disc area * 100

	NS	<10%	<5%	<2%	<1%	<0,5%
NS	23	2	0	0	0	0
<5%	0	0	0	0	0	0
<1%	0	0	1	0	0	0
<0.1%	0	0	0	0	0	0

Table 3.29a The level of statistical significance of the rim-disc ratio (ordinate) and of the PSD (abscissa) for the normal individuals at Visit 5 for the right eye (left column) and left eye (right column). Top: SITA Standard. Middle: SITA Fast. Bottom: SITA SWAP.

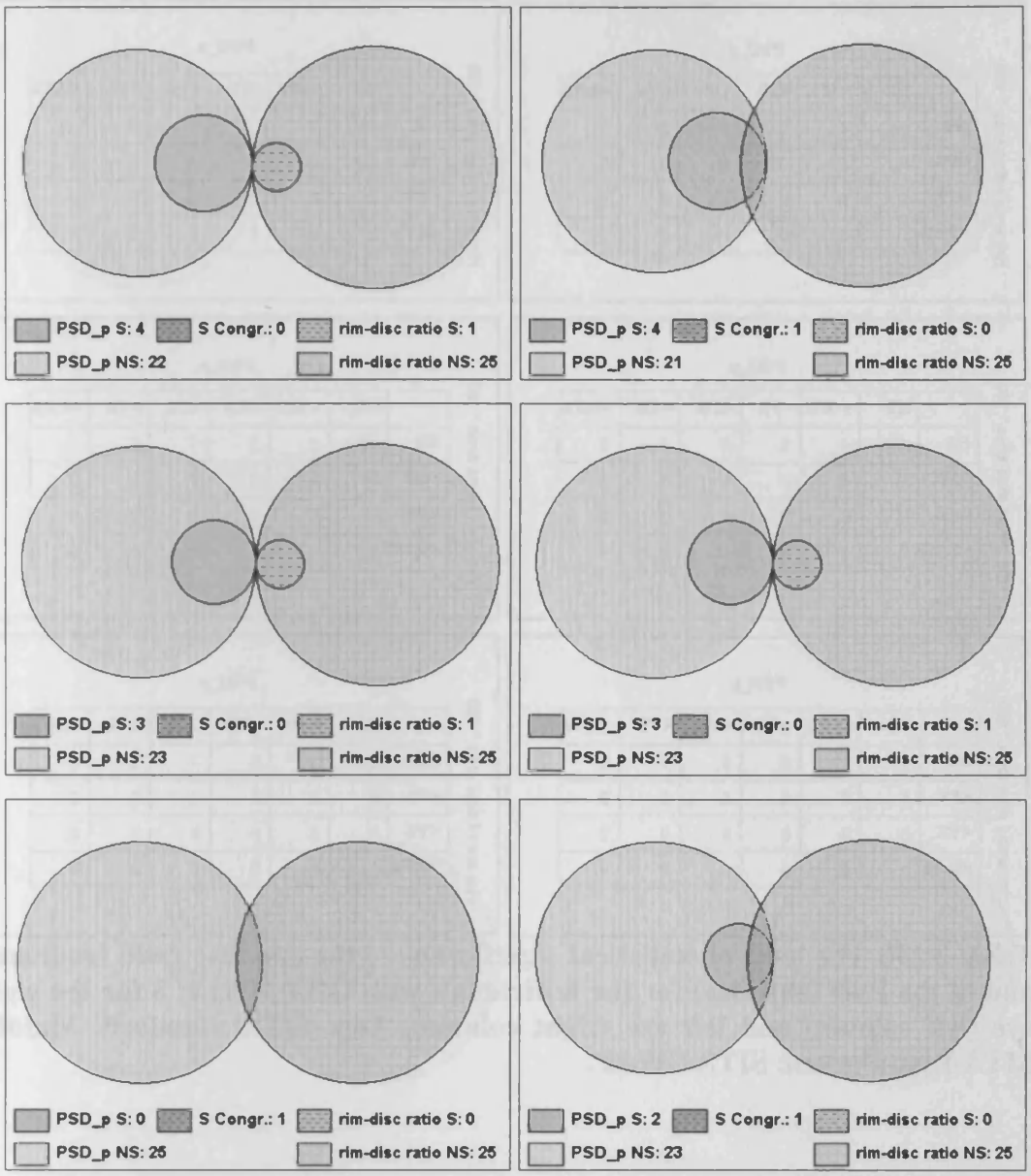

Figure 3.24a Venn diagrams, drawn to scale, illustrating the relationship between the presence (S) or absence of statistical significance (NS) associated with the respective values of the rim-disc ratio and PSD for the normal individuals at Visit 5 for the right eye (left column) and left eye (right column). Top: SITA Standard. Middle: SITA Fast. Bottom: SITA SWAP. The number of individuals in whom both measures indicate statistically significant abnormality (S Congr[uence]) is indicated by the overlap and size of the respective two circles.

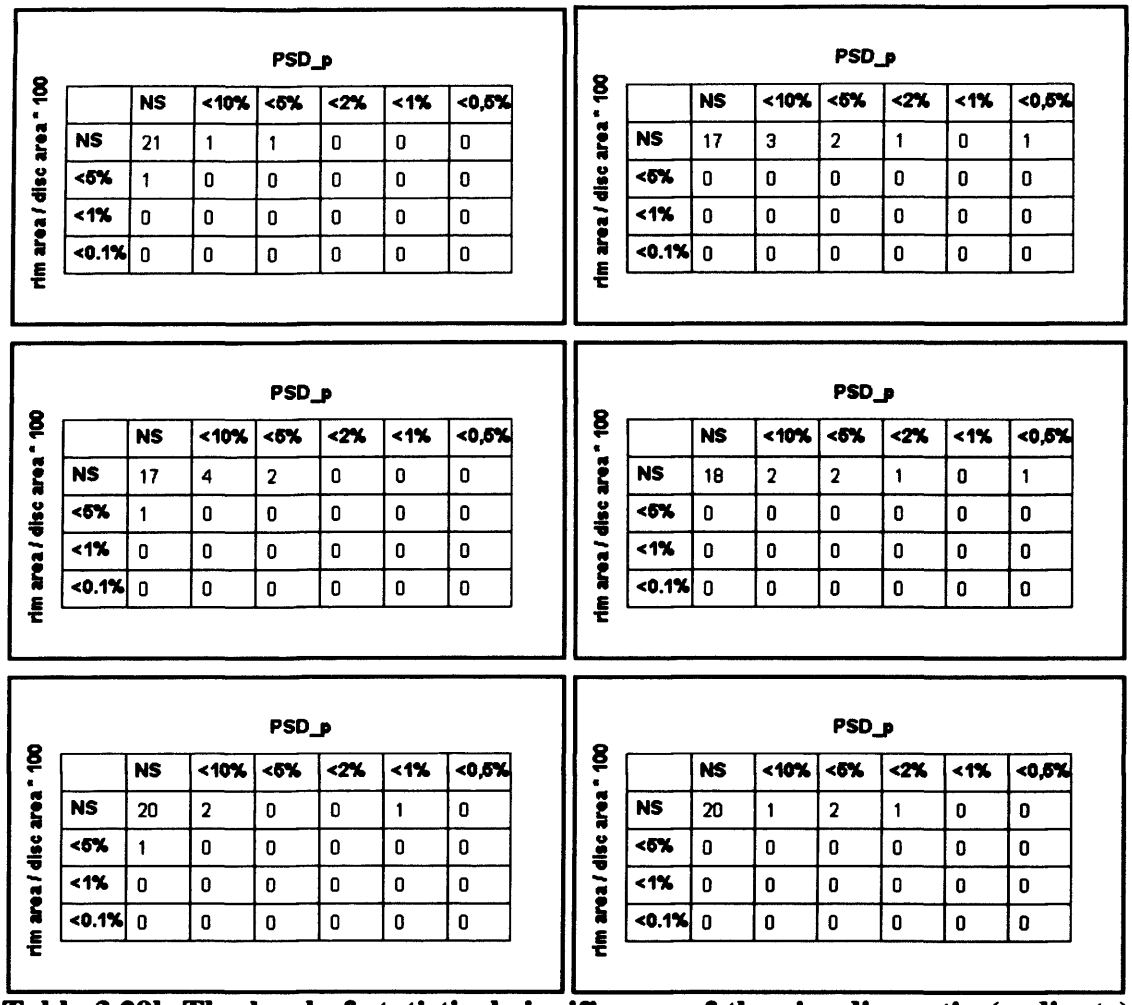

PSD_p

rim area / disc area * 100

	NS	<10%	<5%	<2%	<1%	<0,5%
NS	21	1	1	0	0	0
<5%	1	0	0	0	0	0
<1%	0	0	0	0	0	0
<0.1%	0	0	0	0	0	0

PSD_p

rim area / disc area * 100

	NS	<10%	<5%	<2%	<1%	<0,5%
NS	17	3	2	1	0	1
<5%	0	0	0	0	0	0
<1%	0	0	0	0	0	0
<0.1%	0	0	0	0	0	0

PSD_p

rim area / disc area * 100

	NS	<10%	<5%	<2%	<1%	<0,5%
NS	17	4	2	0	0	0
<5%	1	0	0	0	0	0
<1%	0	0	0	0	0	0
<0.1%	0	0	0	0	0	0

PSD_p

rim area / disc area * 100

	NS	<10%	<5%	<2%	<1%	<0,5%
NS	18	2	2	1	0	1
<5%	0	0	0	0	0	0
<1%	0	0	0	0	0	0
<0.1%	0	0	0	0	0	0

PSD_p

rim area / disc area * 100

	NS	<10%	<5%	<2%	<1%	<0,5%
NS	20	2	0	0	1	0
<5%	1	0	0	0	0	0
<1%	0	0	0	0	0	0
<0.1%	0	0	0	0	0	0

PSD_p

rim area / disc area * 100

	NS	<10%	<5%	<2%	<1%	<0,5%
NS	20	1	2	1	0	0
<5%	0	0	0	0	0	0
<1%	0	0	0	0	0	0
<0.1%	0	0	0	0	0	0

Table 3.29b The level of statistical significance of the rim-disc ratio (ordinate) and of the PSD (abscissa) for the individuals with OHT at Visit 5 for the right eye (left column) and left eye (right column). Top: SITA Standard. Middle: SITA Fast. Bottom: SITA SWAP.

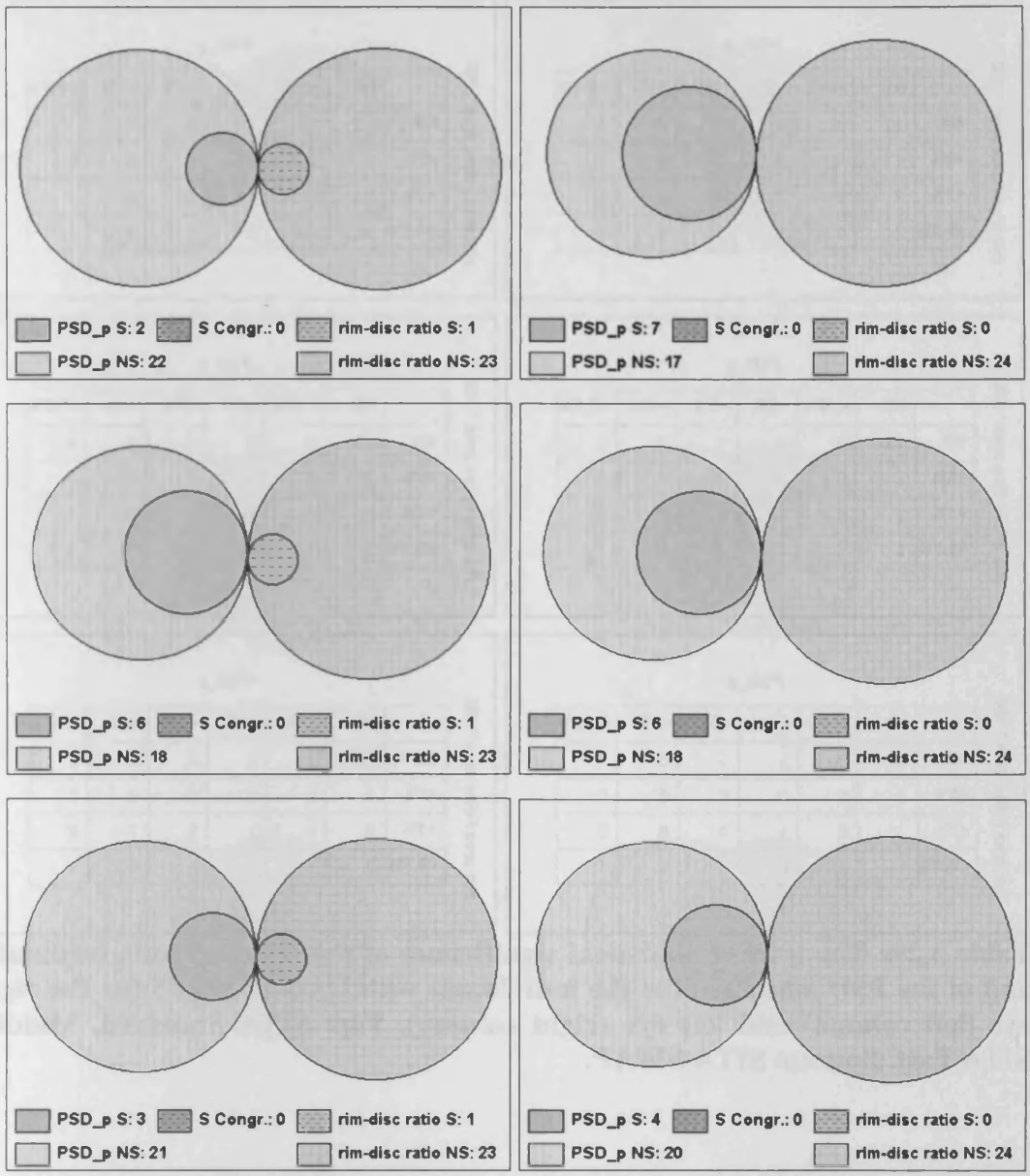

Figure 3.24b Venn diagrams, drawn to scale, illustrating the relationship between the presence (S) or absence of statistical significance (NS) associated with the respective values of the rim-disc ratio and MD for the individuals with OHT at Visit 5 for the right eye (left column) and left eye (right column). Top: SITA Standard. Middle: SITA Fast. Bottom: SITA SWAP. The number of individuals in whom both measures indicate statistically significant abnormality (S Congr[uence]) is indicated by the overlap and size of the respective two circles.

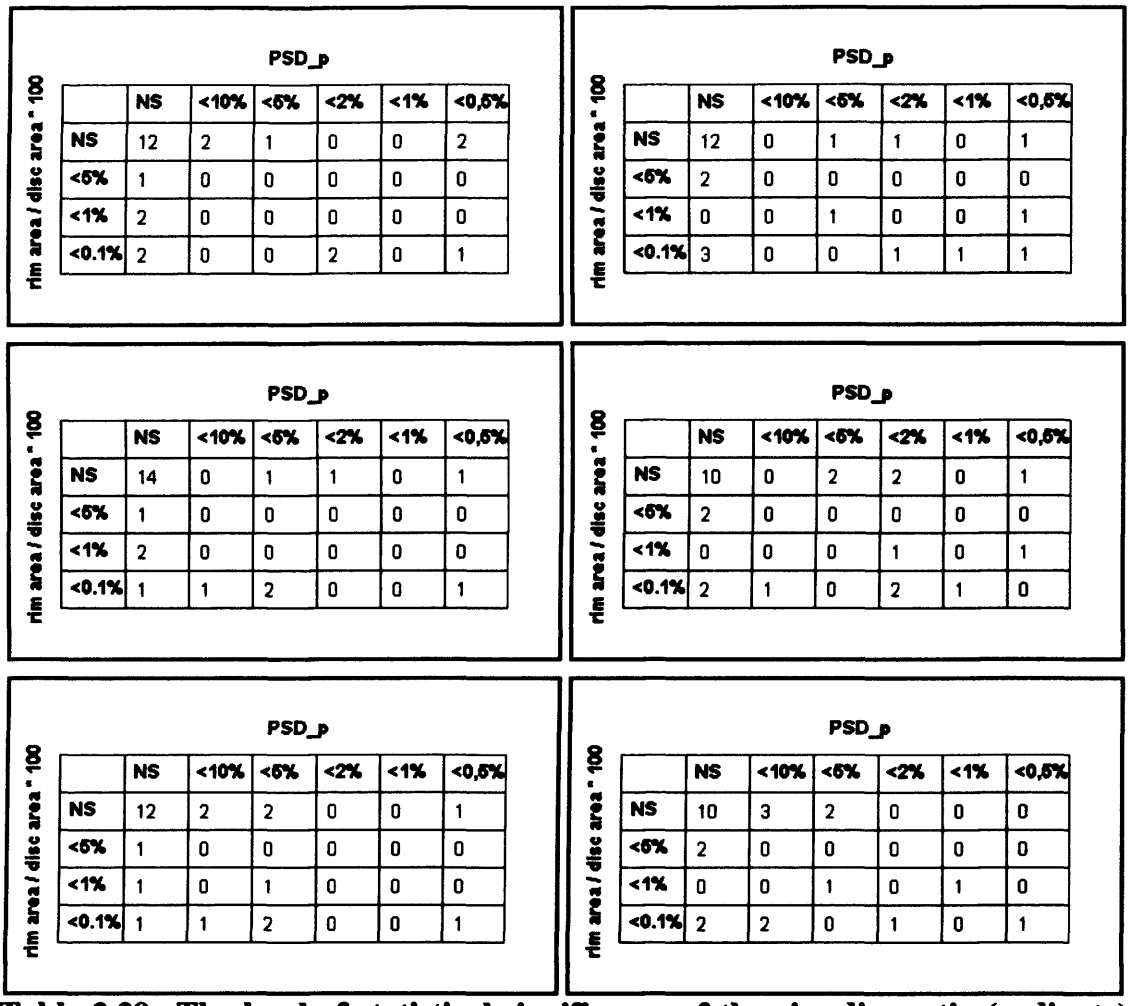

PSD_p / rim area / disc area * 100

	NS	<10%	<5%	<2%	<1%	<0,5%
NS	12	2	1	0	0	2
<5%	1	0	0	0	0	0
<1%	2	0	0	0	0	0
<0.1%	2	0	0	2	0	1

PSD_p / rim area / disc area * 100

	NS	<10%	<5%	<2%	<1%	<0,5%
NS	12	0	1	1	0	1
<5%	2	0	0	0	0	0
<1%	0	0	1	0	0	1
<0.1%	3	0	0	1	1	1

PSD_p / rim area / disc area * 100

	NS	<10%	<5%	<2%	<1%	<0,5%
NS	14	0	1	1	0	1
<5%	1	0	0	0	0	0
<1%	2	0	0	0	0	0
<0.1%	1	1	2	0	0	1

PSD_p / rim area / disc area * 100

	NS	<10%	<5%	<2%	<1%	<0,5%
NS	10	0	2	2	0	1
<5%	2	0	0	0	0	0
<1%	0	0	0	1	0	1
<0.1%	2	1	0	2	1	0

PSD_p / rim area / disc area * 100

	NS	<10%	<5%	<2%	<1%	<0,5%
NS	12	2	2	0	0	1
<5%	1	0	0	0	0	0
<1%	1	0	1	0	0	0
<0.1%	1	1	2	0	0	1

PSD_p / rim area / disc area * 100

	NS	<10%	<5%	<2%	<1%	<0,5%
NS	10	3	2	0	0	0
<5%	2	0	0	0	0	0
<1%	0	0	1	0	1	0
<0.1%	2	2	0	1	0	1

Table 3.29c The level of statistical significance of the rim-disc ratio (ordinate) and of the PSD (abscissa) for the individuals with OAG at Visit 5 for the right eye (left column) and left eye (right column). Top: SITA Standard. Middle: SITA Fast. Bottom: SITA SWAP.

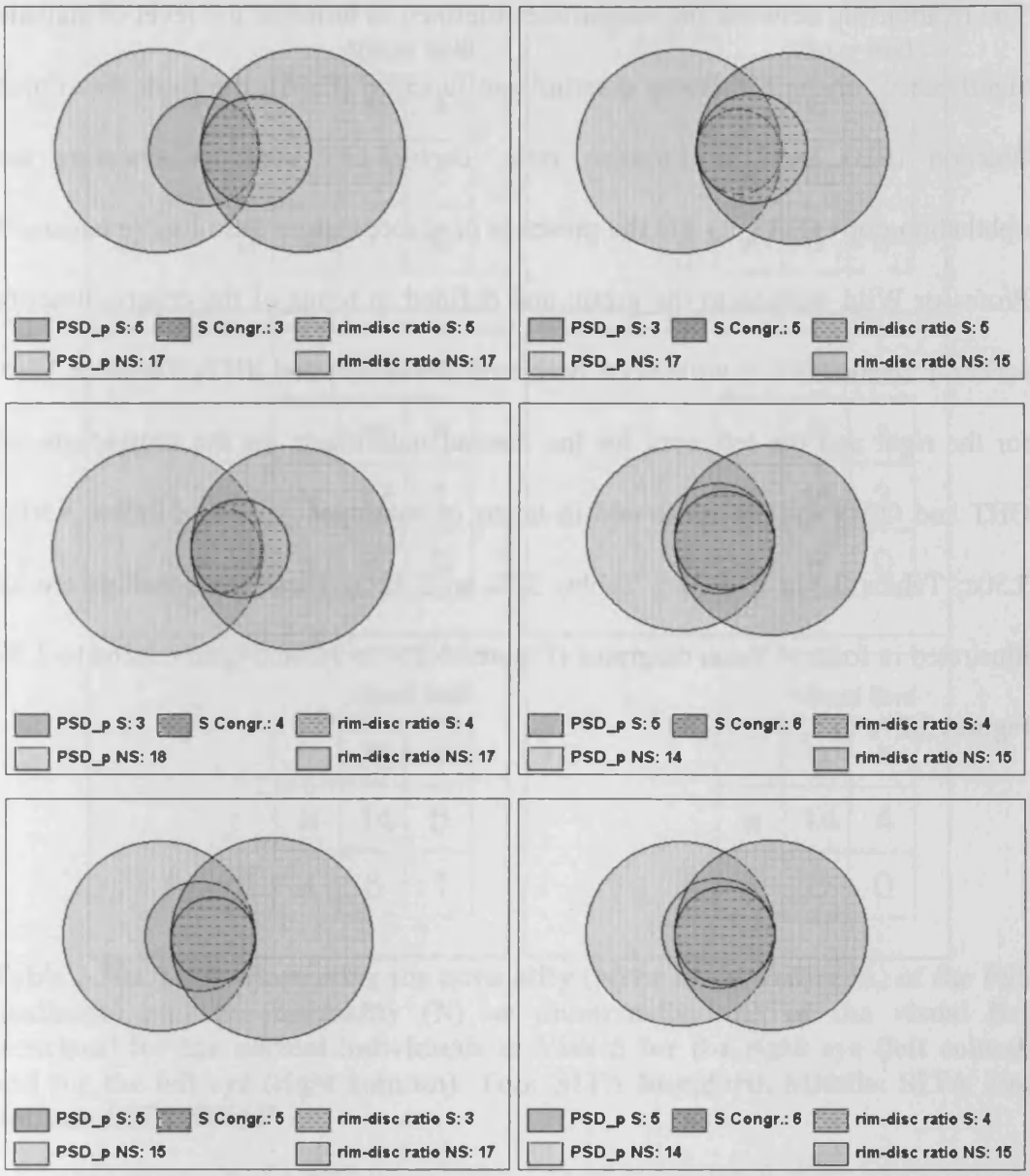

Figure 3.24c Venn diagrams, drawn to scale, illustrating the relationship between the presence (S) or absence of statistical significance (NS) associated with the respective values of the rim-disc ratio and PSD for the individuals with OAG at Visit 5 for the right eye (left column) and left eye (right column). Top: SITA Standard. Middle: SITA Fast. Bottom: SITA SWAP. The number of individuals in whom both measures indicate statistically significant abnormality (S Congr[uence]) is indicated by the overlap and size of the respective two circles.

The relationship between the magnitudes (defined in terms of the level of statistical significance) of the Mikelberg discriminate function (FSM), the Burk discriminate function (RB) and the rim-disc ratio, derived by confocal scanning laser ophthalmoscopy (HRT II) and the presence of glaucomatous field loss (evaluated by Professor Wild masked to the group and defined in terms of the criteria described earlier in Section 3.3.1) with SITA Standard, SITA Fast and SITA SWAP at Visit 5 for the right and the left eyes for the normal individuals for the individuals with OHT and OAG and are illustrated in terms of contingency tables (Tables 3.30a to 3.30c; Tables 3.31a to 3.31c; Tables 3.32 to 3.32c). These relationships are also illustrated in form of Venn diagrams (Figures 3.25a to 3.25c; Figures 3.26a to 3.26c; Figures 3.27a to 3.27c).

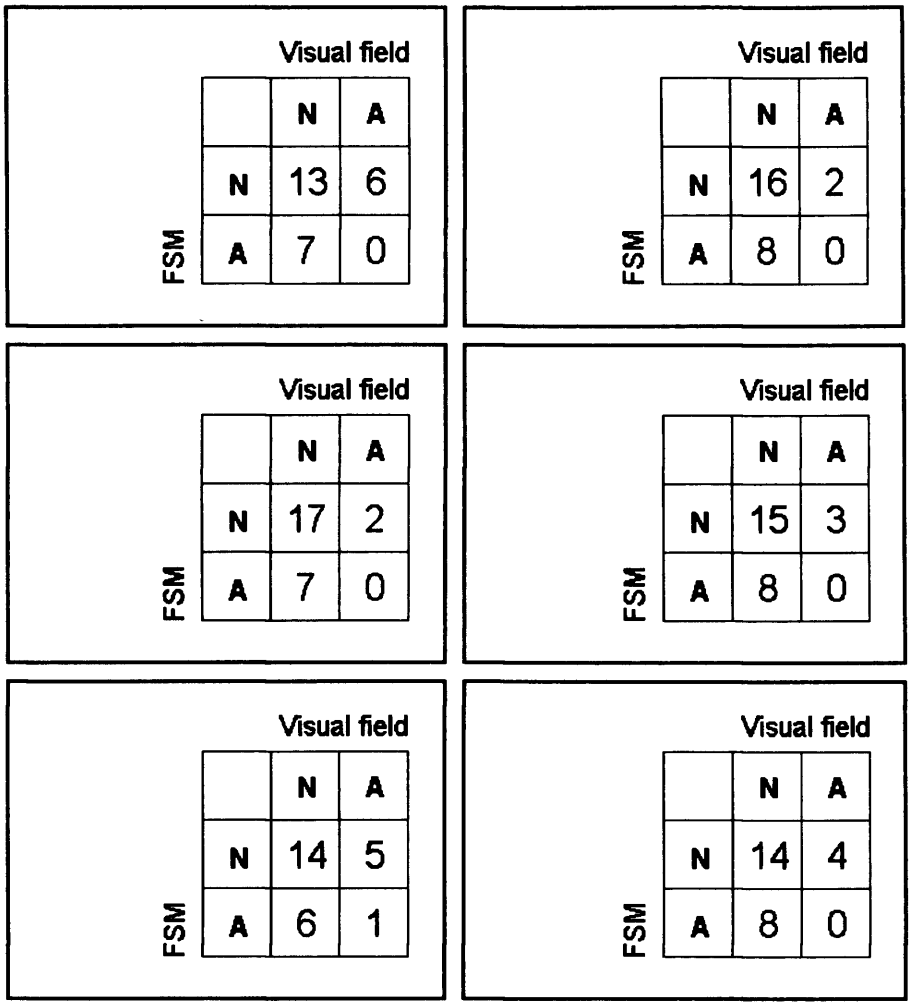

FSM \ Visual field	N	A
N	13	6
A	7	0

FSM \ Visual field	N	A
N	16	2
A	8	0

FSM \ Visual field	N	A
N	17	2
A	7	0

FSM \ Visual field	N	A
N	15	3
A	8	0

FSM \ Visual field	N	A
N	14	5
A	6	1

FSM \ Visual field	N	A
N	14	4
A	8	0

Table 3.30a Table illustrating the normality (N) or abnormality (A) of the FSM (ordinate) and the normality (N) or abnormality (A) of the visual field (abscissa) for the normal individuals at Visit 5 for the right eye (left column) and for the left eye (right column). Top: SITA Standard. Middle: SITA Fast. Bottom: SITA SWAP.

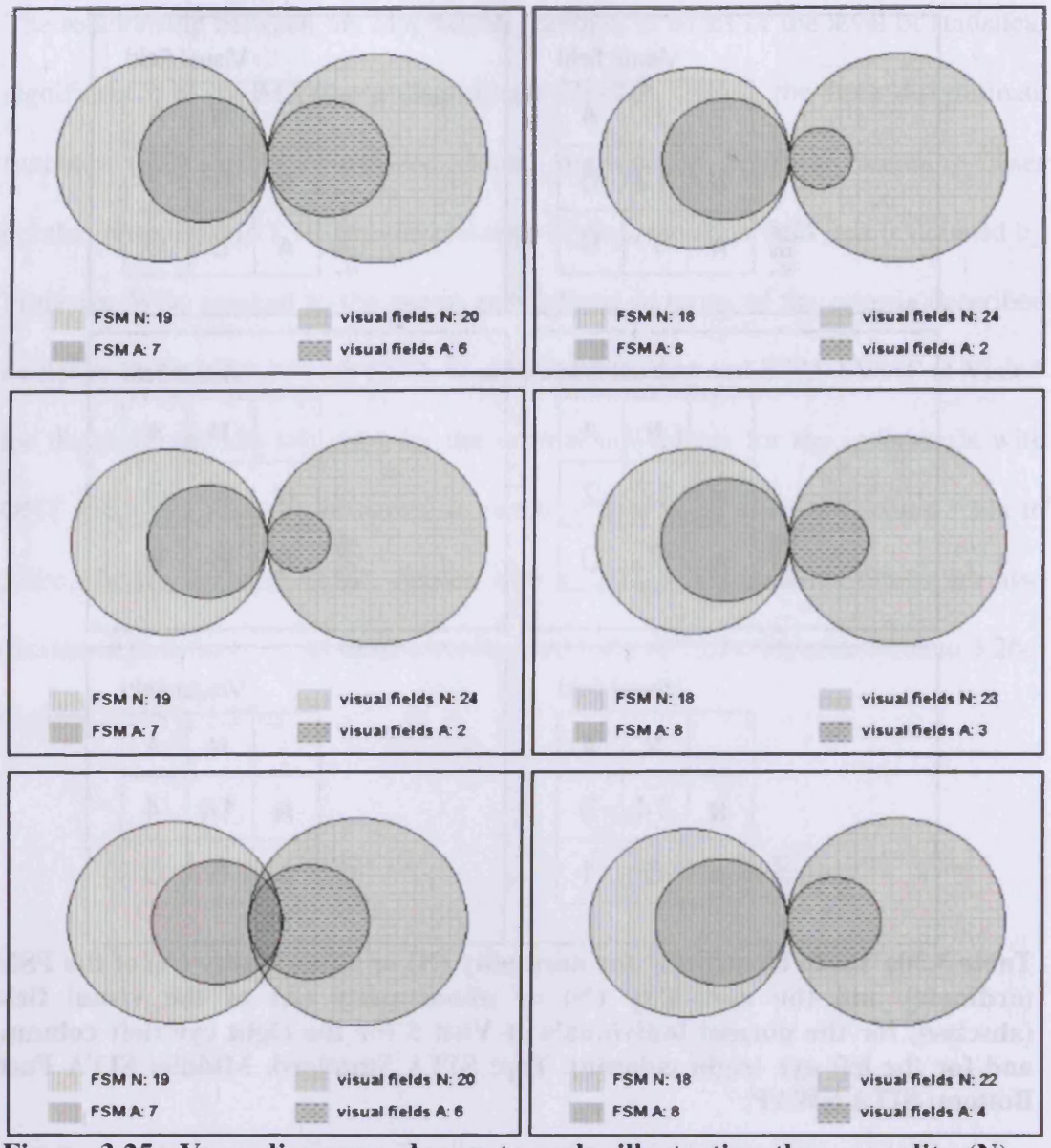

Figure 3.25a Venn diagrams, drawn to scale, illustrating the normality (N) or abnormality (A) of the visual field and the normality (N) or abnormality (A) of the FSM for the normal individuals at Visit 5 for the right eye (left column) and for the left eye (right column). Top: SITA Standard. Middle: SITA Fast. Bottom: SITA SWAP.

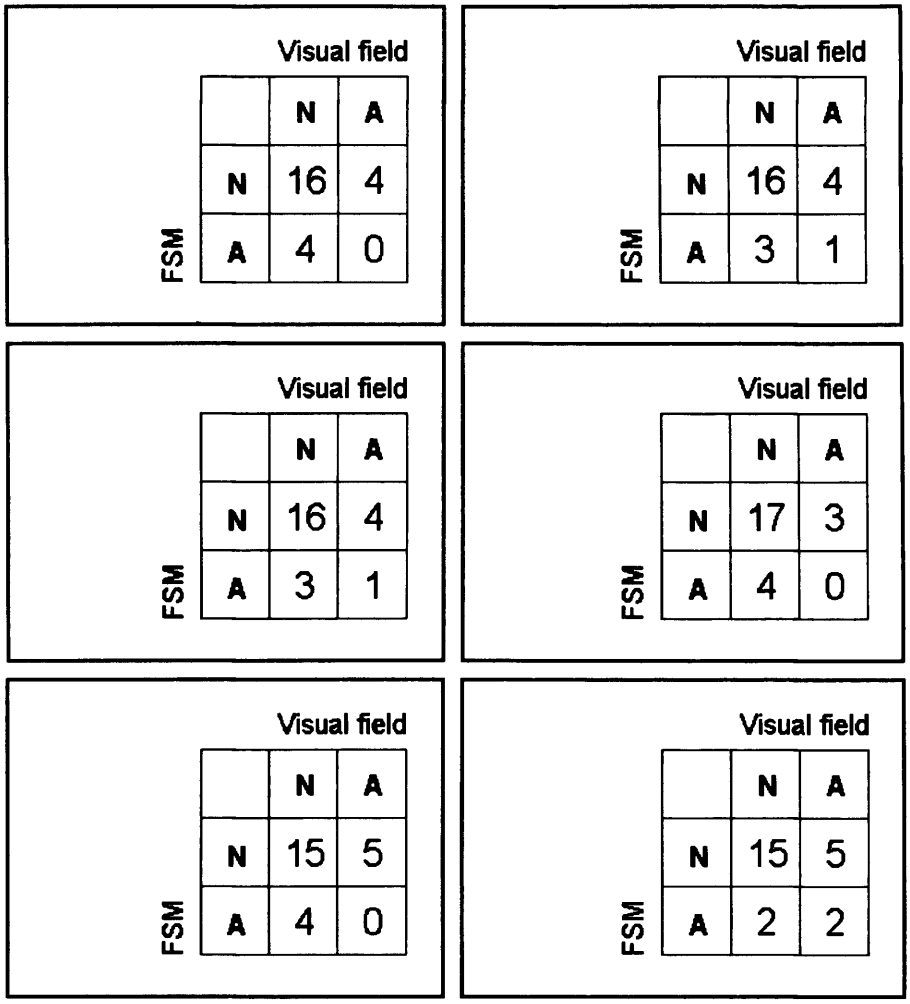

Table 3.30b Table illustrating the normality (N) or abnormality (A) of the FSM (ordinate) and the normality (N) or abnormality (A) of the visual field (abscissa) for the individuals with OHT at Visit 5 for the right eye (left column) and for the left eye (right column). Top: SITA Standard. Middle: SITA Fast. Bottom: SITA SWAP.

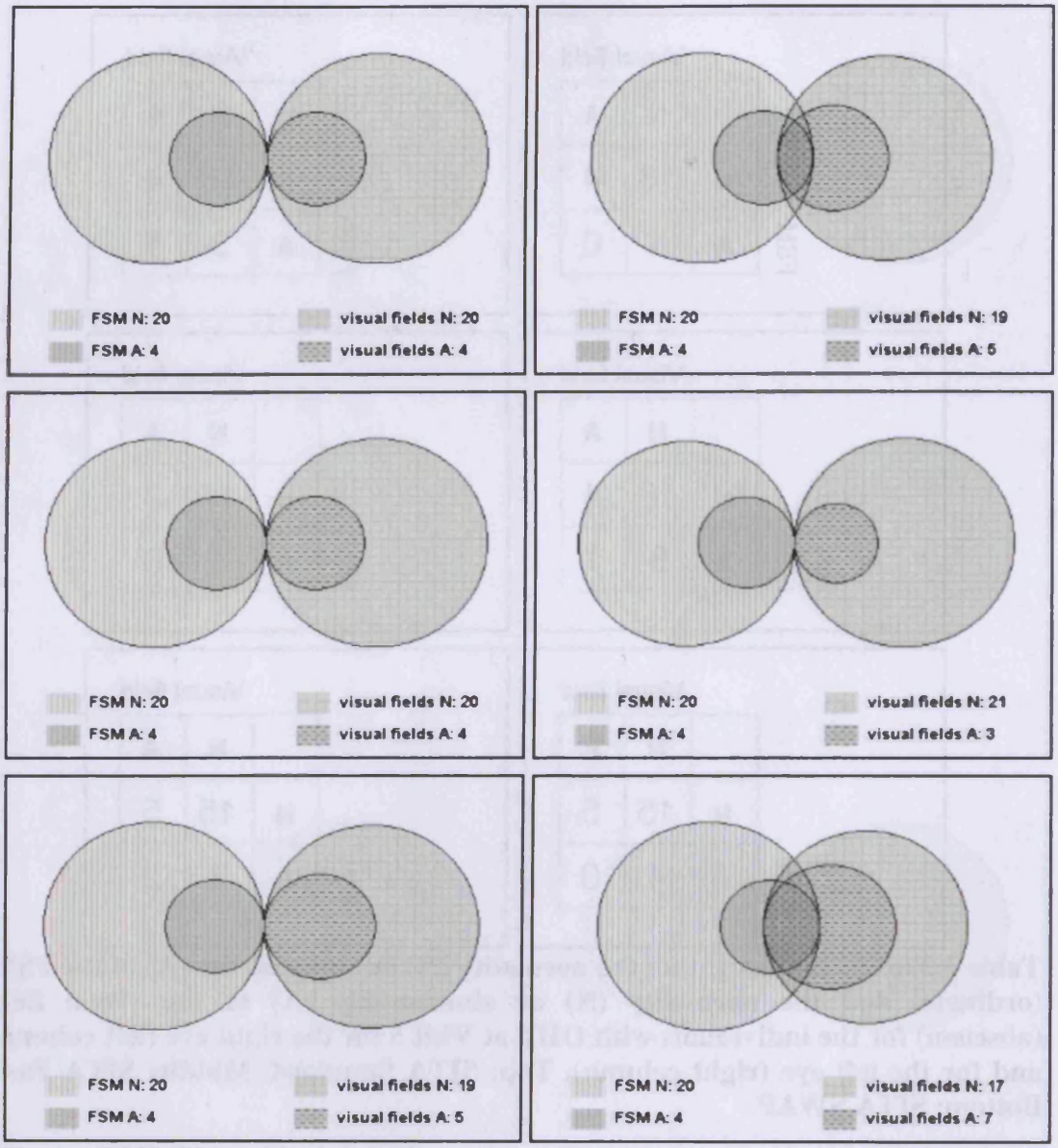

Figure 3.25b Venn diagrams, drawn to scale, illustrating the normality (N) or abnormality (A) of the visual field and the normality (N) or abnormality (A) of the FSM for the individuals with OHT at Visit 5 for the right eye (left column) and for the left eye (right column). Top: SITA Standard. Middle: SITA Fast. Bottom: SITA SWAP.

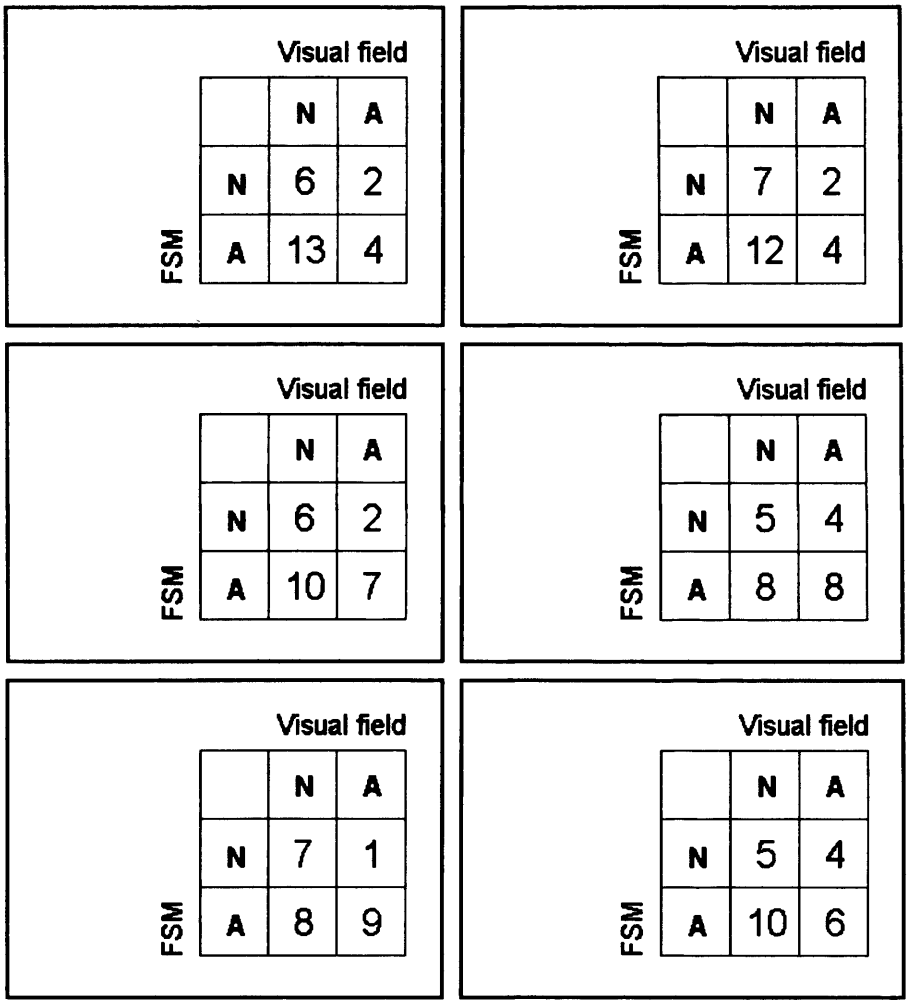

Table 3.30c Table illustrating the normality (N) or abnormality (A) of the FSM (ordinate) and the normality (N) or abnormality (A) of the visual field (abscissa) for the individuals with OAG at Visit 5 for the right eye (left column) and for the left eye (right column). Top: SITA Standard. Middle: SITA Fast. Bottom: SITA SWAP.

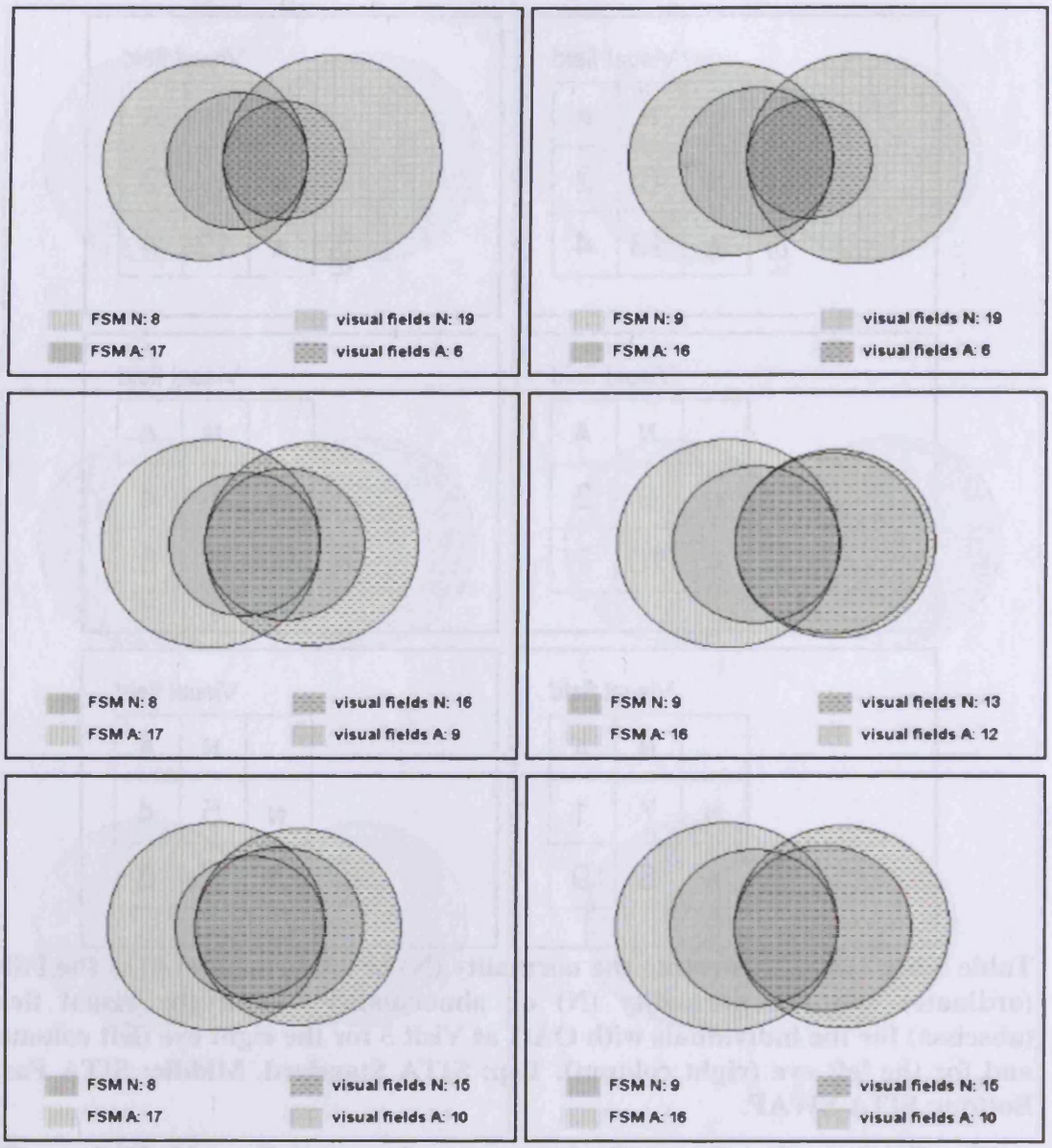

Figure 3.25c Venn diagrams, drawn to scale, illustrating the normality (N) or abnormality (A) of the visual field and the normality (N) or abnormality (A) of the FSM for the individuals with OAG at Visit 5 for the right eye (left column) and for the left eye (right column). Top: SITA Standard. Middle: SITA Fast. Bottom: SITA SWAP.

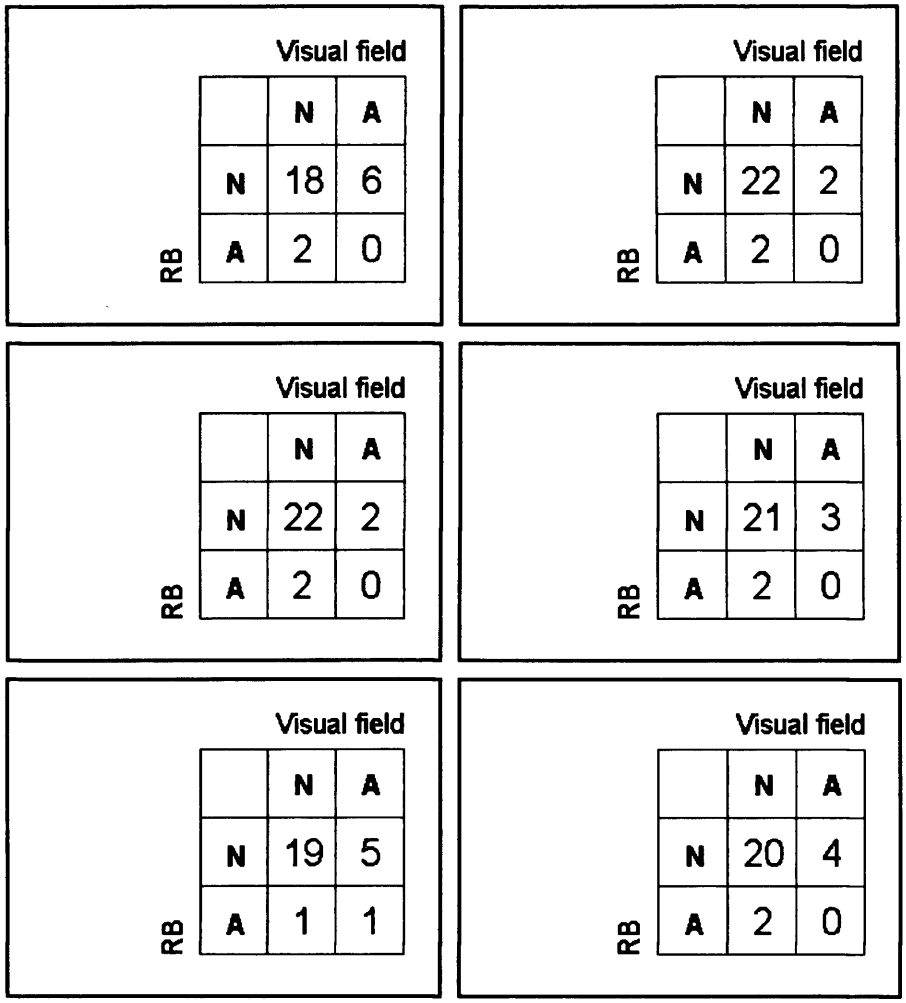

Table 3.31a Table illustrating the normality (N) or abnormality (A) of the RB (ordinate) and the normality (N) or abnormality (A) of the visual field (abscissa) for the normal individuals at Visit 5 for the right eye (left column) and for the left eye (right column). Top: SITA Standard. Middle: SITA Fast. Bottom: SITA SWAP.

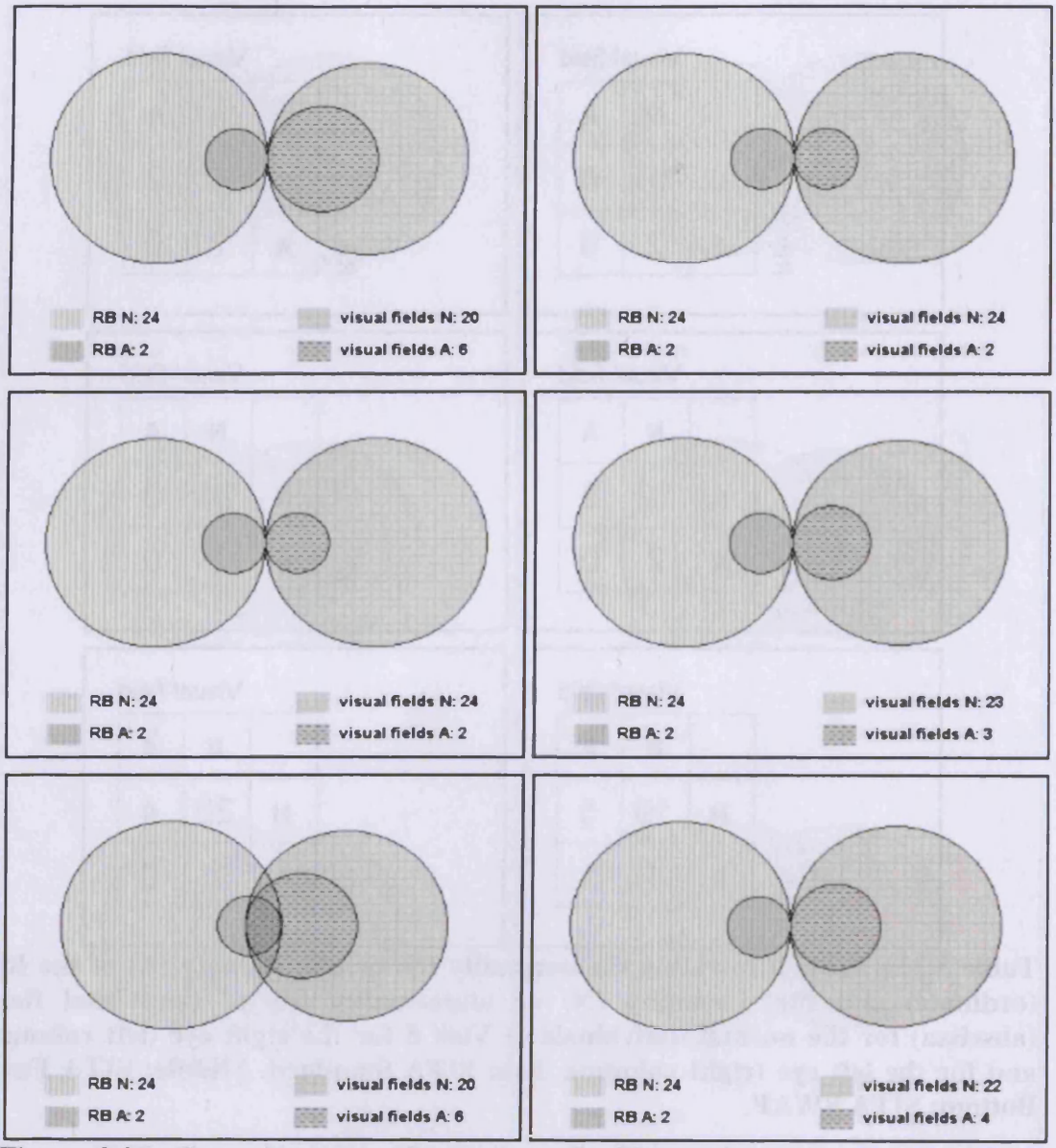

Figure 3.26a Venn diagrams, drawn to scale, illustrating the normality (N) or abnormality (A) of the visual field and the normality (N) or abnormality (A) of the FSM for the normal individuals at Visit 5 for the right eye (left column) and for the left eye (right column). Top: SITA Standard. Middle: SITA Fast. Bottom: SITA SWAP.

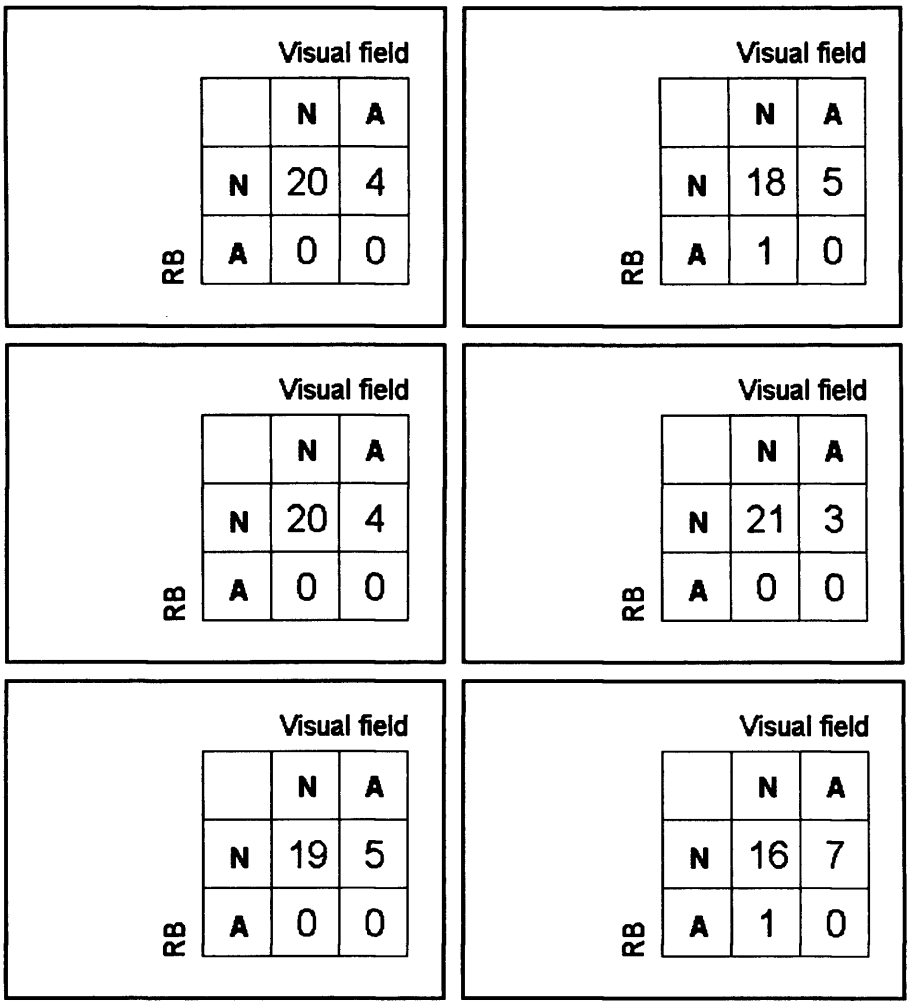

Table 3.31b Table illustrating the normality (N) or abnormality (A) of the RB (ordinate) and the normality (N) or abnormality (A) of the visual field (abscissa) for the individuals with OHT at Visit 5 for the right eye (left column) and for the left eye (right column). Top: SITA Standard. Middle: SITA Fast. Bottom: SITA SWAP.

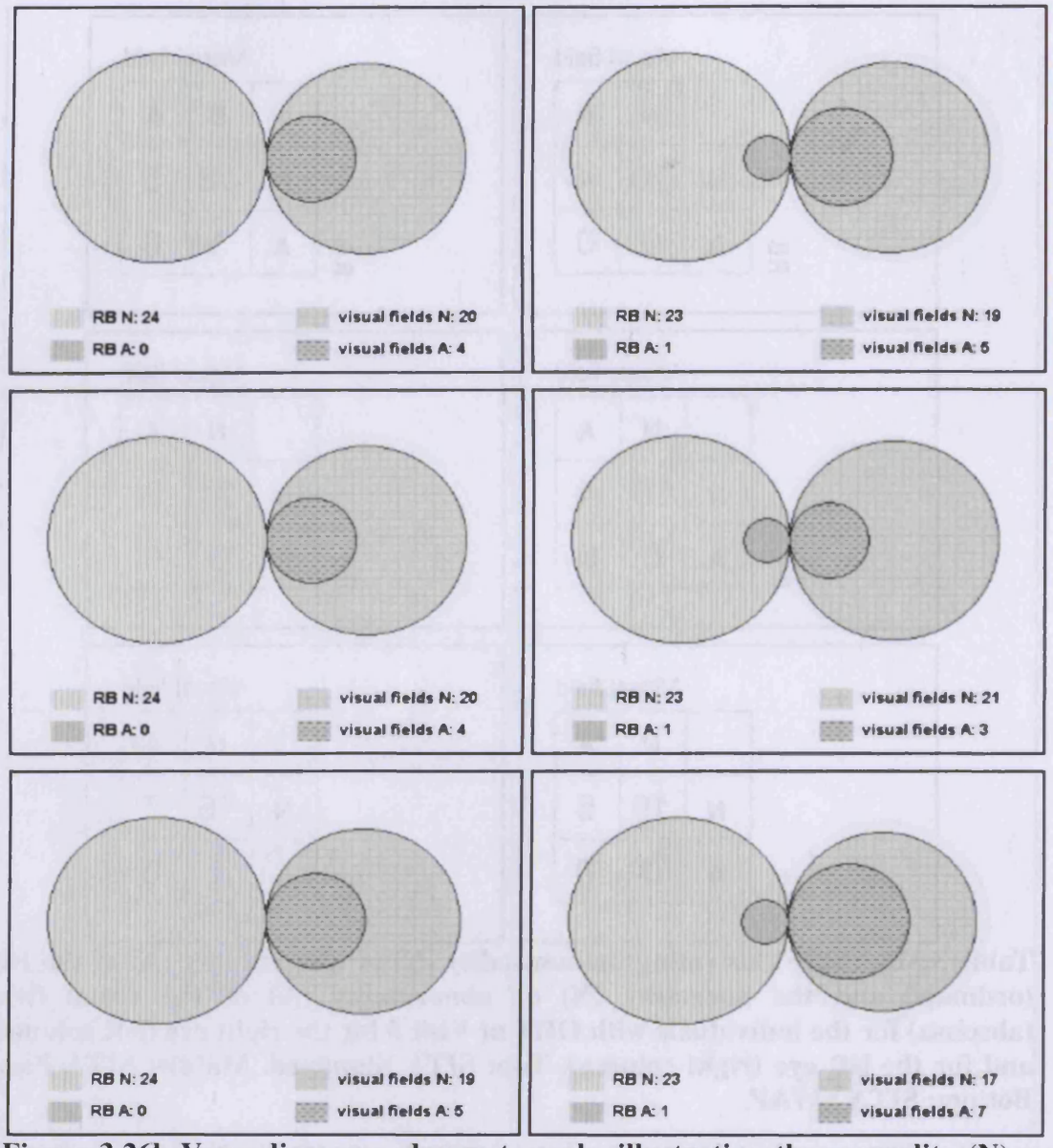

Figure 3.26b Venn diagrams, drawn to scale, illustrating the normality (N) or abnormality (A) of the visual field and the normality (N) or abnormality (A) of the RB for the individuals with OHT at Visit 5 for the right eye (left column) and for the left eye (right column). Top: SITA Standard. Middle: SITA Fast. Bottom: SITA SWAP.

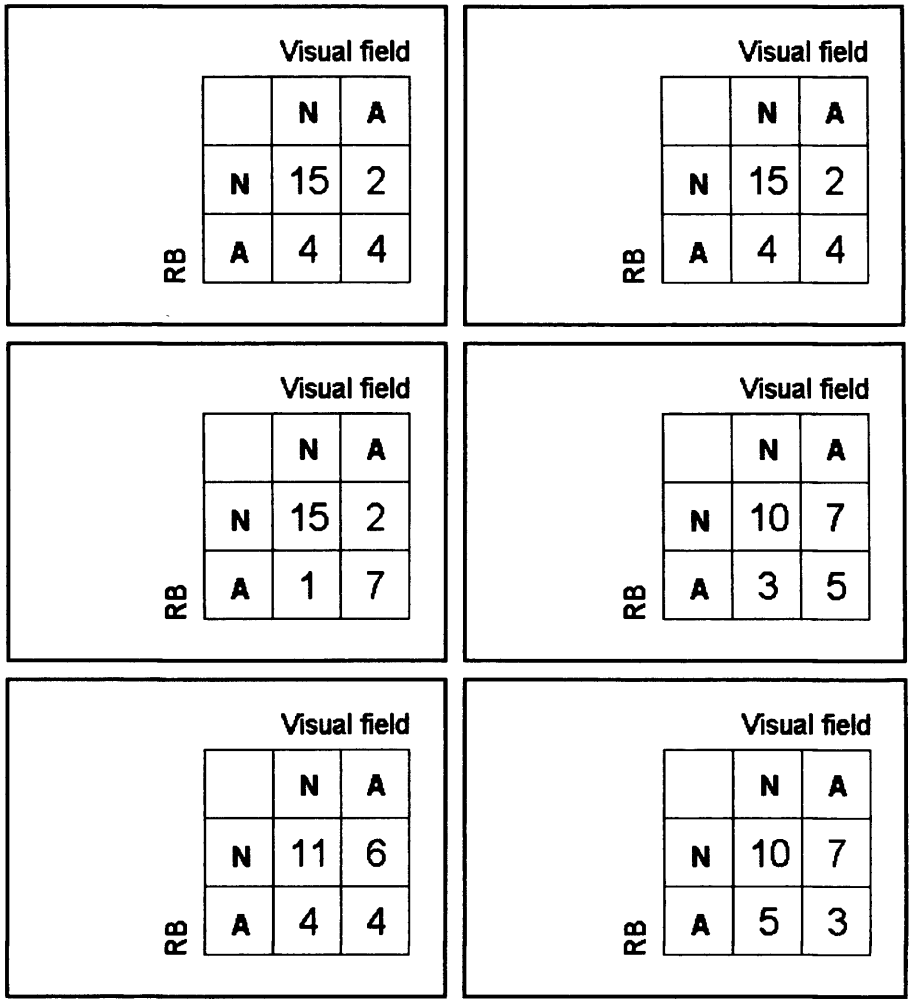

Table 3.31c Table illustrating the normality (N) or abnormality (A) of the RB (ordinate) and the normality (N) or abnormality (A) of the visual field (abscissa) for the individuals with OAG at Visit 5 for the right eye (left column) and for the left eye (right column). Top: SITA Standard. Middle: SITA Fast. Bottom: SITA SWAP.

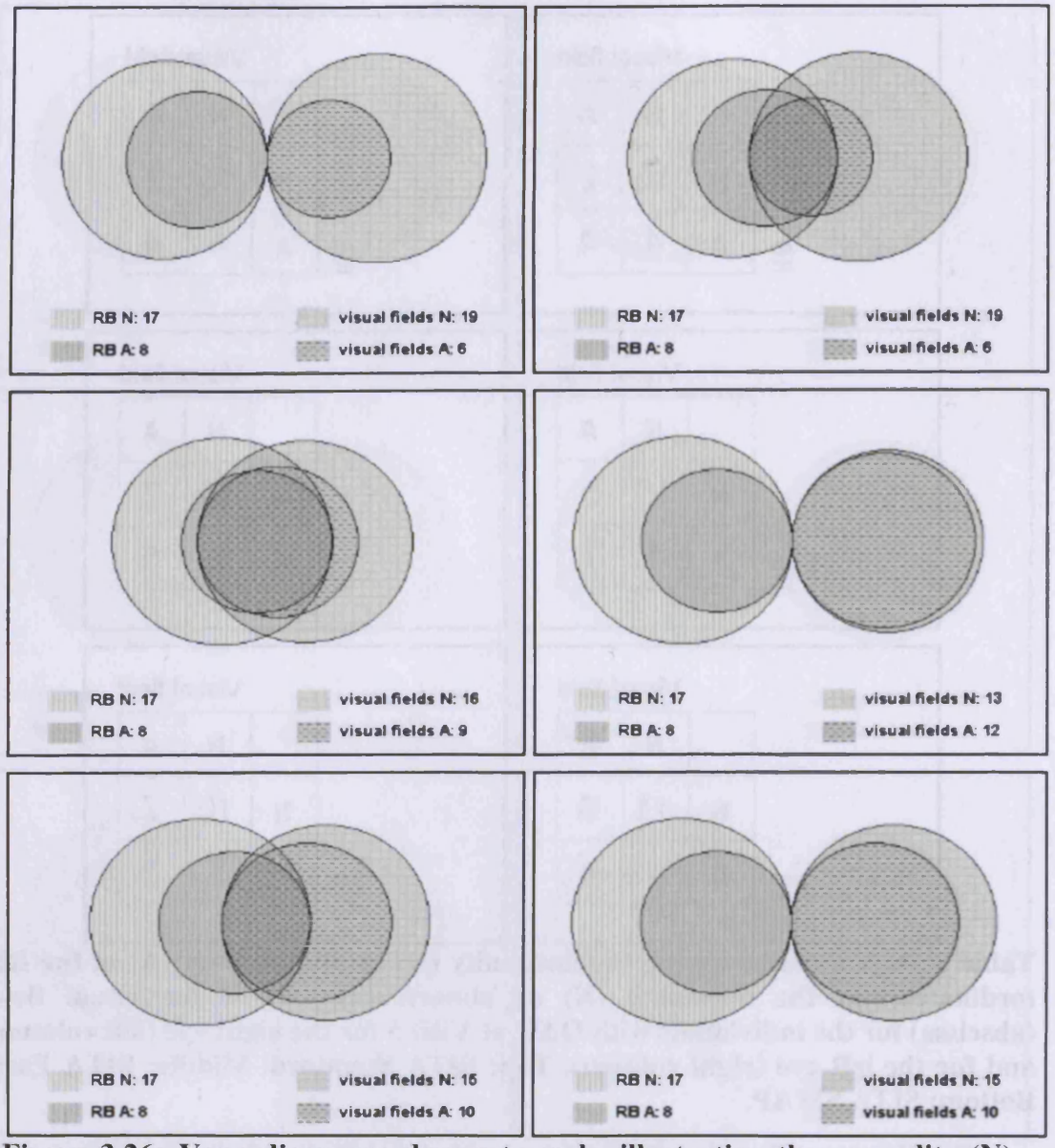

Figure 3.26c Venn diagrams, drawn to scale, illustrating the normality (N) or abnormality (A) of the visual field and the normality (N) or abnormality (A) of the RB for the individuals with OAG at Visit 5 for the right eye (left column) and for the left eye (right column). Top: SITA Standard. Middle: SITA Fast. Bottom: SITA SWAP.

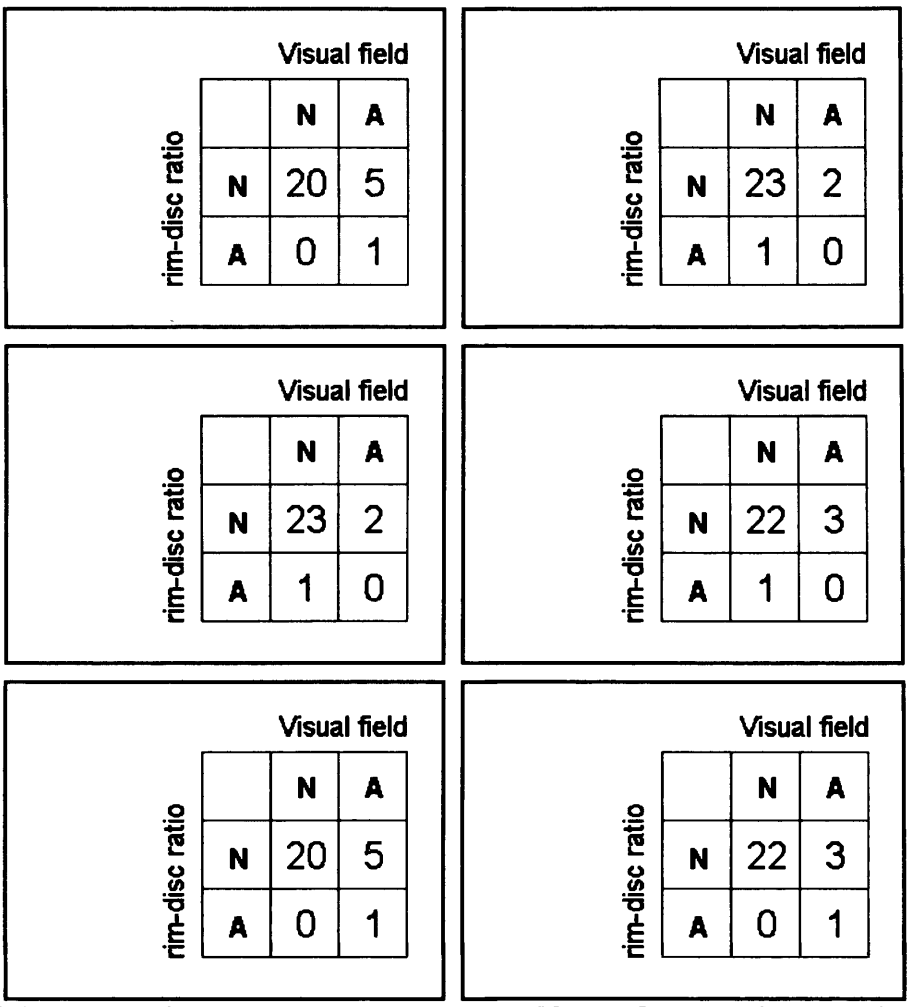

Table 3.32a Table illustrating the normality (N) or abnormality (A) of the rim-disc ratio (ordinate) and the normality (N) or abnormality (A) of the visual field (abscissa) for the normal individuals at Visit 5 for the right eye (left column) and for the left eye (right column). Top: SITA Standard. Middle: SITA Fast. Bottom: SITA SWAP.

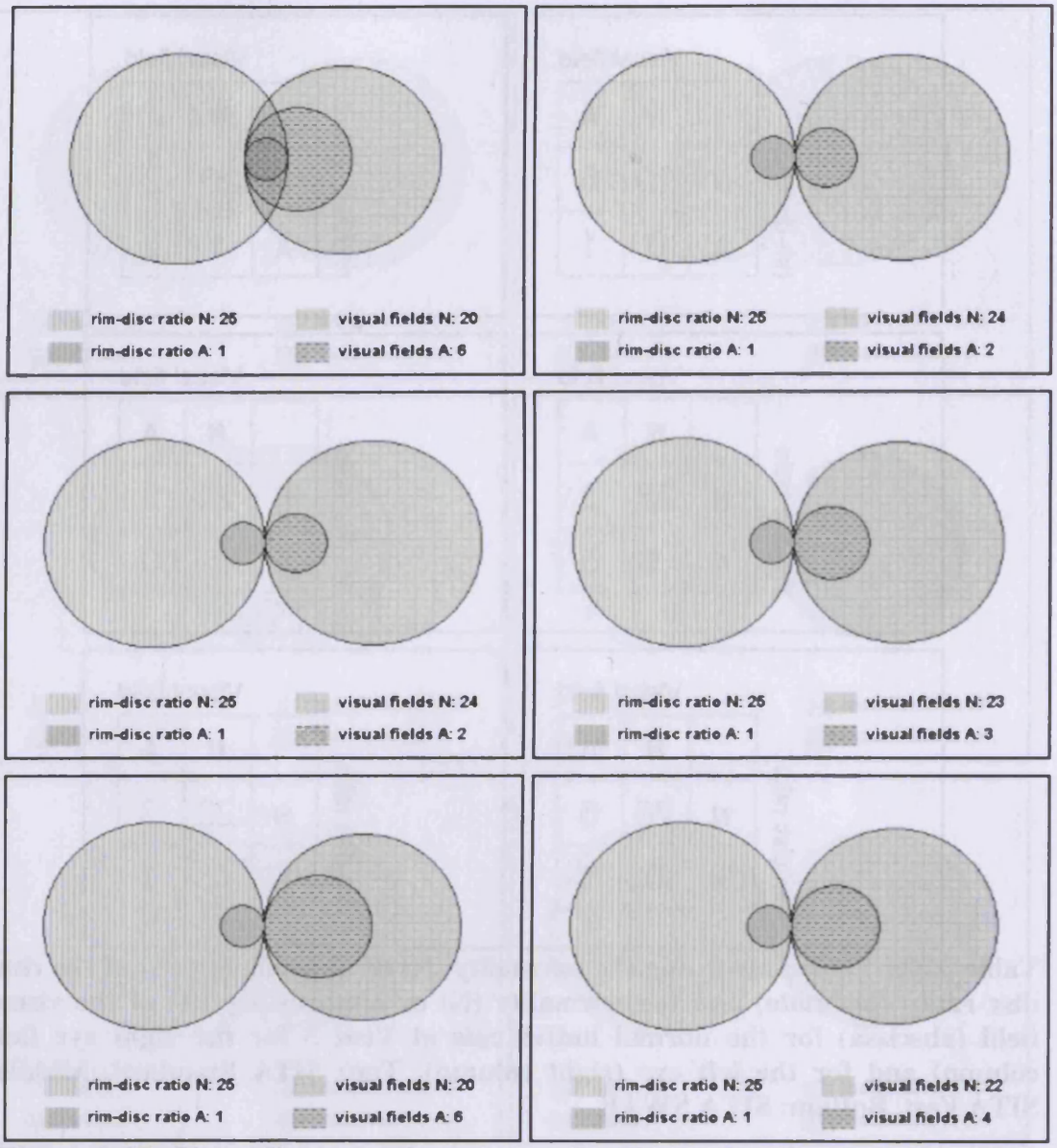

Figure 3.27a Venn diagrams, drawn to scale, illustrating the normality (N) or abnormality (A) of the visual field and the normality (N) or abnormality (A) of the rim-disc ratio for the normal individuals at Visit 5 for the right eye (left column) and for the left eye (right column). Top: SITA Standard. Middle: SITA Fast. Bottom: SITA SWAP.

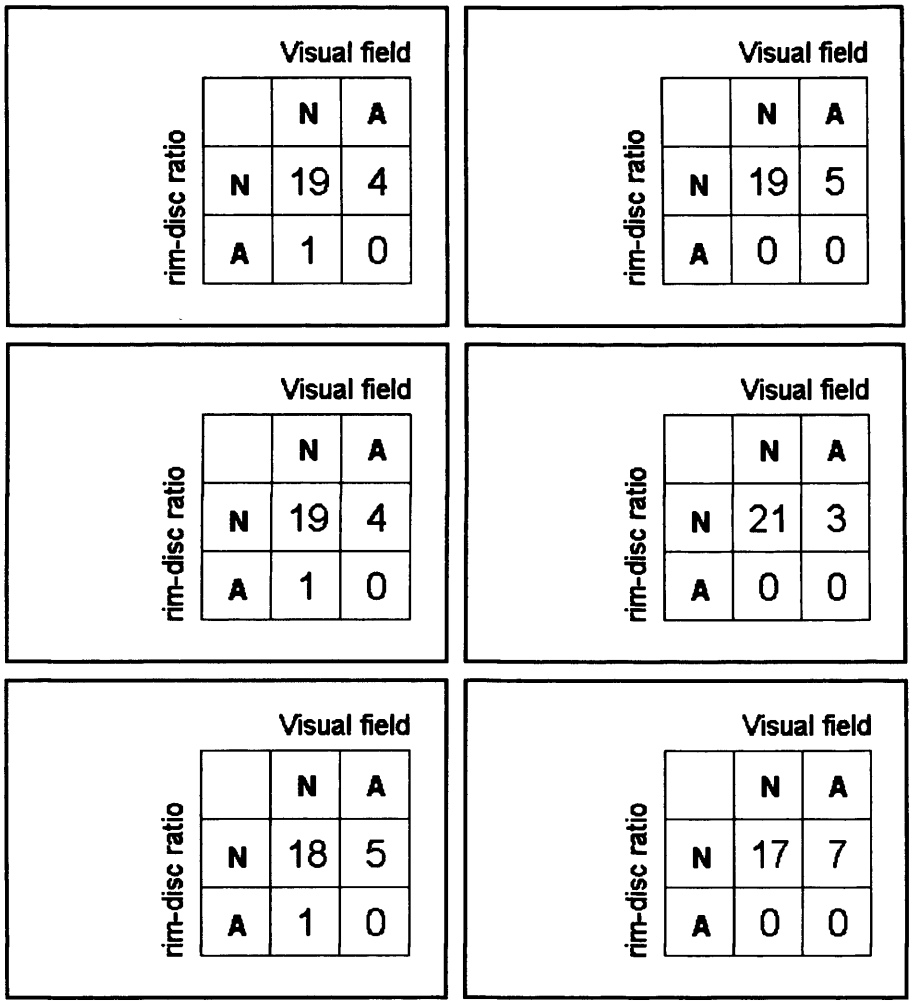

Table 3.32b Table illustrating the normality (N) or abnormality (A) of the rim-disc ratio (ordinate) and the normality (N) or abnormality (A) of the visual field (abscissa) for the individuals with OHT at Visit 5 for the right eye (left column) and for the left eye (right column). Top: SITA Standard. Middle: SITA Fast. Bottom: SITA SWAP.

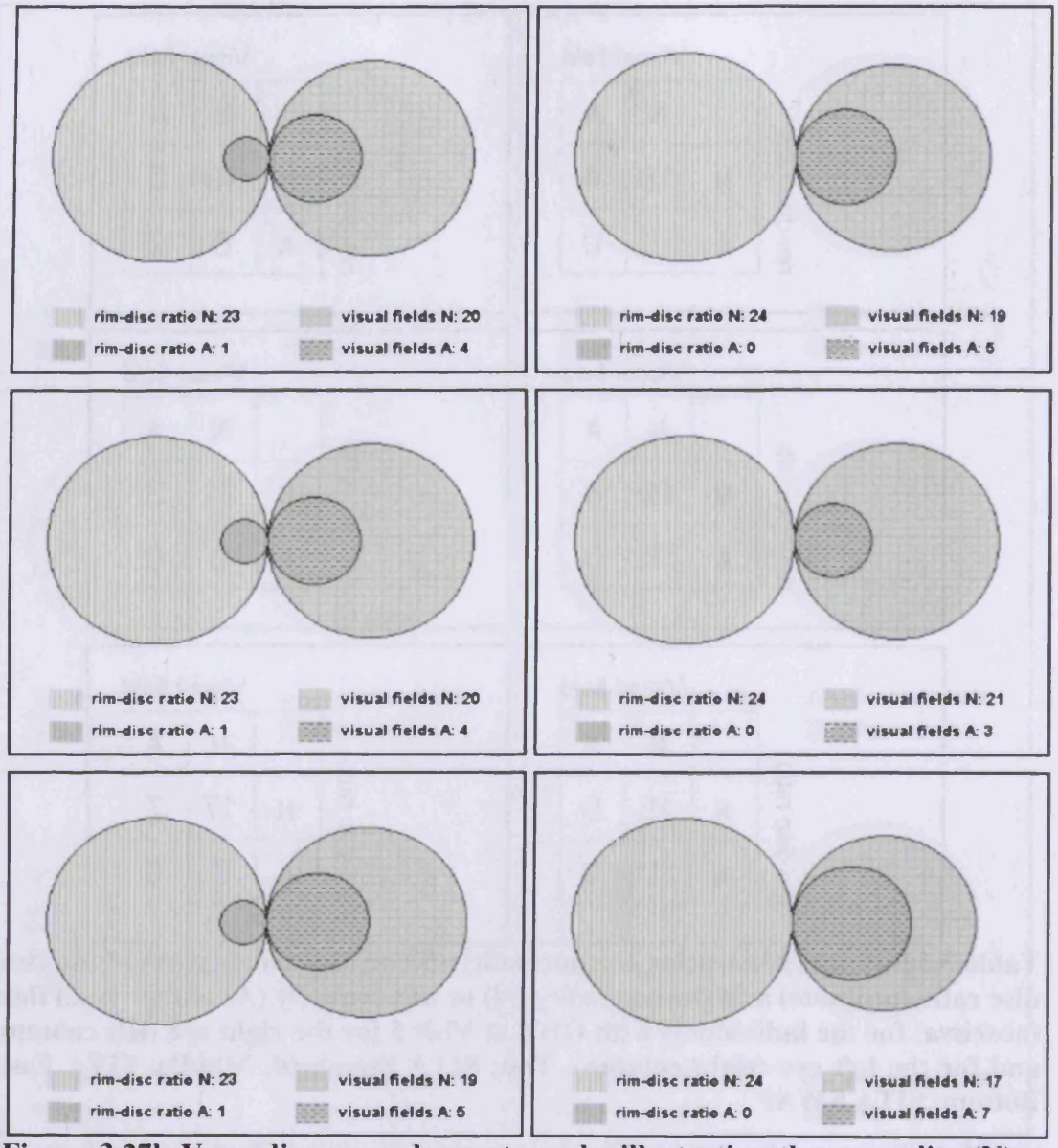

Figure 3.27b Venn diagrams, drawn to scale, illustrating the normality (N) or abnormality (A) of the visual field and the normality (N) or abnormality (A) of the rim-disc ratio for the individuals with OHT at Visit 5 for the right eye (left column) and for the left eye (right column). Top: SITA Standard. Middle: SITA Fast. Bottom: SITA SWAP.

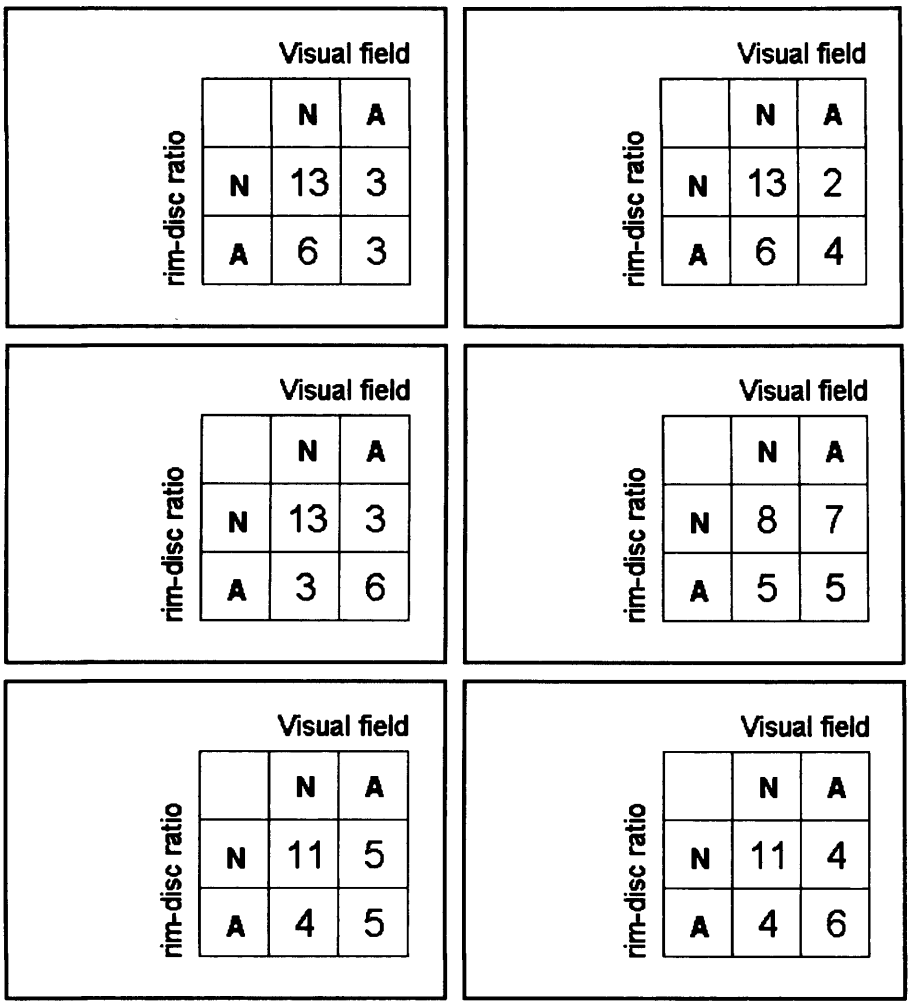

Table 3.32c Table illustrating the normality (N) or abnormality (A) of the rim-disc ratio (ordinate) and the normality (N) or abnormality (A) of the visual field (abscissa) for the individuals with OAG at Visit 5 for the right eye (left column) and for the left eye (right column). Top: SITA Standard. Middle: SITA Fast. Bottom: SITA SWAP.

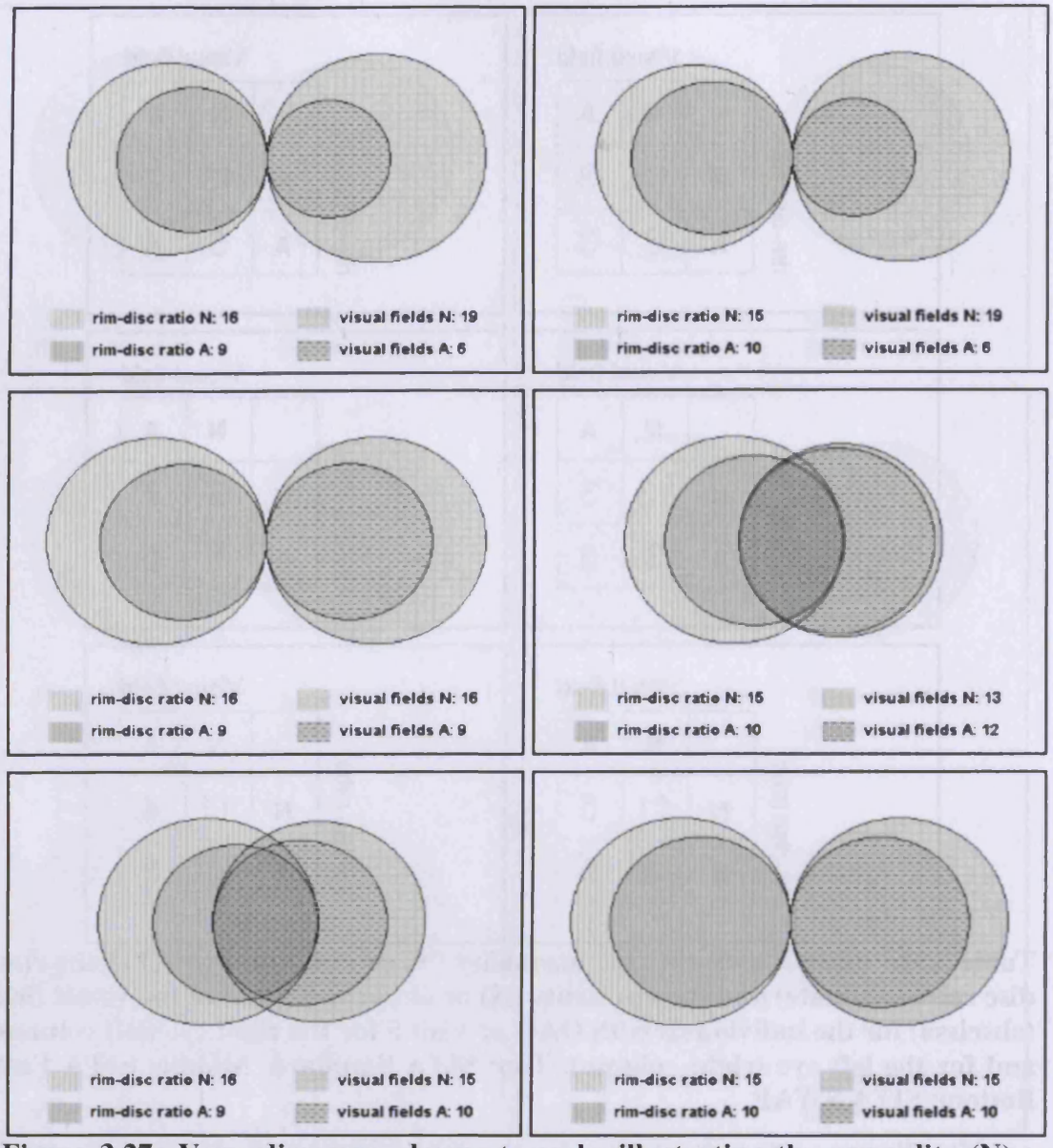

Figure 3.27c Venn diagrams, drawn to scale, illustrating the normality (N) or abnormality (A) of the visual field and the normality (N) or abnormality (A) of the rim –disc ratio for the individuals with OAG at Visit 5 for the right eye (left column) and for the left eye (right column). Top: SITA Standard. Middle: SITA Fast. Bottom: SITA SWAP.

Compared to the clinical diagnosis made by PD Dr med. M. Zulauf, the FSM exhibited the highest sensitivity of the HRT derived stereometric parameters (17 of 25 cases in the right eye and 16 of 25 cases in the left eye correctly) with a moderate specificity (8 of the 26 normal right eyes and 9 of 26 the left eyes incorrectly identified). The RB exhibited better specificity than the FSM. It incorrectly

identified 2 of the 26 normal right eyes and 2 of the 26 left eyes (one individual was incorrectly identified in both eyes and two individuals in one eye). However, the sensitivity was poor (8 cases in each eye of 25 eyes with OAG correctly identified). The rim-disc area exhibited almost 100% specificity but similar sensitivity to that of the RB (8 of 25 right eyes with OAG and 9 of 25 left eyes correctly identified). The MD of the SITA SWAP algorithm gave the worst specificity of the three perimetric algorithms and a similar, but poor, sensitivity to the two SAP algorithms. It correctly designated 22 of the 26 normal right eyes and 20 of the 26 normal left eyes and 5 of the 25 right eyes with OAG and 5 of the 25 left eyes with OAG. As a consequence of the poor sensitivity of the MD of each of the three perimetric algorithms, the corresponding structure-function concordances were poor. The PSD yielded better specificity and sensitivity for each of the three perimetric algorithms. With the SITA SWAP algorithm, 25 of the 26 normal right eyes and 23 of the 26 left eyes and 10 of the 25 right eyes with OAG and 11 of the 25 left eyes were correctly designated. Similar results were obtained for each of the two SAP algorithms. The clinical evaluation gave broadly similar results, in terms of sensitivity and specificity, to the PSD for each of the three algorithms. As a consequence of the poor sensitivities of each of the three perimetric algorithms, the structure-function concordances were, at best, only moderate.

3.5 Discussion

3.5.1 The Learning effect

The results show clear evidence for a learning effect (i.e. in improvement in sensitivity) which was evident for all three algorithms across all three groups and was most pronounced for the SITA SWAP algorithm. In terms of the visual field indices, the learning effect was manifest as an increase in the MD (i.e. it became less

negative) and a slight reduction in the PSD (i.e. it became less positive). Therefore, both the height and the shape of the field tended towards a more normal appearance with repeated examinations. The learning effect, in general, was complete by Visit 3 for both SAP algorithms and possibly at Visit 4 for SWAP.

The improvement in performance was to be expected in the normal individuals for both SAP and SWAP as these individuals were naïve to any type of perimetry. The extent of the improvement in these individuals was restricted by the limited potential range for improvement i. e. normal results can, in essence, only remain normal. Somewhat surprisingly, the individuals with OHT and the individuals with OAG also exhibited, in terms of group means statistics, at least, a slight improvement in the outcome to SAP despite having previously undertaken, on average, 5 to 6 examinations per eye (i.e. 5 to 6 visits) as part of their normal clinical care. The greater improvement for SWAP compared to SAP, irrespective of prior experience of SAP, indicates that the outcome from SWAP relies upon a different perceptual task, i.e. SWAP stimulates the short-wavelength sensitive chromatic pathway and the response requires the detection of chromatic (blue) contrast against the yellow background (Felius et al 1995) compared to SAP which requires the detection of the edge contrast against the white background. Such an improvement for SITA SWAP was compatible with that reported for SWAP undertaken with the Full Threshold algorithm (Wild et al 2006).

The slope of the decline in mean sensitivity with increase in age became steeper by three fold in the right eye and by two fold in the left eye between Visits 1 and 5 for the SITA Standard algorithm. The steepening of the slope between Visits 1 and 5 was less for SITA Fast (1.5 fold for the right eye and 1.8 fold for the left eye). These

findings indicate that the magnitude of the potential improvement in sensitivity declines with increase in age.

The value of the slope for the SITA Standard algorithm at Visit 5 was -0.91dB per decade for the right eye and -1.30dB per decade for the left eye, and compares with that of -0.72dB per decade, determined at the second perimetric visit (i.e. the second examination) by Wild et al (1999a). The corresponding values at Visit 2 in the current study were -0.62dB per decade and -0.82dB per decade.

The slopes for the SITA Fast algorithm at Visit 5 were -0.75dB per decade for the right eye and -0.91dB per decade for the left eye. The slopes at the second visit using SITA Fast were -0.52dB and -0.64dB per decade compared to -0.62dB per decade obtained after the second visual field examination (Wild et al 1999a).

Interestingly, the slope of the decline in sensitivity with increase in age for SITA SWAP remained relatively similar in each eye, or possibly flattened slightly, over the 5 visits. Nevertheless, the slope was markedly steep in each eye compared to the SITA Standard and SITA Fast algorithms (by 2.2 fold in the right eye and 1.9 fold in the left eye at Visit 5 compared to SITA Standard; and by 2.6 fold and by 2.7 fold, respectively, compared to SITA Fast). The slopes for SITA SWAP at Visit 5 were -2.00dB per decade for the right eye and -2.46dB for the left eye per decade compared with -1.96dB per decade for SWAP using the Full Threshold algorithm and -1.80dB per decade using the FASTPAC algorithm (Wild et al 1998).

The hill of vision for both SAP algorithms and for SWAP became steeper with increase in age i.e. the decline in sensitivity became more pronounced with increase in eccentricity. The extent of the steepening was greatest for SITA SWAP and this was similar to that found for the Full Threshold algorithm (Wild et al 1998).

As would be expected, the examination duration became shorter over the five examinations for each algorithm and each diagnostic group. The greatest reduction occurred for the group with glaucoma; the group exhibited a reduction of 30 seconds, averaged across the two eyes, from the base line to the fifth visits (233 vs 203 seconds). In terms of the necessary concentration by a patient, this is a sizable saving of time. In terms of the shorter examination duration, SITA SWAP would seem to be ideal to implement in the clinical setting. However, the greater number of examinations required to overcome the learning effect is a disadvantage of the technique and has cost implications. The latter could be countenanced if SWAP proved to be superior to SAP for the detection of glaucomatous abnormality. However, this does not appear to be the case (van der Schoot et al 2009).

The ratio of the PMS to the CMS was similar between algorithms and across visits. This finding contradicts previous reports on SAP (Wood et al 1987b; Heijl et al 1989c; Wild et al 1989; Kulze et al 1990; Heijl and Bengtsson 1996; Wild et al 1999a). However, the use of Program 24-2 rather than Program 30-2 used in the studies of the learning effect for SAP may account for the lack of a more pronounced peripheral component to the learning effect in the outer annuli of stimulus locations present with Program 30-2 and not present with Program 24-2.

Although the group mean analysis indicated an *overall* improvement in the performance with both SAP algorithms and also, particularly, with the SITA SWAP algorithm, the within individual analysis of the MD (Fig. 3.8a-3.8d) and of the PSD (Fig. 3.9a-3.9d) showed considerable between-individual variation in performance, particularly for SWAP and particularly for the second (left) eye examined.

The upward direction (positive slope) of the 90^{th} , 50^{th} and 10^{th} percentiles of the distribution of the within-algorithm difference in sensitivity between Visits 1 and 5 across all stimulus locations indicated (Fig. 3.10a to Fig. 3.1d) that, as would be expected, the predominant improvement occurred at increasingly intermediate values of sensitivity and this was particularly evident for SWAP.

The truncation of the percentiles at approximately 16dB for SITA Standard and for SITA Fast in the normal individuals, and in the individuals with OHT, arise from the lack of stimulus locations exhibiting sensitivities below this value. Similarly, the scatter below approximately 16dB in the location of the percentiles for SAP in the individuals with OAG arises from the limited number of locations exhibiting reduced sensitivity. The apparent extension of the range of the percentiles for SWAP towards minimal levels of sensitivity, compared to SAP, arises from the different dB scales between SAP and SWAP.

The reduction in the number and/ or severity of the Total and of the Pattern Deviation probability levels between the Visit 1 and Visit 5 reflects the improvement in the absolute values of sensitivity, particularly at the intermediate values of sensitivity, described earlier. This reduction in the number and/ or severity

of the probability levels was most pronounced, as would be expected, for the Total Deviation map. It occurred for all algorithms but was most pronounced for SITA SWAP and for the individuals with OAG. Such an outcome could, in fact, lead to an increased specificity and a reduced sensitivity for both the Total Deviation and the Pattern Deviation analysis but, generally, will result in a less severe appearance to the visual field particularly for the SITA SWAP algorithm in contrast to both SAP algorithms. The improvement in the outcome of SWAP should also be considered in the context of the increased confidence limits for normality of SWAP relative to SAP reported for the Full Threshold and FASTPAC algorithms (Wild et al 1998; Soliman et al 2002) and confirmed in this study for SITA SWAP. However, the individuals with OHT, and also the normal individuals, also exhibited a considerable improvement for SITA SWAP, particularly in the first (right) eye examined. This fact could be explained by the presence of a greater fatigue effect (which is opposed to the learning effect) in the second (left) eye examined. However, the influence of the fatigue effect on each of the three algorithms for SWAP is unknown.

The overriding conclusion from the various analyses was that a residual learning effect was present for SITA SWAP, over and above any learning effect for SAP, and that this residual effect lasted up to the fourth examination. Such an effect essentially renders SITA SWAP obsolete in the clinical environment. Figure 3.28 shows an example of typically improvement with the SITA SWAP algorithm.

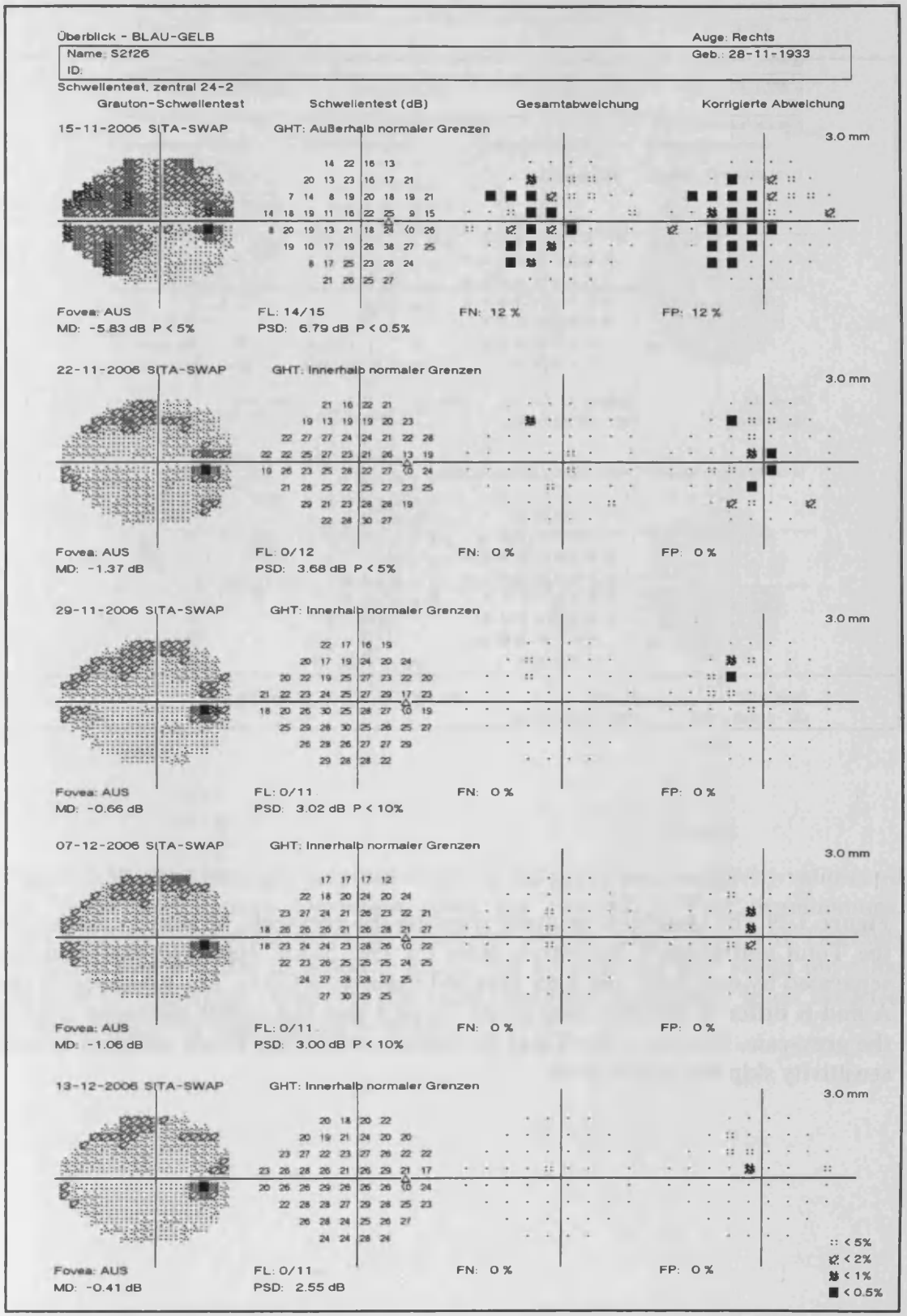

Figure 3.28 A typical example of the learning effect with the SITA SWAP algorithm between Visit 1 and Visit 5 in the right eye of an individual with OAG. The learning effect manifests as an improvement in the MD, the PSD and the Total and Pattern Deviation maps.

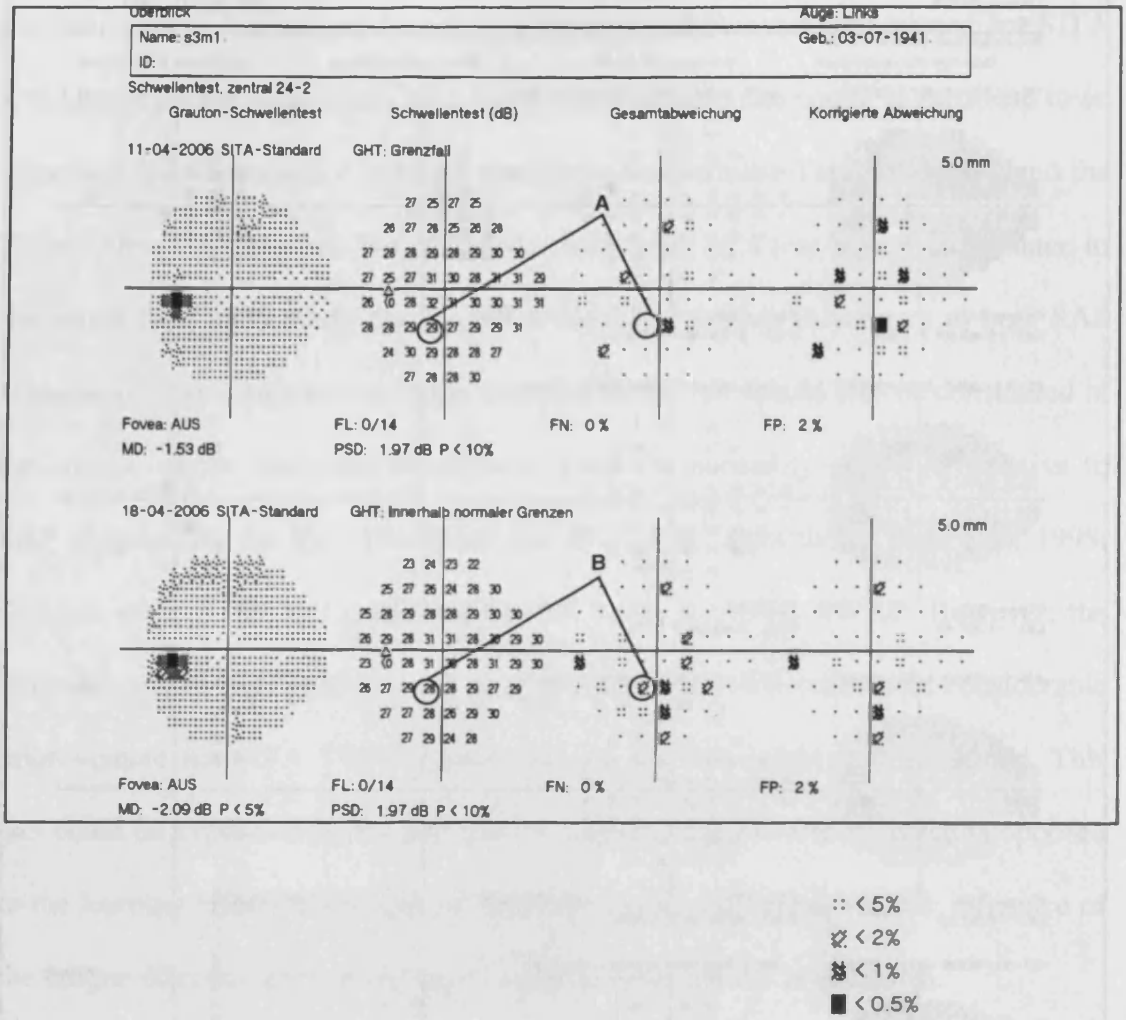

Figure 3.29 The Overview printout showing the greyscale, sensitivity values and the Total and Pattern Deviation plots for two SITA Standard examinations, separated by one week, for a 65 year old male with OAG. The locations circled A and B differ in absolute sensitivity by 1dB and fall within the same level on the greyscale. However, the Total Deviation probability levels assigned to each sensitivity skip the p<5% level.

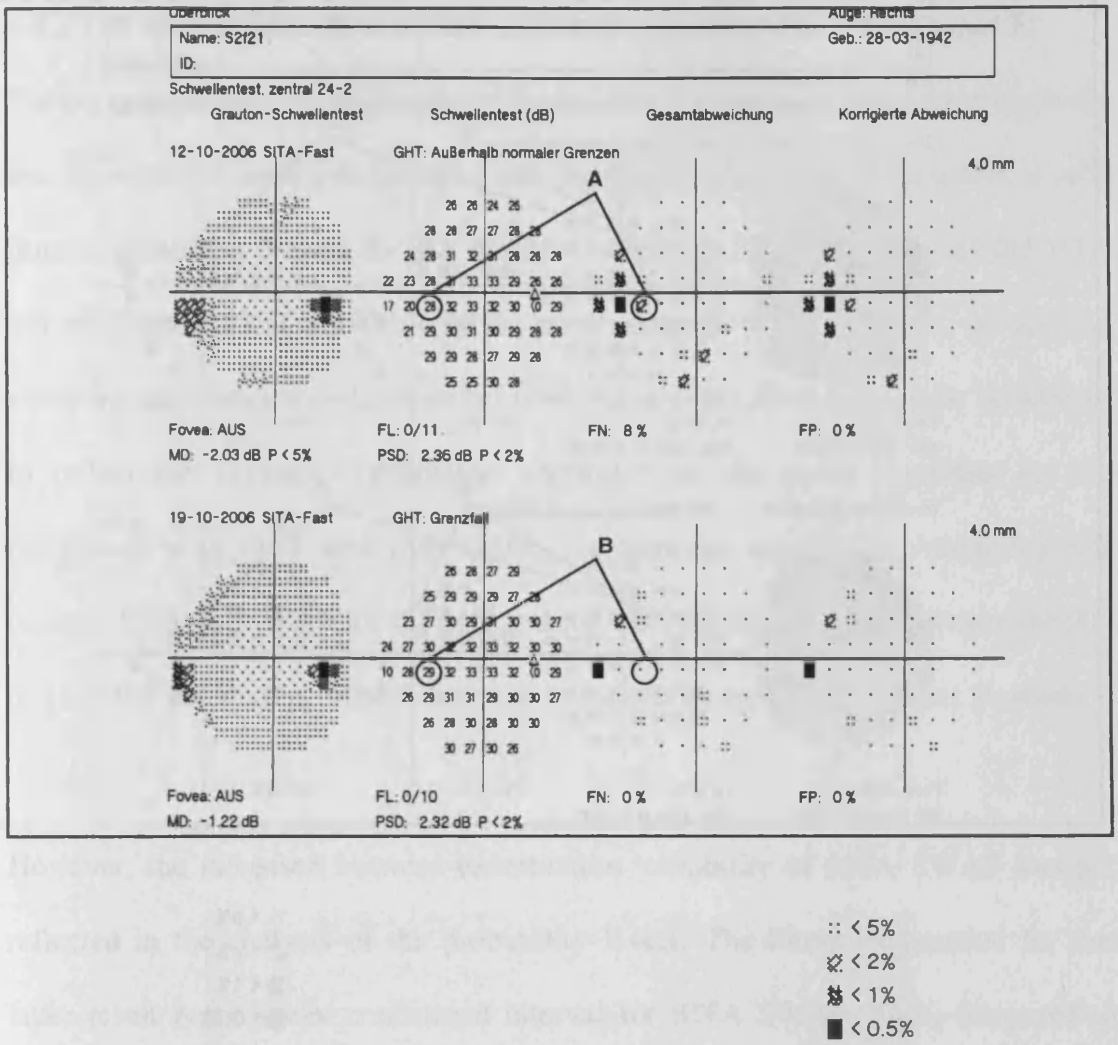

Figure 3.30 The Overview printout showing the greyscale, sensitivity values and the Total and Pattern Deviation plots for two SITA Fast examinations, separated by one week, for a 64 year old female with OAG. The locations circled A and B differ in absolute sensitivity by 1dB and fall within the same level on the greyscale. However, the Total Deviation probability levels assigned to each sensitivity skip the p<5% level.

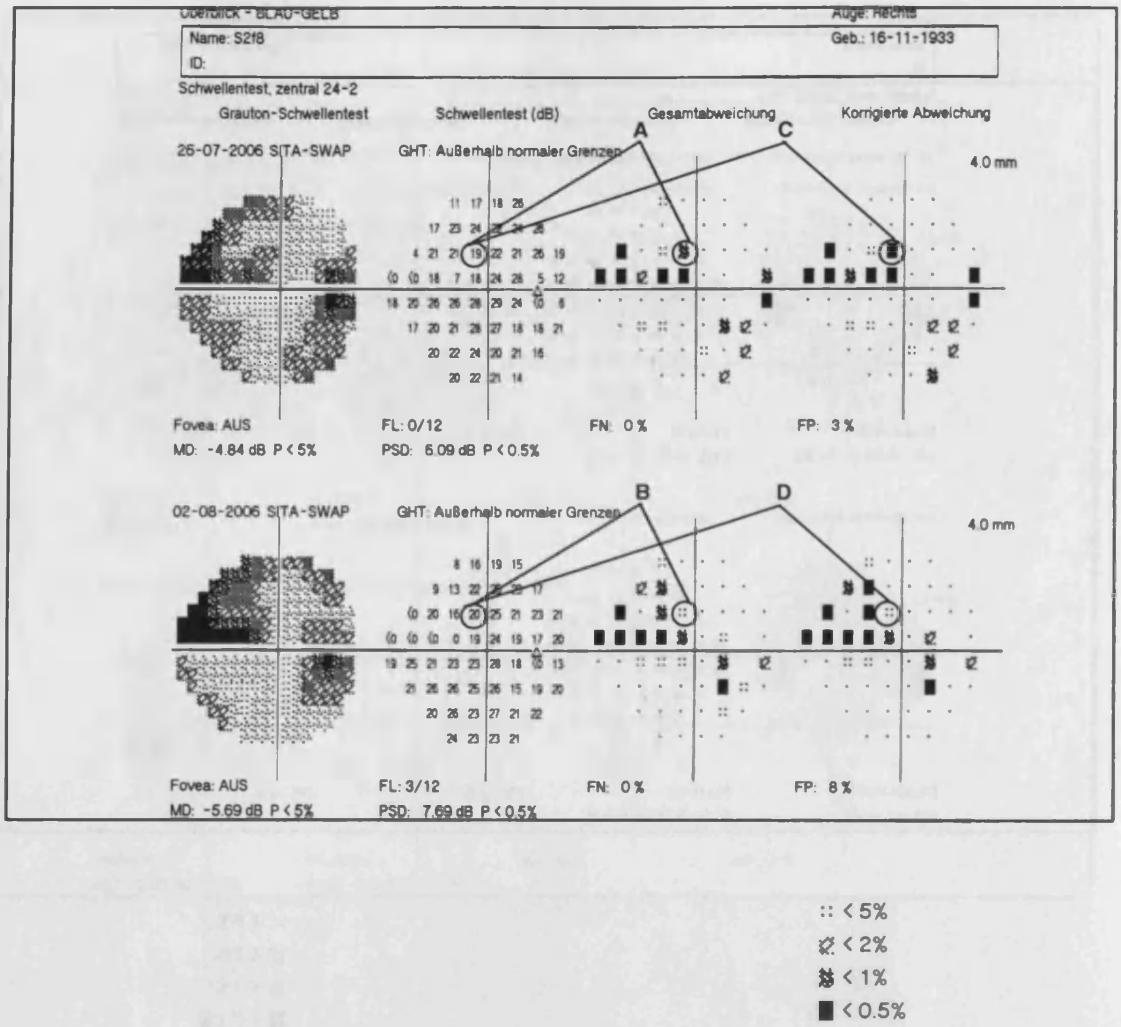

Figure 3.31 The Overview printout showing the greyscale, sensitivity values and the Total and Pattern Deviation plots for two SITA SWAP examination, separated by one week, for a 73 year old female with OAG. The locations circled A, B and C, D differ in absolute sensitivity by 1dB and fall within the same level on the greyscale. However, the Total Deviation probability levels assigned to each sensitivity skip the p<2% level and the Pattern Deviation probability levels skip the p<1% and the p<2% levels.

3.5.2 The within-individual within-algorithm between-visit (Visits 4 and 5) variability

The corresponding analysis between Visits 4 and 5 exhibited a similar but markedly less pronounced trend compared to that between Visits 1 and 5. In effect, a mild improvement was present for the normal individuals for SITA Fast and for SITA SWAP (Figure 3.13a and Table 3.15a) predominantly in the right eye. In essence, therefore, the analyses undertaken between Visits 4 and 5 can, at least be considered to reflect the between-examination variability in the given algorithm for the individuals with OHT and with OAG. The between examination-variability was greatest for SITA SWAP for the MD and for the PSD for the range between the 90^{th} and the 10^{th} percentiles of the difference in sensitivity across all stimulus locations.

However, the increased between-examination variability of SITA SWAP was not reflected in the analysis of the probability levels. The likely explanation for this latter result is the wider confidence interval for SITA SWAP, itself, compared to those for SITA Standard and SITA Fast. The increased between-examination variability of SITA SWAP relative to SAP is a further limitation in the utility of SWAP.

3.5.3 The between-individual within-visit (Visit 5) between-algorithm variability

The between-algorithm difference in the MD at Visit 5 was, as may be expected, narrowest for the two SAP algorithms (Table 3.20); the agreement was better in the second (left) eye examined. The reason for the substantially less agreement between either SAP algorithms and the SITA SWAP is not clear. One reason must lie in the difference in the cohorts used for the determination of the age-corrected normal values from which the MD index is determined. The outcome from each two SAP

algorithms is referenced to the same normative database whilst that for SITA SWAP is referenced to a different database. Given the not unrealistic assumption that the individuals within each database were selected as a result of random sampling, the differences between the MDs for SAP and for SWAP should be minimal. An alternative more likely explanation is that the difference between the MDs is a manifestation of the inherent greater variability of SWAP.

The between-algorithm differences in the PSD at Visit 5 were less than the corresponding differences in the MD. A similar explanation can be proffered for the slightly greater difference in the PSD between the SAP and SITA SWAP algorithms compared to that between the two SITA algorithms. The MD index is included in the calculation of the PSD index; however, the greater difference for SWAP is likely to result again from the greater inherent variability of SWAP.

The underestimation at Visit 5 by the SITA SWAP algorithm of the sensitivity derived by each SAP algorithm was approximately by 5dB at all levels of sensitivity for all groups (Figures 3.16a to 3.16d). The SITA Fast algorithm underestimated the sensitivity derived by SITA Standard algorithm predominantly in the normal group by between approximately 1 and 3dB with the difference increasing as the sensitivity decreased (Figure 3.15a).

In terms of the Total Deviation probability level (Table 3.22), the SITA SWAP algorithm overestimated the extent of apparent abnormality in the height of the visual field relative to the SITA Standard algorithm both in the normal individuals and in the individuals with OHT (by, on average, 1.4 fold and 2.5 fold, respectively)

and relative to the SITA Fast algorithm (by, on average, 2.3 fold and 1.4 fold, respectively). One possible explanation for this finding was that the confidence limits for normality were narrower for SITA SWAP than either of the two SAP algorithms. However, as will be seen in the next paragraph, the Coefficient of Variation (CoV) of the between subject normal variability is substantially larger for SITA SWAP than for either SITA algorithm which indicates that the confidence limits are wider for SITA SWAP. In addition, the between-algorithm difference in the number and severity of the Pattern Deviation probability levels was slightly greater than unity when either SAP algorithm was compared to the SITA SWAP algorithm indicating greater loss for the SAP algorithms. Thus, it is likely that the apparent more frequent and/ or more significant loss by Total Deviation probability analysis for SITA SWAP was due to increased within-examination variability.

The CoV for the individual stimulus locations was substantially greater for SITA SWAP than for either SAP algorithm at Visit 1 and at Visit 5 (Figures 3.17a to 3.17l). Although the magnitudes of the CoV became smaller from Visit 1 to Visit 5 for each algorithm, the CoV for SITA SWAP (Figures 3.18a to 3.18l) remained substantially higher by, on average, approximately twofold (i.e. the values decreased but the between-algorithm ratio remained the approximately the same).

3.5.4 The structure-function relationship

The FSM was the best of the three stereo-metric parameters for the identification of OAG. Such a finding is in agreement with other studies (Bryce et al 2003; Borque et al 2008; Ferreras et al 2008). The SITA SWAP algorithm exhibited the worst specificity and a similar (but poor) sensitivity to the two SAP algorithms when considered in terms of the MD. The specificity and sensitivity of SITA SWAP was

similar for all three groups when evaluated in terms of the PSD and of the clinical evaluation. The poor sensitivity of SWAP resulted in a poor structure-function relationship.

3.6 Conclusion

The pronounced learning effect associated with SITA SWAP compared to that for SAP in individuals experienced in SAP, the greater between-visit variability (between Visits 4 and 5), the greater confidence intervals for normality and the equivalent sensitivity and possibly poorer specificity compared to SAP all mitigate against the clinical use of SITA SWAP both for the detection and the follow-up of glaucomatous visual field loss.

Note

Since this study was undertaken, an e-publication has appeared in abstract form only (Fogagnolo et al 2009) which describes an investigation of the learning effect for the SITA SWAP algorithm. Twenty-seven individuals with OHT and experienced in SAP underwent SITA SWAP with Program 24-2 on each of five occasions each separated by 5 days. The outcome was evaluated in terms of the visual field indices and the GHT. The only improvement in performance over the five visits was that of the foveal sensitivity.

CHAPTER 4

THE PERFORMANCE OF PULSAR PERIMETRY

4.1 Introduction

The concept of Pulsar perimetry was first described at the beginning of the current decade (Gonzalez-Hernandez et al 2000a,b; 2002a,b). Pulsar perimetry evaluates several visual functions, simultaneously, namely, spatial resolution, contrast sensitivity and temporal modulation. The simultaneous examination of these different visual functions had never been undertaken prior to the development of the Pulsar perimeter. The current methods of perimetry only examine one visual function, e.g. spatial resolution using High-pass Resolution Perimetry (HRP) (Frisen 1986; 1987a,b; Frisen and Nikolajeff 1993); contrast perception with a moving sine wave grating (Koenderink and Doorn 1978; Koenderink et al 1978; Regan and Beverley 1983); or temporal functions including Motion perimetry (Leibowitz et al 1972; Koenderink et al 1978; Fitzke et al 1987; Newsome and Pare 1988; Sample and Weinreb 1990; Trick et al 1995; Wall and Ketoff 1995), Flicker perimetry (Tyler 1981; Tytla et al 1990) and Temporal Modulation Perimetry (TMP) (Casson and Johnson 1992; Casson et al 1993a,b; Johnson 1994b). Other studies have investigated foveal function, e. g. the simultaneous testing of CSF and spatial resolution (Arden and Jacobson 1978; Motolko and Phelps 1984; Ross et al 1984). Pulsar perimetry analyzes the combined threshold for high spatial frequencies and high temporal frequencies. In other words, it simultaneously examines the parvocellular and the magnocellular pathways.

4.1.1 The contrast sensitivity function and temporal sensitivity function

The contrast sensitivity function (CSF) for the fovea was first described for the normal eye using sine wave gratings by (Campell and Green 1965) and was later described in OAG (Arden and Jacobson 1978). The changes of the CSF in relation to retinal eccentricity are characterized by a displacement of the curve toward the lower spatial frequencies due to the reduction of resolution in the peripheral retina (Rovamo et al 1978). Examination of the CSF within the central field offers a reasonable approach to the early detection of OAG (Korth et al 1989; Falcao-Reis et al 1990).

The contrast sensitivity is the reciprocal of the contrast threshold. The threshold is derived for different spatial frequencies resulting in a graph that demonstrates contrast sensitivity as a function of the spatial frequency. The typical human CSF reaches its peak sensitivity at about 4 cycles/ degree and decreases in sensitivity on either side (Campell and Robson 1968) i.e. at a frequency of 4 cycles/ degree, a human eye can detect a grating at a lower contrast than at any other frequency.

The temporal sensitivity function (TSF) for a moving sinusoidal grating is highest at approximately 8Hz (where one Hz corresponds to one cycle/ sec) and decreases either side of this value at lower and higher temporal frequencies, respectively (Robson 1966), i.e. stimuli of moderate temporal frequencies can be detected with a smaller modulation depth than stimuli at a lower or a higher temporal frequency.

The critical flicker fusion (CFF) is the highest temporal frequency that can be resolved at a given modulation depth.

4.1.2 Principles of Pulsar perimetry

The current prototype of the Pulsar perimeter consists of an examination screen, namely a 19'computer monitor (Samsung Electronics Co, 416 Maetan-3 Dong, Paldal-Gu, Suwon City, Kyungki-Do, Korea) which is automatically photometrically calibrated by means of photometer (Tektronix J17 Luma Colour) which plugs directly into a USB port. The resolution of the screen is 1024x768 pixels, the frame rate is 60Hz and the colour temperature is 6500°K. The chinrest is situated at 31cm from the screen.

The brightness of the monitor screen is 100asb and the stimulus oscillates above and below the background, i.e. is iso-luminant to the background. The stimulus for the clinical version (T30W) of the Pulsar perimeter consists of a 5 degrees diameter circular waveform, flickering at 30Hz, with decreasing contrast towards the edge, presented for 500msec.

The contrast of the Pulsar stimulus (V) at each point depends upon the global contrast (C), the spatial resolution (SR), the distance from the centre (D) and the radius of the stimulus (R) and is described as:

$$V = C \,.\, cos[(2\pi \,.\, SR \,.\, D)-\pi] \,.\, [1-(D/R)]$$

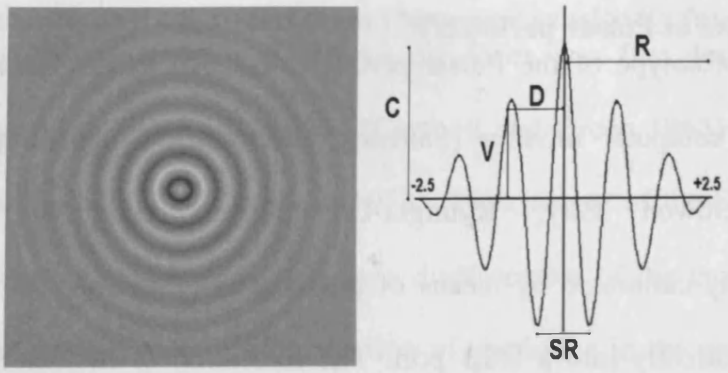

Figure 4.1 The stimulus used in the clinical version of the Pulsar perimeter.

The SR varies over twelve logarithmic levels (between 0.5 cycles/ degree and 6.3 cycles/ degree) and is illustrated in Table 4.1.

Cycl./deg.	0.5	0.6	0.8	1.0	1.3	1.6	2.0	2.5	3.2	4.0	5.0	6.3
dB	0	1	2	3	4	5	6	7	8	9	10	11

Table 4.1 The spatial resolution over the twelve logarithmic levels in cycles/ degree.

The spatial resolution level (dLog) is defined as:

$$dLog = 10Log\ (SR/\ 0.5)$$

The contrast varies over 32 logarithmic levels (between 6% and 100%, 0-31dB).

The contrast level, C, is defined as:

Contrast = -20Log ([central amplitude from background]/[background intensity])

Pulsar perimetry (T30W) simultaneously determines the minimum SR and contrast in 35 steps [spatial-resolution-contrast units (src)]. The legibility of the stimulus is varied by altering both the SR and the contrast. The measurement scale commences at 0src (which is equivalent to 0.5 cycles/ degree of SR and 100% of contrast) and ends at 35src (which is equivalent to 6.3 cycles/ degree of SR and 6% of contrast). The inter-stimulus duration is adapted to the response rate of the patient. Random changes occur in the inter-stimulus duration to avoid rhythmic responses. The stimulus is presented using the TOP algorithm.

The perimeter examines 66 locations in the central visual field, based upon a 6 degrees square grid analogous to HFA Program 30-2, and extending horizontally to 30 degrees in the nasal and temporal regions and vertically to 24 degrees in the superior and inferior regions. The fixation is monitored by the Heijl-Krakau technique and false-positive and false-negative catch trials are also included. The examination duration is approximately 3.5 minutes. The printout contains the results displayed in the standard manner for perimetry i.e. numeric values, grey scale, defect curve, difference values and visual field indices.

4.1.3 Previous studies of Pulsar perimetry

The initial clinical study of Pulsar perimetry (Fernandez-Vidal et al 2002) was undertaken in patients with OHT and showed that Pulsar perimetry, with Program T30W, was seemingly more sensitive for the detection of early field loss compared to SAP. In this latter study, 34 eyes from individuals with OHT and normal visual fields by SAP and 41 eyes from normal patients were included in the study. The group mean MS in the normal individuals was 21.25src (SD=2.70) compared to 18.65src (SD=2.79) in the individuals with OHT. The MD was 0.93src (SD=1.80)

and the LV 6.11src (SD=4.30) for the normal individuals compared to 2.73src (SD=2.30) and 8.46src (SD=5.01), respectively, for the individuals with OHT. These results were statistically significant ($p<0.05$) for both the MD and the LV. Since MD for individuals with OHT was significantly higher than that for normal individuals, it was concluded that Pulsar perimetry may have a greater diagnostic sensitivity than SAP. Furthermore, the smaller differences for LV between the two groups was explained on the basis that initial glaucomatous damage is more diffuse than localized, and therefore is manifest as a greater MD than a LV.

The diagnostic capability of Pulsar perimetry, using Program T30W, was compared to that of Program N30 of the FDT (Carl Zeiss Meditec, Dublin, CA), SAP TOP and to the structural outcome derived by the HRT-II (Heidelberg Engineering GmbH, Dossenheim, Germany) in glaucoma suspects (Gonzalez de la Rosa et al 2007). Forty seven eyes of 47 glaucoma suspects were examined twice with each technique. The results were compared with those of 70 eyes of 70 normal subjects. The group mean MD for SAP in the glaucoma suspect group (0.96dB) was not significantly different from that of the normal individuals (0.8dB), whereas the rim area in the glaucoma suspects ($2.12mm^2$) was significantly higher than in the normal individuals ($1.97mm^2$) ($p<0.01$). For 95.7% specificity, the sensitivity of the FDT MD was 11.7% and for Pulsar perimetry 14.9%, respectively. The FDT PSD exhibited a sensitivity of 9.6% and the Pulsar sLV 30.9%. The reproducibility of the Pulsar MD was 8.5%, and the sLV 17% compared to 6.4%. and 4.3%, respectively, for the FDT.

A comparison of four types of perimetry, SAP (TOP G1), Pulsar perimetry, FDT, TOP flicker perimetry and an assessment of the retinal nerve fibre layer with the GDx was undertaken by in a cohort of individuals with OHT divided into five groups (Méndez et al 2004). The composition of the groups was: Group 1: Octopus TOP G1 (63 eyes of individuals with OHT and 63 eyes of normal individuals); Group 2: Pulsar perimetry (56 eyes of individuals with OHT and 47 eyes of normal individuals); Group 3: FDT threshold perimetry (49 eyes of individuals with OHT and 44 eyes of normal individuals), Group 4: CFF perimetry (53 eyes of individuals with OHT and 59 eyes of normal individuals); Group 5: GDx (58 eyes of individuals with OHT and 46 eyes of normal individuals). The area under the ROC curve for Octopus TOP G1 MD and LV was 0.43 ($p=0.112$) and 0.45 ($p=0.357$); for the Pulsar MD and LV 0.604 ($p<0.05$) and 0.60 ($p=0.097$); for the FDT MD and PSD 0.57 ($p=0.223$), and 0.54 ($p=0.533$) and for the CFF perimetry MD and LV was 0.52 ($p=0.822$) and 0.52 ($p=0.802$). However, at 95% specificity, the sensitivity for the Octopus TOP G1 MD and LV was 3% and 2%, respectively, for the Pulsar MD and LV 18% and 16%, respectively, for the FDT MD and PSD 3% and 14%, respectively, and for the CFF perimetry MD and LV 4% and 4%, respectively.

Thus, there are few studies which have clinically evaluated the Pulsar perimeter and those that have been undertaken are of questionable methodology. Clearly, there is a pressing need to undertake an evaluation of the Pulsar perimeter using a robust experimental design.

4.2 Purpose

The aim of this study, therefore, was to determine the characteristics of Pulsar perimetry in the clinical environment with particular reference to SAP undertaken

with the SITA Standard algorithm. Five specific characteristics were to be investigated, namely, the presence, magnitude and temporal characteristics of any learning effect; the magnitude of the within-algorithm, within individual, between-visit variability; the magnitude of the within-visit between-individual variability between-algorithms; and the structure-function relationship.

4.3 Methods

4.3.1 Case series

The case series comprised 78 consecutively presenting individuals who met the inclusion criteria for enrolment in the study and who, during the recruitment phase, had volunteered to take part in the study. All individuals were provided with verbal and written information concerning the nature of the study, and gave written consent, in accordance with the requirements and approval of the Ethikkommission des Kantons Graubünden, which is, in turn, in accordance with the tenets of the declaration of Helsinki.

The case series consisted of three groups of individuals. One group comprised 25 normal individuals (17 females and 8 males) who were recruited from the optometric practice of the author in Landquart, Switzerland. The mean age was 46.6 years (SD=5.6) and the age range was 41 to 60 years. The second group comprised 26 individuals with OHT (13 females and 13 males) with a mean age of 60.5 years (SD=8.4) and a range of 45 to 72 years. The third group was made up of 27 individuals with OAG (17 females and 10 males) with a mean age of 61.6 years (SD=9.5) and a range of 45 to 77 years. Twenty-two of the 26 individuals with OHT and 22 of the 27 individuals with OAG were drawn from the ophthalmological practice of PD Dr. med. Zulauf, Chur, Switzerland. The remaining 9 individuals

were drawn from the practices of six ophthalmologists within Landquart, Switzerland. The individuals were matched as closely as possible in age.

The number of individuals included within each diagnostic category was based upon the power calculation described in Chapter 3. Twenty-six patients provided 90% power of detecting a 1.0dB difference between visits and/ or between algorithms.

Seventeen of the 26 individuals with OHT and 19 of the 27 individuals with OAG had taken part in the previous study concerning the clinical characteristics of SITA SWAP. The minimum interval between completion of participation in the SITA SWAP study and entry into the study described here was 3 months. None of the normal individuals had undergone any form of perimetry prior to entry into the study described here. The age profile across the three groups is given in Table 4.2.

Age (years)	Number of Normal Individuals	OHT	OAG
40-49	18	3	5
50-59	6	8	5
60-69	1	11	11
70-79	0	4	6

Table 4.2 The number of individuals and distribution of age within each of the three groups.

All the individuals who did not participate in the study of SITA SWAP underwent standard optometric and ophthalmological examinations at baseline comprising the

same procedures as described in Chapter 3. The individuals who participated at the SITA SWAP study and who were willing to participate in this study were included without any further optometric or ophthalmological examination. Most of the normal individuals (22 of the 25) and all of the new individuals with OHT or OAG underwent laser scanning ophthalmoscopy of the ONH with the HRT II (Heidelberg Engineering GmbH, Dossenheim, Germany).

The baseline examination was identical to that undertaken for the SITA SWAP study. The IOP for the normal individuals was measured with the Pascal Dynamic Contour Tonometer (Zeimer Ophthalmic Systems AG, Port, Switzerland). The IOP for the individuals with OHT and for the individuals with OAG was measured with the Goldmann applanation tonometer and all underwent/ had undergone pachometry with the Quantel Pocket I ultrasonic pachometer (Quantel Medical SA, Clermont-Ferrand, France). Each individual was required to exhibit in each eye a visual acuity of 7/10 or better (equivalent to 6/9 or better); a distance refractive error of ≤+/-7.0 dioptres mean sphere and ≤+/-3.0 dioptres cylinder; a normal anterior segment, and lenticular changes no greater than NC2.0, NO2.0, C1.0, or P1.0 according to the LOCS III (Chylack et al 1993). In addition, no individual was receiving systemic medication, or manifested any systemic disease, known to affect the visual field nor had a negative family history of any ocular disease or any systemic diseases with potential ocular involvement.

Normal individuals were categorized on the basis of normal findings from the clinical examination and exhibited an upper limit of ≤20mmHg.

Individuals with OHT were categorized on the basis of a corneal thickness corrected IOP of ≥22mmHg in both eyes on at least two occasions separated by at least one month, or a pre-treatment IOP ≥22 mmHg under similar circumstances, in the presence of normal discs and a normal visual field. The criteria for a normal field were those described in the study of SITA SWAP (Morgan et al 2005), namely: a field exhibiting complete normality by Pattern Deviation probability analysis; a field containing one non-edge location exhibiting apparent abnormality at the $p<2.0\%$ level or worse; or as a field containing up to 3 non-clustered locations in any one horizontal hemifield at the $p<5\%$ level. Locations exhibiting apparent abnormality arising from the presence of obvious artefacts such as lens rim, upper lid contamination, or seed-point (i.e. those at 9°, 9° eccentricity) errors, and those locations immediately adjacent to the blind spot were not considered in the evaluation of the given field.

Two of the 26 individuals were receiving a single topical agent in each eye for IOP control (one a prostaglandin analogue and one a β-receptor blocker/ carbonic anhydrase inhibitor combination). Three of the individuals were receiving a systemic selective β1-adrenergic receptor blocker and 21 had no medical therapy, which can influence IOP. All five patients who had medication, has been treated for at least two months prior to entry into the study with the given regimen and remained on the same regimen throughout the five week period.

As in the study of SITA SWAP, the level of risk of the OHT in the worst eye was classified, post hoc, using the STAR II system (Gordon et al 2007) which determines the level of risk on the basis of the following: the magnitude of the

corneal-thickness-corrected IOP; the more asymmetric disc; a thin corneal thickness; and the mean of the PSD index obtained at the two most recent visual field examinations. The latter was derived from the SITA Standard strategy at Visits 4 and 5 (see Section 4.4.1.1.3, below).

The group comprised 3 individuals at low risk (mean 3.5%, SD=0.7), 16 individuals designated at medium risk (mean 8.8%, SD=3.3) and 7 at high risk (mean 27.6%, SD=9.3). Twenty-one of the 26 individuals with OHT had previous experience of SAP and SWAP. The mean number of visual field examination sessions (i.e. visits) for these 21 individuals was 7.43 (SD=3.37) and the range was to 2 to 14 visits.

The individuals with OAG were categorized on the basis of an optic nerve head characteristic of the disease including generalized or focal thinning of the neuro-retinal rim, disc asymmetry, changes in the lamina cribrosa, pallor, vessel changes or disc margin haemorrhage. The Heidelberg Retina Tomograph reflectance image for the optic nerve heads of each of the 27 individuals with OAG and the values of the parameters for Disc Area, Cup Shape Measure, Height Variation Contour, Linear Cup:Disc ratio and the Mikelberg and Burk Discriminant functions are given in Figure 4.2.

Patient ID	Right eye	DA (mm^2); CSM; HVC (mm); Linear cup/disc ratio; FSM; RB	Left eye	DA (mm^2); CSM; HVC (mm); Linear cup/disc ratio; FSM; RB
1	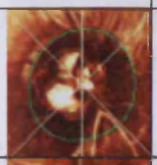	1.83; -0.14; 0.54; 0.59; -0.46; 1.70	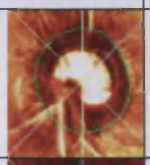	1.51; -0.24; 0.47; 0.61; 0.02; 1.67
2		1.93; -0.13; 0.54; 0.48; 1.51; 1.69		1.80; -0.11; 0.55; 0.57; -1.09; 0.44
4		2.29; 0.07; 0.27; 0.83; -3.21; -0.80		2.32; 0.03; 0.35; 0.83; -3.33; -0.67
5		1.91; 0.04; 0.43; 0.91; -5.32; -2.95		2.06; -0.05; 0.28; 0.81; -2.23; -1.69
6		1.87; -0.22; 0.39; 0.55; 2.47; 1.49		1.71; -0.22; 0.45; 0.54; 1.01; 2.04
7		1.64; -0.21; 0.35; 0.61; -0.80; 0.68	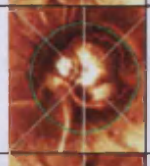	1.85; -0.17; 0.39; 0.64; -0.61; 0.46
8	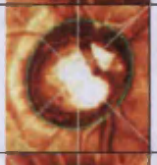	1.93; -0.02; 0.33; 0.79; -2.70; 0.22		1.84; -0.03; 0.40; 0.80; -3.19; 0.26
10	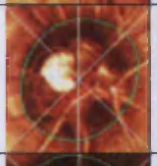	2.43; -0.22; 0.38; 0.53; 2.39; 1.62		2.05; -0.19; 0.35; 0.59; 1.22;1.49
11		3.29; -0.08; 0.30; 0.70; -0.17; -0.54		3.45; -0.03; 0.36; 0.73; -2.12; -0.28
12	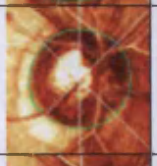	1.92; -0.14; 0.34; 0.61; -0.18; -0.23	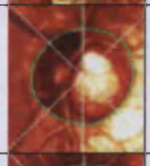	1.91; -0.19; 0.45; 0.59; 0.34; 0.89
13		2.27; -0.09; 0.35; 0.68; -1.31; 1.54	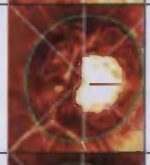	2.85; -0.10; 0.33; 0.66; -0.41; 0.44
14	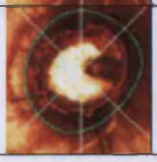	2.41; -0.05; 0.27; 0.75; -2.06; 0.24		2.62; -0.09; 0.33; 0.76; -1.20; 0.76

15		2.35; 0.0; 0.21; 0.81; -2.55; -1.01	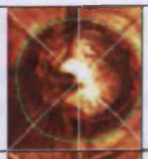	2.71; 0.01; 0.28; 0.75; -2.03; -1.18
16		2.07; -0.14; 0.40; 0.55; 0.66; 1.75		2.12; -0.11; 0.36; 0.65; 0.02; 0.81
18	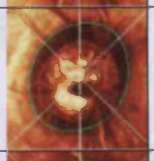	1.80; -0.04; 0.29; 0.70; -1.86; -0.17		2.22; -0.03; 0.17; 0.84; -2.11; -0.97
19	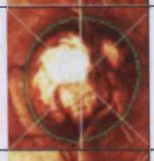	2.84; -0.02; 0.53; 0.63; -0.67; 1.24	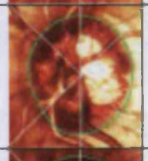	2.55; -0.07; 0.45; 0.56; -0.22; 0.34
20		2.18; -0.02; 0.27; 0.74; -2.23; -0.34		2.76; 0.06; 0.24; 0.80; -3.30; -0.71
21	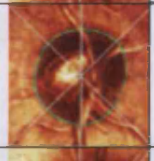	1.61; -0.32; 0.33; 0.48; 2.74; 1.21	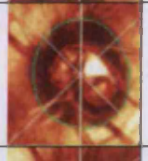	1.92; -0.16; 0.35; 0.56; 0.49; 1.13
22		1.62; -0.15; 1.05; 0.63; -2.27; 3.99		1.33; -0.23; 0.61; 0.32; 1.27; 2.74
26		1.28; -0.19; 0.33; 0.42; 0.60; 1.66		1.29; -0.18; 0.27; 0.32; 0.75; 0.82
27		2.34; -0.10; 0.36; 0.69; -1.15; 0.15		2.26; -0.17; 0.44; 0.57; 2.01; 1.78
28	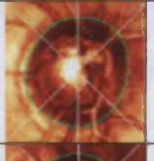	1.96; -0.14; 0.27; 0.61; -0.29; 0.30		1.84; -0.11; 0.25; 0.63; -1.02; -0.02
29		2.01; -0.15; 0.21; 0.74; -0.52; 0.30		2.04; -0.05; 0.33; 0.83; -3.19; 0.02
30		2.06; -0.13; 0.30; 0.61; -0.21; -0.28		1.98; -0.26; 0.32; 0.51; 1.72; 0.89
31	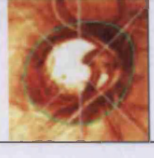	2.06; -0.13; 0.19; 0.66; -0.59; -0.74		2.41; -0.08; 0.46; 0.56; 0.15; 1.16

32	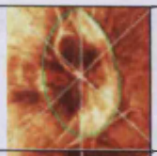	1.78; -0.32; 0.78; 0.15; 6.75; 3.29	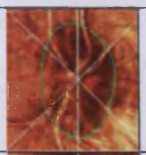	1.67; -0.37; 0.59; 6.63; 3.26
33	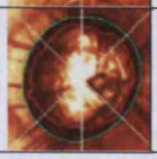	2.70; 0.01; 0.28; 0.85; -3.27; -0.28	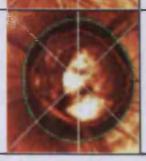	2.57; 0.01; 0.20; 0.79; -2.66; -0.84

Figure 4.2 The Heidelberg Retina Tomograph reflectance images for the ONHs of the 27 individuals with open angle glaucoma. (DA: Disc Area; CSM: Cup Shape Measure; HVC: Height Variation Contour FSM: Mikelberg Discriminant function; RB: Burk Discriminant function). Individuals with case numbers 1 to 25 had taken part in the investigation of SWAP described in Chapter 3.

Seventeen individuals were receiving a single topical agent in each eye for control of IOP (two were receiving a nonselective β-receptor blocker, two an α-adrenergic agonist, eight a prostaglandin analogue, one a prostaglandin analogue/ β-receptor blocker combination and four a β-receptor blocker/ carbonic anhydrase inhibitor combination). One individual required two topical agents for IOP control (a combination of a β-adrenergic receptor blocker/ α-adrenergic receptor agonist and carbonic anhydrase inhibitor). One individual had previously undergone bilateral trabeculectomy and was receiving a systemic β-blocker. Eight individuals had no glaucoma medication (four individuals switched from another diagnostic group, one individual was a new detected glaucoma and three individual suffered from low tension glaucoma).

In those cases where the appearance of the ONH was in doubt, the diagnosis of OAG or OHT was also based, post hoc, upon the appearance of the visual field derived during the study. Glaucomatous visual field loss was defined as for the SITA SWAP study according to the following guidelines: a minimum of one location in the paracentral or nasal step regions corresponding to Sectors 1 or 2, or to

the inferior three locations in Sector 3 of the Glaucoma Hemifield Test exhibiting repeatable abnormality at the $p<0.5\%$ level by Pattern Deviation probability analysis; or as two or more locations situated in a cluster exhibiting repeatable abnormality at the $p<2.0\%$ level, or lower, by Pattern Deviation probability analysis excluding any location in the cluster that was situated in the opposite horizontal hemifield (Morgan et al 2005).

The severity of the visual field loss in the individuals with OAG was graded, post hoc, on the appearance of the eye, with the more severe loss found with the SITA Standard algorithm at the last visit. The staging system was that of Hodapp and colleagues (1993) and modified by Litwak (2001) in terms of the number and severity of the Pattern Deviation probability levels and of the defect depth at the four central locations adjacent to fixation. The use of the MD index was omitted from the classification system in order to emphasize the spatial component in the grading of the field loss. A total of 19 of the 27 individuals exhibited mild loss, two moderate losses and two severe losses, whereas four individuals showed a normal visual field.

Three of the 26 individuals with OHT and six of the 27 individuals with OAG were receiving artificial tears because of minor dry eye problems. None of the 25 normal individuals were receiving artificial tears.

4.3.2 Examination protocol

In addition to the baseline visit, all individuals took part in five further visits. Each of these five visits was separated by one week. Each eye was separately examined with Program 24-2 of the HFA 745i (Carl Zeiss Meditech Inc., Dublin, CA) using the SITA Standard algorithm and with the Pulsar Program CP-T30W using the TOP algorithm. The order of the algorithms within the visit was randomized within individuals and varied over each of the five visits. The visual field of the right eye was always examined before that of the left eye.

Each individual wore their refractive correction together the correction for the viewing distance of the perimeter bowl and for the Pulsar perimetry screen, respectively, in the form of full-aperture trial lenses, if necessary. The time needed to adapt to the SITA Standard algorithm and to the TOP algorithm was each approximately one minute. The non-examined eye was occluded with an opaque patch.

With the HFA, in addition to the standard Heijl-Krakau technique and to the gaze tracker, fixation was monitored continuously via the video monitor. With the Pulsar perimeter, fixation was monitored with the standard Heijl-Krakau technique. The influence of the fatigue effect was reduced by providing a rest period of approximately one minute midway through the examination of each eye and a rest period of approximately five minutes between eyes. During such rest periods the individual remained adapted to the perimeter bowl and to the Pulsar perimetry screen, respectively. Each patient was given the same instructions throughout each examination at each visit to reduce bias. Two perimetrists performed the perimetry, CAC, and the practice nurse BT. The number of individuals in each group assigned

to each perimetrist and to a combination of the two perimetrists is given in Table 4.3.

	Normal	OHT	OAG
CAC and BT	15	9	12
BT, only	6	14	13
CAC, only	4	3	2

Table 4.3 The number of individuals in each group assigned to each perimetrist and to a combination of the two perimetrists.

4.3.3 Analysis

The stimulus locations above and below the physiological blind spot were discarded from the analysis.

4.3.3.1 The learning effect

4.3.3.1.1 Visual field indices

The analysis of the learning effect was undertaken in terms of the magnitudes of the conventional visual field indices MS, MD and PSD for the HFA and the corresponding indices for the Pulsar perimeter MS, MD and sLV within- and between-eyes and between groups, over the five visits. The polarity of the Pulsar MD index was reversed (i.e. all positive values were converted to negative values and vice versa).

A separate ANOVA was undertaken for each type of index. Age, diagnostic group, number of previous examinations with both SAP and SWAP, and the given perimetrist were considered as between-subject factors. Visit, eye and algorithm were considered as within-subject factors. The examination duration was also

analyzed in a similar manner. Post hoc multiple comparisons of means were undertaken to determine the visit at which no further improvement in sensitivity was present, i.e. the learning effect was no longer operative. It was recognized that the MD indices and the PSD and sLV indices, respectively, from the two perimeters were based upon different formulae, upon a different number of stimulus locations and upon different age-corrected normative databases. Nevertheless, it was felt that an analysis based on the above, represented evaluation of the Pulsar perimeter as it would be used in the clinical setting.

4.3.3.1.2 Peripheral mean sensitivity and central mean sensitivity

The analysis of the learning effect was also undertaken in terms of the magnitudes of the proportionate change in peripheral (PMS) and in the central mean sensitivities (CMS) over the five visits for each of the two perimeters using a further repeated measures ANOVA. The outer 14 stimulus locations of the Pulsar's CP-T30W stimulus grid were omitted to achieve compatibility with the Program 24-2 grid of the HFA. The 22 stimulus locations within the central annulus out to 15 degrees eccentricity, horizontally, and 15 degrees vertically were then designated as those locations from which the CMS was calculated (Table 4.8). The remaining 30 locations in the peripheral annulus beyond these eccentricities were designated as those locations from which the PMS was calculated.

4.3.3.1.3 The within-individual within-algorithm between-visit (Visits 1 and 5) difference in sensitivity

Three separate analyses were used to determine the within-individual within-algorithm between-examination variability at Visits 1 and 5. The first analysis calculated the difference in each of the visual field indices, MS; MD and PSD and sLV; between Visits 1 and 5 for each of the three groups and for all three groups,

combined, in terms of the average of the two given respective indices. As mentioned in Section 3.3.3.2, such an approach overcomes the limitations associated with the use of correlation analysis (Bland and Altman, 1986).

The second analysis expressed the within-individual, within-algorithm between-visit difference in sensitivity across each stimulus location in terms of the distribution of the difference in sensitivity at each location between Visits 1 and 5 as a function of the sensitivity at the corresponding stimulus location recorded at Visit 1.

The third analysis expressed the within-individual within-algorithm between-visit difference in sensitivity across each stimulus location in terms of the distribution of the difference in the magnitudes of the Total Deviation probability levels, respectively, between Visits 1 and 5 and illustrated in terms of a contingency table.

4.3.3.2 The within-individual within-algorithm between-visit (Visits 4 and 5) variability

The same three separate analyses were used to determine the within-individual within-algorithm between-examination variability at Visits 4 and 5 as was undertaken between Visits 1 and 5.

4.3.3.3 The within-visit (Visit 5), between-individual variability between algorithms

The within-visit between-individual variability between algorithms at Visit 5 was analysed in four separate ways. The first analysis illustrated the between-algorithm differences in the MD, in the PSD and sLV indices between each algorithm at Visit 5 across the three groups in terms of the average of the two indices.

The second analysis determined the difference in sensitivity between each pair of algorithms at Visit 5 for each stimulus location across all patients in the three groups and expressed, graphically, as the respective difference as a function of the sensitivity at the corresponding stimulus location recorded with the comparison algorithm of the given pair. The third analysis compared the magnitude of the Total Deviation (TD) probability values at each stimulus location across all patients in the three groups between each pair of algorithms at Visit 5. The fourth sub-analysis compared the between-individual variability at each stimulus location in the normal individuals for each algorithm in terms of the CoV.

4.3.3.4 The structure-function relationship

The relationships between the magnitudes of the Mikelberg discriminate function (FSM), the Burk discriminate function (RB) and the rim-disc ratio, derived by confocal scanning laser ophthalmoscopy (HRT II), were compared with the statistical significance of the visual field indices MD and PSD/ sLV at Visit 5 for the right and the left eyes across each diagnostic group and were illustrated in terms of contingency tables and Venn diagrams.

4.4 Results

A total of 1560 visual field examinations were undertaken with the SITA Standard algorithm and with the Pulsar perimeter; no individual exhibited incorrect responses greater than 33% to either the false-positive or the false-negative catch trials. Forty-two examinations with the SITA Standard algorithm exhibited more than 20% fixation losses with the Heijl-Krakau technique and, of these, 31 exhibited more than 30% fixation losses. No examinations recorded with the Pulsar perimeter exhibited fixation losses greater than 20%. No one individual was associated with a large

number of incorrect responses to either the false-negative or false-positive catch trials or with fixation losses.

4.4.1 The learning effect

4.4.1.1 Visual field indices

4.4.1.1.1 Mean Sensitivity

The group mean MS (SD) as a function of the algorithm for each eye of the individuals in each of the three groups is given in Table 4.4.

Algorithm	Visit 1		Visit 2		Visit 3		Visit 4		Visit 5	
	RE	LE	RE	LE	RE	LE	RE	LE	RE	LE
SITA Standard	31.40 (1.36)	31.32 (1.61)	31.41 (1.03)	31.43 (1.08)	31.82 (1.01)	31.48 (0.87)	31.75 (1.08)	31.57 (1.20)	31.97 (1.14)	31.61 (1.09)
Pulsar	21.44 (1.94)	21.76 (1.53)	21.26 (2.10)	21.83 (1.34)	21.51 (1.85)	21.82 (1.55)	21.60 (1.37)	21.88 (1.28)	21.44 (1.98)	21.90 (1.33)
SITA Standard	30.83 (1.23)	30.58 (1.90)	31.11 (1.31)	30.78 (1.47)	31.13 (1.31)	30.77 (1.51)	31.00 (1.55)	30.64 (1.67)	30.94 (1.69)	30.60 (1.64)
Pulsar	19.84 (1.77)	20.04 (1.67)	19.41 (4.27)	19.46 (3.56)	20.12 (1.50)	20.00 (1.52)	20.07 (1.58)	20.11 (1.61)	20.16 (1.48)	20.04 (1.37)
SITA Standard	29.65 (4.25)	29.61 (2.37)	29.80 (4.16)	29.83 (2.45)	29.79 (4.33)	29.83 (2.41)	29.75 (4.27)	29.83 (2.34)	29.92 (4.07)	29.81 (2.44)
Pulsar	18.45 (3.46)	18.18 (3.60)	18.29 (3.64)	18.30 (3.41)	18.18 (3.80)	18.38 (3.35)	18.25 (3.65)	18.32 (3.79)	17.92 (4.11)	18.28 (3.53)

Table 4.4 The group mean MS (SD) at each of the five visits for each eye as a function of the algorithm for the normal individuals (no shading), the individuals with OHT (light shading), and the individuals with OAG (dark shading).

The group mean MS for each eye at each visit for each of the two algorithms is also shown graphically in Figure 4.3a to Figure 4.3c for each of the three groups.

The MS was independent of the of the order of both algorithms within the examination ($p=0.118$). It was similar between the two eyes ($p=0.931$). The MS varied across the three diagnostic groups ($p<0.001$) and, as would be expected, was highest for the normal individuals and least for the group with OAG. The magnitude

of the MS was greater for the SITA Standard algorithm ($p<0.001$) but the difference between the two types of perimetry varied across the three groups being greatest for the group with OAG ($p<0.001$).

On average, the MS for the SITA Standard algorithm improved between Visits 1 and 5 by 0.43dB for the normal individuals, by 0.13dB for those with OHT and by 0.24dB for those with OAG. The corresponding improvement across the three groups for Pulsar perimetry was 0.07dB, 0.16dB and 0.22dB. The improvement in MS, overall, did not reach statistical significance ($p=0.339$). Neither the difference in the improvement between the two algorithms nor the difference in the improvement between the three groups reached statistical significance ($p=0.504$ and $p=0.914$, respectively).

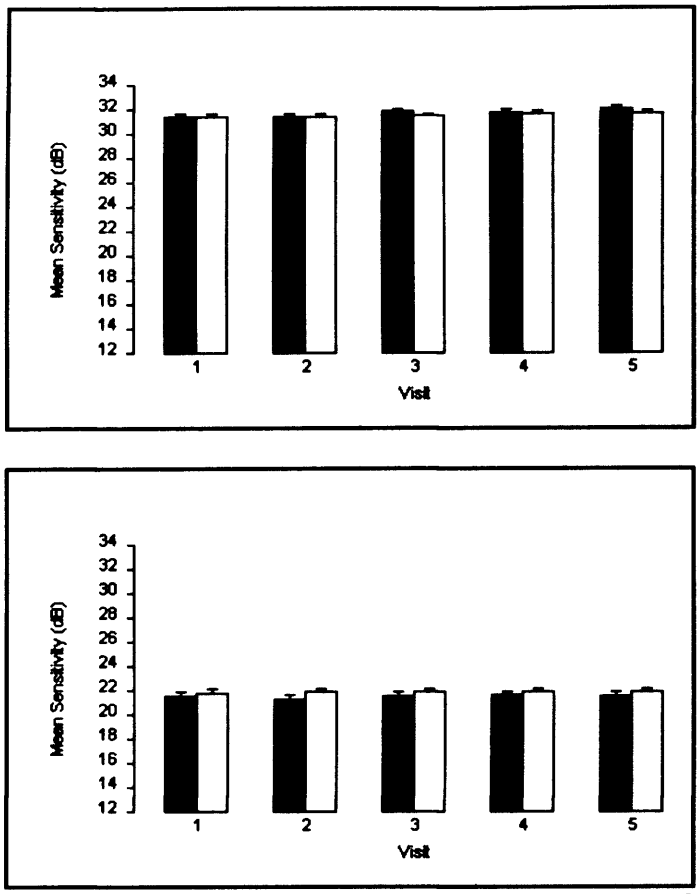

Figure 4.3a The group mean MS (SE) at each of the five visits for each eye as a function of the algorithm for the normal individuals: right eye, dark bars; left eye, open bars. Top: SITA Standard. Bottom: Pulsar perimetry.

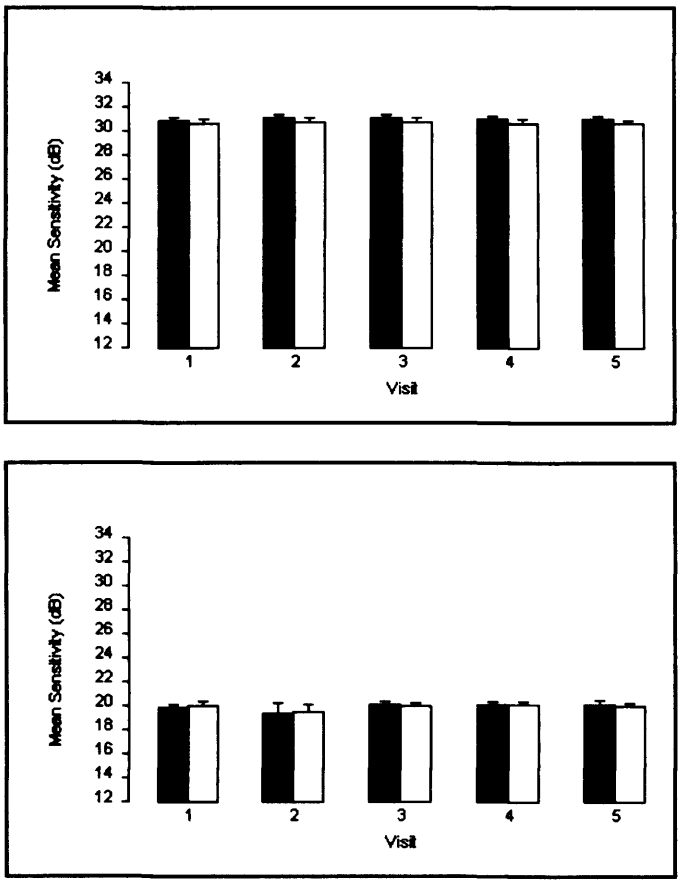

Figure 4.3b The group mean MS (SE) at each of the five visits for each eye as a function of the algorithm for the individuals with OHT: right eye, dark bars; left eye, open bars. Top: SITA Standard. Bottom: Pulsar perimetry.

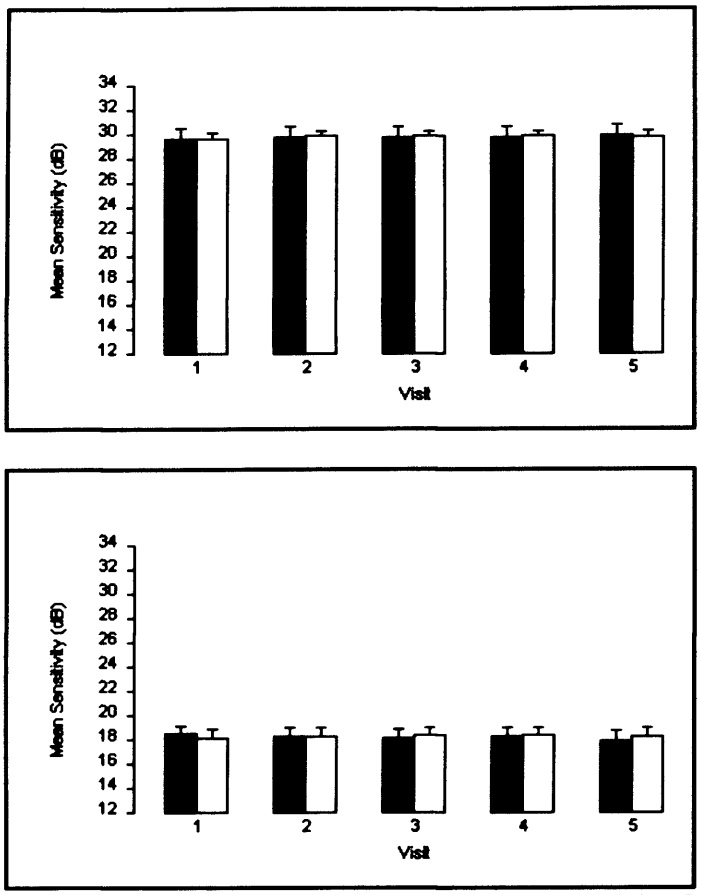

Figure 4.3c The group mean MS (SE) at each of the five visits for each eye as a function of the algorithm for the individuals with OAG: right eye, dark bars; left eye, open bars. Top: SITA Standard. Bottom: Pulsar perimetry.

4.4.1.1.2 Mean Deviation and Mean Defect

The group mean MD (SD) for the SITA Standard algorithm and the group mean MD (SD) for Pulsar stimulus as a function of the algorithm for each eye of the individuals in each of the three groups is shown in Table 4.5.

Algorithm	Visit 1		Visit 2		Visit 3		Visit 4		Visit 5	
	RE	LE	RE	LE	RE	LE	RE	LE	RE	LE
SITA Standard	0.64 (1.18)	0.53 (1.01)	0.62 (0.88)	0.60 (1.12)	0.97 (0.90)	0.69 (0.76)	0.96 (0.89)	0.85 (1.01)	1.17 (1.02)	0.82 (1.00)
Pulsar	0.08 (1.80)	0.43 (1.52)	-0.01 (1.95)	0.49 (1.34)	0.18 (1.34)	0.53 (1.59)	0.51 (1.14)	0.67 (1.18)	0.30 (1.90)	0.61 (1.32)
SITA Standard	0.88 (1.0)	0.65 (1.18)	1.16 (1.10)	0.83 (1.18)	1.16 (1.04)	0.86 (1.19)	1.07 (1.29)	0.75 (1.32)	1.01 (1.49)	0.73 (1.34)
Pulsar	0 (1.50)	0.27 (1.27)	-0.39 (3.80)	-0.30 (3.11)	0.30 (1.27)	0.21 (1.27)	0.24 (1.23)	0.32 (1.22)	0.30 (1.24)	0.25 (1.08)
SITA Standard	-0.20 (4.03)	-0.17 (1.97)	-0.03 (3.91)	0.01 (2.02)	-0.04 (4.03)	0 (2.07)	-0.08 (4.03)	0.01 (1.98)	0.10 (3.82)	-0.17 (2.10)
Pulsar	-1.07 (2.58)	-1.39 (2.90)	-1.39 (3.28)	-1.26 (2.62)	-1.36 (2.94)	-1.18 (2.63)	-1.25 (3.05)	-1.21 (2.98)	-1.60 (3.33)	-1.26 (2.92)

Table 4.5 The group mean MD (SD) at each of the five visits for each eye as a function of the algorithm for the normal individuals (no shading), the individuals with OHT (light shading), the individuals with OAG (dark shading).

The group mean MD for each eye at each visit for each of the two algorithms is also shown graphically in Figures 4.4a to 4.4c for each of the three groups.

Overall, the MD became less positive (i.e. worsened) with increase in age ($p=0.006$). The magnitude of the MD, overall, was independent of the influence of the perimetrist ($p=0.452$) and of the order of both algorithms within the examination ($p=0.098$). It was similar between the two eyes ($p=0.212$). The MD varied across the three diagnostic groups ($p<0.001$) and, as would be expected, was highest (i.e. best) for the normal individuals and least (i.e. worst) for the group with OAG. The MD was higher for those individuals who had had previous experience of perimetry

(p=0.007). The magnitude of the MD was greater for the SITA Standard algorithm (p<0.001) but the difference between the two types of perimetry varied across the three groups being greatest for the group with OAG (p<0.001).

On average, the MD for the SITA Standard algorithm improved between Visits 1 and 5 by 0.41dB for the normal individuals, by 0.11dB for those with OHT and by 0.15dB for those with OAG. The corresponding improvement across the three groups for Pulsar perimetry was 0.20dB, 0.14dB and 0.33dB. The improvement in MD, overall, did not reach statistical significance (p=0.211). Neither the difference in the improvement between the two algorithms nor the difference in the improvement between the three groups reached statistical significance (p=0.453 and p=0.937, respectively).

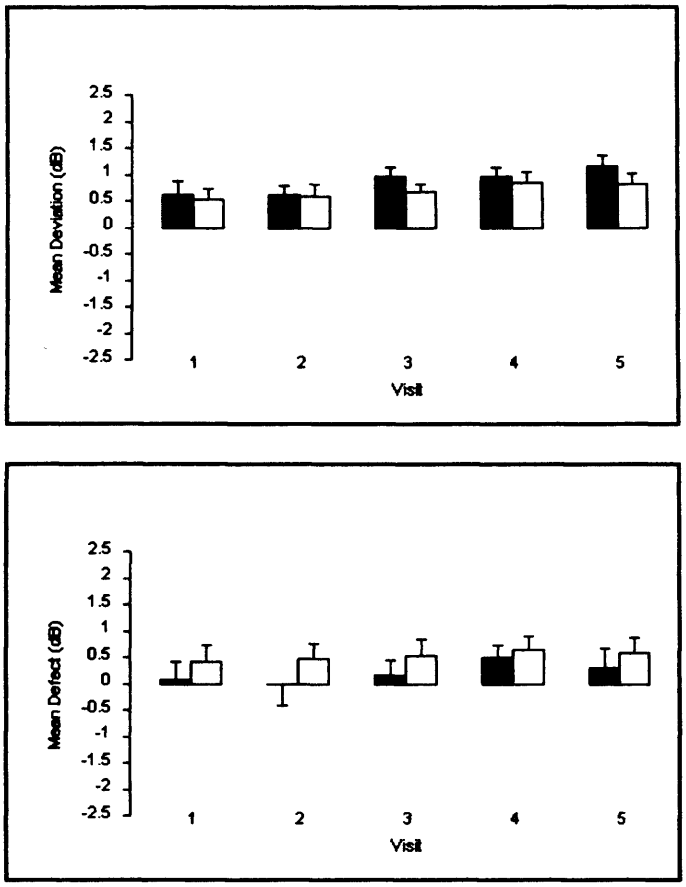

Figure 4.4a The group mean MD (SE) at each of the five visits for each eye as a function of the algorithm for the normal individuals: right eye, dark bars; left eye, open bars. Top: SITA Standard. Bottom: Pulsar perimetry.

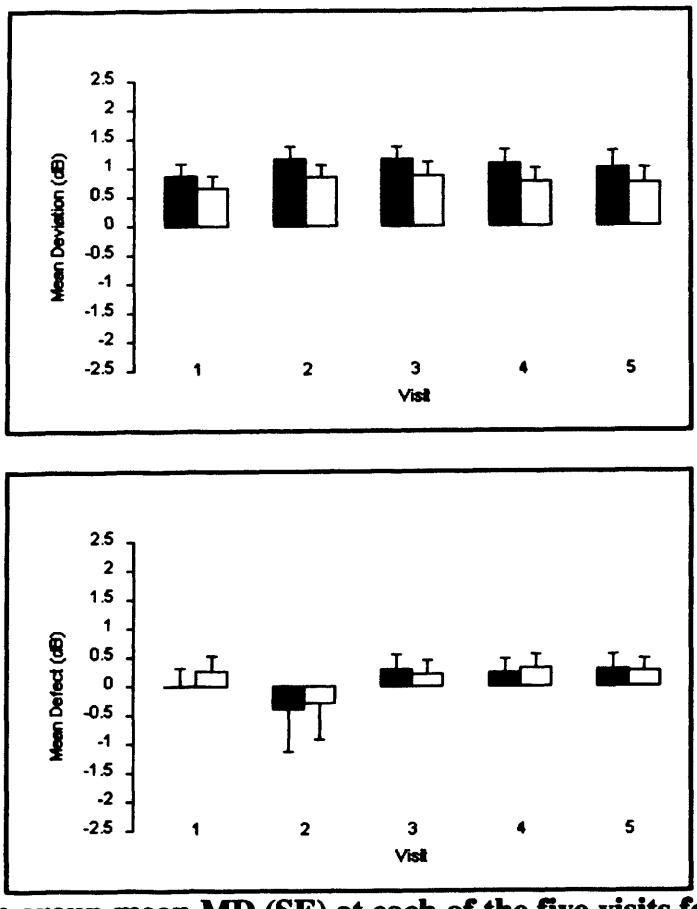

Figure 4.4b The group mean MD (SE) at each of the five visits for each eye as a function of the algorithm for the individuals with OHT: right eye, dark bars; left eye, open bars. Top: SITA Standard. Bottom: Pulsar perimetry.

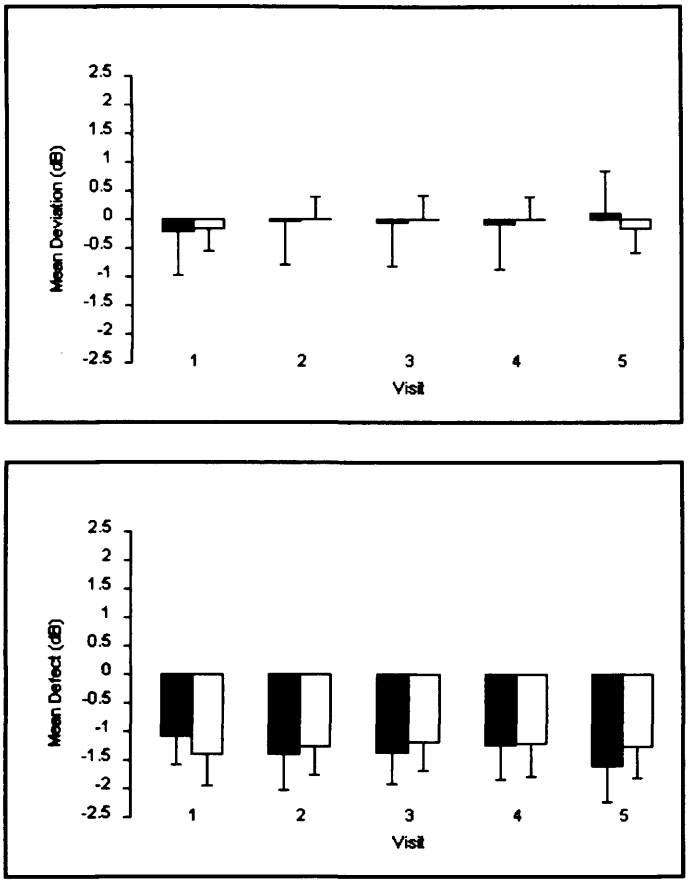

Figure 4.4c The group mean MD (SE) at each of the five visits for each eye as a function of the algorithm for the individuals with OAG: right eye, dark bars; left eye, open bars. Top: SITA Standard. Bottom: Pulsar perimetry.

4.4.1.1.3 Pattern Standard Deviation and square root of the Loss Variance

The group mean PSD (SD) and sLV (SD), respectively, at each of the five visits for each eye of the individuals in each of the three groups, as a function of the two algorithms is shown in Table 4.6.

Algorithm	Visit 1		Visit 2		Visit 3		Visit 4		Visit 5	
	RE	LE	RE	LE	RE	LE	RE	LE	RE	LE
SITA Standard	1.58 (0.38)	1.53 (0.39)	1.46 (0.88)	1.46 (0.38)	1.46 (0.31)	1.50 (0.37)	1.43 (0.34)	1.45 (0.43)	1.41 (0.33)	1.38 (0.31)
Pulsar	2.28 (1.11)	1.91 (0.92)	2.07 (1.11)	1.80 (0.67)	2.22 (1.62)	1.84 (1.11)	2.05 (1.00)	1.76 (0.67)	2.21 (1.40)	1.79 (0.72)
SITA Standard	1.54 (0.39)	1.67 (0.80)	1.39 (0.20)	1.64 (0.76)	1.41 (0.26)	1.71 (0.92)	1.48 (0.31)	1.71 (0.95)	1.40 (0.24)	1.62 (0.69)
Pulsar	2.35 (1.13)	1.97 (0.57)	2.26 (1.17)	2.15 (0.91)	2.14 (0.92)	2.23 (1.12)	2.26 (1.14)	1.96 0.83)	2.16 (1.07)	1.96 (0.78)
SITA Standard	2.17 (2.08)	2.31 (1.72)	2.08 (2.09)	2.17 (1.87)	2.02 (1.90)	2.04 (1.68)	2.04 (1.85)	2.14 (1.65)	2.02 (1.98)	2.11 (1.65)
Pulsar	2.56 (1.06)	2.63 (1.41)	2.50 (0.99)	2.66 (1.33)	2.58 (1.01)	2.70 (1.21)	2.59 (1.10)	2.56 (1.10)	2.70 (1.40)	2.61 (1.17)

Table 4.6 The group mean PSD (SD) and the group mean sLV (SD) at each of the five visits for each eye as a function of the algorithm for the normal individuals (no shading), the individuals with OHT (light shading), the individuals with OAG dark shading).

The group mean PSD and the group mean sLV for each eye at each visit for each of the two algorithms is also shown graphically in Figures 4.5a to 4.5c for each of the three groups.

Overall, the PSD/ sLV became more positive (i.e. worsened) with increase in age ($p=0.006$). The magnitude of the PSD/ sLV, overall, was independent of the influence of the perimetrist ($p=0.452$) and of the order of both algorithms within the examination ($p=0.861$). It was similar between the two eyes ($p=0.550$). The PSD/ sLV varied across the three diagnostic groups ($p<0.001$) and, as would be expected, was highest for the individuals with OAG. The magnitude of the PSD/ sLV was

greater for Pulsar perimetry ($p<0.001$) but the difference between the two types of perimetry was similar across the three groups ($p=0.687$).

On average, the PSD for the SITA Standard algorithm improved between Visits 1 and 5 by 0.17dB for the normal individuals, by 0.10dB for those with OHT and by 0.18dB for those with OAG. The corresponding improvement in sLV across the three groups for Pulsar perimetry was 0.10dB, 0.10dB and -0.06dB. The improvement in PSD/ sLV, overall, did not reach statistical significance ($p=0.445$). Neither the difference in the improvement between the two algorithms nor the difference in the improvement between the three groups reached statistical significance ($p=0.834$ and $p=0.997$, respectively).

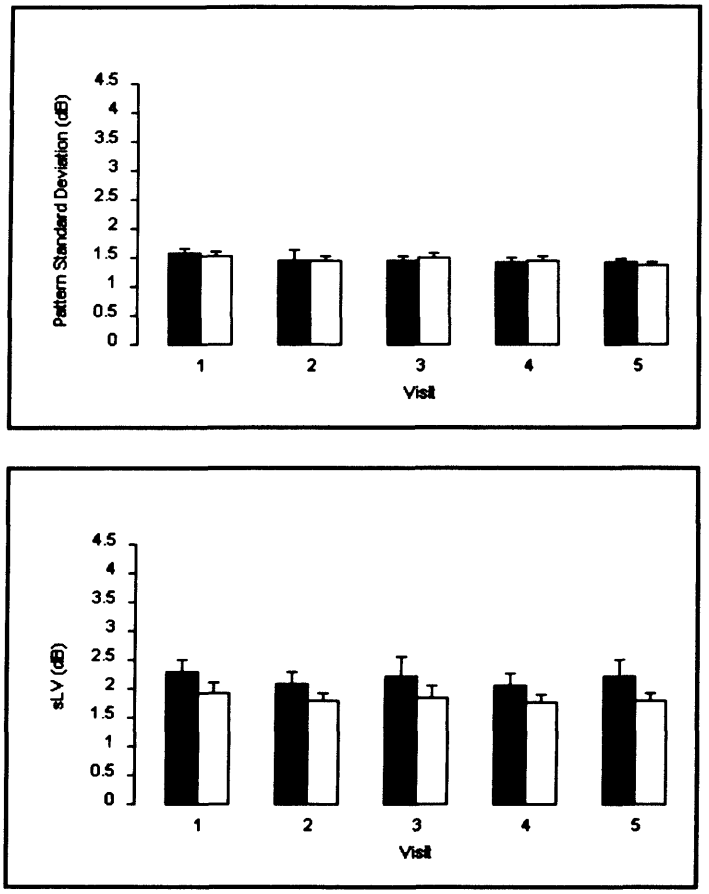

Figure 4.5a The group mean PSD (SE) and the group mean sLV (SD) at each of the five visits for each eye as a function of the algorithm for the normal individuals: right eye, dark bars; left eye, open bars. Top: SITA Standard. Bottom: Pulsar perimetry.

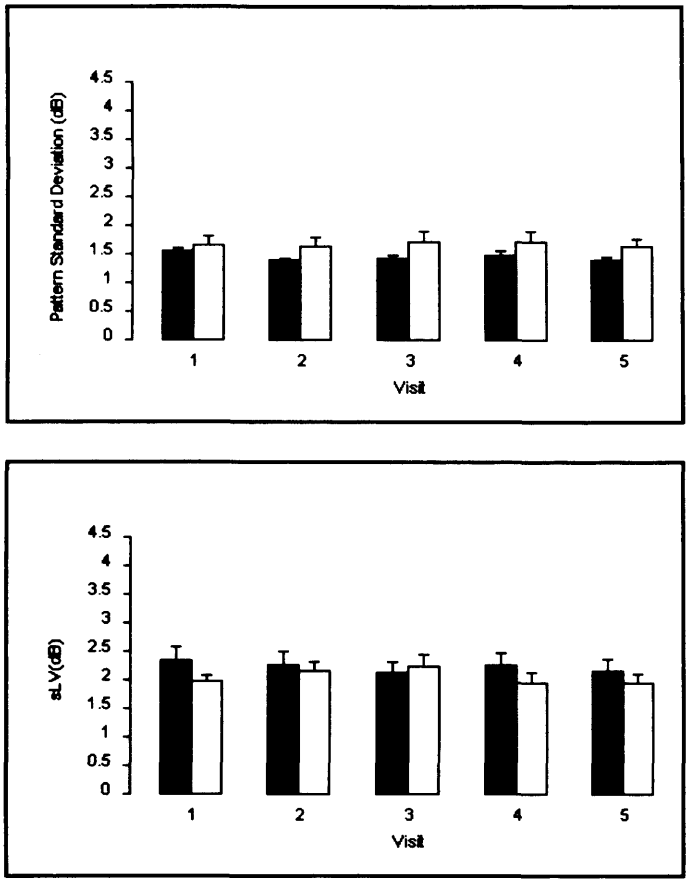

Figure 4.5b The group mean PSD (SE) and the group mean sLV (SD) at each of the five visits for each eye as a function of the algorithm for the individuals with OHT: right eye, dark bars; left eye, open bars. Top: SITA Standard. Bottom: Pulsar perimetry.

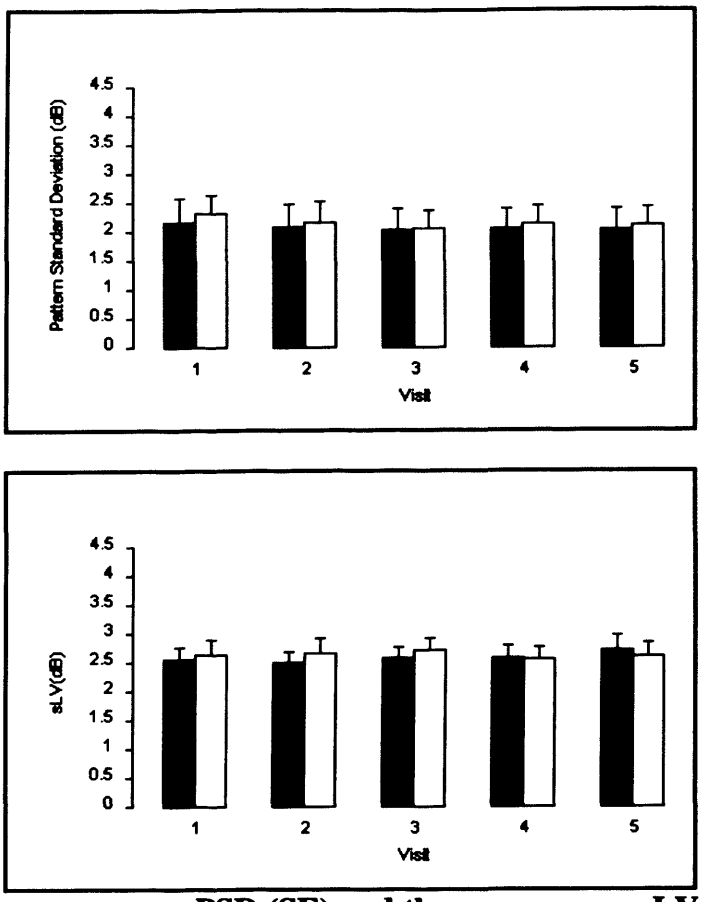

Figure 4.5c The group mean PSD (SE) and the group mean sLV (SD) at each of the five visits for each eye as a function of the algorithm for the individuals with OAG: right eye, dark bars; left eye, open bars. Top: SITA Standard. Bottom: Pulsar perimetry.

4.4.1.1.4 Examination duration

The group mean examination duration (SD) at each of the five visits for each eye of the individuals in each of the three groups, as a function of the two algorithms is shown in Table 4.7.

Algorithm	Visit 1		Visit 2		Visit 3		Visit 4		Visit 5	
	RE	LE	RE	LE	RE	LE	RE	LE	RE	LE
SITA Standard	274 (29)	276 (29)	271 (22)	269 (24)	268 (34)	268 (28)	259 (39)	265 (23)	268 (27)	266 (31)
Pulsar	203 (8)	194 (3)	204 (8)	197 (6)	200 (7)	197 (5)	204 (7)	196 (4)	202 (7)	196 (4)
SITA Standard	281 (28)	280 (30)	269 (31)	267 (26)	272 (32)	272 (33)	280 (42)	277 (40)	272 (38)	275 (32)
Pulsar	204 (9)	198 (6)	203 (9)	197 (7)	204 (6)	199 (7)	204 (8)	198 (9)	204 (8)	199 (6)
SITA Standard	280 (34)	298 (40)	289 (41)	293 (40)	285 (35)	296 (42)	280 (41)	293 (43)	286 (37)	291 (35)
Pulsar	213 (12)	201 (11)	208 (9)	199 (6)	210 (12)	201 (8)	211 (10)	199 (8)	210 (11)	199 (7)

Table 4.7 The group mean examination duration (SD) at each of the five visits for each eye as a function of the two algorithms for the normal individuals (no shading), the individuals with OHT (light shading), the individuals with OAG (dark shading).

The group mean examination duration for each eye at each visit for each of the two algorithms is also shown graphically in Figures 4.6a to 4.6c for each of the three groups.

Overall, the examination duration increased with increase in age ($p=0.006$). The magnitude of the examination duration overall, was independent of the influence of the perimetrist ($p=0.452$) and of the order of both algorithms within the examination ($p=0.543$). It was shorter for the second eye examined ($p=0.010$). The examination duration varied across the three diagnostic groups ($p<0.001$) and was longest for the individuals with OAG. The examination duration was shorter for Pulsar perimetry

($p<0.001$) and the difference between the two types of perimetry was greater for the group with OAG ($p<0.001$).

On average, the examination duration for the SITA Standard algorithm improved between Visits 1 and 5 by 8 seconds for the normal individuals, by 7 seconds for those with OHT and by 0.5 second for those with OAG. The corresponding change in examination duration across the three groups for Pulsar perimetry was -0.5 seconds, -0.5 seconds and 2.5 seconds. The improvement in examination duration, overall, reached statistical significance ($p=0.016$) and the difference in the improvement between the two algorithms was statistically significant ($p=0.028$). However, the difference in the improvement between the three groups was not statistically significant ($p=0.216$).

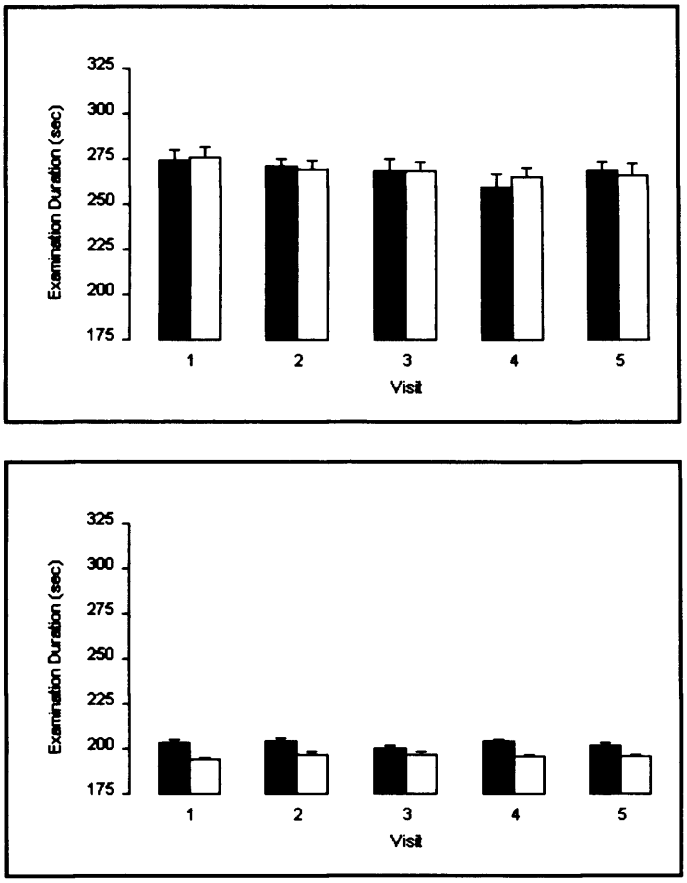

Figure 4.6a The group mean examination duration (SE) at each of the five visits for each eye as a function of the two algorithms for the normal individuals: right eye, dark bars; left eye, open bars. Top: SITA Standard. Bottom: Pulsar perimetry.

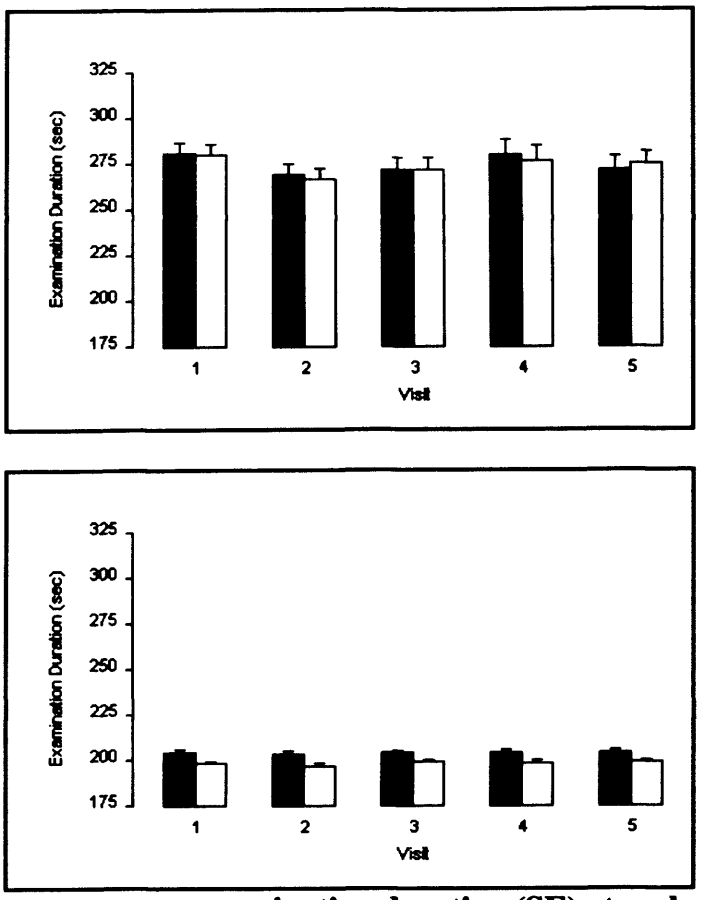

Figure 4.6b The group mean examination duration (SE) at each of the five visits for each eye as a function of the two algorithms for the individuals with OHT: right eye, dark bars; left eye, open bars. Top: SITA Standard. Bottom: Pulsar perimetry.

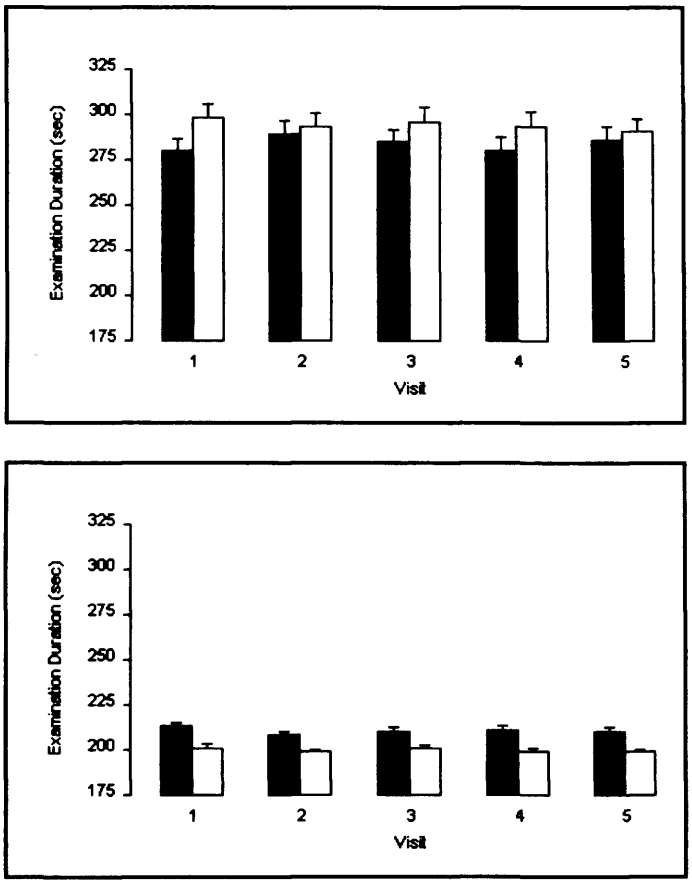

Figure 4.6c The group mean examination duration (SE) at each of the five visits for each eye as a function of the two algorithms for the individuals with OAG: right eye, dark bars; left eye, open bars. Top: SITA Standard. Bottom: Pulsar perimetry.

4.4.1.1.5 Ratio of the peripheral mean sensitivity to the central mean sensitivity
The ratio of the peripheral mean sensitivity (PMS) to the central mean sensitivity (CMS) for each eye of the individuals in each of the three groups is shown in Table 4.8.

Algorithm	Visit 1		Visit 2		Visit 3		Visit 4		Visit 5	
	RE	LE	RE	LE	RE	LE	RE	LE	RE	LE
SITA Standard	0.93 (0.03)	0.93 (0.03)	0.94 (0.02)	0.94 (0.02)	0.94 (0.03)	0.94 (0.02)	0.94 (0.03)	0.94 (0.04)	0.94 (0.03)	0.94 (0.03)
Pulsar	0.72 (0.06)	0.74 (0.04)	0.73 (0.05)	0.75 (0.06)	0.72 (0.06)	0.74 (0.04)	0.73 (0.04)	0.75 (0.05)	0.72 (0.06)	0.74 (0.03)
SITA Standard	0.93 (0.02)	0.92 (0.04)	0.93 (0.02)	0.93 (0.02)	0.93 (0.03)	0.93 (0.03)	0.93 (0.03)	0.92 (0.03)	0.93 (0.02)	0.92 (0.03)
Pulsar	0.72 (0.06)	0.72 (0.06)	0.70 (0.06)	0.71 (0.06)	0.71 (0.03)	0.72 (0.06)	0.71 (0.05)	0.71 (0.05)	0.71 (0.05)	0.72 (0.04)
SITA Standard	0.93 (0.04)	0.92 (0.05)	0.92 (0.03)	0.92 (0.04)	0.93 (0.03)	0.93 (0.04)	0.93 (0.03)	0.92 (0.04)	0.93 (0.04)	0.92 (0.04)
Pulsar	0.72 (0.07)	0.70 (0.06)	0.71 (0.05)	0.71 (0.06)	0.71 (0.06)	0.70 (0.06)	0.71 (0.06)	0.70 (0.05	0.70 (0.09)	0.71 (0.07)

Table 4.8 The group mean ratio of the PMS to the CMS and the ratio of the standard deviations (SD) at each of the five visits for each eye as a function of the two algorithms for the normal individuals (no shading), the individuals with OHT (light shading), the individuals with OAG (dark shading).

The group mean ratio of the PMS to the CMS and the ratio of the standard deviation (SD) for each eye at each visit for each of the two algorithms is also shown graphically in Figures 4.7a to 4.7c for each of the three groups.

Overall, the group mean ratio of the PMS to the CMS decreased with increase in age ($p=0.006$). The magnitude of the ratio, overall, was independent of the influence of the perimetrist ($p=0.452$). The order of both algorithms within the examination ($p=0.762$) and between eyes ($p=0.316$) had little effect. The ratio was higher for the SITA Standard algorithm than for Pulsar perimetry ($p<0.001$). The ratio was highest for the normal individuals ($p<0.001$) and the difference between groups largely arose in the ratio for the Pulsar perimeter. The ratio was stable over the five visits

(p=0.834). On average, the ratio was approximately 0.92 for the SITA Standard algorithm and 0.73 for Pulsar perimetry.

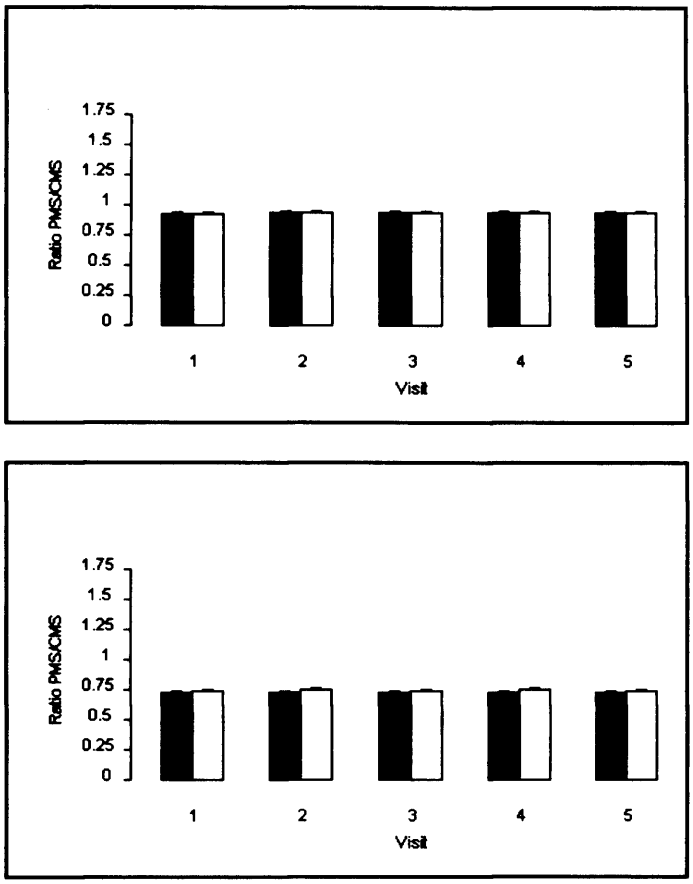

Figure 4.7a The group mean (SE) ratio PMS/CMS at each of the five visits for each eye as a function of the algorithm for the normal individuals: right eye, dark bars; left eye, open bars. Top: SITA Standard. Bottom: Pulsar perimetry.

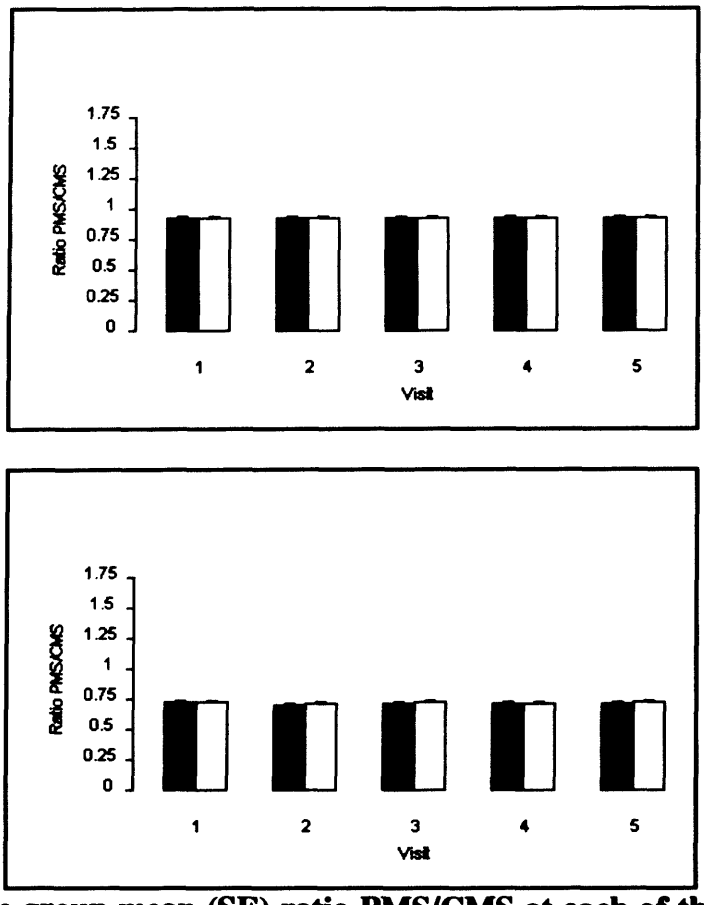

Figure 4.7b The group mean (SE) ratio PMS/CMS at each of the five visits for each eye as a function of the algorithm for the individuals with OHT: right eye, dark bars; left eye, open bars. Top: SITA Standard. Bottom: Pulsar perimetry.

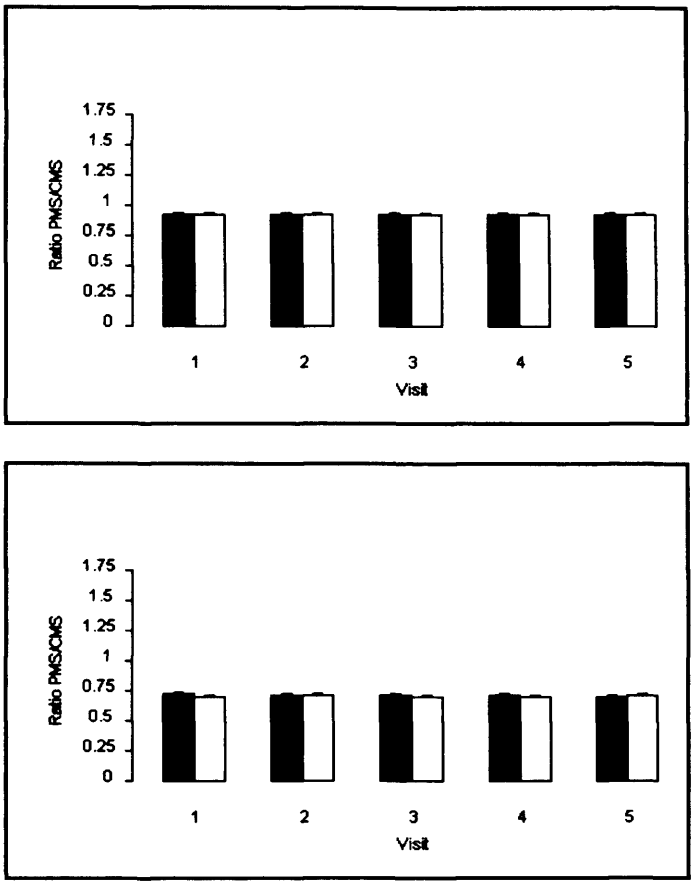

Figure 4.7c The group mean (SE) ratio PMS/CMS at each of the five visits for each eye as a function of the algorithm for the individuals with OAG: right eye, dark bars; left eye, open bars. Top: SITA Standard. Bottom: Pulsar perimetry.

4.4.1.2 The within-individual within-algorithm between-visit (Visits 1 and 5) difference (improvement) in sensitivity

The within-algorithm differences between Visits 1 and 5 in the MD for the SITA Standard algorithm and for Pulsar perimetry are illustrated in Figures 4.8a to Figure 4.8d and are summarised in Table 4.9.

Algorithm	Eye	Normal	OHT	OAG	All groups
SITA Standard	RE	2.68 dB	3.21 dB	3.15 dB	3.06 dB
	LE	3.05 dB	4.02 dB	3.44 dB	3.51 dB
Pulsar	RE	5.07 dB	5.44 dB	8.72 dB	6.73 dB
	LE	3.24 dB	4.37 dB	5.65 dB	4.51 dB

Table 4.9 The within-individual within-algorithm difference in the MD between Visits 1 and 5 expressed as the range of the limits of agreement (defined as the mean of the differences +/- 1.96SD) for the two algorithms for each eye of the three groups of individuals and for the three groups, combined.

The range of the limits of agreement for the MD was wider for Pulsar perimetry across each diagnostic group and was widest for the group with OAG.

SITA Standard

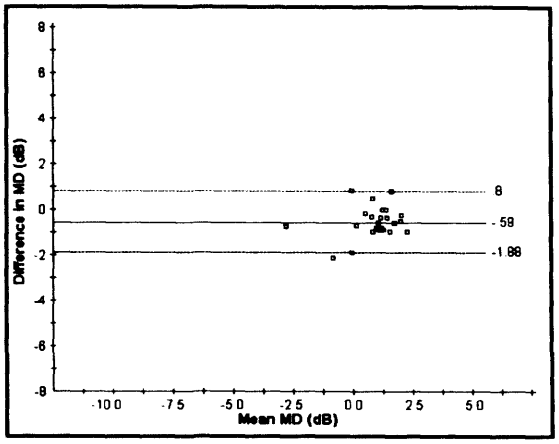

SITA Standard

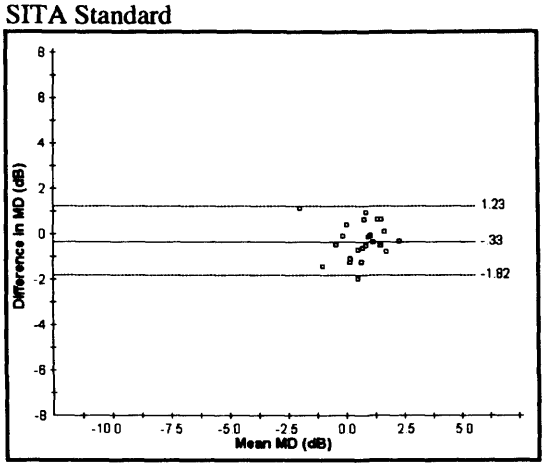

Pulsar

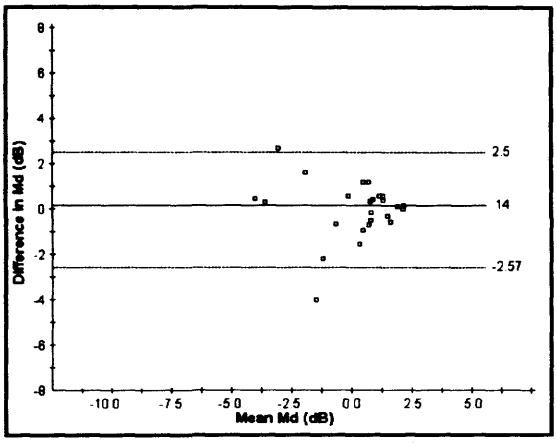

Pulsar

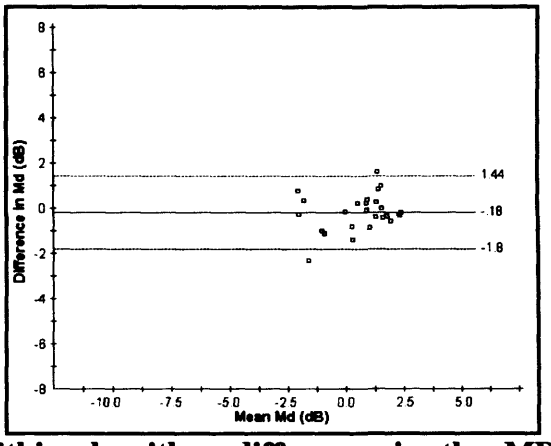

Figure 4.8a The within-individual within-algorithm difference in the MD between Visits 1 and 5 against the mean of the two MDs for the right eye (left column) and for the left eye (right column) for the normal individuals. Top: SITA Standard. Bottom: Pulsar perimetry. The solid line indicates the mean of the differences and the upper and lower dotted lines the mean of the differences +/- 1.96SD, respectively.

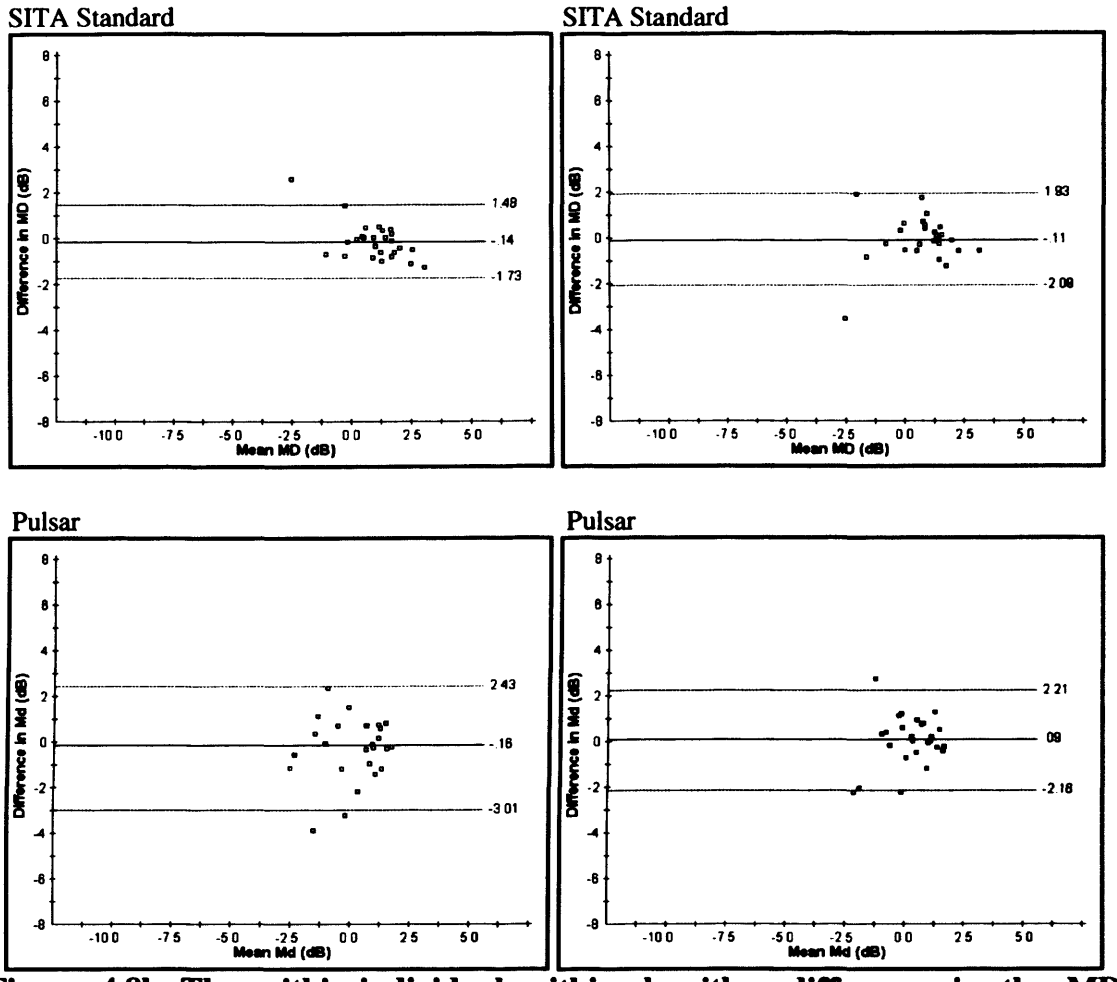

Figure 4.8b The within-individual within-algorithm difference in the MD between Visits 1 and 5 against the mean of the two MDs for the right eye (left column) and for the left eye (right column) for the individuals with OHT. Top: SITA Standard. Bottom: Pulsar perimetry. The solid line indicates the mean of the differences and the upper and lower dotted lines the mean of the differences +/- 1.96SD, respectively.

SITA Standard

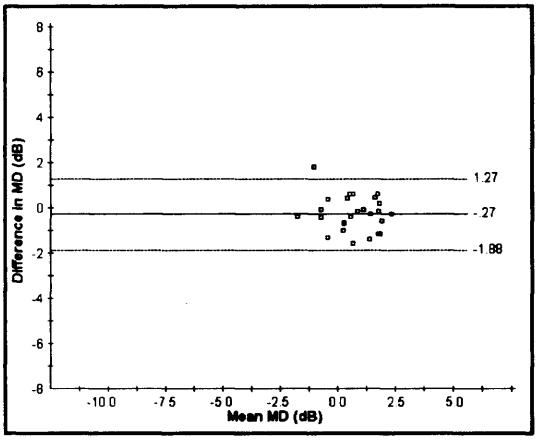

SITA Standard

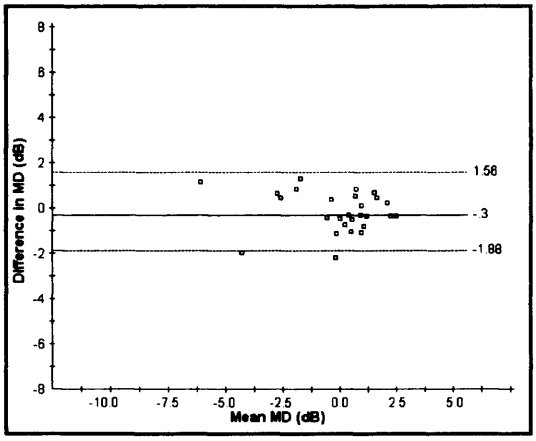

Pulsar

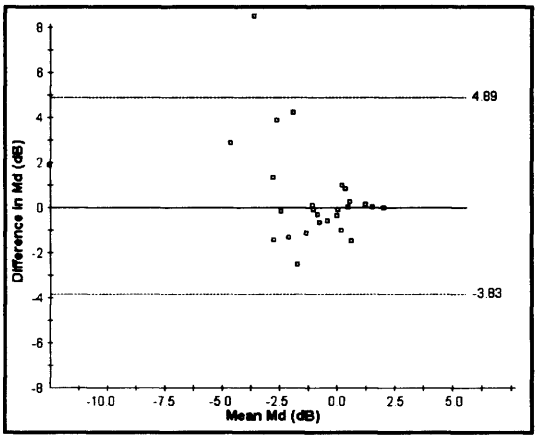

Pulsar

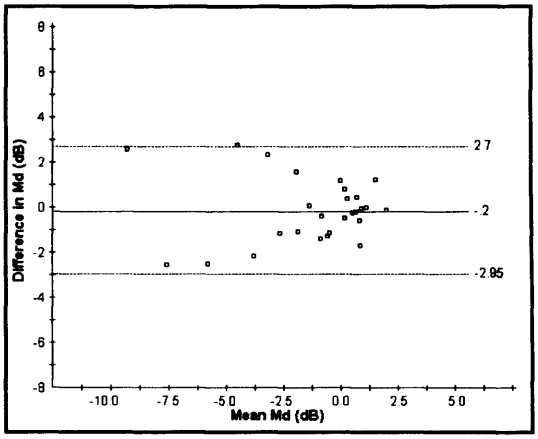

Figure 4.8c The within-individual within-algorithm difference in the MD between Visits 1 and 5 against the mean of the two MDs for the right eye (left column) and for the left eye (right column) for the individuals with OAG. Top: SITA Standard. Bottom: Pulsar perimetry. The solid line indicates the mean of the differences and the upper and lower dotted lines the mean of the differences +/- 1.96SD, respectively.

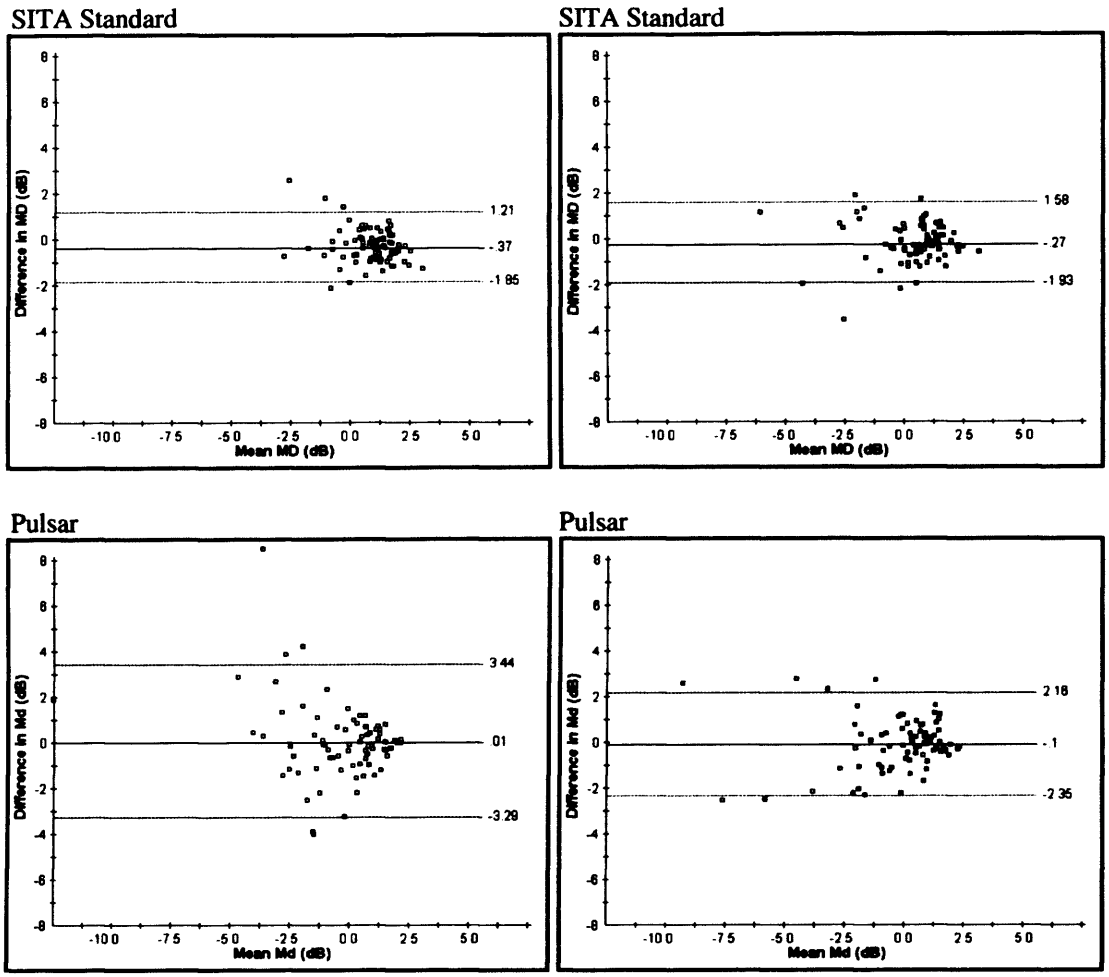

Figure 4.8d The within-individual within-algorithm difference in the MD between Visits 1 and 5 against the mean of the two MDs for the right eye (left column) and for the left eye (right column) for the three groups, combined. Top: SITA Standard. Bottom: Pulsar perimetry. The solid line indicates the mean of the differences and the upper and lower dotted lines the mean of the differences +/- 1.96SD, respectively.

The within-algorithm differences between Visits 1 and 5 in the PSD for the SITA Standard algorithm and in the sLV for Pulsar perimetry are illustrated in Figure 4.9a to Figure 4.9d and summarised in Table 4.10.

Algorithm	Eye	Normal	OHT	OAG	All groups
SITA Standard	**RE**	1.56 dB	1.45 dB	1.48 dB	1.48 dB
	LE	1.02 dB	2.45 dB	3.04 dB	2.34 dB
Pulsar	**RE**	3.52 dB	4.50 dB	5.65 dB	4.63 dB
	LE	2.34 dB	2.60 dB	4.48 dB	3.27 dB

Table 4.10 The within-individual within-algorithm differences in the PSD and in the sLV indices between Visits 1 and 5 expressed as the range of the limits of agreement (defined as the mean of the differences +/- 1.96SD) for the two algorithms for each eye of the three groups of individuals and for the three groups, combined.

The range of the limits of agreement was wider for the sLV of Pulsar perimetry across each diagnostic group and was widest for the group with OAG.

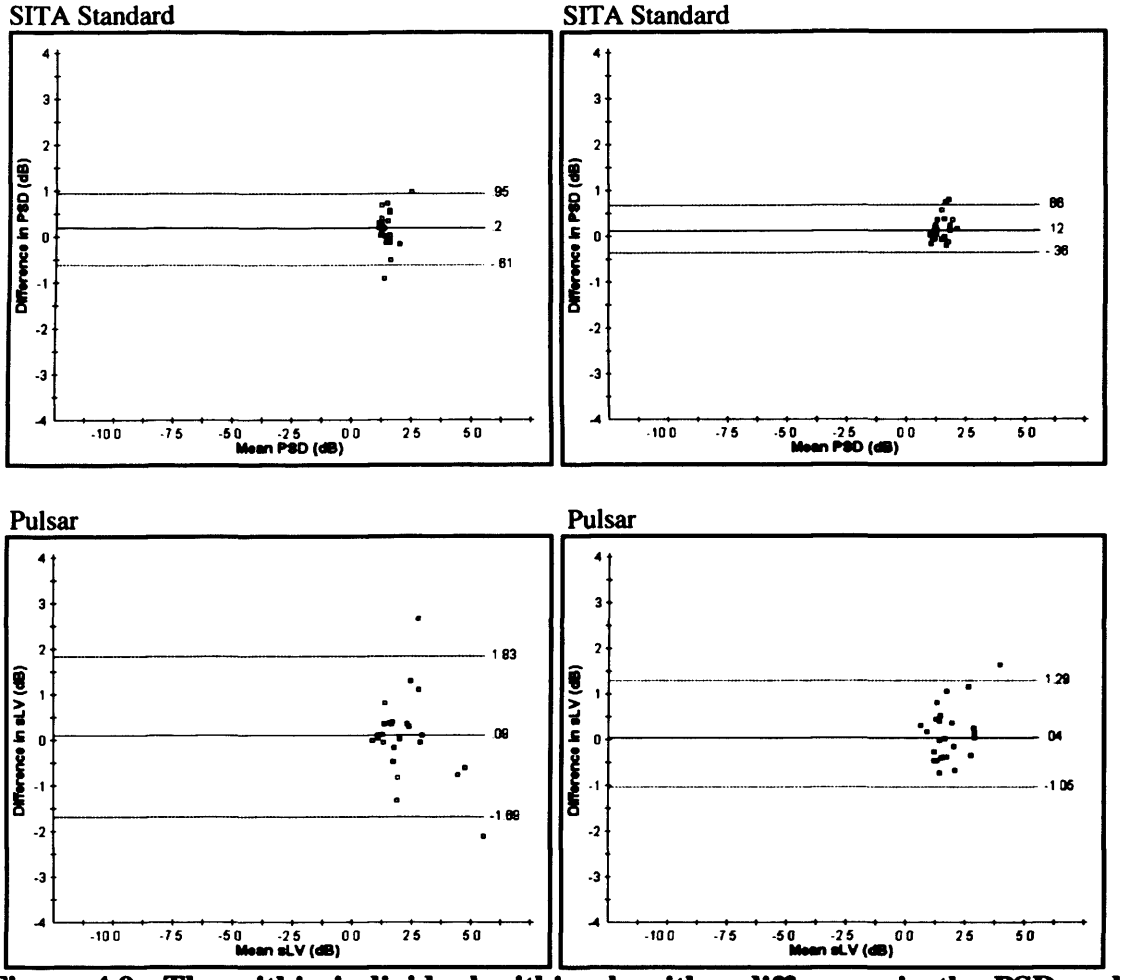

Figure 4.9a The within-individual within-algorithm difference in the PSD and sLV indices between Visits 1 and 5 against the mean of the two PSDs or two sLVs, as appropriate, for the right eye (left column) and for the left eye (right column) for the normal individuals. Top: SITA Standard. Bottom: Pulsar perimetry. The solid line indicates the mean of the differences and the upper and lower dotted lines the mean of the differences +/- 1.96SD, respectively.

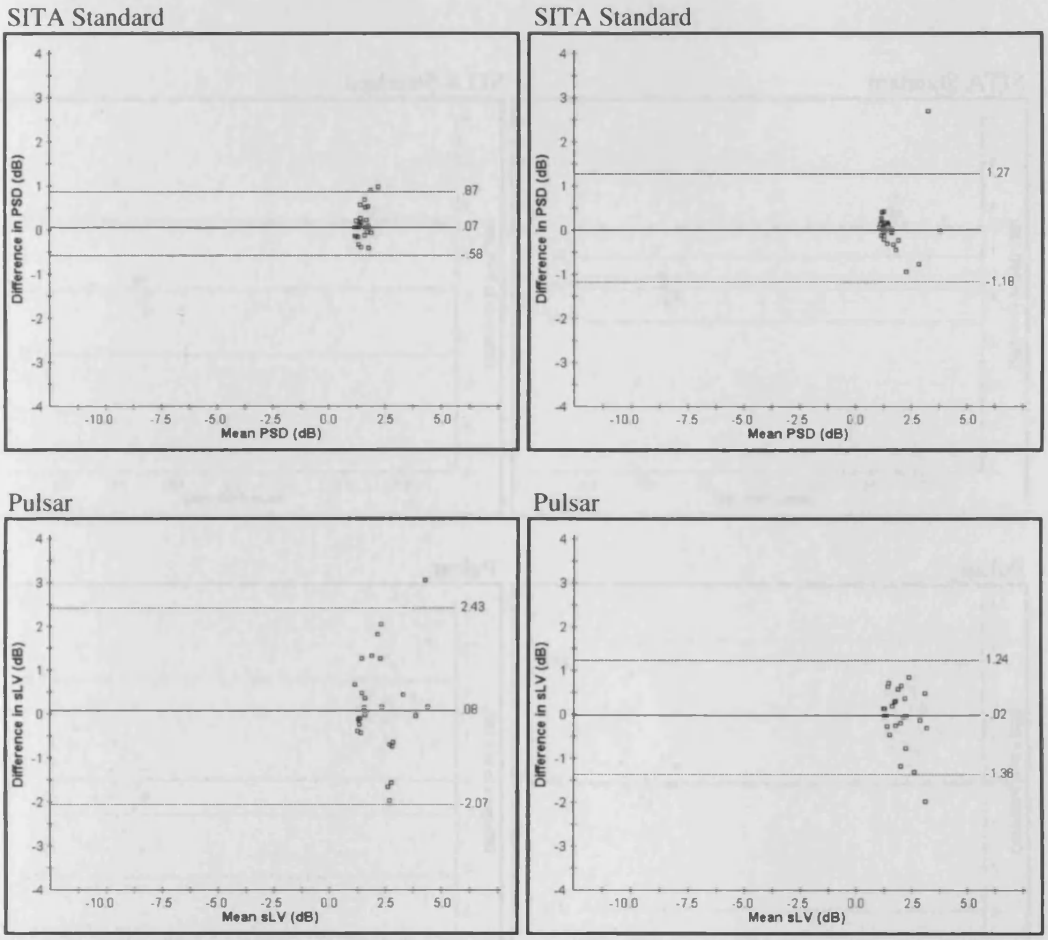

Figure 4.9b The within-individual within-algorithm difference in the PSD and sLV indices between Visits 1 and 5 against the mean of the two PSDs or two sLVs, as appropriate, for the right eye (left column) and for the left eye (right column) for the individuals with OHT. Top: SITA Standard. Bottom: Pulsar perimetry. The solid line indicates the mean of the differences and the upper and lower dotted lines the mean of the differences +/- 1.96SD, respectively.

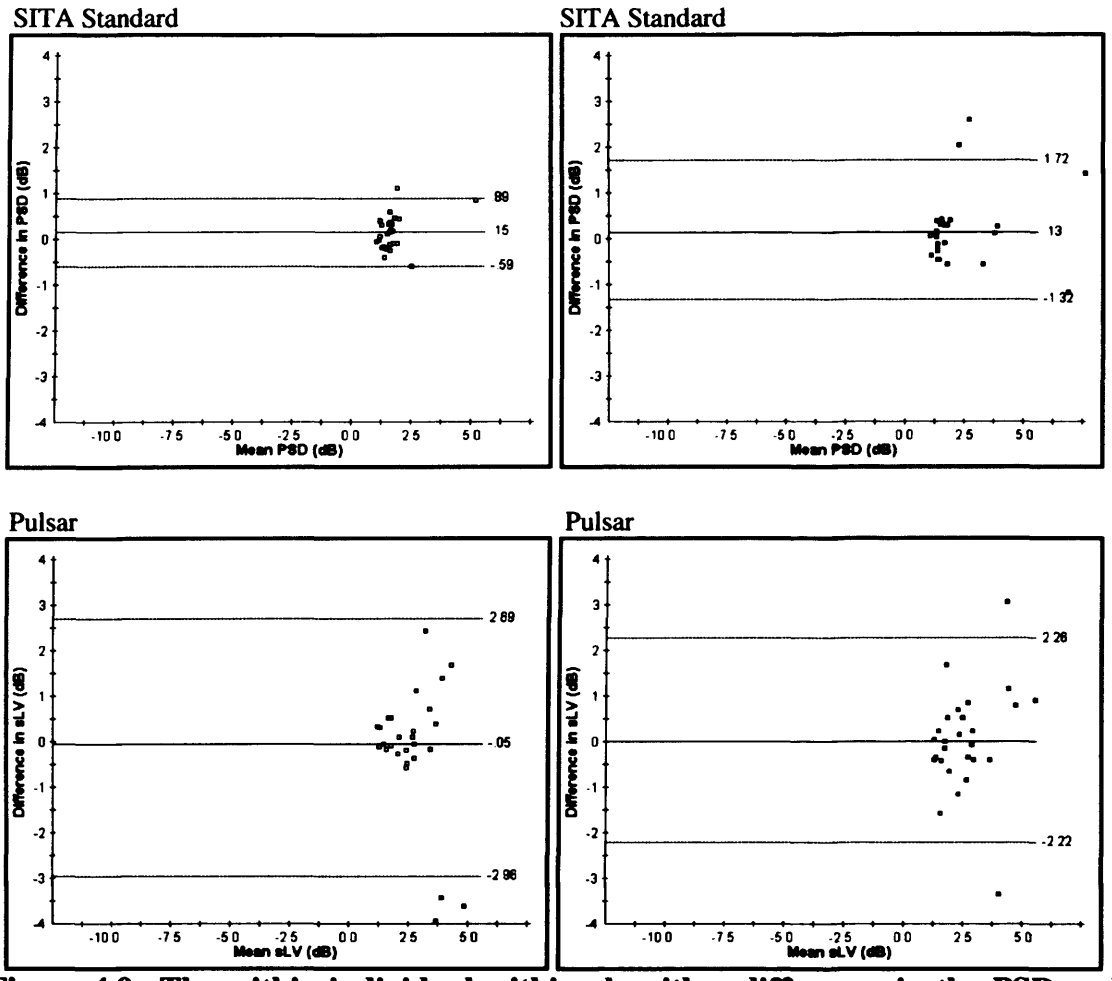

Figure 4.9c The within-individual within-algorithm difference in the PSD and sLV indices between Visits 1 and 5 against the mean of the two PSDs or two sLVs, as appropriate, for the right eye (left column) and for the left eye (right column) for the individuals with OAG. Top: SITA Standard. Bottom: Pulsar perimetry. The solid line indicates the mean of the differences and the upper and lower dotted lines the mean of the differences +/- 1.96SD, respectively.

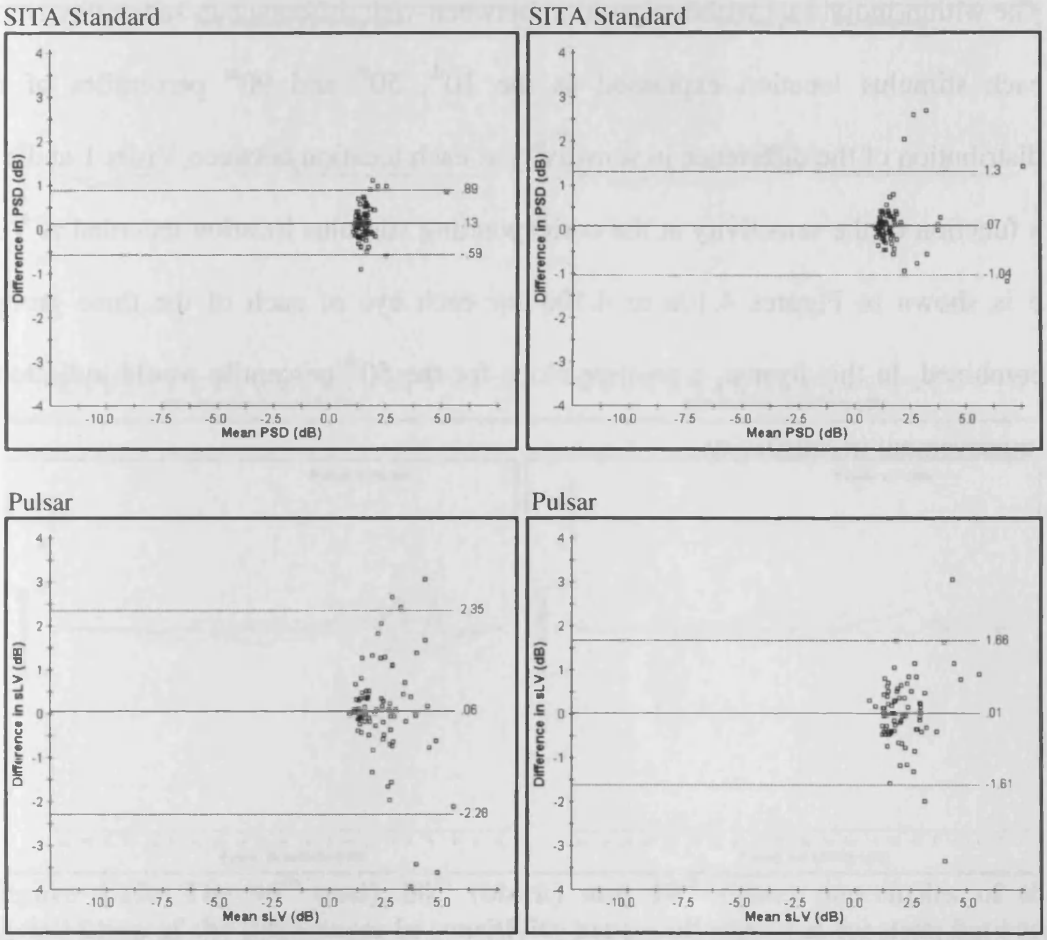

Figure 4.9d The within-individual within-algorithm difference in the PSD and sLV indices between Visits 1 and 5 against the mean of the two PSDs or two sLVs, as appropriate, for the right eye (left column) and for the left eye (right column) for the three groups, combined. Top: SITA Standard. Bottom: Pulsar perimetry. The solid line indicates the mean of the differences and the upper and lower dotted lines the mean of the differences +/- 1.96SD, respectively.

The within-individual within-algorithm between-visit difference in sensitivity across each stimulus location expressed as the 10^{th}, 50^{th} and 90^{th} percentiles of the distribution of the difference in sensitivity at each location between Visits 1 and 5 as a function of the sensitivity at the corresponding stimulus location recorded at Visit 5 is shown in Figures 4.10a to 4.10d for each eye of each of the three groups, combined. In this format, a positive slope for the 50^{th} percentile would indicate an improvement in sensitivity.

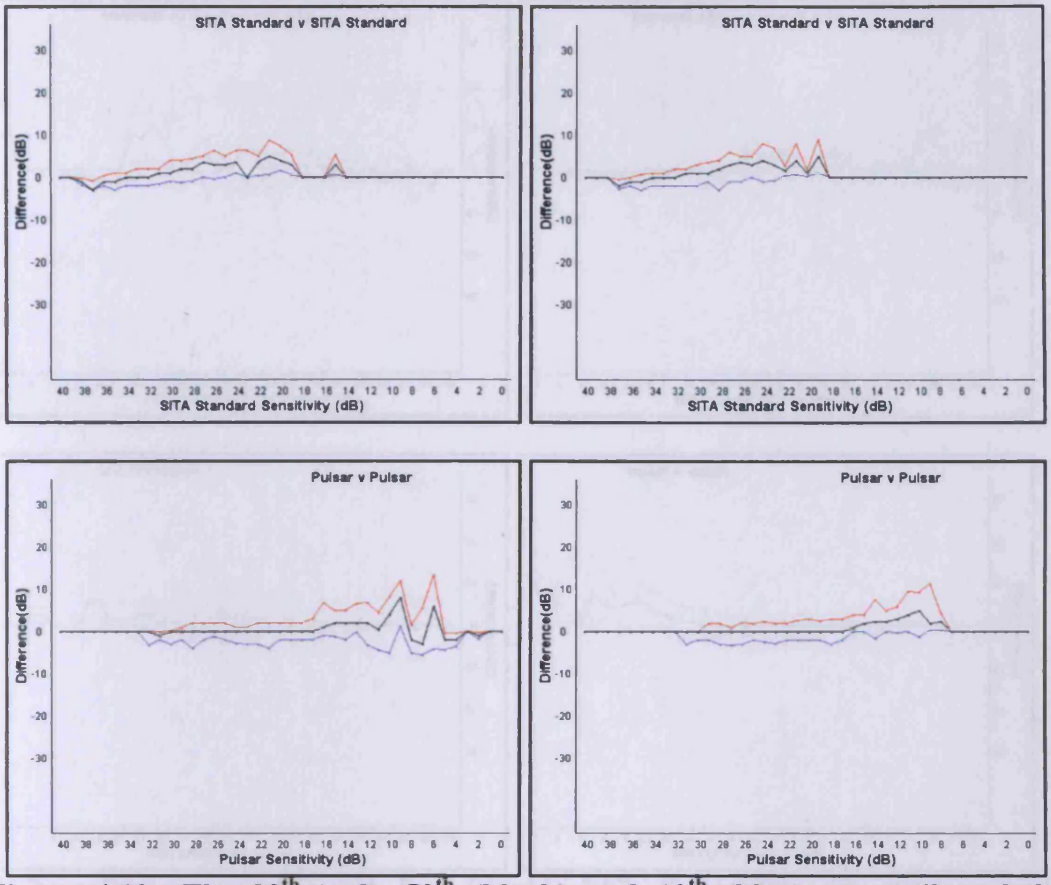

Figure 4.10a The 90th (red), 50th (black) and 10th (blue) percentiles of the distribution of the differences in sensitivity across all stimulus location between Visits 1 and 5 as a function of the sensitivity at the corresponding stimulus location recorded at Visit 5 for the right eye (left column) and for the left eye (right column) for the normal individuals. Top: SITA Standard. Bottom: Pulsar perimetry.

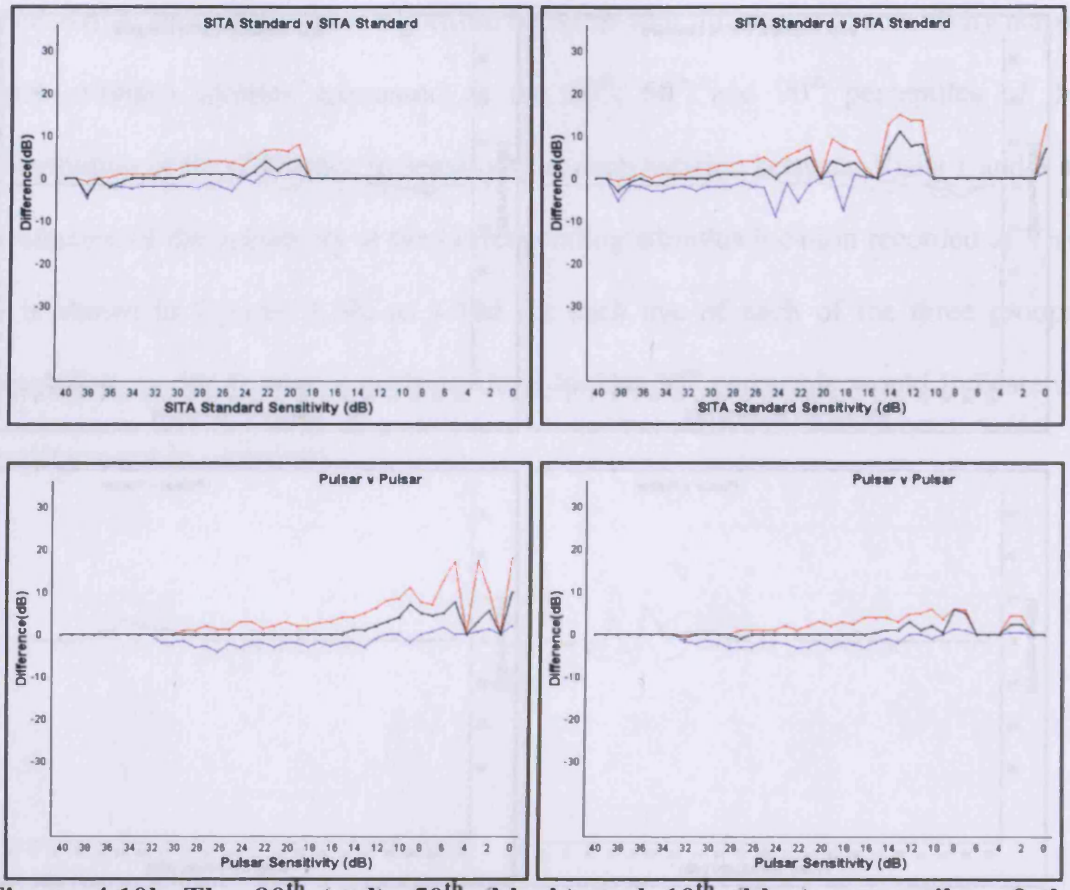

Figure 4.10b The 90th (red), 50th (black) and 10th (blue) percentiles of the distribution of the differences in sensitivity across all stimulus location between Visits 1 and 5 as a function of the sensitivity at the corresponding stimulus location recorded at Visit 5 for the right eye (left column) and for the left eye (right column) for the individuals with OHT. Top: SITA Standard. Bottom: Pulsar perimetry.

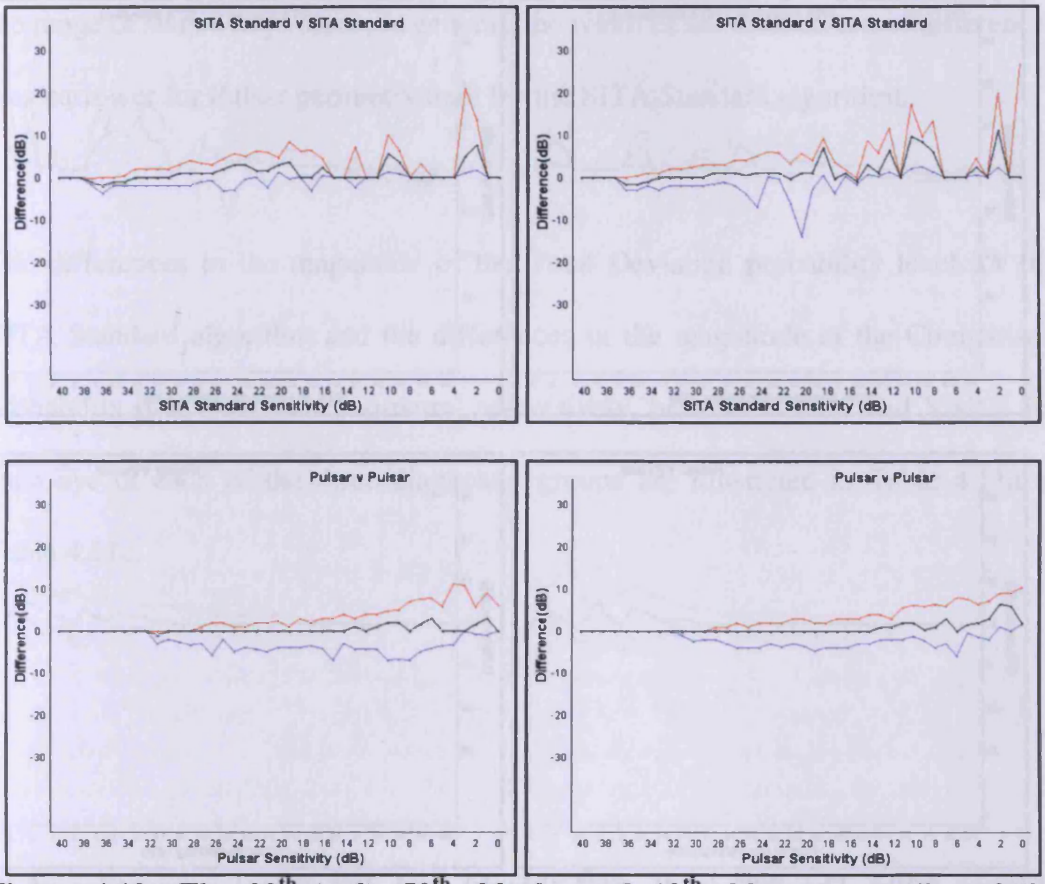

Figure 4.10c The 90th (red), 50th (black) and 10th (blue) percentiles of the distribution of the differences in sensitivity across all stimulus location between Visits 1 and 5 as a function of the sensitivity at the corresponding stimulus location recorded at Visit 5 for the right eye (left column) and for the left eye (right column) for the individuals with OAG. Top: SITA Standard. Bottom: Pulsar perimetry.

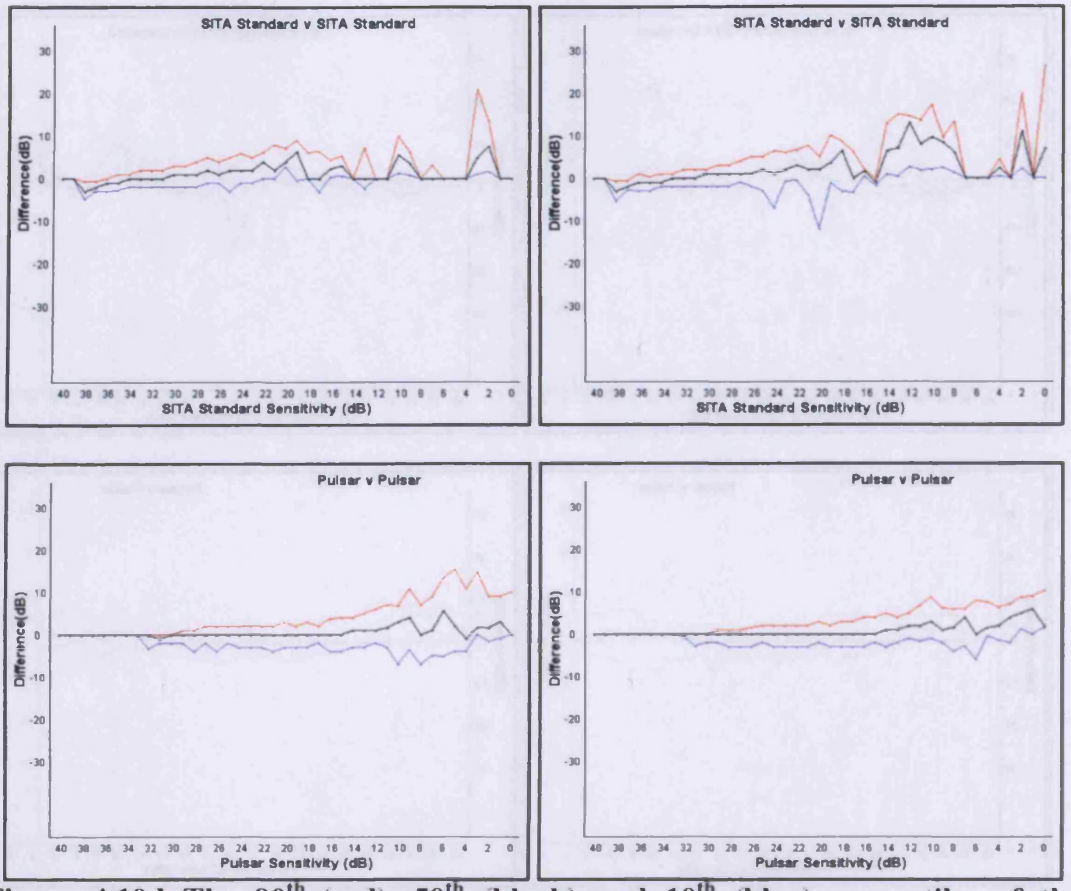

Figure 4.10d The 90th (red), 50th (black) and 10th (blue) percentiles of the distribution of the differences in sensitivity across all stimulus locations between Visit 1 and 5 as a function of the sensitivity at the corresponding stimulus location recorded at Visit 5 for the right eye (left column) and for the left eye (right column) of the individuals in all three diagnostic categories. Top: SITA Standard. Bottom: Pulsar perimetry.

As would be expected, there was least difference at stimulus locations exhibiting high levels of sensitivity for each algorithms i.e. the 10th, 50th and 90th percentiles approximate to zero. As would also be expected, the spread of the distribution of differences widened as the sensitivity declined. The 50th percentile for the normal individuals, exhibited a positive slope for the SITA Standard algorithm in both eyes indicating an improvement in sensitivity between Visits 1 and 5. However, the 50th percentile for Pulsar perimetry approximated to zero for both eyes at all values of sensitivity indicating the absence, in general, of a learning effect over the 5 visits. The 50th percentile for Pulsar perimetry for the individuals with OHT and for the individuals with OAG also approximated to zero for at least the upper two thirds of

the range of sensitivity values. In general, the width of the distribution of differences was narrower for Pulsar perimetry than for the SITA Standard algorithm.

The differences in the magnitude of the Total Deviation probability level for the SITA Standard algorithm and the differences in the magnitude of the Comparison probability plot for Pulsar perimetry, respectively, between Visit 1 and Visit 5 for each eye of each of the three diagnostic groups are illustrated in Table 4.11a to Table 4.11c.

SITA Standard	SITA Standard		
	NS	5%/2%	1%/0,5%
NS	1228	14	2
5%/2%	37	5	0
1%/0,5%	7	6	1

SITA Standard	SITA Standard		
	NS	5%/2%	1%/0,5%
NS	1229	21	4
5%/2%	28	8	1
1%/0,5%	8	1	0

Pulsar	Pulsar		
	NS	5%/2%	1%/0,5%
NS	1171	24	14
5%/2%	29	11	7
1%/0,5%	19	3	22

Pulsar	Pulsar		
	NS	5%/2%	1%/0,5%
NS	1222	19	4
5%/2%	27	6	0
1%/0,5%	20	1	1

Table 4.11a The magnitudes of the Total Deviation probability levels (SITA Standard) and of the Comparison probability levels (Pulsar Perimetry), respectively, between Visit 1 (ordinate) and Visit 5 (abscissa), across all locations for the normal individuals for the right eye (left column) and left eye (right column). Top: SITA Standard. Bottom: Pulsar perimetry. The shading indicates the number of locations exhibiting identical probability levels at the two examinations. The number of locations exhibiting an improvement in probability level at Visit 5 is indicated below the shading. The number of locations exhibiting a deterioration in probability level at Visit 5 is indicated above the shading.

The extent of the improvement in the Total Deviation and Comparison probability levels, respectively, between Visit 1 and Visit 5 for the normal individuals (Table 4.11a) differed between the two types of perimetry. (For the SITA Standard algorithm, 50 locations in the right eye exhibited an improvement and 16 locations exhibited a deterioration [a 3.1 fold overall improvement]; 37 locations in the left eye exhibited an improvement and 26 locations exhibited a deterioration [a 1.4 fold overall improvement]. For Pulsar perimetry, 51 locations in the right eye exhibited an improvement and 45 locations exhibited a deterioration [a 1.1 fold overall improvement]; 48 locations in the left eye exhibited improvement and 23 locations exhibited a deterioration [a 2.1 fold overall improvement]). However, the extent of the improvement for the SITA Standard algorithm was substantially greater for the

right eye than for the left eye, in contrast to Pulsar perimetry where the improvement was greater for the left than for the right eye. The majority of the locations, for each type of perimetry, which exhibited a change in probability level between the two visits, exhibited either an improvement from the 5% and 2% probability levels to normal or a deterioration from normal to the 5% or 2% probability levels.

SITA Standard

SITA Standard	NS	5%/2%	1%/0,5%
NS	1267	30	10
5%/2%	26	9	3
1%/0,5%	6	1	0

SITA Standard

SITA Standard	NS	5%/2%	1%/0,5%
NS	1236	33	9
5%/2%	36	12	4
1%/0,5%	14	5	3

Pulsar

Pulsar	NS	5%/2%	1%/0,5%
NS	1232	25	5
5%/2%	46	5	4
1%/0,5%	26	4	5

Pulsar

Pulsar	NS	5%/2%	1%/0,5%
NS	1287	19	7
5%/2%	23	4	1
1%/0,5%	7	2	2

Table 4.11b The magnitudes of the Total Deviation probability levels (SITA Standard) and of the Comparison probability levels (Pulsar Perimetry), respectively, between Visit 1 (ordinate) and Visit 5 (abscissa), across all locations for the individuals with OHT for the right eye (left column) and left eye (right column). Top: SITA Standard. Bottom: Pulsar perimetry. The shading indicates the number of locations exhibiting identical probability levels at the two examinations. The number of locations exhibiting an improvement in probability level at Visit 5 is indicated below the shading. The number of locations exhibiting a deterioration in probability level at Visit 5 is indicated above the shading.

The extent of the improvement in the Total Deviation and Comparison probability levels, respectively, between Visit 1 and Visit 5 for the individuals with OHT (Table 4.11b) again differed between the two types of perimetry. (For the SITA Standard algorithm, 33 locations in the right eye exhibited an improvement and 43 locations exhibited a deterioration [a 1.3 fold overall deterioration]; 55 locations in the left eye

exhibited an improvement and 46 locations exhibited a deterioration [a 1.2 fold overall improvement]. For Pulsar perimetry, 76 locations in the right eye exhibited an improvement and 34 locations exhibited a deterioration [a 2.2 fold overall improvement]; 32 locations in the left eye exhibited improvement and 27 locations exhibited a deterioration [a 1.2 fold overall improvement]). As was the case with the group of normal individuals, the majority of the locations, for each of the two algorithms, which exhibited a change in probability level between the two visits, exhibited either an improvement from the 5% and 2% probability levels to normal or a deterioration from normal to the 5% or 2% probability levels.

SITA Standard	SITA Standard		
	NS	5%/2%	1%/0,5%
NS	1254	33	4
5%/2%	42	4	7
1%/0,5%	5	3	52

SITA Standard	SITA Standard		
	NS	5%/2%	1%/0,5%
NS	1228	35	9
5%/2%	32	14	13
1%/0,5%	15	8	50

Pulsar	Pulsar		
	NS	5%/2%	1%/0,5%
NS	1109	54	71
5%/2%	44	15	16
1%/0,5%	24	8	63

Pulsar	Pulsar		
	NS	5%/2%	1%/0,5%
NS	1115	47	33
5%/2%	45	14	25
1%/0,5%	21	24	80

Table 4.11c The magnitudes of the Total Deviation probability levels (SITA Standard) and of the Comparison probability levels (Pulsar Perimetry), respectively, between Visit 1 (ordinate) and Visit 5 (abscissa), across all locations for the individuals with OAG for the right eye (left column) and left eye (right column). Top: SITA Standard. Bottom: Pulsar perimetry. The shading indicates the number of locations exhibiting identical probability levels at the two examinations. The number of locations exhibiting an improvement in probability level at Visit 5 is indicated below the shading. The number of locations exhibiting a deterioration in probability level at Visit 5 is indicated above the shading.

The extent of the improvement in the Total Deviation and Comparison probability levels, respectively, between Visit 1 and Visit 5 for the individuals with OAG (Table 4.11c) differed between the two types of perimetry. (For the SITA Standard algorithm, 50 locations in the right eye exhibited an improvement and 44 locations exhibited a deterioration [a 1.1 fold overall improvement]; 55 locations in the left eye exhibited an improvement and 57 locations exhibited a deterioration [exhibited parity]. Somewhat surprisingly, with Pulsar perimetry, 76 locations in the right eye exhibited an improvement and 141 locations exhibited a deterioration [a 1.9 fold overall deterioration]; 90 locations in the left eye exhibited improvement and 105 locations exhibited a deterioration [a 1.2 fold overall deterioration]). Once again, the majority of the locations, for each of the two algorithms, which exhibited a change in probability level between the two visits, exhibited either an improvement from the 5% and 2% probability levels to normal or a deterioration from normal to the 5% or 2% probability levels.

The between-visit difference (between Visits 1 and 5) for SITA Standard and for Pulsar perimetry in each group is summarized in Table 4.12 for the Total Deviation and Comparison probability level, respectively.

Algorithm	Eye	Normal	OHT	OAG
SITA Standard	RE	3.1	-1.3	1.1
	LE	1.4	1.2	1.0
Pulsar	RE	1.1	2.2	-1.9
	LE	2.1	1.2	-1.2

Table 4.12 The summary of the between-visit difference (Visits 1 and 5) expressed in terms of the ratio of the difference in the number of stimulus locations exhibiting an abnormal Total Deviation (Tables 4.11a to 4.11c) and Comparison probability level, at either Visit 1 or Visit 5, or both, for SITA Standard and Pulsar perimetry, respectively. (A positive value indicates an improvement i.e. a reduction in the number of stimulus locations exhibiting a significant, and/ or a less significant, probability level relative to Visit 1 and a negative value indicates a deterioration i.e. an increase in the number of stimulus locations exhibiting a significant and/ or more significant probability level relative to Visit 1).

4.4.2 Within-individual within-algorithm between-visit (Visits 4 and 5) variability

The within-algorithm differences between Visits 4 and 5 in the MD are illustrated in Figure 4.11a to Figure 4.11d and summarised in the Table 4.13.

Algorithm	Eye	Normal	OHT	OAG	All groups
SITA Standard	RE	1.93 dB	3.97 dB	2.50 dB	2.94 dB
	LE	2.98 dB	3.00 dB	1.85 dB	2.62 dB
Pulsar	RE	4.03 dB	4.21 dB	9.45 dB	6.44 dB
	LE	2.43 dB	3.59 dB	6.00 dB	4.26 dB

Table 4.13 The within-individual within-algorithm differences in the MD between Visits 4 and 5 expressed as the range of the limits of agreement (defined as the mean of the differences +/- 1.96SD) for the two algorithms for each eye of the three groups of individuals and for the three groups, combined.

The range of the limits of agreement for the MD between Visits 4 and 5 was again wider for Pulsar perimetry across each diagnostic group and was widest for the group with OAG. With Pulsar perimetry, the range was approximately 1.5 fold wider for the right eye than for the left eye both in the normal individuals and in the individuals with glaucoma and 1.2 fold wider for the individuals with OHT.

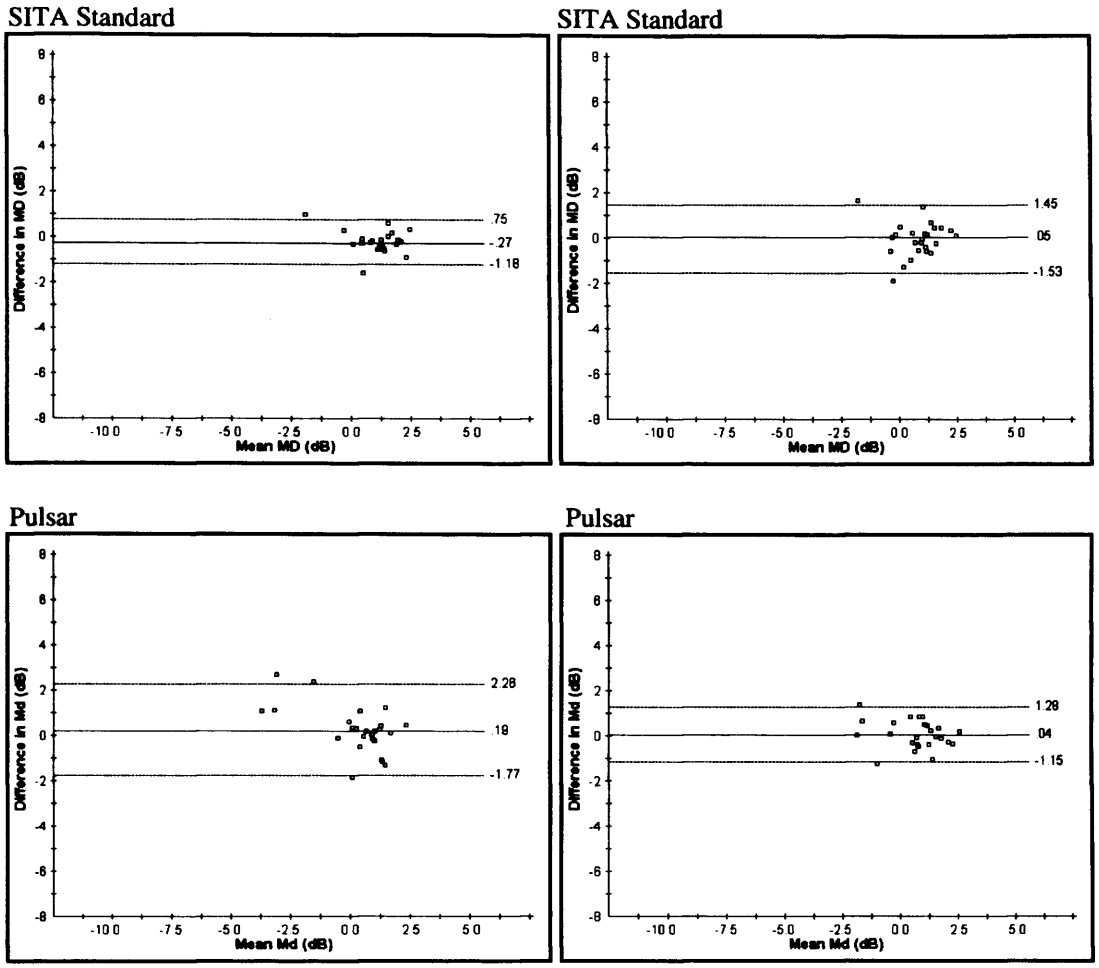

Figure 4.11a The within-individual within-algorithm difference in the MD between Visits 4 and 5 against the mean of the two MDs for the right eye (left column) and for the left eye (right column) for the normal individuals. Top: SITA Standard. Bottom: Pulsar perimetry. The solid line indicates the mean of the differences and the upper and lower dotted lines the mean of the differences +/- 1.96SD, respectively.

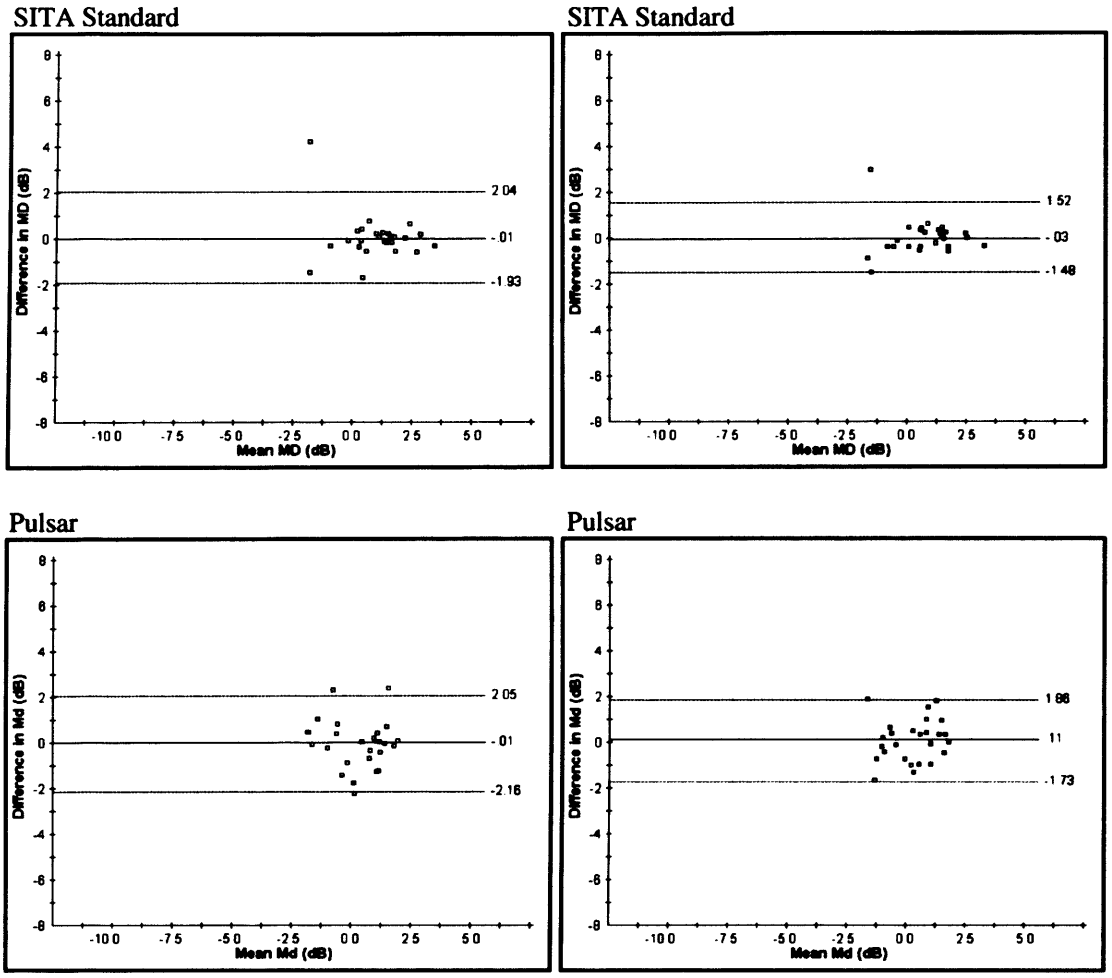

Figure 4.11b The within-individual within-algorithm difference in the MD between Visits 4 and 5 against the mean of the two MDs for the right eye (left column) and for the left eye (right column) for the individuals with OHT. Top: SITA Standard. Bottom: Pulsar perimetry. The solid line indicates the mean of the differences and the upper and lower dotted lines the mean of the differences +/- 1.96SD, respectively.

SITA Standard

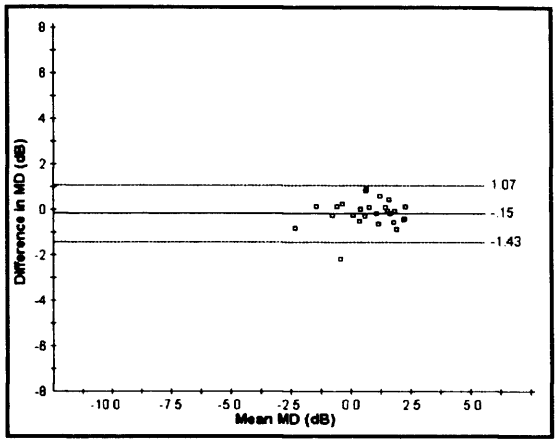

SITA Standard

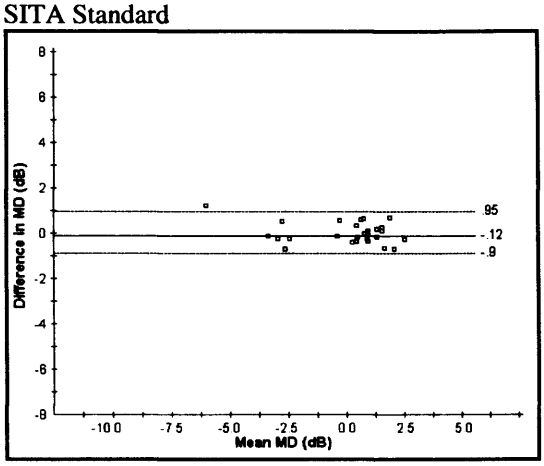

Pulsar

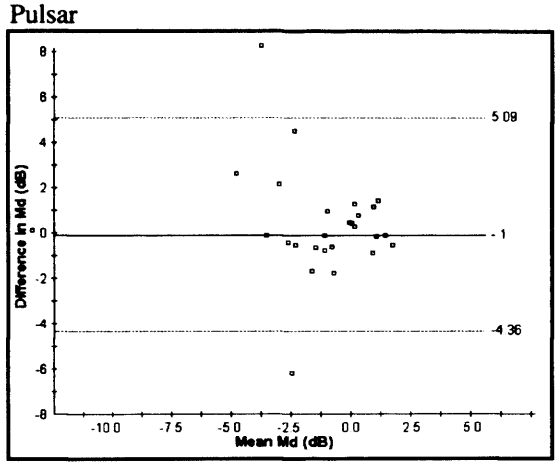

Pulsar

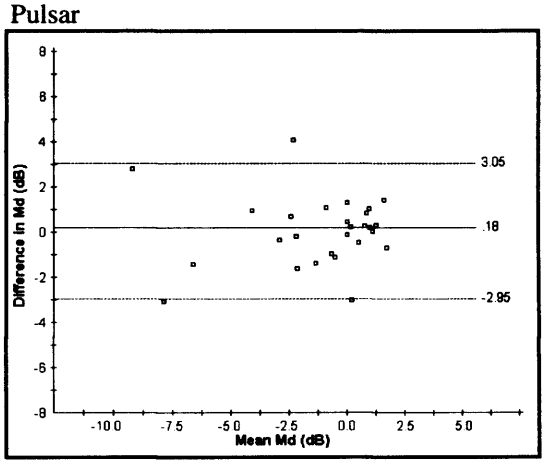

Figure 4.11c The within-individual within-algorithm difference in the MD between Visits 4 and 5 against the mean of the two MDs for the right eye (left column) and for the left eye (right column) for the individuals with OAG. Top: SITA Standard. Bottom: Pulsar perimetry. The solid line indicates the mean of the differences and the upper and lower dotted lines the mean of the differences +/- 1.96SD, respectively.

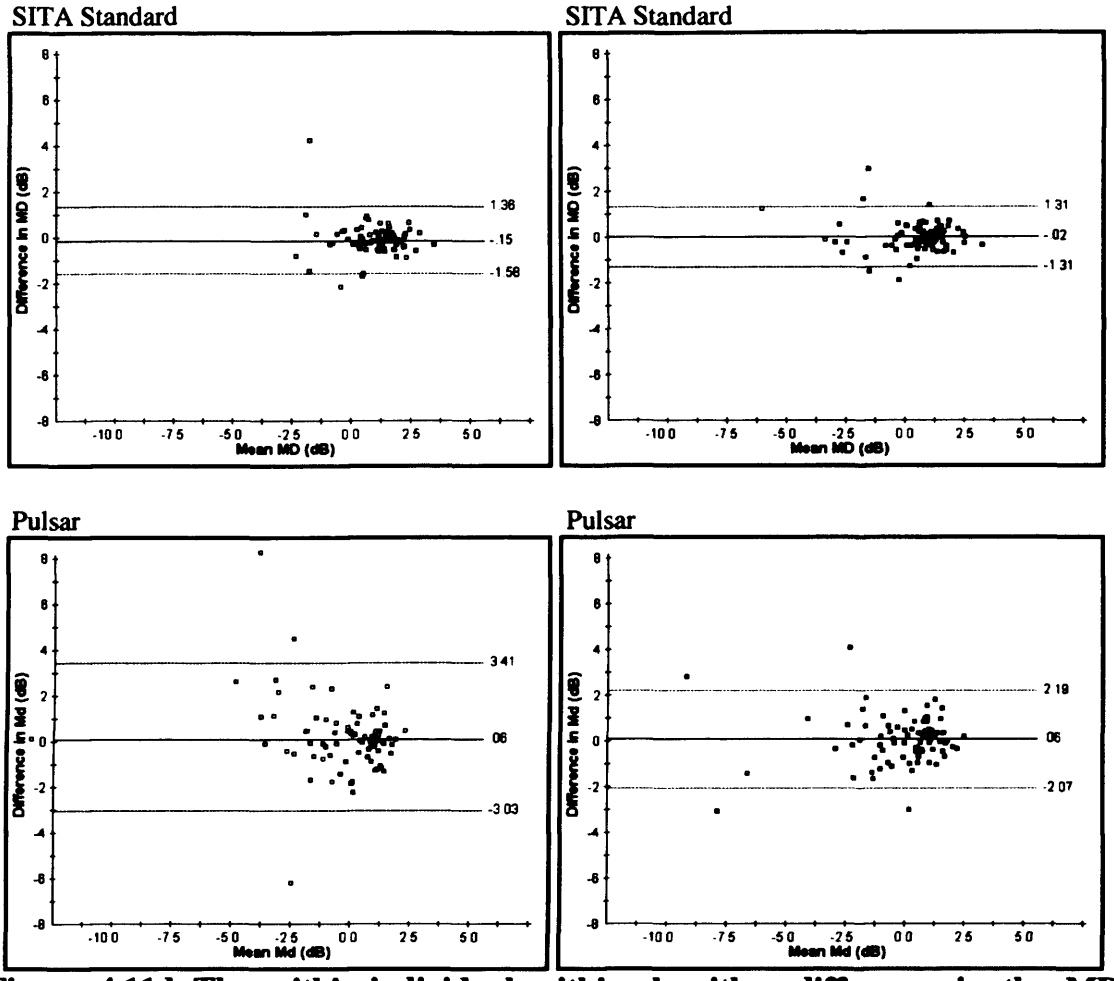

Figure 4.11d The within-individual within-algorithm difference in the MD between Visits 4 and 5 against the mean of the two MDs for the right eye (left column) and for the left eye (right column) for the three groups, combined. Top: SITA Standard. Bottom: Pulsar perimetry. The solid line indicates the mean of the differences and the upper and lower dotted lines the mean of the differences +/- 1.96SD, respectively.

The within-algorithm differences between Visits 4 and 5 in the PSD and in the sLV are illustrated in Figure 4.12a to Figure 4.12d and summarised in the Table 4.14.

Algorithm	Eye	Normal	OHT	OAG	All groups
SITA Standard	RE	1.31 dB	0.98 dB	1.67 dB	1.35 dB
	LE	1.47 dB	1.47 dB	1.50 dB	1.54 dB
Pulsar	RE	3.76 dB	3.43 dB	5.63 dB	4.38 dB
	LE	1.90 dB	2.55 dB	3.97 dB	2.94 dB

Table 4.14 The within-individual within-algorithm differences in the PSD and in the sLV between Visits 4 and 5 expressed as the range of the limits of agreement (defined as the mean of the differences +/- 1.96SD) for the two algorithms for each eye of the three groups of individuals and for the three groups, combined.

The range for the limits of agreement for the sLV of Pulsar perimetry were wider than for the PSD of the SITA Standard algorithm in all three diagnostic groups, were wider for the right eye than for the left eye and were widest for group with OAG.

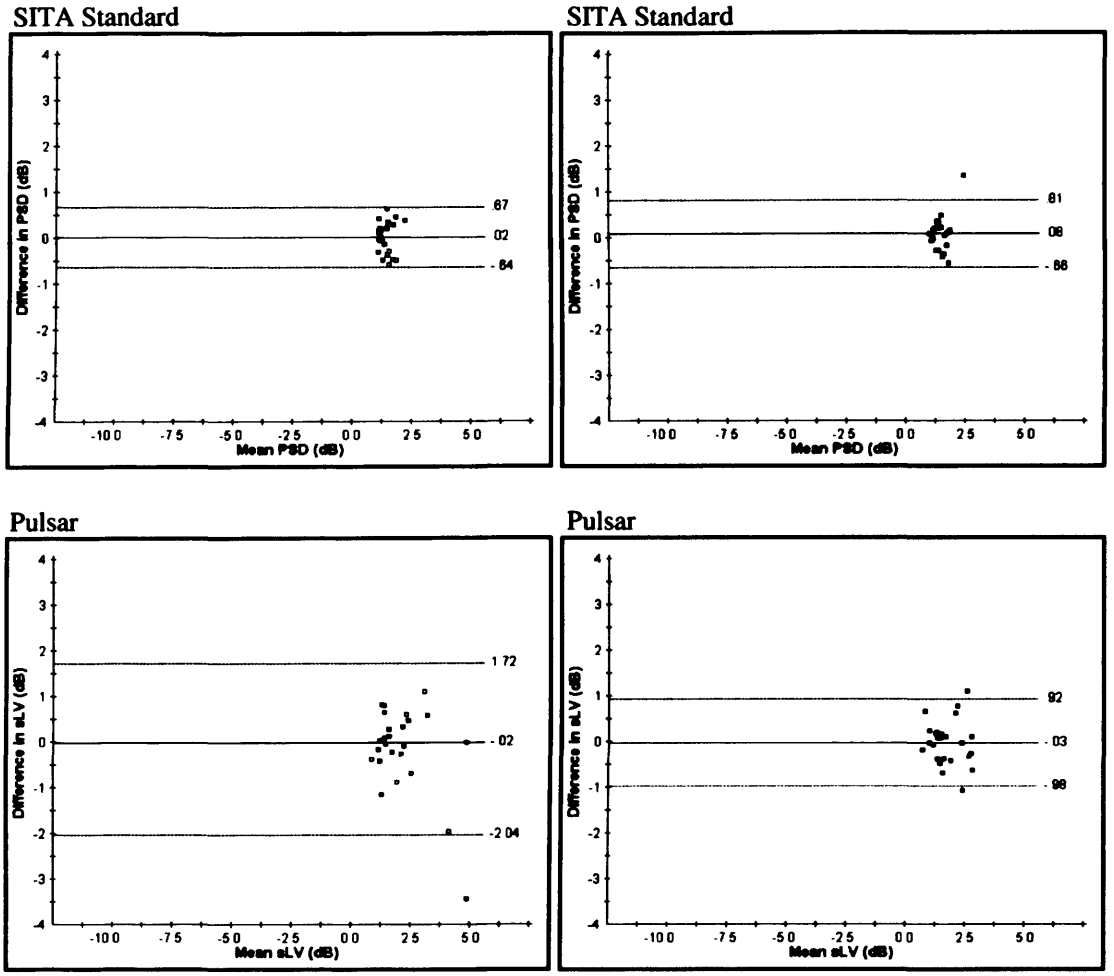

Figure 4.12a The within-individual within-algorithm difference in the PSD and sLV indices between Visits 4 and 5 against the mean of the two PSDs and the two sLVs, respectively, for the right eye (left column) and for the left eye (right column) for the normal individuals. Top: SITA Standard. Bottom: Pulsar perimetry. The solid line indicates the mean of the differences and the upper and lower dotted lines the mean of the differences +/- 1.96SD, respectively.

SITA Standard

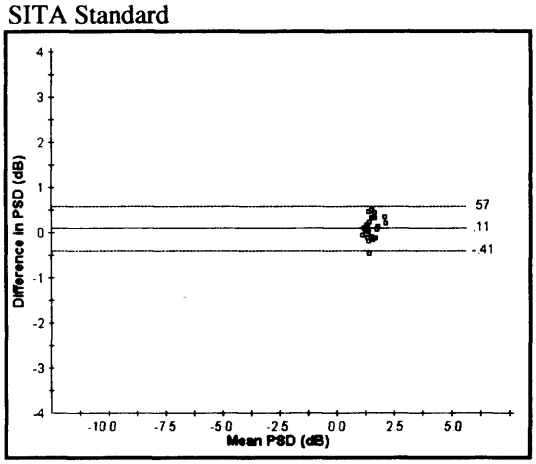

SITA Standard

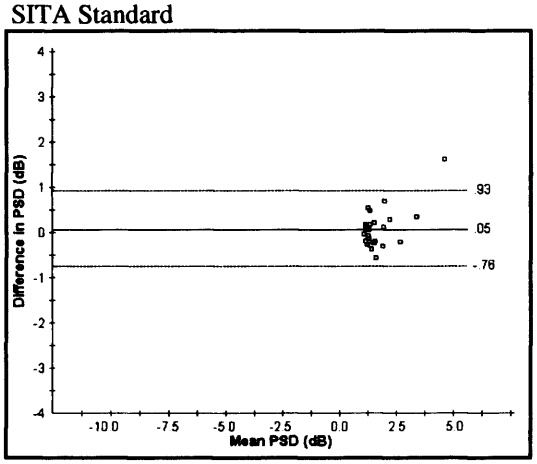

Pulsar

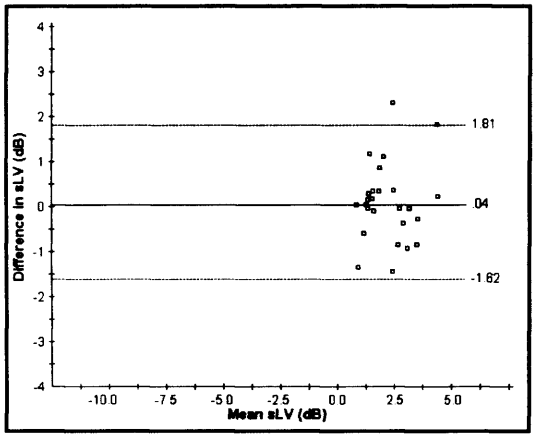

Pulsar

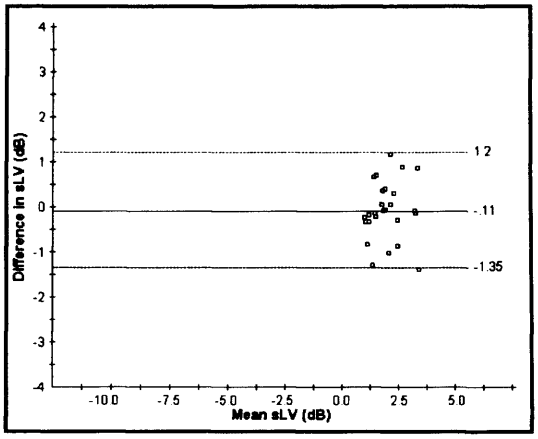

Figure 4.12b The within-individual within-algorithm difference in the PSD and sLV indices between Visits 4 and 5 against the mean of the two PSDs and the two sLVs, respectively, for the right eye (left column) and for the left eye (right column) for the individuals with OHT. Top: SITA Standard. Bottom: Pulsar perimetry. The solid line indicates the mean of the differences and the upper and lower dotted lines the mean of the differences +/- 1.96SD, respectively.

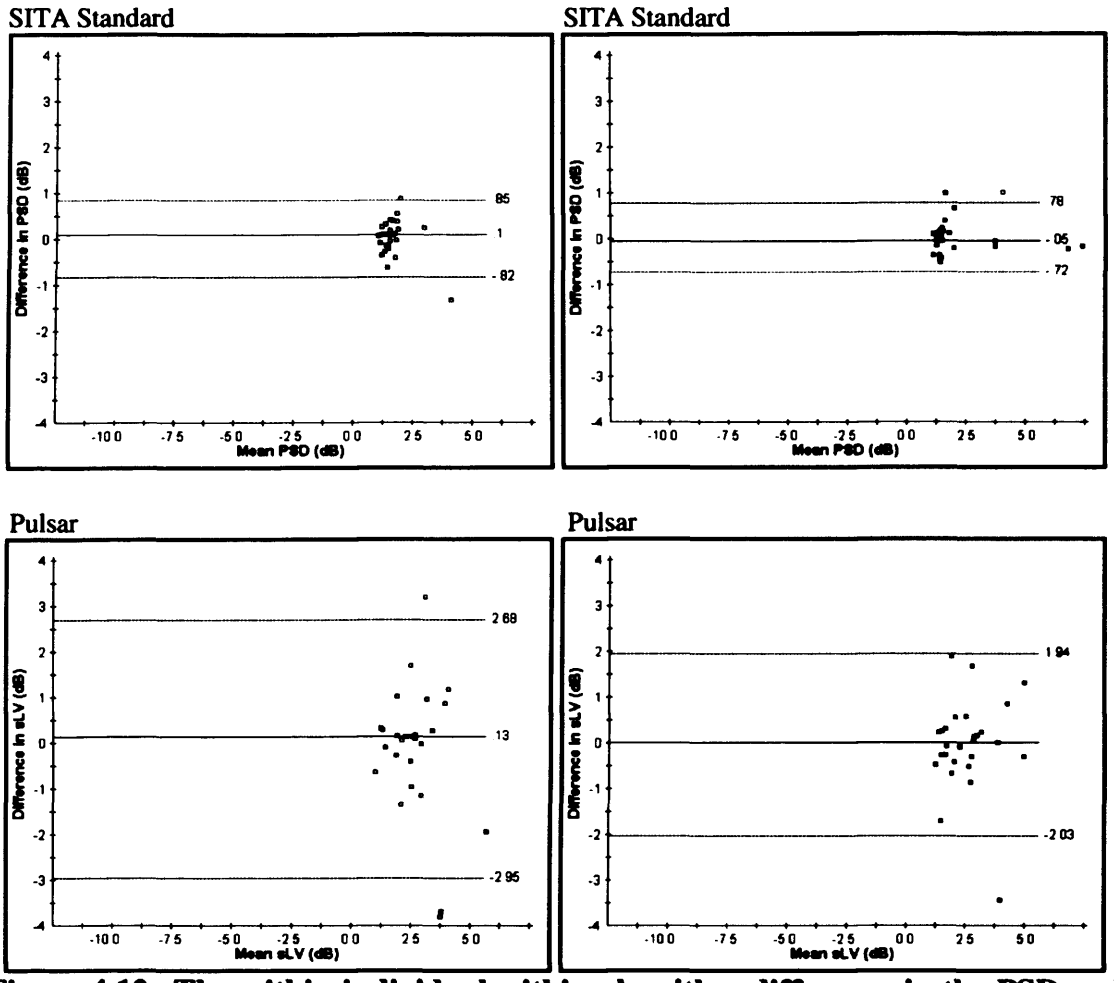

Figure 4.12c The within-individual within-algorithm difference in the PSD and sLV indices between Visits 4 and 5 against the mean of the two PSDs and the two sLVs, respectively, for the right eye (left column) and for the left eye (right column) for the individuals with OAG. Top: SITA Standard. Bottom: Pulsar perimetry. The solid line indicates the mean of the differences and the upper and lower dotted lines the mean of the differences +/- 1.96SD, respectively.

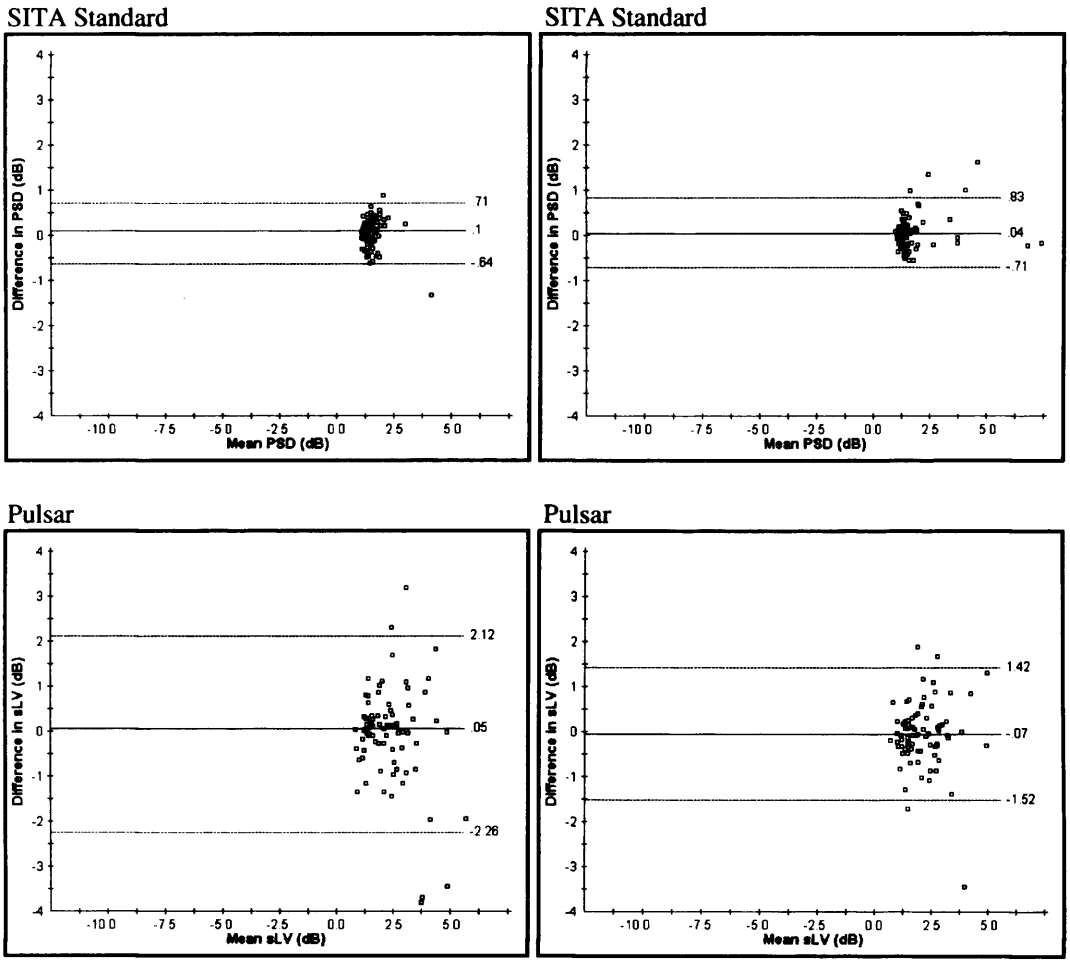

Figure 4.12d The within-individual within-algorithm difference in the PSD and sLV indices between Visits 4 and 5 against the mean of the two PSDs and the two sLVs, respectively, for the right eye (left column) and for the left eye (right column) for all three groups, combined. Top: SITA Standard. Bottom: Pulsar perimetry. The solid line indicates the mean of the differences and the upper and lower dotted lines the mean of the differences +/- 1.96SD, respectively.

The pointwise difference in dB between Visits 4 and 5 for the SITA Standard 24-2 and Pulsar CP-T30W algorithms, for all three diagnostic groups and for the right and left eyes is illustrated in the Figure 4.13a to Figure 4.13d.

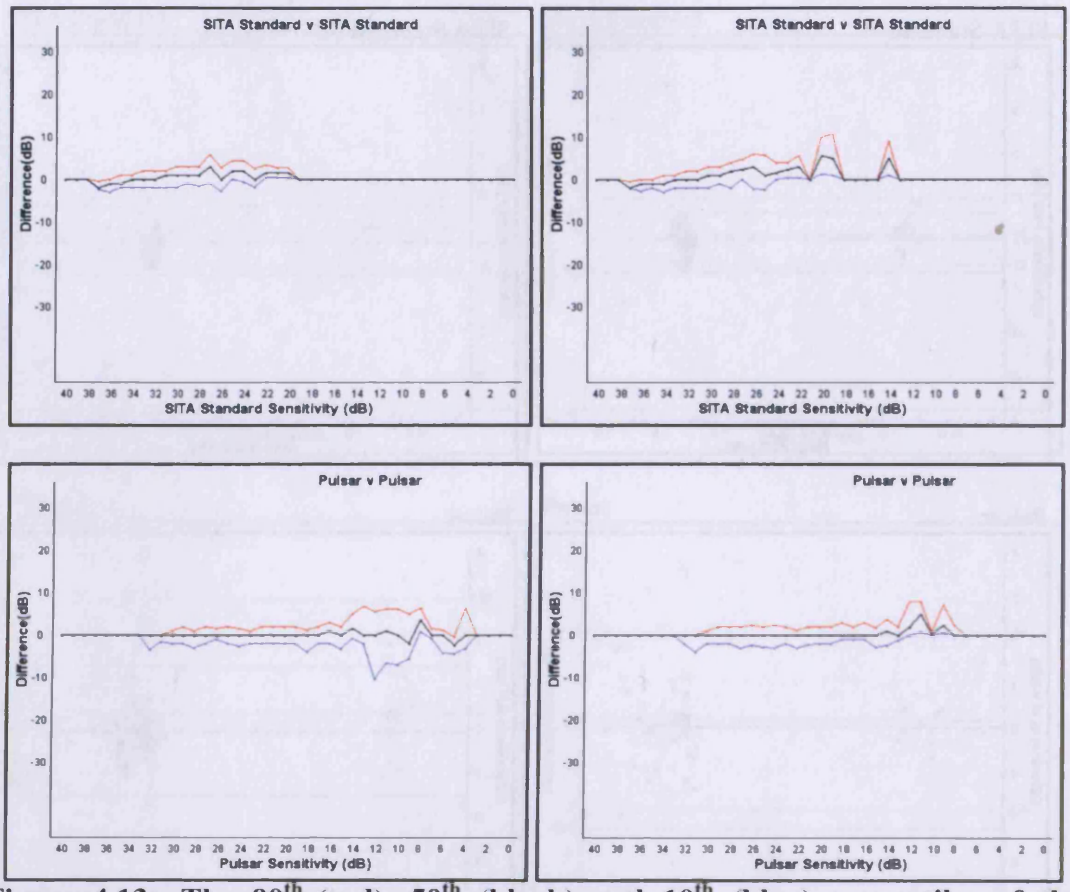

Figure 4.13a The 90th (red), 50th (black) and 10th (blue) percentiles of the distribution of the differences in sensitivity across all stimulus locations between Visit 4 and 5 as a function of the sensitivity at the corresponding stimulus location recorded at Visit 5 for the right eye (left column) and for the left eye (right column) for the normal individuals. Top: SITA Standard. Bottom: Pulsar perimetry.

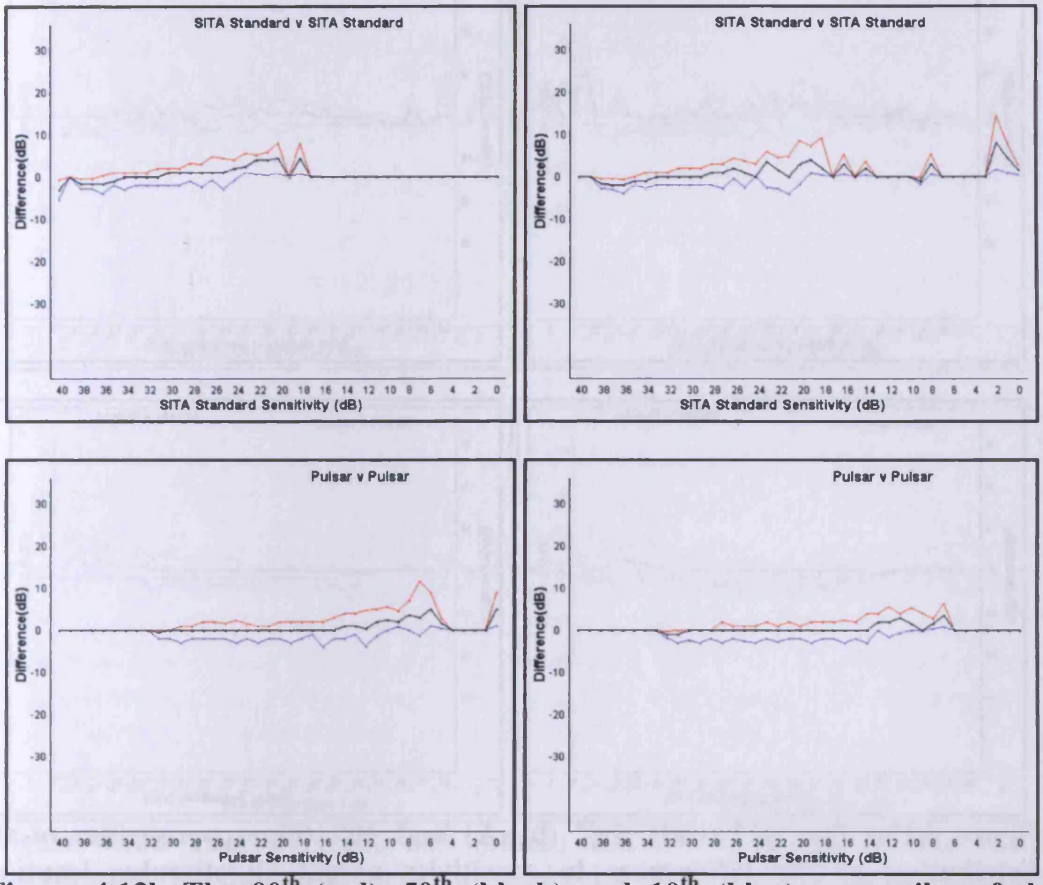

Figure 4.13b The 90th (red), 50th (black) and 10th (blue) percentiles of the distribution of the differences in sensitivity across all stimulus locations between Visit 4 and 5 as a function of the sensitivity at the corresponding stimulus location recorded at Visit 5 for the right eye (left column) and for the left eye (right column) for the individuals with OHT. Top: SITA Standard. Bottom: Pulsar perimetry.

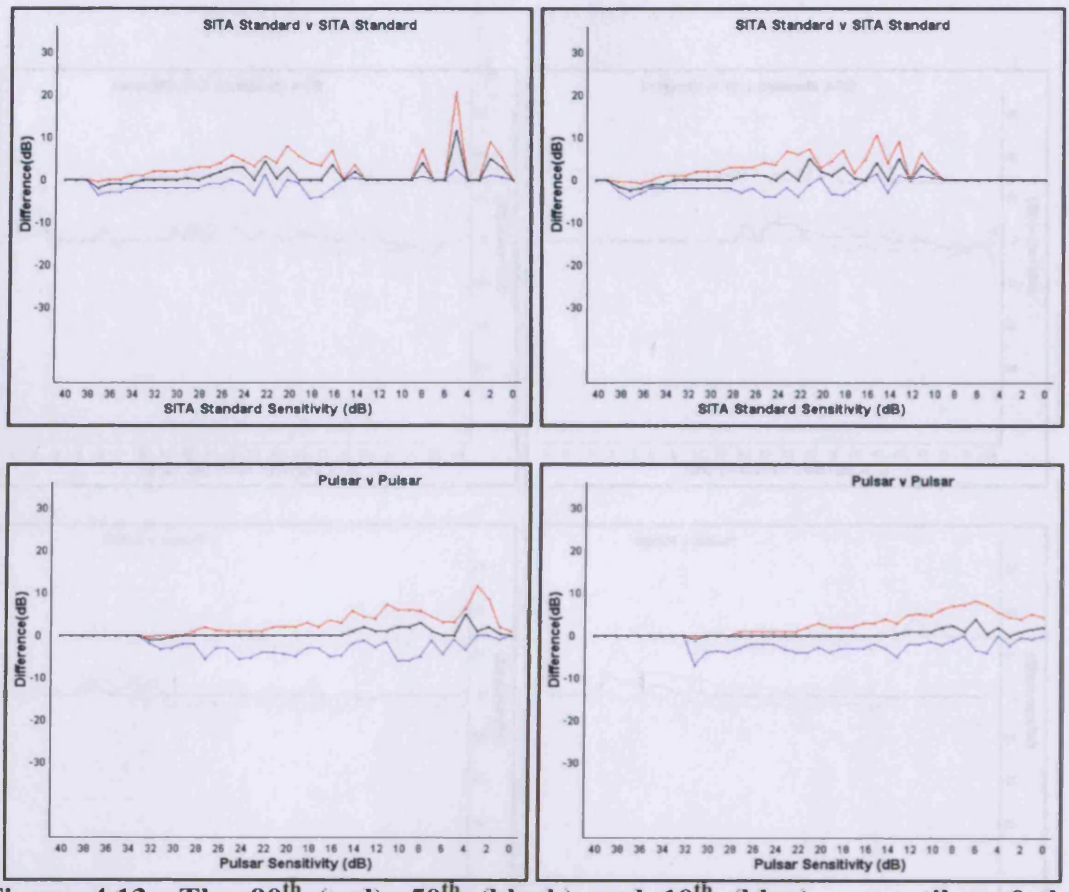

Figure 4.13c The 90th (red), 50th (black) and 10th (blue) percentiles of the distribution of the differences in sensitivity across all stimulus locations between Visit 4 and 5 as a function of the sensitivity at the corresponding stimulus location recorded at Visit 5 for the right eye (left column) and for the left eye (right column) for the individuals with OAG. Top: SITA Standard. Bottom: Pulsar perimetry.

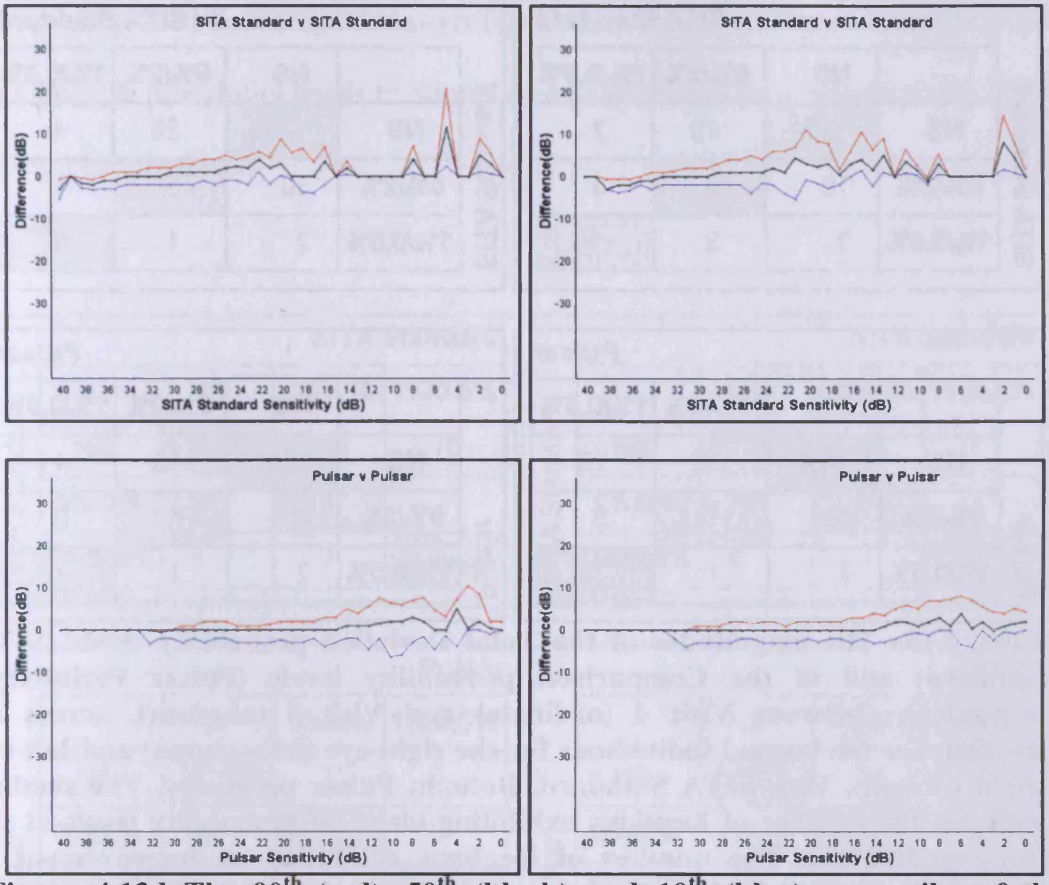

Figure 4.13d The 90th (red), 50th (black) and 10th (blue) percentiles of the distribution of the differences in sensitivity across all stimulus locations between Visit 4 and 5 as a function of the sensitivity at the corresponding stimulus location recorded at Visit 5 for the right eye (left column) and for the left eye (right column) of the individuals in all three diagnostic categories. Top: SITA Standard. Bottom: Pulsar perimetry.

The differences in the magnitude of the Total Deviation probability level (TD) for the HFA and Comparison Probability plot for the Pulsar perimeter, respectively, between Visit 4 and Visit 5 for the SITA Standard 24-2 and the Pulsar CP- T30W algorithms, for all diagnostic groups on both eyes are illustrated in the tables below, Table 4.15a to Table 4.15c.

SITA Standard	NS	5%/2%	1%/0,5%
NS	1254	13	2
5%/2%	16	9	0
1%/0,5%	2	3	1

SITA Standard	NS	5%/2%	1%/0,5%
NS	1233	26	4
5%/2%	30	3	1
1%/0,5%	2	1	0

Pulsar	NS	5%/2%	1%/0,5%
NS	1198	26	20
5%/2%	14	11	8
1%/0,5%	7	1	15

Pulsar	NS	5%/2%	1%/0,5%
NS	1247	19	4
5%/2%	20	6	0
1%/0,5%	2	1	1

Table 4.15a The magnitudes of the Total Deviation probability levels (SITA Standard) and of the Comparison probability levels (Pulsar Perimetry), respectively, between Visit 4 (ordinate) and Visit 5 (abscissa), across all locations for the normal individuals for the right eye (left column) and left eye (right column). Top: SITA Standard. Bottom: Pulsar perimetry. The shading indicates the number of locations exhibiting identical probability levels at the two examinations. The number of locations exhibiting an improvement in probability level at Visit 5 is indicated below the shading. The number of locations exhibiting a deterioration in probability level at Visit 5 is indicated above the shading.

The extent of the improvement in the Total Deviation and Comparison probability levels, respectively, between Visit 4 and Visit 5 for the normal individuals (Table 4.15a) differed between the two types of perimetry. (For the SITA Standard algorithm, 21 locations in the right eye exhibited an improvement and 15 locations exhibited a deterioration [a 1.4 fold overall improvement]; 33 locations in the left eye exhibited an improvement and 31 locations exhibited a deterioration [a 1.1 fold overall improvement]. For Pulsar perimetry, 22 locations in the right eye exhibited an improvement and 54 locations exhibited a deterioration [a 2.5 fold overall deterioration]; 23 locations in the left eye exhibited an improvement and 23 locations exhibited a deterioration [exhibited parity]). Once again, the majority of the stimulus locations, for each of the two algorithms, which exhibited a change in

probability level between the two visits, exhibited either an improvement from the 5% and 2% probability levels to normal or a deterioration from normal to the 5% or 2% probability levels.

SITA Standard			
SITA Standard	NS	5%/2%	1%/0,5%
NS	1270	30	10
5%/2%	24	8	2
1%/0,5%	5	2	1

SITA Standard			
SITA Standard	NS	5%/2%	1%/0,5%
NS	1255	32	7
5%/2%	25	14	3
1%/0,5%	6	4	6

Pulsar			
Pulsar	NS	5%/2%	1%/0,5%
NS	1265	21	8
5%/2%	30	9	3
1%/0,5%	9	4	3

Pulsar			
Pulsar	NS	5%/2%	1%/0,5%
NS	1302	20	7
5%/2%	12	4	1
1%/0,5%	3	1	2

Table 4.15b The magnitudes of the Total Deviation probability levels (SITA Standard) and of the Comparison probability levels (Pulsar Perimetry), respectively, between Visit 4 (ordinate) and Visit 5 (abscissa), across all locations for the individuals with OHT for the right eye (left column) and left eye (right column). Top: SITA Standard. Bottom: Pulsar perimetry. The shading indicates the number of locations exhibiting identical probability levels at the two examinations. The number of locations exhibiting an improvement in probability level at Visit 5 is indicated below the shading. The number of locations exhibiting a deterioration in probability level at Visit 5 is indicated above the shading.

The extent of the improvement in the Total Deviation and Comparison probability levels, respectively, between Visit 4 and Visit 5 for the individuals with OHT (Table 4.15b) again differed between the two types of perimetry. (For the SITA Standard algorithm, 31 locations in the right eye exhibited an improvement and 42 locations exhibited a deterioration [a 1.4 fold overall deterioration]; 35 locations in the left eye exhibited an improvement and 42 locations exhibited a deterioration [a 1.2 fold overall deterioration]. For Pulsar perimetry, 43 locations in the right eye exhibited

an improvement and 32 locations exhibited a deterioration [a 1.3 fold overall improvement]; 16 locations in the left eye exhibited an improvement and 28 locations exhibited a deterioration [a 1.8 fold overall deterioration]). As was also the case for the normal individuals, the majority of the locations, for each of the two algorithms, which exhibited a change in probability level between the two visits, exhibited either an improvement from the 5% and 2% probability levels to normal or a deterioration from normal to the 5% or 2% probability levels.

SITA Standard	SITA Standard		
	NS	5%/2%	1%/0,5%
NS	1256	26	2
5%/2%	33	11	5
1%/0,5%	12	3	56

SITA Standard	SITA Standard		
	NS	5%/2%	1%/0,5%
NS	1219	26	15
5%/2%	42	20	12
1%/0,5%	14	11	45

Pulsar	Pulsar		
	NS	5%/2%	1%/0,5%
NS	1079	44	63
5%/2%	64	21	15
1%/0,5%	34	12	72

Pulsar	Pulsar		
	NS	5%/2%	1%/0,5%
NS	1104	36	22
5%/2%	57	30	12
1%/0,5%	20	19	104

Table 4.15c The magnitudes of the Total Deviation probability levels (SITA Standard) and of the Comparison probability levels (Pulsar Perimetry), respectively, between Visit 4 (ordinate) and Visit 5 (abscissa), across all locations for the individuals with OAG for the right eye (left column) and left eye (right column). Top: SITA Standard. Bottom: Pulsar perimetry. The shading indicates the number of locations exhibiting identical probability levels at the two examinations. The number of locations exhibiting an improvement in probability level at Visit 5 is indicated below the shading. The number of locations exhibiting a deterioration in probability level at Visit 5 is indicated above the shading.

The extent of the improvement in the Total Deviation and Comparison probability levels, respectively, between Visit 4 and Visit 5 for the individuals with OAG (Table 4.15c) again differed between the two types of perimetry. (For the SITA Standard

algorithm, 48 locations in the right eye exhibited an improvement and 33 locations exhibited a deterioration [a 1.5 fold overall improvement]; 67 locations in the left eye exhibited an improvement and 53 locations exhibited a deterioration [a 1.3 fold overall improvement]. For Pulsar perimetry, 110 locations in the right eye exhibited an improvement and 122 locations exhibited a deterioration [a 1.1 fold overall deterioration]; 96 locations in the left eye exhibited an improvement and 70 locations exhibited a deterioration [a 1.4 fold overall improvement]). As was the case for the other two groups, the majority of the locations, for each of the two algorithms, which exhibited a change in probability level between the two visits, exhibited either an improvement from the 5% and 2% probability levels to normal or a deterioration from normal to the 5% or 2% probability levels.

The between-visit difference (between Visits 4 and 5) for SITA Standard and for Pulsar perimetry in each group is summarized in Table 4.16 for the Total Deviation and Comparison probability level, respectively.

Algorithm	Eye	Normal	OHT	OAG
SITA Standard	**RE**	1.4	-1.4	1.5
	LE	1.1	-1.2	1.3
Pulsar	**RE**	-2.5	1.3	-1.1
	LE	1.0	-1.8	1.4

Table 4.16 The summary of the ratio of the between-visit difference (Visits 4 and 5) expressed in terms of the ratio of the difference in the number of stimulus locations exhibiting an abnormal Total Deviation (Tables 4.15a to 4.15c) and Comparison probability level for SITA Standard and Pulsar perimetry, respectively. (A positive value indicates an improvement i.e. a reduction in the number of stimulus locations exhibiting a significant, and/ or a less significant, probability level relative to Visit 4 and a negative value indicates a deterioration i.e. an increase in the number of stimulus locations exhibiting a significant and/ or more significant probability level relative to Visit 4).

4.4.3 The between-individual within-visit (Visit 5) between-algorithm variability

The between-algorithm differences at Visit 5 in the MD are illustrated in Figures 4.14a and 4.14b and are summarised in Table 4.17.

Algorithm	Eye	Normal	OHT	OAG	All groups
SITA Standard v Pulsar	RE	6.76 dB	5.95 dB	9.49 dB	7.67 dB
	LE	4.22 dB	4.95 dB	6.40 dB	5.52 dB

Table 4.17 The between-algorithm differences in the MD at Visit 5 expressed as the range of the limits of agreement (defined as the mean of the differences +/- 1.96SD) for the two algorithms for each eye of the three groups of individuals and for the three groups, combined.

The range of the limits of agreement for the MD was approximately 1.4 fold greater for the right eye compared to the left eye in all three diagnostic groups and was widest for the individuals with OAG. The mean of the differences indicated that the MD for SITA Standard was approximately 0.6dB more positive than that for the Pulsar perimeter.

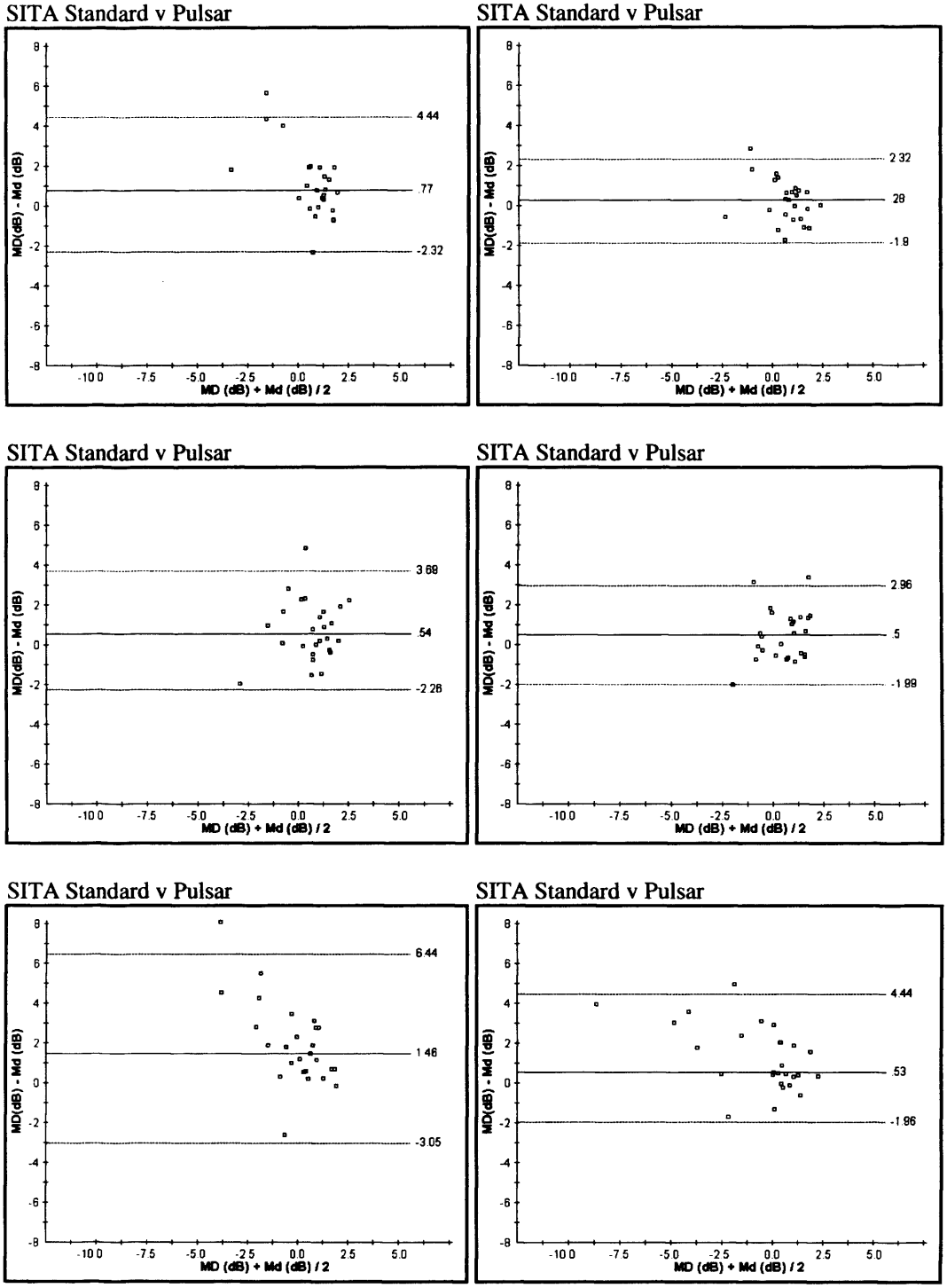

Figure 4.14a The within-individual between-algorithm difference in the MD indices at Visit 5 against the mean of the two MDs for the right eye (left column) and for the left eye (right column). Top: normal individuals. Middle: individuals with OHT. Bottom: individual with OAG. The solid line indicates the mean of the differences and the upper and lower dotted lines the mean of the differences +/- 1.96SD, respectively.

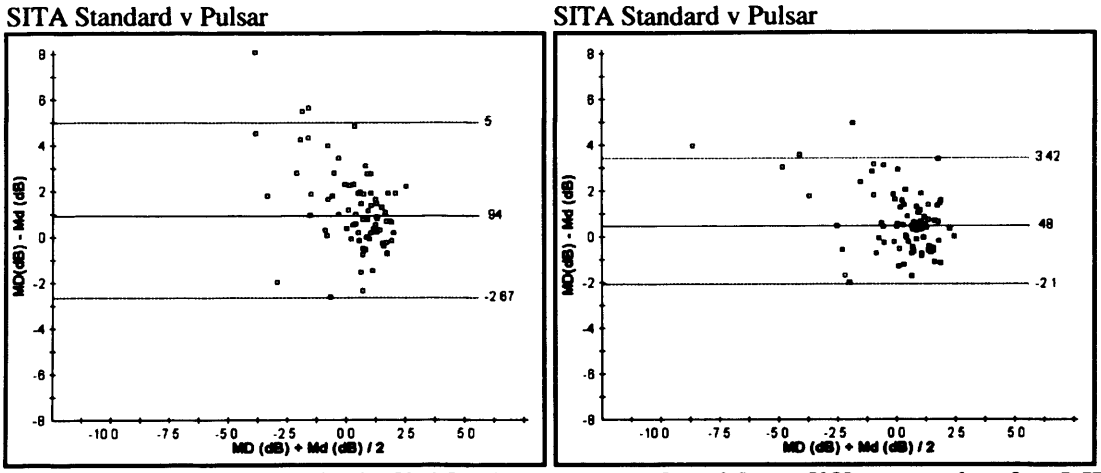

Figure 4.14b The within-individual between-algorithm difference in the MD indices at Visit 5 against the mean of the two MDs for the right eye (left column) and for the left eye (right column) for the three groups, combined. The solid line indicates the mean of the differences and the upper and lower dotted lines the mean of the differences +/- 1.96SD, respectively.

The between-algorithm differences at Visit 5 in the PSD and sLV are illustrated in Figures 4.15a and 4.15b and are summarised in Table 4.18.

Algorithm	Eye	Normal	OHT	OAG	All groups
SITA Standard v Pulsar	RE	5.58 dB	3.99 dB	8.67 dB	6.35 dB
	LE	2.56 dB	3.35 dB	5.23 dB	3.86 dB

Table 4.18 The between-algorithm differences in the PSD and sLV at Visit 5 expressed as the range of the limits of agreement (defined as the mean of the differences +/- 1.96SD) for the two algorithms for each eye of the three groups of individuals and for the three groups, combined.

The range of the limits of agreement between the PSD and sLV was approximately 1.6 fold greater for the right eye compared to the left eye in all three diagnostic groups wider and was widest for the individuals with OAG. The mean of the differences indicated that the sLV for the Pulsar perimeter was approximately 0.6dB more positive than that for the SITA Standard algorithm.

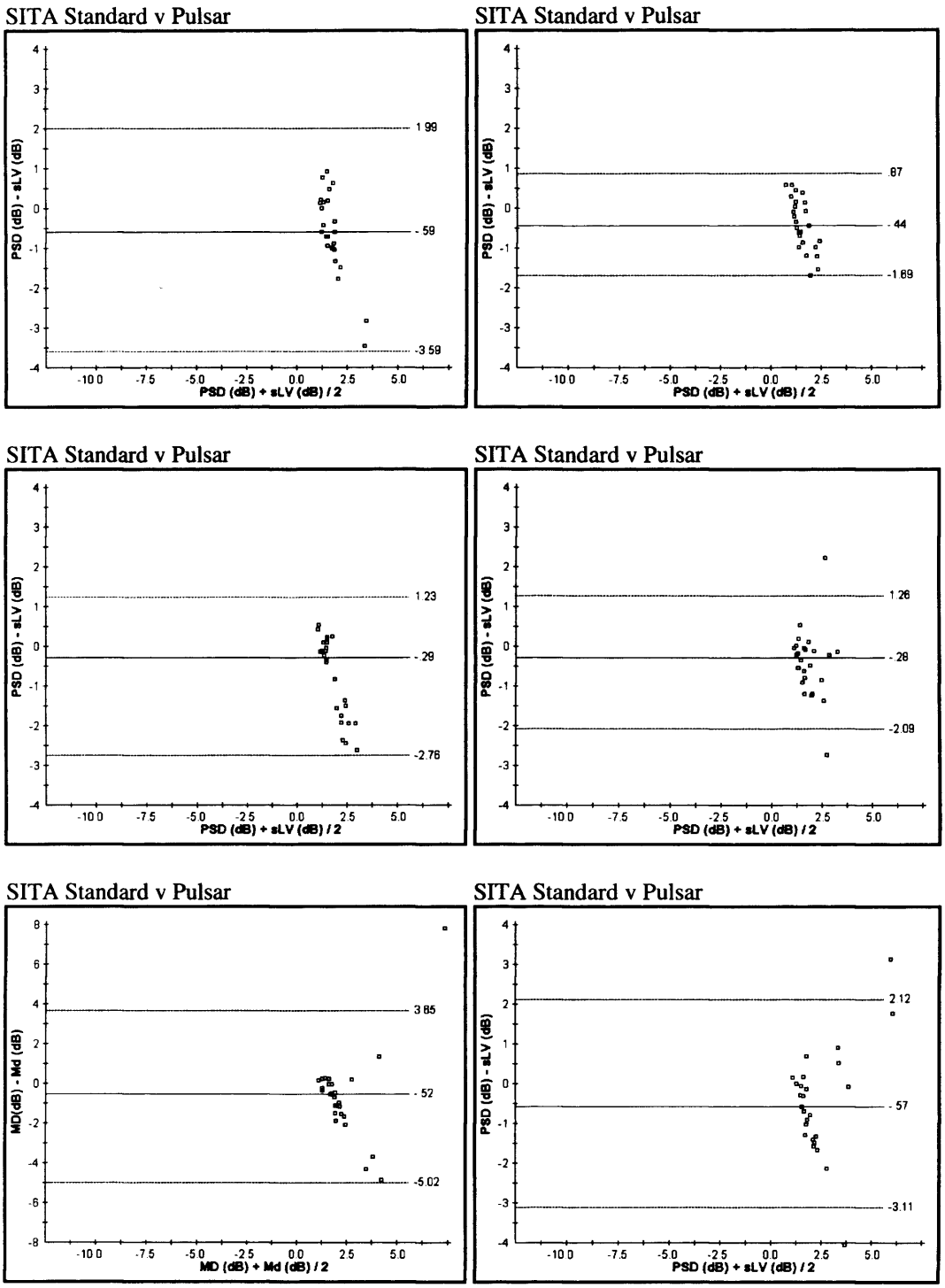

Figure 4.15a The within-individual between-algorithm difference in the PSD and sLV indices at Visit 5 against the mean of the two PSDs and the two sLVs, respectively, for the right eye (left column) and for the left eye (right column). Top: normal individuals. Middle: individuals with OHT. Bottom: individual with OAG. The solid line indicates the mean of the differences and the upper and lower dotted lines the mean of the differences +/- 1.96SD, respectively. Note the difference in the scaling of the ordinate in the right eye for the SITA Standard, Pulsar perimetry comparison.

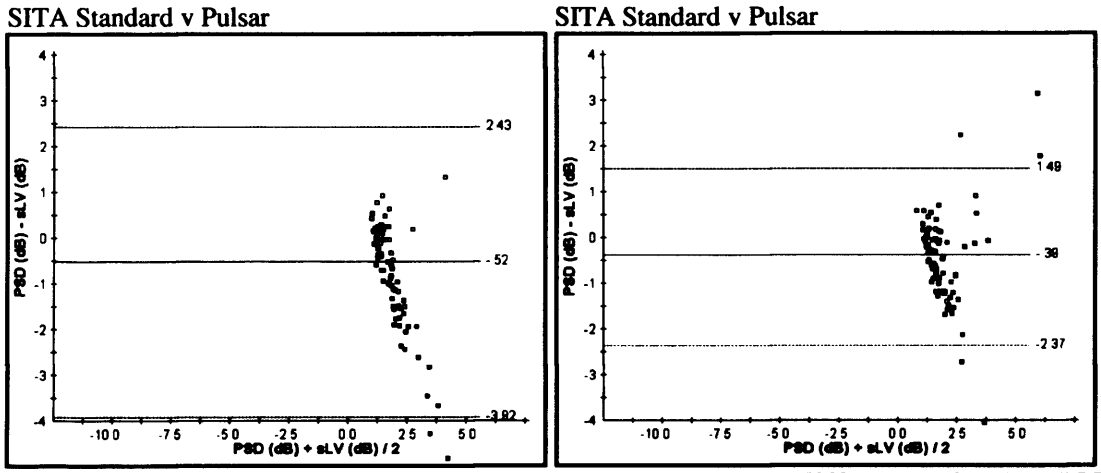

Figure 4.15b The within-individual between-algorithm difference in the PSD and sLV indices at Visit 5 against the mean of the two PSDs and the two sLVs, respectively, for the right eye (left column) and for the left eye (right column) for all three groups, combined. The solid line indicates the mean of the differences and the upper and lower dotted lines the mean of the differences +/- 1.96SD, respectively.

The 10th, 50th and 90th percentiles of the distribution of the variability in sensitivity at each sensitivity level between the SITA Standard 24-2 and the Pulsar CP-T30W algorithms at Visit 5, for each diagnostic group and for both eyes (right and left) are illustrated in Figures 4.16a and 4.16b. The Pulsar perimeter, as might be expected from Table 4.4, yielded a sensitivity in the region of 9-10dB less than that obtained with the SITA Standard algorithm across all three diagnostic groups and this difference was approximately the same at all values of sensitivity between approximately 31 and 18dB derived by the SITA Standard algorithm.

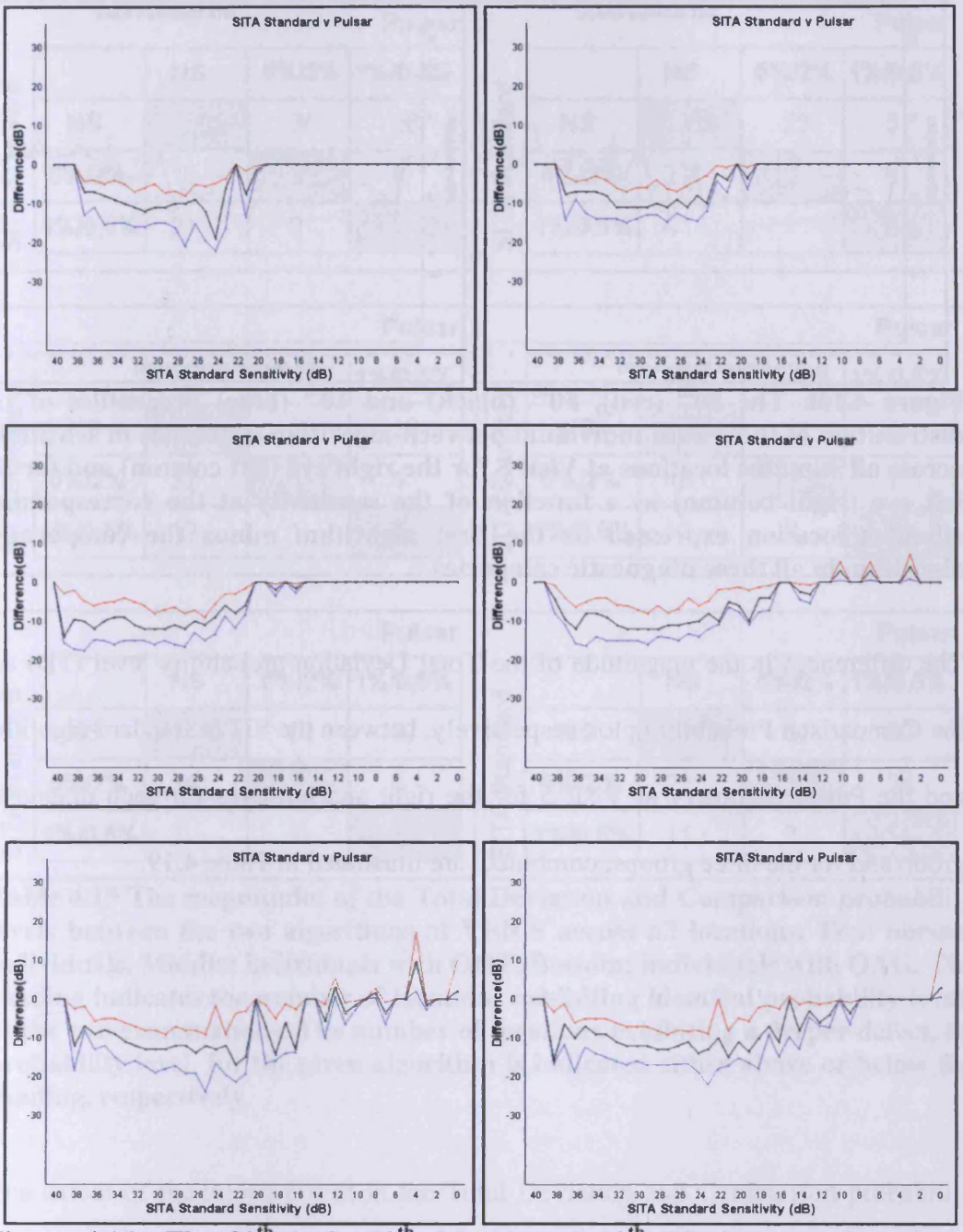

Figure 4.16a The 90th (red), 50th (black) and 10th (blue) percentiles of the distribution of the within-individual between-algorithm difference in sensitivity across all stimulus locations at Visit 5 for the right eye (left column) and for the left eye (right column) as a function of the sensitivity at the corresponding stimulus location expressed as the first algorithm minus the comparative algorithm. Top: normal individual. Middle: individual with OHT. Bottom: individual with OAG.

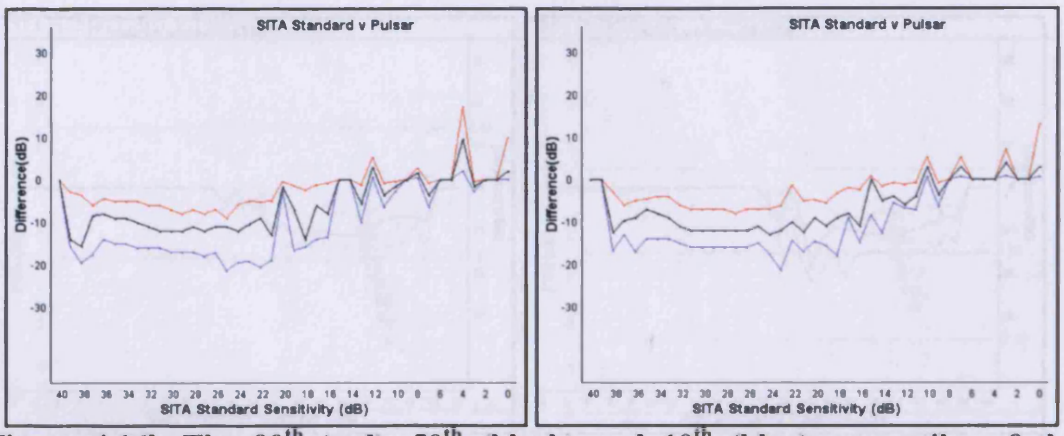

Figure 4.16b The 90th (red), 50th (black) and 10th (blue) percentiles of the distribution of the within-individual between-algorithm difference in sensitivity across all stimulus locations at Visit 5 for the right eye (left column) and for the left eye (right column) as a function of the sensitivity at the corresponding stimulus location expressed as the first algorithm minus the comparative algorithm in all three diagnostic categories.

The differences in the magnitude of the Total Deviation probability level (TD) and the Comparison Probability plot, respectively, between the SITA Standard algorithm and the Pulsar perimetry at Visit 5 for the right and left eyes for each diagnostic group and for the three groups, combined, are illustrated in Table 4.19.

SITA Standard	Pulsar		
	NS	5%/2%	1%/0,5%
NS	1201	35	36
5%/2%	16	3	6
1%/0,5%	2	0	1

SITA Standard	Pulsar		
	NS	5%/2%	1%/0,5%
NS	1238	22	5
5%/2%	27	3	0
1%/0,5%	4	1	0

SITA Standard	Pulsar		
	NS	5%/2%	1%/0,5%
NS	1260	29	10
5%/2%	32	4	4
1%/0,5%	12	1	0

SITA Standard	Pulsar		
	NS	5%/2%	1%/0,5%
NS	1258	21	7
5%/2%	46	2	2
1%/0,5%	13	2	1

SITA Standard	Pulsar		
	NS	5%/2%	1%/0,5%
NS	1148	68	87
5%/2%	24	8	8
1%/0,5%	7	1	55

SITA Standard	Pulsar		
	NS	5%/2%	1%/0,5%
NS	1148	67	60
5%/2%	22	11	24
1%/0,5%	11	7	54

Table 4.19 The magnitudes of the Total Deviation and Comparison probability levels between the two algorithms at Visit 5 across all locations. Top: normal individuals. Middle: individuals with OHT. Bottom: individuals with OAG. The shading indicates the number of locations exhibiting identical probability levels at the two examinations. The number of locations exhibiting a deeper defect, by probability level, for the given algorithm is indicated either above or below the shading, respectively.

The extent of the improvement in the Total Deviation and Comparison probability levels, respectively, at Visit 5 for the normal individuals (Table 4.19) differed between the two types of perimetry. (Pulsar perimetry tended to overestimate the presence of visual field loss for the right eye [by 4.3 fold] compared to that for the SITA Standard algorithm and to underestimate the presence of visual field loss for the left eye [by 1.2 fold]. The corresponding values for the individuals with OHT were in parity for the right eye and overestimated by two fold the left eye. The SITA Standard algorithm tended to overestimate the presence of visual field loss

compared to Pulsar perimetry for the left eye. However, Pulsar perimetry overestimated the presence of apparent visual field loss for each eye of the individuals with OAG [namely by 5.1 fold for the right eye and by 3.8 fold for the left eye]).

The between-algorithm performance for SITA Standard and Pulsar perimetry in terms of the ratio of the difference in the magnitude of the Total Deviation and Comparison probability levels, respectively, is summarized in Table 4.20 and clearly indicates apparent deeper and/ or wider field loss for the individuals with OAG compared to that obtained with the SITA Standard algorithm. However, such a finding needs to be treated with caution given the presence of a similar finding for the right eye of the normal individuals.

Algorithm	Eye	Normal	OHT	OAG
SITA Standard	RE	-4.3	1.0	-5.1
v Pulsar	LE	1.2	2.0	-3.8

Table 4.20 The summary of the between-algorithm performance (Visits 5) for SITA Standard and Pulsar perimetry expressed in terms of the ratio of the difference in the number of stimulus locations exhibiting an abnormal Total Deviation and Comparison probability level, respectively, (Table 4.19) for each group. (A positive value indicates less field loss i.e. either a fewer number of stimulus locations exhibiting a significant, or a less significant, probability level relative to the SITA Standard algorithm and a negative value indicates more field loss i.e. a greater number of stimulus locations exhibiting a significant, or a more significant, probability level relative to the SITA Standard algorithm).

The extent of the within-algorithm variability at each stimulus location for the normal individuals provides some indication of the confidence intervals for normality for the given algorithm. The Coefficient of Variation (CoV) (the standard deviation divided by the mean) at each stimulus location for each of the two

algorithms at Visits 1 and 5 for each eye is given in Figure 4.17a to Figure 4.17h. The use of the CoV overcomes the difference in the dynamic ranges between SAP and Pulsar perimetry. As would be expected, the CoV increased with increase in eccentricity for both types of perimetry and was greater nasally than temporally and greater superiorly than inferiorly. The CoV was larger for Pulsar perimetry than for the SITA Standard algorithm. The CoVs for each type of perimetry were broadly similar between the two visits. The latter difference is illustrated by the ratio of the CoV for each type of perimetry, expressed as the CoV for Pulsar perimetry against the CoV for SITA Standard perimetry. The ratio at each stimulus location for each eye at Visit 1 and at Visit 5 is given in Figure 4.18a to Figure 4.18d. The magnitude of the ratio was 1.5 to 2 in the central region and as much 2 to 3 in the peripheral zones. This indicates firstly that the between-individual normal variability was greater for Pulsar perimetry than for the SITA Standard algorithm and secondly that the increase in the between-individual normal variability with increase in eccentricity was greater for Pulsar perimetry than for the SITA Standard algorithm.

		10.90	12.18	10.55	11.62		
	7.91	5.45	6.03	8.12	8.55	9.17	
8.15	5.88	4.34	3.67	6.32	8.71	8.60	9.93
8.53	6.07	5.20	3.71	3.56	4.52	5.65	7.04
8.43	5.78	4.24	3.42	3.74	3.75	4.98	10.79
7.28	3.78	3.66	5.29	3.87	3.56	6.52	6.43
	6.49	3.14	3.52	5.23	4.89	6.05	
		7.04	6.48	9.74	8.46		

Figure 4.17a The CoV (the SD divided by the mean) expressed as a percentage for the right eye of the normal individuals at each stimulus location for the SITA Standard algorithm at Visit 1.

> 10	> 14	> 18	> 22	> 26	> 30

		11.00	11.19	8.06	8.20		
	9.69	6.78	6.92	5.86	5.62	8.77	
7.92	5.67	4.50	4.16	4.28	5.91	7.06	9.26
11.00	6.15	6.10	3.48	3.50	3.90	4.76	7.12
10.54	5.35	3.87	3.38	4.73	4.03	4.74	4.46
7.70	6.76	4.37	4.24	3.87	4.96	6.22	5.28
	7.77	4.59	4.06	4.50	4.31	5.31	
		6.84	7.37	5.86	6.37		

Figure 4.17b The CoV (the SD divided by the mean) expressed as a percentage for the left eye of the normal individuals at each stimulus location for the SITA Standard algorithm at Visit 1. The figure is represented in right eye format.

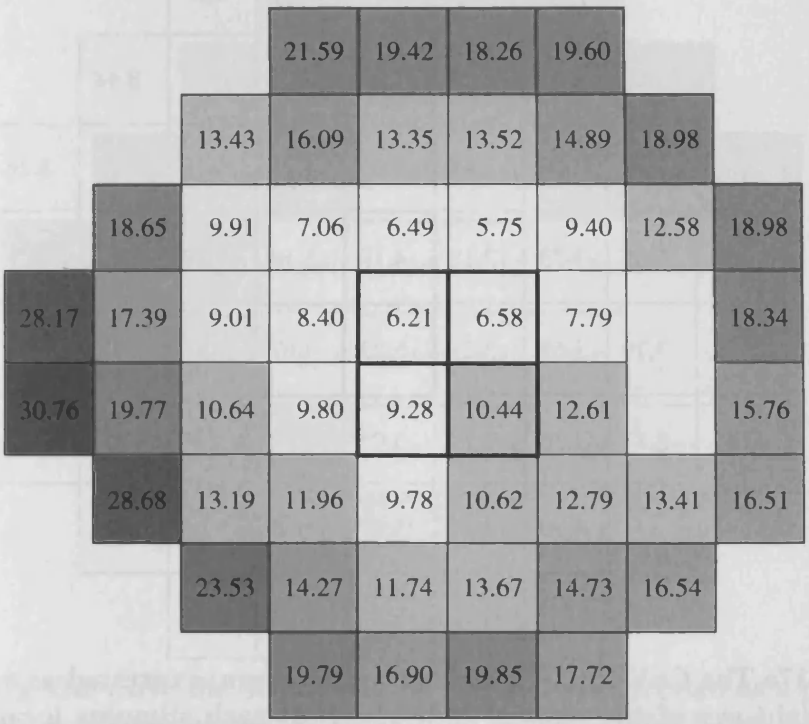

Figure 4.17c The CoV (the SD divided by the mean) expressed as a percentage for the right eye of the normal individuals at each stimulus location for Pulsar perimetry at Visit 1.

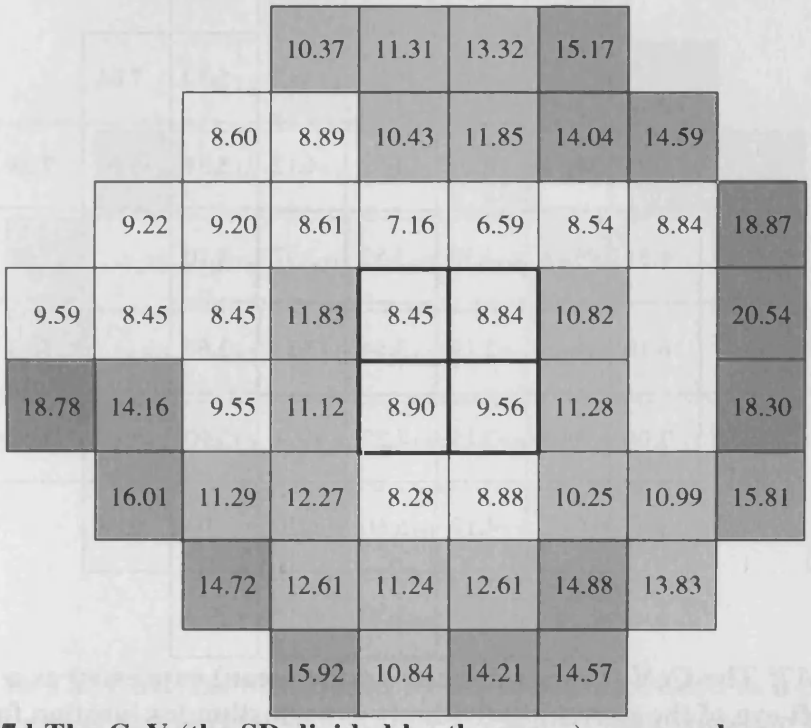

Figure 4.17d The CoV (the SD divided by the mean) expressed as a percentage for the left eye of the normal individuals at each stimulus location for Pulsar perimetry at Visit 1. The figure is represented in right eye format.

		7.91	9.66	10.40	8.19		
	6.64	6.20	7.02	5.87	6.33	8.48	
7.60	3.89	3.48	3.63	4.71	6.16	7.28	8.26
9.22	5.35	3.73	3.18	4.19	5.19	5.29	6.67
7.43	3.79	3.65	3.21	5.23	4.67	4.81	6.75
	5.12	3.36	2.79	5.06	3.67	3.57	7.01	7.71
		4.70	4.37	4.07	4.55	5.65	4.09	
			6.36	6.72	6.51	6.29		

Figure 4.17e The CoV (the SD divided by the mean) expressed as a percentage for the right eye of the normal individuals at each stimulus location for the SITA Standard algorithm at Visit 5.

> 10	> 14	> 18	> 22	> 26	> 30

		7.80	9.88	9.43	8.99		
	7.54	4.25	4.32	5.62	5.50	7.04	
8.24	4.31	3.27	4.62	4.12	5.34	6.63	7.39
9.10	4.61	3.43	4.30	3.55	3.97	4.10	7.02
9.49	6.10	4.29	2.19	3.84	3.52	3.66	5.15
	7.06	3.95	3.15	4.22	4.21	3.90	6.25	5.62
		6.02	4.18	5.60	6.10	4.94	6.88	
			6.13	5.30	6.74	7.13		

Figure 4.17f The CoV (the SD divided by the mean) expressed as a percentage for the left eye of the normal individuals at each stimulus location for the SITA Standard algorithm at Visit 5. The figure is represented in right eye format.

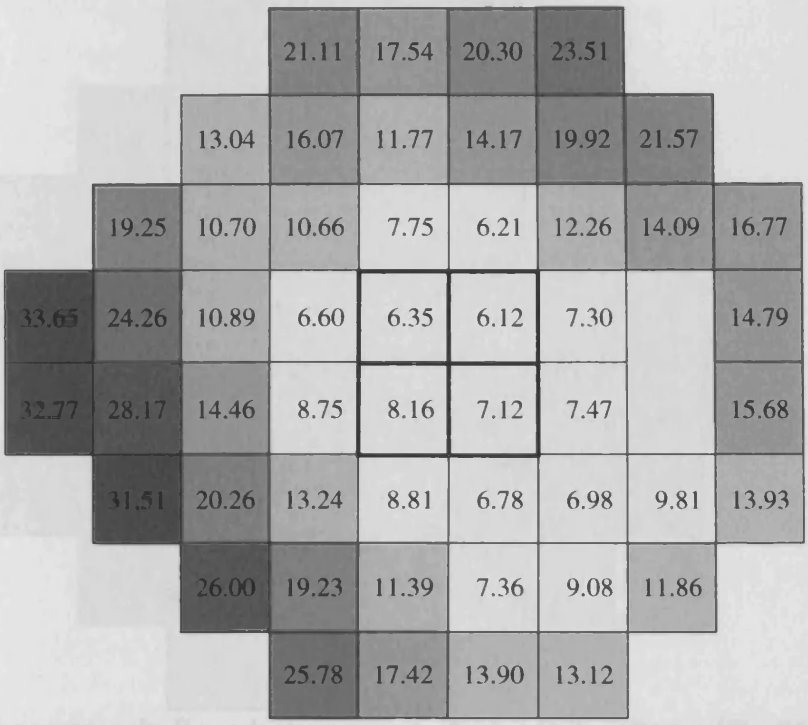

Figure 4.17g The CoV (the SD divided by the mean) expressed as a percentage for the right eye of the normal individuals at each stimulus location for Pulsar perimetry at Visit 5.

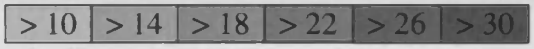

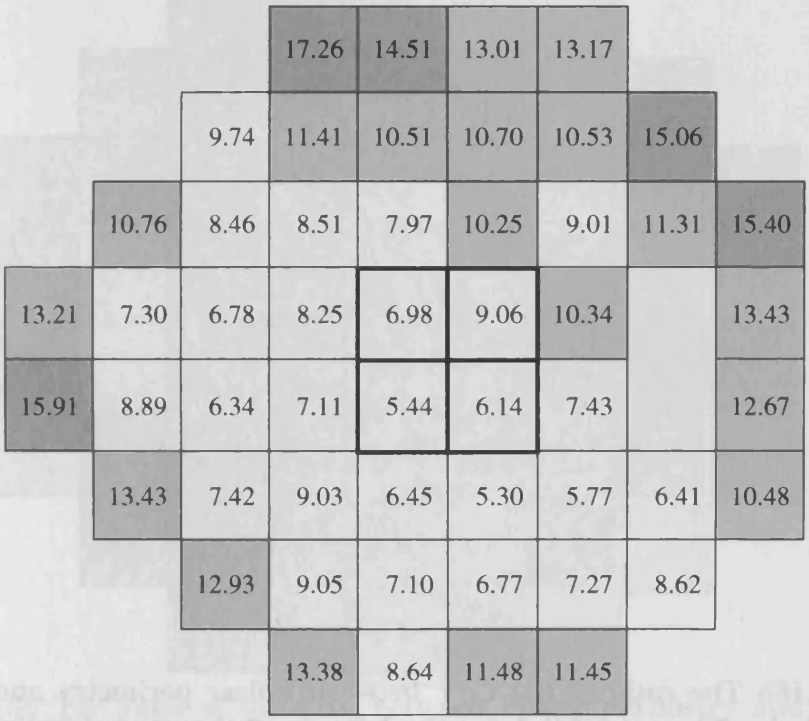

Figure 4.17h The CoV (the SD divided by the mean) expressed as a percentage for the left eye of the normal individuals at each stimulus location for Pulsar perimetry at Visit 5. The figure is represented in right eye format.

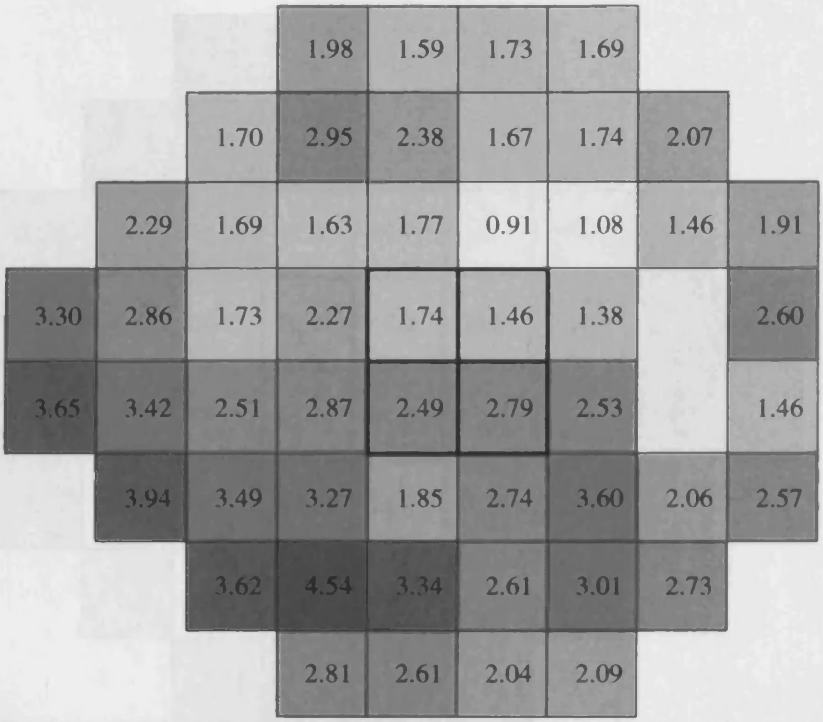

Figure 4.18a The ratio of the CoV between Pulsar Perimetry and the SITA Standard algorithm at Visit 1 for the right eye of the normal individuals.

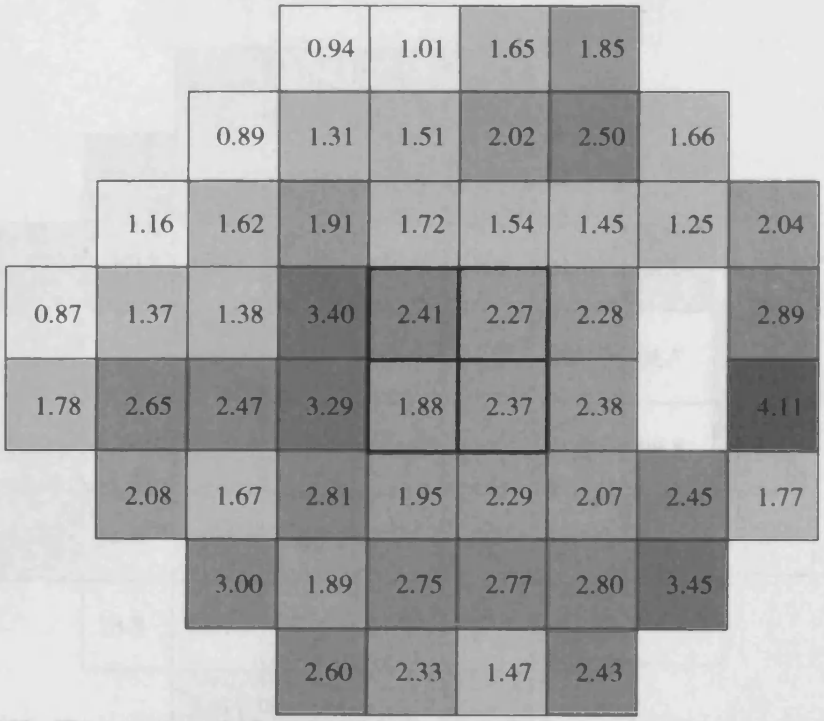

Figure 4.18b The ratio of the CoV between Pulsar perimetry and the SITA Standard algorithm at Visit 1 for the left eye of the normal individuals. The figure is represented in the right eye format.

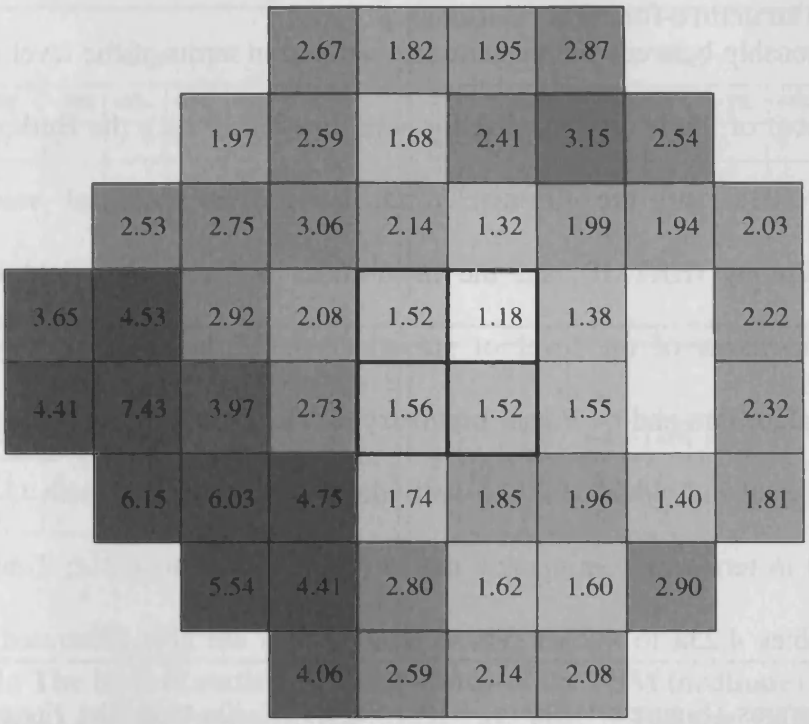

Figure 4.18c The ratio of the CoV between Pulsar perimetry and the SITA Standard algorithm at Visit 5 for the right eye of the normal individuals.

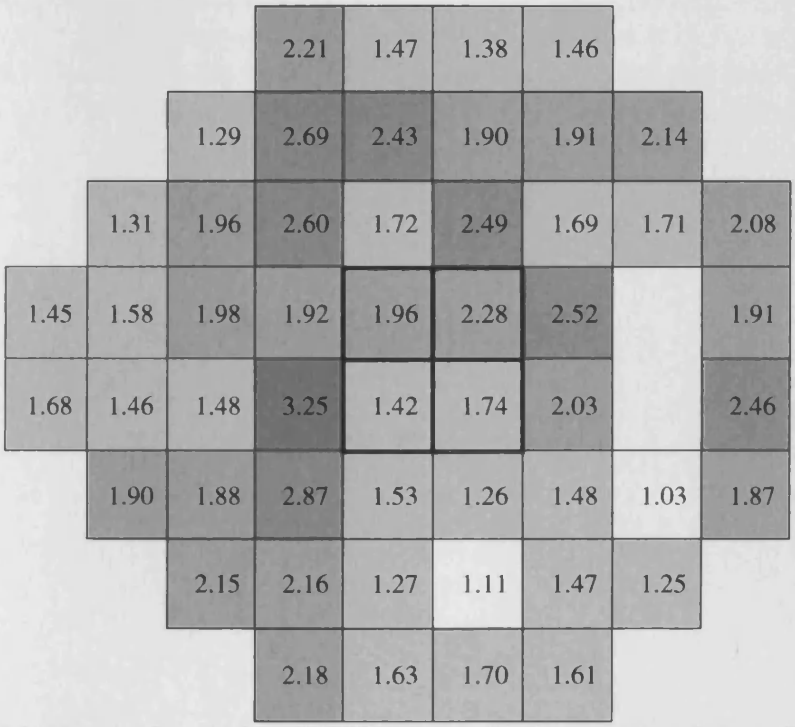

Figure 4.18d The ratio of the CoV between Pulsar perimetry and the SITA Standard algorithm at Visit 5 for the left eye of the normal individuals. The figure is represented in the right eye format.

4.4.4 The structure-function relationship

The relationship between the magnitudes (defined in terms of the level of statistical significance) of the Mikelberg discriminate function (FSM), the Burk discriminate function (RB), and the rim-disc ratio, derived by confocal scanning laser ophthalmoscopy (HRT II) and the magnitudes of the visual field indices MD (defined in terms of the level of statistical significance) derived by the SITA Standard algorithm and by Pulsar perimetry at Visit 5 for the right and the left eyes for the normal individuals for the individuals with OHT and with OAG and are illustrated in terms of contingency tables (Tables 4.21a to 4.21c; Tables 4.22a to 4.22c; Tables 4.23a to 4.23c). These relationships are also illustrated in form of Venn diagrams (Figures 4.19a to 4.19c; Figures 4.20a to 4.20c; Figures 4.21a to 4.21c).

MD_p

FSM	NS	<10%	<5%	<2%	<1%	<0,5%
NS	17	0	0	0	0	0
-	5	0	0	0	0	0

MD_p

FSM	NS	<10%	<5%	<2%	<1%	<0,5%
NS	17	0	0	0	0	0
-	5	0	0	0	0	0

Md_p

FSM	NS	<5%	<1%
NS	17	0	0
-	5	0	0

Md_p

FSM	NS	<5%	<1%
NS	17	0	0
-	5	0	0

Table 4.21a The level of statistical significance of the FSM (ordinate) and of the MD (abscissa) for the normal individuals at Visit 5 for the right eye (left column) and left eye (right column). Top: SITA Standard. Bottom: Pulsar perimetry. The '-'sign indicates a statistically abnormal FSM.

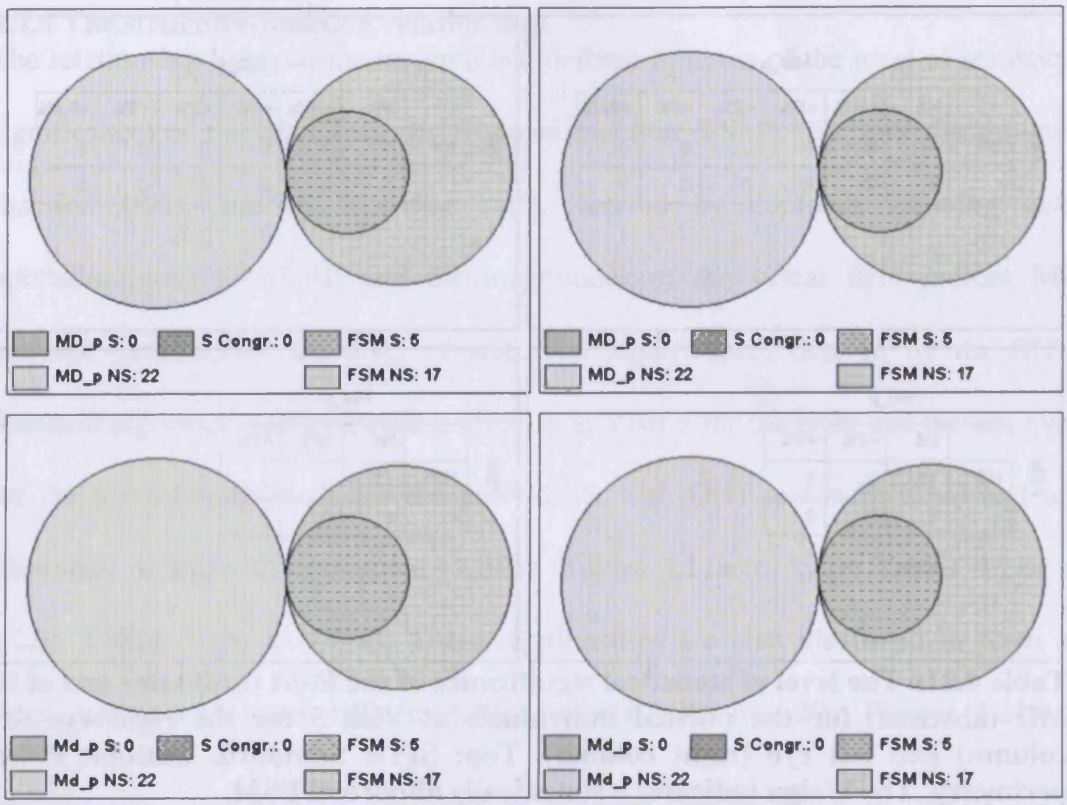

Figure 4.19a Venn diagrams, drawn to scale, illustrating the relationship between the presence (S) or absence of statistical significance (NS) associated with the respective values of FSM and MD for the normal individuals at Visit 5 for the right eye (left column) and left eye (right column). Top: SITA Standard. Bottom: Pulsar perimetry. The number of individuals in whom both measures indicate statistically significant abnormality (S Congr[uence]) is indicated by the overlap and size of the respective two circles.

MD_p

FSM	NS	<10%	<5%	<2%	<1%	<0,5%
NS	18	0	0	0	1	0
-	7	0	0	0	0	0

MD_p

FSM	NS	<10%	<5%	<2%	<1%	<0,5%
NS	16	0	0	1	0	0
-	9	0	0	0	0	0

Md_p

FSM	NS	<5%	<1%
NS	19	0	0
-	7	0	0

Md_p

FSM	NS	<5%	<1%
NS	19	0	0
-	7	0	0

Table 4.21b The level of statistical significance of the FSM (ordinate) and of the MD (abscissa) for the individuals with OHT at Visit 5 for the right eye (left column) and left eye (right column). Top: SITA Standard. Bottom: Pulsar perimetry. The '-'sign indicates a statistically abnormal FSM.

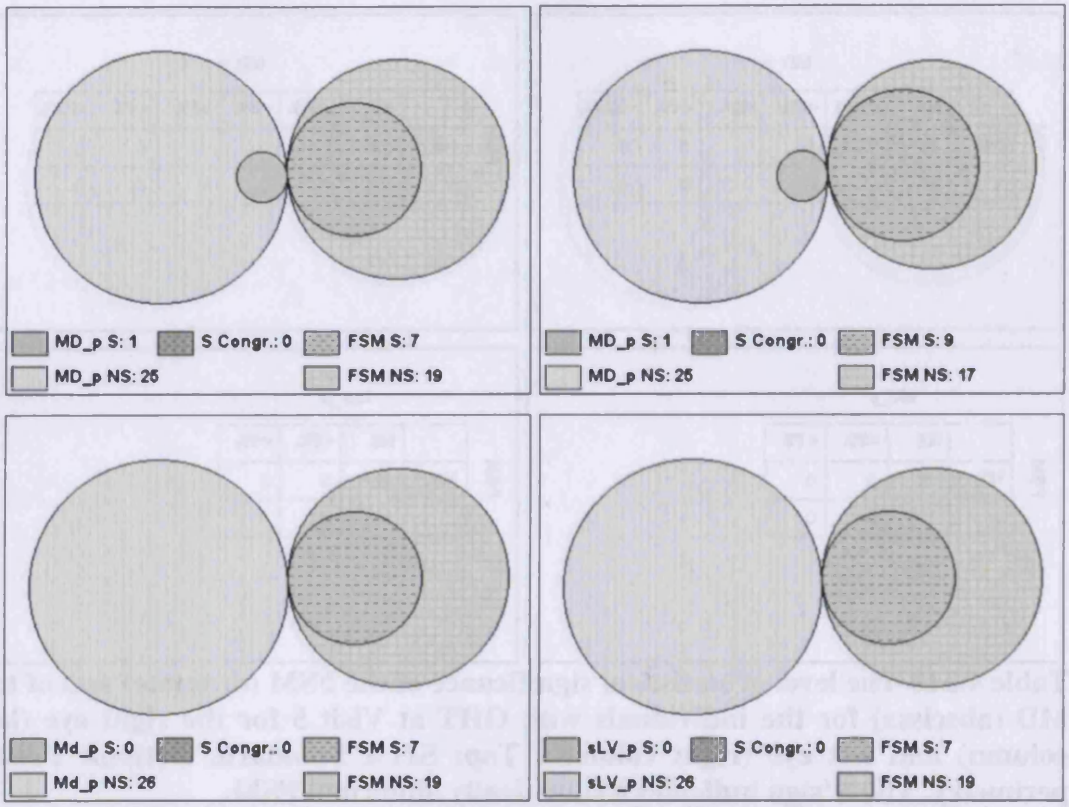

Figure 4.19b Venn diagrams, drawn to scale, illustrating the relationship between the presence (S) or absence of statistical significance (NS) associated with the respective values of FSM and MD for the individuals with OHT at Visit 5 for the right eye (left column) and left eye (right column). Top: SITA Standard. Bottom: Pulsar perimetry. The number of individuals in whom both measures indicate statistically significant abnormality (S Congr[uence]) is indicated by the overlap and size of the respective two circles.

MD_p

FSM	NS	<10%	<5%	<2%	<1%	<0,5%
NS	7	1	0	0	0	0
-	18	0	0	0	0	1

MD_p

FSM	NS	<10%	<5%	<2%	<1%	<0,5%
NS	9	0	1	0	0	0
-	12	0	1	3	0	1

Md_p

FSM	NS	<5%	<1%
NS	8	0	0
-	19	0	0

Md_p

FSM	NS	<5%	<1%
NS	10	0	0
-	17	0	0

Table 4.21c The level of statistical significance of the FSM (ordinate) and of the MD (abscissa) for the individuals with OAG at Visit 5 for the right eye (left column) and left eye (right column). Top: SITA Standard. Bottom: Pulsar perimetry. The '-'sign indicates a statistically abnormal FSM.

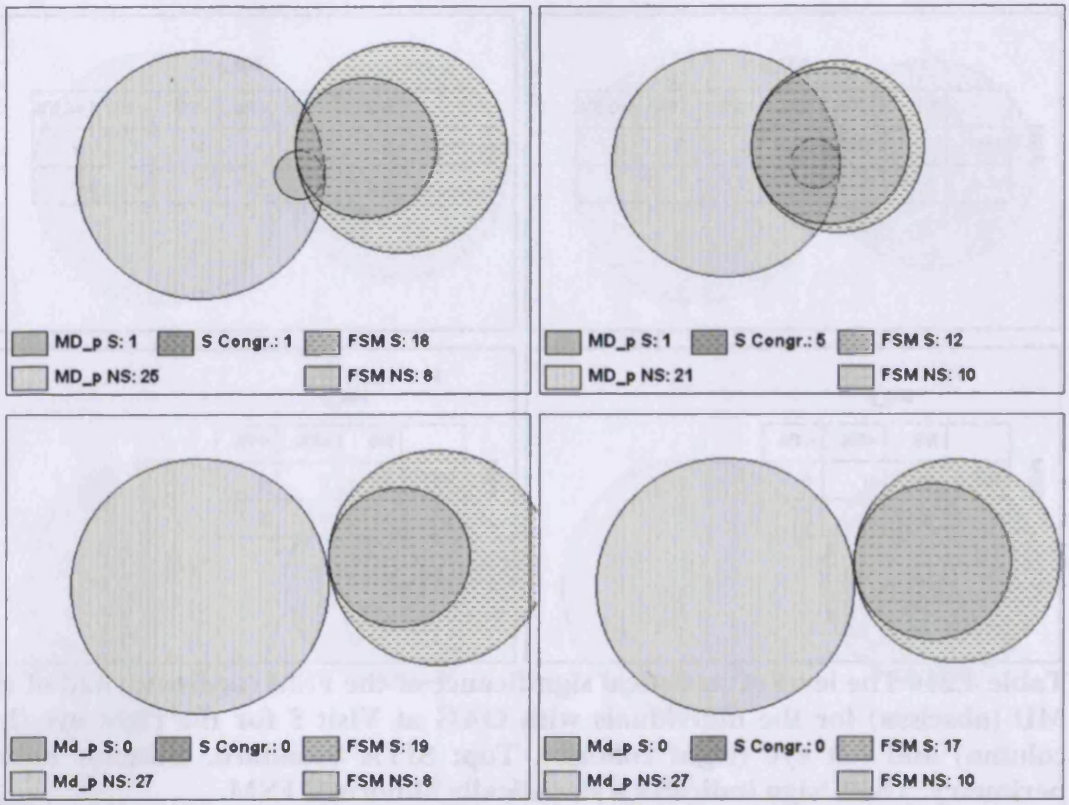

Figure 4.19c Venn diagrams, drawn to scale, illustrating the relationship between the presence (S) or absence of statistical significance (NS) associated with the respective values of FSM and MD for the individuals with OAG at Visit 5 for the right eye (left column) and left eye (right column). Top: SITA Standard. Bottom: Pulsar perimetry. The number of individuals in whom both measures indicate statistically significant abnormality (S Congr[uence]) is indicated by the overlap and size of the respective two circles.

MD_p

RB	NS	<10%	<5%	<2%	<1%	<0,5%
NS	22	0	0	0	0	0
-	0	0	0	0	0	0

MD_p

RB	NS	<10%	<5%	<2%	<1%	<0,5%
NS	22	0	0	0	0	0
-	0	0	0	0	0	0

Md_p

RB	NS	<5%	<1%
NS	22	0	0
-	0	0	0

Md_p

RB	NS	<5%	<1%
NS	22	0	0
-	0	0	0

Table 4.22a The level of statistical significance of the RB (ordinate) and of the MD (abscissa) for the normal individuals at Visit 5 for the right eye (left column) and left eye (right column). Top: SITA Standard. Bottom: Pulsar perimetry. The '-'sign indicates a statistically abnormal RB.

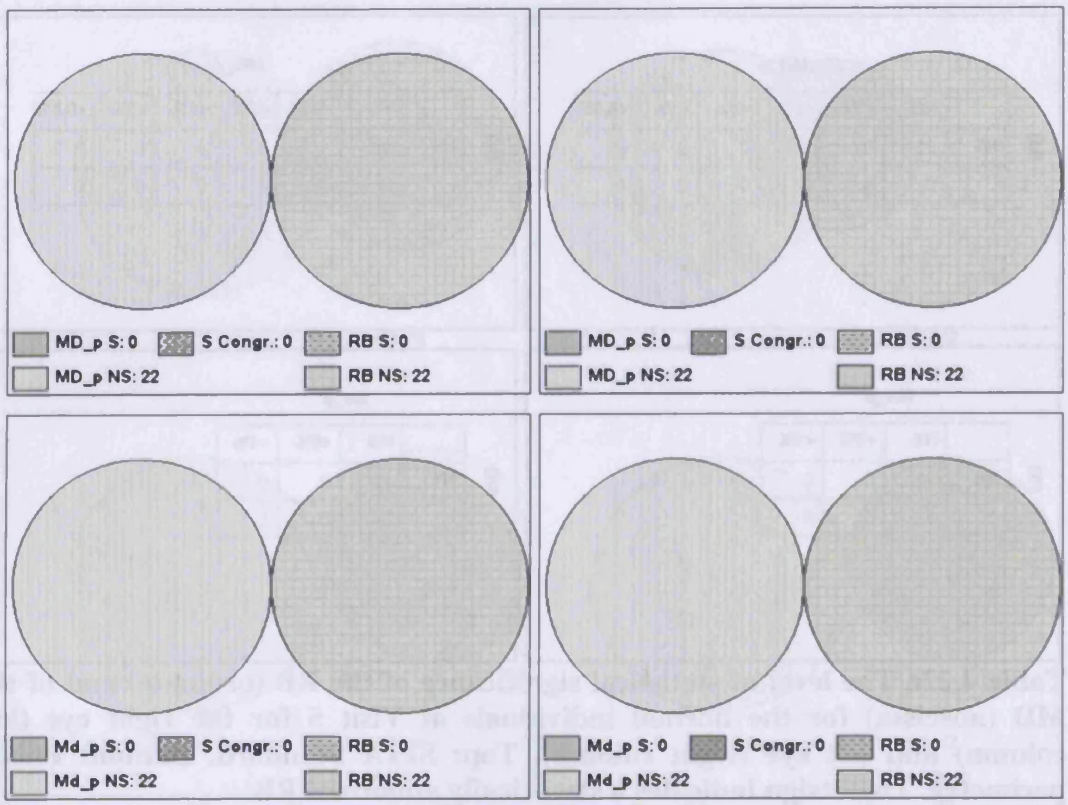

Figure 4.20a Venn diagrams, drawn to scale, illustrating the relationship between the presence (S) or absence of statistical significance (NS) associated with the respective values of RB and MD for the normal individuals at Visit 5 for the right eye (left column) and left eye (right column). Top: SITA Standard. Bottom: Pulsar perimetry. The number of individuals in whom both measures indicate statistically significant abnormality (S Congr[uence]) is indicated by the overlap and size of the respective two circles.

MD_p

RB	NS	<10%	<5%	<2%	<1%	<0,5%
NS	24	0	0	0	1	0
-	1	0	0	0	0	0

MD_p

RB	NS	<10%	<5%	<2%	<1%	<0,5%
NS	25	0	0	1	0	0
-	0	0	0	0	0	0

Md_p

RB	NS	<5%	<1%
NS	25	0	0
-	1	0	0

Md_p

RB	NS	<5%	<1%
NS	26	0	0
-	0	0	0

Table 4.22b The level of statistical significance of the RB (ordinate) and of the MD (abscissa) for the individuals with OHT at Visit 5 for the right eye (left column) and left eye (right column). Top: SITA Standard. Bottom: Pulsar perimetry. The '-'sign indicates a statistically abnormal RB.

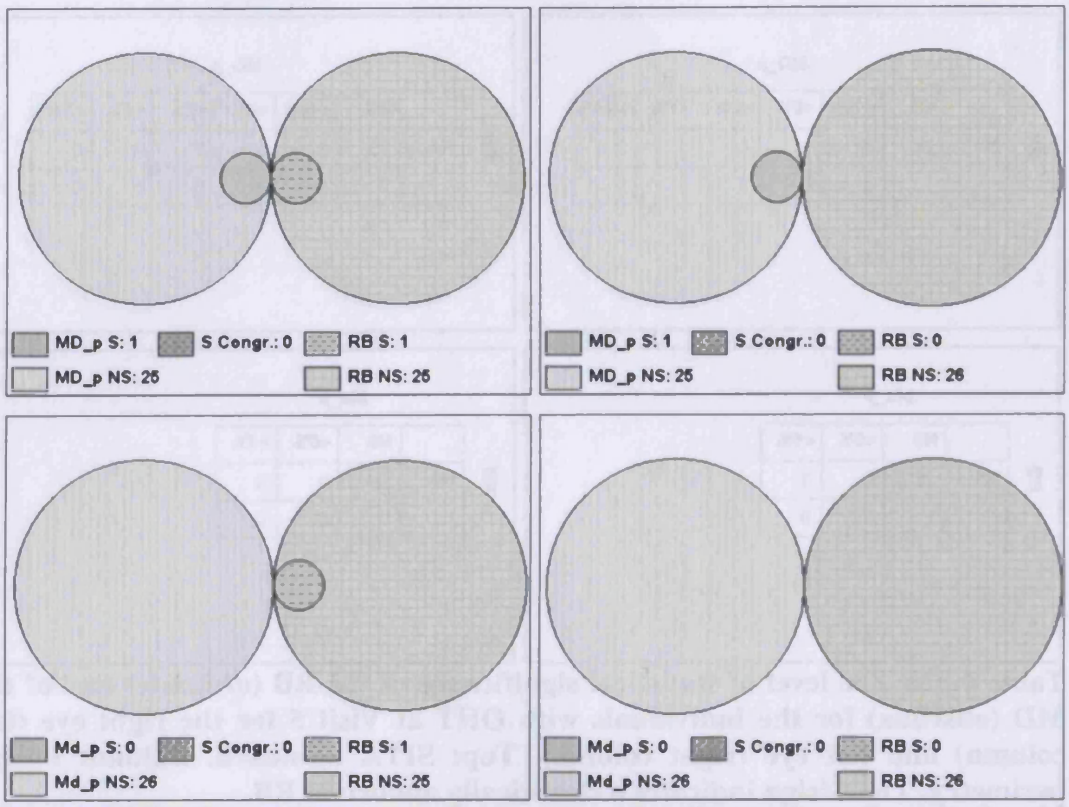

Figure 4.20b Venn diagrams, drawn to scale, illustrating the relationship between the presence (S) or absence of statistical significance (NS) associated with the respective values of RB and MD for the individuals with OHT at Visit 5 for the right eye (left column) and left eye (right column). Top: SITA Standard. Bottom: Pulsar perimetry. The number of individuals in whom both measures indicate statistically significant abnormality (S Congr[uence]) is indicated by the overlap and size of the respective two circles.

MD_p

RB	NS	<10%	<5%	<2%	<1%	<0,5%
NS	17	1	0	0	0	0
-	8	0	0	0	0	1

MD_p

RB	NS	<10%	<5%	<2%	<1%	<0,5%
NS	14	0	1	2	0	0
-	7	0	1	1	0	1

Md_p

RB	NS	<5%	<1%
NS	18	0	0
-	9	0	0

Md_p

RB	NS	<5%	<1%
NS	17	0	0
-	10	0	0

Table 4.22c The level of statistical significance of the RB (ordinate) and of the MD (abscissa) for the individuals with OAG at Visit 5 for the right eye (left column) and left eye (right column). Top: SITA Standard. Bottom: Pulsar perimetry. The '-'sign indicates a statistically abnormal RB.

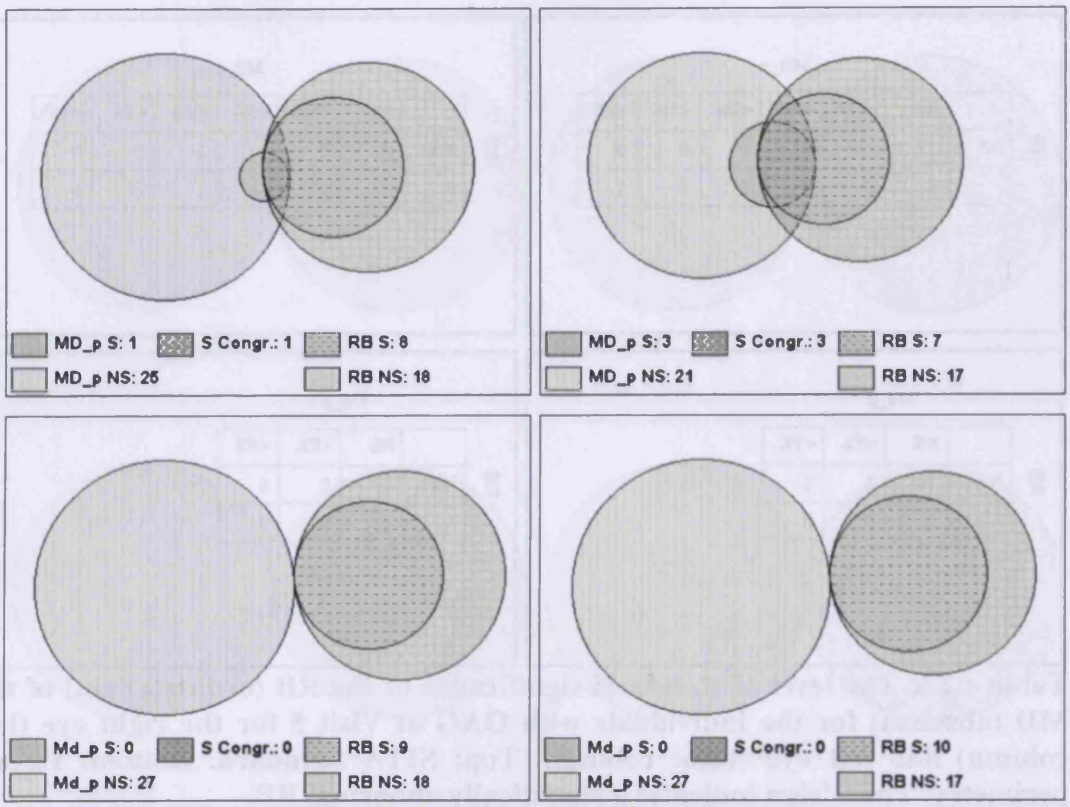

Figure 4.20c Venn diagrams, drawn to scale, illustrating the relationship between the presence (S) or absence of statistical significance (NS) associated with the respective values of RB and MD for the individuals with OAG at Visit 5 for the right eye (left column) and left eye (right column). Top: SITA Standard. Bottom: Pulsar perimetry. The number of individuals in whom both measures indicate statistically significant abnormality (S Congr[uence]) is indicated by the overlap and size of the respective two circles.

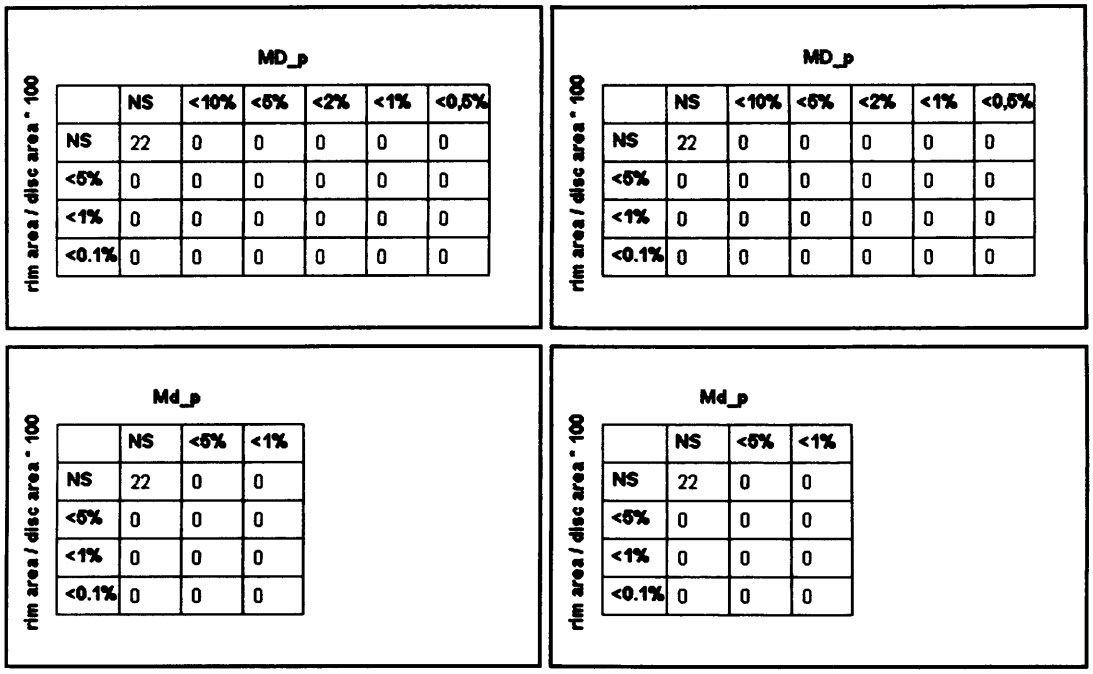

MD_p

rim area / disc area * 100

	NS	<10%	<5%	<2%	<1%	<0,5%
NS	22	0	0	0	0	0
<5%	0	0	0	0	0	0
<1%	0	0	0	0	0	0
<0.1%	0	0	0	0	0	0

MD_p

rim area / disc area * 100

	NS	<10%	<5%	<2%	<1%	<0,5%
NS	22	0	0	0	0	0
<5%	0	0	0	0	0	0
<1%	0	0	0	0	0	0
<0.1%	0	0	0	0	0	0

Md_p

rim area / disc area * 100

	NS	<5%	<1%
NS	22	0	0
<5%	0	0	0
<1%	0	0	0
<0.1%	0	0	0

Md_p

rim area / disc area * 100

	NS	<5%	<1%
NS	22	0	0
<5%	0	0	0
<1%	0	0	0
<0.1%	0	0	0

Table 4.23a The level of statistical significance of the rim-disc ratio (ordinate) and of the MD (abscissa) for the normal individuals at Visit 5 for the right eye (left column) and left eye (right column). Top: SITA Standard. Bottom: Pulsar perimetry.

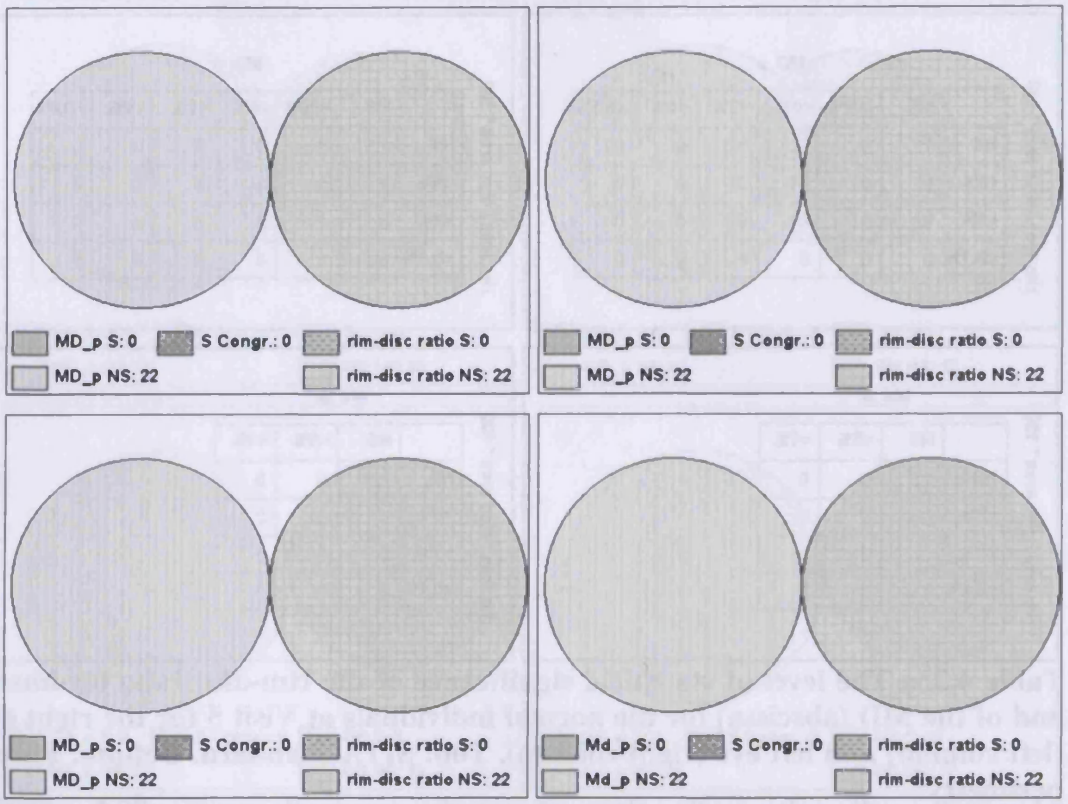

Figure 4.21a Venn diagrams, drawn to scale, illustrating the relationship between the presence (S) or absence of statistical significance (NS) associated with the respective values of the rim-disc ratio and MD for the normal individuals at Visit 5 for the right eye (left column) and left eye (right column). Top: SITA Standard. Bottom: Pulsar perimetry. The number of individuals in whom both measures indicate statistically significant abnormality (S Congr[uence]) is indicated by the overlap and size of the respective two circles.

MD_p

rim area / disc area * 100

	NS	<10%	<5%	<2%	<1%	<0,5%
NS	23	0	0	0	1	0
<5%	2	0	0	0	0	0
<1%	0	0	0	0	0	0
<0.1%	0	0	0	0	0	0

MD_p

rim area / disc area * 100

	NS	<10%	<5%	<2%	<1%	<0,5%
NS	25	0	0	1	0	0
<5%	0	0	0	0	0	0
<1%	0	0	0	0	0	0
<0.1%	0	0	0	0	0	0

Md_p

rim area / disc area * 100

	NS	<5%	<1%
NS	24	0	0
<5%	2	0	0
<1%	0	0	0
<0.1%	0	0	0

Md_p

rim area / disc area * 100

	NS	<5%	<1%
NS	26	0	0
<5%	0	0	0
<1%	0	0	0
<0.1%	0	0	0

Table 4.23b The level of statistical significance of the rim-disc ratio (ordinate) and of the MD (abscissa) for the individuals with OHT at Visit 5 for the right eye (left column) and left eye (right column). Top: SITA Standard. Bottom: Pulsar perimetry.

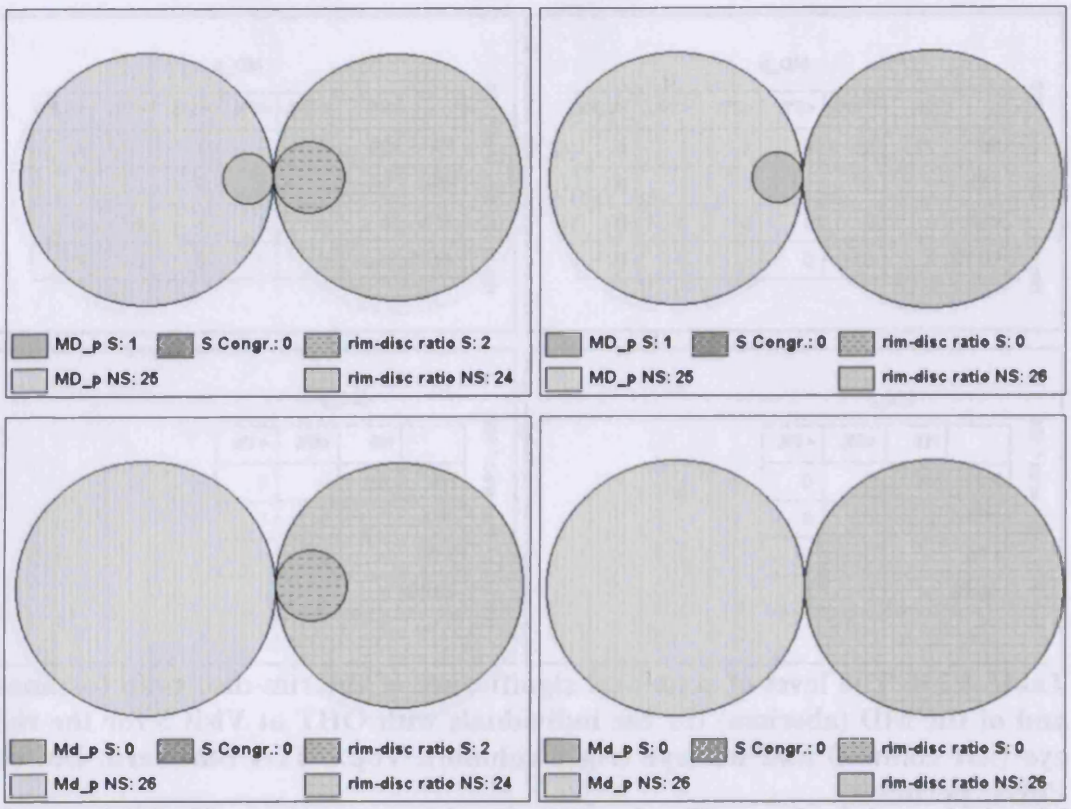

Figure 4.21b Venn diagrams, drawn to scale, illustrating the relationship between the presence (S) or absence of statistical significance (NS) associated with the respective values of the rim-disc ratio and MD for the individuals with OHT at Visit 5 for the right eye (left column) and left eye (right column). Top: SITA Standard. Bottom: Pulsar perimetry. The number of individuals in whom both measures indicate statistically significant abnormality (S Congr[uence]) is indicated by the overlap and size of the respective two circles.

MD_p

rim area / disc area * 100

	NS	<10%	<5%	<2%	<1%	<0,5%
NS	16	1	0	0	0	0
<5%	2	0	0	0	0	0
<1%	2	0	0	0	0	0
<0.1%	5	0	0	0	0	1

MD_p

rim area / disc area * 100

	NS	<10%	<5%	<2%	<1%	<0,5%
NS	16	0	1	0	0	0
<5%	1	0	0	0	0	0
<1%	1	0	1	0	0	0
<0.1%	3	0	0	3	0	1

Md_p

rim area / disc area * 100

	NS	<5%	<1%
NS	17	0	0
<5%	2	0	0
<1%	2	0	0
<0.1%	6	0	0

Md_p

rim area / disc area * 100

	NS	<5%	<1%
NS	17	0	0
<5%	1	0	0
<1%	2	0	0
<0.1%	7	0	0

Table 4.23c The level of statistical significance of the rim-disc ratio (ordinate) and of the MD (abscissa) for the individuals with OAG at Visit 5 for the right eye (left column) and left eye (right column). Top: SITA Standard. Bottom: Pulsar perimetry.

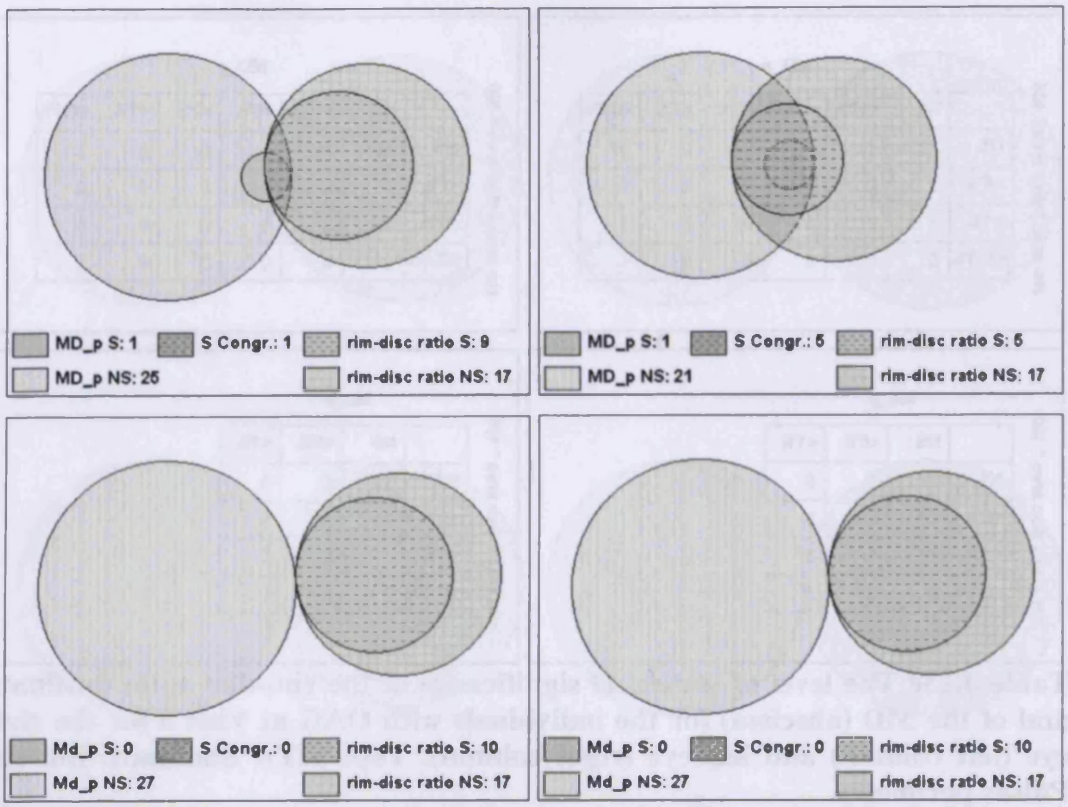

Figure 4.21c Venn diagrams, drawn to scale, illustrating the relationship between the presence (S) or absence of statistical significance (NS) associated with the respective values of rim-disc ratio and MD for the individuals with OAG at Visit 5 for the right eye (left column) and left eye (right column). Top: SITA Standard. Bottom: Pulsar perimetry. The number of individuals in whom both measures indicate statistically significant abnormality (S Congr[uence]) is indicated by the overlap and size of the respective two circles.

The relationship between the magnitudes (defined in terms of the level of statistical significance) of the Mikelberg discriminate function (FSM), the Burk discriminate function (RB) and the rim-disc ratio, derived by confocal scanning laser ophthalmoscopy (HRT II) and the magnitudes of the visual field indices PSD/ sLV (defined in terms of the level of statistical significance) derived by the SITA Standard algorithm and by Pulsar perimetry at Visit 5 for the right and the left eyes for the normal individuals for the individuals with OHT and OAG and are illustrated in terms of contingency tables (Tables 4.24a to 4.24c; Tables 4.25a to 4.25c; Tables 4.26a to 4.26c). These relationships are also illustrated in form of Venn diagrams (Figures 4.22a to 422c; Figures 4.23a to 4.23c; Figures 4.24a to 4.24c).

PSD_p

FSM	NS	<10%	<5%	<2%	<1%	<0,5%
NS	17	0	0	0	0	0
-	3	1	1	0	0	0

PSD_p

FSM	NS	<10%	<5%	<2%	<1%	<0,5%
NS	16	1	0	0	0	0
-	5	0	0	0	0	0

sLV_p

FSM	NS	<5%	<1%
NS	15	0	2
-	5	0	0

sLV_p

FSM	NS	<5%	<1%
NS	17	0	0
-	5	0	0

Table 4.24a The level of statistical significance of the FSM (ordinate) and of the PSD/ sLV (abscissa) for the normal individuals at Visit 5 for the right eye (left column) and left eye (right column). Top: SITA Standard. Bottom: Pulsar perimetry. The '-'sign indicates a statistically abnormal FSM.

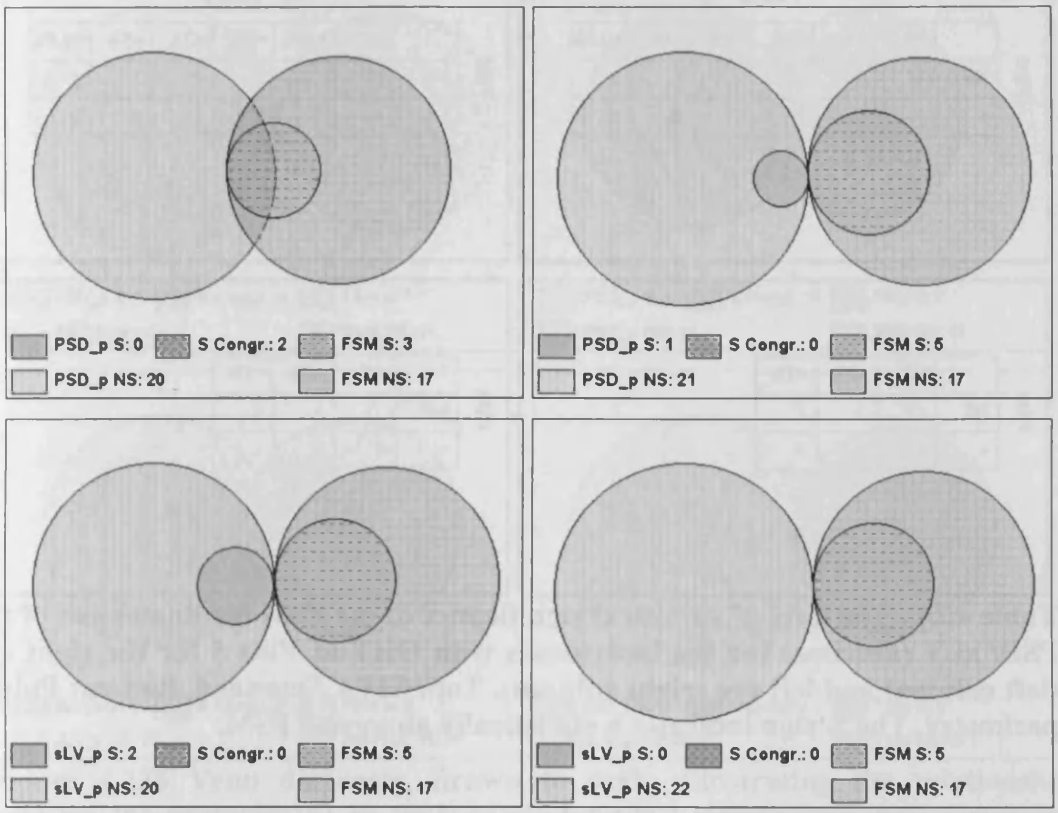

Figure 4.22a Venn diagrams, drawn to scale, illustrating the relationship between the presence (S) or absence of statistical significance (NS) associated with the respective values of FSM and PSD/ sLV for the normal individuals at Visit 5 for the right eye (left column) and left eye (right column). Top: SITA Standard. Bottom: Pulsar perimetry. The number of individuals in whom both measures indicate statistically significant abnormality (S Congr[uence]) is indicated by the overlap and size of the respective two circles.

PSD_p

FSM	NS	<10%	<5%	<2%	<1%	<0,5%
NS	17	2	0	0	0	0
-	7	0	0	0	0	0

PSD_p

FSM	NS	<10%	<5%	<2%	<1%	<0,5%
NS	12	1	2	0	1	1
-	7	1	0	1	0	0

sLV_p

FSM	NS	<5%	<1%
NS	15	3	1
-	6	1	0

sLV_p

FSM	NS	<5%	<1%
NS	17	0	0
-	8	0	1

Table 4.24b The level of statistical significance of the FSM (ordinate) and of the PSD/ sLV (abscissa) for the individuals with OHT at Visit 5 for the right eye (left column) and left eye (right column). Top: SITA Standard. Bottom: Pulsar perimetry. The '-'sign indicates a statistically abnormal FSM.

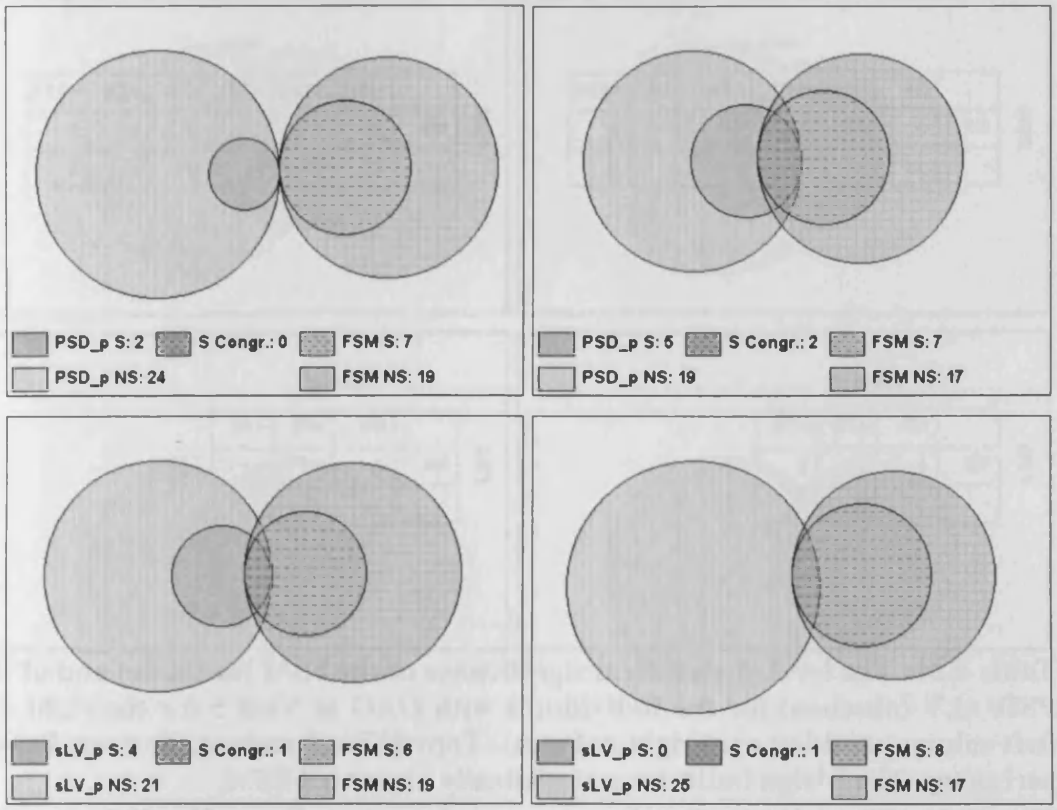

Figure 4.22b Venn diagrams, drawn to scale, illustrating the relationship between the presence (S) or absence of statistical significance (NS) associated with the respective values of FSM and PSD/ sLV for the individuals with OHT at Visit 5 for the right eye (left column) and left eye (right column). Top: SITA Standard. Bottom: Pulsar perimetry. The number of individuals in whom both measures indicate statistically significant abnormality (S Congr[uence]) is indicated by the overlap and size of the respective two circles.

PSD_p

FSM	NS	<10%	<5%	<2%	<1%	<0,5%
NS	8	0	0	0	0	0
-	13	3	0	1	0	2

PSD_p

FSM	NS	<10%	<5%	<2%	<1%	<0,5%
NS	10	0	0	0	0	0
-	11	0	1	0	0	5

sLV_p

FSM	NS	<5%	<1%
NS	8	0	0
-	13	3	3

sLV_p

FSM	NS	<5%	<1%
NS	8	1	1
-	14	1	2

Table 4.24c The level of statistical significance of the FSM (ordinate) and of the PSD/ sLV (abscissa) for the individuals with OAG at Visit 5 for the right eye (left column) and left eye (right column). Top: SITA Standard. Bottom: Pulsar perimetry. The '-'sign indicates a statistically abnormal FSM.

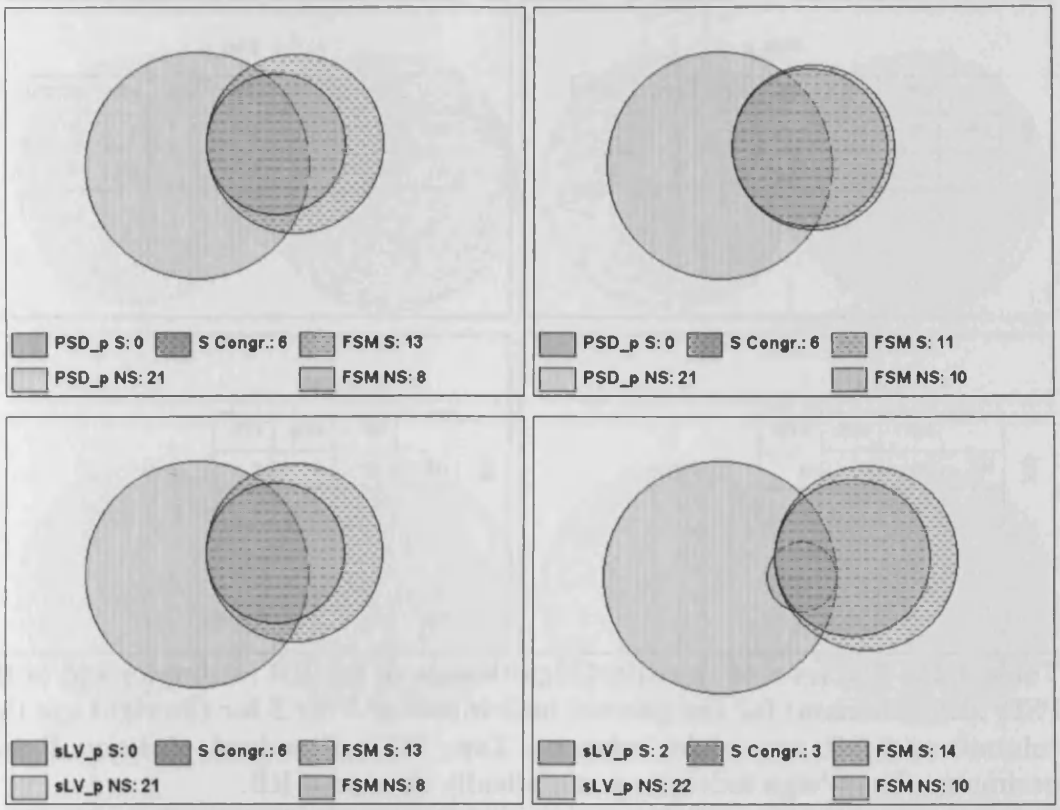

Figure 4.22c Venn diagrams, drawn to scale, illustrating the relationship between the presence (S) or absence of statistical significance (NS) associated with the respective values of FSM and PSD/ sLV for the individuals with OAG at Visit 5 for the right eye (left column) and left eye (right column). Top: SITA Standard. Bottom: Pulsar perimetry. The number of individuals in whom both measures indicate statistically significant abnormality (S Congr[uence]) is indicated by the overlap and size of the respective two circles.

PSD_p

RB \ PSD_p	NS	<10%	<5%	<2%	<1%	<0,5%
NS	20	1	1	0	0	0
-	0	0	0	0	0	0

PSD_p

RB \ PSD_p	NS	<10%	<5%	<2%	<1%	<0,5%
NS	21	1	0	0	0	0
-	0	0	0	0	0	0

sLV_p

RB \ sLV_p	NS	<5%	<1%
NS	20	0	2
-	0	0	0

sLV_p

RB \ sLV_p	NS	<5%	<1%
NS	22	0	0
-	0	0	0

Table 4.25a The level of statistical significance of the RB (ordinate) and of the PSD/ sLV (abscissa) for the normal individuals at Visit 5 for the right eye (left column) and left eye (right column). Top: SITA Standard. Bottom: Pulsar perimetry. The '-'sign indicates a statistically abnormal RB.

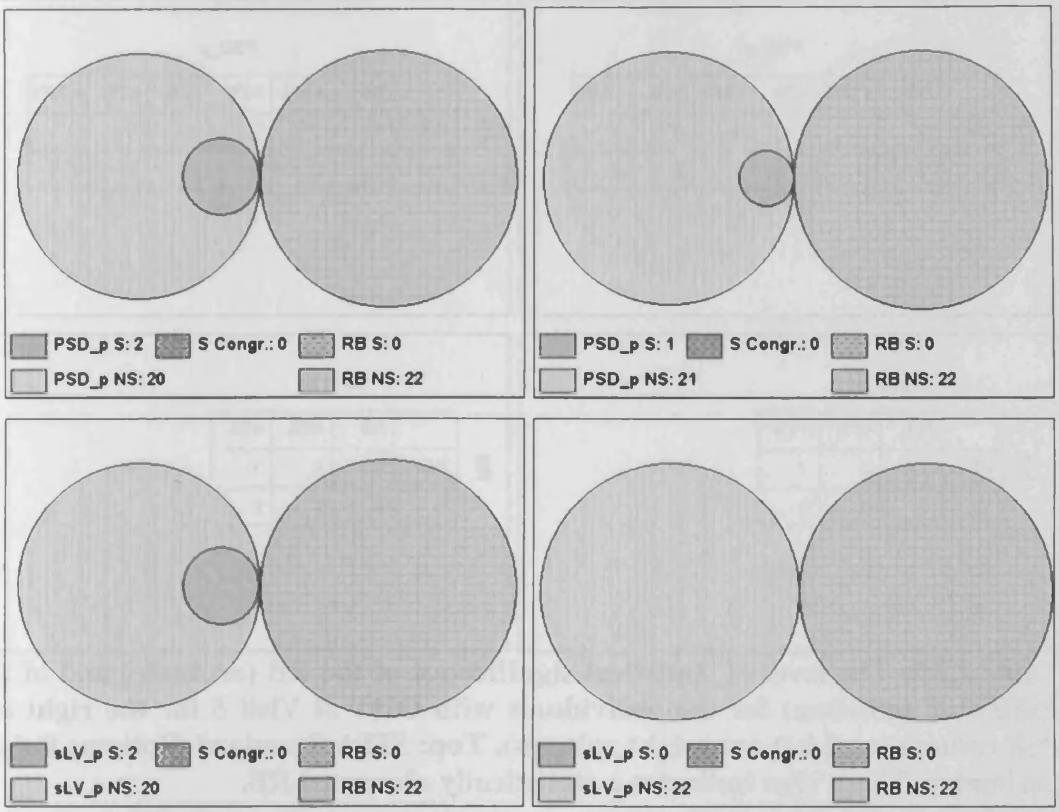

Figure 4.23a Venn diagrams, drawn to scale, illustrating the relationship between the presence (S) or absence of statistical significance (NS) associated with the respective values of RB and PSD/ sLV for the normal individuals at Visit 5 for the right eye (left column) and left eye (right column). Top: SITA Standard. Bottom: Pulsar perimetry. The number of individuals in whom both measures indicate statistically significant abnormality (S Congr[uence]) is indicated by the overlap and size of the respective two circles.

PSD_p

RB	NS	<10%	<5%	<2%	<1%	<0,5%
NS	23	2	0	0	0	0
-	1	0	0	0	0	0

PSD_p

RB	NS	<10%	<5%	<2%	<1%	<0,5%
NS	19	2	2	1	1	1
-	0	0	0	0	0	0

sLV_p

RB	NS	<5%	<1%
NS	20	4	1
-	1	0	0

sLV_p

RB	NS	<5%	<1%
NS	25	0	1
-	0	0	0

Table 4.25b The level of statistical significance of the RB (ordinate) and of the PSD/ sLV (abscissa) for the individuals with OHT at Visit 5 for the right eye (left column) and left eye (right column). Top: SITA Standard. Bottom: Pulsar perimetry. The '-'sign indicates a statistically abnormal RB.

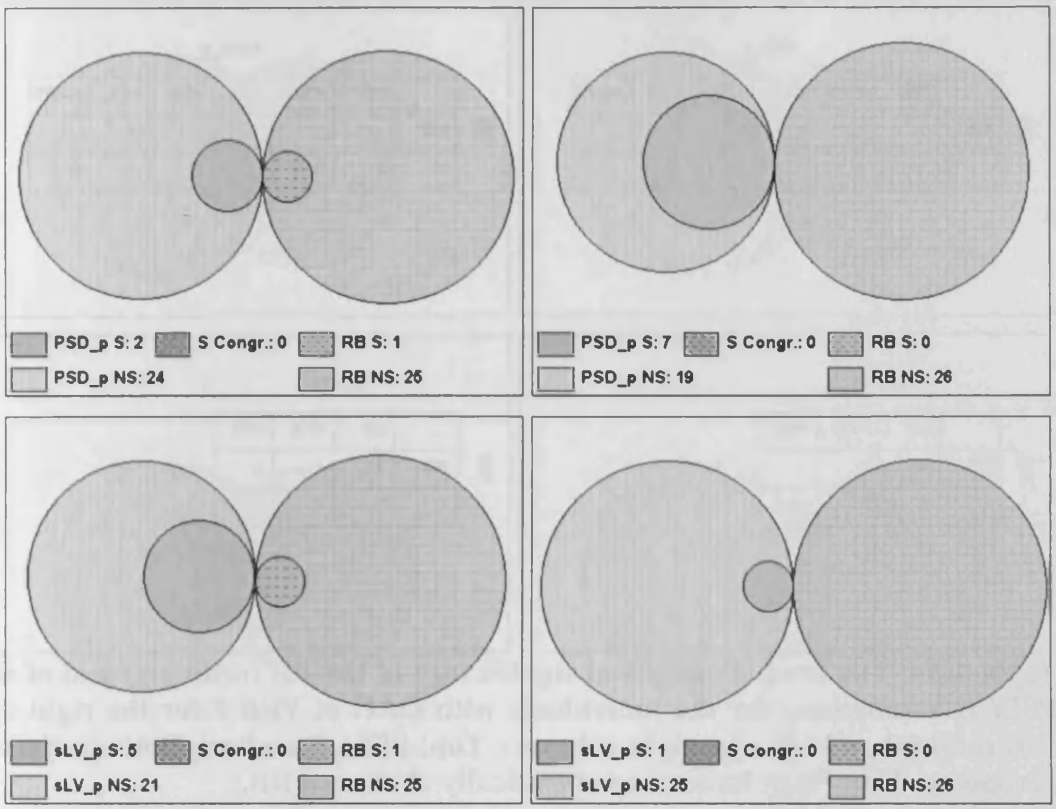

Figure 4.23b Venn diagrams, drawn to scale, illustrating the relationship between the presence (S) or absence of statistical significance (NS) associated with the respective values of RB and PSD/ sLV for the individuals with OHT at Visit 5 for the right eye (left column) and left eye (right column). Top: SITA Standard. Bottom: Pulsar perimetry. The number of individuals in whom both measures indicate statistically significant abnormality (S Congr[uence]) is indicated by the overlap and size of the respective two circles.

PSD_p

RB	NS	<10%	<5%	<2%	<1%	<0,5%
NS	17	1	0	0	0	0
-	4	2	0	1	0	2

PSD_p

RB	NS	<10%	<5%	<2%	<1%	<0,5%
NS	14	0	1	0	0	2
-	7	0	0	0	0	3

sLV_p

RB	NS	<5%	<1%
NS	16	0	2
-	5	3	1

sLV_p

RB	NS	<5%	<1%
NS	13	1	3
-	9	1	0

Table 4.25c The level of statistical significance of the RB (ordinate) and of the PSD/ sLV (abscissa) for the individuals with OAG at Visit 5 for the right eye (left column) and left eye (right column). Top: SITA Standard. Bottom: Pulsar perimetry. The '-'sign indicates a statistically abnormal RB.

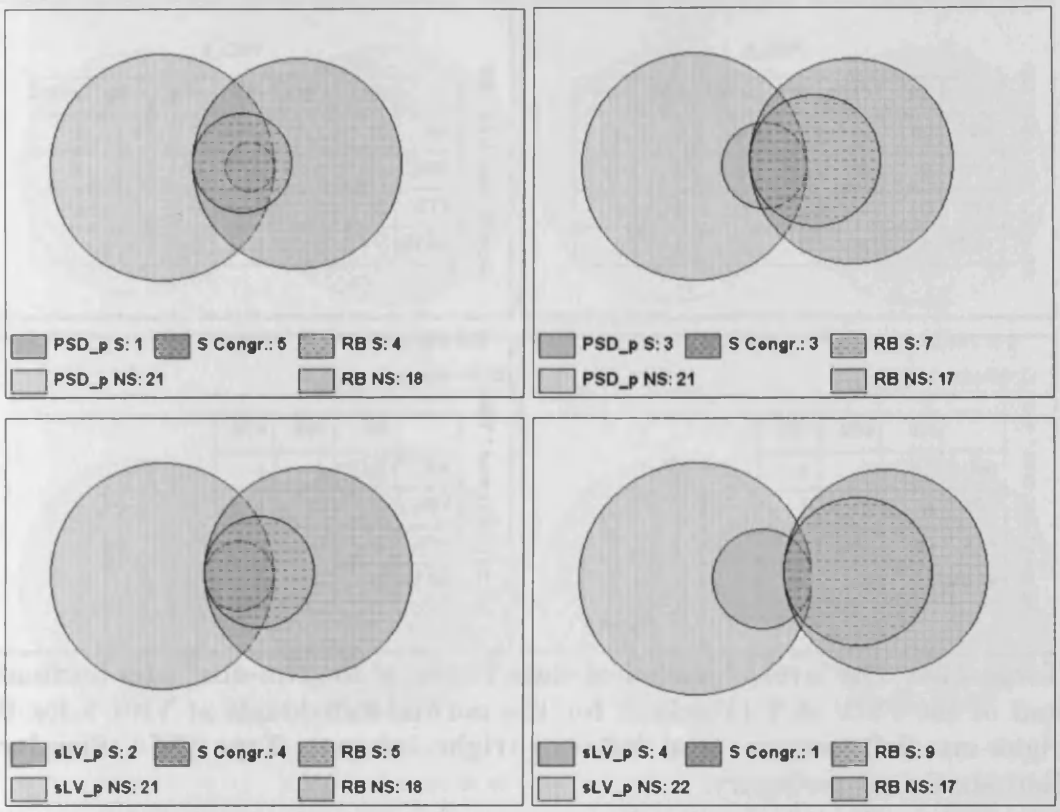

Figure 4.23c Venn diagrams, drawn to scale, illustrating the relationship between the presence (S) or absence of statistical significance (NS) associated with the respective values of RB and PSD/ sLV for the individuals with OAG at Visit 5 for the right eye (left column) and left eye (right column). Top: SITA Standard. Bottom: Pulsar perimetry. The number of individuals in whom both measures indicate statistically significant abnormality (S Congr[uence]) is indicated by the overlap and size of the respective two circles.

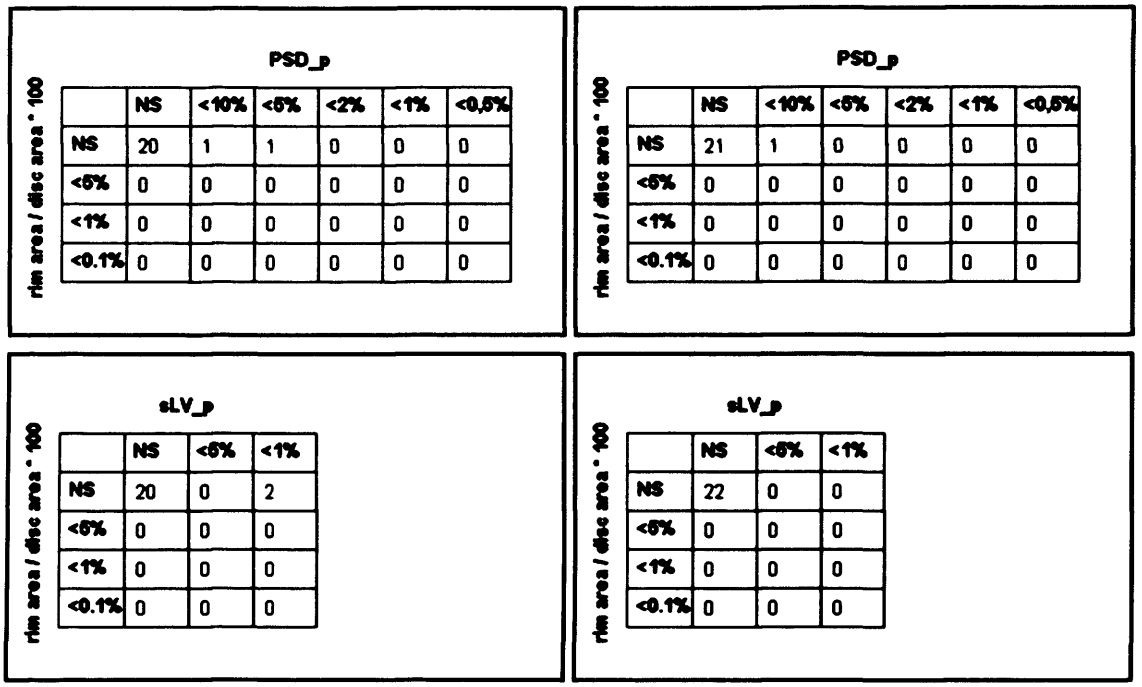

PSD_p

rim area / disc area * 100

	NS	<10%	<5%	<2%	<1%	<0,5%
NS	20	1	1	0	0	0
<5%	0	0	0	0	0	0
<1%	0	0	0	0	0	0
<0.1%	0	0	0	0	0	0

PSD_p

rim area / disc area * 100

	NS	<10%	<5%	<2%	<1%	<0,5%
NS	21	1	0	0	0	0
<5%	0	0	0	0	0	0
<1%	0	0	0	0	0	0
<0.1%	0	0	0	0	0	0

sLV_p

rim area / disc area * 100

	NS	<5%	<1%
NS	20	0	2
<5%	0	0	0
<1%	0	0	0
<0.1%	0	0	0

sLV_p

rim area / disc area * 100

	NS	<5%	<1%
NS	22	0	0
<5%	0	0	0
<1%	0	0	0
<0.1%	0	0	0

Table 4.26a The level of statistical significance of the rim-disc ratio (ordinate) and of the PSD/ sLV (abscissa) for the normal individuals at Visit 5 for the right eye (left column) and left eye (right column). Top: SITA Standard. Bottom: Pulsar perimetry.

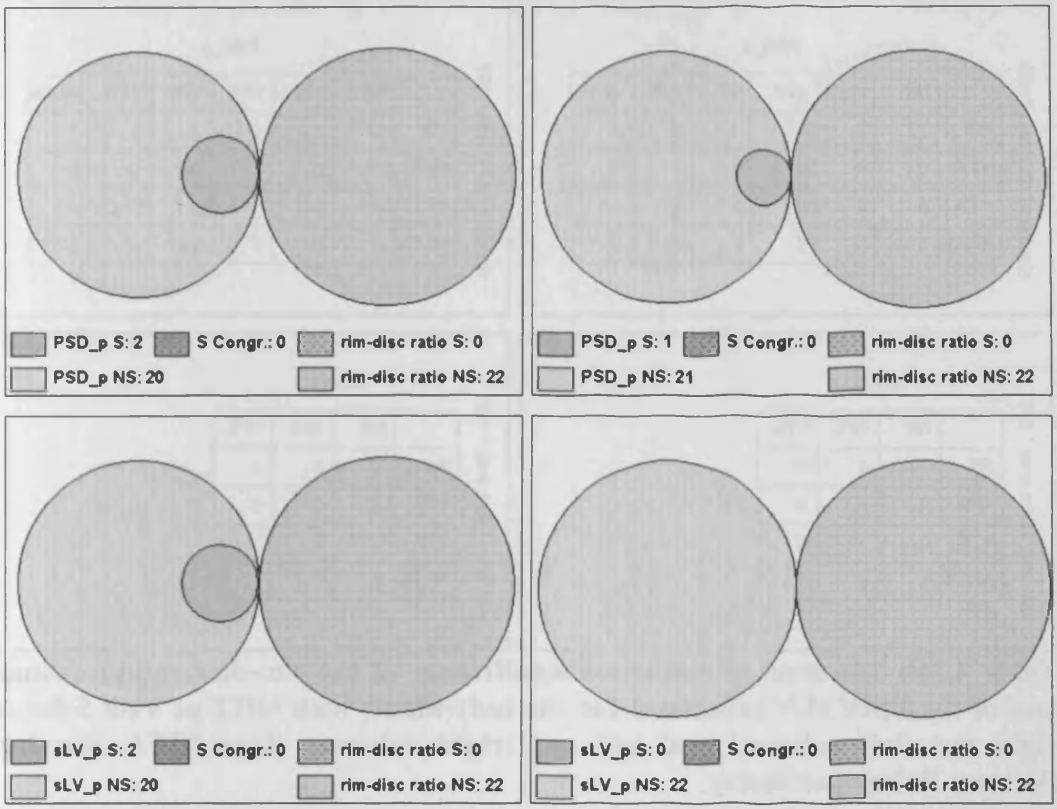

Figure 4.24a Venn diagrams, drawn to scale, illustrating the relationship between the presence (S) or absence of statistical significance (NS) associated with the respective values of the rim-disc ratio and PSD/ sLV for the normal individuals at Visit 5 for the right eye (left column) and left eye (right column). Top: SITA Standard. Bottom: Pulsar perimetry. The number of individuals in whom both measures indicate statistically significant abnormality (S Congr[uence]) is indicated by the overlap and size of the respective two circles.

PSD_p

rim area / disc area * 100

	NS	<10%	<5%	<2%	<1%	<0,5%
NS	22	2	0	0	0	0
<5%	2	0	0	0	0	0
<1%	0	0	0	0	0	0
<0.1%	0	0	0	0	0	0

PSD_p

rim area / disc area * 100

	NS	<10%	<5%	<2%	<1%	<0,5%
NS	19	2	2	1	1	1
<5%	0	0	0	0	0	0
<1%	0	0	0	0	0	0
<0.1%	0	0	0	0	0	0

sLV_p

rim area / disc area * 100

	NS	<5%	<1%
NS	19	4	1
<5%	2	0	0
<1%	0	0	0
<0.1%	0	0	0

sLV_p

rim area / disc area * 100

	NS	<5%	<1%
NS	25	0	1
<5%	0	0	0
<1%	0	0	0
<0.1%	0	0	0

Table 4.26b The level of statistical significance of the rim-disc ratio (ordinate) and of the PSD/ sLV (abscissa) for the individuals with OHT at Visit 5 for the right eye (left column) and left eye (right column). Top: SITA Standard. Bottom: Pulsar perimetry.

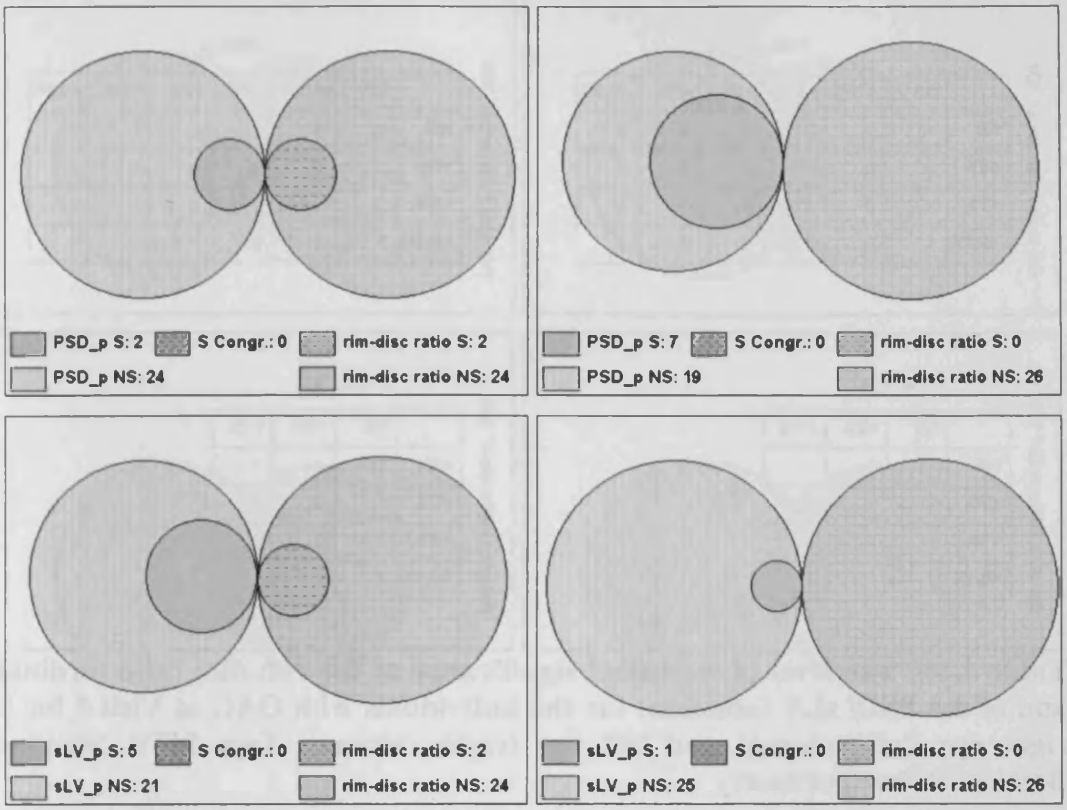

Figure 4.24b Venn diagrams, drawn to scale, illustrating the relationship between the presence (S) or absence of statistical significance (NS) associated with the respective values of the rim-disc ratio and PSD/ sLV for the individuals with OHT at Visit 5 for the right eye (left column) and left eye (right column). Top: SITA Standard. Bottom: Pulsar perimetry. The number of individuals in whom both measures indicate statistically significant abnormality (S Congr[uence]) is indicated by the overlap and size of the respective two circles.

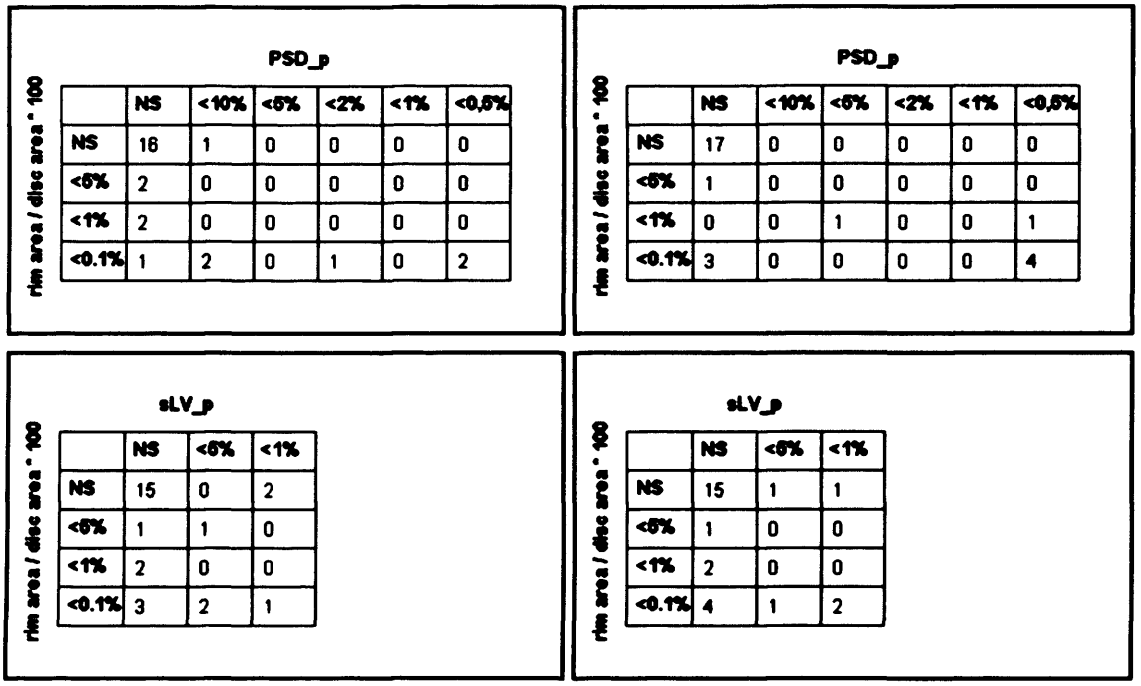

PSD_p

rim area / disc area * 100

	NS	<10%	<5%	<2%	<1%	<0,5%
NS	16	1	0	0	0	0
<5%	2	0	0	0	0	0
<1%	2	0	0	0	0	0
<0.1%	1	2	0	1	0	2

PSD_p

rim area / disc area * 100

	NS	<10%	<5%	<2%	<1%	<0,5%
NS	17	0	0	0	0	0
<5%	1	0	0	0	0	0
<1%	0	0	1	0	0	1
<0.1%	3	0	0	0	0	4

sLV_p

rim area / disc area * 100

	NS	<5%	<1%
NS	15	0	2
<5%	1	1	0
<1%	2	0	0
<0.1%	3	2	1

sLV_p

rim area / disc area * 100

	NS	<5%	<1%
NS	15	1	1
<5%	1	0	0
<1%	2	0	0
<0.1%	4	1	2

Table 4.26c The level of statistical significance of the rim-disc ratio (ordinate) and of the PSD/ sLV (abscissa) for the individuals with OAG at Visit 5 for the right eye (left column) and left eye (right column). Top: SITA Standard. Bottom: Pulsar perimetry.

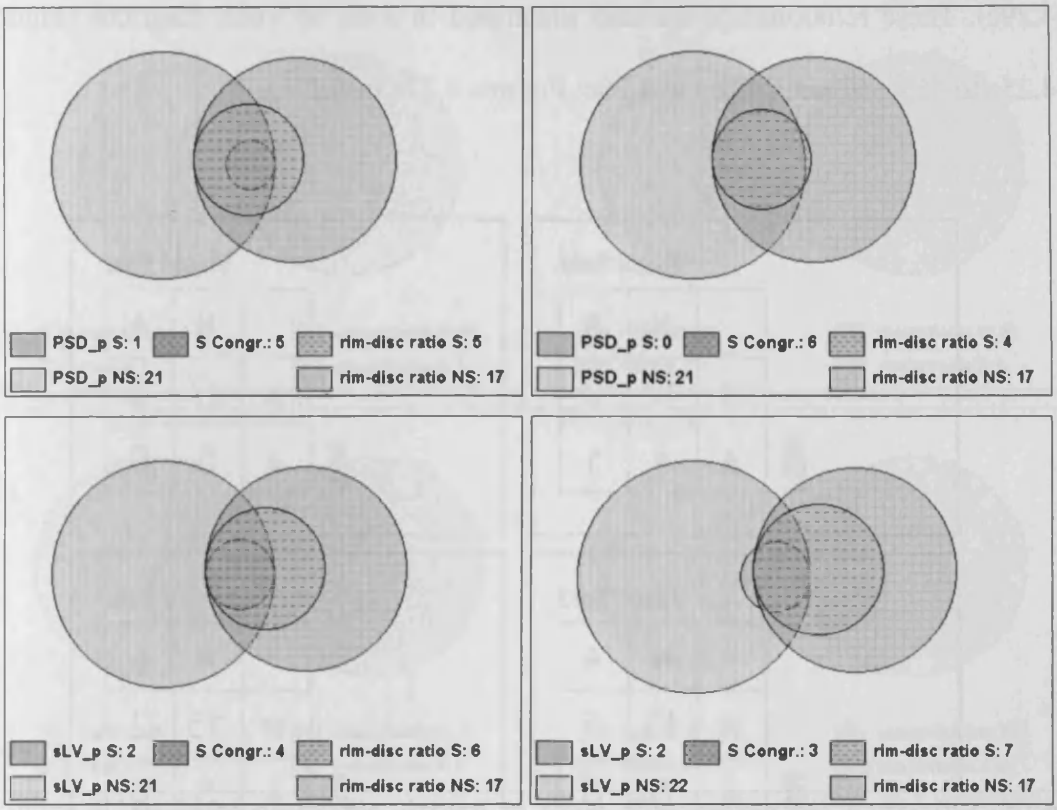

Figure 4.24c Venn diagrams, drawn to scale, illustrating the relationship between the presence (S) or absence of statistical significance (NS) associated with the respective values of the rim-disc ratio and PSD/ sLV for the individuals with OAG at Visit 5 for the right eye (left column) and left eye (right column). Top: SITA Standard. Bottom: Pulsar perimetry. The number of individuals in whom both measures indicate statistically significant abnormality (S Congr[uence]) is indicated by the overlap and size of the respective two circles.

The relationship between the magnitudes (defined in terms of the level of statistical significance) of the Mikelberg discriminate function (FSM), the Burk discriminate function (RB) and the rim-disc ratio, derived by confocal scanning laser ophthalmoscopy (HRT II) and the presence or absence of glaucomatous field loss (evaluated by Professor Wild masked to the group and defined in terms of the criteria described earlier in Section 4.3.1) with the SITA Standard algorithm and with Pulsar perimetry at Visit 5 for the right and the left eyes for the normal individuals, for the individuals with OHT and OAG and are illustrated in terms of contingency tables (Tables 4.27a to 4.27c; Tables 4.28a to 4.28c; Tables 4.29a to

4.29c). These relationships are also illustrated in form of Venn diagrams (Figures 4.25a to 425c; Figures 4.26a to 4.26c; Figures 4.27a to 4.27c).

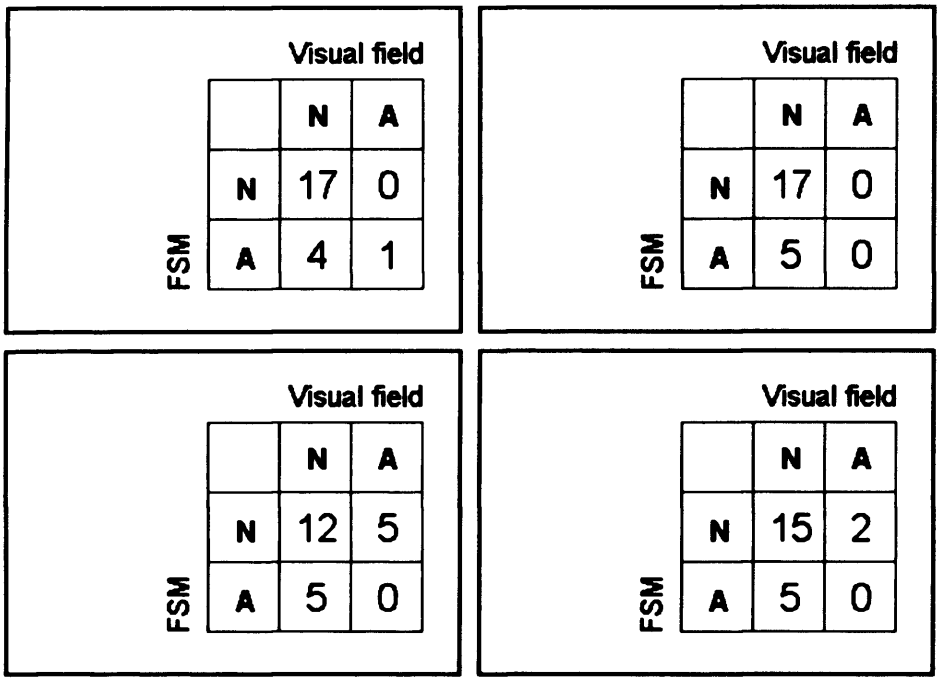

Table 4.27a Table illustrating the normality (N) or abnormality (A) of the FSM (ordinate) and the normality (N) or abnormality (A) of the visual field (abscissa) for the normal individuals at Visit 5 for the right eye (left column) and for the left eye (right column). Top: SITA Standard. Bottom: Pulsar perimetry.

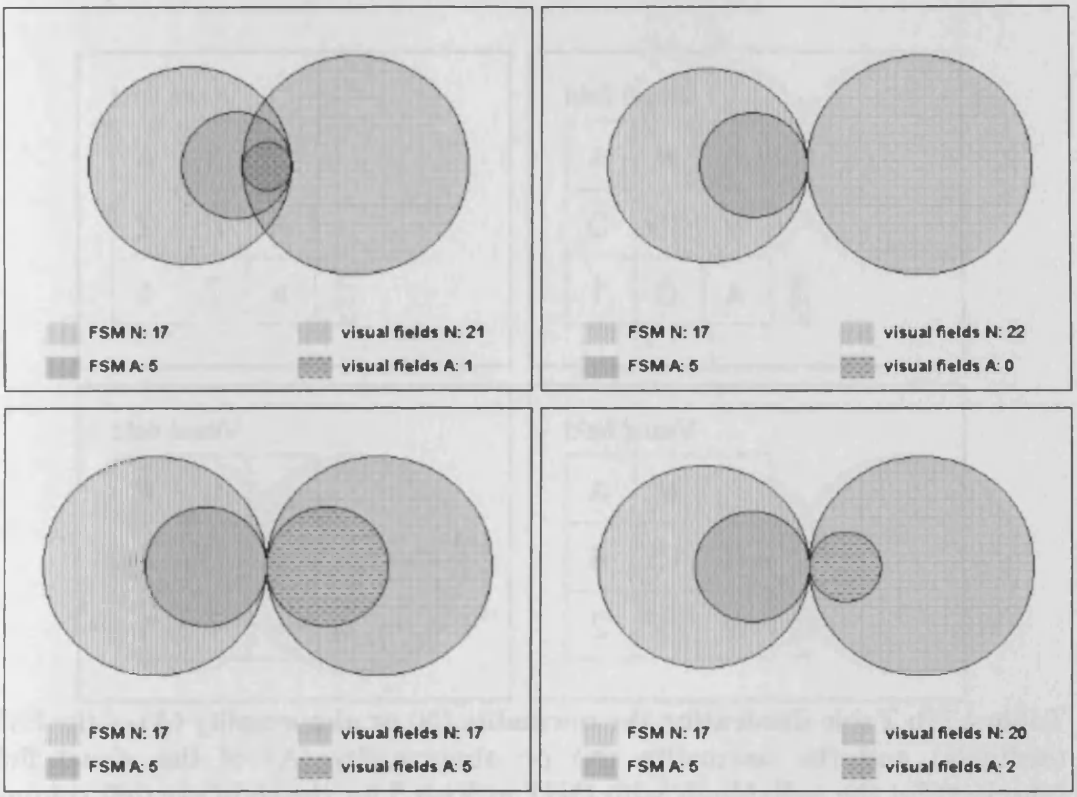

Figure 4.25a Venn diagrams, drawn to scale, illustrating the normality (N) or abnormality (A) of the visual field and the normality (N) or abnormality (A) of the FSM for the normal individuals at Visit 5 for the right eye (left column) and for the left eye (right column). Top: SITA Standard. Bottom: Pulsar perimetry.

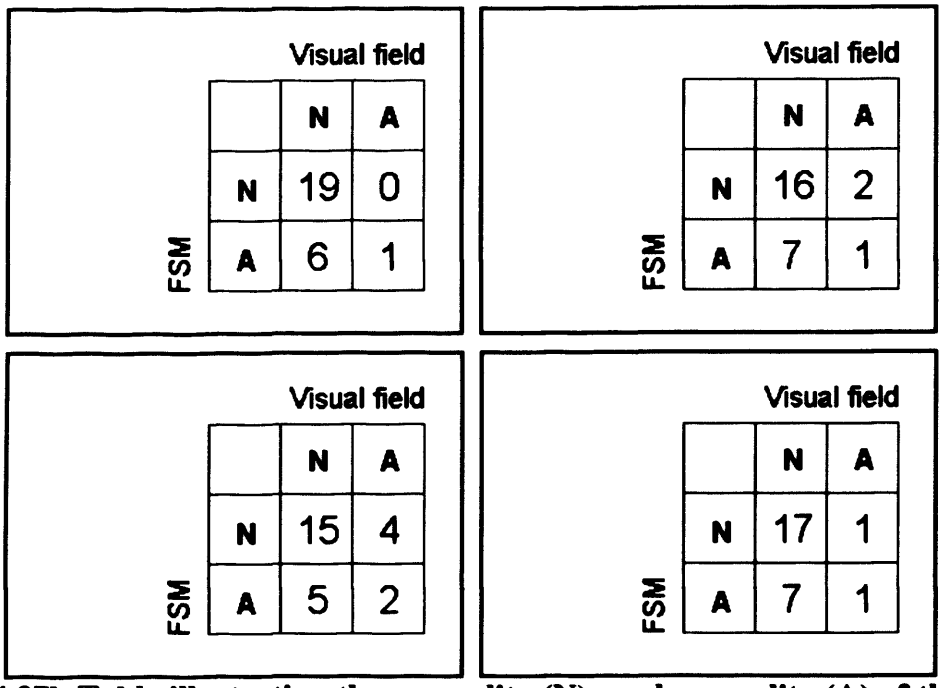

Table 4.27b Table illustrating the normality (N) or abnormality (A) of the FSM (ordinate) and the normality (N) or abnormality (A) of the visual field (abscissa) for the individuals with OHT at Visit 5 for the right eye (left column) and for the left eye (right column). Top: SITA Standard. Bottom: Pulsar perimetry.

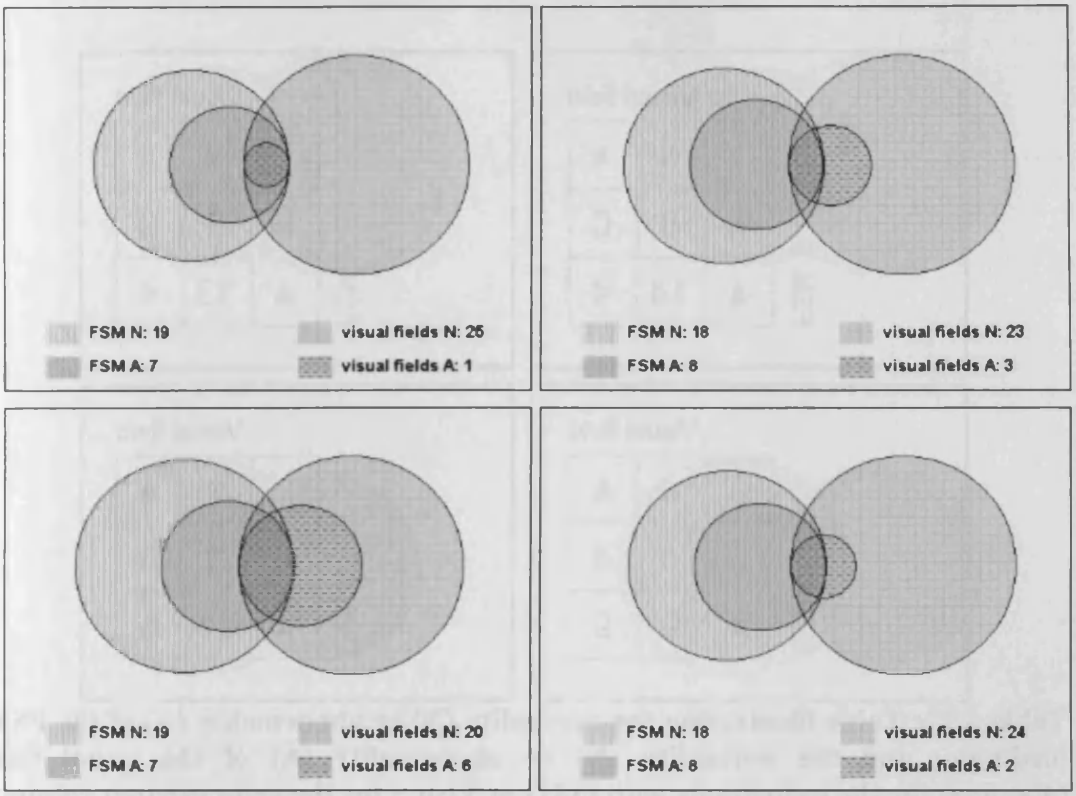

Figure 4.25b Venn diagrams, drawn to scale, illustrating the normality (N) or abnormality (A) of the visual field and the normality (N) or abnormality (A) of the FSM for the individuals with OHT at Visit 5 for the right eye (left column) and for the left eye (right column). Top: SITA Standard. Bottom: Pulsar perimetry.

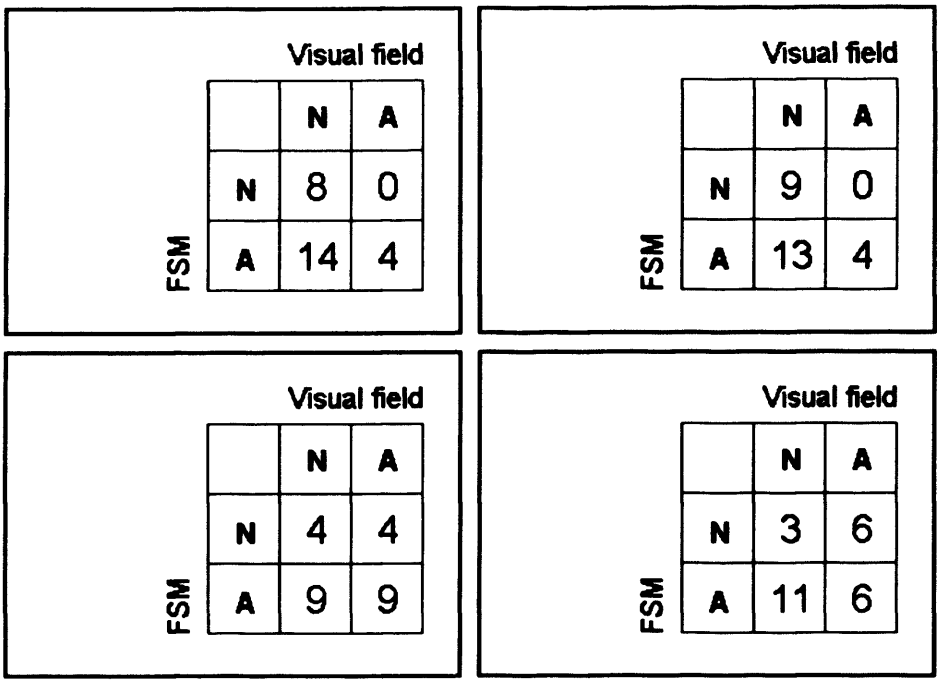

Table 4.27c Table illustrating the normality (N) or abnormality (A) of the FSM (ordinate) and the normality (N) or abnormality (A) of the visual field (abscissa) for the individuals with OAG at Visit 5 for the right eye (left column) and for the left eye (right column). Top: SITA Standard. Bottom: Pulsar perimetry.

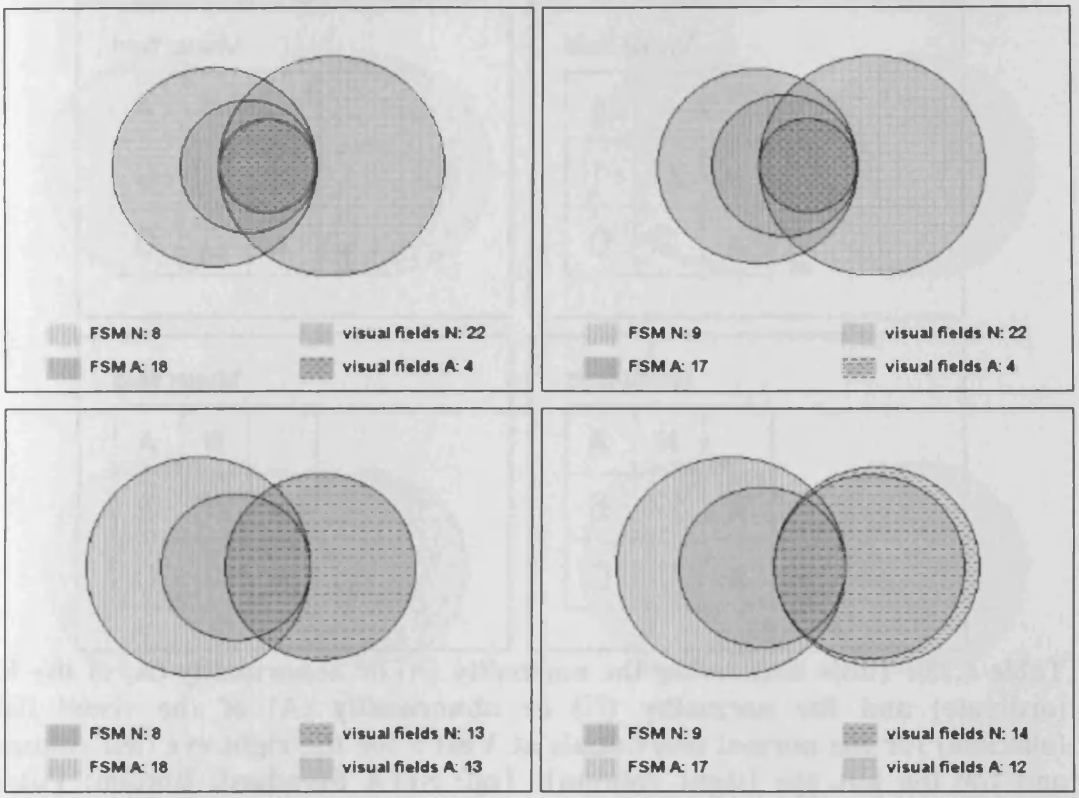

Figure 4.25c Venn diagrams, drawn to scale, illustrating the normality (N) or abnormality (A) of the visual field and the normality (N) or abnormality (A) of the FSM for the individuals with OAG at Visit 5 for the right eye (left column) and for the left eye (right column). Top: SITA Standard. Bottom: Pulsar perimetry.

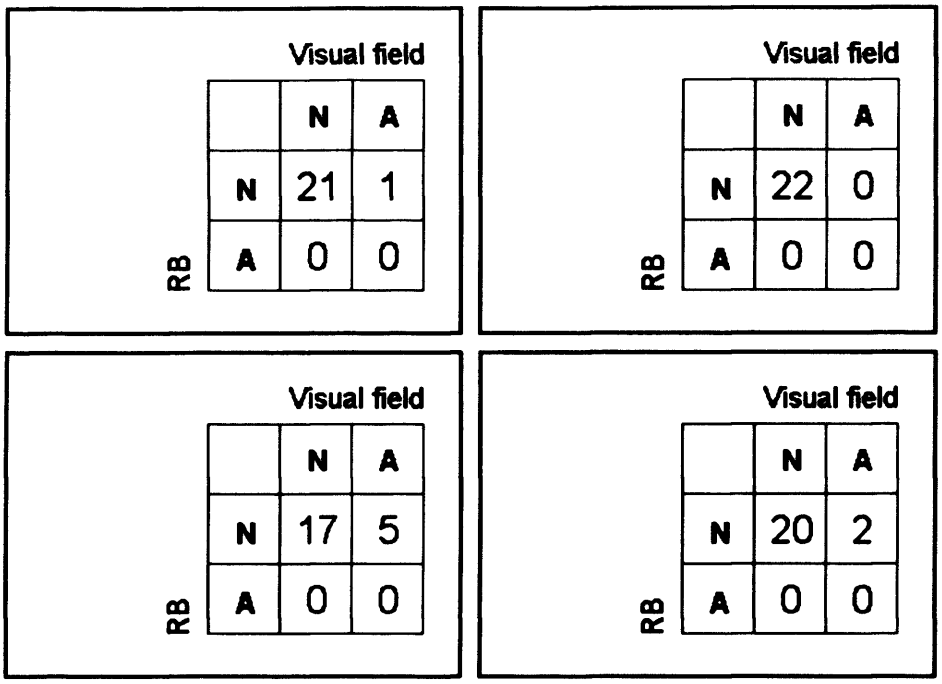

Table 4.28a Table illustrating the normality (N) or abnormality (A) of the RB (ordinate) and the normality (N) or abnormality (A) of the visual field (abscissa) for the normal individuals at Visit 5 for the right eye (left column) and for the left eye (right column). Top: SITA Standard. Bottom: Pulsar perimetry.

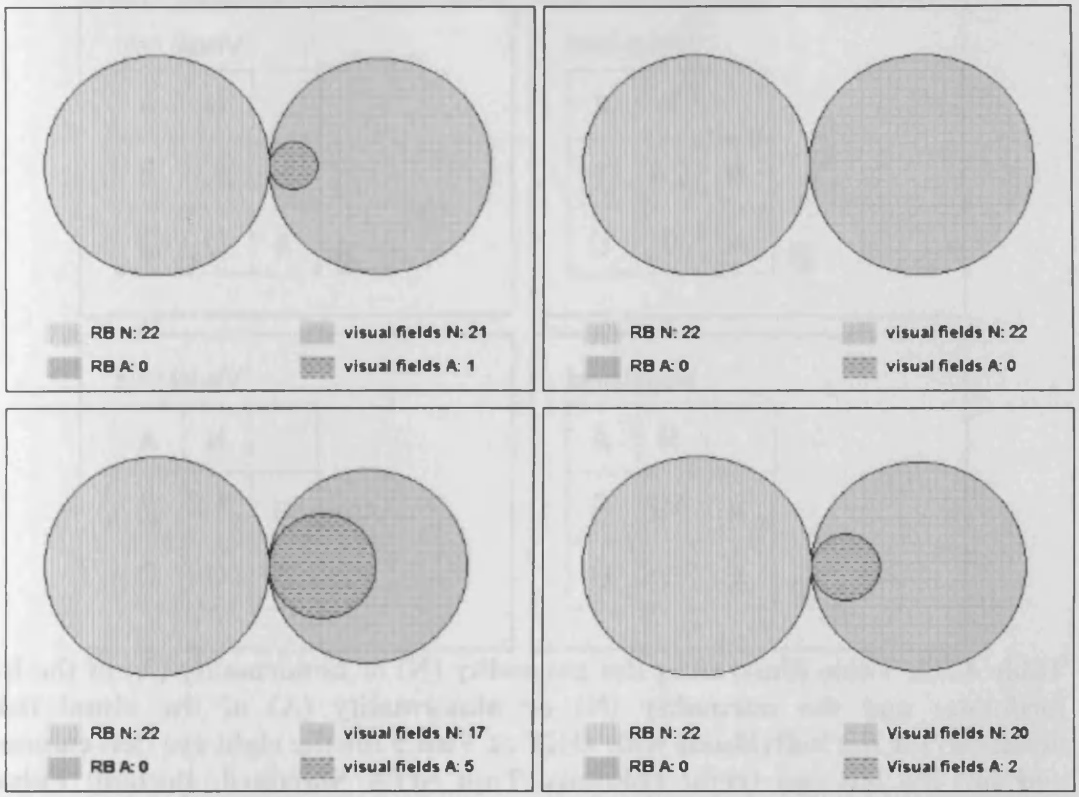

Figure 4.26a Venn diagrams, drawn to scale, illustrating the normality (N) or abnormality (A) of the visual field and the normality (N) or abnormality (A) of the RB for the normal individuals at Visit 5 for the right eye (left column) and for the left eye (right column). Top: SITA Standard. Bottom: Pulsar perimetry.

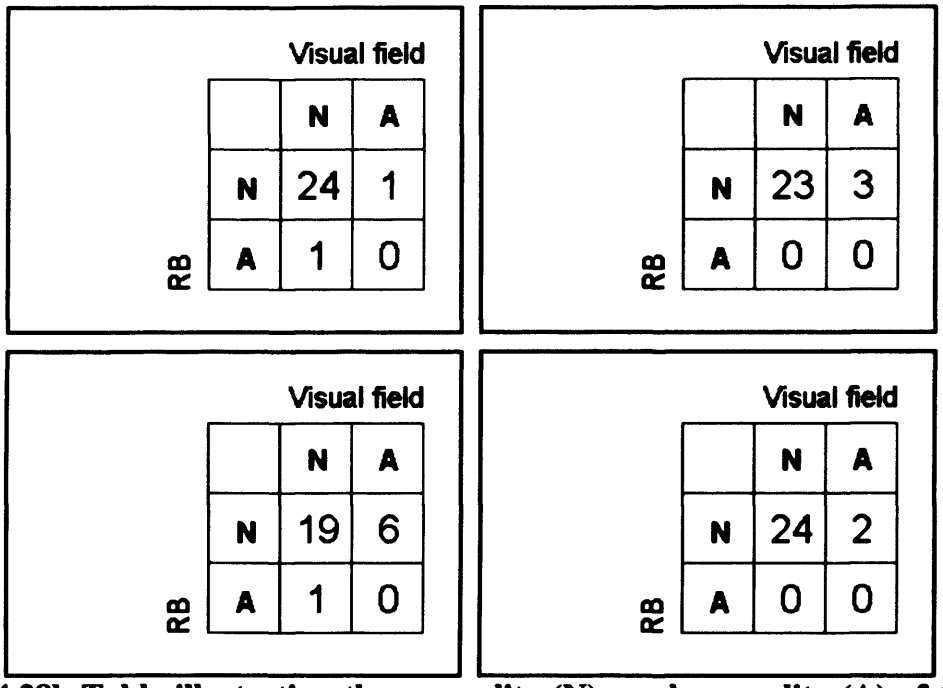

Table 4.28b Table illustrating the normality (N) or abnormality (A) of the RB (ordinate) and the normality (N) or abnormality (A) of the visual field (abscissa) for the individuals with OHT at Visit 5 for the right eye (left column) and for the left eye (right column). Top: SITA Standard. Bottom: Pulsar perimetry.

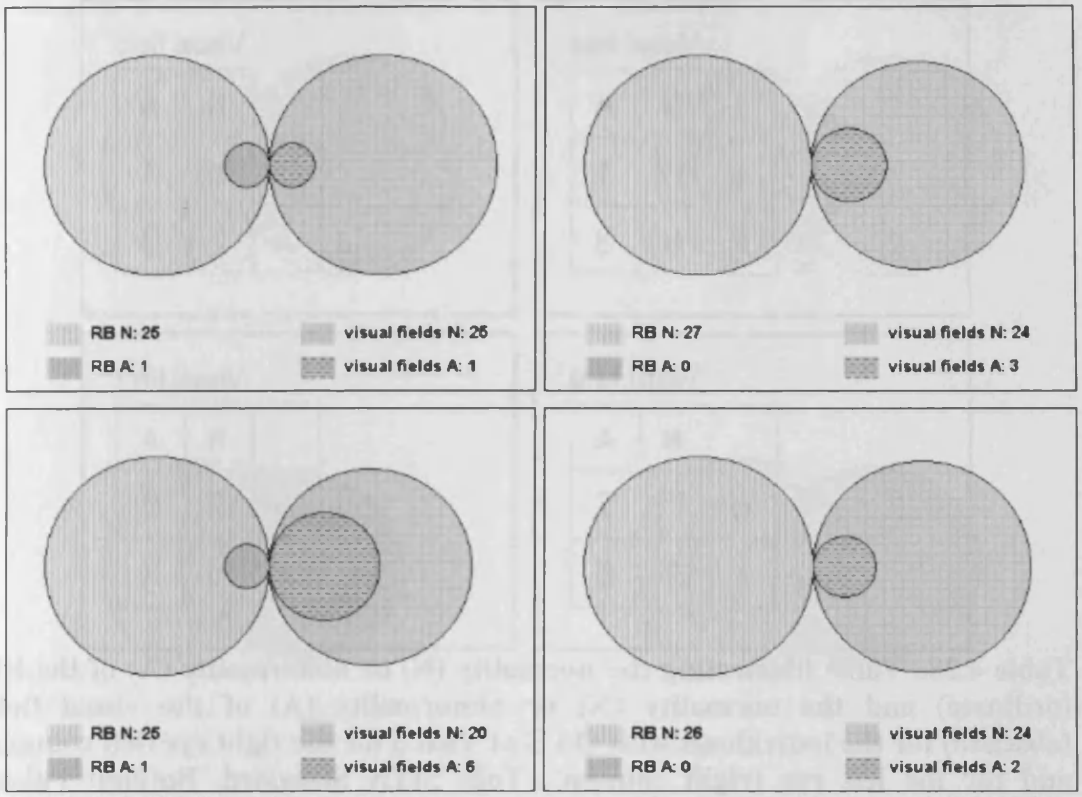

Figure 4.26b Venn diagrams, drawn to scale, illustrating the normality (N) or abnormality (A) of the visual field and the normality (N) or abnormality (A) of the RB for the individuals with OHT at Visit 5 for the right eye (left column) and for the left eye (right column). Top: SITA Standard. Bottom: Pulsar perimetry.

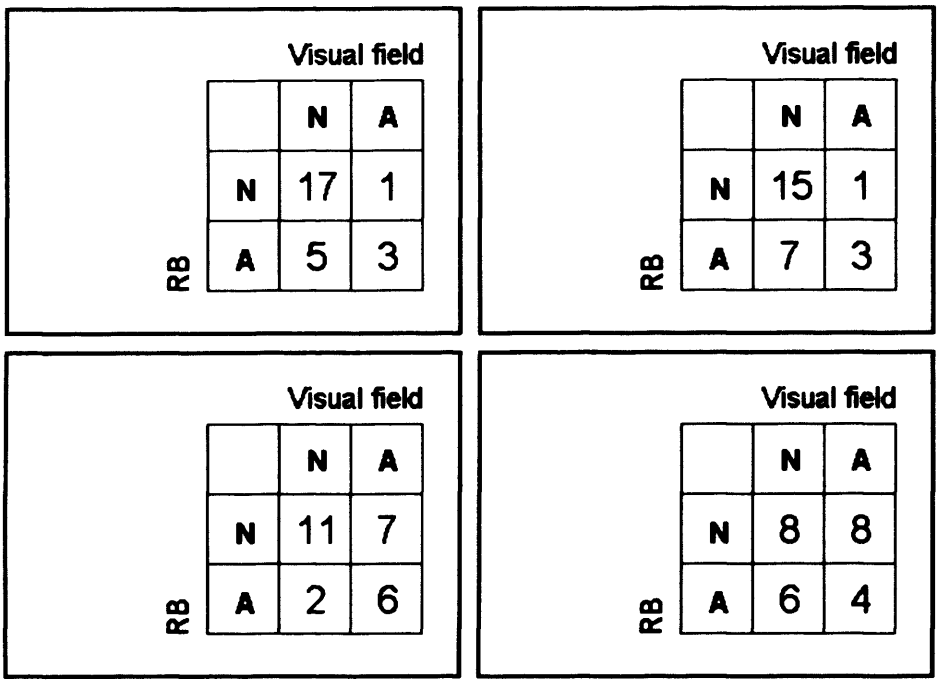

Table 4.28c Table illustrating the normality (N) or abnormality (A) of the RB (ordinate) and the normality (N) or abnormality (A) of the visual field (abscissa) for the individuals with OAG at Visit 5 for the right eye (left column) and for the left eye (right column). Top: SITA Standard. Bottom: Pulsar perimetry.

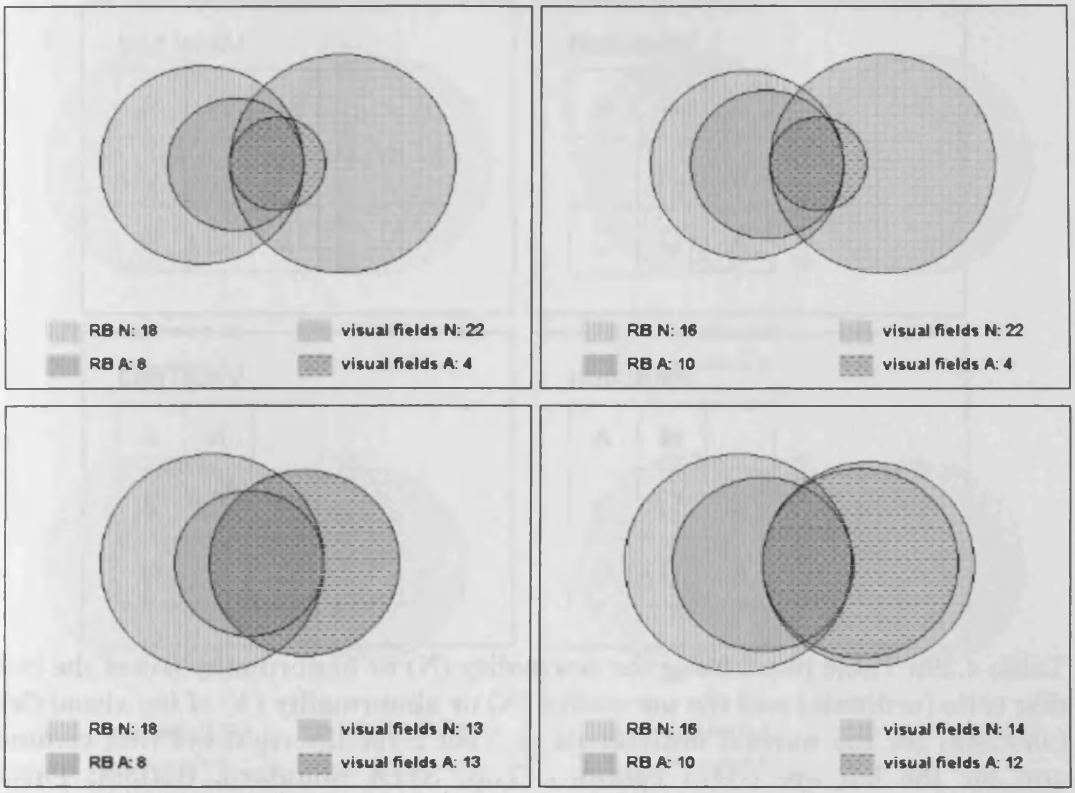

Figure 4.26c Venn diagrams, drawn to scale, illustrating the normality (N) or abnormality (A) of the visual field and the normality (N) or abnormality (A) of the RB for the individuals with OAG at Visit 5 for the right eye (left column) and for the left eye (right column). Top: SITA Standard. Bottom: Pulsar perimetry.

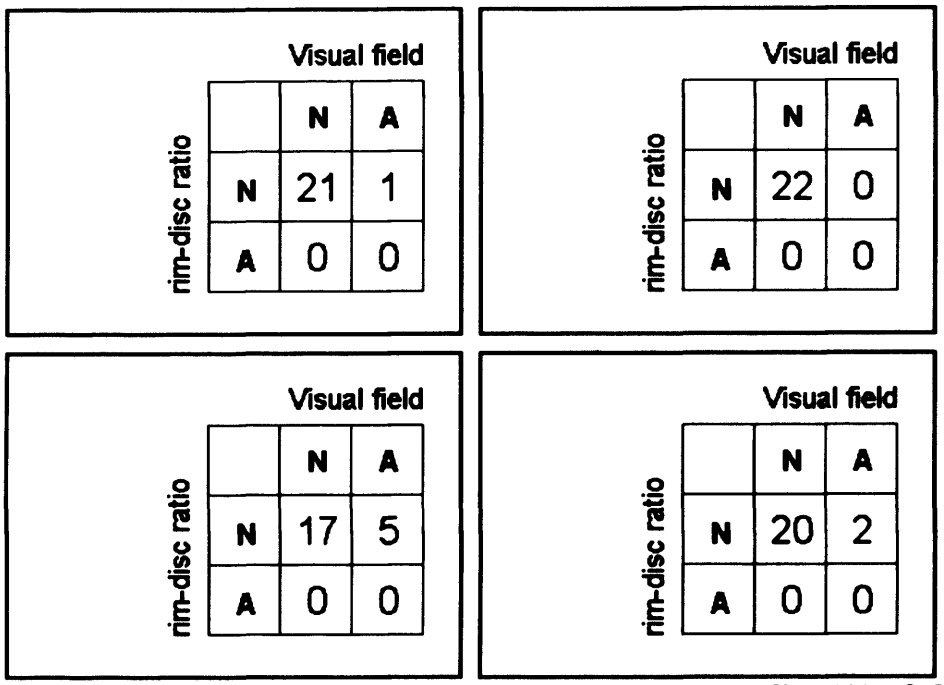

Table 4.29a Table illustrating the normality (N) or abnormality (A) of the rim-disc ratio (ordinate) and the normality (N) or abnormality (A) of the visual field (abscissa) for the normal individuals at Visit 5 for the right eye (left column) and for the left eye (right column). Top: SITA Standard. Bottom: Pulsar perimetry.

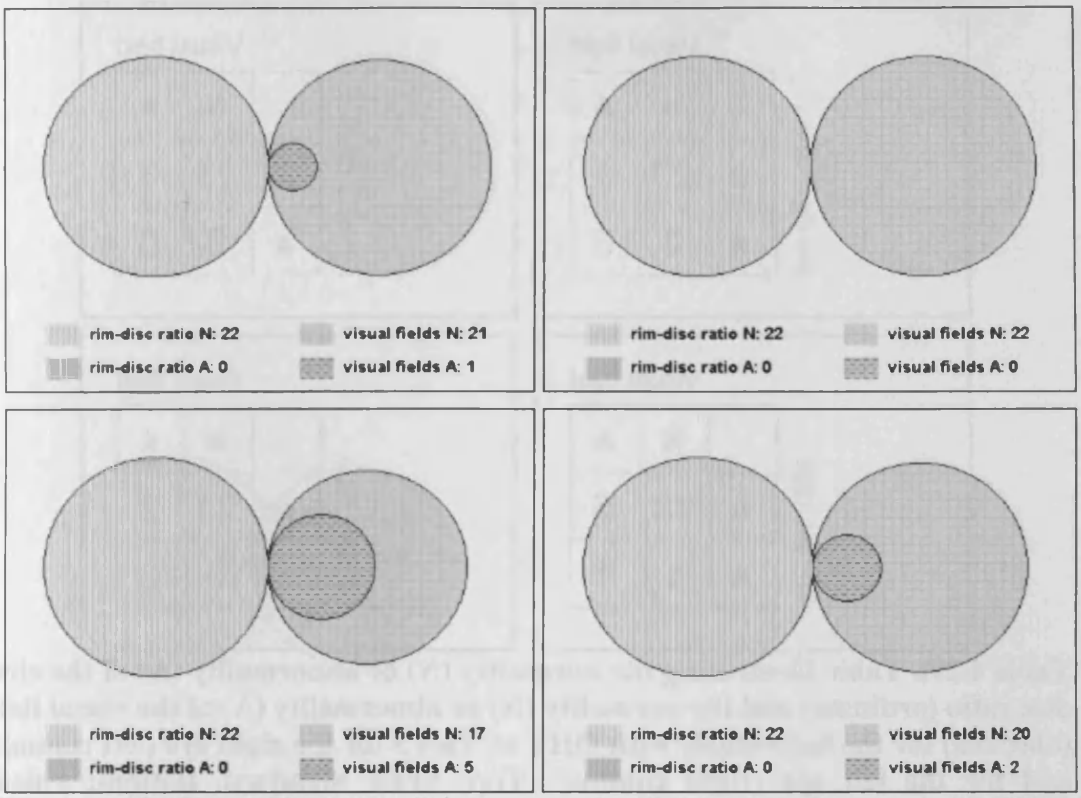

Figure 4.27a Venn diagrams, drawn to scale, illustrating the normality (N) or abnormality (A) of the visual field and the normality (N) or abnormality (A) of the rim-disc ratio for the normal individuals at Visit 5 for the right eye (left column) and for the left eye (right column). Top: SITA Standard. Bottom: Pulsar perimetry.

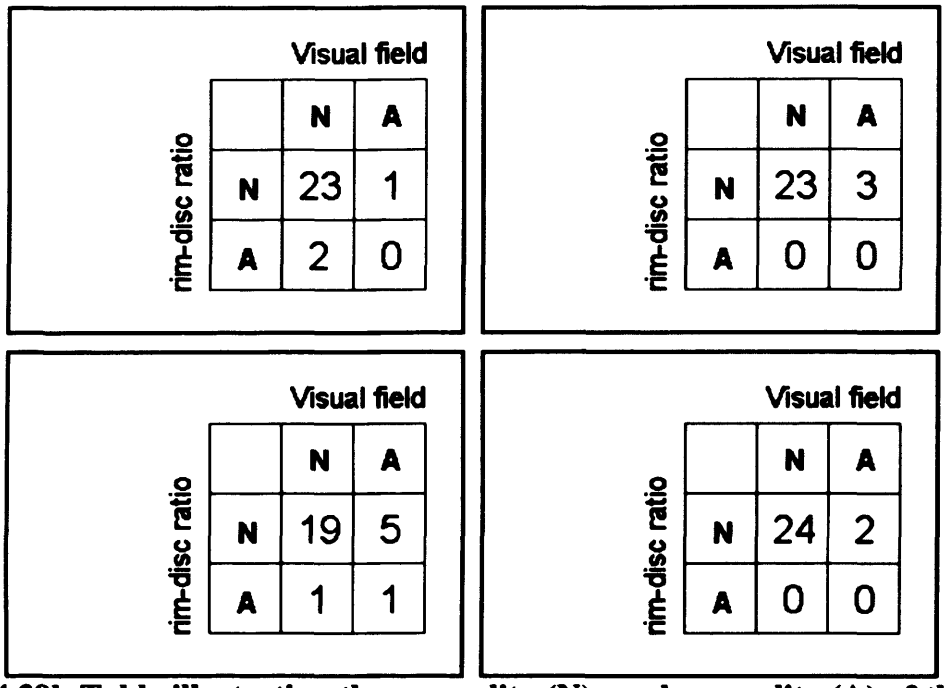

Table 4.29b Table illustrating the normality (N) or abnormality (A) of the rim-disc ratio (ordinate) and the normality (N) or abnormality (A) of the visual field (abscissa) for the individuals with OHT at Visit 5 for the right eye (left column) and for the left eye (right column). Top: SITA Standard. Bottom: Pulsar perimetry.

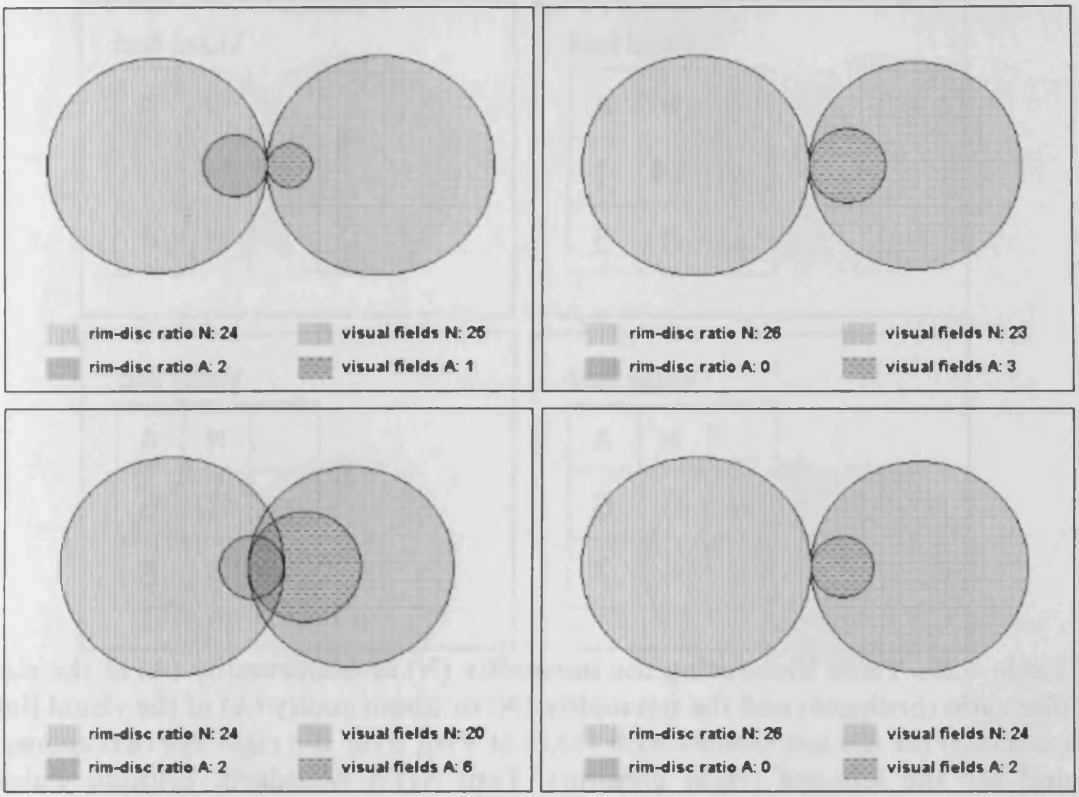

Figure 4.27b Venn diagrams, drawn to scale, illustrating the normality (N) or abnormality (A) of the visual field and the normality (N) or abnormality (A) of the rim-disc ratio for the individuals with OHT at Visit 5 for the right eye (left column) and for the left eye (right column). Top: SITA Standard. Bottom: Pulsar perimetry.

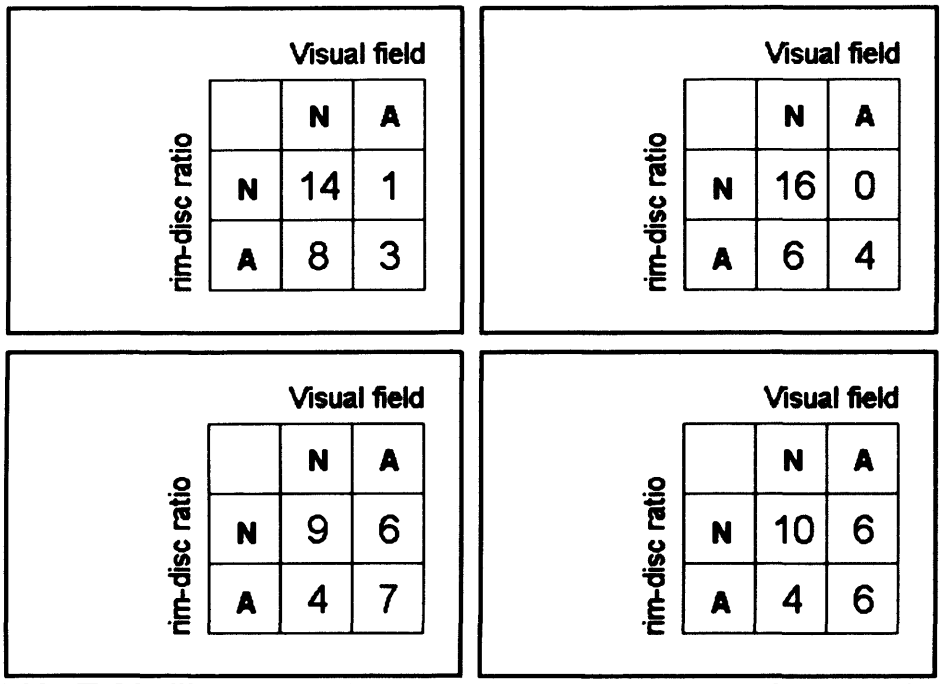

Table 4.29c Table illustrating the normality (N) or abnormality (A) of the rim-disc ratio (ordinate) and the normality (N) or abnormality (A) of the visual field (abscissa) for the individuals with OAG at Visit 5 for the right eye (left column) and for the left eye (right column). Top: SITA Standard. Bottom: Pulsar perimetry.

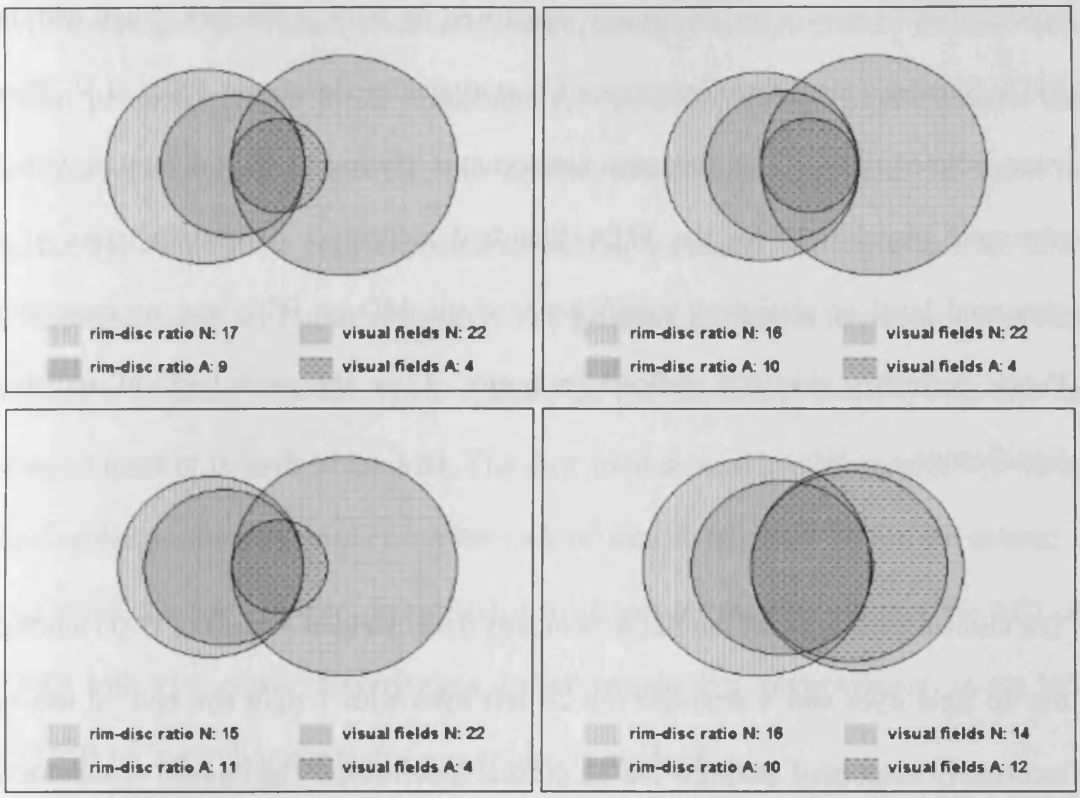

Figure 4.27c Venn diagrams, drawn to scale, illustrating the normality (N) or abnormality (A) of the visual field and the normality (N) or abnormality (A) of the rim-disc ratio for the individuals with OAG at Visit 5 for the right eye (left column) and for the left eye (right column). Top: SITA Standard. Bottom: Pulsar perimetry.

Compared to the clinical diagnosis made by PD Dr med. M. Zulauf, the FSM exhibited the highest sensitivity (19 of 27 cases in the right eye and 17 of 27 cases in the left eye) and the lowest specificity (5 in each eye of 22 normals incorrectly identified) of the HRT derived stereometric parameters. The RB and the rim-disc ratio both exhibited poor sensitivity and 100% specificity. The MDs of the SITA Standard algorithm and of the Pulsar perimeter each exhibited 100% specificity. The MD of the SITA Standard algorithm correctly identified 2 cases of OAG amongst the 27 right eyes and 6 cases amongst the 27 left eyes. No cases of OAG were identified by Pulsar perimetry on the basis of a statistically abnormal MD. The two types of perimetry yielded similar poor sensitivities (6 cases of OAG, each, amongst the right eyes and 6 and 5 cases respectively amongst the left eyes) and high

specificities (2 eyes were incorrectly diagnosed by both perimeters, 1 eye with the SITA Standard algorithm) in terms of a statistically significant PSD/ sLV. There were isolated cases of an abnormal stereometric parameter in conjunction with an abnormal visual field for the SITA Standard algorithm, defined in terms of an abnormal level of statistical significance of the MD or PSD, and no cases with Pulsar perimetry similarly defined in terms of an abnormal level of statistical significance.

The clinical evaluation of the SITA Standard fields yielded 4 cases of OAG amongst the 26 right eyes and 4 amongst the 26 left eyes with 1 right eye and no left eye incorrectly diagnosed amongst the 22 normal individuals. The clinical evaluation of the Pulsar fields yielded 13 cases of OAG amongst the 26 right eyes and 12 amongst the 26 left eyes with 5 right eyes and 2 left eyes incorrectly diagnosed amongst the 22 normal individuals. Consequently, the degree of agreement of the stereometric parameters no different with the clinical evaluation of the field than with evaluation based upon the indices. In addition, the clinical evaluation of the results from Pulsar perimetry identified more cases of glaucomatous field loss than the clinical evaluation of the results from SAP but with poorer specificity.

4.5 Discussion

4.5.1 The learning effect

The ANOVAs for the various visual field indices gave no indication of a learning effect for either type of perimetry. This finding may, perhaps, be explained by the inclusion of a substantial number of individuals (approximately 65%) with either OHT or OAG who had taken part in the study of the learning effect for SWAP. The latter would have been expected to be thoroughly familiar with the requirements of

SAP and might, as 'trained observers', be expected to be immediately familiar with Pulsar perimetry and to yield, immediately, a plausible/ correct result without the necessity for practice. However, the normal individuals, who were all naïve to perimetry, would have been expected to exhibit a (small) learning effect for SAP and, perhaps, also for Pulsar perimetry. The group exhibited an improvement in MS for SITA Standard between Visits 1 and 5 of 0.43dB across the two eyes and an improvement of 0.40dB in the MD. The lack of statistical significance of this latter finding unquestionably arises from the lack of statistical power within the cohort; a sample of 27, for example, is sufficient to detect an improvement in the MD of 3.0dB with 95% power. Nevertheless, the corresponding 'improvement' in the MS and MD for the Pulsar perimetry was clinically negligible.

The lack of a learning effect for Pulsar perimetry in the normal individuals naïve to perimetry implies either that the visual task was 'simple' and did not require any 'training' or that the task was too complex and could not be improved over the five training sessions. The former is an ideal requirement for perimetry whilst the latter is unacceptable. The learning effect between Visits 1 and 5 within the group with OAG of approximately 0.3dB could have arisen from either scenario. However, the analysis of the learning effect in terms of the limits of agreement for the Pulsar MD between Visits 1 and 5 indicates that an equal number of individuals (approximately one third) across the three groups exhibited an improvement, an equal number exhibited a deterioration, and the remaining one third exhibited little difference. The exception to this trend occurred for the sLV in the individuals with OAG: more individuals demonstrated an apparent deterioration than an apparent improvement.

The PMS/CMS ratio was similar across the five visits for each algorithm. The stability of the ratio is in contrast to that reported for SAP (Wood et al 1987b; Heijl et al 1989c; Wild et al 1989; 1999a) where the peripheral zone of the central field exhibited greater improvement than the central zone. The use of Program 24-2 rather than Program 30-2 for the SITA Standard algorithm (i.e. without the stimulus locations at the extremities of the central field) and the use of an identical grid for Pulsar perimetry reduced the potential for an improvement in sensitivity for both types of perimetry.

The spread of the limits of agreement for Pulsar perimetry between Visits 1 and 5 was greater than for the SITA Standard algorithm in absolute terms and considerably greater in proportionate terms given the reduced dynamic range of Pulsar perimetry compared to SAP.

Similar results were found for the limits of agreement for the sLV compared to those for the PSD of the SITA Standard algorithm. Thus, the analysis, in terms of the limits of agreement, explains the lack of statistical significance achieved by the various ANOVAs, i.e. some individuals seemingly improve, some seemingly deteriorate and some seemingly exhibit a similar level of performance. The question remains as to whether the apparent improvements and deteriorations are true measures or merely expressions of variability. In either case, the magnitudes of these changes, both in absolute and in proportionate terms, are clinically unacceptable.

The analysis of the learning effect in terms of the various percentiles of the differences in sensitivity across all stimulus locations was less informative in terms

of the change in sensitivity since the representation was across individuals rather than within individuals. The truncation of the percentiles at approximately 16dB for the SITA Standard algorithm in the normal individuals and in the individuals with OHT arose from the lack of stimulus locations exhibiting sensitivities below this value. Similarly, the scatter below approximately 16dB in the location of the percentiles for SITA Standard in the individuals with OAG arose from the limited number of locations exhibiting reduced sensitivity. The apparent extension of the range of the percentiles towards minimal levels of sensitivity for Pulsar perimetry in all three diagnostic groups, compared to the SITA Standard algorithm, arises from the differences in dynamic range between the two algorithms.

The difference between Visit 1 and Visit 5 in the Total Deviation and in the Comparison probability levels exhibited no particular trend. In the right eye of the normal individuals, the SITA Standard algorithm exhibited an apparent increase in the number and/ or severity of the Total Deviation probability levels at Visit 5. In contrast, the individuals with OAG seemingly exhibited a reduction in the number and/ or severity of the Comparison probability levels for Pulsar perimetry (a 1.9 fold reduction for the right eye and a 1.2 fold reduction for the left eye). It is possible that these latter findings could be explained by a reduction in motivation for perimetry at the last examination. However, it is more likely that the desired information from the analysis (i.e. the signal) is masked by the inherent between-visit variability in the results across all three groups.

One of the individuals with OHT exhibited a repeatable visual field defect by Pulsar perimetry (in the right eye) and only one individual a repeatable defect by SAP (in

the right eye). No comparative studies have yet been published which determine the prevalence of visual field loss by Pulsar perimetry and by SAP. The Pulsar perimeter has been compared to SAP using Program G1 and the TOP algorithm in 17 individuals with OHT with normal visual fields by SAP and in 22 normal individuals (Fernandez-Vidal et al 2002). Pulsar perimetry yielded a poorer (i.e. worse) group mean MD and a larger group mean LV for the individuals with OHT compared to the normal individuals. However, the number of cases (or eyes) with apparent glaucomatous visual field loss was not given.

The age distribution of the normal individuals did not permit an accurate estimation of the slope of the decline in MS with increase in age (Table 4.2). A similar age-related decline in sensitivity between SAP and Pulsar perimetry was found by Gonzalez-Hernandez et al (2000a) and an extension of the age range of the cohort in the current study would enable a comparison of the results with those of the Spanish group.

The examination time for Pulsar perimetry over the five visits was approximately six seconds shorter for the left eye than for the right eye both for the normal individuals and for the individuals with OHT, however, the difference was in the region of 9-10 seconds for the individuals with OAG. The examination duration for Pulsar perimetry was approximately 70 seconds shorter than the SITA Standard algorithm for the normal individuals and for the individuals with OHT and 70 to 90 seconds shorter for the individuals with OAG. The reduction in time for the Pulsar perimetry is most likely to occur from the use of the TOP algorithm rather than from the stimulus, itself. The examination duration arising from the use of the TOP algorithm

is faster than that arising from the use of the SITA Fast algorithm (King et al 2002; Wadood et al 2002). Overall, it would seem that, in terms of the group as a whole, no learning effect was present for Pulsar perimetry. However, some individuals clearly exhibited an improvement in performance over the various visits whilst other seemed to exhibit an apparent reduction in performance. Such results do not auger well for the future clinical application of Pulsar perimetry.

4.5.2 The within-individual within-algorithm between-visit (Visits 4 and 5) variability

The analysis was based on the assumption that the learning effect for both types of perimetry was either clinically minimal or not present. The limits of agreement between Visits 4 and 5 for both MD and PSD/ sLV exhibited the same trend as for those between Visit 1 and 5 for both types of perimetry but were generally narrower for Visits 4 and 5, i.e. they were larger for Pulsar perimetry across all three groups, in both absolute and proportionate terms, than for SITA Standard and were largest for the group with OAG. Such a finding suggests that Pulsar perimetry exhibits greater between-examination variability (i.e. Long-term fluctuation) compared to the SITA Standard algorithm. This, in turn, indicates that Pulsar perimetry will be less useful for the identification of progressive visual field loss compared to SAP with the SITA Standard algorithm.

The difference between Visit 4 and Visit 5 in the Total Deviation and in the Comparison probability levels exhibited no particular trend between the two different algorithms or between the three groups.

4.5.3 The between-individual within-visit (Visit 5) between-algorithm variability

The magnitude of the limits of agreement for the between-algorithm difference in the SITA Standard algorithm and Pulsar perimetry for the MD at Visit 5 spans a range of approximately 9.5dB. The difference largely arises from the magnitude (more positive) of the MD for the SITA algorithm compared to that for Pulsar perimetry. The reason for the more positive MD for the SITA Standard algorithm is not clear but is likely to arise from the differences in the characteristics of the two groups of normal individuals used to derive the two respective sets of age-corrected normal values. The difference in the MD between the two types of perimetry exhibited a slight tendency to increase with increase in severity of the field loss. It is possible that the magnitude of the limits of agreement may also have been influenced by the difference in the dynamic ranges between the two types of perimetry. The limits of agreement for the PSD/ sLV were similarly unacceptably wide and largely arose from the greater magnitude of the sLV compared to the PSD. The larger sLV of Pulsar perimetry would be expected on the basis of the smaller MD.

The difference in dynamic range between the two perimeters is well illustrated in Figures 4.16a to 4.16b where the sensitivity derived by the Pulsar perimeter underestimates the value of sensitivity obtained by the SITA Standard algorithm by approximately 10dB.

The number and/ or severity of the Comparison probability levels for Pulsar perimetry at Visit 5 in the individuals with OAG was approximately 4.5 fold more than for the Total Deviation probability levels of the SITA Standard algorithm

(Table 4.20). This finding can be explained in one of several ways, namely: that Pulsar perimetry is more sensitive than SAP for the detection of glaucomatous abnormality, and/ or that the confidence limits for normality are (proportionately) narrower for Pulsar perimetry than for the SITA Standard algorithm; that compared to SAP, Pulsar perimetry is influenced to a greater extent by abnormalities in the ocular media; or that the confidence limits for normality for Pulsar perimetry are currently incorrect. The current software of the Pulsar perimeter does not enable shape probability analysis (i.e. that equivalent to the Pattern Deviation probability analysis of the HFA and to the Corrected Comparison probability analysis of the Octopus perimeter). The exclusion criteria for the cohort used in the study comprised a cataract greater than NC2.0, NO2.0, C1.0, or P1.0 by LOCS III (Chylack et al 1993). Nevertheless, the influence of cataract upon the Pulsar stimulus warrants further investigation in relation to shape probability analysis. It is also possible that the confidence limits for normality for Pulsar perimetry are incorrect. The latter is a distinct possibility given the underestimation of the MD for Pulsar perimetry. Indeed, the CoV (which gives an indication of the likely confidence limits of a given measure) at each individual stimulus locations in both eyes was greater by, on average, approximately 1.6 fold for Pulsar perimetry compared to the SITA Standard algorithm both at Visit 1 and at Visit 5. Whilst the latter finding must be considered with caution due to the limited size of the cohort, it would imply that the current confidence limits for Pulsar perimetry are too narrow and should be wider than those for SAP with the SITA Standard algorithm. Nevertheless, despite the equivocal nature of the confidence limits for Pulsar perimetry, it is still possible that Pulsar perimetry possesses greater sensitivity for the detection of glaucomatous abnormality. However, it should be noted that only one of the individuals with OHT exhibited repeatable field loss, in one eye only, in

terms of probability analysis by Pulsar perimetry, and one individual exhibited repeatable field loss, in one eye only, with the SITA Standard algorithm.

4.5.4 The structure function relationship

The FSM was the best of the three stereo-metric parameters for the identification of OAG. Such a finding is in agreement with other studies (Bryce et al 2003; Borque et al 2008; Ferreras et al 2008). The clinical evaluation of the results from Pulsar perimetry possibly identified slightly more cases of functional abnormality than SAP at the cost of a reduction in specificity. However, the outcome of the clinical evaluation of the results from Pulsar perimetry need to be treated with caution in the absence of the Corrected Comparison (shape) probability analysis. The agreement between the structural and functional outcomes was poor: only 9 of the 22 right eyes and 6 of the 22 left eyes exhibited abnormality by both FSM and Pulsar perimetry.

4.6 Conclusion

The results of the current study suggest that, within the constraints of the limited size of the cohort, Pulsar perimetry exhibits poorer performance criteria than SAP using the SITA Standard algorithm. Compared to the SITA Standard algorithm, such disadvantages include the apparent heterogeneity in any learning effect; the greater absolute and proportionate difference in the between-examination variability (at Visits 4 and 5); the reduced dynamic range; the uncertainty of the current confidence limits for normality; the absence of any deeper/ additional field loss; and the similar agreement with the stereometric parameters.

On the positive side, Pulsar perimetry was well accepted by the individuals in all three diagnostic groups, was easy to perform and, due to the use of the TOP algorithm, was relatively rapid.

CHAPTER 5

THE EFFECT OF DEFOCUS ON THE PULSAR STIMULUS IN NORMAL INDIVIDUALS AND IN PATIENTS WITH OAG

5.1 Introduction

Defocus decreases the quality of the retinal image by reducing the luminous contrast and changing the luminous gradient at the image margin. Defocus can result from ametropia or from presbyopia. Therefore, it is evident that defocus will impact upon the threshold derived by perimetry. Several factors can influence the relationship between defocus and the measurement of threshold. The effect of defocus is dependent on factors such as stimulus size, stimulus eccentricity, magnitude of defocus, background luminance and pupil size. The application of large stimuli diminishes the effect of ametropia and presbyopia, considerably (Ogle 1960; 1961a; 1961b). However, the use of large stimuli reduces the resolution at which localised abnormality can be detected and, therefore, is not clinically acceptable (Bek and Lund-Andersen 1989). The effect of defocus diminishes with increase in eccentricity (Monjé and Offermann 1955; Fankhauser and Enoch 1962; Maguire 1971). Sensitivity decreases rapidly in the centre, compared to the periphery, with defocus and this effect increases with increase in defocus (Fankhauser and Enoch 1962; Benedetto and Cyrlin 1985). Retinal elevations and depressions can provoke ametropia in these regions (Schmidt 1955; Drance et al 1967; Maguire 1971), which, in turn, can give raise to relative scotomas known as 'refractive scotomas' (Drance et al 1967).

Defocus also occurs because the apparent position of the stimulus is displaced on the retina by the prismatic effect arising from high powered correcting trial lenses (Atchison and Johnston, 1979). But this effect can be neglected, because in relation

to the other factors, it is relatively unimportant. Patients undergoing perimetry should wear contact lenses instead of trial lenses for powers greater than ±10 dioptres and for accurate measurements beyond 30 degrees to 40 degrees eccentricity (Atchison and Johnston 1979; Zalta 1989).

Due to the higher spherical aberrations in individuals with larger pupil sizes, the depth of focus will decrease and will therefore exert less effect on defocus.

5.1.1 Newer aspects of defocus in the context of perimetry

The effect of defocus has been investigated for different aspects of perimetry. One aspect is the distinction between detection acuity, defined as the highest spatial frequency for which luminance gratings can be discriminated from a uniform field, and resolution acuity, defined as the highest spatial frequency for which spatial patterns are perceived (Wang et al 1997). Detection acuity in the periphery varies significantly with the amount of defocus, whereas acuity for grating resolution or letter discrimination in the periphery is unaffected by defocus over a range up to 6 dioptres. These findings support the hypothesis that detection acuity in the periphery is limited by contrast, whereas resolution acuity is limited by neural undersampling. The former finding impacts upon the use of conventional perimetry in the measurement of the differential light sensitivity.

The effect of dioptric blur on 'circular' white stimuli is quantitatively and qualitatively very different between the fovea and in the periphery (Anderson et al 2001). Larger stimuli not only yield a much lower threshold than smaller stimuli but

are more resistant to the effects of optical defocus in both the fovea and the periphery.

Newer perimetric methods (e. g. FDT) have no provision for introducing corrective lenses and this implies that some patients are sometimes probably examined appreciable in the presence of defocus. As described in Section 1.7.1, FDT examines the visual field by means of low-spatial-frequency sine-wave-grating stimuli that are counterphase flickered at high temporal frequency.

As described in Sections 2.2 and 4.1.3, the stimulus for the Pulsar perimeter comprises a 5 degrees diameter circular wave presented for a duration of 500msec, isoluminant to the background, and temporally modulated at 30Hz. The spatial frequency of the circular wave varies in 35 steps from 0.5 cycles/ degree to 6.3 cycles/ degree. The corresponding variation in contrast ranges between 6% and 100%. As such, defocus would be expected to attenuate the sensitivity to the Pulsar stimulus. However, the influence of defocus upon the outcome of Pulsar perimetry is unknown.

5.2 Purpose

The aim of the study was to determine the effect of defocus on sensitivity observed by Pulsar perimetry in normal individuals and in individuals with OAG.

5.3 Methods

5.3.1 Case series

The cohort comprised 31 consecutively presenting individuals who met the inclusion criteria for enrolment in the study and who, during the recruitment phase, had

volunteered to take part in the study. As with the previous studies, all individuals were provided with verbal and written information concerning the nature of the study, and gave written consent, in accordance with the requirements, and approval, of the Ethikkommission des Kantons Graubünden, which in turn adhered to the tenets of the Declaration of Helsinki.

The case series consisted of two groups of individuals. One group comprised 17 normal individuals (10 females and 7 males) who were recruited from Castelberg Optometry in Landquart, Switzerland. The mean age of the group was 63.8 years (SD=8.2, range 45-74 years). Twelve of the 14 individuals with OAG were drawn from the ophthalmological practice of PD Dr. med. Zulauf, Chur, Switzerland. The remaining two individuals were drawn from the practices of two ophthalmologists within Landquart, Switzerland. The mean age of the group was 62.4 years (SD=8.2; range 48-77 years). The age profiles of the two groups are given in Table 5.1.

Age (years)	**Normal Individuals**	**OAG**
40-49	1	2
50-59	5	1
60-69	6	10
70-79	5	1

Table 5.1 The number and age distribution of the individuals within the two groups.

None of the normal individuals had taken part in either of the previous two studies. Nine of the 14 individuals with OAG had taken part in the previous study with

Pulsar perimetry, 7 individuals in the study of SWAP and 5 individuals in both studies.

The number of individuals included within each diagnostic category was not based upon a power calculation but was dictated by the remaining time available for the thesis.

As discussed previously in Chapters 3 and 4, the representative nature of the case series to that within the general population can only be determined from comparisons with other case series compiled for similar studies.

All the normal individuals underwent a standard optometric and ophthalmological examination at baseline comprising the same procedures as described in Chapter 3. The individuals who had participated at the SITA SWAP and/ or Pulsar perimetry studies did not undergo a further optometric and ophthalmological examination.

The IOP of the normal individuals was measured with the Goldmann applanation tonometer and all underwent/ had undergone pachometry with the Quantel Pocket I ultrasonic pachometer (Quantel Medical SA, Clermont-Ferrand, France).

Each individual was required to exhibit in each eye a visual acuity of 7/10 or better (equivalent to 6/9 or better); a distance refractive error of ≤+/-7.0 dioptres mean sphere and ≤+/-3.0 dioptres cylinder; a normal anterior segment; and lenticular changes no greater than NC2.0, NO2.0, C1.0, or P1.0 classified by LOCS III

(Chylack et al 1993). In addition, no individual was receiving systemic medication, or manifested any systemic disease, known to affect the visual field nor had a negative family history of any ocular disease or any systemic diseases with potential ocular involvement.

Normal individuals were, as in the previous two studies, categorized on the basis of normal findings from the clinical examination and exhibited an upper limit of ≤20mmHg. The criteria for a normal field were those described in the previous studies of SITA SWAP and/ or Pulsar perimetry (Morgan et al 2005), namely: a field exhibiting complete normality by Pattern Deviation probability analysis; a field containing one non-edge location exhibiting apparent abnormality at the $p<2.0\%$ level or worse; or as a field containing up to 3 unclustered locations in any one horizontal hemifield at the $p<5\%$ level. Locations exhibiting apparent abnormality arising from the presence of obvious artefacts such as lens rim, upper lid contamination, or seed-point (i.e. those at 9°, 9° eccentricity) errors, and those locations immediately adjacent to the blind spot were not considered in the evaluation of the given field.

The individuals with OAG were categorized on the basis of an optic nerve head characteristic of the disease including generalized or focal thinning of the neuro-retinal rim, disc asymmetry, changes in the lamina cribrosa, pallor, vessel changes or disc margin haemorrhage. The Heidelberg Retina Tomograph reflectance image for the optic nerve heads of each of the 14 individuals with OAG and the values of the parameters for Disc Area, Cup Shape Measure, Height Variation Contour, Linear

Cup:Disc ratio and the Mikelberg and Burk Discriminant functions are given in Figure 5.1.

Patient ID	Right eye	DA (mm^2); CSM; HVC (mm); Linear cup/disc ratio; FSM; RB	Left eye	DA (mm^2); CSM; HVC (mm); Linear cup/disc ratio; FSM; RB
2	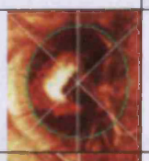	1.93; -0.13; 0.54; 0.48; 1.51; 1.69		1.80; -0.11; 0.55; 0.57; -1.09; 0.44
13	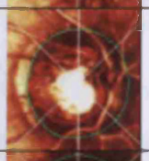	2.27; -0.09; 0.35; 0.68; -1.31; 1.54	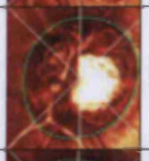	2.85; -0.10; 0.33; 0.66; -0.41; 0.44
14	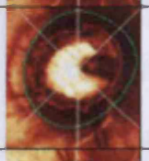	2.41; -0.05; 0.27; 0.75; -2.06; 0.24		2.62; -0.09; 0.33; 0.76; -1.20; 0.76
20		2.18; -0.02; 0.27; 0.74; -2.23; -0.34		2.76; 0.06; 0.24; 0.80; -3.30; -0.71
21		1.61; -0.32; 0.33; 0.48; 2.74; 1.21	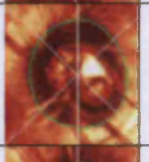	1.92; -0.16; 0.35; 0.56; 0.49; 1.13
24		2.06; -0.09; 0.42; 0.65; -0.22; 1.21		2.18; -0.13; 0.36; 0.70; -0.74; 0.29
25		1.92; -0.07; 0.23; 0.60; -0.55; -0.92		1.69; -0.15; 0.53; 0.55; -0.69; 0.54
27		2.34; -0.10; 0.36; 0.69; -1.15; 0.15		2.26; -0.17; 0.44; 0.57; 2.01; 1.78
28		1.96; -0.14; 0.27; 0.61; -0.29; 0.30	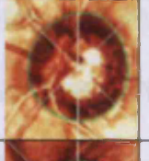	1.84; -0.11; 0.25; 0.63; -1.02; -0.02
29	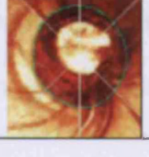	2.01; -0.15; 0.21; 0.74; -0.52; 0.30	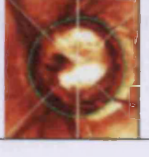	2.04; -0.05; 0.33; 0.83; -3.19; 0.02

30		2.06; -0.13; 0.30; 0.61; -0.21; -0.28	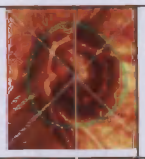	1.98; -0.26; 0.32; 0.51; 1.72; 0.89
34	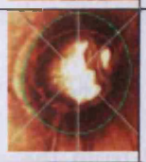	2.39; -0.16; 0.29; 0.71; -0.42; 0.55	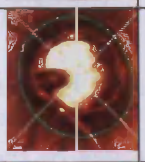	2.51; -0.07; 0.34; 0.72; -1.50; 0.95
35	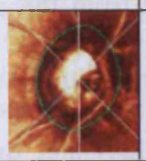	1.47; -0.06; 0.45; 0.67; -2.39; 1.55	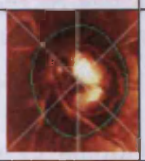	1.81; -0.17; 0.38; 0.64; 0.48; 1.29
36	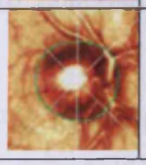	1.20; -0.09; 0.42; 0.54; -1.55; 0.49		1.25; 0.0; 0.44; 0.67; -2.75; 0.31

Figure 5.1 The Heidelberg Retina Tomograph reflectance images for the ONHs of the 14 individuals with open angle glaucoma. (DA: Disc Area; CSM: Cup Shape Measure; HVC: Height Variation Contour FSM: Mikelberg Discriminant function; RB: Burk Discriminant function). Individuals with case numbers 2, 13, 14, 20 and 21 had taken part in both the SWAP and the Pulsar studies (described in Chapters 3 and 4, respectively). Individuals with case numbers 24 and 25 had taken part in the SWAP study and individuals with case numbers 27, 28, 29 and 30 had taken part in the Pulsar study.

Seven individuals with OAG were receiving a single topical agent in each eye for control of IOP (one was receiving a nonselective β-receptor blocker, two an α-adrenergic agonist, two a prostaglandin analogue and two a carbon anhydrase inhibitor). One individual required two topical agents for IOP control (a carbon anhydrase inhibitor/ β-receptor blocker combination and a prostaglandin analogue). One individual had one topical agent for IOP control (a prostaglandin analogue) and a systemic β-receptor blocker and another individual had two topical agents (a carbonic anhydrase inhibitor/ β-receptor blocker combination and a prostaglandin analogue/ β-receptor blocker combination) and a systemic β-receptor blocker. Three individuals were not receiving treatment for IOP (one individual switched from another diagnostic group, one individual was a new detected glaucoma and one individual suffered from low tension glaucoma).

As in Sections 3.3.1 and 4.3.1, the severity of the visual field loss for the individuals with OAG was graded, post hoc, on the appearance of the visual field determined with the SITA Standard algorithm at the last visit based upon the classification of Hodapp and colleagues (1993) and modified by Litwak (2001) for the SITA Standard algorithm. The use of the MD index was omitted from the classification system in order to emphasize the spatial component in the grading of the field loss. Twelve of the 14 individuals exhibited mild visual field loss and two moderate losses.

One of the 17 normal individuals and one of the 14 individuals with OAG were receiving artificial tears because of minor dry eye problems.

5.3.2 Examination protocol

In addition to the baseline visit, all individuals took part in five further visits. Each of these five visits was separated by one week. At each visit, the designated eye was examined with Program 24-2 of the Humphrey Field Analyzer 745i (HFA; Carl Zeiss Meditech Inc., Dublin, CA) using the SITA Standard algorithm and four times with the Pulsar Program CP-T30W (Interzeag AG, Schlieren, Switzerland) using the TOP algorithm. The order of the type of perimetry within the visit was randomized within individuals and was varied over each of the five visits. For each examination with Program CP-T30W, the given individual was examined with the best correction (i.e. no defocus) in full-aperture trial lens form corrected, where necessary, for the viewing distance of the perimeter bowl, and with an additional +2.00DS, +4.00DS and +6.00DS, respectively. The sequence of defocus was randomized within the visit and was varied over each of the five visits. The designated for the normal

individuals was selected at random and for the individuals with OAG was designated as the worst eye.

Each individual adapted to the bowl luminance of the HFA and to the screen luminance of the Pulsar perimeter for at least one minute. The non-examined eye was occluded with an opaque patch.

For the HFA, in addition to the standard Heijl-Krakau technique and to the gaze tracker, fixation was monitored continuously via the video monitor. For Pulsar perimetry, fixation was monitored by the standard Heijl-Krakau technique.

The influence of the fatigue effect was reduced by providing rest periods of approximately one minute in duration at two minute intervals during each examination. During such rest periods the individual remained adapted to the perimeter bowl or to the Pulsar perimetry screen. Each individual was given the same instructions throughout each examination at each visit to reduce operator bias.

Two perimetrists performed the perimetry, Mrs Beatrice Thöny, the practice nurse, and the author. The number of individuals in each group assigned to each perimetrist and to a combination of the two perimetrists is given in Table 5.2.

	Normal	OAG
CAC and BT	7	8
BT, only	6	2
CAC, only	4	4

Table 5.2 The number of individuals in each group assigned to each perimetrist and to a combination of the two perimetrists.

5.3.3 Analysis

The improvement over the 5 visits in the visual field indices, MS, MD, and PSD; in the examination duration and on the ratio of the PMS to the CMS derived by the SITA Standard algorithm was undertaken using separate repeated measures of Analysis of Variance (ANOVA). The age, the designated eye, the perimetrist, the degree of previous experience of visual field examination, pupil size, diagnostic group, order of the type of perimetry and order of defocus were each considered as between-subject factors. The visit was considered as a within-subject factor.

The influence of defocus on the each of the Pulsar perimeter visual field indices, MS, MD, and sLV; on examination duration and on the ratio of the central MS to the peripheral MS was undertaken using separate repeated measures of ANOVA. The age, the designated eye, the perimetrist, the degree of previous experience of visual field examination, pupil size, diagnostic group, order of the type of perimetry and order of defocus were each considered as between-subject factors. The level of defocus and the visit were considered as within-subject factors. The sign convention for the MD derived by the Pulsar perimeter was reversed (i. e. all positive values were converted to negative values and vice versa).

SITA Standard	Visit 1	Visit 2	Visit 3	Visit 4	Visit 5
MS (dB)	30.31 (3.24)	30.02 (1.84)	30.00 (1.87)	30.29 (1.71)	30.34 (1.53)
MD (dB)	0.75 (2.98)	0.41 (1.58)	0.30 (1.65)	0.56 (1.44)	0.49 (1.23)
PSD (dB)	2.63 (2.45)	1.89 (0.76)	1.63 (0.02)	1.59 (0.46)	1.93 (0.74)
Examination duration	327 (78)	301 (45)	284 (31)	281 (34)	290 (29)
PMS/CMS	0.90 (0.06)	0.92 (0.03)	0.93 (0.03)	0.92 (0.03)	0.92 (0.03)
MS (dB)	29.72 (2.02)	30.12 (1.68)	30.30 (1.73)	30.23 (1.51)	30.19 (1.92)
MD (dB)	0.56 (1.72)	0.43 (1.37)	0.62 (1.38)	0.53 (1.14)	0.55 (1.48)
PSD (dB)	2.67 (1.92)	2.31 (1.40)	2.18 (1.56)	2.29 (1.59)	2.50 (1.64)
Examination duration	295 (27)	296 (37)	288 (31)	282 (33)	282 (22)
PMS/CMS	0.92 (0.04)	0.92 (0.04)	0.92 (0.04)	0.92 (0.03)	0.92 (0.03)

Table 5.3 The magnitudes of the MS (SD), MD (SD), PSD (SD), examination duration (SD) and the ratio of the PMS (SD) to the CMS derived by the SITA Standard algorithm in the designated eye at each of the five visits for the normal individuals (no shading) and for the individuals with OAG (shading).

5.4.1.1 Mean Sensitivity

The group mean MS for the designated eye at each visit for the SITA Standard algorithm is also shown graphically in Figure 5.2 for each of the two groups.

Overall, the MS declined with age (p=0.038). It was independent of the difference in the designated eye (p=0.512), the given perimetrist (p=0.615), and the degree of previous experience of visual field examination (p=0. 957). The MS varied with the order of the type of perimetry (p=0.012): it was less positive (i.e. worse) for the individuals who underwent examination with the SITA Standard algorithm after examination with the Pulsar perimeter. The MS was also dependent upon pupil size (p=0.050): it became less positive with decrease in pupil size. As would be expected, the MS was less positive for the group with OAG (p<0.001). However, the MS was

similar across the five visits (p=0.529). The difference in the group mean over the five visits was 0.03dB for the normal individuals and 0.47dB for those with OAG.

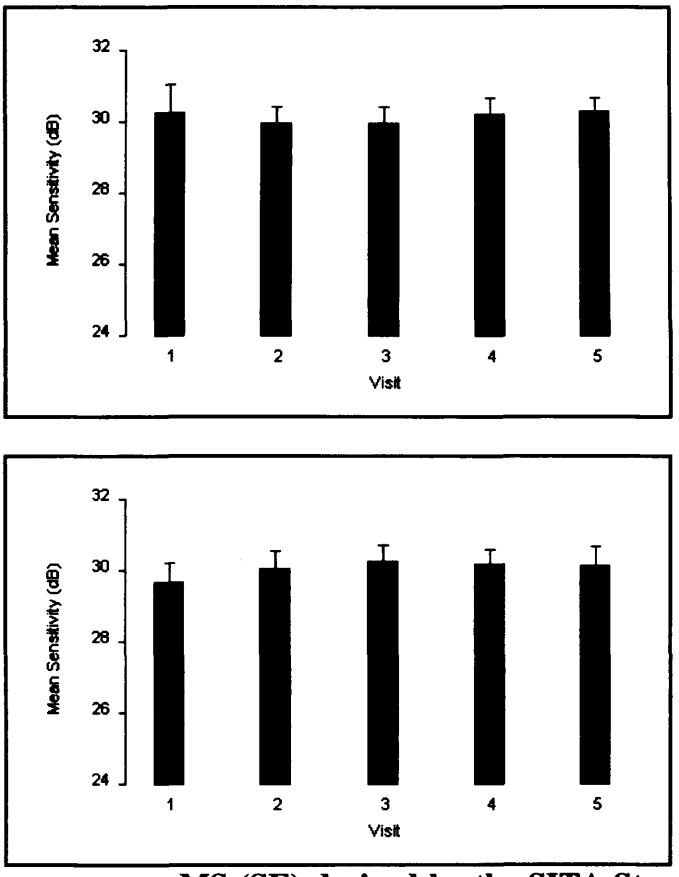

Figure 5.2 The group mean MS (SE) derived by the SITA Standard algorithm in the designated eye at each of the five visits. Top: normal individuals. Bottom: individuals with OAG.

5.4.1.2 Mean Deviation

The group mean MD for the designated eye at each visit for the SITA Standard algorithm is also shown graphically in Figure 5.3 for each of the two groups.

Overall, the MD was independent of age (p=0.445), the difference in the designated eye (p=0.346), the given perimetrist (p=0.862), and the degree of previous experience of visual field examination (p=0.563). The MD varied with the order of the type of perimetry (p=0.009): it was more negative (i.e. worse) for the individual who underwent examination with the SITA Standard algorithm after examination

with the Pulsar perimeter. The MD was also dependent upon pupil size (p=0.034): it became more negative with decrease in pupil size. As would be expected the MD was more negative for the group with OAG (p<0.001). However, the MD was similar across the five visits (p=0.909). The difference in the group mean over the five visits was -0.26dB for the normal individuals and -0.01dB for those with OAG.

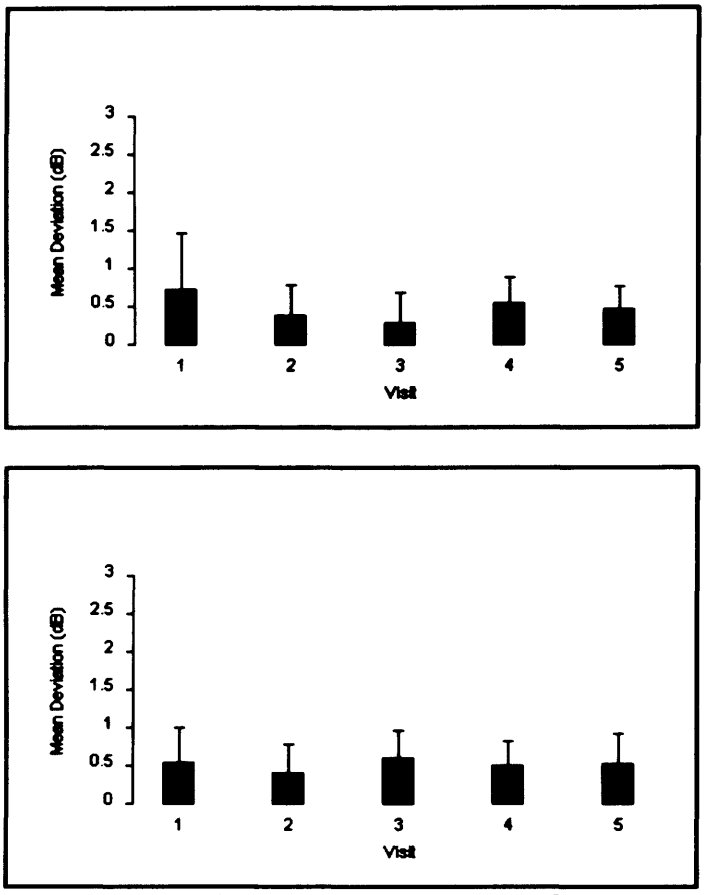

Figure 5.3 The group mean MD (SE) derived by the SITA Standard algorithm in the designated eye at each of the five visits. Top: normal individuals. Bottom: individuals with OAG.

5.4.1.3 Pattern Standard Deviation

The group mean PSD for the designated eye at each visit for the SITA Standard algorithm is also shown graphically in Figure 5.4 for each of the two groups.

Overall, the PSD was independent of age (p=0.888), the difference in the designated eye (p=0.442), the given perimetrist (p=0.998), the degree of previous experience of

visual field examination (p=0.248), order of the type of perimetry (p=0.487). The PSD increased with decrease in pupil size (p=0.012). As would be expected the PSD was different between the two groups (p<0.001) being worst for the group with OAG. The PSD improved across the five visits (p=0.005). The improvement in the group mean was 0.70dB for the normal individuals and 0.17dB for those with OAG.

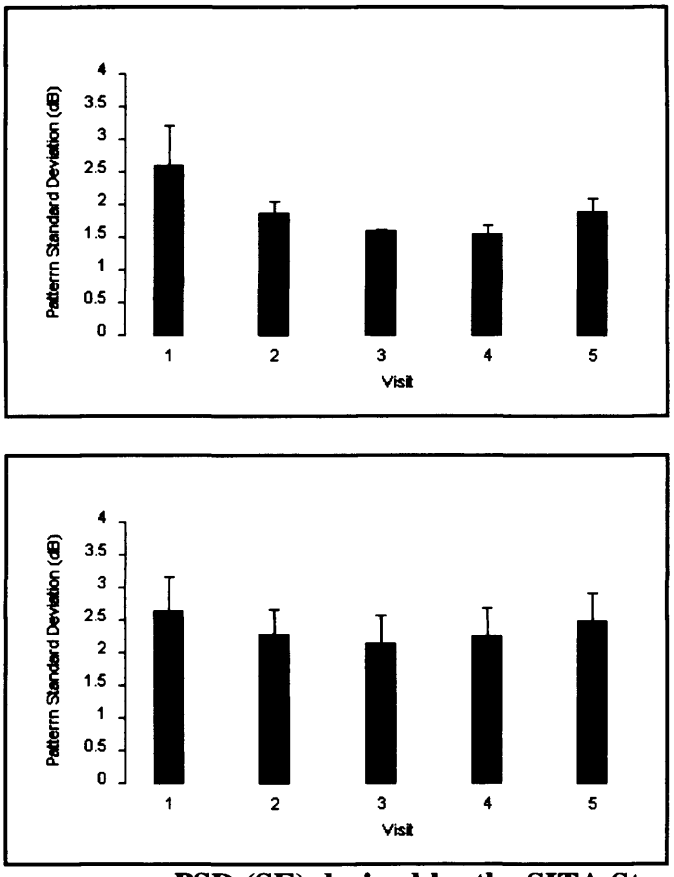

Figure 5.4 The group mean PSD (SE) derived by the SITA Standard algorithm in the designated eye at each of the five visits. Top: normal individuals. Bottom: individuals with OAG.

5.4.1.4 Examination duration

The group mean examination duration for the designated eye at each visit for the SITA Standard algorithm is also shown graphically in Figure 5.5 for each of the two groups.

The relationship between the examination duration, overall, and age exhibited borderline statistical significance (p=0.057). The examination duration was independent of the difference in the designated eye (p=0.514), the degree of previous experience of visual field examination (p=0.516), the order of the type of perimetry (p=0.423) and the given perimetrist (p=0.116). The examination duration became shorter over the five visits (p<0.001). The improvement in the group mean examination duration was 37 seconds for the normal individuals and 7 seconds for the individuals with OAG As might be expected the examination duration was shorter for the group with OAG (p<0.001). The examination duration was also influenced by pupil size (p=0.015) (i.e. the examination duration decreased with increase in pupil size).

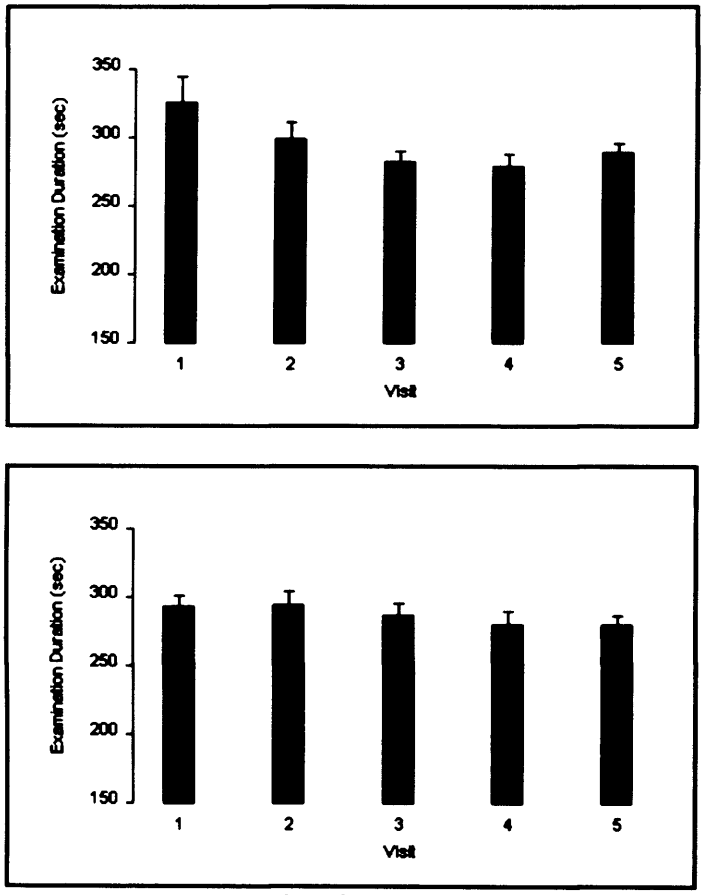

Figure 5.5 The group mean examination duration (SE) derived by the SITA Standard algorithm in the designated eye at each of the five visits. Top: normal individuals. Bottom: individuals with OAG.

5.4.1.5 Ratio of the peripheral mean sensitivity to the central mean sensitivity

The group mean ratio PMS/CMS for the designated eye at each visit for the SITA Standard algorithm is also shown graphically in Figure 5.6 for each of the two groups.

Overall, the ratio of the PMS to the CMS was independent of age (p=0.529), the difference in the designated eye (p=0.791), pupil size (p=0.314), the degree of previous experience of visual field examination (p=0.923), the given perimetrist (p=0.447) and the order of the type of perimetry (p=0.953). It was similar across the five visits (p=0.093) but different between the two groups (p<0.001).

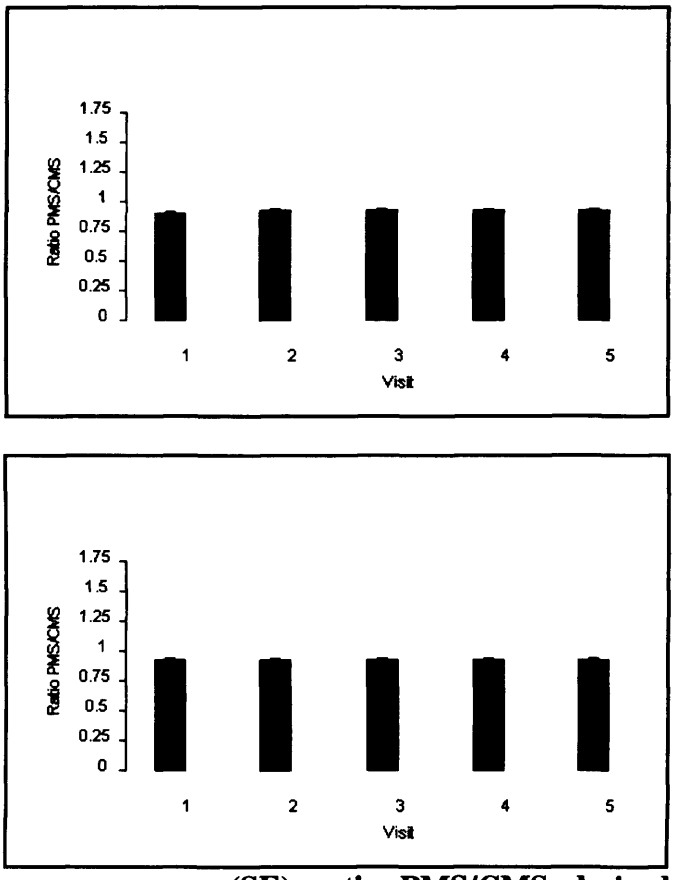

Figure 5.6 The group mean (SE) ratio PMS/CMS derived by the SITA Standard algorithm in the designated eye at each of the five visits. Top: normal individuals. Bottom: individuals with OAG.

5.4.2 The effect of defocus on the visual field indices for Pulsar perimetry

5.4.2.1 Mean Sensitivity

The group mean MS (SD) as a function of defocus at each of the five visits for each of the two groups is shown is shown in Table 5.4.

	Visit 1		Visit 2		Visit 3		Visit 4		Visit 5	
Pulsar normal individuals	0.00 DS	+2.00 DS	0.00 DS	+2.00 DS	0.00 DS	+2.00 DS	0.00 DS	+2.00 DS	0.00 DS	+2.00 DS
	18.76 (2.08)	15.46 (2.79)	18.93 (2.68)	15.67 (2.65)	18.57 (2.44)	16.09 (2.41)	19.07 (1.96)	16.10 (2.46)	19.05 (2.40)	15.78 (2.62)
	+4.00 DS	+6.00 DS	+4.00 DS	+6.00 DS	+4.00 DS	+6.00 DS	+4.00 DS	+6.00 DS	+4.00 DS	+6.00 DS
	12.28 (1.70)	9.90 (1.61)	12.35 (2.19)	10.10 (1.93)	12.56 (2.26)	10.37 (2.67)	12.46 (1.84)	10.60 (3.27)	12.82 (1.66)	10.09 (2.04)
Pulsar individuals with OAG	0.00 DS	+2.00 DS	0.00 DS	+2.00 DS	0.00 DS	+2.00 DS	0.00 DS	+2.00 DS	0.00 DS	+2.00 DS
	17.67 (4.40)	15.58 (3.51)	19.15 (2.93)	15.51 (3.01)	19.15 (2.96)	16.02 (3.38)	18.61 (2.92)	16.20 (3.12)	18.81 (2.97)	16.16 (3.15)
	+4.00 DS	+6.00 DS	+4.00 DS	+6.00 DS	+4.00 DS	+6.00 DS	+4.00 DS	+6.00 DS	+4.00 DS	+6.00 DS
	11.97 (2.77)	10.08 (3.37)	12.19 (3.08)	9.58 (2.49)	12.22 (2.76)	9.64 (2.79)	12.67 (2.81)	10.55 (4.14)	12.55 (2.86)	10.05 (2.46)

Table 5.4 The group mean MS (SD) derived by Pulsar perimetry in the designated eye at each of the five visits as a function of the level of defocus for the normal individuals and for the individuals with OAG. In the prominent rectangles: top left, no defocus; top right, +2.00DS of defocus; bottom left, +4.00DS of defocus; and bottom right +6.00DS of defocus.

Overall, the MS declined with age ($p=0.008$). It was independent of the difference in the designated eye ($p=0.296$), pupil size ($p=0.388$), the given perimetrist ($p=1.000$), the degree of previous experience of visual field examination ($p=0.788$), order of the type of perimetry ($p=0.758$) and of the order of defocus ($p=0.562$). The MS increased over the five visits ($p=0.043$). As would be expected the MS was different between the two groups ($p<0.001$) and became smaller (i.e., worsened) with increase in defocus ($p<0.001$).The group mean MS for the designated eye at each visit for Pulsar perimetry with the four different defocus levels is also shown graphically in Figure 5.7a and Figure 5.7b for each of the two groups.

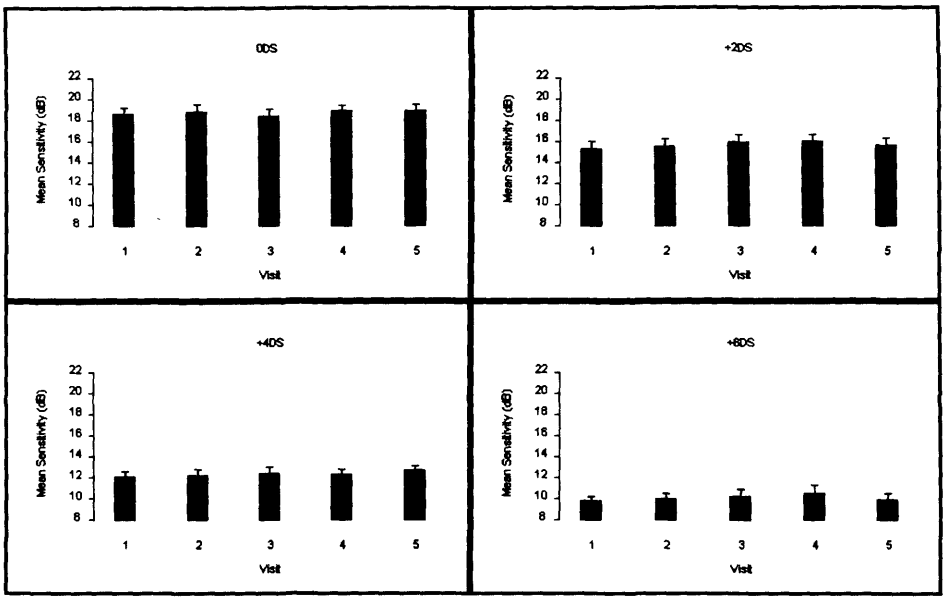

Figure 5.7a Group mean MS (SE) derived by the Pulsar perimeter in the designated eye of the normal individuals as a function of visit for each of the four levels of defocus (top left, no defocus: top right, +2.00DS of defocus; bottom left, +4.00DS of defocus; and bottom right +6.00DS of defocus).

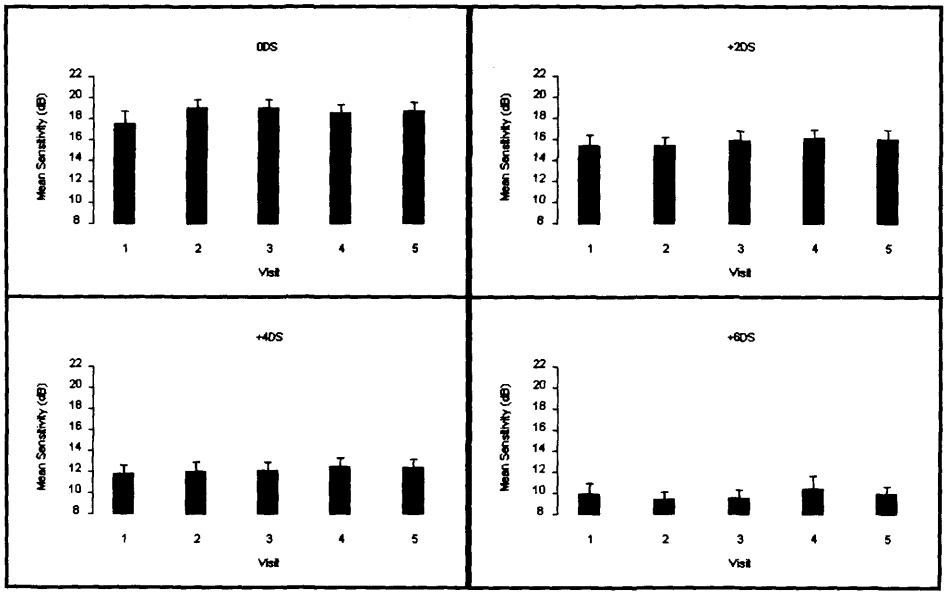

Figure 5.7b Group mean MS (SE) derived by the Pulsar perimeter in the designated eye of the individuals with OAG as a function of visit for each of the four levels of defocus (top left, no defocus: top right, +2.00DS of defocus; bottom left, +4.00DS of defocus; and bottom right +6.00DS of defocus).

5.4.2.2 Mean Defect

The group mean MD (SD) for Pulsar perimetry as a function of the algorithm in each of the two groups and both groups together at each of the five visits are shown in Table 5.5.

	Visit 1		Visit 2		Visit 3		Visit 4		Visit 5	
Pulsar	**0.00 DS**	**+2.00 DS**	**0.00 DS**	**+2.00 DS**	**0.00 DS**	**+2.00 DS**	**0.00 DS**	**+2.00 DS**	**0.00 DS**	**+2.00 DS**
normal	-0.75	-4.07	-0.56	-3.78	-0.93	-3.47	-0.49	-3.42	-0.44	-3.61
individuals	(1.89)	(2.47)	(2.59)	(2.41)	(2.38)	(2.17)	(1.73)	(2.21)	(2.19)	(2.27)
	+4.00 DS	**+6.00 DS**	**+4.00 DS**	**+6.00 DS**	**+4.00 DS**	**+6.00 DS**	**+4.00 DS**	**+6.00 DS**	**+4.00 DS**	**+6.00 DS**
	-7.06	-9.41	-6.92	-9.25	-6.82	-8.88	-6.94	-8.79	-6.51	-9.21
	(1.76)	(1.74)	(2.00)	(2.08)	(2.46)	(2.82)	(2.60)	(3.26)	(2.53)	(2.18)
Pulsar	**0.00 DS**	**+2.00 DS**	**0.00 DS**	**+2.00 DS**	**0.00 DS**	**+2.00 DS**	**0.00 DS**	**+2.00 DS**	**0.00 DS**	**+2.00 DS**
individuals	-1.86	-3.95	-0.41	-3.95	-0.52	-3.60	-0.99	-3.43	-0.87	-3.65
with OAG	(4.20)	(2.98)	(2.62)	(2.58)	(2.72)	(3.01)	(2.85)	(2.65)	(2.43)	(2.76)
	+4.00 DS	**+6.00 DS**	**+4.00 DS**	**+6.00 DS**	**+4.00 DS**	**+6.00 DS**	**+4.00 DS**	**+6.00 DS**	**+4.00 DS**	**+6.00 DS**
	-7.47	-9.42	-7.14	-9.88	-7.26	-9.91	-6.80	-8.95	-7.00	-9.55
	(2.44)	(3.08)	(2.93)	(2.48)	(2.60)	(2.63)	(2.60)	(3.86)	(2.53)	(2.39)

Table 5.5 The group mean MD (SD) derived by Pulsar perimetry in the designated eye at each of the five visits as a function of the level of defocus for the normal individuals and for the individuals with OAG. In the prominent rectangles: top left, no defocus; top right, +2.00DS of defocus; bottom left, +4.00DS of defocus; and bottom right +6.00DS of defocus.

Overall, the MD was independent of age ($p=0.597$), the difference in the designated eye ($p=0.288$), pupil size ($p=0.398$), the given perimetrist ($p=0.983$), the degree of previous experience of visual field examination ($p=0.860$), order of the type of perimetry ($p=0.850$) and of the order of defocus ($p=0.563$). The MD was similar across the five visits ($p=0.125$). As would be expected the MD was different between the two groups ($p<0.001$) and became more negative (i.e. worsened) with increase in defocus ($p<0.001$).The group mean MD for the designated eye at each visit for Pulsar perimetry with the four different defocus levels is also shown graphically in Figure 5.8a and Figure 5.8b for each of the two groups.

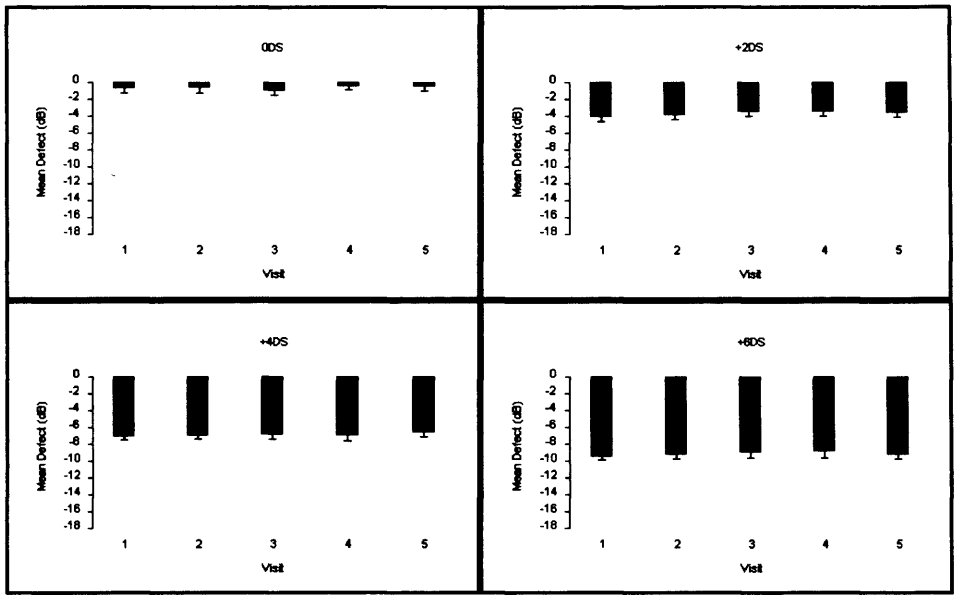

Figure 5.8a Group mean MD (SE) derived by the Pulsar perimeter in the designated eye of the normal individuals as a function of visit for each of the four levels of defocus (top left, no defocus: top right, +2.00DS of defocus; bottom left, +4.00DS of defocus; and bottom right +6.00DS of defocus).

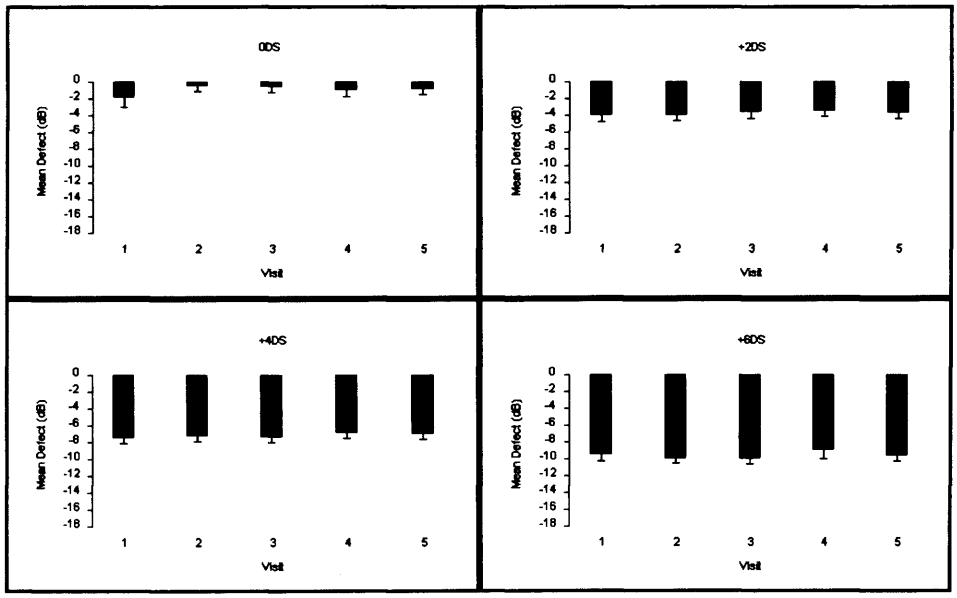

Figure 5.8b Group mean MS (SE) derived by the Pulsar perimeter in the designated eye of the individuals with OAG as a function of visit for each of the four levels of defocus (top left, no defocus: top right, +2.00DS of defocus; bottom left, +4.00DS of defocus; and bottom right +6.00DS of defocus).

5.4.2.3 Square root of the Loss Variance

The group mean sLV (SD) for Pulsar perimetry as a function of the algorithm in each of the two groups and both groups together at each of the five visits are shown in Table 5.6.

	Visit 1		Visit 2		Visit 3		Visit 4		Visit 5	
Pulsar	**0.00 DS**	**+2.00 DS**	**0.00 DS**	**+2.00 DS**	**0.00 DS**	**+2.00 DS**	**0.00 DS**	**+2.00 DS**	**0.00 DS**	**+2.00 DS**
normal	2.52	3.13	2.52	2.89	2.52	2.79	2.51	2.67	2.31	2.63
individuals	(0.96)	(0.97)	(1.79)	(0.84)	(1.29)	(0.81)	(1.30)	(0.85)	(1.39)	(0.97)
	+4.00 DS	**+6.00 DS**	**+4.00 DS**	**+6.00 DS**	**+4.00 DS**	**+6.00 DS**	**+4.00 DS**	**+6.00 DS**	**+4.00 DS**	**+6.00 DS**
	3.06	3.06	3.16	4.28	2.95	3.18	3.24	3.15	2.90	3.15
	(0.61)	(0.65)	(0.48)	(0.70)	(0.65)	(0.41)	(0.90)	(0.74)	(0.58)	(0.74)
Pulsar	**0.00 DS**	**+2.00 DS**	**0.00 DS**	**+2.00 DS**	**0.00 DS**	**+2.00 DS**	**0.00 DS**	**+2.00 DS**	**0.00 DS**	**+2.00 DS**
individuals	2.80	3.22	2.47	3.31	2.71	2.95	2.58	2.92	2.88	3.77
with OAG	(1.21)	(0.66)	(1.15)	(1.28)	(1.30)	(0.91)	(1.19)	(0.95)	(1.16)	(1.28)
	+4.00 DS	**+6.00 DS**	**+4.00 DS**	**+6.00 DS**	**+4.00 DS**	**+6.00 DS**	**+4.00 DS**	**+6.00 DS**	**+4.00 DS**	**+6.00 DS**
	3.09	3.26	3.89	3.20	3.21	3.20	2.99	3.08	3.10	3.47
	(0.92)	(0.69)	(0.61)	(0.86)	(0.78)	(0.67)	(0.61)	(0.78)	(0.45)	(0.78)

Table 5.6 The group mean sLV (SD) derived by Pulsar perimetry in the designated eye at each of the five visits as a function of the level of defocus for the normal individuals and for the individuals with OAG. In the prominent rectangles: top left, no defocus; top right, +2.00DS of defocus; bottom left, +4.00DS of defocus; and bottom right +6.00DS of defocus.

Overall, the sLV was independent of age (p=0.886), the difference in the designated eye (p=0.305), pupil size (p=0.096), the given perimetrist (p=0.973), the degree of previous experience of visual field examination (p=0.630), order of the type of perimetry (p=0.804) and of the order of defocus (p=0.647). The sLV was similar across the five visits (p=0.783). As would be expected the PSD was different between the two groups (p<0.001) and became more negative (i.e. worsened) with increase in defocus (p<0.001).The group mean sLV for the designated eye at each visit for Pulsar perimetry with the four different defocus levels is also shown graphically in Figure 5.9a and Figure 5.9b for each of the two groups.

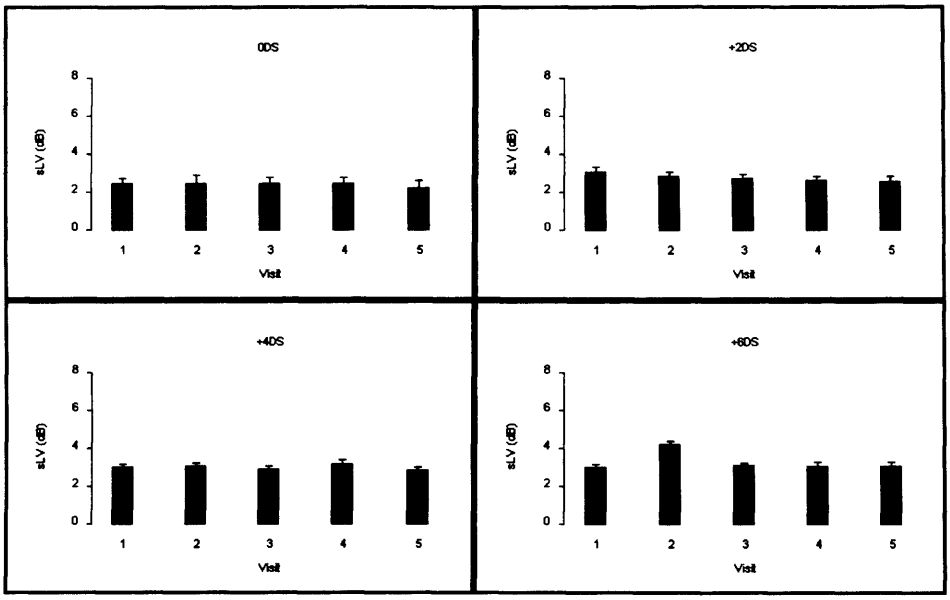

Figure 5.9a Group mean sLV (SE) derived by the Pulsar perimeter in the designated eye of the normal individuals as a function of visit for each of the four levels of defocus (top left, no defocus: top right, +2.00DS of defocus; bottom left, +4.00DS of defocus; and bottom right +6.00DS of defocus).

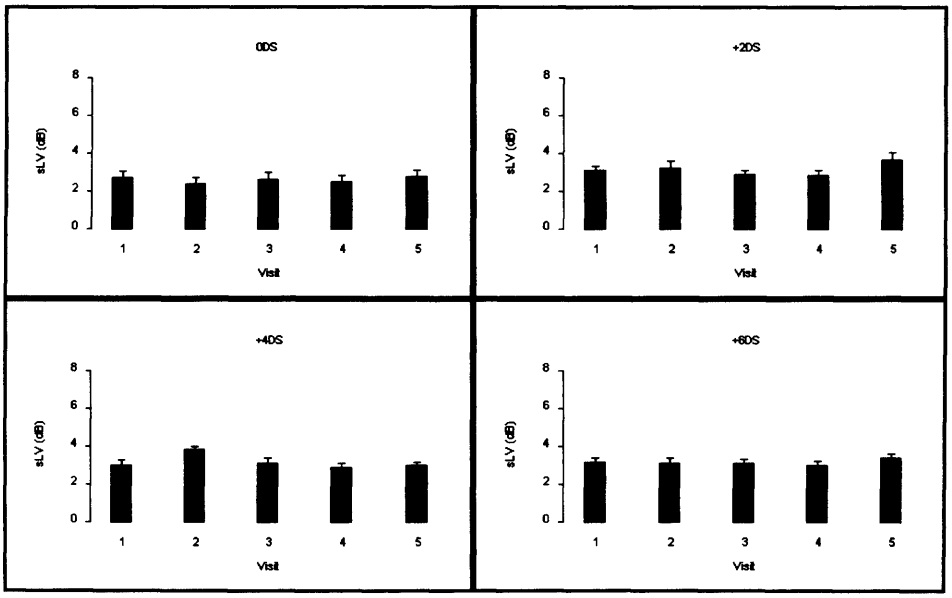

Figure 5.9b Group mean sLV (SE) derived by the Pulsar perimeter in the designated eye of the individuals with OAG as a function of visit for each of the four levels of defocus (top left, no defocus: top right, +2.00DS of defocus; bottom left, +4.00DS of defocus; and bottom right +6.00DS of defocus).

5.4.2.4 Examination duration

The group mean examination duration (SD) as a function of the algorithm in each of the two groups and both groups together at each of the five visits is shown in Table 5.7.

	Visit 1		Visit 2		Visit 3		Visit 4		Visit 5	
Pulsar normal individuals	0.00 DS	+2.00 DS	0.00 DS	+2.00 DS	0.00 DS	+2.00 DS	0.00 DS	+2.00 DS	0.00 DS	+2.00 DS
	199 (5)	201 (11)	198 (5)	200 (8)	198 (6)	202 (16)	199 (5)	202 (13)	200 (6)	200 (6)
	+4.00 DS	+6.00 DS	+4.00 DS	+6.00 DS	+4.00 DS	+6.00 DS	+4.00 DS	+6.00 DS	+4.00 DS	+6.00 DS
	202 (10)	203 (9)	203 (13)	201 (9)	202 (7)	198 (5)	200 (7)	199 (6)	200 (7)	203 (9)
Pulsar individuals with OAG	0.00 DS	+2.00 DS	0.00 DS	+2.00 DS	0.00 DS	+2.00 DS	0.00 DS	+2.00 DS	0.00 DS	+2.00 DS
	200 (9)	200 (6)	201 (8)	200 (9)	200 (8)	199 (6)	199 (5)	197 (5)	200 (6)	200 (5)
	+4.00 DS	+6.00 DS	+4.00 DS	+6.00 DS	+4.00 DS	+6.00 DS	+4.00 DS	+6.00 DS	+4.00 DS	+6.00 DS
	200 (8)	199 (9)	202 (8)	199 (6)	201 (8)	198 (6)	202 (5)	202 (10)	198 (5)	198 (7)

Table 5.7 The group mean examination duration (seconds) (SD) derived by Pulsar perimetry in the designated eye at each of the five visits as a function of the level of defocus for the normal individuals and for the individuals with OAG. In the prominent rectangles: top left, no defocus; top right, +2.00DS of defocus; bottom left, +4.00DS of defocus; and bottom right +6.00DS of defocus.

Overall, the examination duration was independent of age (p=0.543), the difference in the designated eye (p=0.395), the pupil size (p=0.161), the degree of previous experience of visual field examination (p=0.705), and the order of the type of perimetry (p=0.463). However, the duration was shorter for one perimetrist compared to the other (p=0.011). It increased with increase in the magnitude of the defocus (p<0.001). The examination duration was similar across the five visits (p=0.630). As would be expected the examination duration was longer for the individuals with OAG (p<0.001) and became longer with increase in defocus (p<0.001). The group mean examination duration for the designated eye at each visit

for Pulsar perimetry with the four different defocus levels is also shown graphically in Figure 5.10a and Figure 5.10b for each of the two groups.

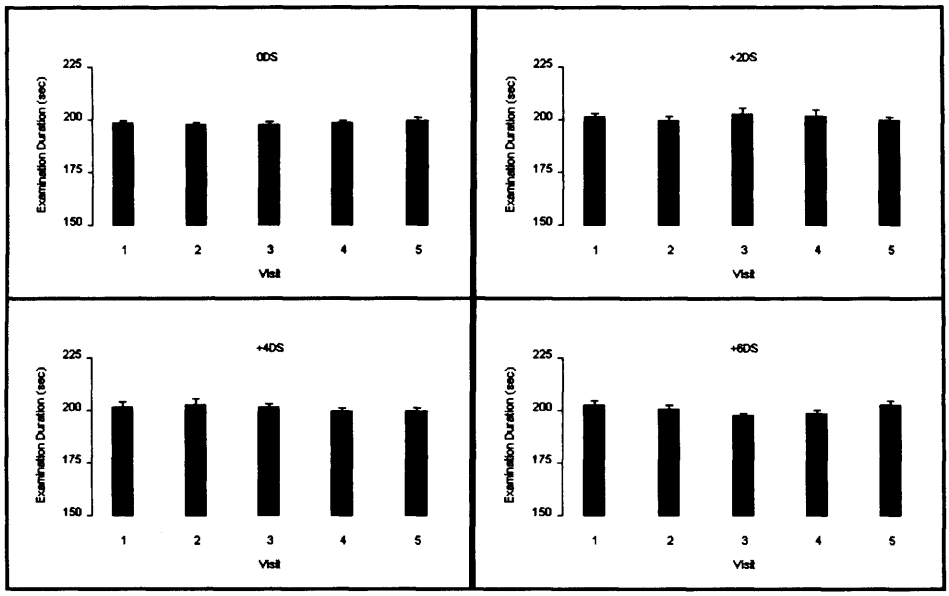

Figure 5.10a Group mean examination duration (SE) derived by the Pulsar perimeter in the designated eye of the normal individuals as a function of visit for each of the four levels of defocus (top left, no defocus: top right, +2.00DS of defocus; bottom left, +4.00DS of defocus; and bottom right +6.00DS of defocus).

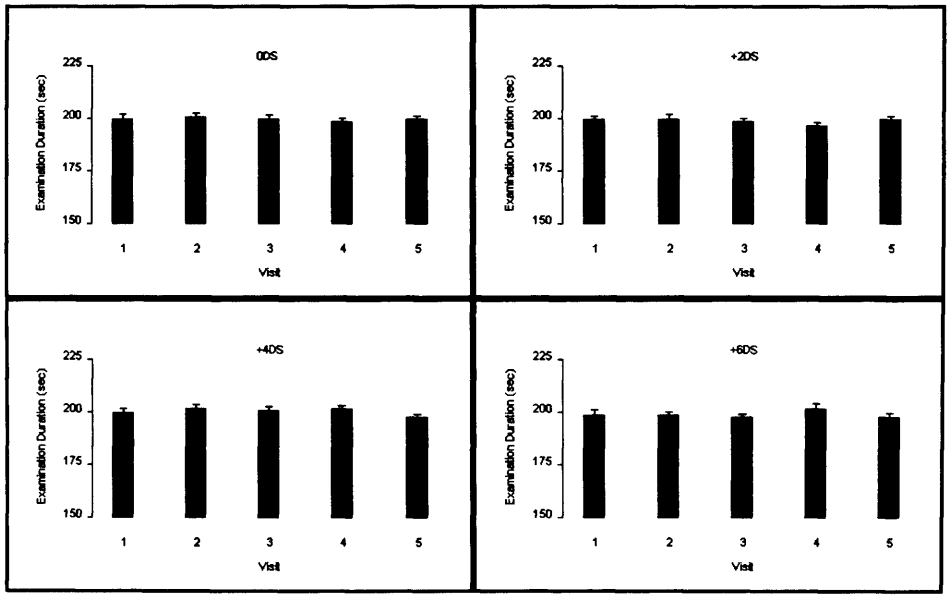

Figure 5.10b Group mean examination duration (SE) derived by the Pulsar perimeter in the designated eye of the individuals with OAG as a function of visit for each of the four levels of defocus (top left, no defocus: top right, +2.00DS of defocus; bottom left, +4.00DS of defocus; and bottom right +6.00DS of defocus).

5.4.2.5 Ratio of the peripheral mean sensitivity to central mean sensitivity

The group mean ratio of the PMS to the CMS as a function of the algorithm in each of the two groups and both groups together at each of the five visits is shown in Table 5.8.

	Visit 1		Visit 2		Visit 3		Visit 4		Visit 5	
Pulsar normal individuals	**0.00 DS**	**+2.00 DS**	**0.00 DS**	**+2.00 DS**	**0.00 DS**	**+2.00 DS**	**0.00 DS**	**+2.00 DS**	**0.00 DS**	**+2.00 DS**
	0.70 (0.07)	0.67 (0.13)	0.68 (0.10)	0.68 (0.12)	0.68 (0.08)	0.69 (0.08)	0.70 (0.07)	0.69 (0.08)	0.70 (0.08)	0.69 (0.11)
	+4.00 DS	**+6.00 DS**	**+4.00 DS**	**+6.00 DS**	**+4.00 DS**	**+6.00 DS**	**+4.00 DS**	**+6.00 DS**	**+4.00 DS**	**+6.00 DS**
	0.66 (0.11)	0.59 0.13)	0.68 (0.12)	0.60 (0.13)	0.69 (0.11)	0.61 (0.17)	0.66 (0.12)	0.57 (0.16)	0.68 (0.10)	0.58 (0.17)
Pulsar individuals with OAG	**0.00 DS**	**+2.00 DS**	**0.00 DS**	**+2.00 DS**	**0.00 DS**	**+2.00 DS**	**0.00 DS**	**+2.00 DS**	**0.00 DS**	**+2.00 DS**
	0.68 (0.12)	0.71 (0.12)	0.71 (0.05)	0.69 (0.10)	0.71 (0.07)	0.69 (0.09)	0.71 (0.05)	0.69 (0.10)	0.70 (0.05)	0.67 (0.11)
	+4.00 DS	**+6.00 DS**	**+4.00 DS**	**+6.00 DS**	**+4.00 DS**	**+6.00 DS**	**+4.00 DS**	**+6.00 DS**	**+4.00 DS**	**+6.00 DS**
	0.65 (0.14)	0.58 (0.17)	0.67 (0.10)	0.59 (0.16)	0.68 (0.11)	0.57 (0.19)	0.67 (0.15)	0.60 (0.16)	0.68 (0.11)	0.59 (0.18)

Table 5.8 The group mean ratio of the PMS (SD) to the CMS derived by Pulsar perimetry in the designated eye at each of the five visits as a function of the level of defocus for the normal individuals and for the individuals with OAG. In the prominent rectangles: top left, no defocus; top right, +2.00DS of defocus; bottom left, +4.00DS of defocus; and bottom right +6.00DS of defocus.

Overall, the ratio of the PMS to the CMS was independent of age (p=0.559), the difference in the designated eye (p=0.130), pupil size (p=0.298), the given perimetrist (p=0.289), the degree of previous experience of visual field, the order of defocus (p=0.023). It was similar across the five visits (p=0.844). The ratio was different between the two groups (p<0.001) and was influenced by increase (i.e. decreased) in defocus (p<0.001). The group mean ratio PMS/ CMS and the ratios SD for the designated eye at each visit for Pulsar perimetry with the four different defocus levels is also shown graphically in Figure 5.11a and Figure 5.11b for each of the two groups.

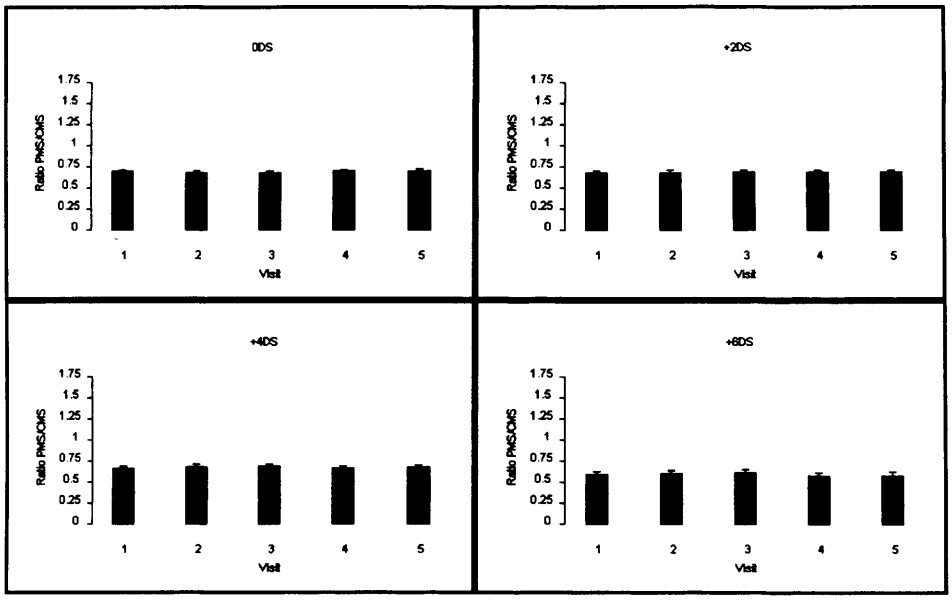

Figure 5.11a Group mean (SE) ratio PMS/CMS derived by the Pulsar perimeter in the designated eye of the normal individuals as a function of visit for each of the four levels of defocus (top left, no defocus: top right, +2.00DS of defocus; bottom left, +4.00DS of defocus; and bottom right +6.00DS of defocus).

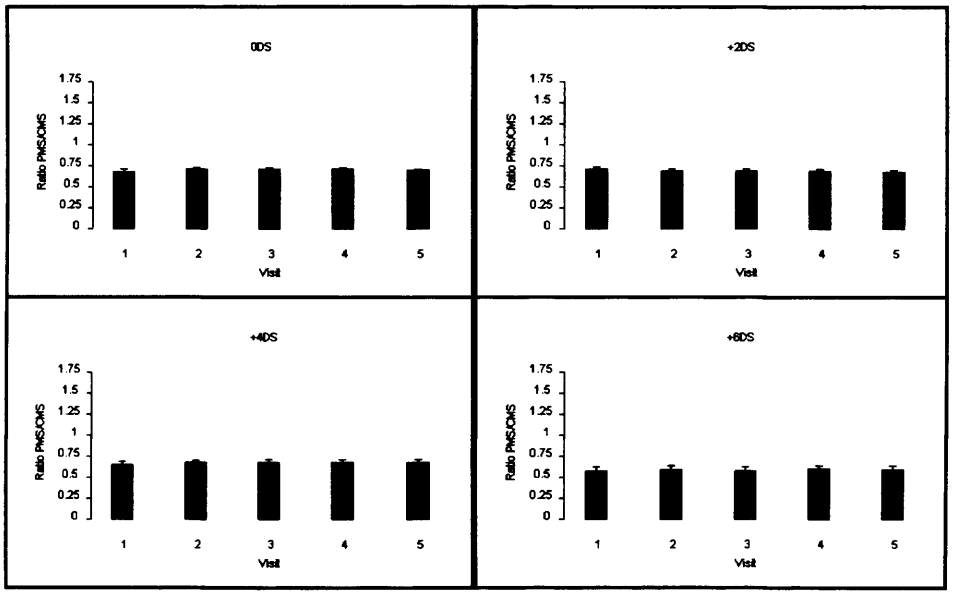

Figure 5.11b Group mean (SE) ratio PMS/CMS derived by the Pulsar perimeter in the designated eye of the individuals with OAG as a function of visit for each of the four levels of defocus (top left, no defocus: top right, +2.00DS of defocus; bottom left, +4.00DS of defocus; and bottom right +6.00DS of defocus).

5.5 The gradient of the decline in sensitivity with defocus

The gradient of the group Mean Sensitivity as a function of defocus for the Pulsar perimetry at each of the five visits is given Table 5.9 for the normal individuals and for the individuals with OAG.

	Visit 1	Visit 2	Visit 3	Visit 4	Visit 5
Normal individuals	-1.4938	-1.4077	-1.4528	-1.4528	-1.4967
	0.9933	0.9924	0.9858	0.9858	0.9985
Individuals with OAG	- 1.3238	- 1.6443	-1.6262	-1.3841	-1.5002
	0.9942	0.9942	0.9958	0.9911	0.9952

Table 5.9 The gradient of the decline of the group MS as function of defocus for the Pulsar perimeter at each of the five visits for the normal individuals (top) and the individuals with OAG (bottom) together with the corresponding value of the Coefficient of Determination (R^2).

The decline in group Mean Sensitivity with increase in defocus was approximately 1.5dB per dioptre of defocus for each of the two groups.

5.5.1 The gradient of the locale decline in sensitivity with defocus at Visit 5

The gradient of the decline in group Mean Sensitivity at each stimulus location with increase in defocus for the normal individuals and for the individuals with OAG at Visit 5 is shown in Figures 5.12a and 5.12b, respectively. The gradient of the decline in sensitivity with increase in defocus flattened with increase in eccentricity for both groups and was flatter for the superior field compared to inferior field in both groups.

			-0.8118 0.9896	-0.6029 0.9062	-0.7559 0.8462	-0.9941 0.9626		
		-1.4500 0.9980	-1.2382 0.9965	-1.0412 0.9969	-1.1412 0.9909	-1.1235 0.9916	-1.0676 0.9768	
	-1.3500 0.9994	-1.5735 9.9963	-1.6235 0.9947	-1.4353 0.9948	-1.5235 0.9945	-1.3618 0.9976	-1.1529 0.9568	-1.3088 0.9097
-1.5882 0.9870	-1.4382 0.9864	-1.5706 0.9565	-1.6971 0.9477	-1.5294 0.9777	-1.7059 0.9929	-1.5735 09826		-1.4147 0.9968
-1.5353 0.9894	-1.6088 0.9857	-1.9859 0.9903	-1.9265 0.9440	-1.7912 0.9722	-1.9794 0.9934	-2.0353 0.9885		-1.5294 0.9940
	-1.5412 0.9914	-2.0029 0.9906	-1.7941 0.9944	-1.6706 0.9879	-1.8912 0.9851	-1.5765 0.9753	-1.2618 0.9954	-1.3588 0.9980
		-1.4794 0.9980	-1.5147 0.9999	-1.5706 0.9966	-1.7971 0.9976	-1.5971 0.9996	-1.4382 0.9973	
			-1.5059 0.9830	-1.8000 0.9796	-1.8676 0.9911	-1.7265 0.9976		

Figure 5.12a The gradient of the group Mean Sensitivity as a function of defocus for the normal individuals at each stimulus location of Pulsar perimetry Program CP-T30W.The lower value is the Coefficient of Determination (R^2). The results are presented in right eye format.

> -1.40	> -1.60	> -1.80	> -2.00	> -2.20	> -2.40

			-0,8821 0.9720	-0.5964 0.9843	-0.6500 0.9573	-0.9143 0.9468		
		-1.3000 0.9717	-1.4821 0.9828	-1.0179 0.9719	-0.9893 0.9466	-0.9393 0.9355	-1.1071 0.9875	
	-1.2643 0.9666	-1.5714 0.9773	-1.7607 0.9960	-1.5036 0.9822	-1.4571 0.9592	-1.2571 0.9857	-1.0036 0.9978	-1.3357 0.9731
-1.3143 0.9657	-1.3821 0.9265	-1.7571 0.9690	-1.9786 0.9840	-1.6536 0.9455	-1.8929 0.9719	-1.8571 0.9931		-1.2893 0.9587
-1.3071 0.9905	-1.4643 0.9682	-2.0286 0.9738	-2.2071 0.9567	-2.0000 0.9441	-2.1571 0.9697	-2.1250 0.9859		-1.3357 0.9668
	-1.5500 0.9929	-2.0607 0.9826	-2.0536 0.9774	-1.7464 0.9590	-1.7714 0.9568	-2.5857 0.9560	-1.0250 0.9541	-1.4321 0.9721
		-1.7464 0.9953	-1.6929 0.9971	-1.6286 0.9950	-1.6643 0.9919	-1.4357 0.9784	-1.2286 0.9534	
			-1.6857 0.9977	-1.8321 0.9932	-1.9071 0.9877	-1.6714 0.9575		

Figure 5.12b The gradient of the group Mean Sensitivity as a function of defocus for the individuals with OAG at each stimulus location of Pulsar perimetry Program CP-T30W. The lower value is the Coefficient of Determination (R^2). The results are presented in right eye format.

5.6 Discussion

5.6.1 The learning effect with the SITA Standard algorithm

In addition to Pulsar perimetry, all individuals underwent SAP at each visit with Program 24-2 of the HFA and the SITA Standard algorithm. SAP was undertaken to familiarise the normal individuals, who were naïve to any form of visual field testing, with perimetry. These data were used to evaluate the learning effect in terms of MS, MD, PSD, examination duration and the PMS/CMS ratio (Table 5.3). As would be expected, the MS and the MD were less positive for the group with OAG, but both indices were similar (i.e. no improvement) for both groups across the five visits, whereas the PSD, which also differed between the two groups, improved across the five visits. The improvement in examination duration was 37 seconds for the normal individuals and only 13 seconds for individuals with OAG, but generally, the examination duration was longer for the group with OAG. The PMS/CMS ratio was similar across the five visits both for the normal individuals and for the individuals with OAG.

5.6.2 The effect of defocus with Pulsar perimetry

The group mean MS ($p<0.001$), MD ($p<0.001$) and sLV ($p<0.001$) each deteriorated with increasing defocus. The slopes of the degradation in the group mean MS and MD both of the normal individuals and of the individuals with OAG were 1.5dB per dioptre of defocus. The corresponding gradient of the decline in group mean MS with increase in defocus for the normal individuals and for the individuals with OAG at each stimulus location flattened with increase in eccentricity and was flatter for the superior field compared to the inferior field in both groups.

The slope of the MS with increasing defocus is identical to that found for SAP using the Octopus perimeter (Luraas et al, unpublished findings). The results are also

compatible with those in the literature for SAP of approximately 1.0dB per dioptre of defocus (Weinreb and Perlman 1986; Heuer et al 1987; Goldstick and Weinreb 1987; Herse 1992; Collin et al 1993).

The corresponding slopes of the degradation for the group mean sLV were 0.27dB and 0.1dB per dioptre of defocus for the normal individuals and for the individuals with OAG, respectively. The group mean examination duration remained at approximately 200sec for both groups and was similar across the five visits. The group mean PMS/CMS ratio decreased slightly with increase in defocus for both groups. However, the omission of the most eccentric annulus containing 14 stimulus locations of the Pulsar CP-T30W stimulus grid compared to those, for example, of HFA Program 24-2, may account for the lack of a more pronounced peripheral component and therefore for a less accentuated ratio.

5.7 Conclusion

The influence of defocus on the outcome of Pulsar perimetry indicates, firstly, that the response is dependent upon a resolution task rather than a detection task and, secondly, that an appropriate refractive correction optimized for the viewing distance of the Pulsar perimeter is essential.

CHAPTER 6

GENERAL SUMMARY OF RESULTS, CONCLUSIONS AND PROPOSALS FOR FUTURE WORK

6.1 Summary of results and conclusions

6.1.1 The performance of SITA SWAP

The Full Threshold and FASTPAC algorithms for SWAP exhibit longer examination durations and greater between-subject normal variability compared to the corresponding algorithms for SAP (Wild et al 1995). The introduction of the SITA Standard and SITA Fast algorithms for SAP have resulted in a notable reduction in the examination duration and the between-subject normal variability compared to the Full Threshold and FASTPAC algorithms. The application of the SITA theory to SWAP was similarly intended to reduce both the examination duration and the between-subject normal variability relative to the Full Threshold and FASTPAC algorithms for SWAP. The study in Chapter 3 describes the performance of the new SITA SWAP relative to the SITA Standard and SITA Fast algorithms. Four different investigations were undertaken in normal individuals, naïve to perimetry, and in individuals with either OHT or with OAG experienced in SAP but naïve to SWAP.

The first investigation concerned the learning effect over 5 consecutive visits each separated by one week, in terms of the: visual field indices; the examination duration; the ratio of the PMS to the CMS; the slope of the decline in MS with increase in age; and the within-algorithm difference in the absolute sensitivity and in the number and/ or severity of the Total and of the Pattern Deviation probability levels. The results of these various analyses revealed clear evidence for a learning

effect in all three algorithms (i.e. an improvement in performance) across all three groups which was most pronounced for the SITA SWAP algorithm. In general, the learning effect was complete by Visit 3 for the SITA Standard and for the SITA Fast algorithms and, in general, at Visit 4 for SITA SWAP. The hill of vision became steeper with increasing age for all three algorithms, but was steepest for SITA SWAP. The overall age-related decline steepened between Visits 1 and 5 for both SITA SAP algorithms (i. e. by three fold for the right eye and by two fold for the left eye for the SITA Standard algorithm and by 1.5 fold for the right eye and by 1.8 fold for the left eye for the SITA Fast algorithm). However, the decline for SITA SWAP remained comparatively stable between Visits 1 and 5. The reason for these findings is not immediately clear.

The second investigation evaluated the within-individual within-algorithm between-visit (Visits 4 and 5) variability. The between-visit variability was greatest for SITA SWAP in terms of the MD and PSD and of the range between the 90^{th} and the 10^{th} percentiles of the difference in sensitivity across all stimulus locations. The greater between-visit variability for SITA SWAP would suggest that this algorithm would be less satisfactory that the two SITA SAP algorithms for identifying progressive glaucomatous loss at least when the loss is identifiable by SAP.

The third investigation evaluated the between-individual within-visit (Visit 5) between-algorithm performance. The underestimation by the SITA SWAP algorithm of the sensitivity derived by each of the two SAP algorithms was approximately by 5dB at all levels of sensitivity for all groups. The apparent greater abnormality in the height of the visual field for SWAP was not reflected either in the difference

between the Total Deviation probability level, or in the Pattern Deviation probability level, between the SITA SWAP algorithm and either the SITA Standard or the SITA Fast algorithms across any of the three groups. This finding is most likely due to the reduced dynamic range of SWAP compared to SAP since the difference between the MD for SITA SWAP and either of the two SITA algorithms is less than the difference in the absolute values of sensitivity. However, the difference is also likely to result from the wider confidence limits for normality for SITA SWAP, compared to each SAP algorithm, associated with the greater reduction in sensitivity for SWAP than for SAP. Indeed, the Coefficient of Variation (CoV) of the within-algorithm between-individual variability was substantially larger for SITA SWAP than for either SITA algorithm indicating that the confidence limits for normality would be wider for SITA SWAP than the other two SITA algorithms. However, the difference in the characteristics of the various cohorts used to determine the age-corrected normal values between the SITA SWAP algorithm and the two SITA algorithms for SAP may also account for some of the discrepancy.

Fourthly, the structure function relationship for SITA SWAP, SITA Standard and SITA Fast assessed in terms of the FSM and RB discriminant functions and in terms of the rim-disc ratio indicated poor structural-functional concordance in OAG largely due to the poor sensitivity of perimetry for the identification of OAG.

The results of the various investigations demonstrate that the learning effect and the between-examination-variability for SITA SWAP were substantially greater compared to either SAP algorithms. In addition, the between-individual within-visit between-algorithm variability was greatest for SITA SWAP compared to either

SITA Standard or SITA Fast which further limits the utility of SWAP. Furthermore, there was no indication from the structure (as assessed by the Heidelberg Retina Tomograph) function relationship that the SITA SWAP algorithm was more closely correlated with structural abnormality than that for either SAP algorithm. Therefore, it would seem that the SITA SWAP algorithm has no clinical advantage compared to SAP, either for discriminating normal individuals from those with OAG nor for use in follow-up examinations. The application of the SITA algorithm to SWAP has resulted in a reduction in the confidence intervals for normality compared to the older Full Threshold and FASTPAC algorithms for SWAP (Bengtsson and Heijl 2003). However, a qualitatively similar reduction in the magnitude of the confidence limits for SAP is present for the SITA algorithms compared to the Full Threshold and FASTPAC algorithms (Wild et al 1999a). As a consequence, the SITA SWAP algorithm is still disadvantaged relative to SAP by the larger confidence intervals. In summary, SWAP, and the SITA SWAP algorithm, itself, will be of little benefit in the clinical setting.

6.1.2 The performance of Pulsar perimetry

The study in Chapter 4 describes the performance of a new technique, Pulsar perimetry. Four different investigations were undertaken in normal individuals, naïve to perimetry, and in individuals with either OHT or with OAG experienced in SAP but naïve to Pulsar perimetry. Approximately 65% of the individuals with OHT or with OAG were also experienced in SWAP having taken part in the study described in Chapter 3.

The first investigation examined the presence of a learning effect for Pulsar perimetry over 5 consecutive visits, each separated by one week. The SITA Standard

algorithm was used as reference i.e. the normal individuals would be expected to show a small learning effect whilst those with OHT or with OAG would be expected to be familiar with the technique. The results for Pulsar perimetry and for SAP were analysed in terms of the visual field indices; the examination duration; the ratio of the PMS to the CMS; and the within-algorithm difference both in the absolute sensitivity and in the number and/ or severity of the Comparison and the Total and Pattern Deviation probability levels, respectively. Little evidence of a learning effect, for the groups as a whole, was found for Pulsar perimetry over the five visits for all three diagnostic groups including the normal individuals. However, considerable differences were present between individuals in all three diagnostic groups across the five visits with some manifesting clear improvements, others little difference and others an apparent worsening in performance. The between-individual variation in performance was widest amongst those with OAG.

Unfortunately, the age distribution of the normal individuals did not permit an appropriate statistical analysis of the age-effect of the slope of decline in mean sensitivity. The reduction the examination duration in all three groups across the five visits was approximately equal.

Despite the greater number of stimulus locations for the Pulsar algorithm CP-T30W compared to the HFA Program 24-2, Pulsar perimetry was approximately 1.3 fold faster than that for the SITA Standard algorithm and Program 24-2. The examination duration was approximately 6 seconds shorter for the left eye than for the right eye both for the normal individuals and for the individuals with OHT and in the region of 9-10 seconds for the individuals with OAG.

The 90^{th}, 50^{th} and 10^{th} percentiles of the distribution of the within-algorithm difference in sensitivity between Visits 1 and 5 across all stimulus locations indicated that a slight improvement occurred at increasingly intermediate values of sensitivity for both algorithms and that the reduction in the number and/ or severity of the probability levels was most pronounced for the SITA Standard algorithm for the right eye in normal individuals, whereas Pulsar perimetry exhibited a deterioration for both eyes in individuals with OAG (i.e. an increase in the number of stimulus locations exhibiting a statistically significant probability level).

The second investigation, which evaluated the within-individual within-algorithm between-visit (Visits 4 and 5) variability, revealed a mild deterioration of the results in the individuals with OAG with Pulsar perimetry. Once again these deteriorations were usually more pronounced for the right eye than for the left eye both in terms of the MD and the sLV and the range between the 90^{th} and 10^{th} percentiles of the difference in sensitivity across all stimulus locations and to a lesser extent in terms of the probability levels. Such between-eye differences suggest a reduced or absent fatigue effect for the second (left) eye examined.

The third investigation evaluated the between-individual within-visit (Visit 5) between-algorithm performance. The between-individual within-visit between-algorithm variability for SITA Standard and Pulsar perimetry was wider for the individuals with OAG and was narrower in all groups in the left eye (i.e. second eye examined) in terms of the MDs, PSD and sLV, respectively. A substantial underestimation of approximately 10dB at all levels of sensitivity in all three groups was found with Pulsar perimetry compared to the SITA Standard algorithm.

However, these discrepancies can be explained in the use of the different dB scales in the two algorithms. Pulsar perimetry demonstrated proportionately more abnormal Comparison probability values compared to those for the SITA Standard Total Deviation probability map in normal individuals for the right eye and in individuals with OAG for both eyes. The CoV for Pulsar perimetry were, on average, approximately 1.6 fold greater in each eye than for SITA Standard across all three groups.

Fourthly, as was the case with the SITA SWAP study (Chapter 3), the structure function relationship for SITA Standard and Pulsar perimetry, assessed in terms of the FSM and RB discriminant functions and in terms of the rim-disc ratio, indicated limited structural-functional concordance in OAG.

It can be concluded that, despite the new perceptual task with Pulsar perimetry, the learning effect across the five visits was minimal. Generally, the within-visit learning effect for Pulsar perimetry led, as a consequence, to more normal results for the left eye (i.e. the second eye examined) than for the right eye (i.e. the first eye examined). Most of the patients preferred Pulsar perimetry over SAP with the SITA Standard algorithm due to the shorter examination duration. The use of Pulsar perimetry might therefore lead to better attendance at the follow-up examinations. However, due to the apparent heterogeneity in any learning effect; the greater absolute and proportionate difference in the between-examination variability; the reduced dynamic range; the uncertainty of the current confidence limits for normality; the absence of any deeper/ additional field loss; and the limited

agreement with the stereometric parameters limits the utility of the Pulsar perimeter for follow-up examinations.

6.1.3 The effect of defocus with Pulsar perimetry

The group mean MS, mean MD and mean sLV each deteriorated significantly with increasing defocus ($p<0.001$). The slopes of the degradation in the group mean MS and MD both of the normal individuals and of the individuals with OAG were 1.5dB per dioptre of defocus. The corresponding slopes of degradation for the group mean sLV were 0.2dB and 0.1dB per dioptre of defocus. The gradient of the decline in sensitivity with increase in defocus flattened with increase in eccentricity for both groups. It was flatter for the superior field compared to inferior field in both groups. The group mean examination duration remained at approximately 200sec for both groups and was similar across the five visits. An appropriate correction for the viewing distance is mandatory when using Pulsar perimetry.

6.2 Proposal for future work

6.2.1 Investigation of the SITA SWAP learning effect after a six month interval

The findings in Chapter 3 revealed a substantially greater learning effect for SITA SWAP than for SITA Standard and for SITA Fast in normal individuals, in individuals with OHT and in individuals with OAG who attended for perimetry in five visits separated by one week. The learning effect for SITA SWAP was, in general, complete by Visit 4. The use of five sessions each separated by one week has become a relatively common protocol by which to investigate the perimetric learning effect (Heijl and Bengtsson 1996; Rossetti et al 2006; Wild et al 2006) and determines the potential for improvement. However such a protocol does not reflect clinical reality where the follow-up visit is normally at either 3, 6 or 12 months. A myriad of alternative experimental designs could have been adopted which reflected

clinical reality more appropriately; however, such designs have to contend with the possibility of progressive loss occurring in OAG. In addition, the majority of such designs could not have been undertaken within the duration of a PhD thesis although this latter point is of minor importance. The retention of any improvement in sensitivity for SAP arising from a short-term training protocol has been investigated at a longer-term follow-up (Wild et al 1991). The study described in Chapter 3 did not investigate the retention of the learning effect for SWAP at a longer-term follow-up, e.g. 6 months. However, given the limitations of SWAP arising from the increased confidence intervals relative to SAP, which will limit the detection of abnormality, and the greater between-examination variability relative to SAP, which will currently limit the detection of progressive loss, such a debate as to the optimum interval between examinations for the study of the learning effect is of academic interest. Nevertheless, a study investigating the retention of the learning effect associated with the SITA SWAP algorithm would be useful.

6.2.2 Long-term fluctuation with SITA SWAP

As mentioned in Chapter 1, the Long-term fluctuation (LF) is the variability of the threshold estimate over several visual field sessions (Bebié et al 1976a; Flammer et al 1984a; Hutchings et al 2000; 2002) after removing the influence of the learning effect and of the age of the patient. The identification of progressive loss by SAP is hindered by the LF. A greater LF for SWAP compared to SAP is present for the Full Threshold algorithm (Wild et al 1995; Kwon et al 1998; Wild et al 1998; Hutchings et al 2000). However, the magnitude of the LF associated with SITA SWAP, has not been studied and although, as described above, the LF is likely to be larger than that for either SITA Standard or SITA Fast, there is no evidence-based knowledge to separate the LF for SWAP from the 'true' progressive loss. However, such an

investigation is not currently possible since the calculation of the LF requires the double determination of the threshold at each of a number of common stimulus locations and this is not possible with the commercially available SITA algorithms. However, given the increased between-examination variability of SITA SWAP relative to SAP for both SITA algorithms, the necessity for a 'noise' reduction technique is paramount.

6.2.3 Development of the Learner's Index for SITA SWAP

The first step in the derivation of the Learner's Index (LI) for SITA SWAP is described in Appendix B1. The magnitude of the learning effect for SWAP necessitates a method whereby the 'measured' representation of the field at baseline is transformed into the 'true' representation of the field which would be present after cessation of the learning effect, thereby avoiding multiple additional visual examinations to 'train' the patient. To avoid the necessity for these training sessions, such an approach requires the prediction of the 'learnt' field from the baseline 'naïve' or measured field. Unfortunately, the mathematical complexity of this topic demanded significant professional input from a mathematician and quickly became beyond the scope of the thesis. The topic is now being studied in-depth by a fellow postgraduate research student within the School.

6.2.4 Estimating the diffuse component of the visual field loss

A method for estimating the diffuse component of visual field loss, defined as the 'false-positive peak' which normally occurs at the 14th highest ranked deviation (of 59 stimulus locations) from the corresponding age-corrected normal value was proposed by Zulauf et al (1996b). The HFA defines the diffuse component in terms of the GH index which, itself, is defined as the 7th highest ranked deviation from the

corresponding age-corrected normal value (see Chapter 1). These two methods for estimating the diffuse component of visual field loss have not been compared for SAP and particularly for SWAP where the absorption of short- wavelengths is a particular problem. The current data set of visual fields derived by SITA Standard, SITA Fast and SITA SWAP is perfectly suited to answer such questions.

6.2.5 Investigation of Pulsar perimetric as a screening tool

Pulsar perimetry may have potential as a screening tool for various ophthalmic diseases and for the examination of the visual field as a requirement for a driving licence. The hardware is simple and therefore affordable, examination duration is relatively short, there is little learning effect compared with SAP (see Chapter 4) and the technique is well accepted by patients. As stated in Chapter 5, an appropriate refraction correction is mandatory. Further studies of the sensitivity and specificity are required to determine whether Pulsar perimetry can be used as a single screening tool or in a battery of various complementary tests.

6.2.6 Investigation into the influence of the cylindrical error and cataract on Pulsar perimetry

As described in Chapter 5, the MS and MD were affected by spherical defocus. The influence of cylindrical error, and of absorption and light scatter arising from cataract, is unknown. Consequently, further studies will be needed to determine the influence of these factors.

6.2.7 Long-term fluctuation with Pulsar perimetry

To distinguish between LF and true progression of glaucomatous visual field decay it is important to describe LF associated with Pulsar perimetry. Currently, the

magnitude of the LF is unknown for Pulsar perimetry. Such information will be necessary if the Pulsar perimeter is to be accepted into clinical practice.

REFERENCES

Adams AJ, Johnson CA and Lewis RA (1991). S-cone pathway sensitivity loss in ocular hypertension and early glaucoma has nerve fiber bundle pattern. In Drum B, Moreland JD and Serra A (eds.). *Colour Vision Deficiencies.* Kluwer Academic Publishers, Dordrecht. 535-542.

Advanced Glaucoma Intervention Study (AGIS) (1994). 2. Visual field test scoring and reliability. *Ophthalmology. 101, 1445-1455.*

Advanced Glaucoma Intervention Study (AGIS) (1998). 4. Comparison of treatment outcomes within race. Seven-year results. *Ophthalmology* 105, 1146-1164.

Airaksinen PJ, Tuulonen A, Valimaki J and Alanko HI (1990). Retinal nerve fiber layer abnormalities and High-pass Resolution Perimetry. *Acta Ophthalmol.* 68, 687-689.

Akar Y, Yucel I, Akar ME, Taskin O and Ozer OH (2005). Menstrual cycle-dependent changes in visual field analysis of healthy women. *Ophthalmologica.* 219, 30-35.

Anderson AJ (2003). Spatial resolution of the Tendency-Oriented Perimetry algorithm. *Invest Ophthalmol Vis Sci.* 44, 1962-1968.

Anderson AJ and Johnson CA (2003). Frequency-Doubling Technology perimetry and optical defocus. *Invest Ophthalmol Vis Sci.* 44, 4147-4152.

Anderson AJ, Johnson CA, Fingert M, Keltner JL, Spry PG, Wall M and Werner JS (2005). Characteristics of the normative database for the Humphrey Matrix perimeter. *Invest Ophthalmol Vis Sci.* 46, 1540-1548.

Anderson AJ and Vingrys AJ (2000). Effect of stimulus duration in Flicker perimetry. *Clin Experiment Ophthalmol.* 28, 223-226.

Anderson AJ and Vingrys AJ (2002). Effect of eccentricity on luminance-pedestal flicker thresholds. *Vision Res.* 42, 1149-1156.

Anderson and O'Brien (1997). Psychophysical evidence for a selective loss of M ganglion cells in glaucoma. *Vision Res.* 37, 1079-1083.

Anderson DR and Patella VM (1999). *Automated static perimetry 2nd Edition.* Mobsy Inc. St. Louis.

Anderson RS, McDowell DR and Ennis FA (2001). Effect of localized defocus on detection thresholds for different sized targets in the fovea and periphery. *Acta Ophthalmol Scand.* 79, 60-63.

Ansari EA, Morgan JE and Snowden RJ (2002). Psychophysical characterisation early functional loss in glaucoma and ocular hypertension. *Br J Ophthalmol.* 86, 1131-1135.

Arden GB and Jacobson JJ (1978) A simple grating test for contrast sensitivity: preliminary results indicate value in screening for glaucoma. *Invest Ophthalmol Vis Sci.* 17, 23-32.

Arnalich-Montiel F, Casas-Llera P, Munoz-Negrete FJ and Rebolleda G (2009). Performance of glaucoma progression analysis software in a glaucoma population. *Graefes Arch Clin Exp Ophthalmol.* 247, 391-397.

Artes PH, Iwase A, Ohno Y, Kitazawa Y and Chauhan BC (2002). Properties of perimetric threshold estimates from Full Threshold, SITA Standard and SITA Fast strategies. *Invest Ophthalmol Vis Sci.* 43, 2654-2659.

Åsman P, Fingert M, Robin A, Wild JM, Pacey IE, Greenfield D, Liebmann J and Ritch R (1999). Kinetic and static fixation methods in automated threshold perimetry. *J Glaucoma.* 8, 290-296.

Åsman P and Heijl A (1992a). Glaucoma Hemifield Test. Automated visual field evaluation. *Arch Ophthalmol.* 110, 812-819.

Åsman P and Heijl A (1992b). Evaluation of methods for automated hemifield analysis in perimetry. *Arch Ophthalmol.* 110, 820-826.

Åsman P and Olsson J (1995). Physiology of cumulative defect curves; consequences in glaucoma perimetry. *Acta Ophthalmol Scan.* 73, 197-201.

Åsman P, Wild JM and Heijl A (2004). Appearance of the Pattern Deviation map as a function of change in area of localized field loss. *Invest Ophthalmol Vis Sci.* 45, 3099-3106.

Asaoka R, Strouthidis NG, Kappou V, Gardiner SK and Garway-Heath DF (2009). HRT-3 Moorfields Reference Plane: effect on Rim Area repeatability and identification of progression. *Br J Ophthalmol* 93, 1510-1513.

Atchison DA (1987). Effect of defocus on visual field measurement. *Ophthalmic Physiol Opt.* 7, 259-265.

Atchison DA and Johnston AW (1979). The alteration in static perimetric thresholds caused by the prismatic effect of ophthalmic lenses. *Aust J Ophthlmol.* 62, 276-278.

Aulhorn and Harms (1972). In: Jamerson D and Hurvich LM (eds.). *Handbook of sensory physiology.* Berlin: Springer, 1972. 7, 102-145.

Austin NW, O'Brien CJ and Wishart PK (1994). Flicker perimetry using a luminance threshold strategy at frequencies from 5-25Hz in glaucoma, ocular hypertension and normal controls. *Curr Eye Res.* 13, 717-723.

Bagga H, Feuer WJ and Greenfield DS (2006). Detection of psychophysical and structural injury in eyes with glaucomatous optic neuropathy and normal Standard automated perimetry. *Arch Ophthalm.*124, 169-176.

Balazsi AG, Rootman J, Drance SM, Schulzer M and Douglas GR (1984). The effect of the age on the nerve fiber population of the human optic nerve. *Am J Ophthalmol. 97,* 760-766.

Bartsch DU, Intaglietta M, Bille JF, Dreher AW, Gharib M and Freeman WR (1989). Confocal laser tomographic analysis of the retina in eyes with macular hole formation and other focal macular diseases. *Am J Ophthalm.* 108, 277-287.

Bathija R, Zangwill L, Berry CC, Sample PA and Weinreb RN (1998). Detection of early glaucomatous structural damage with confocal scanning laser tomography. *J Glaucoma.* 7, 121-127.

Battista J, Badcock DR and McKendrick AM (2009). Spatial summation properties for magnocellular and parvocellular pathways in glaucoma. *Invest Ophthalmol Vis Sci.* 50, 1221-1226.

Bebié H (1990). Computer-assisted evaluation of visual fields. *Graefes Arch Clin Exp Ophthalmol.* 228, 242-245.

Bebié H, Fankhauser F and Spahr J (1976a). Static perimetry: strategies. *Acta Ophthalmol.* 54, 325-338.

Bebié H, Fankhauser F and Spahr J (1976b). Static perimetry: accuracy and fluctuations. *Acta Ophthalmol.* 54, 339-348.

Bebié H, Flammer J and Bebié T (1989). The cumulative defect curve: separation of local and diffuse components of visual field damage. *Graefes Arch Clin Exp Ophthalmol.* 227, 9-12.

Becker ST, Vonthein R, Volpe NJ and Schiefer U (2005). Factors influencing reaction time during automated kinetic perimetry on the Tübingen computer campimeter. *Invest Ophthalmol Vis Sci.* 46, 2633-2638.

Bedell HE and Katz LM (1982). On the necessity of correcting peripheral target luminance for pupillary area. *Am J Optom Physiol Opt.* 59, 767-769.

Bek T and Lund-Andersen H (1989). The influence of stimulus size on perimetric detection of small scotoma. *Graefes Arch Clin Exp Ophthalmol.* 227, 531-534.

Benedetto MD and Cyrlin MN (1985). The effect of blur upon static perimetric thresholds. *Documenta Ophthalmologica, Proceedings Series.* 42, 563-567.

Bengtsson B (2003). A new rapid threshold algorithm for Short-wavelength Automated Perimetry. *Invest Ophthalmol Vis Sci.* 44, 1388-1394.

Bengtsson B and Heijl A (2008). A visual field index for calculation of glaucoma rate of progressions. *Am J Ophthalmol.* 145, 343-353.

Bengtsson B and Heijl A (1998a). Evaluation of a new perimetric threshold strategy, SITA, in patients with manifest and suspect glaucoma. *Acta Ophthalmol Scand.* 76, 268-272.

Bengtsson B and Heijl A (1998b). SITA Fast, a new rapid perimetric threshold test. Description of methods and evaluation in patients with manifest and suspect glaucoma. *Acta Ophthalmol Scand.* 76, 431-437.

Bengtsson B, Heijl A and Olsson J (1998c). Evaluation of a new threshold visual field strategy, SITA, in normal subjects. Swedish Interactive Threshold Algorithm. Acta *Ophthalmol Scand.* 76, 165-169.

Bengtsson B and Heijl A (1999a). Comparing significance and magnitude of glaucomatous visual field defects using the SITA and Full Threshold strategies. *Acta Ophthalmol Scand.* 77, 143-146.

Bengtsson B and Heijl A (1999b). Inter-subject variability and normal limits of the SITA Standard, SITA Fast and the Humphrey Full Threshold computerized perimetry strategies, SITA STATPAC. *Acta Ophthalmol Scand.* 77, 125-129.

Bengtsson B and Heijl A (2000). False-negative responses in glaucoma perimetry: indicators of patient performance or test reliability? *Invest Ophthalmol Vis Sci.* 41, 2201-2204.

Bengtsson B and Heijl A (2003). Normal intersubject threshold variability and normal limits of the SITA SWAP and Full Threshold SWAP perimetric programs. *Invest Ophthalmol Vis Sci.* 44, 5029-5034.

Bengtsson B and Heijl A (2006). Diagnostic sensitivity of fast blue-yellow and Standard automated perimetry in early glaucoma: a comparison between different test programs. *Ophthalmology.* 113, 1092-1097.

Bengtsson B, Lindgren A, Heijl A, Lindgren G, Åsman P and Patella VM (1997a). Perimetric probability maps to separate change caused by glaucoma from that caused by cataract. *Acta Ophthalmol Scand.* 75, 184-188.

Bengtsson B, Olsson J, Heijl A and Rootzen H (1997b). A new generation of algorithms for computerized threshold perimetry, SITA. *Acta Ophthalmol Scand.* 75, 368-375.

Bernardi L, Costa VP and Shiroma LO (2007). Flicker perimetry in healthy subjects: influence of age and gender, learning effect and Short-term fluctuation. *Arq Bras Oftalmol.* 70, 91-99.

Bickler-Bluth M, Trick GL, Kolker AE and Cooper DG (1989). Assessing the utility of reliability indices for automated visual fields. Testing ocular hypertensives. *Ophthalmology.* 96, 616-619.

Birt CM, Shin DH, Samudrala V, Hughes BA, Kim C and Lee D (1997). Analysis of reliability indices from Humphrey visual field test in an urban glaucoma population. *Ophthalmology.* 104, 1126-1130.

Bland J and Altman D (1986). Statistical methods for assessing agreement between two methods of clinical measurement. *The Lancet.* 327, 307-310.

Bloch AM (1885). Expèrience sur la vision. *Comp R Soc Biol 2.* 493.

Blumenthal EZ, Sample PA, Zangwill L, Lee AC, Kono Y and Weinreb RN (2000). Comparison of Long-term variability for standard and Short-wavelength Automated Perimetry in stable glaucoma patients. *Am J Ophthalmol.* 129, 309-313.

Boeglin RJ, Caprioli J and Zulauf M (1992). Long-term fluctuation of the visual field in glaucoma. *Am J Opthalmol.* 113, 396-400.

Boet (1970). Toxic effects of phentothiazines on the eye. *Doc Ophthalmol.* 24, 1-69.

Borque E, Ferreras A, Polo V, Larrosa JM, Alias E and Honrubia (2008). Evaluation of four new discriminant functions for HRT II in glaucoma diagnosis. *Arch Soc Esp Oftalmol.* 83, 349-356.

Bosworth CF, Sample PA, Gupta N, Bathija R and Weinreb RN (1998). Motion automated perimetry identifies early glaucomatous field defects. *Arch Opthalmol.* 116, 1153-1158.

Bosworth CF, Sample PA and Weinreb RN (1997). Perimetric motion thresholds are elevated in glaucoma suspects and glaucoma patients. *Vision Res.* 37, 1989-1987.

Bozkurt B, Yilmaz PT and Irkec M (2008). Relationship between Humphrey 30-2 SITA Standard test, Matrix 30-2 Threshold test, and Heidelberg Retina Tomograph in ocular hypertensive and glaucoma patients. *J Glaucoma.* 17, 203-210.

Brenton RS and Phelps CD (1986). The normal visual field on the Humphrey Field Analyzer. *Ophthalmologica.* 193, 56-74.

Brigatti L and Carioli J (1995). Correlation of visual field with scanning confocal laser optic disc measurements in glaucoma. *Arch Ophthalmol.* 113, 1191-1194.

Brusini P, Salvetat ML, Zeppieri M and Parisi L (2006). Frequency-Doubling Technology perimetry with the Humphrey Matrix 30-2 test. *J Glaucoma.* 15, 77-83.

Bryce AF, Artes PH, McCormick TA, Nicolela MT, LeBlanc RP and Chauhan BC (2003). Comparison of data analysis tools for detection of glaucoma with the Heidelberg Retina Tomograph. *Ophthalmology.* 110, 1145-1150.

Budenz DL, Rhee P, FeuerWJ, McSoley J, Johnson CA and Anderson DR (2002). Sensitivity and specificity of the Swedish Interactive Threshold Algorithm for glaucomatous visual field defects. *Ophthalmology.* 109, 1052-1058.

Buerki E (2006). Update Octopus Perimetrie -Die Polardarstellung der Gesichtsfelddaten. *Ophtha.* 7, 9-12.

Buerki E and Monhart M (2007). An update to Octopus perimetry. *Eur Ophthalmic Review.* 20-22.

Burgansky-Eliash Z, Wollstein G, Patel A, Bilonick RA, Ishikawa H, Kagemann L, Dilworth WD and Schuman JS (2007). Glaucoma detection with Matrix and Standard achromatic perimetry. *Br J Ophthalmol.* 9, 933-938.

Burgansky-Eliash Z, Wollstein G, Patel A, Jones BL, Ishikawa H and Schuman JS (2005). Comparing the ability of visual field testing by Matrix perimetry and Swedish Interactive Thresholding Algorithm (SITA) perimetry to detect glaucoma. *Invest Ophthalmol Vis Sci.* 46: E-Abstract 3725.

Burk RO, Noack H, Rohrschneider K and Völcker HE (1998). Prediction of glaucomatous visual field defect by Reference Plane independent three-dimensional optic nerve head parameters. In Wall M and Wild JM (eds.). *Perimetry Update* 1998/1999, 463-474.

Burk RO, Rohrschneider K, Noack H and Völcker HE (1991). Volumetric analysis of the optic papilla using laser scanning tomography. Parameter definition and comparison of glaucoma and control papilla. *Klin Monatsbl Augenheilkd.* 198, 522-529.

Burk RO, Rohrschneider K and Völcker HE (1990). Posterior segment laser scanning tomography: Contour-line modulation in optic disk analysis. *Proceedings of SPIE.* 1357, 228-235.

Bynke H and Heijl A (1978). Automated computerized perimetry in the detection of neurological visual field defects. A pilot study. *Graefes Arch Clin Exp Ophthalmol.* 206, 11-15.

Calkins DJ (2001). Seeing with S-cones. *Prog Retin Eye Res.* 20, 255-287.

Callaway EM (2005). Structure and function of parallel pathways in the primate early visual system. *J Physiol.* 566, 13-19.

Campbell FW and Green DG (1965). Optical and retinal factors affecting visual resolution. *J Physiol.* 181, 576-593.

Campbell FW and Robson JG (1968). Application of Fourier analysis to the visibility of gratings. *J Physiol.* 197, 551-566.

Caprioli J (2001). Should we use Short-wavelength Automated Perimetry to test glaucoma patients? *Am J Ophthalmol.* 131, 792-794.

Caprioli J and Miller JM (1988). Warman: Visual field improvement with acute reduction of intraocular pressure. *Invest Ophthalmol Vis Sci.* 29, ARVO suppl 422.

Carcieri SM, Jacobs AL and Nirenberg S (2003). Classification of retinal ganglion cells: a statistical approach. *J Neurophysiol.* 90, 1704-1713.

Casas-Llera P, Rebolleda G, Munoz-Negrete FJ, Arnalich-Montiel, Pérez-Lopez M and Fernandez-Buenaga R (2009). Visual field index rate and event-based glaucoma progression analysis: Comparison in a glaucoma population. *Br J Ophthalmol.* Epub ahead of print.

Cascairo MA, Stewart WC and Sutherland SE (1991). Influence of missed catch trials on the visual field in normal subjects. *Graefes Arch Clin Exp Ophthalmol.* 229, 437-441.

Casson EJ and Johnson CA (1992). Temporal Modulation Perimetry in glaucoma and ocular hypertension. *Perimetry Update* 1992/93 books googlecom. 443-451.

Casson EJ, Johnson CA and Nelson-Quigg JM (1993b). Temporal Modulation Perimetry: the effects of aging and eccentricity on sensitivity in normals. *Invest Ophthalmol Vis Sci.* 34, 3096-3102.

Casson EJ, Johnson CA and Shapiro LR (1993a). A longitudinal comparison of Temporal Modulation Perimetry with white-on-white and blue-on-yellow perimetry in ocular hypertension and early glaucoma. *J Opt Soc Am A Opt Image Sci Vis.* 10, 1792-1806.

Cavanagh P, MacLeod DI and Anstis SM (1987). Equiluminance: spatial and temporal factors and the contribution of blue-sensitive cones. *J Opt Soc Am A.* 4, 1428-1438.

Cello KE, Nelson-Quigg JM and Johnson CA (2000). Frequency-Doubling Technology perimetry for detection of glaucomatous visual field loss. *Am J Ophthalmol.* 129, 314-322.

Centofanti M, Fogagnolo P, Oddone F, Orzalesi N, Vetrugno M, Manni G and Rossetti L (2008). Learning effect of Humphrey Matrix Frequency-Doubling Technology Perimetry in patients with ocular hypertension. *J Glaucoma.* 17, 436-441.

Chapron DJ, Gomolin IH and Sweeney KR (2004). Acetazolamide blood concentrations are excessive in the elderly: propensity for acidosis and relationship to renal function. *Br J Ophthalmol.* 88, 714-715.

Chauhan BC (1996). Analysis of changes in the optic nerve head. In Anderson DR and Drance SM (eds.) *Encounters in glaucoma research 3.* Amsterdam/ New York: Kugler Publication, 1996. 195-208.

Chauhan BC, Blanchard JW, Hamilton DC and LeBlanc RP (2000). Technique for detecting serial topographic changes in the optic disc and peripapillary retina using scanning laser tomography. *Invest Ophthalmol Vis Sci.* 41, 775-782.

Chauhan BC, Drance SM and Douglas GR (1990). The use of visual field indices in detecting changes in the visual field in glaucoma. *Invest Ophthalmol Vis Sci.* 31, 512-520.

Chauhan BC and House PH (1991). Intratest variability in conventional and High-pass Resolution Perimetry. *Ophthalmology.* 98, 79-83.

Chauhan BC, House PH, McCormick TA and LeBlanc RP (1999). Comparison of conventional and High-pass Resolution Perimetry in a prospective study of patients with glaucoma and healthy controls. *Arch Ophthalmol.* 117, 24-33.

Chauhan BC, LeBlanc RP, McCormick TA, Mohandas RN and Wijsman K (1993a). Correlation between the optic disc and results obtained with conventional, High-pass Resolution and Pattern Discrimination Perimetry in glaucoma. *Can J Ophthalmol.* 28, 312-316.

Chauhan BC, LeBlanc RP, McCormick TA and Rogers JB (1993c). Comparison of High-pass Resolution Perimetry and Pattern Discrimination Perimetry to conventional perimetry in glaucoma. *Can J Ophthalmol.* 28, 306-311.

Chauhan BC, Mohandas RN, Whelan JH and McCormick TA (1993d). Comparison of reliability indices in conventional High-pass Resolution Perimetry. *Ophthalmology.* 100, 1089-1094.

Chauhan BC, Tompkins JD, LeBlanc RP and McCormick TA (1993b). Characteristics of Frequency of Seeing curves in normal subjects, patients with suspected glaucoma and patients with glaucoma. *Invest Ophthalmol Vis Sci.* 34, 3534-3540.

Chen XM (1992). Frequency distribution of earliest glaucomatous visual field defects. *Zhonghua Yan Ke Za Zhi.* 28, 206-208.

Chen YY, Chen PP, Xu L, Ernst PK, Wang L and Mills RP (1998). Correlation of peripapillary nerve fiber layer thickness by scanning laser polarimetry with visual field defects in patients with glaucoma. *J Glaucoma.* 7, 312-316.

Cho NC, Poulsen GL, Ver Hoeve JN and Nork TM (2000). Selective loss of S-cones in diabetic retinopathy. *Arch Ophthalmol.* 118, 1393-1400.

Choplin NT and Edwards RP (1999). Basic principles of visual field interpretation. In: Choplin NT and Edwards RP (eds.). *Visual field testing with the Humphrey Field Analyser.* New Jersey: Thorofare. 1999. 77-113

Choplin NT, Sherwood MB and Spaeth GL (1990). The effect of stimulus size on the measured threshold values in automated perimetry. *Opththamology.* 97, 371-374.

Chylack LT, Wolfe JK, Singer DM, Leske MC, Bullimore MA, Bailey IL, Friend J, McCarthy D and Wu SY (1993). The Lens Opacities Classification System III. The longitudinal study of cataract study group. *Arch Ophthlmol.* 111, 831-836.

Clement CI, Goldberg I, Healey PR and Graham S (2009). Humphrey Matrix Frequency- Doubling Perimetry for detection of visual field defects in open-angle glaucoma. *Br J Ophthalmol.* 93, 582-588.

Contestabile MT, Perdicchi A, Amodeo S, Recupero V and Recupero SM (2007). The influence of learning effect on Frequency-Doubling Technology Perimetry (Matrix). *J Glaucoma.* 16, 297-301.

Collin HB, Banks R and Dimitratos M (1993). The effect of refractive error on perimetric thresholds using the Humphrey Field Analyzer. *Clinical and experimental optometry.* 76, 162-171.

Cook CA, Koretz JF, Pfahnl A, Hyun J and Kaufman PL (1994). Aging of the human crystalline lens and anterior segment. *Vision Res.* 34, 2945-2954.

Cowan RA, Hartnell GG, CP Lowdell, Baird IM and Leak AM (1984). Metabolic acidosis induced by carbonic anhydrase inhibitors and salicylates in patients with normal renal functions. *Br Med (Clin Res Ed).* 289, 347-348.

Curcio CA, Allen KA, Sloan KR, Lerea CL, Hurley JB, Klock IB and Milam AH (1991). Distribution and morphology of human cone photoreceptors stained with anti-blue opsin. *J Comp Neurol.* 312, 610-624.

Dacey DM (1993a). Morphology of a small-field bistratified ganglion cell type in the macaque and human retina. *Vis neurosci.* 10, 1081-1098.

Dacey DM (1993b). The mosaic of midget ganglion cells in the human retina. *J Neurosci.* 13, 5334-5355.

Dacey DM (1999). Primate retina: cell types, circuits and colour opponency. *Prog Retin Eye Res.* 18, 737-763.

Dacey (2000). Parallel pathways for spectral coding in primate retina. *Annu Rev Neurosci.* 23, 743-775.

Dacey DM and Lee BB (1994). The 'blue-on' opponent pathway in primate retina originates from a distinct bistratified ganglion cell type. *Nature.* 367, 731-735.

Dacey DM and Petersen MR (1992). Dendritic field size and morphology of midget and parasol ganglion cells of the human retina. *Proc Natl Acad Sci USA.* 89, 9666-9670.

De Jong LA, Snepvangers CE, van de Berg TJ and Langerhorst CT (1990). Blue-yellow perimetry in the detection of early glaucomatous damage. *Doc Ophthalmol.* 75, 303-314.

De Valois RL, Abramov I and Jacobs GH (1966). Analysis of response patterns of LGN cells. *J Opt Soc Am.* 56, 966-977.

Deghislage C, Van Malderen L and Zeyen TG (2008). False negative results in glaucoma detection with Heidelberg Retina Tomograph II. *Clin. Ophthalmol.* 2, 153-157.

Delori FC and Burns SA (1996). Fundus reflectance and the measurement of crystalline lens density. *J Opt Soc Am A Opt Image Sci Vis.* 13, 215-226.

Demirel S and Johnson CA (2000). Isolation of short-wavelength sensitive mechanisms in normal and glaucomatous visual field regions. *J Glaucoma.* 9, 63-73.

Demirel S and Johnson CA (2001). Incidence and prevalence of Short-wavelength Automated Perimetry deficits in ocular hypertensive patients. *Am J Ophthalmol.* 131, 709-715.

Denler-Harles M, Wild JM, Cole MD, O'Neill EC and Crews SJ (1990). The influence of forward light scatter on the visual field indices in glaucoma. *Graefes Arch Clin Exp Ophthalmol.* 228, 326-331.

Devaney KO and Johnson HA (1980). Neuron loss in the aging visual cortex of man. *J Gerontol.* 35, 836-841.

Dichtl A, Jonas JB and Naumann GOH (2004). Retinal nerve fiber layer thickness in human eyes. *Graefes Arch Clin Exp Ophthalmol.* 237, 474-479.

Dolderer J. Vonthein, Johnson CA, Schiefer U and Hart W (2007). Scotoma mapping by semi-automat kinetic perimetry: the effects of stimulus properties and the speed of subjects responses. *Acta Ophthalmol Scan.* 94. 338-344.

Dolman CL, McCormick AQ and Drance SM (1980). Aging of the optic nerve. *Arch Ophthalmol.* 98, 2053-2058.

Doshi S and Harvey W (2003). *Investigative techniques and ocular examination.* Butterworth-Heinemann, Edingburgh, London, New York, Oxford, Philadelphia, St. Louis, Sydney, Toronto.

Drance SM, Douglas G, Schulzer M and Wijsman C (1989). The learning effect of the Frisén High-pass Resolution Perimeter. In Heijl A (eds.). *Perimetry Update* 1988/89. 199-201.

Drance SM (1974). Editorial: The optic disc and visual field in glaucoma. *Can J Ophthalmol.* 9, 389-390.

Drance SM (1975). Correlation of optic nerve and visual field defects in simple glaucoma. *Trans Ophthalmol Soc UK*: 95, 288-296.

Drance SM, Weehler C and Pattullo M (1967). The use of static perimetry in the early detection of glaucoma. *Can J Ophthalmol.* 2, 249-258.

Drasdo N and Fowler CW (1974). Non-linear projection of the retinal image in a wide-angle schematic eye. *Br J Ophthalmol.* 58, 709-714.

Duggan C, Sommer A, Auer C and Burkhard K (1985). Automated differential threshold perimetry for detecting glaucomatous visual field loss. *Am J Ophthalmol.* 100, 420-423.

Durez P, Fraselle V, Houssiau F, Thonnard JL and Nielsens MP (2006). Extended report: Validation of the abilhand questionnaire as a measure of manual ability in patients with rheumatoid arthritis. *Annals of the Rheumatic Diseases.* 66, 1098-1105.

Edgar DF, Crabb DP, Rudnicka AR, Lawrenson JG, Guttridge NM and O'Brien CJ (1999). Effects of Dipivefrin and Pilocarpine on pupil diameter, automated perimetry and LogMAR acuity. *Graefes Arch Clin Exp Ophthalmol.* 237, 117-124.

Eisner A and MacLeod DI (1980). Blue-sensitive cones do not contribute to luminance. *Opt Soc Am.* 70, 121-123.

Ennis FA and Johnson CA (2002). Are High-pass Resolution Perimetry thresholds sampling limited or optically limited? *Optom Vis Sci.* 79, 506-511.

Easterbrook M and Trope G (1989). Value of Humphrey perimetry in the detection of early Chloroquine retinopathy. *Lens Eye Toxic Res.* 6, 255-68.

Evans DW, Harris A, Chung HS, Cantor LB and Garzozi HJ (1999). Effects of long-term hypotensive therapy with nonselective beta-blocker on ocular hemodynamics in primary open-angle glaucoma. *Journal of glaucoma.* 8, 1-81

Falco-Reis F, O'Donoghue E, Buceti R, Hitchings RA and Arden GB (1990). Peripheral contrast sensitivity in glaucoma and ocular hypertension. *Br J Ophthalmol.* 74, 712-716.

Famiglietti EV (2005). 'Small-tufted' ganglion cells and two visual systems for the detection of object motion in rabbit retina. *Vis Neurosci.* 22, 509-534.

Fankhauser (1979). Problems related to the design of automatic perimeters. *Doc Ophthalmol.* 47, 89-138.

Fankhauser F, Koch P and Roulier A (1972). On automation of perimetry. *Graefe's Arch Clin Exp Ophthalmol.* 126-150.

Fankhauser F (1993). Influence of missed catch trials on the visual field in normal subjects. *Graefes Arch Clin Exp Ophthalmol.* 231, 58-59.

Fankhauser F and Bebié H (1979). Threshold fluctuation, interpolation and spatial resolution in perimetry. Dr. W. Junk Publisers. *Documenta Ophthalmologica.* Proceeding Series 19. Proceeding of the 3th International Visual Field Symposium. The Hague. 295-309.

Fankhauser F and Enoch JM (1962). The effects of blur upon perimetric thresholds. A method for determining a quantitative estimate of retinal contour. *Arch Ophthalmol.* 68, 240-251.

Fankhauser F and Haeberlin H. 1980. Dynamic range and stray light. An estimate of the falsifying effects of stray light in perimetry. *Doc Ophthalmol.* 50, 143-167.

Farber DB, Flannery JG, Lolley RN and Bok D (1985). Distribution patterns of photoreceptors, protein and cyclic nucleotides in the human retina. *Invest Ophthalmol Vis Sci.* 26, 1558-1568.

Felius J, de Jong LA, van den Berg TJ and Greve EL (1995). Functional characteristics of blue-on-yellow perimetric thresholds in glaucoma. *Invest Ophthalmol Vis Sci.* 36, 1665-1674.

Fernandez-Vidal A, Garcia Feijoo J, Gonzalez de la Rosa M and Garcia Sanchez J (2002). Initial findings with ocular hypertension. *Arch Soc Esp Oftalmol.* 77, 321-326.

Ferrera VP, Nealey TA and Maunsell JH (1994). Responses in macaque visual area V4 following inactivation of the parvocellular and magnocellular LGN pathways. *J Neurosci.* 14, 2080-2088.

Ferreras A, Pajarin A, Polo V, Larrosa J, Pablo L and Honrubia F (2007). Diagnostic ability of the Heidelberg Retina Tomograph 3 classifications Glaucoma Probability Score versus Moorfields Regression Analysis. *Ophthalmology.* 114, 1981-1987.

Ferreras A, Pablo LE, Pajarin AB, Larrosa JM, Polo V and Pueyo V (2008). Diagnostic ability of the Heidelberg Retina Tomograph 3 for glaucoma. *Am J Ophthalmol.* 145, 354-359.

Fingert M and Lewis TL (2001). *Primary care of the glaucomas 2nd Edition.* McGraw-Hill Companies, Inc.

Fitzke FW and Poinoosawmy D (1987). Peripheral displacement thresholds in normals, ocular hypertensives and glaucoma. *Doc Ophthalmol Proc Ser.* 49, 447-452.

Fitzke FW, Hitchings D, Poinoosawmy D, McNaught AI and Crabb DP (1996). Analysis of visual field progression in glaucoma. *Br J Ophthalmol.* 80, 40-48.

Flammer J and Drance SM (1983a). Effect of Acetazolamide on the differential threshold. *Arch Ophthalmol.* 101, 1378-1380.

Flammer J and Drance SM (1983b). The effect of a number of glaucoma medication on the differential light threshold. *Doc Ophthalmol. Proc Ser.* 35, 145-148.

Flammer J, Drance SM, Augustiny L and Funkhouser A (1985). Quantification of glaucomatous visual field defects with automated perimetry. *Invest Ophthalmol Vis Sci.* 26, 176-181.

Flammer J, Drance SM, Fankhauser F and Augustiny L (1984b). Differential light threshold in automated static perimetry. Factors influencing Short-term fluctuation. *Arch Ophthalmol.* 102, 876-879.

Flammer J, Drance SM and Schulzer M (1984c). Covariates of the Long-term fluctuation of the differential light threshold. *Arch Ophthalmol.* 102, 880-882.

Flammer J, Drance SM and Zulauf M (1984a). Differential light threshold. Short- and Long-term fluctuation in patients with glaucoma, normal controls and patients with suspected glaucoma. *Arch Ophthalmol.* 102, 704-706.

Flammer J, Robert Y and Gloor B (1986). Influence of Pindolol and Timolol treatment on the visual fields of glaucoma patients. *Journal of Ocular Pharmacology and Therapeutics.* 2, 305-311.

Flanagan JG, Moss ID, Wild JM, Hudson C, Prokopich L, Whitaker D and O'Neill EC (1993b). Evaluation of FASTPAC: a new strategy for threshold estimation with Humphrey Field Analyzer. *Graefes Arch Clin Exp Ophthalmol.* 231, 465-469.

Flanagan JG, Wild JM and Wood JM (1988). Stimulus configuration and the format of the normal sensitivity gradient. *Doc Ophthalmol.* 69, 371-383.

Flanagan JG, Wild JM and Trope GE (1993a) The visual field indices in primary open-angle glaucoma. *Invest Ophthalmol Vis Sci.* 34, 2266-2274.

Fogagnolo P, McNaught, Centofanti M, Rossetti L and Orzalesi (2007). The effects of intraocular pressure reduction on perimetric variability in glaucomatous eyes. *Invest Ophthalmol Vis Sci.* 48, 4557-4563.

Fogagnolo P, Tanga L, Rossetti L, Oddone F, Manni G, Orzalesi N and Centofanti M (2009). Mild learning effect of Short-wavelength Automated Perimetry using SITA program. *J Glaucoma.* Epub ahead of print.

Frisen L (1986). Vanishing optotypes. New type of acuity test letters. *Arch Ophthalmol.* 104, 1194-1198.

Frisen L (1987a). A computer-graphics visual field screener using High-pass spatial frequency resolution targets and multiple feedback devices. *Doc Ophthalmol proc Ser.* 49, 441-446.

Frisen L (1987b). High-pass resolution targets in peripheral vision. *Ophthalmology.* 94, 1104-1108.

Frisen L (1988). Acuity perimetry: estimation of neural channels. *Int Ophthalmol.* 12, 169-174.

Frisen L (1993). High-pass Resolution Perimetry. A clinical review. *Doc Ophthalmol.* 83, 1-25.

Frisen L and Nikolajeff F (1993). Properties of High-pass Resolution Perimetry targets. *Acta Ophthalmol.* 71, 320-326.

Funkhouser A, Flammer J, Fankhauser F, Hirsbrunner HP (1992a). A comparison of five methods for estimating general glaucomatous visual field depression. *Graefes Arch Clin Exp Ophthalmol.* 230, 101-106.

Funkhouser AT (1991). A new diffuse loss index for estimating general glaucomatous visual field depression. *Doc Ophthalmol.* 77, 57-72.

Funkhouser AT, Fankhauser F and Weale RA (1992b). Problems related to diffuse versus localized loss in perimetry of glaucomatous visual fields. *Graefes Arch Clin Exp Ophthalmol.* 230, 243-247.

Gaffney M (1993). Refractive errors and automated perimetry: discussion and case studies. *J Ophthalmic Nurs Technol.* 12, 167-171.

Gardiner SK and Crabb DP (2002a). Examination of different pointwise linear regression methods for determining visual field progression. *Invest Ophthalmol Vis Sci.* 43, 1400-1407.

Gardiner SK and Crabb DP (2002b). Frequency of testing for detecting visual field progression. *Br J Ophthalmol.* 86, 560-564.

Gardiner SK, Demirel S and Johnson CA (2008). Is there evidence for continued learning over multiple years in perimetry? *Optom Vis Sci.* 85, 1043-1048

Gardiner SK, Demirel S, Johnson CA and Turpin A (2006). Why are SITA-SWAP sensitivities higher than those from Full Threshold SWAP? *Acta Opthalmol Scand.* 84, 575.

Gardiner SK, Johnson CA and Cioffi GA (2005). Evaluation of the structure-function relationship in glaucoma. *Invest Ophthalmol Vis Sci.* 46, 3712-3717.

Gartner S and Henkind P (1981). Aging and degeneration of the human macula. 1. Outer nuclear layer and photoreceptors. *Br J Ophthalmol.* 65, 23-28.

Garway-Heath DF, Caprioli J, Fitzke FW and Hitchings RA (2000). Scaling the hill of vision: the physiological relationship between light sensitivity and ganglion cell numbers. *Invest Ophthalmol Vis Sci.* 41, 1774-1782.

Gherezghiher T, Hey JA and Koss MC (2009). Systemic blood pressure and intraocular pressure relationship. *Journal of Ocular Pharmacology and Therapeutics.* 4, 2009

Girkin CA, Emdadi A, Sample PA, Blumenthal EZ, Lee AC, Zangwill LM and Weinreb RN (2000). Short-wavelength Automated Perimetry and Standard perimetry in the detection of progressive optic disc cupping. *Arch Ophthalmol.* 118, 1231-1236.

Glass E, Schaumberger M and Lachenmayr BJ (1995). Simulation for FASTPAC and the standard 4-2dB Full Threshold strategy of the Humphrey Field Analyzer. *Invest Ophthalmol Vis Sci.* 36, 1847-1854.

Gloor BP and Vokt BA (1985). Long-term fluctuations versus actual field loss in glaucoma patients. *Dev Ophthalmol.* 12, 48-69.

Gloster J (1979). Quantitative studies of visual field loss and cupping of the optic disc. There relevance to the management of chronic simple glaucoma. *Trans Ophthalmol Soc UK.* 99, 82-83.

Glovinsky Y, Quigley HA and Dunkelberger GR (1991). Retinal ganglion cell loss is size dependent in experimental glaucoma. *Invest Ophthalmol Vis Sci.* 32, 484-491.

Glovinsky Y, Quigley HA and Pease ME (1993). Foveal ganglion cell loss is size dependent in experimental glaucoma. *Invest Ophthalmol Vis Sci.* 34, 395-400.

Goldberg I (1981). Optic and visual field changes in primary open angle glaucoma. *Aust J Ophthalmol.* 9, 223-229.

Goldmann H (1945). Grundlagen exakter Perimetrie. *Ophthalmologica.* 3, 187.

Goldmann H (1946). Demonstration unseres neuen Projektionskugelperimeteres samt theoretischen und klinischen Bemerkungen über Perimetrie. *Ophthalmologica.* 109, 57-70.

Goldstick BJ and Weinreb RN (1987). The effect of refractive error on automated global analysis Program G-1. *Am J Ophthalmol.* 15, 229-232.

Gonzalez de la Rosa M, Gonzalez-Hernandez M, Aguilar-Estevez J, Diaz-Aleman T and Armas-Plasencia R (2007). Diagnostic capability of Pulsar, FDT and HRT II in glaucoma suspects. *Arch Soc Esp Ophthalmol.* 82, 413-422.

Gonzalez de la Rosa M, Martinez A, Sanchez M, Mesa C, Cordoves L and Losada MJ (1996). Accuracy of the Tendency-Oriented Perimetry (TOP) in the Octopus 1-2-3 Perimeter. In Wall M and Wild JM (eds.). *Perimetry Update 1996/97.* Amsterdam/ New York: Kugler Publ., 1997. 119-223.

Gonzalez de la Rosa M, Morales J, Dannheim F, Papst E, Papst N, Seiler T, Matsumoto CYL, Mermoud A and Prünte C (2003a). Multicenter evaluation of Tendency-Oriented Perimetry (TOP) using G1 grid. *Eur J Ophthalmol.* 13, 32-41.

Gonzalez de la Rosa M and Pareja A (1997). Influence of the fatigue effect on the mean deviation measurement in perimetry. *Eur J Ophthalmol.*7, 29-34.

Gonzalez-Hernandez M, Abreu A, Sanchez M and Gonzalez de la Rosa M (2002a). Combined spatial, contrast and temporal function perimetry in early glaucoma and ocular hypertension. In Henson D and Wall M (eds.). *Perimetry Update 2002/03.* The Hague, the Netherlands: Kugler Publ., 2004. 247.

Gonzalez-Hernandez M, Fernandez-Vidal A, Garcia-Feijoo J and Gonzalez de la Rosa M (2002b). Perimetric measurement of contrast sensitivity functions. In Henson D and Wall M (eds.). *Perimetry Update 2003.* Proceedings of the 15th International Perimetric Society Meeting, Stratford-upon-Avon, England. The Hague, the Netherlands: Kugler Publ., 2002. 345-352.

Gonzalez-Hernandez M, Rios AP, Rodriguez M and Gonzalez de la Rosa M (2000a). Combined spatial resolution and contrast perimetry in normal subjects. In Wall M and Mills RP (eds.). *Perimetry Update 2000/2001.* The Hague, the Netherlands: Kugler Publ., 2001. 109-114.

Gonzalez-Hernandez M, Rios AP, Rodriguez M and Gonzalez de la Rosa M (2000b). Pulsar perimeter, introduction to multi-component perimetry. 7th International Octopus user visual field symposium, Thun, June 2000.

Gordon MO and Kass MA (1999). The Ocular Hypertension Treatment Study: design and baseline description of the participants. *Arch Ophthalmol.* 117, 573-583.

Gordon MO, Beiser JA, Brandt JD, Heuer DK, Higginbotham EJ, Johnson CA, Keltner JL, Miller JP, Parish II RK, Wilson MR, and Kass MA (2002). The Ocular Hypertension Treatment Study: baseline factors that predict the onset of primary open-angle glaucoma. *Arch Ophthalmol.*120, 714-720.

Gordon MO, Torri V, Miglior S, Beiser JA, Floriani I, Miller JP, Gao F, Adamsons I, Poli D, D'Aostino RB and Kass MA (2007). Validated prediction model for the development of primary open-angle glaucoma in individuals with ocular hypertension. *Ophthalmology.* 114, 10-19.

Gouras P (1968). Identification of cone mechanisms in Monkey ganglions cells. *J Physiol.* 199, 533-547.

Graham SL and Drance SM (1995). Interpretation of High-pass Resolution Perimetry with a Probability plot. *Graefes Arch Clin Exp Ophthalmol.* 233, 140-149.

Gramer E, Kontic D and Kriegelstein GK (1981). Computer perimetry of glaucomatous visual field defects at different stimulus sizes. Ophthalmologica. 183, 162-167.

Greenfield DS, Bagga H and Knighton RW (2003). Macular thickness changes in glaucomatous optic neuropathy detected using optical coherence tomography. *Arch Ophthalmol.* 121, 41-46.

Greenstein VC, Hood DC, Ritch R, Steinberger D and Carr RE (1989). S (blue) cone pathway vulnerability in retinitis pigmentosa, diabetes and glaucoma. *Invest Ophthalmol Vis Sci.* 30, 1732-1737.

Greve EL (1973). Single and multiple stimulus static perimetry in glaucoma; the two phases of perimetry. Thesis. *Doc Ophthalmol.* 36, 1-355.

Greve EL (1975). Static perimetry. *Ophthalmologica.* 171, 26-38.

Greve EL (1979). Peritest Docu. *Ophthalm. Proc. Series.* Ed. EL Greve Dr. W Junk Publ. The Hague. 19, 79-88.

Greve EL (1980). Peritest Docu. *Ophthalm. Proc. Series.* Ed. EL Greve Dr. W Junk Publ. The Hague. 22, 71-74.

Guthauser U, Flammer J, and Niesel P (1987). Relationship between cataract density and visual field damage. In Greve EL and Heijl A (eds.). Doc Ophthalmol Proc Ser 49. 7th International Visual Field Symposium. Dordrecht Martinus Nijhoff/ Dr. W Junk. 39-41.

Ham WT Jr, Mueller HA, Ruffolo JJ Jr, Guerry D and Guerry RK (1982). Action spectrum for retinal injury from near-ultraviolet radiation in the aphakic monkey. *Am J Ophthalmol.* 93, 299-306.

Hart WM Jr, Yablonski M, Kass MA and Becker B (1979). Multivariate analysis of the risk of glaucomatous visual field loss. *Arch Ophthalmol.* 97, 1455-1458.

Hart WM Jr, and Becker B (1982). The onset and evolution of glaucomatous visual field defects. *Ophthalmology.* 89, 268-279.

Hart WM Jr and Gordon MO (1983). Calibration of the Dicon Auto Perimeter 2000 compared with that of the Goldmann perimeter. *Am J Ophthalmol.* 96, 744-750.

Harwerth RS, Smith EL 3rd and Chandler M (1999). Progressive visual field defects from experimental glaucoma: measurements with white and colored stimuli. *Optom Vis Sci.* 76, 558-570.

Hashimoto S, Matsumoto C, Arimura E, Takada S, Okuyama S and Shimomura Y (2003). Clinical evaluation of the Octopus 101 Kinetic Program. *Nippon Ganka Kiyo.* 54, 200-204.

Heeg GP, Ponsioen TL and Jansonius NM (2003). Learning effect, normal range and test-retest variability of Frequency-Doubling perimetry as a function of age, perimetric experience and the presence or absence of glaucoma. *Ophthalmic Physiol Opt.* 23, 535-540.

Heijl A (1976). Automatic perimetry in glaucoma visual field screening. A clinical study. *Graefes Arch Clin Exp Ophthalmol.* 200, 21-37.

Heijl A (1977a). Time changes of contrast thresholds during automatic perimetry. *Acta Ophthalmol.* 55, 696-708.

Heijl A (1977b). Studies on computerized perimetry. *Acta Ophthalmol.* Suppl. 132, 1-42.

Heijl A (1985). The Humphrey Field Analyzer: Concepts and clinical results. *Doc Ophthalmol Proc Ser.* 43, 55-64.

Heijl A and Bengtsson B (1996). The effect of perimetric experience in patients with glaucoma. *Arch Ophthalmol.* 114, 19-22.

Heijl A, Bengtsson B, Hyman L, Leske MC (2009). Natural history of open-angle glaucoma. *Ophthalmology.* Epub ahead of print.

Heijl A and Drance SM (1983). Changes in differential threshold in patients with glaucoma during prolonged perimetry. *Br J Ophthalmol.* 67, 512-516.

Heijl A and Krakau CE (1975a). An automatic static perimeter, design and pilot study. *Acta Ophthalmol.* 53, 293-310.

Heijl A and Krakau CE (1975b). An automatic perimeter for glaucoma visual field screening and control: Construction and clinical cases. *Albrecht Von Graefes Arch. Klin Exp Ophthalmol.* 197, 13-23.

Heijl A and Krakau CE (1977). A note of fixation during perimetry. *Acta Ophthalmol.* 55, 854-861.

Heijl A, Lindgren A and Lindgren G (1989b). Test-retest variability in glaucomatous visual fields. *Am J Ophthalmol.* 108, 130-135.

Heijl A, Lindgren A and Lindgren G (1990a). Extended empirical statistical package for evaluation of single and multiple fields in glaucoma: Statpac 2. In Mills R and Heijl A (eds.). *Perimetry Update 1990/91.* Amsterdam: Kugler Publ. 1991. 303-315.

Heijl A, Lindgren A and Lindgren G (1990b). Reply. *Am J Ophthalmol.* 109-110.

Heijl A, Lindgren A and Olsson J (1987a). Normal variability of statistic perimetric threshold values across the central visual field. *Arch Ophthalmol.* 105, 1544-1549.

Heijl A, Lindgren G and Olsson J (1989c). The effect of perimetric experience in normal subjects. *Arch Ophthalmol.* 107, 81-86.

Heijl A, Lindgren G, Olsson J and Åsman P (1987b). A package for the statistical analysis of visual fields. *Doc Ophthalmol Proc Ser.* 49, 153-168.

Heijl A, Lindgren G, Olsson J and Åsman P (1989a). Visual field interpretation with empiric probability maps. *Arch Opthalmol.* 107, 204-208.

Hendry SH and Yoshioka T (1994). A neurochemically distinct third channel in the macaque dorsal lateral geniculate nucleus. *Science.* 264, 575-577.

Henson D and Artes PH (2002). New developments in supra-threshold perimetry. *Ophthalmic and Physiol Optics.* 22, 463.

Hermann A, Paetzold J, Vonthein R, Krapp, Rauscher S and Schiefer U (2008). Age dependent normative values for differential luminance sensitivity in automated static perimetry using the Octopus 101. *Acta Ophthalmol.* 86, 446-455.

Heron G, Adams AJ and Husted R (1988). Central visual fields for short-wavelength sensitive pathways in glaucoma and ocular hypertension. *Invest Ophthalmol Vis Sci.* 29, 64-72.

Herse PR (1992). Factors influencing normal perimetric thresholds obtained using the Humphrey Field Analyzer. *Invest Ophthalmol Vis Sci.* 33, 611-617.

Heuer DK, Anderson DR, Feuer WJ and Gressel MG (1987). The influence of refraction accuracy on automated perimetric threshold measurements. *Ophthalmology.* 94, 1550-1553.

Heuer DK, Anderson DR, Feuer WJ, Knighton RW, Gressel MG and Fantes FE (1988). The influence of simulated light scattering on automated perimetric threshold measurements. *Arch. Ophthalmol Vis Sci.* 106, 1247-1251.

Hitschings RA and Anderton S (1983). Identification of glaucomatous visual field defects from examination of monocular photographs of the optic disc. *Br J Ophthalmol.* 67, 822-825.

Hitchings RA and Spaeth GL (1977). The optic disc in glaucoma II: Correlation of the appearance of the optic disc with the visual field. *Br J Ophthalmol.* 61, 107-113.

Hodapp E, Parrish II RK and Anderson D (1993). *Clinical decisions in glaucoma.* St. Louis, Mobsy-Year Book, Inc, 11-63.

Holmin C (1982). Optic disc evaluation versus the visual field in chronic glaucoma. *Acta Ophthalmol.* 60, 275-283.

Holmin C and Krakau CE (1979). Variability of glaucomatous visual field defects in computerized perimetry. *Albrecht von Graefes Arch Klin Exp Ophthalmol.* 210, 235-250.

Hong S, Na K, Kim CY and Seong GJ (2007). Learning effect of Humphrey Matrix perimetry. *Can J Ophthalmol.* 42, 707-711.

Horani A, Frenkel S, Yahalom C, Farber MD, Ticho U and Blumenthal EZ (2002). The learning effect in visual field testing of healthy subjects using Frequency-Doubling Technology. *J Glaucoma.* 11, 511-516.

Huang CQ, Carolan J, Redline D, Taravati P, Woodward KR, Johnson CA, Wall M and Keltner JL (2008). Humphrey Matrix perimetry in optic nerve and chiasmal disorders: comparison with Humphrey SITA Standard 24-2. *Invest Ophthalmol Vis Sci.* 49, 917-923.

Hudson C and Wild JM (1992). Assessment of physiological statokinetic dissociation by automated perimetry. *Invest Ophthalmol Vis Sci.* 33, 3162-3168.

Hudson C, Wild JM and Archer-Hall J (1993). Maximizing the dynamic range of the Humphrey Field Analyzer for blue-on-yellow perimetry. *Ophthalmic Physiol Opt.* 13, 405-408.

Hudson C, Wild JM and O'Neill EC (1994). Fatigue effects during a single session of automated static threshold perimetry. *Invest Ophthalmol Vis Sci.* 35, 268-280.

Hutchings N, Hosking SL, Wild JM and Flanagan JG (2001). Long-term fluctuation in Short-wavelength Automated Perimetry in glaucoma suspects and glaucoma patients. *Invest Ophthalmol Vis Sci.* 42, 2332-2337.

Hutchings N, Wild JM, Hussey MK, Flanagan JG and Trope GE (2000). The Long-term fluctuation of the visual field in stable glaucoma. *Invest Ophthalmol Vis Sci.* 41, 3429-3436.

Hutchings N, Wild JM, Hussey MK and Trope GE (1993). The homogeneous and heterogeneous components of the Long-term fluctuation in glaucomatous field loss. *Invest Ophthalmol Vis Sci.* 34, 1263.

Hutchison PH, Artes PH and Chauhan BC (2004). Test-retest variability of the new Frequency-Doubling Technology (Humphrey Matrix) perimeter in patients with glaucoma. *Invest Ophthalmol Vis Sci.* 45: E-abstract 2138.

Iester M (2000). Frequency-Doubling Technique in patients with ocular hypertension and glaucoma. *Ophthalmology.* 107, 288-294.

Iester M, Capris P, Pandolfo A, Zingirian M and Traverso CE (2000). Learning effect, Short-term fluctuation and Long-term fluctuation in Frequency-Doubling Technique. *Am J Opthalmol.* 130, 160-164.

Iester M, Mikelberg FS, Courtight P and Drance SM (1997b). Correlation between the visual field indices and the Heidelberg Retina Tomograph parameters. *J Glaucoma.* 6, 78-82.

Iester M, Mikelberg FS, Courtrigth P, Burk RO, Caprioli J, Jonas JB, Weinreb RN and Zangwill L (2001). Interobserver variability of optic disk variables measured by confocal scanning laser tomography. *Am J Ophthalmol.* 132, 57-62.

Iester M; Mikelberg FS and Drance SM (1997a). The effect of optic disc size on diagnostic precision with the Heidelberg Retina Tomograph. *Ophthalmology.* 104, 545-548.

Iester M, Perdicchi A, Capris E, Siniscalco A, Calabria and Recupero SM (2008). Comparison between discriminant analysis models and 'Glaucoma Probability Score' for the detection of glaucomatous optic nerve head changes. *J Glaucoma*. 17, 535-540.

Iester M, Swindale NV and Mikelberg FS (1997c). Sector-based analysis of optic nerve head shape parameters and visual field indices in healthy and glaucomatous eyes. *J Glaucoma*. 6, 370-376.

Isayama T, O'Brien BJ, Ugalde I, Muller JF, Frenz A, Arora V, Tsiaras W and Berson DM (2009). Morphology of retinal ganglion cells in the ferret (Mustela puorius furo). *J Comp Neurol*. 1, 459-450.

Janknecht P and Funk J (1994). Optic nerve head analyser and Heidelberg Retina Tomograph: accuracy and reproducibility of topographic measurements in a model eye and in volunteers. *Br J Ophthalmol*. 78, 760-768.

Johnson CA (1994a). Selective vs nonselective losses in glaucoma. *J Glaucoma*. 3, 32-44.

Johnson CA, Adams AJ, Casson EJ and Brandt JD (1993a). Blue-on-yellow perimetry can predict the development of glaucomatous visual field loss. *Arch Ophthalmol*. 111, 645-650.

Johnson CA, Adams AJ, Casson EJ and Brandt JD (1993b). Progression of early glaucomatous visual field loss as detected by blue-on-yellow and standard white-on-white automated perimetry. *Arch Ophthalmol*. 111, 651-656.

Johnson CA, Adams AJ and Lewis RA (1989). Evidence for a neural basis of age-related visual field loss in normal observers. *Invest Ophthalmol Vis Sci*. 30, 2056-2064.

Johnson CA, Adams AJ, Twelker JD and Quigg JM (1988b). Age-related changes in the central visual field for short-wavelength sensitive pathways. *J Opt Soc Am A*. 5, 2131-2139.

Johnson CA, Adams CW and Lewis RA (1988a). Fatigue effects in automated perimetry. *Applied Optics*. 27, 1030-1037.

Johnson CA, Brandt JD, Khong AM and Adams AJ (1995a). Short-wavelength Automated Perimetry in low-, medium- and high-risk ocular hypertensive eyes. Initial baseline results. *Arch Ophthalmol*. 113, 70-76.

Johnson CA, Cioffi GA, Drance SM, Gasterland D, Mills RP, Ashburn F, Hnik P and Van Coevorden RE (1997). A multicenter comparison study of the Humphrey Field Analyzer I and the Humphrey Field Analyzer II. *Ophthalmol*. 104, 1910-1917.

Johnson CA, Cioffi GA and Van Buskirk EM (1999). Frequency-Doubling Technology perimetry using a 24-2 stimulus presentation pattern. *Optom Vis Sci.* 76, 571-581.

Johnson CA, Howard DL, Marshall D and Shu H (1993c). A noninvasive video-based method for measuring lens transmission properties of the human eye. *Optom Vis Sci.* 70, 944-955.

Johnson CA and Marshall D Jr (1995). Aging effects for opponent mechanisms in the central visual field. *Optom Vis Sci.* 72, 75-82.

Johnson CA and Marshall D Jr and Eng KE (1994b). Displacement threshold perimetry in glaucoma using a Macintosh computer system and a 21 inch monitor. In Mill RP and Wall M (eds.). *Perimetry Update 1994/95.* 103-110.

Johnson CA, Sample PA, Cioffi GA, Liebmann JR and Weinreb RN (2002). Structure and function evaluation (SAFE): I. criteria for glaucomatous visual field loss using Standard automated perimetry (SAP) and Short-wavelength Automated Perimetry (SWAP). *Am J Ophthalmol.* 134, 177-185.

Johnson CA, Sample PA, Zangwill LM, Vasile CG, Cioffi GA, Liebmann JR and Weinreb RN (2003). Structure and function evaluation (SAFE): II. Comparison of optic disk and visual field characteristics. *Am J Ophthalmol.* 135, 148-154.

Johnson CA and Samuels SJ (1997). Screening for glaucomatous visual field loss with Frequency-Doubling Perimetry. *Invest Ophthalm Vis Sci.* 38, 413-425.

Kamal DS, Garaway-Heath DF, Hitchings RA and Fitzke FW (2000). Use of sequential Heidelberg Retina Tomograph images to identify changes at the optic disc in ocular hypertensive patients at risk of developing glaucoma. *Br J Ophthamol.* 84, 993-998.

Kamal DS, Viswanathan AC, Garway-Heath DF, Hitchings RA, Poinoosawmy D and Bunce C (1999). Detection of optic disc change with the Heidelberg Retina Tomograph before confirmed visual field change in ocular hypertensives converting to early glaucoma. *Br J Ophthalmol.* 83, 290-294.

Kanamori A, Nakamura M, Escano MF, Seya R, Maeda H and Negi A (2003). Evaluation of the glaucomatous damage on retinal nerve fiber layer thickness measured by optical coherence tomography. *Am J Ophthalmol.* 135, 513-520.

Kass MA, Heuer DK, Higginbotham EJ, Johnson CA, Keltner JL, Miller JP, Parish II RK, Wilson MR and Gordon MO (2002). The Ocular Hypertension Treatment Study: a randomized trial determines that topical ocular hypotensive medication

delays or prevents the onset of primary open-angle glaucoma. *Arch Opthalmol.* 120, 829-830.

Katz J (2000). A comparison of the Pattern- and Total Deviation-based glaucoma change probability programs. *Invest Ophthalmol Vis Sci.* 41, 1012-1016.

Katz J, Gilbert D, Quigley HA and Sommer A (1997). Estimating progression of visual field loss in glaucoma. *Ophthalmology.* 104, 1017-1025.

Katz J, Congdon N and Friedman DS (1999). Methodological variations in estimating apparent progressive visual field loss in clinical trials of glaucoma treatment. *Arch Ophthalmol.* 117, 1137-1142.

Katz J, Quigley HA and Sommer A (1995b). Repeatability of the Glaucoma Hemifield Test in automated perimetry. *Invest Ophthalmol Vis Sci.* 36, 158-1664.

Katz J and Sommer A (1987). A longitudinal study of the age-adjusted variability of automated visual fields. *Arch Ophthalmol.* 105, 1083-1086.

Katz J and Sommer A (1988). Reliability indexes of automated perimetric tests. *Arch Ophthalmol.* 106, 1252-1254.

Katz J and Sommer A (1990). Reliability of automated perimetric tests. *Arch Ophthalmol.* 108, 777-778.

Katz J, Sommer A, Gasterland D and Anderson AJ (1991b). Comparison of analytic algorithms for detecting glaucomatous visual field loss. *Arch Ophthalmol.* 109, 1684-1689.

Katz J, Sommer A, and Witt K (1991a). Reliability of visual field results over repeated testing. *Ophthalmology.* 98, 70-75.

Katz J, Tielsch JM, Quigley HA and Sommer A (1995a). Automated perimetry detects visual field loss before manual Goldmann perimetry. *Ophthalmology.* 102, 21-26.

Katz J, Spaeth GL, Cantor LB, Poryzees EM and Steinmann WC (1989). Reversible optic disk cupping and visual field improvement in adults with glaucoma. *Am J Ophthalmol.* 107, 485-492.

Kelly DH (1981). Nonlinear visual responses to flickering sinusoidal gratings. *J Opt Soc Am.* 71, 1051-1055.

Keltner JL and Johnson CA (1995). Short-wavelength Automated Perimetry in neuro-ophthalmologic disorders. *Arch Ophthalmol.* 113, 475-481.

Keltner JL, Johnson CA and Balestrery FG (1979). Suprathreshold Static perimetry: Initial clinical trials with the Fieldmaster automated perimeter. *Arch Ophthalmol.* 97, 260-272.

Kerrigan-Baumrind LA, Quigley HA, Pease ME, Kerrigan DF and Mitchell RS (2000). Number of ganglion cells in glaucoma eyes compared with threshold visual field tests in the same persons. *Invest Ophthalmol Vis Sci.* 41, 741-748.

Kilbride PE, Hutman LP, Fishman M and Read JS (1986). Foveal cone pigment density difference in the aging human eye. *Vision Res.* 26, 321-325.

Kimura T, Kawabata K, Ohyama S, Hasegawa S, Fujimaki T and Murakami A (2005). Comparative studies in Humphrey Field Analyzer, FDT screener and Humphrey Matrix for the detection of normal tension glaucoma. *Invest Ophthalmol Vis Sci.* 46: E-Abstract 3722.

King-Smith P and Carden D (1976). Luminance and opponent-colour contributions to visual detection and adaptation and to temporal and spatial integration. *J Opt Soc Am.* 66, 709-717.

King A, Taguri A, Wadood A and Azuara-Blanco A (2002). Comparison of two fast strategies, SITA Fast and TOP, for the assessment of visual fields in glaucoma patients. *Graefes Arch Clin Exp Ophthalmol.* 240, 481-487.

Klimaschka T and Weber J (1994). Test time and efficiency of the dynamic strategy in glaucoma perimetry. In Mills RP and Wall M (eds.). *Perimetry update 1994/95.* Proceedings of the 11th International Perimetric Society Meeting, Washington DC, USA, 1994. Amsterdam/ New York: Kugler Publications, 1995. 259-261.

Koch K, McLean J, Berry M, Sterling P. Balasubramanian V and Freed MA (2004). Efficiency of information transmission by retinal ganglion cells. *Curr Biol.* 7, 1523-1530.

Koenderink JJ, Bouman MA, Bueno de Mesquita AE and Slappendel S (1978). Perimetry of contrast detection thresholds of moving spatial sine wave patterns. I. The near peripheral visual field (eccentricity 0 degrees-8 degrees). *J Opt Soc Am.* 68, 845-849.

Koenderink JJ and Doorn AJ (1978). Visual detection of spatial contrast; influence of location in the visual field, target extent and illuminance level. *Biological Cybernetics.* 30, 157-167.

Kono Y, Sample PA, Emdadi A and Weinreb RN (2000). Comparative study between pointwise and ranked threshold distribution analyses of change in serial fields for Short-wavelength Automated Perimetry. *J Glaucoma.* 9, 419-427.

Kooijman AC (1983). Light distribution on the retina of a wide-angle theoretical eye. *JOSA*. 73, 1544-1550.

Korth M, Horn F, Stork B and Jonas JB (1989). Spatial and spatialtemporal contrast sensitivity of normal and glaucomas eyes. *Graefes Arch Clin Exp Ophthalmol.* 227, 428-435.

Koskela PU, Airaksinen PJ and Tuulonen A (1990). The effect of jogging on visual field indices. *Acta Ophthalmol.* 68, 91-93.

Kratochvilova P (2002). Computer perimetry- rapid TOP (Tendency-Oriented Perimetry) and normal threshold methods in clinical practice- comparison of results. *Cesk Slov Oftalmol.* 58, 158-193.

Kruse FE, Burk RO, Volcker HE, Zinser G and Harbarth U (1989). Reproducibility of topographic measurements of the optic nerve head with laser tomographic scanning. *Ophthalmology.* 96, 1320-1324.

Kulze JE, Stewart WC and Sutherland SE (1990). Factors associated with a learning effect in glaucoma patients using automated perimetry. *Acta Ophthalmol.* 68, 681-686.

Kwon YH, Park HJ, Jap A, Ugurlu S and Caprioli J (1998). Test-retest variability of blue-on-yellow perimetry is greater than white-on-white perimetry in normal subjects. *Am J Ophthalmol.* 126, 29-36.

Lachenmayr BJ, Drance SM, Chauhan BC, House PH and Lalani S (1991b). Diffuse and localized glaucomatous field loss in Light-sense, Flicker and Resolution perimetry. *Graefes Arch Clin Exp Ophthalmol.* 229, 267-273.

Lachenmayr BJ, Drance SM, Douglas GR and Mikelberg FS (1991a). Light-sense, Flicker and Resolution perimetry in glaucoma: a comparative study. *Graefes Arch Clin Exp Ophthalmol.* 229, 246-251.

Lachenmayr BJ and Drance (1992b). Diffuse field loss and central visual function in glaucoma. *Ger J Ophthalmol.* 1, 67-73.

Lachenmayr BJ, Drance SM and Airaksinen PJ (1992c). Diffuse field loss and diffuse retinal nerve fiber loss in glaucoma. *Ger J Ophthalmol.* 1, 22-25.

Lachenmayr BJ and Gleissner M (1992a). Flicker perimetry resists retinal image degradation. *Invest Ophthalmol Vis Sci.* 33, 3539-3542.

Lachenmayr BJ (1994). The role of temporal threshold criteria in psychophysical testing in glaucoma. *Curr Opin Ophthalmol.* 5, 58-63.

Lachkar Y, Barrault O, Lefrancois A and Demailly P (1998). Rapid Tendency-Oriented Perimeter (TOP) with the Octopus visual field analyzer. *J Fr Ophthalmol.* 21, 180-184.

Langerhorst CT, Van den Berg TJ, Veldman E and Greve EL (1987). Population study of global and local fatigue with prolonged threshold testing in automated perimetry. In Greve EL and Heijl A (eds.). *Perimetry Update.* 7th International Visual Field Symposium. Dordrecht Mirtinus Nijhoff/ Dr. W Junk. 1987. 657-662.

Latham K, Whitaker D, Wild JM and Elliot DB (1993). Magnification perimetry. *Invest Ophthalmol Vis Sci.* 34, 1691-1701.

Lee BB and Sun H (2003). The physiological origin of chromatic response components in signals of the magnocellular pathway of the macaque. *Invest Ophthalmol Vis Sci.* 44, E-Abstract 3250.

Leibowitz HW, Johnson CA and Isabelle E (1972). Peripheral motion detection and refractive error. *Science.* 177, 1207-1208.

Lennie P (1980). Parallel visual pathways: a review. *Vision Res.* 20, 561-594.

Leske MC, Heijl A, Hyman L and Bengtsson B (1999). Early Manifest Glaucoma Trial: design and baseline data. *Ophthalmology.* 106, 2144-2153.

Leske MC, Heijl A, Hussein M, Bengtsson B, Hyman L and Komaroff E (2003). Factors for glaucoma progression and the effect of treatment: the Early Manifest Glaucoma Trial. Arch *Ophthalmol.* 121, 48-56.

Lewis RA, Hayreh SS and Phelps CD (1983). Optic disk and visual field correlations in primary open-angle and low-tension glaucoma. *Am J Ophthalmol.* 96, 148-152.

Lewis RA, Johnson CA, Keltner JL and Labermeier PK (1986). Variability of quantitative automated perimetry in normal observers. *Ophthalmology.* 93, 878-881.

Lichter PR, Musch DC, Gillespie BW, Guire KE, Janz NK, Wren PA, and Mills RP (2001). Interim clinical outcomes in the Collaborative Initial Glaucoma Treatment Study comparing initial treatment randomized to medications or surgery. *Ophthalmology.* 108, 1943-1953.

Linberg KA, Lewis GP, Shaaw C, Rex TS and Fisher SK (2001). Distribution of S- and M-cones in normal and experimentally detached cat retina. *J Comp Neurol.* 430, 343-356.

Lindenmuth KA, Skuta GL, Rabbani R and Musch DC (1989). Effects of pupillary constriction on automated perimetry in normal eyes. *Ophthalmology.* 96, 1298-1301.

Lindenmuth KA, Skuta GL Rabbani R, Musch DC and Bergstrom TJ (1990). Effects of pupillary dilatation on Automated perimetry in normal patients. *Ophthalmology.* 97, 367-370.

Litwak A (2001). *Glaucoma Handbook.* Butterworth-Heinemann, Boston. 138.

Livingstone MS and Hubel DH (1987). Psychophysical evidence for separate channels for the perception of form, color, movement and depth. *J Neurosci.* 7, 3416-3468.

Livingstone MS and Hubel DH (1988). Segregation of form, color, movement and depth: anatomy, physiology and perception. *Science.* 240, 740-749.

Luo XG, Chiu K, Lau FH, Lee VE, Yung KK and So KF (2009). The selective vulnerability of retinal ganglion cells in rat chronic ocular hypertension model at early phase. *Cell Mol Neurobiol.* Epub ahead of print.

Luo XG Heidinger V, Picaud S, Lambrou G, Dreyfus H, Sahel j and Hicks D (2001). Selective excitotoxic cells in vitro. *Invest Ophthalmol Vis Sci.* 42, 1096-1106.

Lutze M and Bresnick GH (1991). Lenses of diabetic patients 'yellow' at an accelerated rate similar to older normals. *Invest Ophthalmol Vis Sci.* 32, 194-199.

Maddess T, Goldberg I, Dobonson J, Wine S and James AC (1995). Clinical trials of the frequency illusion as an indicator of glaucoma (ARVO abstracts). *Invest Ophthalmol Vis Sci.* 36 (suppl), 335.

Maddess T and Henry GH (1992). Performance of nonlinear visual units in ocular hypertension and glaucoma. *Clin Vis Sci.* 7, 371-383.

Maeda H, Nakamura M and Negi A (2001). Selective reduction of the S-cone component of the electroretinogram in Posner-Schlossman syndrome. *Eye.* 15, 163-167.

Madea H, Nakaura M and Negi A (2000). New perimetric threshold test algorithm with Dynamic strategy and Tendency-Oriented Perimetry (TOP) in glaucomatous eyes. *Eye.* 14, 747-751.

Maguire C (1971). Ametropia in the visual field. *Trans Ophthalmol Soc UK.* 91, 663-678.

Mardin CY, Horn FK, Jonas JB and Budde WM (1999). Perimetric glaucoma diagnosis by confocal scanning laser tomography of the optic disc. *Br J Ophthalmol.* 83, 299-304.

Marraffa M, Marchini G, Albertini R and Bonomi L (1989). Comparison of different screening methods for the detection of visual field defects in early glaucoma. *Int Ophthalmol.* 13, 43-45.

Martin PR and Grunert U (1999). Analysis of the short wavelength-sensitive (blue) cone mosaic in the primate retina: comparison of New World and Old World monkeys. *J Comp Neurol.* 406, 1-14.

Martin PR, White AJ, Goodchild AK, Wilder HD and Sefton AE (1997). Evidence that blue-on cells are part of the third geniculocortical pathway in primates. *Eur J Neurosci.* 9, 1536-1541.

Martin XD and Rabineau P (1989). Vasoconstrictive effect of topical Timolol on human retinal arteries. *Graefe's Archive for Clinical and Experimental Ophthalmology.* 227, 526-530.

Martinez A, Pareja A, Mantolan C, Sanchez M, Cordoves L and Gonzalez de la Rosa M (1996). Results of the Tendency-Oriented Perimetry (TOP) in normal population. *Vision Res Sup Jermov.* 36, 153.

Martinez GA, Sample PA and Weinreb RN (1995). Comparison of High-pass Resolution Perimetry and Standard automated perimetry in glaucoma. *Am J Ophthalmol.* 119, 195-201.

McKendrick AM (2005). Recent developments in perimetry: test stimuli and procedures. *Clin Exp Optom.* 88.2, 73-80.

McKendrick AM and Turpin A (2005). Advantages of terminating Zippy Estimation by Sequential Testing (ZEST) with dynamic criteria for white-on-white perimetry. *Optom Vis Sci.* 82, 981-987.

McMillan TA, Stewart WC and Hunt HH (1992). Association of reliability with reproducibility of the glaucomatous visual field. *Acta Ophthalmol.* 70, 665-670.

McNaught AI, Crabb DP, Fitzke FW and Hitchings RA (1995). Modelling series of visual fields to detect progression in normal–tension glaucoma. *Graefes Arch Clin Exp Ophthalmol.* 233, 750-755.

Méndez CH, Feijoo JG, Vidal-Fernandez A, Gonzalez de la Rosa M, Martinez de la Casa J, Saenz-Frances F and Garcia-Sanchez J (2004). Laser polarimetry and white/ white, Pulsar, FDT and Flicker perimetries in ocular hypertension. *Publication on Pulsar.* International Perimetric Society Meeting Barcelona 2004.

Merigan WH and Maunsell JH (1993). How parallel are the primate visual pathway? *Annu Rev Neurosci.* 16, 369-402.

Meyer JH and Funk J (1995). High-pass Resolution Perimetry and Light-sense perimetry in open-angle glaucoma. *Ger J Ophthalmol.* 4, 222-227.

Miglior S, Brigatti L, Lonati C, Rossetti L, Pierrottet C and Orzalesi N (1996). Correlation between the progression of the optic disc and visual field changes in glaucoma. *Curr Eye Res.* 15, 145-149.

Mikelberg FS and Drance SM (1984). The mode of progression of visual field defects in glaucoma. *Am J Ophthalmol.* 98, 443-445.

Mikelberg FS, Drance SM, Schulzer MD and Wijsman K (1987). The effect of miosis on visual field indices. In Greve EL and Heijl A (eds.). 7th International Visual Field Symposium. *Doc Ophthalmol Proc Ser 49.* Dordrecht: Martinus Nijhoff/ Dr. W Junk. 645-649.

Mikelberg FS, Parfitt C, Swindale N, Graham SL, Drance SM and RG (1995). Ability of the Heidelberg Retina Tomograph to detect early glaucomatous visual field loss. *J Glaucoma.* 4, 242-247.

Mikelberg FS, Wijsman K and Schulzer M (1993). Reproducibility of topographic parameters obtained with the Heidelberg Retina Tomograph. *J Glaucoma.* 2, 101-103.

Mills RP (1984). A comparison of Goldmann, Fieldmaster 200, and Dicon AP2000 perimeters in a screening mode. *Ophthalmology.* 91, 347-354.

Mistlberger A (2002). Assessment of the optic disc anatomy and nerve fiber layer thickness in ocular hypertensive subjects with normal Short-wavelength Automated Perimetry. *Ophthalmology.* 109, 1362-1366.

Mok KH, Lee VW and So KF (2003). Retinal nerve fiber layer measurement by optical coherence tomography in glaucoma suspects with Short-wavelength Automated Perimetry abnormalities. *J Glaucoma.* 12, 45-49.

de Monasterio FM, Schein SJ and McCrane EP (1981). Staining of blue-sensitive cones of the macaque retina by a fluorescent dye. *Science.* 213, 1278-1281.

de Monasterio FM, McCrane EP, Newlander JK and Schein SJ (1985). Density profile of bleu-sensitive cones along the horizontal meridian of macaque retina. *Invest Ophthalmol Vis Sci. 26*, 289-302.

Monhart M, Buerki E, Bebié H and Palmowski-Wolfe A (2006). Calculation of the abnormal response area as an indicator of visual field changes. *Invest Ophthalmol Vis Sci.* 47: E-Abstract 3982.

Monjé M and Offermann R (1955). Über die Empfindlichkeit der Netzhaut bei Refraktionsanomalien. *Graefes Arch Clin Exp Ophthalmol.* 155, 63-78.

Morales J, Weitzman ML and Gonzalez de la Rosa M (2000). Comparison between Tendency-Oriented Perimetry (TOP) and Octopus Threshold perimetry. *Ophthalmology.* 107, 134-142.

Morgan JE, Sheen NJL, North RV, Goyal R, Morgan S, Ansari E and Wild JM (2005). Discrimination of glaucomatous optic neuropathy by digital stereoscopicopic analysis. *Ophthalmology.* 112, 855-862.

Morgan RK, Feuer WJ and Anderson DR (1991). Statpac 2 Glaucoma Change Probability. *Arch Ophthalmol.* 109, 1690-1692.

Moss ID and Wild JM (1994). The influence of induced forward light scatter on the normal blue-on-yellow perimetric profile. *Graefes Arch Clin Exp Ophthalmol.* 232, 409-414.

Moss ID, Wild JM and Whitaker DJ (1995). The influence of age-related cataract on blue-on-yellow perimetry. *Invest Ophthalmol Vis Sci.* 36, 764-773.

Motolko MA and Phelps CD (1984). Contrast sensitivity in asymmetric glaucoma. *Int Ophthalmol.* 7, 45-59.

Musch DC, Lichter PR, Guire KE and Standardi CL (1999). The Collaborative Initial Glaucoma Treatment Study: Study design, methods, and baseline characteristics of enrolled patients. *Ophthalmology.* 106, 653-662.

Newkirk MR, Gardiner SK, Demirel S and Johnson CA (2006). Assessment of false positives with the Humphrey Field Analyzer II perimeter with the SITA algorithm. *Invest Ophthalmol Vis Sci.* 47, 4632-4637.

Newsome WT and Pare EB (1998). A selective impairment of motion perception following lesions of the middle temporal visual area (MT). *J Neurosci.* 8 , 2201-2211.

Nordmann JP, Brion F, Hamard Pand Mouton-Chopin D (1998). Evaluation of the Humphrey perimetry programs SITA Standard and SITA Fast in normal probands and patients with glaucoma. *J Fr Ophthalmol* 21, 549-554.

van Norren D and van Meel GJ (1985). Density of human cone photopigments as function of age. *Invest Ophthalmol Vis Sci.* 26, 1014-1016.

Nouri-Mahdavi K, Brigatti L, Weitzman M and Caprioli J (1997). Comparison of methods to detect visual field progression in glaucoma. *Ophthalmology.* 104, 1228-1236.

Nowak DA, Grefkes C, Dafotakis M, Eichhoff S, Küst J, Karbe H, Gereon R and Fink MD (2008). Effect of low-frequency repetitive transcranial magnetic stimulation of the contralesional primary motor cortex on movement kinematics and neural activity in subcortical stroke. *Arch Neurol.* 65(6), 741-747.

Nowak DA, Grefkes C, Dafotakis M, Küst J, Karbe H and Fink GR (2007). Dexterity is impaired at both hands following unilateral subcortical middle cerebral artery stroke. *Eur J Neurosci.* 25, 3173-3184.

Nowomiejska K, Paetzold J, Krapp E, Rejdak R, Zagorski Z and Schiefer U (2004b). Comparison of SKP (semi-automated kinetic perimetry) and SASP (suprathreshold automated static perimetry) techniques in patients with advanced glaucoma. *Klin Oczna.* 106, 231-233.

Nowomiejska K, Paetzold J, Zagorski Z and Schiefer U (2004c). Recent developments in kinetic perimetry. *Klin Oczna.* 106, 798-801.

Nowomiejska K, Rejdak R, Zarnowski, Krapp E, Paetzold J, Schiefer U and Zagorski Z (2004a). Quantification of isopters using semiautomated kinetic perimetry (SKP) in glaucoma patients with advanced retinal nerve fiber layer (RNFL) loss. *Klin Oczna.* 106, 228-230.

Nowomiejska K, Vonthein R, Krapp E, Rauscher S, Hermann A, Paetzold J and Schiefer U (2003). High resolution assessment of kinetic isopters on the stimulus size and luminance surface. *Invest Ophthalmol Vis Sci.* 44: E-Abstract 1955.

Nowomiejska K, Vonthein R, Paetzold J, Zagorski Z, Kardon R and Schiefer U (2005). Comparison between semiautomated kinetic perimetry and conventional Goldmann manual kinetic perimetry in advanced field loss. *Ophthalmology.* 112, 1343-1354.

O'Brien C, Poinoosawmy D, Wu J and Hitschings R (1994). Evaluation of the Humphrey FASTPAC Threshold program in glaucoma. *Br J Ophthalmol.* 78, 516-519.

O'Brien and Schwartz (1992). Point by point linear regression analysis of automated visual fields in primary open angle glaucoma. In Mills RP (eds.). *Perimetry Update 1992/93*. Proceeding of the 10th International Perimetric Society Meeting, Kyoto, Japan 1992. 149-152.

Oddone F, Centofanti M, Rossetti L, Iester M, Fogagnolo P, Capris E and Manni G (2008). Exploring the Heidelberg Retinal Tomograph 3 diagnostic accuracy across disc sizes and glaucoma stages: a multicenter study. *Ophthalmology*. 115, 1358-1365.

Ogle KN (1960). Blurring of the retinal image and contrast thresholds in the fovea. *J Opt Soc Am*. 50, 307-315.

Ogle KN (1961a). Foveal contrast thresholds with blurring of the retinal image and increasing size of test stimulus. *J Opt Soc Am* 51, 862-869.

Ogle KN (1961b). Peripheral contrast thresholds and blurring of the retinal image for a point light source. *J Opt Soc Am*. 51, 1265-1268.

Olsson J (1991). *Statistics in perimetry*. Doctoral thesis.

Olsson J, Åsman P and Heijl A (1997b). A perimetric learner's index. *Acta Ophthalmol Scand*. 75, 665-668.

Olsson J, Bengtsson B and Heijl A (1998). Frequency of seeing curve in Short-wavelength Automated Perimetry (SWAP). *Invest Ophthalmol Vis Sci*. 39, S 494. Abstract nr 2268.

Olsson J, Bengtsson B, Heijl A and Rootzen H (1997a). An improved method to estimate frequency of false positive answers in computerized perimetry. *Acta Ophthalmol Scand*. 75, 181-183.

Olsson J, Bengtsson B and Rootzen H (1994). Improving estimation of false positive and false negative responses in computerized perimetry. In Mills RP and Wall M (eds.). *Perimetry Update 1994/95*. Proceeding of the 11th International Perimetric Society Meeting, Washington DC, 1994. 219.

Olsson J, Bengtsson B and Rootzen H (1993). Frequency of seeing in computerised perimetry. In Mills PR (eds.). *Perimetry Update 1993*. Amsterdam/ New York: Kugler. 551-556.

Olsson J and Rootzen H (1994). An image model for quantal response analysis in perimetry. *Scandinavian journal of statistics*. 21, 375-387.

Olsson J, Rootzen H and Heijl A (1988). Maximum likelihood estimation of the frequency of false positive and false negative answers from the up-and-down staircases of cumputerized threshold perimetry. In Heijl A (eds.). *Perimetry Update 1988/89.* Proceeding of the 13th International Perimetric Society Meeting, Vancouver, 1988. 245.

Park HJ and Youn DH (1994). Quantitative analysis of changes of automated perimetric thresholds after papillary dilatation and induced myopia in normal subjects. *Korean J Ophthalmol.* 8, 53-60.

Parrish RK, Schiffman J and Anderson DR (1984). Static and kinetic visual field testing. Reproducibility in normal volunteers. *Arch Ophthalmol.* 102, 1497-1502.

Patel A, Wollstein G, Ishikawa H and Schuman JS (2007). Comparison of visual field defects using Matrix perimetry and standard achromatic perimetry. *Ophthalmology.* 114, 480-487.

Pieroth L, Schuman JS, Hertzmark E, Hee MR, Wilkins JR, Coker J, Mattox C, Pedut-Kloizman R, Puliafito CA, Fujimoto JG and Swanson E (1999). Evaluation of focal defects of the nerve fiber layer using optical coherence tomography. *Ophthalmology.* 106, 570-579.

Pierre-Filho PD, Gomes PR, Pierre ET and Pierre LM (2009). Learning effect in visual field testing of healthy subjects using Humphrey Matrix Frequency-Doubling Technology perimetry. *Eye.* Epub ahead of print.

Poli A, Strouthidis NG, HO TA and Garway-Heath DF (2008). Analysis of HRT images: comparison of References Plane. *Invest Ophthalmol Vis Sci.* 49, 3970-3975.

Polo V, Abecia E, Pablo LE, Pinilla I, Larrosa JM and Honrubia FM (1998). Short-wavelength Automated Perimetry and retinal nerve fiber layer evaluation in suspected case of glaucoma. *Arch Ophthalmol.* 116, 1295-1298.

Polo V, Abecia E, Pablo LE, Pinilla I, Larrosa JM and Honrubia FM (2001). Functional and structural measurements in a multifactorial glaucoma risk model. *Acta Ophthalmol Scand.* 79, 10-14.

Portney GL and Krohn MA (1978). Automated perimetry: Background, instruments and methods. *Surv Ophthalmol.* 22, 271-278.

Quigley HA, Dunkelberger GR and Green WR (1988). Chronic human glaucoma causing selectively greater loss of large optic nerve fibres. *Ophthalmology.* 95, 357-363.

Quigley HA, Sanchez RM, Dunkelberger GR, L'Hernault NL and Baginski TA (1987). Chronic glaucoma selectively damages large optic nerve fibres. *Invest Ophthalmol Vis Sci.* 28, 913-920.

Racette L, Medeiros FA, Zangwill LM, Ng D, Weinreb RN and Sample PA (2008). Diagnostic accuracy of the Matrix 24-2 and original N-30 Frequency-Doubling Technology tests compared with Standard automated perimetry. *Invest Ophthalmol Vis Sci.* 49, 954-960.

Read RM and Spaeth GL (1974). The practical clinical appraisal of the optic disc in glaucoma: the natural history of cup progression and some specific disc-field correlations. *Trans Am Acad Ophthalmol Otolaryngol.* 78, 255-274.

Regan D and Beverley KI (1983). Visual fields described by contrast sensitivity, by acuity and by relative sensitivity to different orientations. *Invest Ophthalmol Vis Sci.* 24, 754-759.

Reitner A, Tittl M, Ergun E and Baradaran-Dilmaghani R (1996). The efficient use of perimetry for neuro-ophthalmic diagnosis. *Br J Ophthalmol.* 80, 903-905.

Robson JG (1966). Spatial and temporal contrast-sensitivity functions of the visual system. *J Opt Soc Am.* 56, 1141-1149.

Rohrschneider K, Burk RO, Kruse FE and Volcker HE (1994). Reproducibility of the optic nerve head topography with a new laser tomographic scanning device. *Ophthalmology.* 101, 1044-1049.

Ross JE, Bron, AJ and Clarke DD (1984). Contrast sensitivity and visual disability in chronic simple glaucoma. *Br J Ophthalmol.* 68, 821-827.

Rossetti L, Fogagnolo P, Miglior S, Centofanti M, Vetrugno M and Orzalesi N (2006). Learning effect of Short-wavelength Automated Perimetry in patients with ocular hypertension. *J Glaucoma.* 15, 399-404.

Rossi A, Montanari P, Mosca M, Luccarelli S and Ratiglia R (2005). Comparison of optic nerve head measurements obtained by HRT II and functional parameters. *Invest Ophthalmol Vis Sci.* 6, E-Abstract-2540.

Rovamo J, Virsu V and Näsänen R (1978). Cortical magnification factor predicts the photopic contrast sensitivity of peripheral vision. *Nature.* 271, 54-56.

Rutishauser C, Flammer J and Haas A (1989). The distribution of normal values in automated perimetry. *Graefes Arch Clin Exp Ophthalmol.* 227, 513-517.

Sagdullaev BT and McCall MA (2005). Stimulus size and intensity alter fundamental receptive-field properties of mouse retinal ganglion cells in vivo. *Vis neurosci.* 22, 649-659.

Sakai T, Matsushima M, Shikishima K and Kitahara K (2007). Comparison of Standard automated perimetry with Matrix Frequency-Doubling Technology in patients with resolved optic neuritis. *Ophthalmology.* 114, 949-956.

Sample PA, Ahn DS, Lee PC and Weinreb RN (1992a). High-pass Resolution Perimetry in eyes with ocular hypertension and primary open-angle glaucoma. *Am J Ophthalmol.* 113, 309-316.

Sample PA, Cook JN and Weinreb RN (1993a). Variability and sensitivity of short-wavelength colour visual fields in normal and glaucoma eyes. In: *Non-invasive assessment of the visual system.* Tech Digest Ser., 292-295.

Sample PA, Taylor JDN, Martinez GA, Lusky M and Weinreb RN (1993b). Short wavelength colour visual fields in glaucoma suspects at risk. *Am J Ophthalmol.* 115: 225-223.

Sample PA, Esterson FD and Weinreb RN (1989). A practical method for obtaining an index of lens density with an automated perimeter. *Invest Ophthalmol Vis Sci.* 30, 786-787.

Sample PA, Esterson FD, Weinreb RN and Boynton RM (1988). The aging lens: in vivo assessment of light absorption in 84 human eyes. *Invest Ophthalmol Vis Sci.* 29, 1306-1311.

Sample PA, Irak I, Martinez GA and Yamagishi (1997). Asymetries in the normal short-wavelength visual field: implications for Short-wavelength Automated Perimetry. *Am J Ophthalmol.* 124, 46-52.

Sample PA, Johnson CA, Haegerstrom-Portnoy G and Adams AJ (1996). Optimum parameters for Short-wavelength Automated Perimetry. *J Glaucoma.* 5, 375-383.

Sample PA and Weinreb RN (1990). Color perimetry for assessment of primary open-angle glaucoma. *Invest Ophthalmol Vis Sci.* 31, 1869-1875.

Sample PA and Weinreb RN (1992b). Progressive color visual field loss in glaucoma. *Invest Ophthalmol Vis Sci.* 33, 2068-2071.

Sanabria O, Feuer WJ and Anderson DR (1991). Pseudo-loss of fixation in automated perimetry. *Ophthalmology.* 98, 76-78.

Sanchez-Galeana CA, Bowd C, Zangwill LM, Sample PA and Weinreb RN (2004). Short-wavelength Automated Perimetry results are correlated with optical coherence tomography retinal nerve fiber layer thickness measurements in glaucomatous eyes. *Ophthalmology*. 111, 1866-1872.

Scheibel ME, Lindsay RD, Tomiyasu U and Scheibel AB (1975). Progressive dendritic changes in aging human cortex. *Exp Neurol*. 47, 392-403.

Scheuerle AF, Schmidt E and Burk ROW (2001). Polar contour-line of optic disc border reaches Mean Retina Height (MRH) in normal eyes in laser scanning tomography using the Heidelberg Retina Tomograph (HRT). *Invest Ophthalmol Vis Sci*. 42, 135.

Scheuerle AF and Schmidt E (2004). *Atlas of laser scanning Ophthalmoscopy*. Springer-Verlag Berlin, Heidelberg, New York.

Schiefer U, Nowomiejska K, Krapp E, Patzold J and Johnson CA (2006). K-Train a computer-based interactive training program with an incorporated certification system for practicing kinetic perimetry: evaluation of acceptance and success rate. *Graefes Arch Clin Exp Ophthalmol*. 244, 1300-1309.

Schiefer U, Nowomiejska K, Schiller J, Krapp E, Vonthein R and Paetzold J (2004). An interactive, computer-based training software for practicing kinetic perimetry in virtual patients. *Invest Ophthalmol Vis Sci*. 45: E-Abstract 233.

Schiefer U, Schiller J, Paetzold J, Dieterich TJ, Vonthein R and Besch D (2001). Evaluation of advanced visual field defects by computer assisted kinetic perimetry. *Klin Monatsbl Augenheilkd*. DOI: 10. 1055/s-2001-11255, 13-20.

Schiefer U, Pascual JP, Edmunds B, Feudner E, Hoffmann EM, Johnson CA, Lagrèze WA, Pfeiffer N, Sample PA, Staubach F, Weleber RG, Vonthein R, Krapp E and Paetzold J (2009). Comparison of the new perimetric GATE strategy with conventional Full Threshold and SITA Standard strategies. *Invest Ophthalmol Vis Sci*. 50, 488-494.

Schimiti RB, Arcieri ES, Avelino RR, Matsuo T and Costa VP (2006). Full Threshold vs. SITA in glaucomatous patients undergoing automated perimetry for the first time. *Arq Bras Oftalmol*. 69, 145-150.

Schmidt T (1955). Perimetrie relativer Skotome. *Ophthalmologica*. 129, 303-315.

van der Schoot J, Reus NJ, Colen TP and Lemij HG (2009). The ability of Short-wavelength Automated Perimetry to predict conversion to glaucoma. *J Glaucoma*. Epub ahead of print.

Schuman JS, Hee MR, Puliafito CA, Wong C, Pedult-Kloizman T, Lin TP, Hertzmark E, Izatt JA, Swanson EA and Fujimoto JG (1995). Quantification of nerve fiber layer thickness in normal and glaucomatous eyes using optical coherence tomography. *Arch Ophthalmol* 113, 586-596.

Searle AE, Wild JM, Shaw DE and O'Neill, EC (1991). Time-related variation in normal automated static perimetry. Ophthalmology. 98, 701-707.

Seitz AR, Nanez JE Sr, Holloway SR and Watanabe T (2006). Perceptual learning of motion leads to faster flicker perception. *PLoS ONE.* 1, e28.

Sekhar GC, Naduvilath TJ, Lakkai M, Jaykumar AJ, Pandi GT, Mandal AK and Honavar SG (2000). Sensitivity of Swedish Interactive Algorithm in Humphrey visual field testing. *Ophthalmology.* 107, 1303-1308.

Shabana N, Cornilleau Pérès V, Carkeet A and Chew PT (2003). Motion perception in glaucoma patients: a review. *Surv Ophthalmol.* 48, 92-106.

Shah NN, Bowd C, Medeiros FA, Weinreb RN, Sample PA, Hoffmann EM and Zangwill LM (2006). Combining structural and functional testing for detection of glaucoma. *Ophthalmology.* 113, 1593-1602.

Shapley R (1990). Visual sensitivity and parallel retinocortical channels. *Annu Rev. Psychol.* 41, 635-658.

Shapley R and Perry VH (1986). Cat and monkey retinal ganglion cells and their visual functional roles. *TINS.* Elsevier Science Publihers B.V. Amsterdam 0378-591286502.00.

Sharma AK, Goldberg I, Graham SL and Mohsin M (2000). Comparison of the Humphrey Swedish Thresholding Algorithm (SITA) and Full Threshold strategies. *J Glaucoma.* 9, 20-27.

Shirakashi M, Abe H, Sawagucchi S and Funaki S (1997). Measurement of thickness of retinal nerve fibre layer by scanning laser polarimetry and High-pass Resolution Perimetry in patients with primary open-angle or normal-tension glaucoma. *Acta Opthalmol Scand.* 75, 641-644.

Shirakashi M, Funaki S, Funaki H, Yaoeda K and Abe H (1999). Measurement of retinal nerve fibre layer by scanner laser polarimetry and High-pass Resolution Perimetry in normal tension glaucoma with relatively high or low intraocular pressure. *Br J Ophthalmol.* 83, 353-357.

Shutt HK, Boyd TA and Salter AB (1967). The relationship of visual fields, optic disc appearances and age in non-glaucomatous and glaucomatous eyes. *Can J Ophthalmol.* 2, 83-90.

Siatkowski RM, Lam BL, Anderson DR, Feuer WJ and Halikman AM (1996). Automated suprathreshold static perimetry screening for detecting neuro-ophthalmologic disease. *Ophthalmology.* 103, 907-917.

Siik S, Airaksinen PJ, Tuulonen A, Alanko HI and Nieminen H (1991). Lens autofluorescence in healthy individuals. *Acta Ophthalmol.* 69, 187-192.

Soliman MA, de Jong LA, Ismaeil AA, van den Berg T and de Smet M (2002). Standard achromatic perimetry, Short-wavelength Automated Perimetry in glaucoma suspects and glaucoma patients. *Ophthalmology.* 109, 444-454.

Spaeth GL (1967). Potassium, acetazolmide, and intraocular pressure. *Arch Ophthalmol* 78; 578-582.

Spaeth GL (1985). The effect of change in intraocular pressure on the natural history of glaucoma: lowering intraocular pressure in glaucoma can result in improvement of visual fields. *Trans Ophthalmol Soc UK.* 104, 256-262.

Spahr J and Fankhauser F (1974a). On automation of perimetry. Problems and solutions. *L' Année therapeutique et Clinique en Ophthalmologie.* 25, 337-347.

Spahr J and Fankhauser F (1974b). OCTOPUS-an automated perimeter. *Rev Sensory Disability.* 18, 5-8.

Sponsel WE, Arango S, Trigo Y and Mensah J (1998). Clinical classification of glaucomatous visual field loss by Frequency-Doubling perimetry. *Am J Ophthalmol.* 125, 830-836.

Spry PG and Johnson CA (2002). Identification of progressive glaucomatous visual field loss. *Survey of Ophthalmology.* 47, 158-173.

Spry PG, Johnson CA, Bates AB, Turpin A and Chauhan BC (2002). Spatial and temporal processing of threshold data for detection of progressive glaucomatous visual field loss. *Arch Opthalmol.* 120, 173-180.

Spry PG, Hussin HM and Sparrow JM (2005b). Clinical evaluation of Frequency-Doubling Technology perimetry using the Humphrey Matrix 24-2 Threshold strategy. *Br J Ophthalmol.* 89, 1031-1035.

Spry PG, Johnson CA, Mansberger SL and Cioffi GA (2005a). Psychophysical investigation of ganglion cell loss in early glaucoma. *J Glaucoma.* 14, 11-19.

Stiles W (1939). The directional sensitivity of the retina and the spectral sensitivities of the rods and cones. *Proceedings of the Royal Society of London (Series B).* 127, 64-105.

Stiles W (1959). Color vision the approach through increment-threshold sensitivity. *Proc Nat Acad Sci, USA.* 45, 100-114.

Strouthidis NG, Scott A, Viswanathan AC, Crabb DP and Garway-Heath (2007). Monitoring glaucomatous visual field progression: The effect of a novel spatial filter. *Invest Ophthalmol Vis Sci.* 48, 251-257.

Suzumura H (1988). Visual fatigue-like effect in glaucomas with repeated threshold measurement. *Nippon Ganka Zasshi.* 92, 220-224.

Szmajda BA, Grünert U and Martin PR (2008). Retinal ganglion cell inputs to the koniocellular pathway. *J Comp Neurol.* 20, 251-258.

Taibbi G, Fogagnolo P, Orzalesi N and Rossetti (2009). Reproducibility of the Heidelberg Retina Tomograph III glaucoma probability score. *J Glaucoma.* 18, 247-252.

Teesalu P, Airaksinen PJ, Tuulonen A, Nieminen H and Alanko H (1997a). Flurometry of the crystalline lens for correcting blue-on-yellow perimetry results. *Invest Ophthalmol Vis Sci.* 38, 697-703.

Teesalu P, Vihanninjoki K, Airaksinen PJ and Tuulonen A (1998). Hemifield association between blue-on-yellow visual field and optic nerve head topographic measurements. *Graefes Arch Clin Exp Ophthalmol.* 236, 339-345.

Teesalu P, Vihanninjoki K, Airaksinen PJ, Tuulonen A and Laara E (1997b). Correlation of blue-on-yellow visual fields with scanning confocal laser optic disc measurement. *Invest Ophthalmol Vis Sci.* 38, 2452-2459.

Thomas D, Thomas R, Muliyil JP and Georg R (2001). Role of Frequency-Doubling perimetry in detecting neuro-ophthalmic visual field defects. *Am J Ophthalmol.* 131, 734-741.

Tomita G, Maeda M, Sogano S and Kitazawa Y (1993). An analysis of the relationship between High-pass Resolution Perimetry and neuroretinal rim area in normal-tension glaucoma. *Acta Ophthalmol* . 71, 196-200.

Traquair HM (1927). Cited in: *Traquair's clinical perimetry:* 13th Edition, 1957. London, Kimpton.

Tremblay F, Mireault AC, Létourneau A, Pierrat A and Bourrassa S (2002).Tactile perception and manual dexterity in computer users. *Somatosensory and Motor Research.* 19, 1010-1018.

Trible J, Schultz R, Robinson J and Rothe T (2000). Accuracy of glaucoma detection with Frequency-Doubling perimetry. *Am J Ophthalmol.* 129, 740-745.

Trick GL, Steinman SB and Amyot M (1995). Motion perception deficits in glaucomatous optic neuropathy. *Vision Res.* 35, 2225-2233.

Trong PK and Rieke F (2008). Origin of correlated activity between parasol retinal ganglion cells. *Nat Neurosci.* 11, 1343-1351.

Trope GE and Britton R (1987). A comparison of Goldmann and Humphrey automated perimetry in patients with glaucoma. *Br J Ophthalmol.* 71, 489-493.

Tsai CS, Zangwill L, Sample PA, Garden V, Bartsch DU and Weinreb RN (1995). Correlation of peripapillary retinal height and visual field in glaucoma and normal subjects. *J Glaucoma.* 4, 110-116.

Turpin A, McKendrick AM, Johnson CA and Vingrys AJ (2002). Performance of efficient test procedures for Frequency-Doubling Technology perimetry in normal and glaucomatous eyes. *Invest Ophthalmol Vis Sci.* 43, 709-715.

Turpin A, McKendrick AM, Johnson CA and Vingrys AJ (2003). Properties of perimetric threshold estimates from Full Threshold, ZEST and SITA-like strategies as determined by computer simulation. *Invest Ophthalmol Vis Sci.* 44, 4787-4795.

Tyler CW (1981). Specific deficits of flicker sensitivity in glaucoma and ocular hypertension. *Invest Ophthalmol Vis Sci.* 20, 204-212.

Tyrrell R and Owens D (1988). A rapid technique to assess the resting states of the eyes and other threshold phenomena: the Modified Binary Search (MOBS). *Behav Res Methods Instr Comp.* 20, 137-141.

Tytla ME, Trope GE and Buncic JR (1990). Flicker sensitivity in treated ocular hypertension. *Ophthalmology.* 97, 36-43.

Uchida H, Brigatti L and Caprioli J (1996). Detection of structural damage from glaucoma with confocal laser image analysis. *Invest Ophthalmol Vis Sci.* 37, 2393-2401.

Uchida H, Tomita G, Shibahara G, Sugiyama K and Kitazawa Y (1998). Diagnostic capabilities of a classification program of the Heidelberg Retina Tomograph for early glaucomatous changes. *Nippon Ganka Gakkai Zasshi.* 102, 333-339.

Vesti E, Johnson CA and Chauhan BC (2003). Comparison of different methods for detecting glaucomatous visual field progression. *Invest Ophthalmol Vis Sci.* 44, 3873-3879.

Vingrys AJ and Pianta MJ (1999). A new look at threshold estimation algorithms for automated static perimetry. *Optom Vis Sci.* 76, 588-595.

Volbrecht VJ, Nerger JL, Imhoff SM and Ayde CJ (2000). Effect of the short-wavelength sensitive cone mosaic and rods on the locus of unique green. *J Opt Soc Am A Opt Image Sci Vis.* 17, 628-634.

Vonthein R, Rauscher S, Paeztold J, Nowomiejska K, Krapp E, Hermann A, Sadowski B, Chaumette C, Wild JM and Schiefer U (2007). The normal age-corrected and reaction time-corrected isopter derived by semi-automated kinetic perimetry. *Ophthalmology.* 114, 1065-1072.

Wadood AC, Azuara-Blanco A, Aspinall P, Taguri A and King AJ (2002). Sensitivity and specificity of Frequency-Doubling Technology, Tendency-Oriented Perimetry and Humphrey Swedish Interactive Threshold Algorithm-fast perimetry in a glaucoma practice. *Am J Ophthalmol.* 133, 327-332.

Wall M, Jennisch CS and Munden PM (1997a). Motion perimetry identifies nerve fiber bundle like defects in ocular hypertension. *Arch Ophthalmol.* 115, 26-33.

Wall M and Ketoff KM (1995). Random dot motion perimetry in patients with glaucoma and in normal subjects. *Am J Ophthalmol.* 120, 587-596.

Wall M, Kutzko KE and Chauhan BC (1997b). Variability in patients with glaucomatous visual field damage is reduced using size V stimuli. *Invest Ophthalmol. Vis Sci.* 38, 426-435.

Wall M, Lefante J and Conway M (1991). Variability of High-pass Resolution Perimetry in normals and patients with idiopathic intracranial hypertension. *Invest Ophthalmol Vis Sci.* 32, 3091-3095.

Wall M; Maw RJ; Stanek KE and Chauhan BC (1996). The psychometric function and reaction time of automated perimetry in normal and abnormal areas of the visual field in patients with glaucoma. *Invest Ophthalmol Vis Sci.* 37, 878-885.

Wang J, Wu DZ and Fitake FW (1996). A study of motion perception in primary open angle glaucoma. *Yan Ke Xue Bao.* 12, 46-50.

Wang YZ, Thibos LN and Bradley A (1997). Effects of refractive error on detection acuity and resolution acuity in peripheral vision. *Invest Ophthalmol Vis Sci.* 38, 2134-2143.

Weber J (1990). A new strategy for automated static perimetry. *Fortschr Ophthalmol.* 1, 37-40.

Weber J and Klimaschka T (1995). Test time and efficiency of the dynamic strategy in glaucoma perimetry. *Ger J Ophthalmol.* 4, 25-31.

Weber J and Rau S (1992). The properties of perimetric thresholds in normal and glaucomatous eyes. *Ger J Ophthalmol.* 1, 79-85.

Weijland A, Fankhauser F, Bebie H and Flammer J (2004). *Automated perimetry, visual field digest, fifth edition.* Haag-Streit AG.

Weinreb RN, Lindsey JD and Sample PA (1994). Lateral geniculate nucleus in glaucoma. *Am J Ophthalmol.* 118, 126-129.

Weinreb RN, Lusky M, Bartsch DU and Morsman D (1993). Effect of repetitive imaging on topographic measurements of the optic nerve head. *Arch Ophthalmol.* 111, 636-638.

Weinreb RN and Perlman JP (1986). The effect of refractive correction on automated perimetric thresholds. *Am J Ophthalmol.* 101, 706-709.

Weinreb RN, Shakiba S and Sample PA (1995). Association between quantitative nerve fibre layer measurement and visual field loss in glaucoma. Am J Ophthalmol. 120, 732-738.

Weinreb RN, Zangwill L, Berry CC, Bathija R and Sample PA (1998). Detection of glaucoma with scanning laser polarimetry. *Arch Ophthalmol.* 116, 1583-1589.

Werner EB, Adelson A and Krupin T (1988). Effect of patient experience on the results of automated perimetry in clinically stable glaucoma patients. *Ophthalmology.* 95, 764-767.

Werner EB, Krupin T, Adelson A and Feitl ME (1990). Effect of patient experience on the results of automated perimetry in glaucoma suspect patients. *Ophthalmology.* 97, 44-48.

Werner EB, Petrig B, Krupin T and Bishop KI (1989), Variability of automated visual fields in clinically stable glaucoma patients. *Invest Ophthalmol Vis Sci.* 30, 1083-1089.

Werner JS (1982). Development of scotopic sensitivity and the absorption spectrum of the human ocular media. *J Opt Soc Am.* 72, 247-258.

Westcott MC, Fitzke FW and Hitchings RA (1998). Abnormal motion displacement thresholds are associated with fine scale luminance sensitivity loss in glaucoma. *Vision Res.* 38, 3171-3180.

Wiesel TN and Hubel DH (1966). Spatial and chromatic interactions in the lateral geniculate body of the rhesus monkey. *J Neurophysiol.* 29, 1115-1156.

Wikler KC and Rakic P (1990). Distribution of photoreceptor subtypes in the retina of diurnal and nocturnal primates. *J Neurosci.* 10, 3390-3401.

Wild JM, Betts T, Ross K and Kenwood C (1988). Influence of antihistamines on central visual field assessment. In Heijl A (eds.). *Perimetry update 1988/89*: Proceedings of the 13th International Perimetric Society meeting, Vancouver, 1988. 439.

Wild JM (2001). Short-wavelength Automated Perimetry. *Acta Ophthalmol Scan.* 79, 546-559.

Wild JM, Cubbidge RP, Pacey IE and Robinson R (1998). Statistical aspects of the normal visual field in Short-wavelength Automated Perimetry. *Invest Ophthalmol Vis Sci.* 39, 54-63.

Wild JM, Dengler-Harles M, Searle AE, O'Neill EC and Crews SJ (1989). The influence of the learning effect on automated perimetry in patients with suspected glaucoma. *Acta Ophthalmol.* 67, 537-545.

Wild JM and Hudson C (1995). The attenuation of blue-on-yellow perimetry by the macular pigment. *Ophthalmology.* 102, 911-917.

Wild JM, Hussey MK, Flanagan JG and Trope GE (1993). Pointwise topographical and longitudinal modelling of the visual field in glaucoma. *Invest Ophthalmol Vis Sci.* 34, 1907-1916.

Wild JM, Hutchings N, Hussey MK, Flanagan JG and Trope GE (1997). Pointwise univariate linear regression of perimetric sensitivity against follow-up time in glaucoma. *Ophthalmology.* 104, 808-815.

Wild JM, Kim LS, Pacey IE and Cunliffe IA (2006). Evidence for a learning effect in Short-wavelength Automated Perimetry. *Ophthalmology.* 113, 206-215.

Wild JM and Moss ID (1996). Baseline alteration in blue-on-yellow normal perimetric sensitivity. *Graefes Arch Clin Exp Ophthalmol.* 234, 141-149.

Wild JM, Moss ID, Whitaker D and O'Neill EC (1995). The statistical interpretation of blue-on-yellow visual field loss. *Invest Ophthalmol Vis Sci.* 36, 1398-1410.

Wild JM, Pacey IE, Hancock SA and Cunliffe IA (1999a). Between-algorithm, between-individual differences in normal perimetric sensitivity: Full Threshold, FASTPAC and SITA. Swedish Interactive Threshold Algorithm. *Invest Ophthalmol Vis Sci.* 40, 1152-1161.

Wild JM, Pacey IE, O'Neill EC and Cunliffe IA (1999b). The SITA perimetric threshold algorithms in glaucoma. *Invest Ophthalmol Vis Sci.* 40, 1998-2009.

Wild JM, Searle AE, Dengler-Harles M and O'Neill AI (1991). Long-term follow-up of baseline learning and fatigue effects in the automated perimetry of glaucoma and ocular hypertensive patients. *Acta Ophthalmol.* 69, 210-216.

Wild JM, Wood JM and Flanagan JG (1987). Spatial summation and the cortical magnification of perimetric profiles. *Ophthalmologica.* 195, 88-96.

Wildberger W and Robert Y (1998). Visual fatigue during prolonged visual field testing in optic neuropathies. *Neuro-Ophthalmology.* 8, 167-174.

Wollstein G, Garway-Heath DF, Fontana L and Hitchings RA (2000). Identifying early glaucomatous changes. Comparison between expert clinical assessment of optic disc photographs and confocal scanning ophthalmoscopy. *Ophthalmology.* 107, 2272-2277.

Wollstein G, Garway-Heath DF and Hitchings RA (1998). Identification of early glaucoma cases with the scanning laser ophthalmoscope. *Ophthalmology.* 105, 1557-1563.

Wood JM, Wild JM and Crews SJ (1987a). Induced intraocular light scatter and the sensitivity gradient of the normal visual field. *Graefes Arch Clin Exp Ophthalmol.* 225, 369-373.

Wood JM, Wild JM, Hussey MK and Crews SJ (1987b). Serial examination of the normal visual field using Octopus automated projection perimetry. Evidence for a learning effect. Acta Ophthalmol. 65, 326-333.

Wood JM, Wild JM, Smerdon DL and Crews SJ (1989). Alteration in the shape of the automated perimetric profile arising from cataract. *Graefes Arch Clin Exp Ophthalmol.* 227, 157-161.

Wu DC, Schwartz B and Nagin P (1987). Trend analyses of automated visual fields. *Doc Ophthalmol Proc Ser.* 49, 175.

van Wyk M, Wässle H and Taylor WR (2009). Receptive field properties of ON- and OFF-ganglion cells in the mouse retina. *Vis Neurosci.* 26, 297-308.

Yamagishi N, Anton A, Sample PA, Zangwill L, Lopez A and Weinreb RN (1997). Mapping structural damage of the optic disc to the visual field defect in glaucoma. *Am J Ophthalmol.* 123, 667-676.

Yamamoto S, Kamiyama M, Nitta K, Yamada T and Hayasaka S (1996). Selective reduction of the S cone electroretinogram in diabetes. *Br J Ophthalmol.* 80, 973-975.

Yeh T, Smith VC and Pokorny (1989). The effect of background luminance on cone sensitivity functions. *Invest Ophthalmol Vis Sci.* 30, 2077-2086.

Yoshiyama KK and Johnson CA (1997). Which method of Flicker perimetry is most effective for detection of glaucomatous visual field loss? *Invest Ophthalmol Vis Sci.* 38, 2270-2277.

Young WO, Stewart WC, Hunt H and Crosswell H (1990). Static threshold variability in the peripheral visual field in normal subjects. *Graefes Arch Clin Exp Ophthalmol.* 228, 454-457.

Yücel YH, Zhang Q, Weinreb RN, Kaufman PL and Gupta N (2003). Effects of retinal ganglion cell loss on magno-, parvo-, koniocellular pathways in the lateral geniculate nucleus and visual cortex in glaucoma. *Prog Retin Eye Res.* 22, 465-481.

Yudcovitch L (2006). Use of Short-wavelength and Frequency-Doubling Perimetry for glaucoma diagnosis and management. http://www.optpacificu.edu.

Zalta AH (1989). Lens rim artefact in automated threshold perimetry. *Ophthalmol.* 96, 1302-1311.

Zarkovic A, Mora J, McKelvie J and Gamble G (2007). Relationship between second generation Frequency-Doubling Technology and Standard automated perimetry in patients with glaucoma. *Clin Experiment Ophthalmol.* 35, 808-811.

Zeimer RC, Lim HKI and Ogura Y (1987). Evaluation of an objective method for the in vivo measurement of changes in light transmittance of the human crystalline lens. *Exp Eye Res.* 45, 969-976.

Zeyen TG and Caprioli J (1993). Progression of disc and field damage in early glaucoma. *Arch Ophthalmol.* 11, 62-65.

Zeyen TG, Raymond M and Caprioli J (1992). Disc and field damage in patients with unilateral visual field loss from primary open-angle glaucoma. *Doc Ophthalmol.* 82, 279-286.

Zhong Y, Chen L, Cheng Y and Huang (2008). Influence of learning effect on blue-on-yellow perimetry. *Eur J Ophthalmol.* 18, 392-9.

Zinser G, Van Resandt W, Dreher AW, Weinreb RN, Harbarth U, Schroeder H and Burk RO (1989). Confocal laser tomographic scanning of the eye. *Proc SPIE.* 1161, 337.

Zulauf M, Becht C and Bernoulli (1996b). False-positive peak of the Bebié curve as a reliability parameter In Wall M and Heijl A (eds.). *Perimetry Update 1996/97.* Amsterdam/ New York: Kugler Publications, 1997. 185-190.

Zulauf M, Caprioli J, Hoffman DC and Tressler CS (1990). Fluctuation of the differential light sensitivity in clinically stable glaucoma patients. In: Mills RP, Heijl A (eds.). *Perimetry Update 1990/91.* Amsterdam: Kugler and Ghedini, 1991. 183-188.

Zulauf M, Fechlmann P and Flammer J (1994). Efficiency of the standard Octopus bracketing procedure compared to that of the 'Dynamic strategy' of Weber. In Mills RP and Wall M (eds.). *Perimetry update 1994/95.* Amsterdam/ New York: Kugler Publications, 1995. 422-437.

Zulauf M, Fechlmann P and Flammer J (1996a). Perimetry with normal Octopus technique and Weber 'dynamic' technique. Initial results with reference to reproducibility of measurements in glaucoma patients. *Ophthalmologe.* 93, 420-427.

Zulauf M, Flammer J and Singer C (1986). The influence of alcohol on the outcome of automated static perimetry. *Graefes Arch Clin Exp Ophthalmol.* 224, 525-528.

APPENDIX: A.1 PUBLICATIONS

Zulauf M and **Castelberg CA** (2005). Aktuelle Perimetriemethoden zur Beurteilung einer Progression. In: *Search on Glaucoma.* Progressionsfaktoren beim Glaukom. Excerpta Medica, Amsterdam, Niederlande. 14-25.

Zulauf M and **Castelberg CA** (2006). Dynamik der Gesichtsfeld-Veränderung beim Glaukom. In: *Search on Glaucoma.* Chronobiologie und Chronopharmakologie beim Glaukom. Excerpta Medica, Amsterdam, Niederlande. 72-83.

APPENDIX: A.2 ABSTRACTS

Castelberg CA, Zulauf M and Wild JM (2007). Residual learning effect limits the utility of Short-wavelength Automated Perimetry (SWAP) using the Swedish Interactive Threshold Algorithm (SITA). *ARVO.* E-1626.

Castelberg CA, Zulauf M and Wild JM (2008). The learning effect with the Pulsar perimeter in normal individuals, in patients with ocular hypertension and in patients with open angle glaucoma. *ARVO.* E-1101.

Castelberg CA, Zulauf M and Wild JM (2009). The effect of defocus on the Pulsar perimetry in normal individuals and in patients with open angle glaucoma. *ARVO.* E-5293.

APPENDIX: A.3 LECTURES

Castelberg CA (2006). Neue Wege in der Gesichtsfeldmessung. *Meeting of the locale group of ophthalmologists.* August 31, 2006, Chur, Switzerland.

Castelberg CA (2008). Effects of defocusing in Pulsar perimetry. *Octopus symposium.* October 29- November 1, 2008, Berne, Switzerland.

APPENDIX: B.1 MATHEMATICAL KEY OF THE LEARNER'S INDEX

In order to attempt to establish a LI for SITA SWAP and Pulsar perimetry, the deciphering of the Olsson and colleagues (1997b) LI for the HFA 30-2 Full Threshold programme was necessary. The generous Dr. Kern, mathematician from the eidg. Schnee- u. Lawinenforschungsinstitut, Davos, Switzerland supplied us with the following notations:

All persons in the trained group received a vector $s=(s_1, s_2, s_3, s_4, s_5)$ with the values of the mean deviations of the age-corrected average threshold for all of the five concentric zones noted as ACAT (age-corrected average threshold). The averaged values of the measurements of the trained group for all of the five concentric zones are noted with a vector:

(1) $$\bar{s}=(\bar{s}_1, \bar{s}_2, \bar{s}_3, \bar{s}_4, \bar{s}_5)$$

The matrix of the covariance Σ is calculated according to

(2) $$\sigma_{ij}=\{(s_i - \bar{s}_i)(s_j - \bar{s}_j)\}$$

whereby σ_{ij} is the notation on the i-th line of the j-th column of the matrix of the covariance $\boldsymbol{\Sigma}$. This matrix has the dimension of 5x5, because both indices i and j go from 1 to 5.

For example, σ_{23} is the middle product of the deviations of the values from the trained subjects of the mean of the zones 2 and 3. To find the value 'σ_{23}', it is necessary to calculate the product $(s_2 - \bar{s}_2)\ (s_3 - \bar{s}_3)$ for every subject of the trained group and therefore to create the mean of all these values.

In this way, it is necessary to proceed in all possible combinations of i and j and the matrix of covariance Σ will be obtained:

(3)
$$\Sigma = \begin{pmatrix} \sigma_{11}, \sigma_{12}, \sigma_{13}, \sigma_{14}, \sigma_{15} \\ \sigma_{21}, \sigma_{22}, \sigma_{23}, \sigma_{24}, \sigma_{25} \\ \sigma_{31}, \sigma_{32}, \sigma_{33}, \sigma_{34}, \sigma_{35} \\ \sigma_{41}, \sigma_{42}, \sigma_{43}, \sigma_{44}, \sigma_{45} \\ \sigma_{51}, \sigma_{52}, \sigma_{53}, \sigma_{54}, \sigma_{55} \end{pmatrix}$$

Using the formula (2) it becomes visible that the values in the diagonal of the matrix (that means for i=j), the variance of the measurements in contrast to the ACAT, lay in the zone i.

Therefore, the inverse matrix of covariance Σ^{-1} is defined as follows:

(4)
$$\Sigma\Sigma^{-1} = 1$$

where

(5) $$1=\begin{pmatrix}10000\\01000\\00100\\00010\\00001\end{pmatrix}$$

corresponds to the matrix of unity. The matrix of unity is the analogue to 1 in the numbers. By the multiplication of one matrix by the matrix of unity, the original matrix will be obtained again.

The inverse matrix of covariance is according to the equation 4 the analogue matrix to the construction of the fraction $\frac{1}{a}$ originated from the number a. For its determination a standardized numerical procedure was used.

Similar to $\bar{s}$ for the trained subjects, mean values of the deviation of ACAT from the learner group (without training) are calculated and the received values for the zones 1-5 into the vector $\mu=(\mu_1, \mu_2, \mu_3, \mu_4, \mu_5)$ are noted.

The measurement values of the deviation from ACAT for an individual are therefore noted in the vector $\chi=(\chi_1, \chi_2, \chi_3, \chi_4, \chi_5)$. The indices from χ and μ correspond to the concentric zones again.

The meaning of the LI:

The definition of the LI is the relationship between the deviation of the measurements of a concrete subject without training and the averaged deviation of a trained subject.

The LI is defined as

(6) $$LI=\frac{\mu^T \Sigma^{-1}x}{\mu^T \Sigma^{-1}\mu}$$

An intuitive comprehension can be obtained when one imagines that the whole sum of measurement values can be imposed without the classification in the different concentric zones. Thus, in this case $i=j=1$ and

(7) $$\Sigma^{-1}=\sigma_{11}^{-1}=\left\{\left(s_1-\bar{s}_1\right)^2\right\}^{-1}=\frac{1}{\mathrm{var}(s)}$$

The inverse matrix of covariance is therefore only the reciprocal of the variance of s. The vector μ^T becomes simply the mean of the deviations of the untrained group and χ is the measurement value of a concrete subject.

Therefore, in this simple case we can write:

(8) $$LI_1=\frac{\mu\chi / \mathrm{var}(s)}{\mu^2 / \mathrm{var}(s)}$$

Therefore, if the measurement value χ of a subject is close to the mean μ of the learner group without training, LI will tend toward 1. On the contrary, if χ tends to be small, (only a small deviation from ACAT), then LI will go toward 0.

Through the classification in different zones, information about the spatial distribution of the deviation from ACAT will be obtained. With help of Σ^{-1}, a relationship can be established between the spatial deviations of a concrete subject and those of the whole untrained group and compared with those of the trained subjects. Formula 6 allows the statement of how much the spatial distribution χ of the deviation of an individual deviates from the averaged spatial distribution μ of an untrained learner, if they are placed in a relationship with each other by means of the correlation of the deviations of trained individuals.

The math.-procedure:

The way of writing $\mu^T \Sigma^{-1} \chi$ in the numerator of the formula 6 stands for that first of all the vector μ has to be multiplied by the column of the matrix Σ^{-1}. The result is a vector, which in turn is multiplied by the vector χ, out of which a numeric value is obtained. The procedure for the denominator in formula 6 is similar.